

AMM

# Plasticity and Geotechnics

Hai-Sui Yu



Springer

---

# **PLASTICITY AND GEOTECHNICS**

# Advances in Mechanics and Mathematics

---

## VOLUME 13

---

*Series Editors:*

David Y. Gao

*Virginia Polytechnic Institute and State University, U.S.A.*

Ray W. Ogden

*University of Glasgow, U.K.*

*Advisory Editors:*

I. Ekeland

*University of British Columbia, Canada*

S. Liao

*Shanghai Jiao Tung University, P.R. China*

K.R. Rajagopal

*Texas A&M University, U.S.A.*

T. Ratiu

*Ecole Polytechnique, Switzerland*

David J. Steigmann

*University of California, Berkeley, U.S.A.*

W. Yang

*Tsinghua University, P.R. China*

---

# **PLASTICITY AND GEOTECHNICS**

By

HAI-SUI YU  
University of Nottingham, UK

 Springer

Library of Congress Control Number: 2006928849

ISBN-10: 0-387-33597-8      e-ISBN: 0-387-33599-4

ISBN-13: 978-0-387-33597-1

Printed on acid-free paper.

---

AMS Subject Classifications: 74-xx, 65-xx, 70-xx

---

© 2006 Springer Science+Business Media, LLC

All rights reserved. This work may not be translated or copied in whole or in part without the written permission of the publisher (Springer Science+Business Media, LLC, 233 Spring Street, New York, NY 10013, USA), except for brief excerpts in connection with reviews or scholarly analysis. Use in connection with any form of information storage and retrieval, electronic adaptation, computer software, or by similar or dissimilar methodology now known or hereafter developed is forbidden.

The use in this publication of trade names, trademarks, service marks, and similar terms, even if they are not identified as such, is not to be taken as an expression of opinion as to whether or not they are subject to proprietary rights.

Printed in the United States of America.

9 8 7 6 5 4 3 2 1

[springer.com](http://springer.com)

To Xiu-Li, Christina and Thomas  
for inspiration, encouragement and forbearance

*“What is new is the inter-relation of concepts,  
the capacity to create new types of calculation,  
and the unification of the bases for judgement.”*  
A.N. Schofield and C.P. Wroth (1968)

## TABLE OF CONTENTS

<b>Foreword</b>	<b>xvii</b>
<b>Preface</b>	<b>xix</b>

### PART I: FUNDAMENTALS

<b>1 INTRODUCTION</b>	<b>1</b>
1.1 SCOPE AND AIMS	1
1.2 A BRIEF HISTORICAL OUTLINE	1
1.2.1 Elastic-plastic stress-strain relations	2
1.2.2 Plastic solution techniques	3
1.3 CONTINUUM VERSUS DISCRETE APPROACHES	4
1.4 SIGN CONVENTIONS	5
REFERENCES	5
<b>2 ELEMENTS OF CONTINUUM MECHANICS</b>	<b>10</b>
2.1 INTRODUCTION	10
2.2 STRESS STATE AND EQUILIBRIUM	10
2.2.1 Two-dimensional elements	10
2.2.2 Three-dimensional elements	14
2.3 STRAIN AND COMPATIBILITY	18
2.3.1 Two-dimensional elements	18
2.3.2 Three-dimensional elements	18
2.4 ELASTIC STRESS-STRAIN RELATIONS	19
2.4.1 Plane stress conditions	19
2.4.2 Plane strain conditions	20
2.4.3 Three-dimensional conditions	20
2.5 SUMMARY	21
REFERENCES	21
<b>3 FOUNDATIONS OF THE THEORY OF PLASTICITY</b>	<b>22</b>
3.1 INTRODUCTION	22

3.2	YIELD CRITERION	22
3.3	PLASTIC POTENTIAL AND PLASTIC FLOW RULE	23
3.4	PRINCIPLE OF MAXIMUM PLASTIC WORK	24
3.5	STRAIN HARDENING AND PERFECT PLASTICITY	25
3.6	DRUCKER'S STABILITY POSTULATE	27
3.7	ISOTROPIC AND KINEMATIC HARDENING	29
3.7.1	Isotropic hardening	29
3.7.2	Kinematic hardening	30
3.7.3	Mixed hardening	31
3.8	GENERAL STRESS-STRAIN RELATIONS	32
3.8.1	Isotropic hardening	32
3.8.2	Kinematic hardening	34
3.9	HISTORICAL REMARKS	37
	REFERENCES	38
<b>4</b>	<b>GENERAL ELASTIC-PLASTIC THEOREMS</b>	<b>40</b>
4.1	INTRODUCTION	40
4.2	THE PRINCIPLE OF VIRTUAL WORK	40
4.3	UNIQUENESS THEOREMS	43
4.3.1	Uniqueness of stress rates and strain rates	43
4.3.2	Uniqueness of stresses	45
4.4	MINIMUM AND VARIATIONAL PRINCIPLES	47
4.4.1	Elastic materials	47
4.4.2	Elastic-plastic materials	51
4.5	THEOREMS OF PLASTIC COLLAPSE FOR LIMIT ANALYSIS	54
4.5.1	Introduction	54
4.5.2	Constant stress theorem at plastic collapse	55
4.5.3	Lower bound theorem of plastic collapse	56
4.5.4	Upper bound theorem of plastic collapse	58
4.5.5	Extension to non-associated plastic flow	59
4.5.6	Historical remarks	61
4.6	SHAKEDOWN THEOREMS	62
4.6.1	Melan's lower bound shakedown theorem	63

	Table of Contents	ix
4.6.2	Koiter's upper bound shakedown theorem	64
4.6.3	Historical remarks and further extensions	66
REFERENCES		66
<b>PART II: CONSTITUTIVE RELATIONS</b>		
<b>5</b>	<b>PERFECT PLASTICITY</b>	<b>69</b>
5.1	INTRODUCTION	69
5.2	ELASTIC MODELS	70
5.2.1	Linear elasticity	70
5.2.2	Nonlinear elasticity	71
5.3	PLASTICITY MODELS FOR COHESIVE SOILS	72
5.3.1	Tresca model	72
5.3.2	von Mises model	74
5.4	PLASTICITY MODELS FOR FRICTIONAL MATERIAL	75
5.4.1	Mohr-Coulomb model	76
5.4.2	Drucker-Prager model	79
5.4.3	Lade-Duncan and Matsuoka-Nakai models	80
5.4.4	Hoek-Brown model	82
REFERENCES		83
<b>6</b>	<b>ISOTROPIC HARDENING AND CRITICAL STATE THEORY</b>	<b>86</b>
6.1	INTRODUCTION	86
6.2	THE CONCEPT OF CRITICAL STATES	87
6.3	CAM CLAY AND MODIFIED CAM CLAY	88
6.3.1	Cam clay model	88
6.3.2	Modified Cam clay model	93
6.3.3	Limitations of Cam clay and Modified Cam clay	93
6.4	THE STATE PARAMETER INTERPRETATION	95
6.4.1	The state parameter concept	95
6.4.2	Cam clay and modified Cam clay in terms of the state parameter	97
6.5	YU'S UNIFIED CRITICAL STATE MODEL	99
6.5.1	A general stress-state relation for clay and sand	100
6.5.2	Incremental stress-strain relations for state parameter models	104

## Table of Contents

6.5.3	A unified state parameter model – CASM	105
6.5.4	Model constants and their identification	110
6.5.5	Prediction and validation	111
6.5.6	Remarks	127
6.6	EXTENSION OF CASM TO INCLUDE SHEAR HARDENING	129
6.7	EXTENSION OF CASM TO INCLUDE VISCOPLASTICITY	132
6.8	EXTENSION OF CASM FOR UNSATURATED SOILS	133
6.8.1	Elastic strains	134
6.8.2	Yield surfaces	136
6.8.3	Stress-dilatancy relation and plastic potential	137
6.8.4	Plastic strains	138
6.8.5	Hardening laws	138
6.9	EXTENSION OF CASM FOR BONDED GEOMATERIALS	139
6.10	FORMULATIONS FOR GENERAL STRESS STATES	142
	REFERENCES	145
<b>7</b>	<b>MULTI-SURFACE AND BOUNDING SURFACE PLASTICITY</b>	<b>153</b>
7.1	INTRODUCTION	153
7.2	THE MULTI-SURFACE CONCEPT	154
7.2.1	One-dimensional loading and unloading	154
7.2.2	General loading	154
7.3	MULTI-SURFACE PLASTICITY MODELS FOR SOILS	160
7.3.1	Total stress multi-surface modelling of undrained clay	160
7.3.2	Multi-surface modelling of frictional soils	164
7.4	THE BOUNDING SURFACE CONCEPT	168
7.5	BOUNDING SURFACE MODELS FOR SOILS	170
7.5.1	Two surface kinematic hardening formulation for clay	170
7.5.2	Radial mapping formulation of bounding surface plasticity	177
7.5.3	Bounding surface formulation for clay with three surfaces	180
7.6	UNIFIED BOUNDING SURFACE MODEL	182
7.6.1	Bounding surface formulation for monotonic loading – CASM-b	183
7.6.2	Bounding surface formulation for cyclic loading – CASM-c	186
7.6.3	Performance of CASM-c for simulating cyclic triaxial tests	188

REFERENCES	194
<b>8 NON-COAXIAL PLASTICITY</b>	<b>197</b>
8.1 INTRODUCTION	197
8.2 EVIDENCE OF NON-COAXIAL SOIL BEHAVIOUR	197
8.2.1 Simple shear	198
8.2.2 Torsional shear in hollow cylinder apparatus	199
8.2.3 DEM simulation of simple shear of a granular assembly	201
8.3 A YIELD VERTEX NON-COAXIAL THEORY	202
8.4 NON-COAXIAL THEORY BASED ON DOUBLE SHEARING	205
8.4.1 A class of non-coaxial plasticity theories in plane strain	206
8.4.2 Incremental non-coaxial stress-strain relationship	208
8.4.3 Extension of non-coaxial plasticity theories to axisymmetry	209
8.5 COMPARISON OF VERTEX AND DOUBLE SHEARING THEORIES	211
8.6 NUMERICAL SIMULATION OF SIMPLE SHEAR	213
8.6.1 Mohr-Coulomb model with the generalised double shear theory	213
8.6.2 The critical state model CASM with the yield vertex flow rule	223
REFERENCES	228
<b>9 PLASTICITY WITHOUT A PRIOR YIELD CRITERION</b>	<b>232</b>
9.1 INTRODUCTION	232
9.2 THE MATHEMATICAL THEORY OF ENVELOPES	232
9.2.1 Stress and strain variables	233
9.2.2 Energy balance, yield function and flow rule	234
9.2.3 Examples	234
9.3 THE ENDOCHRONIC THEORY	237
9.3.1 General formulation for cohesive soils under undrained conditions	238
9.3.2 Formulation for cohesionless soils	241
9.4 HYPOPLASTICITY	242
9.4.1 The basic hypoplastic equation	242
9.4.2 Determination of model constants	243
9.4.3 Improved hypoplastic equations	244
9.5 HYPERPLASTICITY	245
9.5.1 Derivation of von Mises plasticity	246

9.5.2	Derivation of Cam clay plasticity	247
9.5.3	Remarks	248
REFERENCES		249

### PART III: SOLUTION TECHNIQUES

<b>10</b>	<b>RIGOROUS ANALYSIS OF ELASTIC-PLASTIC PROBLEMS</b>	<b>251</b>
10.1	INTRODUCTION	251
10.2	EXPANSION OF CAVITIES IN AN INFINITE MEDIUM	251
10.3	CAVITY EXPANSION SOLUTION FOR TRESCA MATERIALS	258
10.3.1	Expansion of a spherical cavity in a finite medium	259
10.3.2	Similarity solutions for cavity expansion in an infinite medium	263
10.4	SIMILARITY SOLUTIONS FOR MOHR-COULOMB MATERIALS	263
10.4.1	Soil properties	264
10.4.2	Elastic solution in the outer elastic zone	265
10.4.3	Stress solution in the plastic zone	265
10.4.4	Elastic-plastic displacement analysis	266
10.4.5	Neglecting the convected part of stress rate	270
10.4.6	Results and discussion	270
10.5	ELASTIC-PLASTIC LOADING OF A PLANE STRAIN WEDGE	276
10.5.1	The wedge problem and governing equations	276
10.5.2	The fully elastic solutions	278
10.5.3	The initial yield and the elastic-plastic boundary	279
10.5.4	Elastic-plastic solutions	279
10.6	PLASTIC FLOW PAST A SMOOTH CONE	281
10.6.1	Kinematically determined axially symmetric stress and deformation fields	282
10.6.2	Governing equations in spherical polar coordinates	285
10.6.3	A class of exact solutions	287
10.6.4	Plastic flow past an infinite cone	289
REFERENCES		291
<b>11</b>	<b>SLIP LINE ANALYSIS</b>	<b>293</b>
11.1	INTRODUCTION	293
11.2	STRESS FIELDS IN PLASTIC REGIONS	294

	Table of Contents	xiii
11.2.1	Basic equations in terms of stresses	294
11.2.2	Solution using the method of characteristics	296
11.2.3	Slip line solutions for simple cases	296
11.2.4	Stress boundary conditions	298
11.2.5	Simple slip line fields	300
11.2.6	Boundary value problems and construction of slip line fields	301
11.3	VELOCITY FIELDS IN PLASTIC REGIONS	303
11.3.1	Velocity fields for associated flow rules	303
11.3.2	Velocity fields for non-associated flow rules	305
11.3.3	Discontinuities in velocity	307
11.3.4	Stress conditions on velocity characteristics	309
11.4	GEOTECHNICAL STABILITY EXAMPLES	310
11.4.1	Bearing capacity of embankments – stress fields	310
11.4.2	Bearing capacity of embankments – velocity fields	311
11.4.3	Bearing capacity of embankments – Hill's mechanism	313
11.4.4	Shallow foundations on a cohesive-frictional soil	315
11.4.5	Retaining walls on a cohesive-frictional soil	317
11.4.6	Pseudo-steady wedge penetration into a cohesive-frictional soil	318
11.4.7	Solutions accounting for non-associated flow rules	320
11.4.8	Special solutions for a purely cohesive soil	322
11.5	PLASTIC ANISOTROPY	322
11.5.1	Solutions for a general anisotropic cohesive-frictional material	323
11.5.2	Solution for a purely cohesive material	325
11.6	AXISYMMETRIC PROBLEMS	326
11.6.1	Basic equations in terms of stresses	327
11.6.2	Solution using the method of characteristics	328
	REFERENCES	328
<b>12</b>	<b>LIMIT ANALYSIS</b>	<b>331</b>
12.1	INTRODUCTION	331
12.2	BASIC PROCEDURES OF LIMIT ANALYSIS	332
12.2.1	Lower bound method of limit analysis	332
12.2.2	Upper bound method of limit analysis	335
12.2.3	Upper bound method and limit equilibrium analysis	337

12.2.4	General remarks	339
12.3	LOWER BOUND ANALYSIS USING LINEAR PROGRAMMING	339
12.3.1	Plane strain finite element formulations	340
12.3.2	Axisymmetric finite element formulations	345
12.3.3	Plane strain finite element formulations for jointed media	351
12.3.4	Plane strain finite element formulations for anisotropic soils	359
12.3.5	Plane strain finite element formulations for reinforced soils	361
12.4	UPPER BOUND ANALYSIS USING LINEAR PROGRAMMING	364
12.4.1	Formulation based on constant finite elements	364
12.4.2	Formulation based on linear strain finite elements	386
12.5	LIMIT ANALYSIS USING NONLINEAR PROGRAMMING	393
12.5.1	Limit analysis for a general yield criterion	393
12.5.2	Finite element approximation of velocity fields	397
12.5.3	The iterative solution algorithm	399
	REFERENCES	402
<b>13</b>	<b>SHAKEDOWN ANALYSIS</b>	<b>408</b>
13.1	INTRODUCTION	408
13.2	THE CONCEPT AND THEOREMS OF SHAKEDOWN	409
13.2.1	Simple illustration of the concept of shakedown	409
13.2.2	The lower and upper bound theorems of shakedown	412
13.3	SHAKEDOWN OF ROLLING AND SLIDING LINE CONTACTS	414
13.3.1	Elastic stress fields	414
13.3.2	Shakedown solutions in Tresca materials	416
13.3.3	Shakedown solutions in Mohr-Coulomb materials	419
13.4	SHAKEDOWN OF ROLLING AND SLIDING POINT CONTACTS	421
13.4.1	Problem definition of a point contact	422
13.4.2	The elastic stress field caused by a Hertz stress distribution	422
13.4.3	The residual stress field and static shakedown condition	423
13.4.4	Numerical results and discussion	425
13.5	SHAKEDOWN ANALYSIS USING LINEAR PROGRAMMING	427
13.5.1	Finite element formulation	428
13.5.2	Numerical application to shakedown analysis of pavements	434
13.6	SHAKEDOWN ANALYSIS USING NONLINEAR PROGRAMMING	441

Table of Contents	xv
13.6.1 Shakedown analysis for a general yield criterion	441
13.6.2 Finite element approximation of velocity fields	446
13.6.3 The iterative solution algorithm	448
REFERENCES	452
<b>14 FINITE ELEMENT ANALYSIS</b>	<b>456</b>
14.1 INTRODUCTION	456
14.2 PROCEDURES OF NONLINEAR FINITE ELEMENT ANALYSIS	456
14.3 ACCURATE FINITE ELEMENTS FOR SOIL PLASTICITY	458
14.3.1 Introduction	458
14.3.2 Theory	461
14.3.3 The use of new displacement interpolation function	465
14.3.4 Finite element formulations	467
14.3.5 Implementation in a standard finite element code	471
14.3.6 Numerical examples	474
14.3.7 Conclusions	479
14.4 SOLUTION SCHEMES FOR LOAD-DISPLACEMENT EQUATIONS	483
14.4.1 Incremental solution strategy	483
14.4.2 Iterative solution strategy	483
14.4.3 Incremental solution strategy with automatic step size control	485
14.5 INTEGRATION OF STRESS-STRAIN EQUATIONS	488
14.5.1 Elastic-plastic stress-strain relationship	488
14.5.2 Explicit integration method	489
14.5.3 Implicit integration method	492
14.6 LARGE DEFORMATION ANALYSIS	493
14.6.1 Introduction	493
14.6.2 Finite element formulations for large deformation	494
14.7 NUMERICAL EXAMPLES	498
14.7.1 Finite element analysis of critical state geomaterials	498
14.7.2 Finite element analysis of non-coaxial geomaterials	508
14.7.3 Finite element analysis of bonded geomaterials	510
REFERENCES	512
<b>INDEX</b>	<b>517</b>

## FOREWORD

by John B. Burland CBE, FRS, FREng  
Emeritus Professor of Soil Mechanics, Imperial College London

Geomaterials are very complex and theoretical soil and rock mechanics involves making important idealisations of the real material - in order to analyse it is always necessary to idealise. The process of analysis may be thought of as an exercise in modelling and as such may be carried out at various degree of sophistication ranging from the purely intuitive through to the very complex depending on the problem.

The key to successful engineering modelling lies in having a clear grasp of the nature of the idealisations that have been made and their influence on the calculated solutions. A well known class of ideal material is the porous elastic solids. By modelling the ground from such a material it is possible to find solutions to a wide range of practical problems. The good engineer does not believe that the soil really is elastic but by adopting such an idealisation it is often possible to arrive at valuable approximations to, and insights into, the behaviour of the real material.

Plastic materials form a wide ranging class of ideal materials which are much more 'soil-like' or 'rock-like' in their behaviour than their elastic counterparts. The theory of plasticity as applied to metals has reached its maturity and many books are available to guide practising engineers and students alike in its applications. The application of plasticity theory to geomaterials has been developing rapidly in recent years. Even for an expert in the field of plasticity it is difficult to keep up with the many developments that have, and are taking place. Practising geotechnical engineers, researchers and students could be forgiven for feeling a sense of bewilderment at the range of models now available and the claims made for them.

It is most timely that Professor Yu should have provided this comprehensive review of plasticity theory for geomaterials and its applications to geotechnical modelling. The first part of the book deals with the fundamentals of the theory of plasticity and in particular the general elastic-plastic theorems and principles. In the words of Professor Yu: "*It would be hard to overstate the importance of general theorems in the development and application of the theory of plasticity.*" Formal proofs are developed for all the major theorems and principles that underpin the theory including the Principle of Virtual Work, the Uniqueness Theorems, Minimum and Variational Principles, Theorems of Plastic Collapse for Limit Analysis and the Shakedown Theorems. Readers who are relatively unsophisticated mathematically should not be put off by the formal mathematical treatment adopted as the physical

implications of the results are explained and some valuable historical insights are woven into the story.

The second part of the book traces the development of plasticity models from the classical perfect plasticity models of Mohr-Coulomb, Tresca, von Mises through a range of Critical State isotropic hardening models and multi-surface and bounding surface models to some more recent models involving non-coaxiality of stress and strain increment and “*plasticity without a prior yield criterion.*” Of particular interest is the detailed development of Professor Yu’s unified Critical State Model known as CASM.

The third part of the book deals with solution techniques. These range from the rigorous analysis of some elastic-plastic problems, slip line analysis and limit analysis, moving on to less well known shakedown analysis and ending with a full chapter on the use of Finite Element Analysis. This final chapter places particular emphasis on the significant improvements in accuracy that can be achieved using new displacement interpolation functions developed by Professor Yu and which can be easily incorporated into standard codes.

Mention was made earlier of the bewildering number of plasticity models that are now available for tackling geotechnical problems. This book will serve as a most valuable source of reference to many of these models which are presented in a unified and rigorous manner, emphasising their strengths, weaknesses and applications in a balanced and objective way. It will prove invaluable to engineers, teachers and students working in this challenging and exciting subject.

J.B.B.

## PREFACE

The theory of plasticity is concerned with the mathematical study of stress and strain in plastically deformed materials. In their Preface to the Proceedings of the Symposium on Plasticity and Soil Mechanics held in Cambridge on 13-15 September 1973, Peter Wroth and Andrew Palmer stated:

*"Plasticity theory was developed by people who thought in terms of metals, and for about twenty years workers in soil mechanics have been looking at the theory, rather as outsiders, and asking whether it had anything to offer them."*

Since that time, however, enormous progress has been made towards thoughtful and sensitive application and development of plasticity theory, backed by careful experiments, in geotechnical engineering. Although further progress is still expected, the whole framework of plasticity theory for geomaterials may have reached a good degree of maturity. At present, few, if any, would doubt the usefulness and importance of plasticity theory in geotechnical analysis and design.

This book arose from my belief that there is an urgent need for the geotechnical community to have a unified and coherent presentation of plasticity theory for geomaterials and its applications to geotechnical analysis. Accordingly, the book attempts to summarise and present, in one volume, the major developments achieved to date in the field of plasticity theory and its geotechnical applications. The book covers classical, recent and modern developments of appropriate constitutive theories of stress-strain relations for geomaterials and a wide range of analytical and computational techniques that are available for solving geotechnical design problems. My main concern in writing this book has been to bring out the key concepts behind the most useful theoretical developments, the inter-relation of these concepts and their use and implementation in analytical and numerical procedures that are needed for solving practical problems in geotechnical engineering.

The book is intended primarily as a reference book for civil, geotechnical and mining engineers, researchers and students who are concerned with plasticity theory and its engineering applications. It may also be adopted as a text book for postgraduate or advanced undergraduate courses in plasticity theory. Given plasticity theory has widespread applications in many disciplines, the book should be of direct interest to researchers and engineers in the fields of continuum mechanics, mechanical and chemical engineering who are concerned with granular materials.

As indicated by its table of contents, the book is divided into three parts. The first part, Chapters 1 to 4, covers fundamental elements of continuum mechanics and

classical plasticity theory. The second part, containing Chapters 5 to 9, describes all the major theories that have been developed for deriving non-linear stress-strain relations for geomaterials. The final part of the book, containing Chapters 10 to 14, presents a wide range of solution techniques that are available for solving boundary value problems in geotechnical engineering.

The book is the result of many years of study, research, teaching and reflection. I have benefited much from collaborations with many colleagues and students - their contribution speaks for itself. Those concerned will know that I appreciate their assistance and help with considerable gratitude. I would particularly like to thank, among many, the late Peter Wroth, Jim Mitchell, John Burland, Mike Jamiolkowski, Tony Spencer, Kerry Rowe, Mark Randolph, Ted Brown, Steve Brown, John Carter, Ian Collins, Scott Sloan, Guy Houslsby, Brian Simpson, Robert Mair, Antonio Gens, Harry Poulos, Wai-Fai Chen and Malcolm Bolton for their personal influence on shaping my approach to research and teaching in plasticity theory and geotechnical engineering. I also benefited from discussions with the late John Booker, Chandra Desai, Poul Lade, Yannis Dafalias, Roberto Nova, Gerd Gudehus, Alan Ponter, Peter Kleeman, Andrew Whittle, Pieter Vermeer, David Harris, Fernando Schnaid, Wei Wu, Glenn McDowell, Rodrigo Salgado, Len Herrmann, Colin Thornton, Ken Been, Radoslaw Michalowski, Patrick Selvadurai, Ian Moore, Harvey Burd and Andrew Abbo on various aspects of plasticity theory.

It should be mentioned that consulting the classic book on plasticity by Rodney Hill, Professor of Applied Mathematics at the University of Nottingham from 1953 to 1962, has always been a fruitful and inspirational experience for me. I am very grateful to Tony Spencer, Antonio Gens, Glenn McDowell, Nick Thom, Wei Wu, Rodrigo Salgado and Fernando Schnaid for reading through earlier versions of the book and for their valuable comments. My students Cuong Khong, Huaxiang Li, Xun Yuan, Yunming Yang, Jun Wang and Ringo Tan have also provided helpful suggestions. I wish to thank all members of the staff and students, past and present, at the Nottingham Centre for Geomechanics (NCG) for making it a supportive, scholarly and creative environment under which this book could be produced. Special thanks are extended to David Gao for his encouragement, and to John Mardle and Robert Saley of Springer for their support throughout this project.

Finally it is a pleasure to record my deep appreciation to Professor John Burland for writing a Foreword and for his support and encouragement over the years.

Hai-Sui Yu  
West Bridgford, Nottingham

# CHAPTER 1

## INTRODUCTION

### 1.1 SCOPE AND AIMS

This book is concerned with plasticity theory of geomaterials (i.e. clay, sand, silt, rock etc) and its application to geotechnical analysis and design. In a classic book, Hill (1950) gives the following concise definition for plasticity theory:

*“The theory of plasticity is the name given to the mathematical study of stress and strain in plastically deformed solids. It takes as its starting point certain experimental observations of the macroscopic behaviour of a plastic solid in uniform state of combined stress. The task of the theory is two fold: first, to construct explicit relations between stress and strain agreeing with the observations as closely and as universally as need be; and second, to develop mathematical techniques for calculating non-uniform distributions of stress and strain in bodies permanently distorted in any way.”*

This definition is followed in the present book which will focus on developments of appropriate constitutive theories of stress-strain relations for geomaterials and various analytical and computational solution techniques that can be used to solve geotechnical design problems involving plastic deformation.

Since the subject now has a very wide scope and is still undergoing a steady development, it will be a difficult task to write a ‘definitive’ book that would cover every aspect of the development. Instead of covering the whole field cursorily, this book aims to bring together, in one volume, key concepts behind some of the most useful developments in plasticity theory for geomaterials and to discuss their applications to geotechnical analysis. The emphasis is on recent achievements, the inter-relation of key concepts together with their connections to classical metal plasticity, as well as the research work that I have been involved with over the past two decades. Despite this selective nature, the book still gives a comprehensive and unified account of plasticity theory for geomaterials. It is hoped that this publication will facilitate further development and application of plasticity theory in geotechnical engineering.

### 1.2 A BRIEF HISTORICAL OUTLINE

In this section, a very brief review is given on the development of the subject of plasticity theory of geomaterials. In view of the above discussion, it is instructive

to treat elastic-plastic stress-strain relations and plastic solution techniques separately.

### 1.2.1 Elastic-plastic stress-strain relations

The foundation of classical plasticity theory was laid by the 1950s and 1960s after several decades of theoretical and experimental research on plastic behaviour of metals. A review of this early development can be found in Nadai (1950), Hill (1950), Drucker (1950), Prager (1955) and Naghdi (1960). Key concepts of this foundation include the assumption of coaxiality of the principal stress and strain rate tensors by de Saint-Venant (1870), plastic potential theory by von Mises (1928) and Melan (1938), maximum plastic work principle by Hill (1948), Drucker's stability postulate (Drucker, 1952, 1958), and kinematic hardening laws by Prager (1955) and Ziegler (1959).

The early development of plasticity theory of geomaterials has been built upon this foundation achieved in metal plasticity. Unlike metal plasticity, however, volume changes during loading play a key role in modelling plastic behaviour of geomaterials. The work on soil hardening by Drucker *et al.* (1957) and that on soil yielding by Roscoe *et al.* (1958) laid the foundations for critical state theory, a concept that underpins much of the later developments in plasticity theory for geomaterials (Schofield and Wroth, 1968; Roscoe and Burland, 1968; Wroth and Housby, 1985; Yu, 1998).

More recent developments of metal plasticity include important concepts such as bounding surface plasticity (Dafalias and Popov, 1975; Krieg, 1975), multi-surface plasticity (Mroz, 1967; Iwan, 1967), and endochronic theory (Valanis, 1971). All these concepts have been applied with considerable success in modelling geomaterials over the last two decades. Other notable concepts that have been used to develop plastic stress-strain relations for geomaterials are double shearing theory (Spencer, 1964; de Josselin de Jong, 1971; Harris, 1995; Yu and Yuan, 2005, 2006), yield vertex theory (Rudnicki and Rice, 1975; Yang and Yu, 2006a,b), thermomechanical approach (Housby, 1982; Maugin, 1992; Collins and Housby, 1997), mathematical theory of envelopes (Chandler, 1985), and hypoplastic theory (Green, 1956; Kolymbas, 1991). Apart from stress space-based formulations, Naghdi and Trapp (1975) and Yoder and Iwan (1981) show that plasticity models can also be formulated in strain space. Although the strain space approach was used by a few geotechnical researchers (Zheng *et al.*, 1986; Simpson, 1992; Einav, 2004), its application in geotechnical engineering has so far been very rare.

Most stress-strain relations currently in use are developed based on experimental observations of the macroscopic behaviour of geomaterials in a uniform state of

combined stress in the laboratory (e.g. Jamiolkowski *et al.*, 1985; Mitchell, 1993). In recent years, however, there has been an increasing use of micromechanics and the discrete element method (DEM) (Cundall and Strack, 1979; Thornton, 2000; McDowell and Bolton, 1998; McDowell and Harireche, 2002; Jiang *et al.*, 2005; Jiang and Yu, 2006) for validating or providing physical insights for continuum plasticity theories.

### 1.2.2 Plastic solution techniques

Once a suitable stress-strain relation is developed, it needs to be combined with equilibrium equations and compatibility conditions for solving geotechnical boundary value problems. In general, these governing equations are too complex to be solved analytically. Analytical solutions are possible only for problems with very simple geometry and boundary conditions such as cavity expansion problems solved by Hill (1950) and Yu (2000a). For most problems of practical interest, however, numerical methods (e.g. finite element methods, finite difference methods, boundary element methods, and discrete element methods) will have to be employed (e.g. Sloan and Randolph, 1982; Brown, 1987; Gens and Potts, 1988; Zienkiewicz *et al.*, 1998; Carter *et al.*, 2000; Yu, 2000b).

Many geotechnical designs rely on two key calculations: stability analysis and deformation analysis (Terzaghi, 1943; Wroth and Houlsby, 1985). The former is to ensure that geotechnical structures are safe and stable and the latter is to ensure that deformation experienced by a geotechnical structure under working loads is not excessively large. In the past, geotechnical stability analysis has been carried out largely based on a perfectly plastic material model. This is because that for perfectly plastic behaviour, the slip line method and bound theorems of limit and shakedown analysis developed in the classical plasticity theory allow the failure and stability calculations to be carried out in a relatively simple manner (Hill, 1950; Sokolovski, 1965; Koiter, 1960; Davis, 1968; Chen, 1975; Salencon, 1977).

With respect to deformation analysis, past practice has been based on elastic analysis (Poulos and Davis, 1974). This is now recognized to be inaccurate for many cases as experimental research suggests that behaviour of geomaterials is highly nonlinear and plastic, even at very small strain (Burland, 1989). Therefore an appropriate deformation analysis would need to be based on the use of nonlinear elasticity and accurate plastic stress-strain relations.

There is no doubt that a most important development over the last three decades in geotechnical analysis has been the widespread application of finite element methods in both stability and deformation calculations (Naylor *et al.*, 1981; Chen and Mizuno, 1990; Zienkiewicz *et al.*, 1998; Potts and Zdravkovic, 1999; Carter

*et al.*, 2000). Finite element analysis is particularly popular because it is very general and is capable of incorporating any material stress-strain relations. The finite element method can easily account for both material and geometric nonlinearities, which are often present in boundary value problems facing the geotechnical engineer.

### 1.3 CONTINUUM VERSUS DISCRETE APPROACHES

Mechanics is the science that deals with the interaction between force and motion. In understanding the difference between continuum (i.e. macroscopic) and discrete (i.e. microscopic) approaches, the following remarks of Spencer (1980) may prove instructive:

*“Modern physical theories tell us that on the microscopic scale matter is discontinuous; it consists of molecules, atoms and even smaller particles. However, we usually have to deal with pieces of matter which are very large compared with these particles; this is true in everyday life, in nearly all engineering applications of mechanics, and in many applications in physics. In such cases we are not concerned with the motion of individual atoms and molecules, but only with their behaviour in some average sense. In principle, if we knew enough about the behaviour of matter on the microscopic scale it would be possible to calculate the way in which material behaves on the macroscopic scale by applying appropriate statistical procedures. In practice, such calculations are extremely difficult; only the simplest systems can be studied in this way, and even in these simple cases many approximations have to be made in order to obtain results.”*

Continuum solid mechanics is concerned with the mechanical behaviour of solids on the macroscopic scale. It ignores the discrete nature of matter and treats material as uniformly distributed throughout regions of space. For reasons outlined above, continuum mechanics has been for many years and, in my view, will continue to be the main theoretical basis for modelling mechanical behaviour of geomaterials.

As noted earlier, we have seen an increasing use of discrete mechanics (i.e. the microscopic approach) in recent years. In geotechnical engineering, this trend stems from the development of the Discrete Element Method (DEM) by Cundall and Strack (1979) for modelling granular material. The discrete element method was originally intended as a research tool for investigating the micro-mechanics of granular materials in order to identify the appropriate physically sound continuum model that then might be used in finite element analysis of boundary value problems. As stated by Thornton (2000), however, little progress has been made towards achieving this long term goal. Despite this slow progress, DEM simulations have

provided useful insights into the behaviour of granular materials at the grain scale (Rothenburg and Bathurst, 1992; Cundall, 2000; Thornton, 2000; Jiang *et al.*, 2005; Jiang and Yu, 2006). Thornton (2000) was right to point out that such information obtained from DEM simulations about what happens inside granular materials could lead to reassessment of the underlying concepts and assumptions embedded in traditional continuum mechanics.

In view of the above discussion, this book is mainly concerned with continuum theories of plasticity. However, microscopic information derived from analytical micro-mechanical studies or discrete element modelling will also be used to aid our development whenever possible.

#### 1.4 SIGN CONVENTIONS

Much of the theory of plasticity was initially developed for metals for which tensile stresses are usually considered to be positive. Unfortunately the opposite sign convention is usually adopted in geomechanics because compressive normal stresses are more common than tensile ones. In general, this book adopts the conventional geomechanics sign notation. As in the book of Davis and Selvadurai (1996), however, there are exceptions to this convention particularly in some of the later chapters that deal with elastic-plastic solutions (e.g. Chapters 8, 10, 12 and 13). This should not cause confusion as we will make it clear at each stage of the text whenever a tension positive notation is employed.

#### REFERENCES

Brown, E.T. (1987). *Analytical and Computational Methods in Engineering Rock Mechanics*, “Expanded version of the lectures given at the John Bray Colloquium”, Allen & Unwin, London.

Burland, J.B. (1989). Small is beautiful: the stiffness of soils at small strains, *Can. Geotech. J.*, Vol 26, 499-516.

Carter, J.P., Desai, C.S., Potts, D.M., Schweiger, H.F. and Sloan, S.W. (2000). Computing and computer modelling in geotechnical engineering, *Proc. of GeoEng2000*, Vol I, 1157-1252.

Chandler, H.W. (1985). A plasticity theory without Drucker’s postulate, suitable for granular materials, *J. Mech. Phys. Solids*, Vol 33, 215-226.

Chen, W.F. (1975). *Limit Analysis and Soil Plasticity*, Elsevier, Amsterdam.

Chen, W.F. and Mizuno, E. (1990). *Nonlinear Analysis in Soil Mechanics*. Elsevier, Amsterdam.

Collins, I.F. and Houlsby, G.T. (1997). Application of thermomechanical principles to the modelling of geotechnical materials, *Proc. R. Soc. A.*, Vol 453, 1975-2001.

Cundall, P.A. (2000). A discontinuous future for numerical modelling in geomechanics, *Proc. ICE: Geotech. Eng.*, Vol 149, 41-47.

Cundall, P.A. and Strack, O.D.L. (1979). A discrete numerical model for granular assemblies, *Geotechnique.*, Vol 29, 47-65.

Dafalias, Y.F. and Popov, E.P. (1975). A model of nonlinearly hardening materials for complex loadings, *Acta Mech.*, Vol 21, 173-192.

Davis, E.H. (1968). Theories of plasticity and the failure of soil masses, In: *Soil Mechanics: Selected Topics*, (Editor: I. K. Lee), Butterworths, London, 341-380.

Davis, R.O. and Selvadurai, A.P.S. (1996). *Elasticity and Geomechanics*, Cambridge University Press.

de Josselin de Jong, G. (1971). The double sliding, free rotating model for granular assemblies, *Geotechnique.*, Vol 21, 155-162.

de Saint-Venant, B (1870). Memoire sur l'établissement des équations différentielles des mouvements intérieurs opérés dans les corps solides ductiles au delà des limites où l'élasticité pourrait les ramener à leur premier état, *C.R. Acad. Sci. (Paris)*, Vol 70, 473-480.

Drucker, D.C. (1950). Stress-strain relations in the plastic range: a survey of the theory and experiment, *Report for Office of Naval Research Contract N7-onr-358*, December, Brown University.

Drucker, D.C. (1952). A more fundamental approach to plastic stress-strain relations, In: *Proc. 1st US Nat. Congr. Appl. Mech.*, ASME, New York, 487-491.

Drucker, D.C. (1958). The definition of a stable inelastic material, *J. Appl. Mech.*, ASME, Vol 26, 101-106.

Drucker, D.C., Gibson, R.E. and Henkel, D.J. (1957). Soil mechanics and working hardening theories of plasticity, *Trans. ASCE*, Vol 122, 338-346.

Einav, I. (2004). Thermomechanical relations between stress space and strain space models, *Geotechnique*, Vol 54, 315-318.

Gens, A. and Potts, D.M. (1988). Critical state models in computational geomechanics. *Eng. Comput.*, Vol 5, 178-197.

Green, A.E. (1956). Hypo-elasticity and plasticity, *Proc. R. Soc. A.*, Vol 234, 46-59.

Harris, D. (1995). A unified formulation for plasticity models of granular and other materials, *Proc. R. Soc. A.*, Vol 450, 37-49.

Hill, R. (1948). A variational principle of maximum plastic work in classical plasticity, *Q.J. Mech. Appl. Math.*, Vol 1, 18-28.

Hill, R. (1950). *The Mathematical Theory of Plasticity*, Clarendon Press, Oxford.

Houlsby, G.T. (1982). A derivation of the small-strain incremental theory of plasticity from thermodynamics, *Proc. IUTAM Conf. on Deformation and Failure of Granular Materials*, Delft, 109-118.

Iwan, W.D. (1967). On a class of models for the yielding behaviour of continuous and composite systems, *J. Appl. Mech.*, Vol 34, 612-617.

Jamiolkowski, M., Ladd, C.C., Germaine, J.T. and Lancellotta, R. (1985). New developments in field and laboratory testing of soils, Theme Lecture, *Proc. 11th Int. Conf. on Soil Mech. Found. Eng.*, San Francisco, Vol 1, 57-153, Balkema.

Jiang, M.J., Harris, D. and Yu, H.S. (2005). Kinematic models for non-coaxial granular materials: Part I and Part II, *Int. J. Num. Anal. Meth. Geomech.*, Vol 29, 643-689.

Jiang, M.J. and Yu, H.S. (2006). Application of the discrete element method to modern geomechanics, In: *Modern Trends in Geomechanics*, (Editors: W. Wu and H.S. Yu), Springer.

Koiter, W.T. (1960). General theorems for elastic-plastic solids, In: *Progress in Solid Mechanics*, (Editors: I.N. Sneddon and R. Hill), Vol 1, 167-221.

Kolymbas, D. (1991). An outline of hypoplasticity, *Arch. Appl. Mech.*, Vol 61, 143-151.

Krieg, R.D. (1975). A practical two-surface plasticity theory, *J. Appl. Mech.*, Vol 42, 641-646.

Maugin, G.A. (1992). *The Thermomechanics of Plasticity and Fracture*, Cambridge University Press.

McDowell, G.R. and Bolton, M.D. (1998). On the micromechanics of crushable aggregates, *Geotechnique*, Vol 48, 667-679.

McDowell, G.R. and Harireche, O. (2002). Discrete element modelling of yielding and nominal compression of sand, *Geotechnique*, Vol 52, 299-304.

Melan, E (1938). Zur plastizität des raumlichen Kontinuums, *Ing. Arch.*, Vol 9, 116-125.

Mitchell, J.K. (1993). *Fundamentals of Soil Behaviour*, 2nd edition, John Wiley & Sons, New York.

Mroz, Z (1967). On the description of anisotropic hardening, *J. Mech. Phys. Solids.*, Vol 15, 163-175.

Nadai, A. (1950). *Theory of Flow and Fracture of Solids*, 2nd Edition, McGraw-Hill, New York.

Naylor, D.J., Pande, G.N., Simpson, B. and Tabb, R. (1981). *Finite Elements in Geotechnical Engineering*, Pineridge Press, Swansea.

Naghdi, P.M. (1960). Stress-strain relations in plasticity and thermoplasticity, In: *Plasticity*, (Editors: E.H. Lee and P.S. Symonds), Pergamon Press, 121-169.

Naghdi, P.M. and Trapp, J.A. (1975). The significance of formulating plasticity theory with reference to loading surfaces in strain space. *Int. J. Eng. Sci.*, Vol 13, 785-797.

Prager, W. (1955). The theory of plasticity – a survey of recent achievements, *Proc. Inst. Mech. Eng.*, London, 3-19.

Potts, D. M. and Zdravkovic, L. (1999). *Finite Element Analysis in Geotechnical Engineering: Theory*, Thomas Telford, London.

Poulos, H.G. and Davis, E.H. (1974). *Elastic Solutions for Soil and Rock Mechanics*, John Wiley, New York.

Roscoe, K.H. and Burland, J.B. (1968). On generalised stress strain behaviour of wet clay. In: *Engineering Plasticity* (edited by Heyman and Leckie), 535-609.

Roscoe, K.H., Schofield, A.N. and Wroth, C.P. (1958). On yielding of soils, *Geotechnique*, Vol 8, 28.

Rothenburg, L. and Bathurst, R.J. (1992). Micromechanical features of granular assemblies with planar elliptical particles, *Geotechnique*, Vol 42, 79-95.

Rudnicki, J.W. and Rice, J.R. (1975). Conditions for the localisation of deformation in pressure-sensitive dilatant materials, *J. Mech. Phys. Solids.*, Vol 23, 371-394.

Salencon, J. (1977). *Applications of the Theory of Plasticity in Soil Mechanics*, Wiley, Chichester.

Schofield, A.N. and Wroth, C.P. (1968). *Critical State Soil Mechanics*, McGraw-Hill, London.

Simpson, B. (1992). Retaining structure: displacement and design, *Geotechnique*, Vol 42, 539-576.

Sloan, S.W. and Randolph, M.F. (1982). Numerical prediction of collapse loads using finite element methods. *Int. J. Num. Anal. Meth. Geomech.*, Vol 6, 47-76.

Sokolovskii, V.V. (1965). *Statics of Granular Media*, Pergamon, Oxford.

Spencer, A.J.M. (1964). A theory of the kinematics of ideal soils under plane strain conditions, *J. Mech. Phys. Solids.*, Vol 12, 337-351.

Spencer, A.J.M. (1980). *Continuum Mechanics*. Dover Publications, New York.

Terzaghi, K. (1943). *Theoretical Soil Mechanics*, Wiley, New York.

Thornton, C. (2000). Microscopic approach contributions to constitutive modelling. In: *Constitutive Modelling of Granular Materials*, (Editor: D. Kolymbas), Springer 193-208.

Valanis, K.C. (1971). A theory of viscoplasticity without a yield surface, *Arch. Mech.*, Vol 23, 517-534.

von Mises, R (1928). Mechanik der plastischen Formaenderung von Kristallen, *Z. angew. Math. Mech.*, Vol 8, 161-185.

Wroth, C.P. and Houlsby, G.T. (1985). Soil mechanics – property characterisation and analysis procedures, *Proc. 11th Int Conf of ISSMFE*, Theme Lecture, Vol 1, 1-55.

Yang, Y. and Yu, H.S. (2006a). Numerical simulations of simple shear with non-coaxial soil models, *Int. J. Num. Analy. Meth. Geomech.*, Vol 30, 1-19.

Yang, Y. and Yu, H.S. (2006b). A non-coaxial critical state soil model and its application to simple shear simulations, *Int. J. Num. Analy. Meth. Geomech.* (in press).

Yoder, P.J. and Iwan, W.D. (1981). On the formulation of strain-space plasticity with multiple loading surfaces. *J. Appl. Mech.*, Vol 48, 773-778.

Yu, H.S. (1998). CASM: A unified state parameter model for clay and sand. *Int. J. Num. Analy. Meth. Geomech.*, Vol 22, 621-653.

Yu, H.S. (2000a). *Cavity Expansion Methods in Geomechanics*, Kluwer Academic Publishers.

Yu, H.S. (2000b). *Theoretical Methods in Geomechanics*, DSc Thesis, University of Newcastle, Australia.

Yu, H.S. and Yuan, X. (2005). The importance of accounting for non-coaxial behaviour in modelling soil-structure interaction, *Proc. 11th Int Conf. of IACMAG*, (Editors: G Barla and M. Barla), Patron Editore, Invited Issue Paper, Vol 4, 709-718.

Yu, H.S. and Yuan, X. (2006). On a class of non-coaxial plasticity models for granular soils, *Proc. R. Soc. A.*, Vol 462, 725-748.

Zheng, Y., Chu, J. and Xu, Z. (1986). Strain space formulation of the elasto-plastic theory and its finite element implementation. *Comput. Geotech.* Vol 2, 373-388.

Ziegler, H. (1959). A modification of Prager's hardening rule. *Quart. Appl. Math.* Vol 17, 55.

Zienkiewicz, O.C., Chan, A.H.C., Pastor, M., Schrefler, B.A. and Shiomi, T. (1998). *Computational Geomechanics*, Wiley.

## CHAPTER 2

### ELEMENTS OF CONTINUUM MECHANICS

#### 2.1 INTRODUCTION

This chapter reviews some of the key elements of continuum mechanics that are essential to both the understanding and development of the theory of plasticity. These concepts are mainly concerned with the analysis of stress and strain, equilibrium equations and compatibility conditions, as well as elastic stress-strain relations. The reader is referred to other texts such as Prager (1961), Fung (1965), Timoshenko and Goodier (1970), Spencer (1980) and Malvern (1969) for a detailed treatment of continuum mechanics.

#### 2.2 STRESS STATE AND EQUILIBRIUM

##### 2.2.1 Two-dimensional elements

As shown in Figure 2.1, the stress state for a two-dimensional element is defined by four stress components  $\sigma_{xx}$ ,  $\sigma_{yy}$ ,  $\sigma_{xy}$  and  $\sigma_{yx}$ . The moment equilibrium demands that two shear stresses are equal in magnitude, namely  $\sigma_{xy} = \sigma_{yx}$ . Note that compressive stresses are treated as positive here.

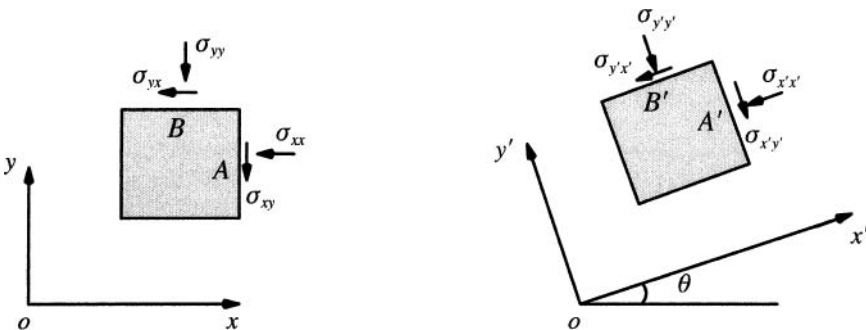


Figure 2.1: Stress state for two-dimensional elements

These stress components can be displaced as elements of a square matrix:

$$\begin{bmatrix} \sigma_{xx} & \sigma_{xy} \\ \sigma_{yx} & \sigma_{yy} \end{bmatrix}$$

The two most frequent cases of two-dimensional engineering problems are those of plane stress and plane strain. For the case of plane stress, the stresses normal to the  $xy$  plane are assumed to be identically zero. On the other hand, the case of plane strain only has non-zero strain components in the  $xy$  plane. In this case, the normal stress in the direction normal to the  $xy$  plane may be determined from the stresses acting on the  $xy$  plane ( $\sigma_{xx}, \sigma_{yy}, \sigma_{xy}$ ) through elastic stress-strain relations that will be discussed later in this chapter. Whilst plane stress is a good assumption for simplifying many engineering problems in structural and mechanical engineering, plane strain is most relevant in geotechnical engineering. This is because many important geotechnical problems, such as embankments and tunnels, may be adequately analysed as a two-dimensional plane strain problem.

### (a) Transformation of stresses and principal stresses

Now let us investigate the stress components at the point with respect to a new coordinate system ( $x'y'$ ), which is obtained by rotating the original coordinate system ( $xoy$ ) anticlockwise by an angle of  $\theta$  (see Figure 2.1). It can be easily shown that the stresses in these two coordinate systems are related by the following equations:

$$\sigma_{x'x'} = \frac{\sigma_{xx} + \sigma_{yy}}{2} + \frac{\sigma_{yy} - \sigma_{xx}}{2} \cos 2\theta - \sigma_{xy} \sin 2\theta \quad (2.1)$$

$$\sigma_{y'y'} = \frac{\sigma_{xx} + \sigma_{yy}}{2} - \frac{\sigma_{yy} - \sigma_{xx}}{2} \cos 2\theta + \sigma_{xy} \sin 2\theta \quad (2.2)$$

$$\sigma_{x'y'} = \sigma_{xy} \cos 2\theta + \frac{\sigma_{yy} - \sigma_{xx}}{2} \sin 2\theta \quad (2.3)$$

The principal stresses are those acting on a principal plane where shear stress is zero. The principal planes can be determined by setting equation (2.3) to zero, which gives:

$$\tan 2\theta = \frac{2\sigma_{xy}}{\sigma_{xx} - \sigma_{yy}} \quad (2.4)$$

Substituting the above solution into equations (2.1) and (2.2) leads to the expressions for the two principal stresses:

$$\sigma_1 = \frac{\sigma_{xx} + \sigma_{yy}}{2} + \sqrt{\left(\frac{\sigma_{xx} - \sigma_{yy}}{2}\right)^2 + \sigma_{xy}^2} \quad (2.5)$$

$$\sigma_2 = \frac{\sigma_{xx} + \sigma_{yy}}{2} - \sqrt{\left(\frac{\sigma_{xx} - \sigma_{yy}}{2}\right)^2 + \sigma_{xy}^2} \quad (2.6)$$

where  $\sigma_1$  and  $\sigma_2$  are also known as the major and minor principal stresses respectively.

The transformation of stresses, analytically expressed by the above equations, can also be simply achieved by using a Mohr-circle construction. Assume that the positive plane normal to the x direction is denoted by A and the positive plane normal to the y direction by B. Whilst compressive normal stresses are regarded as positive, shear stresses acting clockwise are treated as positive.

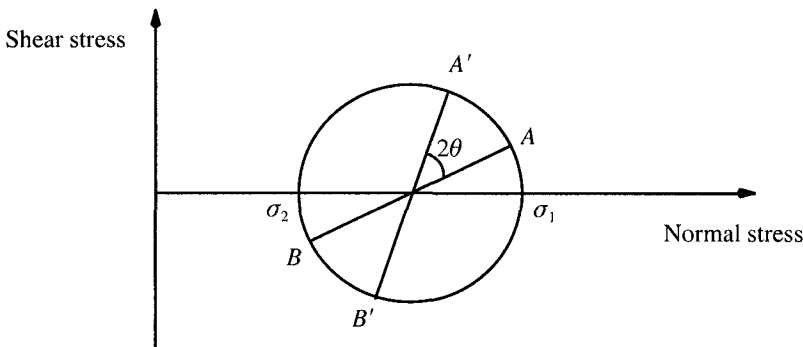


Figure 2.2: Transformation of stresses using a Mohr-circle construction

Using the Mohr-circle construction shown in Figure 2.2, the stresses on the plane A and B are defined by the coordinates of points A and B in the Mohr-circle. The stresses for the corresponding planes  $A'$  and  $B'$  with respect to a new coordinate system  $(x'oy')$  are equal to the coordinates of the points  $A'$  and  $B'$  in the Mohr-circle. It is noted that the points  $A'$  and  $B'$  are arrived by rotating the points A and B respectively by two times the angle between the coordinate systems  $(xoy)$  and  $(x'oy')$ .

By definition, the principal stresses are the coordinates of the interaction points between the Mohr-circle and the normal stress axis.

### (b) Equations of interior stress equilibrium

By accounting for stress variation with coordinates, equations of stress equilibrium can be established. It is instructive to first consider all the stresses in the x direction, as shown in Figure 2.3. The quantity  $X$  is assumed to be the body force (i.e. force per unit volume). The equation of force equilibrium in the x direction leads to the following equation of stresses:

$$\frac{\partial \sigma_{xx}}{\partial x} + \frac{\partial \sigma_{xy}}{\partial y} = X \quad (2.7)$$

Similarly consideration of the force equilibrium in the  $y$  direction gives the second equation of stresses:

$$\frac{\partial \sigma_{xy}}{\partial x} + \frac{\partial \sigma_{yy}}{\partial y} = Y \quad (2.8)$$

where  $Y$  denotes the body force in the  $y$  direction.

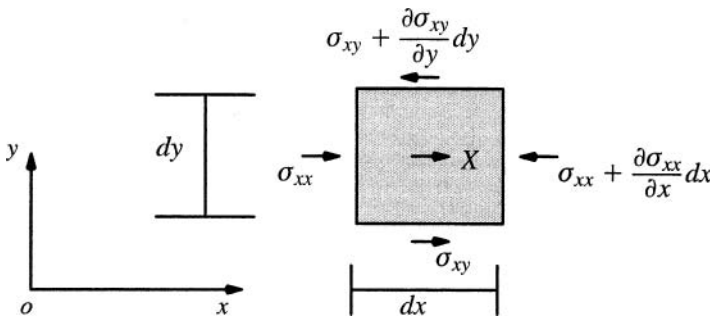


Figure 2.3: Equation of stress equilibrium

Equations (2.7) and (2.8) are known as the equations of interior stress equilibrium for two-dimensional problems.

### (c) Equations of boundary stress equilibrium

When some part of a boundary is subject to tractions (shear and normal components), they need to be in equilibrium with interior stresses acting surrounding that part of the boundary.

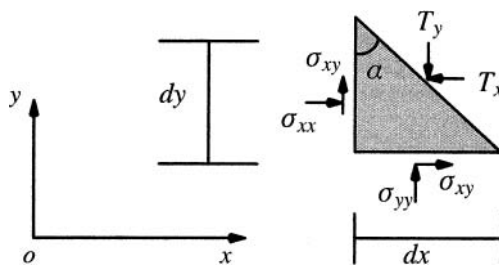


Figure 2.4: Equilibrium of interior stresses with tractions applied on a boundary

Let us assume that the orientation of the boundary with known tractions is denoted by the angle  $\alpha$ , as shown in Figure 2.4. The equilibrium of the triangular element requires:

$$\sigma_{xx} \cos \alpha + \sigma_{xy} \sin \alpha = T_x \quad (2.9)$$

$$\sigma_{xy} \cos \alpha + \sigma_{yy} \sin \alpha = T_y \quad (2.10)$$

where  $T_x$  and  $T_y$  are the applied traction components in the  $x$  and  $y$  directions.

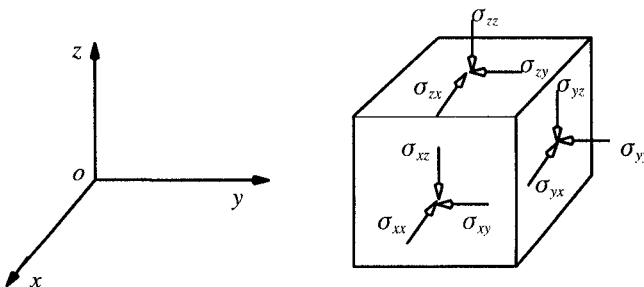


Figure 2.5: Stress state for three-dimensional elements

## 2.2.2 Three-dimensional elements

### (a) Stress tensor

The state of stress for a three-dimensional point is defined by a matrix containing nine stress components shown in Figure 2.5. The nine components of the stress at any point form a second order tensor, known as the stress tensor  $\sigma_{ij}$ , where  $i$  and  $j$  take integral values 1, 2 and 3. In this way, the stress components can be expressed as elements of a square matrix:

$$\begin{bmatrix} \sigma_{xx} & \sigma_{xy} & \sigma_{xz} \\ \sigma_{yx} & \sigma_{yy} & \sigma_{yz} \\ \sigma_{zx} & \sigma_{zy} & \sigma_{zz} \end{bmatrix} = \begin{bmatrix} \sigma_{11} & \sigma_{12} & \sigma_{13} \\ \sigma_{21} & \sigma_{22} & \sigma_{23} \\ \sigma_{31} & \sigma_{32} & \sigma_{33} \end{bmatrix} = \sigma_{ij} \quad (2.11)$$

As in the two-dimensional case, moment equilibrium demands the following relationships on shear stresses:

$$\sigma_{xy} = \sigma_{yx} ; \quad \sigma_{xz} = \sigma_{zx} ; \quad \sigma_{yz} = \sigma_{zy} \quad (2.12)$$

As a result there are only six independent stress components: three normal stresses ( $\sigma_{xx}, \sigma_{yy}, \sigma_{zz}$ ) and three shear stresses ( $\sigma_{xy}, \sigma_{yz}, \sigma_{xz}$ ).

### (b) Principal stresses

The state of stress at a point in three dimensions can also be defined by three principal stresses  $\sigma_1, \sigma_2$  and  $\sigma_3$ . These principal stresses are linked to the components of the stress tensor by the following cubic equation:

$$\sigma^3 - I_1\sigma + I_2\sigma + I_3 = 0 \quad (2.13)$$

where  $I_1, I_2$  and  $I_3$  are known as the first, second and third stress invariant respectively, which are defined as follows:

$$I_1 = \sigma_{xx} + \sigma_{yy} + \sigma_{zz} \quad (2.14)$$

$$I_2 = \sigma_{xx} \sigma_{yy} + \sigma_{yy} \sigma_{zz} + \sigma_{zz} \sigma_{xx} - \sigma_{xy}^2 - \sigma_{yz}^2 - \sigma_{xz}^2 \quad (2.15)$$

$$I_3 = \sigma_{xx} \sigma_{yy} \sigma_{zz} - \sigma_{xx} \sigma_{yz}^2 - \sigma_{yy} \sigma_{xz}^2 - \sigma_{zz} \sigma_{xy}^2 + 2\sigma_{xy} \sigma_{yz} \sigma_{xz} \quad (2.16)$$

The stress tensor in terms of the principal stresses takes the form

$$\begin{bmatrix} \sigma_1 & 0 & 0 \\ 0 & \sigma_2 & 0 \\ 0 & 0 & \sigma_3 \end{bmatrix} = \sigma_{ij} \quad (2.17)$$

In this case the stress invariants are linked to the principal stresses as follows

$$I_1 = \sigma_1 + \sigma_2 + \sigma_3 \quad (2.18)$$

$$I_2 = \sigma_1 \sigma_2 + \sigma_2 \sigma_3 + \sigma_3 \sigma_1 \quad (2.19)$$

$$I_3 = \sigma_1 \sigma_2 \sigma_3 \quad (2.20)$$

### (c) The mean stress and deviatoric stresses

The mean stress of a stressed point is defined as the average of normal stresses in three directions, which can be expressed as follows:

$$p = \frac{1}{3}(\sigma_{xx} + \sigma_{yy} + \sigma_{zz}) = \frac{1}{3}I_1 \quad (2.21)$$

The deviatoric components of the stress are defined by

$$s_{ij} = \sigma_{ij} - p\delta_{ij} \quad (2.22)$$

where  $\delta_{ij}$  is the *Kronecker delta* whose value is 1 when  $i = j$  and is equal to 0 otherwise.

The three invariants of deviatoric stress are

$$J_1 = s_{kk} = 0 \quad (2.23)$$

$$\begin{aligned} J_2 &= \frac{1}{2}s_{ij}s_{ij} = \frac{1}{3}(I_1^2 + 2I_3) \\ &= \frac{1}{6}[(\sigma_1 - \sigma_2)^2 + (\sigma_2 - \sigma_3)^2 + (\sigma_3 - \sigma_1)^2] \end{aligned} \quad (2.24)$$

$$\begin{aligned} &= \frac{1}{6}[(\sigma_{xx} - \sigma_{yy})^2 + (\sigma_{yy} - \sigma_{zz})^2 + (\sigma_{zz} - \sigma_{xx})^2] \\ &\quad + \sigma_{xy}^2 + \sigma_{yz}^2 + \sigma_{xz}^2 \end{aligned} \quad (2.25)$$

$$J_3 = \frac{1}{3}s_{ij}s_{jk}s_{ki} = \frac{1}{27}(2I_1^3 + 9I_1I_2 + 27I_3) \quad (2.26)$$

It is noted that in the theory of soil plasticity, the most useful stress invariants are  $I_1$ ,  $J_2$  and  $J_3$ . Physically,  $I_1$  indicates the effect of mean stress,  $J_2$  represents the magnitude of shear stress, and  $J_3$  determines the direction of shear stress. As will be discussed in the rest of this book, all these three quantities (mean stress, shear stress and shear stress direction) have a key role to play in the theory of elastic-plastic stress-strain relations.

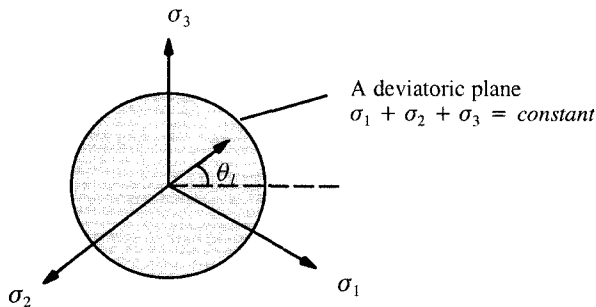


Figure 2.6: Lode angle on a deviatoric plane

The three principal stresses can be determined from the stress invariants as follows

$$\sigma_1 = \frac{1}{3}I_1 + \frac{2}{\sqrt{3}}\sqrt{J_2} \sin (\theta_l + 120^\circ) \quad (2.27)$$

$$\sigma_2 = \frac{1}{3}I_1 + \frac{2}{\sqrt{3}}\sqrt{J_2} \sin (\theta_l) \quad (2.28)$$

$$\sigma_3 = \frac{1}{3}I_1 + \frac{2}{\sqrt{3}}\sqrt{J_2} \sin (\theta_l - 120^\circ) \quad (2.29)$$

where  $\theta_l$  is known as the Lode angle defined in Figure 2.6 as

$$\theta_l = \tan^{-1} \left[ \frac{1}{\sqrt{3}} \left( \frac{2\sigma_3 - \sigma_1 - \sigma_2}{\sigma_1 - \sigma_2} \right) \right] \quad (2.30)$$

or

$$\theta_l = -\frac{1}{3} \sin^{-1} \left[ \frac{3\sqrt{3}}{2} \left( \frac{J_3}{J_2^{3/2}} \right) \right] \quad (2.31)$$

which ranges between  $-30^\circ$  and  $30^\circ$ .

In soil mechanics (Roscoe and Burland, 1968; Muir Wood, 1990), the mean stress  $p$  is often used in pair with a generalised shear stress  $q$  defined below

$$q = \frac{1}{\sqrt{2}} [(\sigma_1 - \sigma_2)^2 + (\sigma_2 - \sigma_3)^2 + (\sigma_3 - \sigma_1)^2]^{1/2} \quad (2.32)$$

$$= \sqrt{3J_2} \quad (2.33)$$

which reduces to

$$q = \sigma_1 - \sigma_3 \quad (2.34)$$

for the triaxial loading condition where  $\sigma_2 = \sigma_3$ .

In terms of  $p$  and  $q$ , the principal stresses are

$$\sigma_1 = p + \frac{2}{3}q \sin (\theta_l + 120^\circ) \quad (2.35)$$

$$\sigma_2 = p + \frac{2}{3}q \sin (\theta_l) \quad (2.36)$$

$$\sigma_3 = p + \frac{2}{3}q \sin (\theta_l - 120^\circ) \quad (2.37)$$

#### (d) Equations of stress equilibrium

By taking account of stress variation with coordinates, the force equilibrium conditions in three directions will lead to the following well-known equation of stress equilibrium:

$$\frac{\partial \sigma_{xx}}{\partial x} + \frac{\partial \sigma_{xy}}{\partial y} + \frac{\partial \sigma_{xz}}{\partial z} = X \quad (2.38)$$

$$\frac{\partial \sigma_{yx}}{\partial x} + \frac{\partial \sigma_{yy}}{\partial y} + \frac{\partial \sigma_{yz}}{\partial z} = Y \quad (2.39)$$

$$\frac{\partial \sigma_{zx}}{\partial x} + \frac{\partial \sigma_{zy}}{\partial y} + \frac{\partial \sigma_{zz}}{\partial z} = Z \quad (2.40)$$

where  $X$ ,  $Y$  and  $Z$  are the body forces acting in the  $x$ ,  $y$  and  $z$  directions respectively.

## 2.3 STRAIN AND COMPATIBILITY

### 2.3.1 Two-dimensional elements

Let us use  $u$  and  $v$  to denote the displacement components in the  $x$  and  $y$  directions of a point in two dimensions. It can be easily shown that the normal strains in both directions are linked to the displacements by the following relationship:

$$\varepsilon_{xx} = \frac{\partial u}{\partial x} \quad (2.41)$$

$$\varepsilon_{yy} = \frac{\partial v}{\partial y} \quad (2.42)$$

In addition, the shear strain is given by

$$\varepsilon_{xy} = \frac{1}{2} \left( \frac{\partial u}{\partial y} + \frac{\partial v}{\partial x} \right) \quad (2.43)$$

These strain components can be displayed as elements of a square matrix:

$$\begin{bmatrix} \varepsilon_{xx} & \varepsilon_{xy} \\ \varepsilon_{yx} & \varepsilon_{yy} \end{bmatrix}$$

It is noted that the definition of a well-used shear strain (termed the engineering shear strain) is given by

$$\gamma_{xy} = 2\varepsilon_{xy} = \frac{\partial u}{\partial y} + \frac{\partial v}{\partial x} \quad (2.44)$$

The strain components  $\varepsilon_{xx}$ ,  $\varepsilon_{yy}$  and  $\varepsilon_{xy}$  are not independent and they are linked by the following condition (known as the compatibility condition):

$$\frac{\partial^2 \varepsilon_{xx}}{\partial y^2} + \frac{\partial^2 \varepsilon_{yy}}{\partial x^2} = 2 \frac{\partial^2 \varepsilon_{xy}}{\partial x \partial y} \quad (2.45)$$

which is obtained from equations (2.41) to (2.43) by eliminating  $u$  and  $v$ .

### 2.3.2 Three-dimensional elements

In three dimensions, the displacement components in the  $x$ ,  $y$  and  $z$  directions are denoted by  $u$ ,  $v$  and  $w$  respectively. The components of strain can be expressed by a strain tensor:

$$\begin{bmatrix} \varepsilon_{xx} & \varepsilon_{xy} & \varepsilon_{xz} \\ \varepsilon_{yx} & \varepsilon_{yy} & \varepsilon_{yz} \\ \varepsilon_{zx} & \varepsilon_{zy} & \varepsilon_{zz} \end{bmatrix} = \begin{bmatrix} \varepsilon_{11} & \varepsilon_{12} & \varepsilon_{13} \\ \varepsilon_{21} & \varepsilon_{22} & \varepsilon_{23} \\ \varepsilon_{31} & \varepsilon_{32} & \varepsilon_{33} \end{bmatrix} = \varepsilon_{ij} \quad (2.46)$$

where

$$\varepsilon_{xy} = \varepsilon_{yx} ; \quad \varepsilon_{xz} = \varepsilon_{zx} ; \quad \varepsilon_{yz} = \varepsilon_{zy} \quad (2.47)$$

The strain components are related to the displacement field as follows:

$$\varepsilon_{xx} = \frac{\partial u}{\partial x} \quad (2.48)$$

$$\varepsilon_{yy} = \frac{\partial v}{\partial y} \quad (2.49)$$

$$\varepsilon_{zz} = \frac{\partial w}{\partial z} \quad (2.50)$$

$$\varepsilon_{xy} = \frac{1}{2} \left( \frac{\partial u}{\partial y} + \frac{\partial v}{\partial x} \right) \quad (2.51)$$

$$\varepsilon_{xz} = \frac{1}{2} \left( \frac{\partial u}{\partial z} + \frac{\partial w}{\partial x} \right) \quad (2.52)$$

$$\varepsilon_{yz} = \frac{1}{2} \left( \frac{\partial v}{\partial z} + \frac{\partial w}{\partial y} \right) \quad (2.53)$$

In addition to equation (2.45), two more conditions of strain compatibility can be obtained:

$$\frac{\partial^2 \varepsilon_{yy}}{\partial z^2} + \frac{\partial^2 \varepsilon_{zz}}{\partial y^2} = 2 \frac{\partial^2 \varepsilon_{yz}}{\partial y \partial z} \quad (2.54)$$

$$\frac{\partial^2 \varepsilon_{xx}}{\partial z^2} + \frac{\partial^2 \varepsilon_{zz}}{\partial x^2} = 2 \frac{\partial^2 \varepsilon_{xz}}{\partial x \partial z} \quad (2.55)$$

## 2.4 ELASTIC STRESS-STRAIN RELATIONS

Although this book is concerned with stress-strain relations in the plastically deforming region, it is fundamental to understand the stress-strain relations in the elastic region (widely known as Hooke's law).

### 2.4.1 Plane stress conditions

Some engineering practical problems can be simplified as a plane stress problem in which the stress in one direction (e.g. the  $z$  direction) is so small that it can be ignored, namely  $\sigma_{zz} = 0$ . In this case, the strain components can be related to the stress components in the following way:

$$\varepsilon_{xx} = \frac{1}{E} (\sigma_{xx} - \nu \sigma_{yy}) \quad (2.56)$$

$$\varepsilon_{yy} = \frac{1}{E} (\sigma_{yy} - \nu \sigma_{xx}) \quad (2.57)$$

$$\varepsilon_{xy} = \frac{1 + \nu}{E} \sigma_{xy} \quad (2.58)$$

where  $E$  and  $\nu$  are material constants known as the Young's modulus and Poisson's ratio respectively. These linear stress-strain relations can also be expressed in the following way:

$$\sigma_{xx} = \frac{E}{1 - \nu^2} (\varepsilon_{xx} + \nu \varepsilon_{yy}) \quad (2.59)$$

$$\sigma_{yy} = \frac{E}{1 - \nu^2} (\varepsilon_{yy} + \nu \varepsilon_{xx}) \quad (2.60)$$

$$\sigma_{xy} = \frac{E}{1 - \nu^2} (1 - \nu) \varepsilon_{xy} \quad (2.61)$$

#### 2.4.2 Plane strain conditions

Many geotechnical engineering problems can be adequately analysed as a plane strain problem in which the strain in one direction, say the  $z$  direction, is very small so that it can be ignored, namely  $\varepsilon_{zz} = 0$ . In this case, the stress-strain relations are given by:

$$\sigma_{xx} = \frac{(1 - \nu)E}{(1 + \nu)(1 - \nu^2)} (\varepsilon_{xx} + \frac{\nu}{1 - \nu} \varepsilon_{yy}) \quad (2.62)$$

$$\sigma_{yy} = \frac{(1 - \nu)E}{(1 + \nu)(1 - \nu^2)} (\varepsilon_{yy} + \frac{\nu}{1 - \nu} \varepsilon_{xx}) \quad (2.63)$$

$$\sigma_{xy} = \frac{E}{1 + \nu} \varepsilon_{xy} \quad (2.64)$$

#### 2.4.3 Three-dimensional conditions

In three dimensions, the elastic normal stress-strain relations take the following simple form:

$$\varepsilon_{xx} = \frac{1}{E} [\sigma_{xx} - \nu(\sigma_{yy} + \sigma_{zz})] \quad (2.65)$$

$$\varepsilon_{yy} = \frac{1}{E} [\sigma_{yy} - \nu(\sigma_{xx} + \sigma_{zz})] \quad (2.66)$$

$$\varepsilon_{zz} = \frac{1}{E} [\sigma_{zz} - \nu(\sigma_{xx} + \sigma_{yy})] \quad (2.67)$$

The shear stresses are related to the shear strains by the following relations

$$\varepsilon_{xy} = \frac{1 + \nu}{E} \sigma_{xy} = \frac{\sigma_{xy}}{2G} \quad (2.68)$$

$$\varepsilon_{yz} = \frac{1 + \nu}{E} \sigma_{yz} = \frac{\sigma_{yz}}{2G} \quad (2.69)$$

$$\varepsilon_{xz} = \frac{1 + \nu}{E} \sigma_{xz} = \frac{\sigma_{xz}}{2G} \quad (2.70)$$

in which  $G$  is shear modulus of the material.

## 2.5 SUMMARY

- (1) The state of stress at a point is defined by a stress tensor with nine stress components. However only six of them, three normal stresses and three shear stresses, are independent due to moment equilibrium. These stresses need to satisfy three equations of equilibrium.
- (2) Deformation of a point can be described by strains. In three dimensions, there are also three normal strains and three shear strains. These strains are also linked by compatibility conditions.
- (3) The relationship between stresses and strains can be very complex and mainly depends on material types and loading conditions. For linear elastic materials, the relationship between stresses and strains is governed by Hooke's law.

## REFERENCES

Fung, Y.C. (1965). *Foundations of Solid Mechanics*. Prentice Hall, New Jersey.

Malvern, L.E. (1969). *Introduction to the Mechanics of a Continuous Medium*. Prentice Hall, New Jersey.

Muir Wood, D. (1990). *Soil Behaviour and Critical State Soil Mechanics*, Cambridge University Press.

Prager, W. (1961). *Introduction to Mechanics of Continua*. Ginn and Company.

Roscoe, K.H. and Burland, J.B. (1968). On generalised stress strain behaviour of wet clay. In: *Engineering Plasticity* (edited by Heyman and Leckie), 535-609.

Spencer, A.J.M. (1980). *Continuum Mechanics*. Dover Publications, New York.

Timoshenko, S.P. and Goodier, J.N. (1970). *Theory of Elasticity*. 3rd edition, McGraw-Hill.

## CHAPTER 3

# FOUNDATIONS OF THE THEORY OF PLASTICITY

### 3.1 INTRODUCTION

This chapter describes some of the fundamental elements of the theory of plasticity. These elements include yield conditions, plastic potential and flow rule, principle of maximum plastic work, isotropic hardening and Drucker's stability postulate, kinematic and mixed hardening, and general stress-strain relations. These concepts form the foundations of the theory of plasticity. A good review of these fundamental concepts can be found in Hill (1950), Prager (1955) and Naghdi (1960). It should be stressed that the general stress-strain relations described here are only valid for small deformation, but their extension to large deformation will be covered in Chapter 14 when used in finite element analysis of large deformation problems.

### 3.2 YIELD CRITERION

A condition that defines the limit of elasticity and the beginning of plastic deformation under any possible combination of stresses is known as the yield condition or yield criterion. In the elastic region, all the deformation will be recovered once the applied stress is removed (i.e. unloading of stress to zero). However once the yield condition is reached, some of the deformation will be permanent in the sense that it cannot be recovered even after the stress is removed completely. This part of the deformation is known as plastic deformation and the remaining deformation is recoverable upon removal of the stress and is known as elastic deformation.

For the simple case of one-dimensional loading, the yield criterion is defined by a stress value beyond which plastic deformation will occur. In other words, the criterion of yield is graphically represented by *a point*. For the case of two dimensional loading, the yielding will occur when the combination of stresses applied in the two loading directions touches *a curve*. In the same way, for the case of three dimensional loading, plastic deformation will occur once the combination of the stresses applied in the three directions touches *a surface* (often known as a yield surface). In short, the yield criterion is generally represented by a surface in stress space. When the stress state is within the yield surface, material behavior is said to be elastic. Once the stress state is on the yield surface, plastic deformation will be produced.

Mathematically, a general form of yield criterion (or surface) can be expressed in terms of either the stress tensor or the three stress invariants as follows:

$$f(\sigma_{ij}) = f(I_1, I_2, I_3) = 0 \quad (3.1)$$

### 3.3 PLASTIC POTENTIAL AND PLASTIC FLOW RULE

A key question that the theory of plasticity sets out to answer is how to determine the plastic deformation (or plastic strains) once the stress state is on the yield surface. The most widely used theory is to assume that the plastic strain rate (or increment) can be determined by the following formula (von Mises, 1928; Melan, 1938; Hill, 1950):

$$d\epsilon_{ij}^p = d\lambda \frac{\partial g}{\partial \sigma_{ij}} \quad (3.2)$$

where  $d\lambda$  is a positive scalar, and

$$g = g(\sigma_{ij}) = g(I_1, I_2, I_3) = 0 \quad (3.3)$$

is known as the plastic potential, which may or may not be the same as the yield surface. Equation (3.2) is referred to as a plastic flow rule that basically defines the ratios of the components of the plastic strain rate. This plastic flow rule was based on the observation by de Saint-Venant (1870) that for metals the principal axes of the plastic strain rate coincide with those of the stress. This is the so-called coaxial assumption, which has been the foundation of almost all the plasticity models used in engineering. It must be noted that recent experimental data suggests that the coaxial assumption is generally not valid for soils (see Chapter 8 for details).

If the plastic potential is the same as the yield surface, then the plastic flow rule (3.2) is called the associated flow (or normality) rule. Otherwise it is called non-associated flow rule. The associated flow rule follows from considerations of the plastic deformation of polycrystalline aggregates in which individual crystals deform by slipping over preferred planes (Bishop and Hill, 1951).

If the unit normal to the plastic potential approaches a finite number of linearly independent limiting values as the stress point approaches the singular point in question, Koiter (1953) proposes the following generalized flow rule

$$d\epsilon_{ij}^p = \sum_{i=1}^n d\lambda_i \frac{\partial g_i}{\partial \sigma_{ij}} \quad (3.4)$$

where  $d\lambda_i$  are nonnegative and  $\partial g_i / \partial \sigma_{ij}$  are the linearly independent gradients.

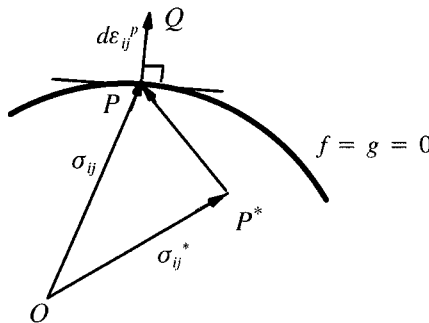


Figure 3.1: Maximum plastic work principle

### 3.4 PRINCIPLE OF MAXIMUM PLASTIC WORK

Suppose the plastic strain rate  $d\epsilon_{ij}^p$  is given and the corresponding stress state,  $\sigma_{ij}$ , determined from the normality rule and the yield criterion, is represented by a point P in the stress space, Figure 3.1. If  $\sigma_{ij}^*$  is an arbitrary state of stress represented by a point  $P^*$  on or inside the yield surface, then the difference between the incremental plastic works done by the two stress states on the actual plastic strain rate is

$$dW_p = (\sigma_{ij} - \sigma_{ij}^*) d\epsilon_{ij}^p \quad (3.5)$$

Equation (3.5) represents the scalar product of the vector  $P^*P$  and  $PQ$ . If the yield surface is strictly *convex*, the angle between these vectors is acute and the scalar product is positive. Therefore

$$(\sigma_{ij} - \sigma_{ij}^*) d\epsilon_{ij}^p \geq 0 \quad (3.6)$$

This condition, due to von Mises (1928) and Hill (1948, 1950), is known as the maximum plastic work principle or theorem. It states that the actual work done in a given plastic strain rate (or increment) is greater than the fictitious work done by an arbitrary state of stress not exceeding the yield limit. Alternatively the maximum plastic work principle can be stated as follows: the plastic work done in a given plastic strain rate has a maximum value in the actual state, with respect to varying stress systems satisfying the yield criterion (Hill, 1948, 1950). As will be seen later in this book, the maximum plastic work theorem (3.6) is the basis for a number of important theorems concerning elastic-plastic solids. For example, it can be shown that the stress field in a material that obeys the maximum plastic work principle is always unique.

In short, the maximum plastic work principle is a mathematical statement of the following two important ideas: (a) The yield surface is convex; (b) The plastic strain rate (or increment) is normal to the yield surface.

### 3.5 STRAIN HARDENING AND PERFECT PLASTICITY

Plastic deformation leads to the hardening of a material and the increase of its elastic limit (i.e. the stress limit under which only elastic deformation occurs). In other words, the yield surface will generally not be fixed in stress space, rather it will expand or contract depending on previous plastic deformation and loading history. Let us for the present consider the case when plastic deformation only changes the size of the yield surface equally in all directions but not its shape (which is known as isotropic hardening). If the yield surface is expanding in size, the material is said to be hardening (i.e. making it more difficult to yield). On the other hand, if the yield surface is contracting in size, then the material is said to be undergoing softening (i.e. making it easier to yield).

The change of the size of the yield surface is often related to some measure or integral of plastic strain rates. The most common measures include the total plastic work per unit volume, the accumulated plastic strain (Hill, 1950), the volumetric plastic strain rate (Schofield and Wroth, 1968; Yu, 1998), or a combination of volumetric and shear plastic strain rates (Wilde, 1977; Yu *et al.*, 2005). The yield surface for a strain-hardening or softening material is also called *the loading surface*. Mathematically, the loading surface, which changes with plastic deformation, may be expressed by

$$f(\sigma_{ij}, \varepsilon_{ij}^P) = 0 \quad (3.7)$$

where  $\varepsilon_{ij}^P$  denotes the plastic strain tensor.

If the yield surface does not change with stress history (i.e. fixed), the material is known a perfectly plastic solid. This is a special case of strain-hardening materials. For a perfectly plastic material, the behaviour is elastic when the stress state lies inside the yield surface. Plastic strains will occur as long as the stress state lies on or travels along the yield surface. The complete stress conditions for plastic and elastic behaviour may be stated as

$$\text{Elastic : } f(\sigma_{ij}) < 0 \quad \text{or} \quad df = \frac{\partial f}{\partial \sigma_{ij}} d\sigma_{ij} < 0 \quad (3.8)$$

$$\text{Plastic : } f(\sigma_{ij}) = 0 \quad \text{and} \quad df = \frac{\partial f}{\partial \sigma_{ij}} d\sigma_{ij} = 0 \quad (3.9)$$

The elastic behaviour of a strain-hardening solid is the same as that of a perfectly plastic one. Therefore the conditions for initial yield must be the same. Indeed, the difference between the two concerns only the mechanism for continuing plastic flow, plus the fact that the conditions for current yielding will depend on the plastic history of the material. The complete stress conditions for plastic and elastic behaviour for a strain-hardening material are

$$\text{Elastic : } f(\sigma_{ij}, \varepsilon_{ij}^p) < 0 \quad \text{or} \quad df = \frac{\partial f}{\partial \sigma_{ij}} d\sigma_{ij} \leq 0 \quad (3.10)$$

$$\text{Plastic : } f(\sigma_{ij}, \varepsilon_{ij}^p) = 0 \quad \text{and} \quad df = \frac{\partial f}{\partial \sigma_{ij}} d\sigma_{ij} > 0 \quad (3.11)$$

Note that in the above conditions,  $df$  is evaluated only with respect to the increments in the stress components (that is, with constant plastic strains, see Kachanov, 1974).

For solving boundary value problems involving elastic-plastic behaviour, it is essential to clearly determine what behaviour will result from a further stress increment when the stress state is already on the yield surface. Three possible conditions exist and they are

$$\text{Unloading : } f(\sigma_{ij}, \varepsilon_{ij}^p) = 0 \quad \text{and} \quad df = \frac{\partial f}{\partial \sigma_{ij}} d\sigma_{ij} < 0 \quad (3.12)$$

$$\text{Neutral loading : } f(\sigma_{ij}, \varepsilon_{ij}^p) = 0 \quad \text{and} \quad df = \frac{\partial f}{\partial \sigma_{ij}} d\sigma_{ij} = 0 \quad (3.13)$$

$$\text{Loading : } f(\sigma_{ij}, \varepsilon_{ij}^p) = 0 \quad \text{and} \quad df = \frac{\partial f}{\partial \sigma_{ij}} d\sigma_{ij} > 0 \quad (3.14)$$

It is commonly assumed that for both unloading and neutral loading, material behaviour is purely elastic. Plastic behaviour occurs only when the loading condition is satisfied.

Based on the loading conditions (3.12)-(3.14), Hill (1950) shows that a general expression for plastic strain rates can be assumed to be

$$d\varepsilon_{ij}^p = G_{ij} df \quad (3.15)$$

where  $G_{ij}$  is a symmetric tensor, which is supposed to be a function of the stress components and possibly of the previous strain history, but not of the stress rate (or

increment). This last assumption is very significant as it means that the ratios of the components of the plastic strain rate are functions of the current stress but not of the stress rate. This can be satisfied by assuming  $G_{ij}$  to be of the following form

$$G_{ij} = h \frac{\partial g}{\partial \sigma_{ij}} \quad (3.16)$$

where  $h$  and  $g$  are scale functions of the stress tensor, and possibly also of the strain history.  $g$  is also known as plastic potential. With equation (3.16), the plastic strain rate can be determined by the following equation

$$d\epsilon_{ij}^p = h \frac{\partial g}{\partial \sigma_{ij}} \, df \quad (3.17)$$

which was first used by Melan (1938).

### 3.6 DRUCKER'S STABILITY POSTULATE

The notations of normality and convexity outlined earlier are just mathematical ideas. In an attempt to provide a missing link between material behaviour and these mathematical ideas, Drucker (1952, 1958) introduced a fundamental stability postulate. In essence, Drucker's stability postulate is a generalization of simple facts which are valid for certain classes of materials, and is not a statement of any thermodynamic principle, as it is often presented (Green and Naghdi, 1965).

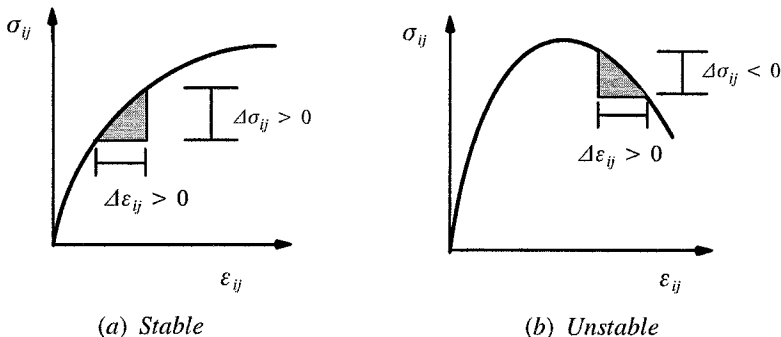


Figure 3.2: Drucker's stability postulate

Figure 3.2 shows two types of typical stress-strain behaviour observed in experiments on real engineering materials. In case (a), the stress increases with increasing strain and the material is actually hardening from the beginning to the end. In other

words, an additional loading (i.e.,  $\Delta\sigma_{ij} > 0$ ) gives rise to an additional strain (i.e.,  $\Delta\varepsilon_{ij} > 0$ ), with the product  $\Delta\sigma_{ij} \Delta\varepsilon_{ij} > 0$ . The additional stress  $\Delta\sigma_{ij}$  therefore does positive work as represented by the shaded triangle in the figure. Behaviour of this kind is called *stable*.

In case (b), the deformation curve has a descending branch which follows a strain-hardening section. In the descending section, the strain increases with decreasing stress. In other words, the additional stress does negative work (i.e.,  $\Delta\sigma_{ij} \Delta\varepsilon_{ij} < 0$ ). Behaviour of this kind is called *unstable*.

In the light of this basic fact, Drucker (1952, 1958) introduced the idea of a *stable plastic material*. This postulate, when applied to an element of elastic-plastic materials in equilibrium under the action of surface loads and body forces, may be stated as follows:

*Consider an element initially in some state of stress, to which by an external agency an additional set of stresses is slowly applied and slowly removed. Then, during the application of the added stresses and in a cycle of application-and-removal of the added stresses, the work done by the external agency is non-negative.*

If we assume that the existing state of stress (on or inside a loading surface in the stress space) be denoted by  $\sigma_{ij}^*$ , Drucker's stability postulate, as stated above, can be shown to lead to the following two important inequalities (Drucker, 1952, 1960):

$$(\sigma_{ij} - \sigma_{ij}^*) d\varepsilon_{ij}^P \geq 0 \quad (3.18)$$

$$d\sigma_{ij} d\varepsilon_{ij}^P \geq 0 \quad (3.19)$$

where (3.18) is in fact the same as the maximum plastic work principle described before in (3.6). It is noted that the equality sign in both (3.18) and (3.19) holds only during neutral loading.

In simpler terms, a material that is stable in Drucker's sense would have the following properties: (a) The yield surface must be convex; (b) The plastic strain rate must be normal to the yield surface (i.e. with an associated flow rule); (c) The rate of strain hardening must be positive or zero (i.e. an additional stress must cause an additional strain); (d) The maximum plastic work principle is valid.

Although Drucker's postulate only covers certain types of real stress-strain behaviour for engineering materials, it does provide a neat way of unifying a whole set of features of plastic stress-strain relations. It must be stressed that while Drucker's postulate implies that the material must obey Hill's maximum plastic work (3.18),

the reverse is not true. This is because Drucker's stability postulate also requires a non-decreasing hardening rate, (3.19).

### 3.7 ISOTROPIC AND KINEMATIC HARDENING

Hardening in the theory of plasticity means that the yield surface changes, in size or location or even in shape, with the loading history (often measured by some form of plastic deformation). When the initial yield condition exists and is identified, the rule of hardening defines its modification during the process of plastic flow.

Most plasticity models currently in use assume that the shape of the yield surface remains unchanged, although it may change in size or location. This restriction is largely based on mathematical convenience, rather than upon any physical principle or experimental evidence. The two most widely used rules of hardening are known as isotropic hardening and kinematic (or anisotropic) hardening.

#### 3.7.1 Isotropic hardening

The rule of isotropic hardening assumes that the yield surface maintains its shape, centre and orientation, but expands or contracts uniformly about the centre of the yield surface.

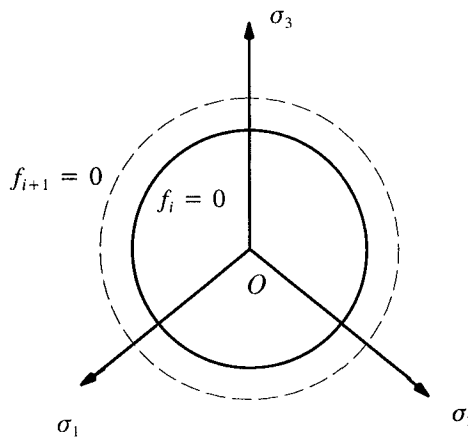


Figure 3.3: Isotropic hardening with uniform expansion of the yield surface

A yield surface with its centre at the origin may be generally described by the following function

$$f = f(\sigma_{ij}) - R(\alpha) = 0 \quad (3.20)$$

where  $R$  represents the size of the yield surface, depending on plastic strains through the hardening parameter  $\alpha$ . As shown in Hill (1950), the two earliest and most widely used hardening parameters are the accumulated equivalent plastic strain

$$\alpha = \int \sqrt{\frac{2}{3}} (d\epsilon_{ij}^P d\epsilon_{ij}^P)^{1/2} \quad (3.21)$$

and the plastic work

$$\alpha = \int \sigma_{ij} d\epsilon_{ij}^P \quad (3.22)$$

Figure 3.3 shows an example of isotropic hardening where the yield surface is uniformly expanding during the process of plastic flow when a stress increment is applied from step  $i$  to  $i+1$ . The size of the yield surface at any stage of loading is determined as long as an evolution rule defining the relationship between  $R$  and  $\alpha$  is defined.

### 3.7.2 Kinematic hardening

The term *kinematic hardening* was introduced by Prager (1955) to construct the first kinematic hardening model. In this first model, it was assumed that during plastic flow, the yield surface translates in the stress space and its shape and size remain unchanged. This is consistent with the Bauschinger effect observed in the uniaxial tension-compression.

Assume that the initial yield surface can be described by

$$f = f(\sigma_{ij} - \alpha_{ij}) - R_0 = 0 \quad (3.23)$$

where  $\alpha_{ij}$  represents the coordinates of the centre of the yield surface, which is also known as the back stress.  $R_0$  is a material constant representing the size of the original yield surface. It can be seen that as the back stress  $\alpha_{ij}$  changes due to plastic flow, the yield surface translates in the stress space while maintaining its initial shape and size.

It is clear now that the formulation of a kinematic hardening model involves assuming an evolution rule of the back stress  $\alpha_{ij}$  in terms of  $\epsilon_{ij}^P$ ,  $\sigma_{ij}$  or  $\alpha_{ij}$ .

The first simple kinematic hardening model was proposed by Prager (1955). This classical model assumes that the yield surface keeps its original shape and size

and moves in the direction of plastic strain rate tensor (see Figure 3.4). Mathematically it can be expressed by the following linear evolution rule

$$d\alpha_{ij} = c \, d\epsilon_{ij}^P \quad (3.24)$$

where  $c$  is a material constant.

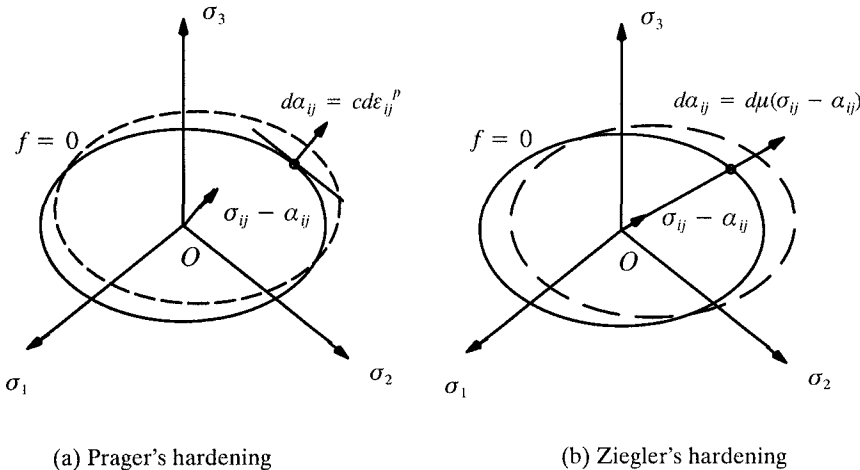


Figure 3.4: Prager's and Ziegler's kinematic hardening

Whilst Prager's model is reasonable for one-dimensional problems, it does not seem to give consistent predictions for two- and three-dimensional cases (Ziegler, 1959). The reason is that the yield function takes different forms for one-, two- and three-dimensional cases. To overcome this limitation, Ziegler (1959) suggested that the yield surface should move in the direction as determined by the vector  $\sigma_{ij} - \alpha_{ij}$ , see Figure 3.4. Mathematically Ziegler's model can be expressed as follows

$$d\alpha_{ij} = d\mu (\sigma_{ij} - \alpha_{ij}) \quad (3.25)$$

where  $d\mu$  is a material constant.

### 3.7.3 Mixed hardening

The term *mixed hardening* is used to indicate cases when the yield surface not only expands or contracts but also translates in the stress space upon plastic loading (see Figure 3.5). This means that both the centre and size of the yield surface will depend on plastic strain. In this case, the yield function can be expressed by

$$f = f(\sigma_{ij} - \alpha_{ij}) - R(\alpha) = 0 \quad (3.26)$$

where the size of the yield surface can be assumed to be a function of either plastic strain or plastic work., while either Prager's rule (3.24) or Ziegler's rule (3.25) may be used to control the translation of the yield surface upon loading.

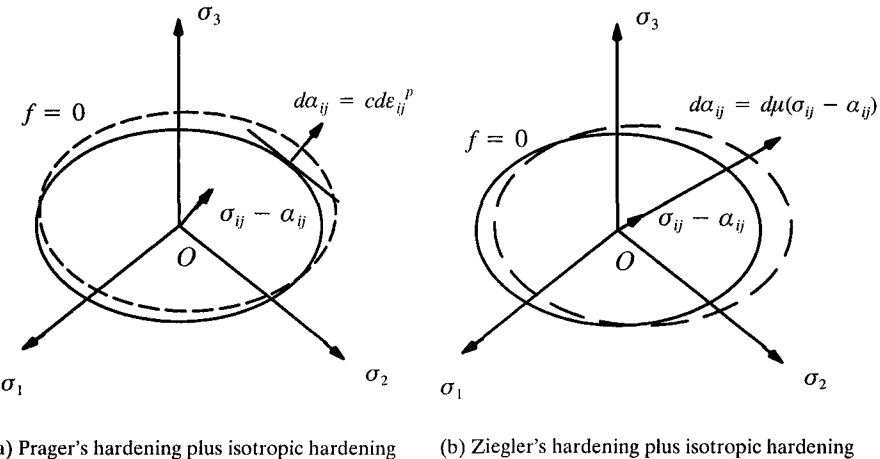


Figure 3.5: Mixed hardening

### 3.8 GENERAL STRESS-STRAIN RELATIONS

In order to determine the complete relation between stress and strain for elastic-plastic solids, we still need to assume *consistency* condition (Prager, 1949). For perfectly plastic solids, consistency condition means that the stress state remains on the yield surface. For strain-hardening materials, consistency means that during plastic flow the stress state must remain on the subsequent yield surface (or loading surface). In other words, loading from a plastically deforming state will lead to another plastically deforming state.

#### 3.8.1 Isotropic hardening

For isotropic hardening material, the yield function can be described by

$$f(\sigma_{ij}, \alpha) = 0 \quad (3.27)$$

then Prager's consistency condition requires

$$\frac{\partial f}{\partial \sigma_{ij}} d\sigma_{ij} + \frac{\partial f}{\partial \alpha} d\alpha = 0 \quad (3.28)$$

Since the hardening parameter is a function of plastic strains, so the consistency condition (3.28) can be further written as follows:

$$\frac{\partial f}{\partial \sigma_{ij}} d\sigma_{ij} + \frac{\partial f}{\partial \alpha} \frac{\partial \alpha}{\partial \varepsilon_{ij}^p} d\varepsilon_{ij}^p = 0 \quad (3.29)$$

For the special case of perfectly plastic solids, the second term of (3.28) will be zero.

The plastic strain rate can be determined from a plastic potential by equation (3.17), which is in fact the same as the plastic flow rule (3.2). This flow rule suggests that once a plastic potential is given, the plastic strain rate will be assumed to be normal to the plastic potential. However the non-negative quantity  $h$  or  $d\lambda$  needs to be determined in order for the plastic strain rate to be calculated. The consistency condition (3.28) can be used to determine  $d\lambda$ .

A general procedure for deriving a complete stress-strain relation for perfectly plastic and hardening materials is given below:

- (1) To divide the total strain rate (or increment) into elastic and plastic strain rates, namely

$$d\varepsilon_{ij} = d\varepsilon_{ij}^e + d\varepsilon_{ij}^p \quad (3.30)$$

- (2) Hooke's law is used to link the stress rate with elastic strain rate by elastic stiffness matrix  $D_{ijkl}$  as follows

$$d\sigma_{ij} = D_{ijkl} d\varepsilon_{kl}^e = D_{ijkl} (d\varepsilon_{kl} - d\varepsilon_{kl}^p) \quad (3.31)$$

- (3) The general non-associated plastic flow rule is used to express equation (3.31) in the following form

$$d\sigma_{ij} = D_{ijkl} (d\varepsilon_{kl} - d\lambda \frac{\partial g}{\partial \sigma_{kl}}) \quad (3.32)$$

- (4) By substituting equation (3.32) into the consistency condition (3.29), we obtain

$$d\lambda = \frac{1}{H} \frac{\partial f}{\partial \sigma_{ij}} D_{ijkl} d\varepsilon_{kl} \quad (3.33)$$

where  $H$  is given by

$$H = \frac{\partial f}{\partial \sigma_{ij}} D_{ijkl} \frac{\partial g}{\partial \sigma_{kl}} - \frac{\partial f}{\partial \alpha} \frac{\partial \alpha}{\partial \varepsilon_{ij}^P} \frac{\partial g}{\partial \sigma_{ij}} \quad (3.34)$$

(5) By substituting equation (3.33) into equation (3.32), we obtain a complete relation between a stress rate and a strain rate as follows

$$d\sigma_{ij} = D_{ijkl}^{ep} d\varepsilon_{kl} \quad (3.35)$$

where the elastic-plastic stiffness matrix  $D_{ijkl}^{ep}$  is defined by

$$D_{ij}^{ep} = D_{ijkl} - \frac{1}{H} D_{ijmn} \frac{\partial g}{\partial \sigma_{mn}} \frac{\partial f}{\partial \sigma_{pq}} D_{pqkl} \quad (3.36)$$

The above procedure is valid for both strain-hardening and perfectly plastic solids. It is noted that for the case of perfectly plastic solids, the yield surface remains unchanged so that (3.34) takes the following simpler form

$$H = \frac{\partial f}{\partial \sigma_{ij}} D_{ijkl} \frac{\partial g}{\partial \sigma_{kl}} \quad (3.37)$$

### 3.8.2 Kinematic hardening

For kinematic hardening material, the yield function may be expressed as

$$f = f(\sigma_{ij} - \alpha_{ij}) - R_0 = 0 \quad (3.38)$$

where  $\alpha_{ij}$  denote the coordinates of the centre of the yield surface, often known as the back stress tensor.

*Prager's translation rule*

Let us now consider the kinematic hardening law proposed by Prager first, then

$$d\alpha_{ij} = c d\varepsilon_{ij}^P = c d\lambda \frac{\partial g}{\partial \sigma_{ij}} \quad (3.39)$$

where  $g$  denotes the plastic potential.

With Prager's consistency condition applied to the yield function (3.38), we have

$$\frac{\partial f}{\partial \sigma_{ij}} d\sigma_{ij} + \frac{\partial f}{\partial \alpha_{ij}} d\alpha_{ij} = 0 \quad (3.40)$$

The assumed form of the yield function (3.38) gives

$$\frac{\partial f}{\partial \sigma_{ij}} = - \frac{\partial f}{\partial \alpha_{ij}} \quad (3.41)$$

With equations (3.39) and (3.41), equation (3.40) can be rewritten as

$$\frac{\partial f}{\partial \sigma_{ij}} d\sigma_{ij} = \frac{\partial f}{\partial \sigma_{ij}} c d\lambda \frac{\partial g}{\partial \sigma_{ij}} \quad (3.42)$$

which gives the plastic multiplier

$$d\lambda = \frac{1}{c} \frac{\frac{\partial f}{\partial \sigma_{ij}} d\sigma_{ij}}{\frac{\partial f}{\partial \sigma_{ij}} \frac{\partial g}{\partial \sigma_{ij}}} = \frac{1}{c} \frac{df}{\frac{\partial f}{\partial \sigma_{ij}} \frac{\partial g}{\partial \sigma_{ij}}} \quad (3.43)$$

Then the increments of the back stress tensor and the plastic strains are determined by

$$d\alpha_{ij} = c d\epsilon_{ij}^p = c d\lambda \frac{\partial g}{\partial \sigma_{ij}} = \frac{df}{\frac{\partial f}{\partial \sigma_{ij}} \frac{\partial g}{\partial \sigma_{ij}}} \frac{\partial g}{\partial \sigma_{ij}} \quad (3.44)$$

$$d\epsilon_{ij}^p = \frac{1}{c} \frac{\frac{\partial g}{\partial \sigma_{ij}}}{\frac{\partial f}{\partial \sigma_{ij}} \frac{\partial g}{\partial \sigma_{ij}}} df \quad (3.45)$$

By using an elastic stress-strain relation, we can determine the elastic strain rate

$$d\epsilon_{ij}^e = C_{ijkl} d\sigma_{kl} \quad (3.46)$$

where  $C_{ijkl}$  is the elastic compliance matrix. The total strain rate is the sum of the elastic and plastic parts

$$d\epsilon_{ij} = C_{ijkl} d\sigma_{kl} + \frac{1}{c} \frac{\frac{\partial g}{\partial \sigma_{ij}}}{\frac{\partial f}{\partial \sigma_{ij}} \frac{\partial g}{\partial \sigma_{ij}}} df \quad (3.47)$$

which can be further written as

$$d\varepsilon_{ij} = C_{ijkl}^{ep} d\sigma_{kl} \quad (3.48)$$

where the elastic-plastic compliance matrix is

$$C_{ijkl}^{ep} = C_{ijkl} + \frac{1}{c} \frac{\frac{\partial g}{\partial \sigma_{ij}} \frac{\partial f}{\partial \sigma_{kl}}}{\frac{\partial f}{\partial \sigma_{ij}} \frac{\partial g}{\partial \sigma_{ij}}} \quad (3.49)$$

It is worth noting that equation (3.48) can be inverted to give

$$d\sigma_{ij} = [C_{ijkl}^{ep}]^{-1} d\varepsilon_{kl} = D_{ijkl}^{ep} d\varepsilon_{kl} \quad (3.50)$$

*Ziegler's translation rule*

Ziegler's translation rule is

$$d\alpha_{ij} = d\mu (\sigma_{ij} - \alpha_{ij}) \quad (3.51)$$

where  $d\mu$  is a constant to be determined.

With Prager's consistency condition applied to the yield function (3.38), we have

$$\frac{\partial f}{\partial \sigma_{ij}} d\sigma_{ij} = \frac{\partial f}{\partial \sigma_{ij}} (\sigma_{ij} - \alpha_{ij}) d\mu \quad (3.52)$$

which gives

$$d\mu = \frac{\frac{\partial f}{\partial \sigma_{ij}} d\sigma_{ij}}{\frac{\partial f}{\partial \sigma_{ij}} (\sigma_{ij} - \alpha_{ij})} = \frac{df}{\frac{\partial f}{\partial \sigma_{ij}} (\sigma_{ij} - \alpha_{ij})} \quad (3.53)$$

The increment of the back stress tensor is therefore given by

$$d\alpha_{ij} = d\mu (\sigma_{ij} - \alpha_{ij}) = \frac{df}{\frac{\partial f}{\partial \sigma_{ij}} (\sigma_{ij} - \alpha_{ij})} (\sigma_{ij} - \alpha_{ij}) \quad (3.54)$$

It is worth noting that the plastic strain is not involved in the consistency condition with Ziegler's hardening. Therefore the plastic strain cannot be derived from the consistency condition. However it is normally assumed (Melan, 1938) that a

plastic modulus exists so that the plastic strain can be derived from a plastic potential following the form of equation (3.17)

$$d\epsilon_{ij}^p = \frac{1}{K_p} \frac{\frac{\partial g}{\partial \sigma_{ij}}}{\frac{\partial f}{\partial \sigma_{ij}} \frac{\partial g}{\partial \sigma_{ij}}} df \quad (3.55)$$

where  $K_p$  is a material constant known as the plastic modulus which can be determined from the uniaxial compression or tension test. Comparing equation (3.55) with equation (3.45) suggests that the plastic modulus plays the same role as the material constant  $c$  in the case with Prager's hardening rule.

### 3.9 HISTORICAL REMARKS

As rightly pointed out by Koiter (1960), it is often difficult to trace the origin of particular ideas in view of the long and often erratic history of the mathematical theory of plasticity, in particular with regard to the fundamental stress-strain relations. No attempt is made here to give a comprehensive review of the initial history of the plasticity theory. Rather a brief sketch will be given on the major landmarks in the early stage of the development of plastic stress-strain relations. For more detailed discussion, the reader is referred to the reviews given by Hill (1950), Prager (1949, 1955), Prager and Hodge (1951), Koiter (1960), Kachanov (1974) and Martin (1975) among others.

Although the work by Tresca (1864) on the yield criterion of metal is widely regarded as the birth of the classical theory of plasticity, fundamental research on the failure or yielding of soils had been carried out much earlier by Coulomb (1773) and applied by Rankine (1853) to solve earth pressure problems in retaining walls. de Saint-Venant (1870) was the first to develop constitutive relations for perfectly plastic solids. In particular, the coaxial assumption (i.e., requiring coaxiality of the stress tensor and plastic strain tensor) made by de Saint-Venant proved to be a foundation for the classical theory of plasticity with regard to stress-strain relations. A more realistic yield criterion than Tresca's function for metal was proposed by von Mises in 1913. The maximum plastic work principle appears to be first proved by von Mises (1928) and Hill (1948) and then supported by Bishop and Hill (1947) from the behaviour of a single crystal. The development of stress-strain relations for hardening materials in incremental form proceeded very slowly. The first general stress-strain relations for solids with hardening was achieved by Melan (1938) and independently by Prager (1949). To provide a unified theoretical basis for the theory of plasticity, Drucker (1952, 1958) proposed a stability postulate, which includes the principle of maximum plastic work as one of its consequences. Drucker's

stability postulate has since been widely used to develop constitutive models for a certain class of plastic solids. In addition, Ziegler (1958) proposed a rather different approach which attempts to bring the theory of plasticity under the scope of Onsager's principle for irreversible thermodynamic processes. This last approach has received more attention in recent years (e.g. Collins and Houlsby, 1997).

## REFERENCES

Bishop, J.F.W. and Hill, R (1951). A theory of the plastic distortion of a polycrystalline aggregate under combined stresses, *Phil. Mag.*, Vol 42, 414-427.

Collins, I.F. and Houlsby, G.T. (1997). Application of thermomechanical principles to the modelling of geotechnical materials, *Proc. R. Soc. A.*, Vol 453, 1975-2001.

Coulomb, C.A. (1773). Essai sur une application des regles des maximis et minimis a quelques problemes de statique relatifs a l'architecture, *Mem. pres. par div. savants*, Vol 7, 343-382.

de Saint-Venant, B (1870). Memoire sur l'établissement des equations differentielles des mouvements interieurs opérés dans les corps solides ductiles au delà des limites où l'élasticité pourrait les ramener à leur premier état, *C.R. Acad. Sci. (Paris)*, Vol 70, 473-480.

Drucker, D.C. (1952). A more fundamental approach to plastic stress-strain relations, In: *Proc. 1st US Nat. Congr. Appl. Mech.*, ASME, New York, 487-491.

Drucker, D.C. (1958). The definition of a stable inelastic material, *J. Appl. Mech.*, ASME, Vol 26, 101-106.

Green, A.E. and Naghdi, P.M. (1965). A general theory for an elastic plastic continuum, *Arch. Rat. Mech. Anal.*, Vol 18, 251-281.

Hill, R (1948). A variational principle of maximum plastic work in classical plasticity, *Q.J. Mech. Appl. Math.*, Vol 1, 18-28.

Hill, R (1950). *The Mathematical Theory of Plasticity*, Clarendon Press, Oxford.

Kachanov, L.M. (1974). *Fundamentals of the Theory of Plasticity*. Mir Publishers, Moscow.

Koiter, W.T. (1953). Stress-strain relations, uniqueness and variational theorems for elastic-plastic materials with a singular yield surface, *Quart. Appl. Math.*, Vol 11, 350-354.

Koiter, W.T. (1960). General theorems for elastic-plastic solids, In: *Progress in Solid Mechanics*, (Editors: I.N. Sneddon and R. Hill), Vol 1, 167-221.

Martin, J.B. (1975). *Plasticity: Fundamentals and General Results*, MIT Press, Cambridge.

Melan, E (1938). Zur plastizität des raumlichen Kontinuums, *Ing. Arch.*, Vol 9, 116-125.

Naghdi, P.M. (1960). Stress-strain relations in plasticity and thermoplasticity, In: *Plasticity*, (Editors: E.H. Lee and P.S. Symonds), Pergamon Press, 121-169.

Prager, W (1949). Recent developments of the mathematical theory of plasticity, *J. Appl. Phys.*, Vol 20, 235.

Prager, W (1955). The theory of plasticity – a survey of recent achievements, *Proc. Inst. Mech. Eng.*, London, 3-19.

Prager, W. and Hodge, P.G. (1951). *The Theory of Perfectly Plastic Solids*, John Wiley and Sons, New York.

Rankine, W.J. (1857). On the stability of loose earth. *Phil. Trans. R. Soc.*, Vol 147, 9-27.

Schofield, A.N. and Wroth, C.P. (1968). *Critical State Soil Mechanics*, McGraw-Hill, London.

Tresca, H. (1864). Sur l'écoulement des corps solides soumis à de fortes pressions, *C.R. Acad. Sci. (Paris)*, Vol 59, 754.

von Mises, R (1928). Mechanik der plastischen Formänderung von Kristallen, *Z. angew. Math. Mech.*, Vol 8, 161-185.

Wilde, P. (1977). Two-invariants dependent model of granular media. *Arch. Mech.*, Vol 29, 445-458.

Yu, H.S. (1998). CASM: A unified state parameter model for clay and sand. *Int. J. Num. Analy. Meth. Geomech.*, Vol 22, 621-653.

Yu, H.S., Khong, C.D., Wang, J. and Zhang, G. (2005). Experimental evaluation and extension of a simple critical state model for sand. *Granular Matter*, Vol 7, 213-225.

Ziegler, H. (1958). An attempt to generalise Onsager's principle, and its significance for rheological problems. *J. Appl. Math. Phys. (ZAMP)*, Vol 9, 748.

Ziegler, H. (1959). A modification of Prager's hardening rule. *Quart. Appl. Math.* Vol 17, 55.

## CHAPTER 4

### GENERAL ELASTIC-PLASTIC THEOREMS

#### 4.1 INTRODUCTION

It would be hard to overstate the importance of general theorems in the development and application of the theory of plasticity. Although the literature on the general theorems is quite extensive (Martin, 1975), the most widely used theorems are still limited. They include the principle of virtual work, uniqueness theorems, minimum principles for stress and strain rates, plastic collapse theorems, and shakedown theorems. A most striking feature of the general theorems is their complementary character. In other words, to each minimum principle (such as collapse or shakedown theorem of a static type in terms of stress variables) corresponds a similar theorem of a kinematic type in terms of strain variables. An exception has to be made only for the uniqueness theorem for perfectly plastic solids, where non-unique strain rates may correspond to unique stress rates (Hill, 1950; Koiter, 1960).

Although significant progress has been made in the development of general theorems for large deformation of elastic-plastic solids (Hill, 1958), their application for solution solving remains difficult and limited. In contrast, the general theorems for small deformation of elastic-plastic solids had already approached their definitive form when Koiter (1960) was presenting his unified treatment of these theorems over forty years ago.

This chapter presents a concise treatment of some of the most widely used general theorems for elastic-plastic solids. The discussion will be restricted to small deformation for the reason mentioned above. While our presentation closely follows Hill (1950), Koiter (1960) and Kachanov (1974), some more recently developed theorems, which have already found practical applications, are also included.

For simplicity, Cartesian tensor notation has been used in most of the literature on the subject of general theorems. We will also follow this tradition. The reader who is not familiar with it is referred to Chapter 8 of the book by Prager and Hodge (1951).

#### 4.2 THE PRINCIPLE OF VIRTUAL WORK

The principle of virtual work (also known as the basic energy equation, Kachanov, 1974) is an alternative form of expressing equilibrium and compatibility condi-

tions. Since the principle does not involve stress-strain relations, it is applicable to both elastic and elastic-plastic solids. The principle of virtual work is important for at least two reasons: (a) it is a basic tool in establishing most other general plastic theorems; (b) it serves as a more convenient basis for numerical solutions of elastic-plastic solids.

Let us consider a body of volume  $V$  bounded by a surface  $S$ . We now apply prescribed values of tractions (forces)  $T_0$  and displacements  $u_0$  over separate regions of the surface  $S_T$  and  $S_u$  respectively (see Figure 4.1).

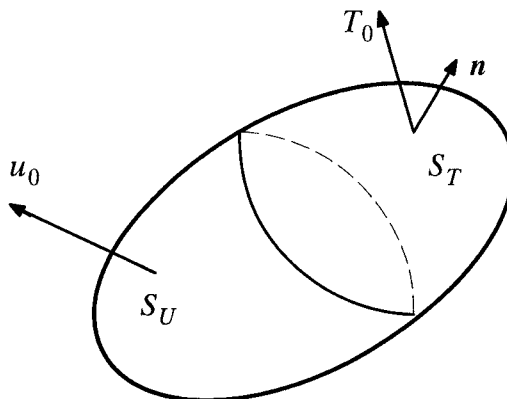


Figure 4.1: Principle of virtual work

The boundary conditions are therefore expressed as follows

$$u_i = u_{0i} \quad \text{on} \quad S_U \quad (4.1)$$

$$\sigma_{ij}n_j = T_{0i} \quad \text{on} \quad S_T \quad (4.2)$$

where  $i$  ( $i = 1, 2, 3$ ) is used to denote the three axes.

In addition to the prescribed forces and displacements on the surface, it is also assumed that the body  $V$  is subjected to a body force field defined by the vector  $b_i$  and the effect of dynamics is ignored. Therefore the equilibrium equations for the body  $V$  can be written as follows

$$\sigma_{ij,j} + b_i = 0 \quad (4.3)$$

where the subscript comma denotes partial differentiation with respect to the appropriate spatial variable (Prager and Hodge, 1951).

Now we define a *virtual displacement field* as the difference between two neighbouring kinematically admissible displacement fields (that satisfy both external boundary conditions and any internal constraints such as incompressibility for incompressible materials). Given a virtual displacement field is a small difference, it can be denoted by  $du_i$ . The virtual strain field associated with the virtual displacement field can be obtained as

$$d\varepsilon_{ij} = \frac{1}{2}(du_{i,j} + du_{j,i}) \quad (4.4)$$

For a complete solid body, the principle of virtual work is mathematically given by the following basic energy equation

$$\iint_V \iint_V \sigma_{ij} d\varepsilon_{ij} dV = \iint_V \iint_V b_i du_i dV + \iint_{S_T} T_{0i} du_i dS \quad (4.5)$$

where the left-hand side is the internal work done by stress fields on the virtual strain field and the right-hand side is the external work done by the prescribed tractions and body force on the virtual displacement field. It is important to note that the surface integral is over  $S_T$  only, since on  $S_U$  the displacements are prescribed so that the virtual displacements must be zero. This makes the external work done on the virtual displacement field over the surface  $S_U$  as zero.

To prove the principle of virtual work (4.5), we can use the stress boundary condition (4.2) to write the surface integral in the form

$$\iint_{S_T} T_{0i} du_i dS = \iint_{S_T} \sigma_{ij} du_i n_j dS \quad (4.6)$$

Let  $F$  be a scalar, vector, or tensor field which is continuously differentiable in closed domain  $V$  bounded by a closed surface  $S$  with the outward unit normal vector  $n_j$ . Then Green's or Gauss's theorem can be used to transform a surface integral to a volume integral

$$\iint_S F n_j dS = \iint_V \iint_V F_{,j} dV \quad (4.7)$$

It can then shown that

$$\iint_S \sigma_{ij} du_i n_j dS = \iint_V \iint_V (\sigma_{ij} du_i)_{,j} dV \quad (4.8)$$

$$= \iint_V \iint_V du_i \sigma_{ij,j} dV + \iint_V \iint_V \sigma_{ij} d\varepsilon_{ij} dV \quad (4.9)$$

As a result, the external work done by the tractions and body force (i.e. the right-hand side of equation (4.5)) can be expressed as follows

$$\begin{aligned} \iint_V \int b_i \, du_i \, dV + \iint_{S_T} T_{0i} \, du_i \, dS &= \\ = \iint_V \int du_i (\sigma_{ij,j} + b_i) \, dV + \iint_V \int \sigma_{ij} \, d\epsilon_{ij} \, dV & \quad (4.10) \end{aligned}$$

Noting that the first term of the right-hand side of equation (4.10) is zero due to equilibrium, we have proved that the external work done is identical to the internal work done by the stress field.

It should be noted that the basic energy equation is valid for any *virtual* displacement fields (i.e. they do not have to be the actual one!) as long as they are kinematically admissible and compatible with the strain fields through equation (4.4). The strain fields could be independent of the stress fields.

So far we have proved that the basic energy equation is valid for any pair of virtual displacement and strain fields. In the same way, we can easily show that the following principle of virtual work in terms of a virtual velocity field  $v_i$  and associated strain rate field  $\dot{\epsilon}_{ij}$  is also true

$$\iint_V \int \sigma_{ij} \dot{\epsilon}_{ij} \, dV = \iint_V \int b_i v_i \, dV + \iint_{S_T} T_{0i} v_i \, dS \quad (4.11)$$

where the virtual velocity field and strain rate field are related by

$$\dot{\epsilon}_{ij} = \frac{1}{2}(v_{i,j} + v_{j,i}) \quad (4.12)$$

## 4.3 UNIQUENESS THEOREMS

Engineering problems are often involved with finding a solution for stress and strain changes in an elastic-plastic body caused by the application of an additional traction or/and displacement fields on the surface surrounding the body. In this section we will investigate the conditions in which the small changes in stress and strain in the body are *uniquely* determined by the given boundary conditions and the stress-strain relations formulated for the elastic-plastic solids.

### 4.3.1 Uniqueness of stress rates and strain rates

Let us assume that the external body forces  $b_i$ , the surface tractions  $T_{0i}$  on the part of the surface  $S_T$  where the tractions are applied, and the surface displacements  $u_{0i}$

on the part of the surface  $S_u$  where the displacements are specified, are increased by known rates  $\dot{b}_i$ ,  $\dot{T}_{0i}$  and  $\dot{u}_{0i}$ . The solution for stress rates will have to satisfy the following requirements:

(1) The stress rates satisfy the equations of equilibrium in the entire body

$$\dot{\sigma}_{ij,j} + \dot{b}_i = 0 \quad (4.13)$$

(2) The stress rates satisfy the stress boundary conditions on  $S_T$

$$\dot{\sigma}_{ij}n_j = \dot{T}_{0i} \quad (4.14)$$

(3) The corresponding strain rates  $\dot{\varepsilon}_{ij}$  are compatible with the velocity field  $v_i = \dot{u}_i$

$$\dot{\varepsilon}_{ij} = \frac{1}{2}(v_{i,j} + v_{j,i}) = \frac{1}{2}(\dot{u}_{i,j} + \dot{u}_{j,i}) \quad (4.15)$$

(4) The displacement increments (or velocities) satisfy the boundary conditions on  $S_u$

$$\dot{u}_i = \dot{u}_{0i} \quad (4.16)$$

It will be shown that the following uniqueness theorem is valid:

*The uniqueness theorem states that no more than one solution for stress rates can exist that will be able to satisfy all the requirements given above.*

This uniqueness theorem for stress rates appears to be first proved by Melan (1938) for both strain hardening and perfectly plastic solids. However Melan's proof for perfectly plastic solids has been overlooked by later researchers, such as Greenberg (1949), who have again independently provided proof for the theorem for perfectly plastic materials (Hill, 1950).

The uniqueness theorem can be proved by showing that the assumption of the existence of two distinct solutions for stress rates,  $\dot{\sigma}_{ij}^{(1)}$  and  $\dot{\sigma}_{ij}^{(2)}$ , leads to a contradiction. The principle of virtual work can be used to obtain the following equation

$$\begin{aligned} \iint_V (\dot{\sigma}_{ij}^{(1)} - \dot{\sigma}_{ij}^{(2)}) (\dot{\varepsilon}_{ij}^{(1)} - \dot{\varepsilon}_{ij}^{(2)}) \, dV = \\ \iint_S (\dot{\sigma}_{ij}^{(1)} - \dot{\sigma}_{ij}^{(2)}) (\dot{u}_i^{(1)} - \dot{u}_i^{(2)}) n_j \, dS \end{aligned} \quad (4.17)$$

If the change in geometry can be ignored (see Hill, 1950), the right-hand side of the above equation is zero because the given boundary conditions give

$$\dot{u}_i^{(1)} - \dot{u}_i^{(2)} = 0 \quad \text{on } S_U \quad (4.18)$$

$$(\dot{\sigma}_{ij}^{(1)} - \dot{\sigma}_{ij}^{(2)}) n_j = 0 \quad \text{on } S_T \quad (4.19)$$

Using equations (4.18) and (4.19), equation (4.17) reduces to

$$\int \int \int_V (\dot{\sigma}_{ij}^{(1)} - \dot{\sigma}_{ij}^{(2)}) (\dot{\epsilon}_{ij}^{(1)} - \dot{\epsilon}_{ij}^{(2)}) dV = 0 \quad (4.20)$$

On the other hand, the integral (4.20) will be shown to be positive unless  $\dot{\sigma}_{ij}^{(1)} = \dot{\sigma}_{ij}^{(2)}$ , and this will therefore lead to a contradiction.

First let's consider the elastic strain rates

$$\begin{aligned} (\dot{\sigma}_{ij}^{(1)} - \dot{\sigma}_{ij}^{(2)}) (\dot{\epsilon}_{ij}^{(1e)} - \dot{\epsilon}_{ij}^{(2e)}) &= \\ C_{ijkl} (\dot{\sigma}_{ij}^{(1)} - \dot{\sigma}_{ij}^{(2)}) (\dot{\sigma}_{kl}^{(1)} - \dot{\sigma}_{kl}^{(2)}) &> 0 \end{aligned} \quad (4.21)$$

which is positive unless  $\dot{\sigma}_{ij}^{(1)} = \dot{\sigma}_{ij}^{(2)}$  and where  $C_{ijkl}$  is the tensor of elastic coefficients.

For both perfectly and strain-hardening plastic materials, the following inequality holds for the plastic part of the integral

$$\begin{aligned} (\dot{\sigma}_{ij}^{(1)} - \dot{\sigma}_{ij}^{(2)}) (\dot{\epsilon}_{ij}^{(1p)} - \dot{\epsilon}_{ij}^{(2p)}) &= \\ (\sigma_{ij}^{(1)} - \sigma_{ij}^{(2)}) \dot{\epsilon}_{ij}^{(1p)} + (\sigma_{ij}^{(2)} - \dot{\sigma}_{ij}^{(1)}) \dot{\epsilon}_{ij}^{(2p)} &\geq 0 \end{aligned} \quad (4.22)$$

Therefore we have proved that for both perfectly plastic and strain-hardening materials, the solution for stress rates is unique. For strain-hardening materials the strain rate in any element is uniquely determined by the stress rate. This feature ensures that the solution for strain rates is also unique for strain-hardening materials. *However a similar conclusion may not be drawn for the strain rate in a perfectly plastic solid* (Hill, 1950). This lack of uniqueness may be removed by regarding the perfectly plastic material as the limiting case of a work-hardening material (Koiter, 1960).

### 4.3.2 Uniqueness of stresses

It is useful to know if the consistent distribution of stresses produced by applied surface displacements is unique, or if it depends upon the state of stress beforehand. To answer this question, Hill (1948, 1950) proved that for a rigid-plastic solid there is not more than one consistent stress solution for which the whole mass deforms plastically.

Suppose that  $(\sigma_{ij}^{(1)}, \dot{u}_i^{(1)})$  and  $(\sigma_{ij}^{(2)}, \dot{u}_i^{(2)})$  could be two consistent solutions corresponding to the same boundary conditions. It can be shown that

$$\begin{aligned} \int \int \int_V (\sigma_{ij}^{(1)} - \sigma_{ij}^{(2)}) (\dot{\varepsilon}_{ij}^{(1)} - \dot{\varepsilon}_{ij}^{(2)}) \, dV = \\ \int \int_S (\sigma_{ij}^{(1)} - \sigma_{ij}^{(2)}) (\dot{u}_i^{(1)} - \dot{u}_i^{(2)}) \, n_j \, dS = 0 \end{aligned} \quad (4.23)$$

if

$$(T_{0i}^{(1)} - T_{0i}^{(2)}) (\dot{u}_i^{(1)} - \dot{u}_i^{(2)}) \, dS = 0 \quad (4.24)$$

on the surface. This condition is satisfied when either the surface displacements or the external forces (tractions) are prescribed.

If the two solutions are possible for the whole mass to be in the plastic state, then they must satisfy the yield criterion, for example,

$$f(\sigma_{ij}^{(1)}) = f(\sigma_{ij}^{(2)}) = R(\alpha) \quad (4.25)$$

throughout the whole mass.  $R(\alpha)$  denotes the size of the yield surface (and therefore the state of hardening) just before the application of additional displacements or forces. By using an associated flow rule and noting the rigid-plastic assumption, we have

$$\begin{aligned} (\sigma_{ij}^{(1)} - \sigma_{ij}^{(2)}) (\dot{\varepsilon}_{ij}^{(1)} - \dot{\varepsilon}_{ij}^{(2)}) &= (\sigma_{ij}^{(1)} - \sigma_{ij}^{(2)}) (\dot{\varepsilon}_{ij}^{(1p)} - \dot{\varepsilon}_{ij}^{(2p)}) \\ &= (\sigma_{ij}^{(1)} - \sigma_{ij}^{(2)}) [d\lambda^{(1)} \frac{\partial f}{\partial \sigma_{ij}^{(1)}} - d\lambda^{(2)} \frac{\partial f}{\partial \sigma_{ij}^{(2)}}] \\ &= (\sigma_{ij}^{(1)} - \sigma_{ij}^{(2)}) d\lambda^{(1)} \frac{\partial f}{\partial \sigma_{ij}^{(1)}} + (\sigma_{ij}^{(2)} - \sigma_{ij}^{(1)}) d\lambda^{(2)} \frac{\partial f}{\partial \sigma_{ij}^{(2)}} \end{aligned} \quad (4.26)$$

As noted by Hill (1950), for the present purpose, there is no need to write  $d\lambda$  as  $hdf$  when the material hardens. By considering the two terms in the right-hand side of equation (4.26), it is obvious that as long as the yield surface is convex they are all positive unless the two solutions for the stresses are the same,  $\sigma_{ij}^{(1)} = \sigma_{ij}^{(2)}$ . We have therefore proved that in a rigid-plastic material, there cannot be two distinct plastic stress solutions that satisfy the same boundary conditions.

## 4.4 MINIMUM AND VARIATIONAL PRINCIPLES

Consider a function that depends on a number of variables. A minimum principle asserts that the function will become minimum over all admissible values of its variables when they are equal to a certain set of values. On the other hand, a variational principle need not assert an extreme at all, even a local one, but only gives the condition that the function obeying it is stationary. It is therefore obvious that a minimum principle is stronger than a variational principle. Both of these types of principles are useful for obtaining approximate solutions for complex engineering problems where the exact solutions are unknown or difficult to obtain. This is why some minimum and variational principles have served as the theoretical basis for many powerful numerical methods in engineering.

### 4.4.1 Elastic material

It is instructive to consider the minimum principles for elastic material before presenting their counterparts for elastic-plastic material. It is well-known that in the theory of elasticity the principles of minimum potential energy and minimum complementary energy have played a very important role. The precise form of the minimum principle will depend on the particular relations between the variables of the problems. As pointed out by Hodge (1958), however, certain features are common to all of the principles, and other features are clearly analogous. In fact, the minimum and variational principles for elastic material are prototypes of most of the principles that will be presented for elastic-plastic material. For this reason, the well-known elastic minimum principles are given in this section for the purpose of comparison.

Let  $(\sigma_{ij}, \varepsilon_{ij})$  be the actual stress and strain fields in an elastic body that has been loaded from a stress-free state by prescribed surface tractions  $T_{0i}$  over a part of its surface  $S_T$ , and by prescribed displacements  $u_{0i}$  over the remainder of the surface  $S_u$ .

#### (a) The minimum and variational principles for the stress field

Consider a pair of stress and strain fields  $(\sigma_{ij}^s, \varepsilon_{ij}^s)$  which are statically admissible (Prager and Hodge, 1951), so that the equations of equilibrium, the stress-strain relations, and stress boundary conditions are satisfied, but the displacement compatibility is not obeyed. The first elastic minimum principle may be expressed by the following statement: the expression

$$\Pi_1 = \frac{1}{2} \int \int \int_V \sigma_{ij}^s \varepsilon_{ij}^s dV - \int \int_{S_U} \sigma_{ij}^s n_j u_{0i} dS \quad (4.27)$$

defined for all statically admissible stress fields, becomes a minimum when the statically admissible stress field is equal to the actual stress field  $\sigma_{ij}$ .

To prove this minimum principle, the principle of virtual work and stress and displacement boundary conditions can be used to give

$$\begin{aligned} \int \int \int_V (\sigma_{ij}^s - \sigma_{ij}) \varepsilon_{ij} dV &= \int \int_S (\sigma_{ij}^s - \sigma_{ij}) n_j u_i dS \\ &= \int \int_{S_U} (\sigma_{ij}^s - \sigma_{ij}) n_j u_{0i} dS \end{aligned} \quad (4.28)$$

By noting the reciprocity relation  $\sigma_{ij}^s \varepsilon_{ij} = \sigma_{ij} \varepsilon_{ij}^s$ , it can also be shown that (Hill, 1950)

$$\frac{1}{2} (\sigma_{ij}^s \varepsilon_{ij}^s - \sigma_{ij} \varepsilon_{ij}) \geq (\sigma_{ij}^s - \sigma_{ij}) \varepsilon_{ij} \quad (4.29)$$

By combining equations (4.28) and (4.29), we obtain the following inequality

$$\begin{aligned} \frac{1}{2} \int \int \int_V (\sigma_{ij}^s \varepsilon_{ij}^s - \sigma_{ij} \varepsilon_{ij}) dV &\geq \int \int \int_V (\sigma_{ij}^s - \sigma_{ij}) \varepsilon_{ij} dV \\ &= \int \int_{S_U} (\sigma_{ij}^s - \sigma_{ij}) n_j u_{0i} dS \end{aligned} \quad (4.30)$$

which can be rearranged to give

$$\begin{aligned} \Pi_1 &= \frac{1}{2} \int \int \int_V \sigma_{ij}^s \varepsilon_{ij}^s dV - \int \int_{S_U} \sigma_{ij}^s n_j u_{0i} dS \\ &\geq \frac{1}{2} \int \int \int_V \sigma_{ij} \varepsilon_{ij} dV - \int \int_{S_U} \sigma_{ij} n_j u_{0i} dS \end{aligned} \quad (4.31)$$

where the equality holds only when  $\sigma_{ij}^s = \sigma_{ij}$ . This provides a proof for the elastic minimum principle in terms of the stress field (also known as the principle of minimum complementary energy).

The corresponding variational principle for this elastic minimum principle states that the following expression

$$\begin{aligned}\Pi_1 &= \frac{1}{2} \int \int \int_V \sigma_{ij}^s \epsilon_{ij}^s dV - \int \int_{S_U} \sigma_{ij}^s n_j u_{0i} dS \\ &= \int \int \int_V E^s dV - \int \int_{S_U} \sigma_{ij}^s n_j u_{0i} dS\end{aligned}\quad (4.32)$$

becomes a stationary value when the varying statically admissible stress field  $\sigma_{ij}^s$  is equal to the actual stress field  $\sigma_{ij}$ .

To prove this, the expression (4.32) is further transformed into the following form

$$\Pi_1 = \int \int \int_V (E^s - \sigma_{ij}^s \epsilon_{ij}) dV - \int \int_{S_T} T_{0i} u_i dS \quad (4.33)$$

which has a stationary value provided

$$\frac{\partial \Pi_1}{\partial \sigma_{ij}^s} = 0 \quad (4.34)$$

A sufficient condition to ensure equation (4.34) is to insist

$$\frac{\partial (E^s - \sigma_{ij}^s \epsilon_{ij})}{\partial \sigma_{ij}^s} = 0 \quad \Rightarrow \quad \frac{\partial E^s}{\partial \sigma_{ij}^s} = \epsilon_{ij} \quad (4.35)$$

at every point of the elastic mass. Assuming the stress field and strain field are linearly related, the condition (4.35) gives

$$\frac{\partial E^s}{\partial \sigma_{ij}^s} = \epsilon_{ij}^s = \epsilon_{ij} \quad (4.36)$$

This proves that the expression  $\Pi_1$  will assume a stationary value when the stress (and strain) field is equal to the actual stress (and strain) field. As discussed earlier, this variational principle is weaker than the corresponding minimum principle (4.31).

### (b) The minimum and variational principles for the strain field

Now consider a pair of stress and strain fields  $(\sigma_{ij}^k, \epsilon_{ij}^k)$  which are kinematically admissible (Prager and Hodge, 1951), so that the displacement compatibility, the stress-strain relations, and displacement boundary conditions are satisfied, but the equations of equilibrium are not obeyed. The second elastic minimum principle may be expressed by the following statement: the expression

$$I_2 = \frac{1}{2} \int \int \int_V \sigma_{ij}^k \varepsilon_{ij}^k dV - \int \int_{S_T} u_i^k T_{0i} dS \quad (4.37)$$

defined for all kinematically admissible strain fields, takes a minimum value when the kinematically admissible strain field is equal to the actual strain field  $\varepsilon_{ij}$ .

To prove this minimum principle, the principle of virtual work and stress and displacement boundary conditions can be used to give

$$\begin{aligned} \int \int \int_V (\varepsilon_{ij}^k - \varepsilon_{ij}) \sigma_{ij} dV &= \int \int_S (u_i^k - u_i) \sigma_{ij} n_j dS \\ &= \int \int_{S_T} (u_i^k - u_i) T_{0i} dS \end{aligned} \quad (4.38)$$

By noting the reciprocity relation

$$(\varepsilon_{ij}^k - \varepsilon_{ij}) \sigma_{ij} = (\sigma_{ij}^k - \sigma_{ij}) \varepsilon_{ij} \quad (4.39)$$

and using the inequality (4.29), we obtain

$$\frac{1}{2} (\sigma_{ij}^k \varepsilon_{ij}^k - \sigma_{ij} \varepsilon_{ij}) \geq (\varepsilon_{ij}^k - \varepsilon_{ij}) \sigma_{ij} \quad (4.40)$$

By using equations (4.28) and (4.29), we obtain the following inequality

$$\begin{aligned} \frac{1}{2} \int \int \int_V (\sigma_{ij}^k \varepsilon_{ij}^k - \sigma_{ij} \varepsilon_{ij}) dV &\geq \int \int \int_V (\varepsilon_{ij}^k - \varepsilon_{ij}) \sigma_{ij} dV \\ &= \int \int_{S_T} (u_i^k - u_i) T_{0i} dS \end{aligned} \quad (4.41)$$

which can be rearranged to give

$$\begin{aligned} I_2 &= \frac{1}{2} \int \int \int_V \sigma_{ij}^k \varepsilon_{ij}^k dV - \int \int_{S_T} u_i^k T_{0i} dS \\ &\geq \frac{1}{2} \int \int \int_V \sigma_{ij} \varepsilon_{ij} dV - \int \int_{S_T} u_i T_{0i} dS \end{aligned} \quad (4.42)$$

As in the first minimum principle, the equal sign is only for the case when the kinematically admissible strain field is equal to the actual strain field.

By following the same procedure as used for the first minimum principle, the variational principle corresponding to the second minimum principle (4.42) can also be proved easily.

So far we have only considered the minimum and variational principles for the stress and strain fields. However similar principles can be proved in the same manner for the stress and strain rates.

#### 4.4.2 Elastic-plastic material

Before proceeding to present the minimum and variational principles for elastic-plastic materials, it is useful to give below the definitions introduced by Prager and Hodge (1951) and Drucker *et al.* (1951):

##### *Statically admissible stress rate fields*

A stress rate distribution  $\dot{\sigma}_{ij}^s$  is termed statically admissible if it satisfies the equations of equilibrium, yield criterion, and the stress boundary conditions. The strain rate field, which is obtained from such a stress rate field by stress-strain relations, is denoted by  $\dot{\varepsilon}_{ij}^s$ .

##### *Kinematically admissible strain rate fields*

A strain rate distribution  $\dot{\varepsilon}_{ij}^k$  is termed kinematically admissible if it satisfies the compatibility, plastic flow rule, and displacement boundary conditions. The stress rate field, which is obtained from such a strain rate field by stress-strain relations, is denoted by  $\dot{\sigma}_{ij}^k$ . This stress rate field does not generally satisfy the equations of equilibrium or the stress boundary conditions.

##### **(a) The minimum principle for the stress rate field**

Consider a pair of stress and strain rate fields  $(\dot{\sigma}_{ij}^s, \dot{\varepsilon}_{ij}^s)$  which are statically admissible, so that the equations of equilibrium, the stress-strain relations, and stress boundary conditions are satisfied, but the displacement compatibility is not obeyed. The minimum principle for the stress rate field may be expressed by the following statement: the expression

$$\Pi_3 = \frac{1}{2} \int \int \int_V \dot{\sigma}_{ij}^s \dot{\varepsilon}_{ij}^s dV - \int \int_{S_U} \dot{\sigma}_{ij}^s n_j \dot{u}_{0i} dS \quad (4.43)$$

defined for all statically admissible stress rate fields, assumes a minimum when the statically admissible stress rate field is equal to the actual stress rate field  $\dot{\sigma}_{ij}$ .

The above minimum principle can be further stated as the following inequality

$$\Pi_3 = \frac{1}{2} \int \int \int_V \dot{\sigma}_{ij}^s \dot{\varepsilon}_{ij}^s dV - \int \int_{S_U} \dot{\sigma}_{ij}^s n_j \dot{u}_{0i} dS$$

$$\geq \frac{1}{2} \int \int \int_V \dot{\sigma}_{ij} \dot{\varepsilon}_{ij} dV - \int \int_{S_U} \dot{\sigma}_{ij} n_j \dot{u}_{0i} dS \quad (4.44)$$

It is obvious that this is in the same form as the first elastic minimum principle.

To prove this minimum principle, we need to show that the following expression is positive (Koiter, 1960)

$$\frac{1}{2} \int \int \int_V [\dot{\sigma}_{ij}^s \dot{\varepsilon}_{ij}^s - \dot{\sigma}_{ij} \dot{\varepsilon}_{ij}] dV - \int \int_{S_U} [\dot{\sigma}_{ij}^s - \dot{\sigma}_{ij}] n_j \dot{u}_{0i} dS$$

By the use of the virtual work equation, the above expression can be transformed into

$$\begin{aligned} & \frac{1}{2} \int \int \int_V [\dot{\sigma}_{ij}^s \dot{\varepsilon}_{ij}^s - \dot{\sigma}_{ij} \dot{\varepsilon}_{ij}] dV - \int \int_{S_U} [\dot{\sigma}_{ij}^s - \dot{\sigma}_{ij}] n_j \dot{u}_{0i} dS \\ &= \frac{1}{2} \int \int \int_V [\dot{\sigma}_{ij}^s \dot{\varepsilon}_{ij}^s - \dot{\sigma}_{ij} \dot{\varepsilon}_{ij} - 2(\dot{\sigma}_{ij}^s - \dot{\sigma}_{ij}) \dot{\varepsilon}_{ij}] dV \end{aligned} \quad (4.45)$$

It can now be easily shown that the integrand in the right hand side of equation (4.45) is always positive unless  $\dot{\sigma}_{ij}^s = \dot{\sigma}_{ij}$ . First of all, the evaluation of the integrand in (4.45) for the elastic parts of the strain rates gives

$$C_{ijkl} (\dot{\sigma}_{ij}^s - \dot{\sigma}_{ij})(\dot{\sigma}_{kl}^s - \dot{\sigma}_{kl}) \geq 0 \quad (4.46)$$

by noting the symmetry of the elastic coefficients  $C_{ijkl}$ , the equality sign in (4.46) holds only when  $\dot{\sigma}_{ij}^s = \dot{\sigma}_{ij}$ .

For perfectly plastic materials, it is obvious that the integrand of (4.45) is non-negative as the first two terms are zero and the last term is non-negative due to the principle of maximum plastic work. For a strain-hardening material, the integrand of (4.45) can be reduced to the following for the plastic parts of the strain rates

$$\dot{\sigma}_{ij}^s \dot{\varepsilon}_{ij}^s + \dot{\sigma}_{ij} \dot{\varepsilon}_{ij} - 2\dot{\sigma}_{ij}^s \dot{\varepsilon}_{ij} \quad (4.47)$$

which is never negative for all possible cases (i.e. loading, unloading, plastic and elastic loading) (see page 64 of Hill, 1950; page 188 of Koiter, 1960). This therefore proves the inequality (4.44).

### (b) The minimum principle for the strain rate field

Now consider a pair of stress and strain rate fields  $(\dot{\sigma}_{ij}^k, \dot{\varepsilon}_{ij}^k)$  which are kinematically admissible, so that the displacement compatibility, the stress-strain relations, and

displacement boundary conditions are satisfied, but the equation of equilibrium and yield criterion are not obeyed. The minimum principle for the strain rate field may be expressed by the following statement: the expression

$$\Pi_4 = \frac{1}{2} \int \int \int_V \dot{\sigma}_{ij}^k \dot{\varepsilon}_{ij}^k dV - \int \int \int_{S_T} u_i^k \dot{T}_{0i} dS \quad (4.48)$$

defined for all kinematically admissible strain rate fields, takes a minimum value when the kinematically admissible strain rate field is equal to the actual strain rate field  $\dot{\varepsilon}_{ij}$ .

Mathematically, the above minimum principle can be stated by the following inequality

$$\begin{aligned} \Pi_4 &= \frac{1}{2} \int \int \int_V \dot{\sigma}_{ij}^k \dot{\varepsilon}_{ij}^k dV - \int \int \int_{S_T} u_i^k \dot{T}_{0i} dS \\ &\geq \frac{1}{2} \int \int \int_V \dot{\sigma}_{ij} \dot{\varepsilon}_{ij} dV - \int \int \int_{S_T} u_i \dot{T}_{0i} dS \end{aligned} \quad (4.49)$$

To prove this minimum principle, we need to show that the following expression is positive

$$\frac{1}{2} \int \int \int_V [\dot{\sigma}_{ij}^k \dot{\varepsilon}_{ij}^k - \dot{\sigma}_{ij} \dot{\varepsilon}_{ij}] dV - \int \int \int_{S_u} [\dot{u}_i^k - \dot{u}_i] \dot{T}_{0i} dS$$

By the use of the virtual work equation, the above expression can be transformed into

$$\begin{aligned} &\frac{1}{2} \int \int \int_V [\dot{\sigma}_{ij}^k \dot{\varepsilon}_{ij}^k - \dot{\sigma}_{ij} \dot{\varepsilon}_{ij}] dV - \int \int \int_{S_u} [\dot{u}_i^k - \dot{u}_i] \dot{T}_{0i} dS \\ &= \frac{1}{2} \int \int \int_V [\dot{\sigma}_{ij}^k \dot{\varepsilon}_{ij}^k - \dot{\sigma}_{ij} \dot{\varepsilon}_{ij} - 2(\dot{\varepsilon}_{ij}^k - \dot{\varepsilon}_{ij})\dot{\sigma}_{ij}] dV \end{aligned} \quad (4.50)$$

By following a very similar procedure as for the minimum principle for the stress rate field, it can be shown that the integrand of the right hand side of equation (4.50) is positive unless  $\dot{\varepsilon}_{ij}^k = \dot{\varepsilon}_{ij}$ .

### (c) Historical remarks

The minimum principle for the stress rate field (4.44) is substantially due to Hodge and Prager (1948) for a strain-hardening material, and to Greenberg (1949) for a

perfectly plastic material. The corresponding variational principle, which states that the expression (4.43) assumes a stationary value for the actual stress rate field, was proved earlier and is largely due to Prager (1942) for a special yield criterion and Hill (1950) for a general yield criterion.

The minimum principle for the strain rate field (4.49) is due to Greenberg (1949) for both strain-hardening and perfectly plastic materials. Again its corresponding variational principle, which states that the expression (4.48) assumes a stationary value for the actual strain rate field, was proved earlier by Prager (1942).

## 4.5 THEOREMS OF PLASTIC COLLAPSE FOR LIMIT ANALYSIS

### 4.5.1 Introduction

Consider that an elastic-perfectly plastic structure is subjected to some external loads on its surface that are gradually increasing. When the loads reach a certain critical value, plastic collapse (i.e. indefinitely increasing deformations under constant loads), makes the structure unable to sustain any further increase of the external loads. Such critical state is called a limit load state. For the purpose of engineering design, the engineer needs to estimate the limit or collapse load for a given structure.

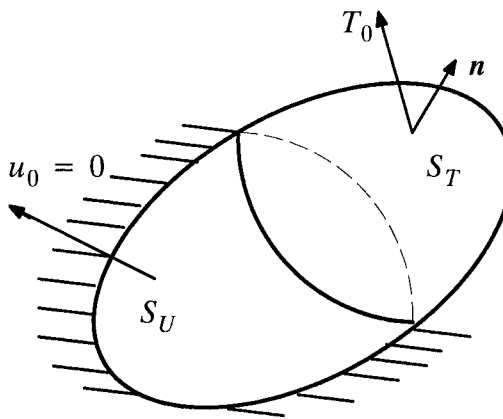


Figure 4.2: Theorems of plastic collapse

Since its development in the 1950s, the method of limit analysis has quickly been applied in civil and mechanical engineering to estimate the collapse load that an

elastic-perfectly plastic structure can sustain. Limit analysis is a quick and direct method of estimating collapse loads, and therefore is particularly attractive to the practising engineer due to their lack of resource for conducting a more involved step by step analysis. The method of limit analysis is based on two theorems of plastic collapse for elastic-perfectly plastic solids. These are known as the lower and upper bound theorems of limit analysis.

As noted by Hodge (1958), the theorems of limit analysis represent a different type of minimum principle. While the principles of minimum potential and complementary energy treat the external forces (or surface tractions) as fixed and minimise the energy, limit analysis is concerned with certain multipliers of the tractions. If a perfectly plastic solid is to be loaded by a set of tractions  $T_{0i}$  (Figure 4.2), we consider the tractions  $mT_{0i}$  as  $m$  is slowly increased from zero. This is also known as proportional loading. Although  $T_{0i}$  may be set as some arbitrary values, it may prove convenient to set them as the unit values of the tractions so that the value of  $m$  is a direct indication of surface tractions (Davis, 1968).

For simplicity, the discussion of the theorems of limit analysis will be restricted to the most important case where the prescribed surface displacements on  $S_u$  are zero (so that *the reaction force does no work*). The reader may verify that the theorems remain valid if parts of  $S_u$  undergo rigid-body displacements and if the resultants of the external loads on these parts of  $S_u$  are specified (Koiter, 1960). If the prescribed displacement on parts or all of the surface  $S_u$  is not equal to zero, then the surface tractions operating on these parts should also be included as the surface tractions. In other words, the surface tractions we refer to include *those reaction forces that do work*. In this case, the definition of  $S_T$  should be extended accordingly (Lubliner, 1990).

If the value of  $m$  is sufficiently small, say  $0 < m < m_e$ , the structure will be entirely elastic. As  $m$  is equal to  $m_e$  the structure starts to become plastic. If  $m$  is greater than  $m_e$  part of the structure will become plastic, but the elastic part of the structure is sufficiently large to support the additional load. However when  $m$  reaches a critical value (called collapse load factor),  $m_c$ , a limit state (i.e. plastic collapse) will occur where the deformation continues to increase with the load remaining constant. The purpose of this section is to present two theorems that can be used to obtain a lower bound and an upper bound on the exact collapse load factor  $m_c$ .

#### 4.5.2 Constant stress theorem at plastic collapse

Before presenting the lower and upper bound theorems of plastic collapse, it is necessary to describe the theorem that asserts that the stress field remains constant at plastic collapse. In formal terms, the theorem can be stated as follows:

If all changes in geometry occurring during collapse are neglected, all stresses are found to remain constant during collapse. In other words, all strains are plastic at collapse.

To prove this theorem, we can apply the principle of virtual work to obtain the following

$$\int \int \int_V \dot{\sigma}_{ij} \dot{\varepsilon}_{ij} dV = \int \int_{S_T} \dot{m}_c T_{0i} v_i dS = 0 \quad (4.51)$$

after noting that at plastic collapse the load factor remains constant so its rate is zero.

Since the strain rate is the sum of an elastic part and a plastic part, equation (4.51) can be rewritten as

$$\int \int \int_V (\dot{\sigma}_{ij} \dot{\varepsilon}_{ij}^e + \dot{\sigma}_{ij} \dot{\varepsilon}_{ij}^p) dV = 0 \quad (4.52)$$

For elastic-perfectly plastic solids obeying the associated flow law, it is well-known that the second term of the integrand in the above equation is zero, namely

$$\dot{\sigma}_{ij} \dot{\varepsilon}_{ij}^p = 0 \quad (4.53)$$

for either unloading (when the plastic strain rate is zero) or loading (when the plastic strain rate is normal to the stress rate for associated plastic flow). Using the elastic stress-strain relation, it is easy to note that equations (4.52) and (4.53) can be satisfied only if

$$\dot{\sigma}_{ij} = 0 \quad \Rightarrow \quad \sigma_{ij} = \text{constant} \quad (4.54)$$

at the state of plastic collapse. It then follows that at collapse the elastic strain will be zero and all the strain will be plastic.

This constant stress theorem at collapse suggests that the collapse load factor will be the same for both elastic-perfectly plastic solids (Drucker *et al.*, 1952) and rigid-perfectly plastic material (Hill, 1951).

#### 4.5.3 Lower bound theorem of plastic collapse

This section establishes a lower bound theorem that can be used to obtain a lower bound on the exact collapse load factor  $m_c$ . For the lower bound theorem, a statically admissible stress field is defined as one which is in equilibrium with the surface tractions  $m_c T_{0i}$  and nowhere violates the yield condition. In addition, the load factor  $m_c^s$  is defined as a statically admissible collapse load factor that corresponds to a statically admissible stress field. The lower bound theorem states:

If all changes in geometry occurring during collapse are neglected, a statically admissible collapse load factor is always less than or equal to the exact collapse load factor ( $m_c^s \leq m_c$ ). The equality sign is valid only when the statically admissible stress field is the true stress field. In other words, the load factor derived from a statically admissible stress field is a lower bound on the true collapse load factor.

To prove this lower bound theorem, we consider

$$\int \int \int_V (\sigma_{ij} - \sigma_{ij}^s) d\varepsilon_{ij} dV$$

where the true stress and strain (purely plastic) fields at plastic collapse are denoted by  $(\sigma_{ij}, d\varepsilon_{ij})$  and the statically admissible stress field is denoted by  $\sigma_{ij}^s$  which is in equilibrium with the load factor  $m_c^s$ . From Figure 4.3 and the principle of maximum plastic work, it is obvious that the above expression is non-negative, namely

$$\int \int \int_V (\sigma_{ij} - \sigma_{ij}^s) d\varepsilon_{ij} dV \geq 0 \quad (4.55)$$

By the principle of virtual work, we have

$$\int \int \int_V (\sigma_{ij} - \sigma_{ij}^s) d\varepsilon_{ij} dV = (m_c - m_c^s) \int \int_{S_T} T_{0i} du_i dS \geq 0 \quad (4.56)$$

which leads to the lower bound theorem

$$m_c^s \leq m_c \quad (4.57)$$

if we note that the plastic work done by the surface tractions  $T_{0i}$  is positive.

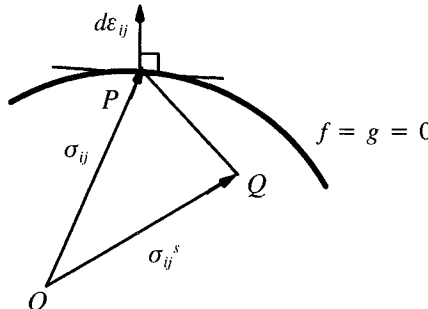


Figure 4.3: The lower bound theorem

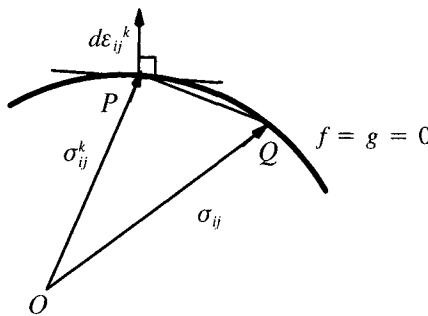


Figure 4.4: The upper bound theorem

#### 4.5.4 Upper bound theorem of plastic collapse

We now consider an upper bound theorem that can be used to obtain an upper bound on the exact collapse load factor  $m_c$ . For the upper bound theorem, a kinematically admissible velocity field is defined as one which satisfies the boundary condition on  $S_u$ . In addition, the load factor  $m_c^k$  is defined as a kinematically admissible collapse load factor that corresponds to a kinematically admissible velocity field. The upper bound theorem states:

*If all changes in geometry occurring during collapse are neglected, a kinematically admissible collapse load factor is always greater or equal to the exact collapse load factor ( $m_c^k \geq m_c$ ). The equality sign is valid only when the kinematically admissible velocity field is the true velocity field. In other words, the load factor derived from a kinematically admissible velocity field is an upper bound on the true collapse load factor.*

To prove this upper bound theorem, we consider

$$\iiint_V (\sigma_{ij}^k - \sigma_{ij}) d\epsilon_{ij}^k dV$$

where the true stress field at plastic collapse is denoted by  $\sigma_{ij}$  and the kinematically admissible strain rate field is denoted by  $d\epsilon_{ij}^k$ . The stress field  $\sigma_{ij}^k$  is associated with the kinematically admissible strain rate field  $d\epsilon_{ij}^k$  by the associated flow law, Figure 4.4. In general this stress field will not be in equilibrium. From the principle of maximum plastic work, it is obvious that the expression is non-negative, namely

$$\int \int \int_V (\sigma_{ij}^k - \sigma_{ij}) d\varepsilon_{ij}^k dV \geq 0 \quad (4.58)$$

If we define a kinematically admissible load factor  $m_c^k$  so that

$$\int \int \int_V \sigma_{ij}^k d\varepsilon_{ij}^k dV = m_c^k \int \int_{S_T} T_{0i} du_i^k dS \quad (4.59)$$

then by the principle of virtual work, we obtain

$$\int \int \int_V (\sigma_{ij}^k - \sigma_{ij}) d\varepsilon_{ij}^k dV = (m_c^k - m_c) \int \int_{S_T} T_{0i} du_i^k dS \geq 0 \quad (4.60)$$

which leads to the upper bound theorem

$$m_c^k \geq m_c \quad (4.61)$$

provided that the kinematically admissible velocity field is chosen so that

$$\int \int_{S_T} T_{0i} du_i^k dS \geq 0 \quad (4.62)$$

which is very easy to do in practice.

#### 4.5.5 Extension to non-associated plastic flow

As shown in the preceding sections, the proof of the theorems of plastic collapse is based on the principle of maximum plastic work. As a result, they are only valid for materials obeying an associated plastic flow rule. However real materials in geotechnical engineering behave more closely to a non-associated plastic material. It is therefore not a surprise that some effort has been devoted in the past to extend the basic lower and upper bound theorems to non-associated materials (e.g. Palmer, 1966; Davis, 1968; Collins, 1969). Despite much effort, there has been no breakthrough in this area. Two of the more useful results are summarised here.

##### (a) Radenkovic's upper bound theorem

This theorem can be stated as follows:

*The collapse load (or an upper bound for the collapse load) for a structure made of an associated material is an upper bound for the collapse load of the structure made of a non-associated material obeying the same yield criterion.*

This theorem follows readily from the fact that the true collapse load for a non-associated material must be statically admissible for an associated material (because statically stress fields are independent of the plastic flow rule), and therefore less than the true collapse load for the associated material.

### (b) Collins' generalised upper bound theorem

In an attempt to develop a method for obtaining upper bounds when the interface behaviour is governed by Coulomb's criterion, Collins (1969) noted that

*The velocity boundary conditions do not need to be satisfied precisely for the upper bound theorem to be valid. In particular if one chooses the admissible velocity field to be such that on a plane interface the velocity component in the direction of the resultant surface traction is constant over the interface, then such a velocity field provides an upper bound to the total normal load in the presence of Coulomb friction.*

To prove this upper bound theorem, we consider a volume  $V$  of a rigid-plastic solid and assume its surface is divided into two parts. On one part  $S_T$ , some or all of the traction components are prescribed. The rest of the surface  $S_u$  corresponds to the frictional interface which may be subject to certain types of velocity conditions. Collins' theorem is used mainly to obtain upper bounds on the normal component of the surface reaction forces due to the prescribed surface velocity conditions.

The general upper bound, when applied to the situation with both the prescribed surface tractions  $T_{0i}$  on  $S_T$  and the reaction forces  $R_i$  on  $S_u$ , takes the following form

$$\iint_{S_u} R_i u_i^k dS \leq \iint_V \int \sigma_{ij}^k \varepsilon_{ij}^k dV - \iint_{S_T} T_{0i} u_i^k dS \quad (4.63)$$

Now suppose we consider a planar interface where  $u_n^k$  and  $u_t^k$  are the normal and tangential components of the prescribed displacements. The corresponding reaction forces  $R_i$  have both normal and tangential components  $R_n$  and  $R_t$ . Further we assume that these two components are related by Coulomb's frictional criterion so that

$$|R_t| = c_w - s_n R_n \tan \phi_w \quad (4.64)$$

where  $s_n = 1$  if  $R_n$  points out of the body (i.e. tension) and  $s_n = -1$  if  $R_n$  points into the body (i.e. compression). The quantities  $c_w$  and  $\phi_w$  denote the cohesion and friction angle on the interface. Using equation (4.64), the basic upper bound inequality can be re-written as

$$\begin{aligned}
& \int \int_{S_u} (s_n u_n^k - s_t s_n u_t^k \tan \phi_w) R_n dS \\
& \leq \int \int \int_V \sigma_{ij}^k \varepsilon_{ij}^k dV - \int \int_{S_T} T_{0i} u_i^k dS - s_t \int \int_{S_u} c_w u_t^k dS \quad (4.65)
\end{aligned}$$

where the sign  $s_t$  is defined so that  $|R_t| = s_t R_t$  and  $s_t = 1$  if  $R_t$  has a clockwise direction around the boundary of the body and  $s_t = -1$  otherwise. The right side of this inequality can be evaluated for any trial velocity field  $u_t^k$  as  $c_w$  is known.

Suppose now we are interested in finding an upper bound for the total normal reaction force  $F_n$  on  $S_u$  namely

$$F_n = \int \int_{S_u} R_n dS \quad (4.66)$$

which could be tensile ( $s_n = 1$ ) or compressive ( $s_n = -1$ ). The inequality (4.65) provides such an overestimate for any trial displacement field which has the property that

$$s_n u_n^k - s_t s_n u_t^k \tan \phi_w = \text{constant} \quad (4.67)$$

on the surface  $S_u$ . In general this will not satisfy the actual displacement boundary condition on the surface  $S_u$ .

In short it appears that our criterion in choosing the trial displacement field should not be that it satisfies the actual boundary conditions, but rather that it should satisfy equation (4.67) to give an upper bound on the quantity of interest. This generalised upper bound theorem has been incorporated by Yu and Sloan (1994) in a finite element formulation for upper bound limit analysis.

#### 4.5.6 Historical remarks

The theorems of plastic collapse were first formulated by Gvozdev (1936) for applications in structural mechanics but this original Russian paper was overlooked by subsequent researchers in the field. The lower bound theorem in its general form was then independently established by Feinberg (1948) and proved by Hill (1948) by applying the principle of maximum plastic work to a finite volume of perfectly plastic material. A more complete statement of both lower and upper bound theorems and their proof was presented by Hill (1951) three years later. In these studies, the assumption of rigid-plastic materials was necessary. In a landmark paper, Drucker *et al.* (1952) first noted that the stress state remains constant at plastic col-

lapse and therefore proved that the lower and upper bound theorems of limit analysis are also valid for elastic-plastic material.

It should be noted that some years before Hill's groundbreaking work, Melan (1938) had already established a more general statical theorem (now known as the lower bound shakedown theorem) for elastic-plastic solids subjected to variable loads. In fact, Melan's shakedown theorem contains the lower bound theorem of plastic collapse as a special case. However this fact seems to have escaped notice by subsequent researchers in the field, possibly because Melan's highly original papers suffered from a rather abstruse argument (Koiter, 1960).

Finally it is stressed that both the upper and lower bound theorems of plastic collapse are based on the key assumption of small deformation at failure. While this assumption is adequate for many problems of practical interest, it may not apply to certain problems. Limited research into the effect of large deformation on structural limit analysis by Onat and Haythornthwaite (1960) and Gao (1991) suggests that geometry changes can work for or against the loading capacity of a structure.

#### 4.6 SHAKEDOWN THEOREMS

When an elastic-plastic structure is subjected to a variable loading programme between given extreme values, its behaviour may fall into one of the following types:

- (1) If the structure is loaded cyclically in tension and compression and also the loading in both directions produces plastic deformation, then it is likely that fracture will occur as the result of plastic deformations alternating in sign. This is called *alternating plasticity* or low-cycled fatigue.
- (2) If the structure is loaded cyclically between two extreme values and also the extreme load values are sufficiently large, then it is likely that each loading cycle will produce plastic deformation. This *progressive plastic flow* is likely to lead to unacceptably large deformation after a large number of cycles, which is also known as *incremental failure*.
- (3) If the structure is loaded cyclically between two extreme values and also the extreme load values are sufficiently small, then it is likely that at early stage of the loading each cycle will produce plastic deformation, and thereafter continuing loading produces no further plastic flow. If this happens, then the structure is said to have reached a state of *shakedown*, at which the structure will behave in a purely elastic manner.

In light of the above discussion, it is obvious that determining whether an elastic-plastic structure will shakedown for given extreme load values is a problem of great practical importance. Its direct solution is difficult but has been helped greatly by

two theorems developed by Melan (1938) and Koiter (1960). Like the lower and upper bound theorems of plastic collapse, these two basic shakedown theorems can also be used to obtain a lower bound and an upper bound for the shakedown load limits under which the structure will shakedown.

For simplicity, the discussion of the basic shakedown theorems will be restricted to the most important case where the prescribed surface displacements on  $S_u$  are zero. Therefore elastic-plastic structures will be subjected to some surface tractions that vary between extreme values.

#### 4.6.1 Melan's lower bound shakedown theorem

Melan's lower bound theorem can be stated as follows:

*An elastic-perfectly plastic structure will shakedown for given extreme load values if and only if there exists a state of time-independent self-stress (i.e. residual stress) that nowhere violates the yield criterion when it is superimposed on the state of elastic stresses of the structure caused by the extreme load values.*

where the state of self-stress or residual stresses is in equilibrium with zero external loads. It is also noted that the state of elastic stresses, to be superimposed on the state of self-stress, is determined from the external loads by assuming that the structure is made of an elastic material.

We consider an elastic-perfectly plastic structure that has already shaken down under a loading programme that varies in time within a certain range of the surface tractions. For simplicity, it is assumed that the loading is applied sufficiently slowly so that the effect of inertia may be small and therefore ignored. At the state of shakedown, the plastic strain field  $\varepsilon_{ij}^p$  remains constant in time and defines a time-independent self-stress or residual stress field  $\varrho_{ij}$ . This residual stress field, when combined with the elastic stress field  $\sigma_{ij}^e$ , does not violate the yield criterion throughout the structure

$$f(\sigma_{ij}) = f(\sigma_{ij}^e + \varrho_{ij}) \leq 0 \quad (4.68)$$

It follows from Melan's lower bound theorem that shakedown will occur in the given load range if a time-independent self-stress field  $\bar{\varrho}_{ij}$ , not necessarily equal to the actual residual stress field at shakedown  $\varrho_{ij}$ , can be found such that

$$f(\bar{\sigma}_{ij}) = f(\sigma_{ij}^e + \bar{\varrho}_{ij}) \leq 0 \quad (4.69)$$

To prove this theorem, we consider the essentially positive elastic strain energy corresponding the residual stresses,  $\varrho_{ij} - \bar{\varrho}_{ij}$ ,

$$A = \frac{1}{2} \int \int \int_V C_{ijkl} (\varrho_{ij} - \bar{\varrho}_{ij}) (\varrho_{kl} - \bar{\varrho}_{kl}) dV \quad (4.70)$$

The derivative of A with respect to time is

$$\frac{dA}{dt} = \int \int \int_V (\varrho_{ij} - \bar{\varrho}_{ij}) \dot{\varepsilon}_{ijr}^e dV \quad (4.71)$$

where  $\dot{\varepsilon}_{ijr}^e$  is the elastic strain rate due to the residual stress rate. It is noted that the total strain is the sum of the elastic strain due to the external load,  $\varepsilon_{ij}^e$ , the elastic strain due to the residual stress,  $\varepsilon_{ijr}^e$ , and the plastic strain due to the residual stress,  $\varepsilon_{ij}^p$ . As a result, equation (4.71) can be reduced to

$$\frac{dA}{dt} = \int \int \int_V (\varrho_{ij} - \bar{\varrho}_{ij}) (\dot{\varepsilon}_{ij} - \dot{\varepsilon}_{ij}^e - \dot{\varepsilon}_{ij}^p) dV \quad (4.72)$$

Since the state of residual stresses,  $\varrho_{ij} - \bar{\varrho}_{ij}$ , is self-equilibrating, and the strain rate field,  $\dot{\varepsilon}_{ij} - \dot{\varepsilon}_{ij}^e$ , is kinematically admissible, equation (4.72) can be further simplified by the principle of virtual work

$$\frac{dA}{dt} = - \int \int \int_V (\varrho_{ij} - \bar{\varrho}_{ij}) \dot{\varepsilon}_{ij}^p dV = - \int \int \int_V (\sigma_{ij} - \bar{\sigma}_{ij}) \dot{\varepsilon}_{ij}^p dV \quad (4.73)$$

It now follows from the principle of maximum plastic work that  $\dot{A} = dA/dt$  will be negative as long as plastic strains occur in the actual loading programme. However as an elastic strain energy, A cannot be negative, and therefore plastic deformation cannot continue indefinitely. In other words, at some stage the structure must shakedown to a state of residual stresses with *constant plastic strains*.

It is important to note that in the above proof of Melan's theorem, nothing is said about the magnitude of the plastic deformations which may occur before the structure reaches its shakedown state. This issue is of practical importance and will be briefly discussed at the end of this chapter.

#### 4.6.2 Koiter's upper bound shakedown theorem

Koiter's upper bound theorem can be stated as follows

*An elastic-perfectly plastic structure will not shakedown for given extreme load values (i.e. it will fail ultimately due to progressive plastic flow) if any kinematically admissible plastic strain rate cycle  $\dot{\varepsilon}_{ij}^k$  and any external loads  $T_{0i}$  within the prescribed limits can be found so that*

$$\int_0^t dt \iint_{S_T} T_{0i} \dot{u}_i^k dS > \int_0^t dt \iiint_V \sigma_{ij}^k \dot{\varepsilon}_{ij}^k dV \quad (4.74)$$

which provides an upper bound for the shakedown load limit. This theorem can be proved indirectly as follows.

The inequality (4.74), with the principle of virtual work applied to its left-hand side, can be rewritten as

$$\int_0^t dt \iiint_V \sigma_{ij}^e \dot{\varepsilon}_{ij}^k dV > \int_0^t dt \iiint_V \sigma_{ij}^k \dot{\varepsilon}_{ij}^k dV \quad (4.75)$$

which can be further reduced to

$$\int_0^t dt \iiint_V [\sigma_{ij}^e \dot{\varepsilon}_{ij}^k - \sigma_{ij}^k \dot{\varepsilon}_{ij}^k] dV > 0 \quad (4.76)$$

If, however, shakedown has taken place, then from Melan's theorem a time-independent residual stress field,  $\varrho_{ij}$ , must exist so that

$$f(\sigma_{ij}) = f(\sigma_{ij}^e + \varrho_{ij}) \leq 0 \quad (4.77)$$

By the principle of maximum plastic work, we have

$$\sigma_{ij}^k \dot{\varepsilon}_{ij}^k \geq (\sigma_{ij}^e + \varrho_{ij}) \dot{\varepsilon}_{ij}^k \quad (4.78)$$

Therefore

$$\int_0^t dt \iiint_V [\sigma_{ij}^e \dot{\varepsilon}_{ij}^k + \varrho_{ij} \dot{\varepsilon}_{ij}^k - \sigma_{ij}^k \dot{\varepsilon}_{ij}^k] dV \leq 0 \quad (4.79)$$

Since the residual stress field  $\varrho_{ij}$  is self-equilibrated (with zero external loads on  $S_T$  and zero displacements on  $S_u$ ), the application of the virtual work equation gives

$$\iiint_V \varrho_{ij} \dot{\varepsilon}_{ij}^k = 0 \quad (4.80)$$

With equation (4.80), the expression (4.79) can be further reduced to

$$\int_0^t dt \iiint_V [\sigma_{ij}^e \dot{\varepsilon}_{ij}^k - \sigma_{ij}^k \dot{\varepsilon}_{ij}^k] dV \leq 0 \quad (4.81)$$

This contradicts inequality (4.76) and therefore shakedown cannot take place as long as inequality (4.74) is satisfied. We have therefore proved Koiter's kinematic shakedown theorem.

#### 4.6.3 Historical remarks and further extensions

The lower bound shakedown theorem for structures under variable loads was first established by Bleich (1932) for simply indeterminate structures. This work was later generalised by Melan (1938) to a general three-dimensional elastic-perfectly plastic structure. It is noted that Melan's original proof was rather complex and considerable simplifications of Melan's proof were achieved by Symonds (1951) and Koiter (1960). The upper bound shakedown theorem was established by Koiter (1960). However Koiter's theorem bears some resemblance to the earlier method of Symonds and Neal (1951).

An extension of the basic lower bound shakedown theorem to kinematic-hardening materials has been made by Ponter (1976). Although Melan's theorem yields a sufficient condition for shakedown, the accumulation of plastic strain and displacement which occurs during the history of loading is not known. The displacement bounding theorems established by Capurso (1974) and Ponter (1972) provide some indication of the accumulated plastic deformation before the state of shakedown is achieved. In fact, the displacement bounding theorem of Capurso (1974) has been used by Shiau and Yu (2000) to estimate the value of plastic deformation at shakedown of pavements under moving traffic loads.

#### REFERENCES

Bleich, H. (1932). Über die Bemessung statisch unbestimmter Stahltragwerke unter Berücksichtigung des elastisch-plastischen Verhaltens des Baustoffes, *Bauingenieur*, Vol 19/20, 261.

Capurso, M. (1974). A displacement bounding principle in shakedown of structures subjected to cyclic loads. *Int. J. Solids Structures*, Vol 10, 77-92.

Collins, I.F. (1969). The upper bound theorem for rigid plastic solids generalised to include Coulomb friction, *J. Mech. Phys. Solids*, Vol 17, 323-338.

Davis, E.H. (1968). Theories of plasticity and the failure of soil masses, In: *Soil Mechanics: Selected Topics*, (Editor: I. K. Lee), Butterworths, London, 341-380.

Drucker, D.C., Greenberg, H.J. and Prager, W. (1951). The safety factor of an elastic-plastic body in plane strain, *J. Appl. Mech.*, ASME, Vol 18, 371-378.

Drucker, D.C., Prager, W. and Greenberg, H.J. (1952). Extended limit design theorems for continuous media, *Quart. Appl. Math.*, Vol 9, 381-389.

Feinberg, S.M. (1948). The principle of limiting stresses (in Russian), *Prikl. Mat. Mekh.*, Vol 12, 63.

Gao, Y. (1991). Extended bounding theorems for nonlinear limit analysis, *Int. J. Solids and Structures*, Vol 27, 523-531.

Greenberg, H.J. (1949). Complementary minimum principles for an elastic-plastic material, *Quart. Appl. Math.*, Vol 7, 85-95.

Gvozdev, A.A. (1936). La determination de la charge de ruine pour les systemes hyperstatiques subissant des deformations plastiques, *Proc. Conf. Plastic Deformation, Ac Sc. USSR*, 19.

Hill, R. (1948). A variational principle of maximum plastic work in classical plasticity, *Q.J. Mech. Appl. Math.*, Vol 1, 18-28.

Hill, R. (1950). *The Mathematical Theory of Plasticity*, Clarendon Press, Oxford.

Hill, R. (1951). On the state of stress in a plastic-rigid body at the yield point, *Phil. Mag.*, Vol 42, 868-875.

Hill, R. (1958). A general theory of uniqueness and stability in elastic-plastic solids, *J. Mech. Phys. Solids*, Vol 6, 236.

Hodge, P.G. (1958). The mathematical theory of plasticity, In: *Elasticity and Plasticity*, John Wiley and Sons, New York, 51-144.

Hodge, P.G. and Prager, W. (1948). A variational principle for plastic materials with strain hardening, *J. Math. Phys.*, Vol 27, 1-10.

Kachanov, L.M. (1974). *Fundamentals of the Theory of Plasticity*. Mir Publishers, Moscow.

Koiter, W.T. (1960). General theorems for elastic-plastic solids, In: *Progress in Solid Mechanics*, (Editors: I.N. Sneddon and R. Hill), Vol 1, 167-221.

Lubliner, J. (1990). *Plasticity Theory*, Macmillan Publishing Company, New York.

Martin, J.B. (1975). *Plasticity: Fundamentals and General Results*, MIT Press, Cambridge.

Melan, E (1938). Zur plastizitat des raumlichen Kontinuums, *Ing. Arch.*, Vol 9, 116-125.

Onat, E.T. and Haythornthwaite, R.M. (1956). The load-carrying capacity of circular plate at large deflection. *J. Appl. Mech.*, Vol 23, 49-55.

Palmer, A.C. (1966). A limit theorem for materials with non-associated flow laws, *J. Mechanique*, Vol 5, 217-222.

Ponter, A.R.S. (1972). An upper bound on the small displacement of elastic perfectly plastic structures. *J. Appl. Mech.*, Vol 39, 959-963.

Ponter, A.R.S. (1976). A general shakedown theorem for inelastic materials. *Proc. 3rd Int. Conf. Struct. Mech. Reactor Technology*, Section L, Imperial College, London.

Prager, W. (1942). Fundamental theorems of a new mathematical theory of plasticity, *Duke Math. J.*, Vol 9, 228.

Prager, W. (1949). Recent developments of the mathematical theory of plasticity, *J. Appl. Phys.*, Vol 20, 235.

Prager, W. (1955). The theory of plasticity – a survey of recent achievements, *Proc. Inst. Mech. Eng.*, London, 3-19.

Prager, W. and Hodge, P.G. (1951). *The Theory of Perfectly Plastic Solids*, John Wiley and Sons, New York.

Shiau, S.H. and Yu, H.S. (2000). Load and displacement predictions for shakedown analysis of layered pavements. *Transport. Res. Rec.*, Vol 1730, 117-124.

Symonds, P.S. (1951). Shakedown in continuous media. *J. Appl. Mech.*, Vol 18, 85.

Symonds, P.S. and Neal, B.G. (1951). Recent progress in the plastic methods of structural analysis. *J. Franklin. Inst.*, Vol 252, 383-407.

Yu, H.S. and Sloan, S.W. (1994). Upper bound limit analysis of a rigid plastic body with frictional interfaces. *Int. J. Mech. Sci.*, Vol 36, 219-229.

## CHAPTER 5

### PERFECT PLASTICITY

#### 5.1 INTRODUCTION

This chapter is concerned with the theory of perfectly plastic solids for application in soil and rock mechanics. In fact, before the theory of plastic stress-strain relations was developed for metals (de Saint-Venant, 1870; Levy, 1870), the concept of perfect plasticity had already been used to solve geotechnical stability problems involving earth pressures and retaining walls by Coulomb (1773) and Rankine (1857). However, without a stress-strain relation, it is not possible to use the theory of plasticity to estimate deformation. This is why in the early stage of the development of soil mechanics and geotechnical engineering, almost all the calculations were concerned with the stability of structures and earthworks. In these analyses, the soil was considered to be a rigid-perfectly plastic solid, and simple calculations led to an estimate of the maximum load the structure can sustain before collapse.

To help understand the influence of early soil mechanics (i.e. the theory of earth pressure) on the development of the theory of plasticity, it is instructive to recall an excellent, concise account made by Prager (1955) in his James Clayton Lecture delivered at the Institution of Mechanical Engineers, London:

*"The foundations of the theory of plasticity were laid about eighty years ago by Saint-Venant, Levy and Boussinesq. The development of hydrostereodynamics or plasticodynamics, as the new field was called, was strongly influenced by the already well-established theory of earth pressure, to which Levy, Saint-Venant, and Boussinesq were then making contributions. Tresca's yield condition (Tresca, 1868), adopted by these authors, can be regarded as a special case of the condition on which Coulomb (1773) had based his theory of earth pressure nearly a century before, and the important concept of the limiting equilibrium of a continuum had been established by Rankine's work on such equilibria in loose earth (Rankine, 1857). Much of the theory of earth pressure, however, had been perfected before Cauchy's fundamental investigations on elasticity has clarified the specifications of stress and strain, and brought out the important role of the stress-strain relations in any branch of mechanics of continua. In the theory of earth pressure the introduction of stress-strain relations was obviated by the restriction to the consideration of limiting equilibria and the appeal to a heuristic extreme principle implied in Coulomb's work and more clearly formulated by Mose-*

ley. It is fortunate that the pioneers of the theory of plasticity did not copy this unsatisfactory feature of the theory of earth pressure but introduced instead a flow rule relating the stress to the strain. Research in plasticity was thereby forced to pursue an independent course and, as a result of this, the theory of plasticity is now able to pay some of the debt of gratitude it owes to the theory of earth pressure: the general theory of limit analysis, developed during recent years as a subject in plasticity, has shed much needed light on the foundations of the theory of earth pressure.”

In fact, with the aid of the modern terminology of limit analysis (Hill, 1951; Drucker *et al.*, 1952), the method used by Coulomb (1773) for calculating the thrust exerted by the soil on a retaining wall by assuming a failure surface may be regarded as an upper bound method. On the other hand, the approach adopted by Rankine (1857) for determining active and passive earth pressures by considering a limiting stress field may be regarded as a lower bound method (Wroth, 1973).

The theory of perfect plasticity assumes that soil or rock can be modelled as an elastic-perfectly plastic solid. As described in Chapter 2, it consists of the following three basic elements:

- (1) A linear or nonlinear law to define the elastic stress-strain relation.
- (2) A yield criterion to define the onset of plastic flow.
- (3) A plastic flow rule to define the plastic stress-strain relation.

A large number of criteria have been proposed to describe the yielding and strength of geomaterials (i.e. soil and rock) under a general loading condition. Based on these criteria, theories of perfect plasticity have been developed. No attempt is made here to cover all these models. Instead we will focus on a few that have been used most widely in geotechnical analysis. They include models based on the yield criteria proposed by Tresca (1864), von Mises (1913), Coulomb (1773), Drucker and Prager (1952), Lade and Duncan (1975), Matsuoka and Nakai (1974, 1982), and Hoek and Brown (1980).

## 5.2 ELASTIC MODELS

### 5.2.1 Linear elasticity

For a linear, isotropic elastic material, the stress-strain relations can be expressed using Hooke’s law in a total form as follows

$$\varepsilon_{ij} = \frac{1 + \nu}{E} \sigma_{ij} + \frac{\nu}{E} \sigma_{kk} \delta_{ij} \quad (5.1)$$

$$\sigma_{ij} = \frac{E}{1 + \nu} \varepsilon_{ij} + \frac{\nu E}{(1 - \nu)(1 + 2\nu)} \varepsilon_{kk} \delta_{ij} \quad (5.2)$$

When applied in conjunction with a plastic model, it is more useful to have the elastic stress-strain relations written in a rate (or incremental) form, namely

$$\dot{\varepsilon}_{ij} = \frac{1+\nu}{E} \dot{\sigma}_{ij} + \frac{\nu}{E} \dot{\sigma}_{kk} \delta_{ij} \quad (5.3)$$

$$\dot{\sigma}_{ij} = \frac{E}{1+\nu} \dot{\varepsilon}_{ij} + \frac{\nu E}{(1-\nu)(1+2\nu)} \dot{\varepsilon}_{kk} \delta_{ij} \quad (5.4)$$

In (5.1)-(5.4), Hooke's elastic stress-strain relations are expressed in terms of Young's modulus and Poisson's ratio. Alternatively, they can be expressed in terms of bulk modulus  $K$  and shear modulus  $G$  as follows

$$\dot{\varepsilon}_{ij} = \frac{1}{9K} \dot{\sigma}_{kk} \delta_{ij} + \frac{1}{2G} \dot{s}_{ij} \quad (5.5)$$

$$\dot{\sigma}_{ij} = K \dot{\varepsilon}_{kk} \delta_{ij} + 2G \dot{e}_{ij} \quad (5.6)$$

where

$$s_{ij} = \sigma_{ij} - \frac{\sigma_{kk}}{3} \delta_{ij} \quad (5.7)$$

$$e_{ij} = \varepsilon_{ij} - \frac{\varepsilon_{kk}}{3} \delta_{ij} \quad (5.8)$$

$$K = \frac{E}{2(1-2\nu)} \quad (5.9)$$

$$G = \frac{E}{2(1+\nu)} \quad (5.10)$$

### 5.2.2 Nonlinear elasticity

Soil or rock rarely behaves as a linear elastic material. So a better approach would be to model them as a nonlinear elastic-plastic material. To fully define the elastic-plastic stress-strain relation for a geomaterial, it is necessary to specify a nonlinear, incremental, elastic stress-strain relation.

Two methods may be used to construct a nonlinear elastic stress-strain relation. They are known as Green's hyperelastic theory and hypoelastic theory.

#### (a) Hyperelasticity

The theory of hyperelasticity assumes that there exists a *strain energy function*,  $U_s(\varepsilon_{ij})$ , and a *complementary energy function*,  $U_c(\sigma_{ij})$ , such that

$$\sigma_{ij} = \frac{\partial U_s}{\partial \varepsilon_{ij}} \quad \text{and} \quad \varepsilon_{ij} = \frac{\partial U_c}{\partial \sigma_{ij}} \quad (5.11)$$

The above equation yields a one-to-one relationship between stress and strain. The rate form of this stress-strain equation is given below

$$\dot{\sigma}_{ij} = \frac{\partial^2 U_s}{\partial \varepsilon_{ij} \partial \varepsilon_{kl}} \dot{\varepsilon}_{kl} = D_{ijkl} \dot{\varepsilon}_{kl} \quad (5.12)$$

$$\dot{\varepsilon}_{ij} = \frac{\partial^2 U_c}{\partial \sigma_{ij} \partial \sigma_{kl}} \dot{\sigma}_{kl} = C_{ijkl} \dot{\sigma}_{kl} \quad (5.13)$$

A key feature of hyperelasticity is that no energy can be generated through load cycles and therefore thermodynamic laws are always satisfied. The main objection to the theory of hyperelasticity is that it may require many material constants, which could be difficult or expensive to determine in practice. Another major limitation of the theory is that it cannot model load history dependence as equations (5.12) and (5.13) imply that tangent moduli of the material are identical for loading and unloading. Applications of this type of theory to soil modelling are given by Housby (1985) and Borja *et al.* (1997) among others.

### (b) Hypoelasticity

In the theory of hypoelasticity, it is assumed that the incremental stress and strain tensors are linearly related by variable material moduli that are functions of the current stress or strain state. Mathematically we have

$$\dot{\sigma}_{ij} = D^e_{ijkl}(\sigma_{mn}) \dot{\varepsilon}_{kl} \quad (5.14)$$

where the material matrix could be a function of both stress and strain. Therefore the hypoelastic behaviour is stress history dependent. It should be noted that in hypoelasticity it is not guaranteed that thermodynamic laws are always satisfied (e.g. Zytnski *et al.*, 1978). Nevertheless this type of nonlinear elastic models is widely used in geotechnical analysis.

## 5.3 PLASTICITY MODELS FOR COHESIVE SOILS

For cohesive soils, the two most widely used plasticity models are those proposed by Tresca (1864) and von Mises (1913) initially for metals. Experience suggests that under undrained conditions, fully saturated cohesive soils (i.e. clay) can be modelled accurately by either Tresca or von Mises plasticity theory.

### 5.3.1 Tresca model

After a series of experiments on metals, Tresca (1864) concluded that yielding occurred when the maximum shear stress reached a certain value. In proposing this,

Hill (1950) suggested that Tresca was probably influenced by a more general law for the failure of soils, proposed many years earlier by Coulomb (1773). Tresca's yield criterion is

$$f = \sigma_1 - \sigma_3 - 2S_u = 0 \quad (5.15)$$

where  $\sigma_1 \geq \sigma_2 \geq \sigma_3$  and  $S_u$  is the undrained shear strength. From a computational point of view, it is more useful to write the above equation in terms of the second invariant of deviatoric stress and Lode's angle as follows

$$f = \sqrt{J_2} \cos \theta_l - S_u = 0 \quad (5.16)$$

As shown in Figure 5.1, the Tresca yield surface is a regular hexagon on a deviatoric plane.

When a saturated clay is loaded under undrained conditions, the volume remains constant. As a result it is suitable to adopt an associated plastic flow rule by treating the yield function (5.16) as the plastic potential as well. Therefore

$$g = \sqrt{J_2} \cos \theta_l - S_u = 0 \quad (5.17)$$

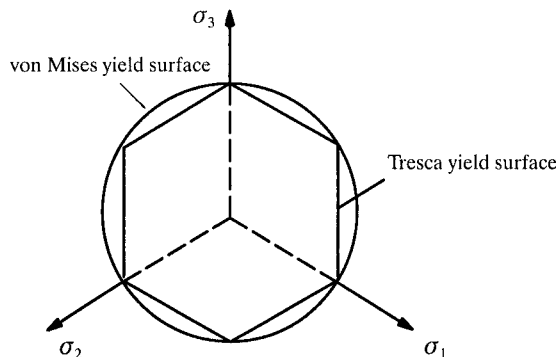


Figure 5.1: Tresca and von Mises yield criteria on a deviatoric plane

As described in Chapter 3, the complete relation between a stress rate and a strain rate for an elastic-perfectly plastic solid may be expressed as follows

$$\dot{\sigma}_{ij} = D_{ijkl}^{ep} \dot{\varepsilon}_{kl} \quad (3.56)$$

where the elastic-plastic stiffness matrix  $D_{ijkl}^{ep}$  is defined by

$$D_{ijkl}^{ep} = D_{ijkl} - \frac{1}{H} D_{ijmn} \frac{\partial g}{\partial \sigma_{mn}} \frac{\partial f}{\partial \sigma_{pq}} D_{pqkl} \quad (3.57)$$

in which

$$H = \frac{\partial f}{\partial \sigma_{ij}} D_{ijkl} \frac{\partial g}{\partial \sigma_{kl}} \quad (3.58)$$

To determine the complete stress-strain relation for Tresca materials, we need to determine  $\partial f / \partial \sigma_{ij}$  and  $\partial g / \partial \sigma_{ij}$ , which can be obtained using the chain rule

$$\frac{\partial f}{\partial \sigma_{ij}} = \frac{\partial f}{\partial J_2} \frac{\partial J_2}{\partial \sigma_{ij}} + \frac{\partial f}{\partial \theta_l} \frac{\partial \theta_l}{\partial \sigma_{ij}} \quad (5.18)$$

$$= \frac{\cos \theta_l}{2\sqrt{J_2}} \frac{\partial J_2}{\partial \sigma_{ij}} - \sqrt{J_2} \sin \theta_l \frac{\partial \theta_l}{\partial \sigma_{ij}} \quad (5.19)$$

$$\frac{\partial g}{\partial \sigma_{ij}} = \frac{\partial g}{\partial J_2} \frac{\partial J_2}{\partial \sigma_{ij}} + \frac{\partial g}{\partial \theta_l} \frac{\partial \theta_l}{\partial \sigma_{ij}} \quad (5.20)$$

$$= \frac{\cos \theta_l}{2\sqrt{J_2}} \frac{\partial J_2}{\partial \sigma_{ij}} - \sqrt{J_2} \sin \theta_l \frac{\partial \theta_l}{\partial \sigma_{ij}} \quad (5.21)$$

where  $\partial J_2 / \partial \sigma_{ij}$  and  $\partial \theta_l / \partial \sigma_{ij}$  are independent of the form of yield functions and plastic potentials as they only depend on the definitions of the second invariant of deviatoric stress and Lode's angle.

It is noted however from Figure 5.1 that Tresca's yield function and plastic potential are not differentiable at certain corner points. These singularities deserve special treatment as they are important for some practical problems. Several approaches exist for dealing with these singularities. One of the classical approaches was developed by Nayak and Zienkiewicz (1972) and consists of using only one yield function in combination with a rounding off procedure for points at which two planes of the yield function meet (the so-called corner point). Sloan and Booker (1984) adopted a modified surface to round off the corners so that a smooth yield surface may be obtained. Although these approaches have proven to be effective to some extent, they are mathematically inconvenient and physically somewhat artificial. A rigorous method has been proposed by Yu (1994) for stress states sited on the corners.

### 5.3.2 von Mises model

A slightly better alternative to the Tresca yield criterion is the criterion proposed by von Mises (1913). von Mises suggested that yielding occurred when the second invariant of deviatoric stress reached a critical value. von Mises' yield criterion is expressed as follows:

$$f = \sqrt{J_2} - k = 0 \quad (5.22)$$

or

$$f = (\sigma_1 - \sigma_2)^2 + (\sigma_2 - \sigma_3)^2 + (\sigma_3 - \sigma_1)^2 - 6k^2 = 0 \quad (5.23)$$

where  $k$  is the undrained shear strength of the soil in pure shear. As shown in Figure 5.1, the von Mises yield surface is a circle on a deviatoric plane. Like the Tresca yield surface, the von Mises yield criterion does not depend on the mean stress. A physical interpretation of the von Mises yield criterion was that equation (5.22) implies that yielding begins when the elastic energy of distortion reaches a critical value (Hill, 1950).

By suitably choosing the value of the strength parameter  $k$  in equation (5.22), we can make the von Mises circle pass through the corners of the Tresca hexagon (as shown in Figure 5.1), which happens when

$$k = \frac{S_u}{\cos \theta_l} = \frac{2}{\sqrt{3}} S_u \quad (5.24)$$

By comparing Tresca's and von Mises' yield criteria, it is obvious that the von Mises yield criterion generally implies a slightly higher undrained shear strength. The difference depends on Lode's angle that indicates the direction of shear stress.

For undrained loading, the plastic volumetric strain is zero so that an associated flow rule is adequate, namely

$$g = \sqrt{J_2} - k = 0 \quad (5.25)$$

which, together with equation (5.22), leads to

$$\frac{\partial f}{\partial \sigma_{ij}} = \frac{\partial f}{\partial J_2} \frac{\partial J_2}{\partial \sigma_{ij}} = \frac{1}{2\sqrt{J_2}} \frac{\partial J_2}{\partial \sigma_{ij}} \quad (5.26)$$

$$\frac{\partial g}{\partial \sigma_{ij}} = \frac{\partial g}{\partial J_2} \frac{\partial J_2}{\partial \sigma_{ij}} = \frac{1}{2\sqrt{J_2}} \frac{\partial J_2}{\partial \sigma_{ij}} \quad (5.27)$$

## 5.4 PLASTICITY MODELS FOR FRICTIONAL MATERIAL

For cohesive-frictional soil and rock, neither Tresca's nor von Mises' yield criterion is adequate. This is because the key feature of yielding of frictional materials is their mean pressure dependence. In other words, a correct yield criterion for any frictional material would be a function of the first stress invariant or mean pressure. In this respect, the oldest and still the most useful yield criterion for cohesive fric-

tional materials is the empirical proposal made by Coulomb (1773) in his investigations of retaining walls.

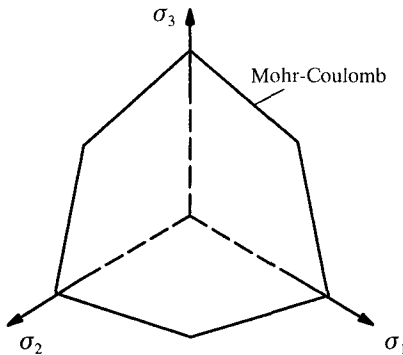


Figure 5.2: Mohr-Coulomb yield surface on a deviatoric plane

#### 5.4.1 Mohr-Coulomb model

The yield criterion proposed by Coulomb (1773) is in terms of shear stress  $\tau$  and normal stress  $\sigma_n$  acting on a plane. It suggests that the yielding begins as long as the shear stress and the normal stress satisfy the following equation

$$|\tau| = c + \sigma_n \tan \phi \quad (5.28)$$

where  $c$  and  $\phi$  are the cohesion and internal angle of friction for the soil.

In terms of the principal stresses, Coulomb's yield criterion can be expressed by

$$f = \sigma_1 - \sigma_3 - (\sigma_1 + \sigma_3) \sin \phi - 2c \cos \phi = 0 \quad (5.29)$$

for  $\sigma_1 \geq \sigma_2 \geq \sigma_3$ .

In terms of the stress invariants and Lode's angle, the Mohr-Coulomb yield criterion (5.29) can be written as

$$f = \sqrt{J_2} - \frac{m(\theta_l, \phi)}{3} I_1 - m(\theta_l, \phi) c \cos \phi = 0 \quad (5.30)$$

where

$$m(\theta_l, \phi) = \frac{\sqrt{3}}{(\sqrt{3} \cos \theta_l + \sin \theta_l \sin \phi)} \quad (5.31)$$

Alternatively, equation (5.30) can also be expressed in terms of the generalised shear stress  $q$  and the mean stress  $p$  as follows

$$f = q - \sqrt{3} p m(\theta_b, \phi) \sin \phi - \sqrt{3} m(\theta_b, \phi) c \cos \phi = 0 \quad (5.32)$$

by noting  $q = \sqrt{3J_2}$  and  $p = I_1/3$ .

With the Mohr-Coulomb model, it is often assumed that the plastic potential takes the same form as the yield function but the friction angle is replaced by the dilation angle (which is a smaller angle). Therefore

$$g = \sqrt{J_2} - \frac{m(\theta_b, \psi) \sin \psi}{3} I_1 - m(\theta_b, \psi) c \cos \psi = 0 \quad (5.33)$$

where  $\psi$  is the dilation angle and

$$m(\theta_b, \psi) = \frac{\sqrt{3}}{(\sqrt{3} \cos \theta_b + \sin \theta_b \sin \psi)} \quad (5.34)$$

To link the plastic potential and the yield function, a stress-dilatancy equation must be used which defines the relationship between the angles of friction and dilation. Perhaps the most successful stress-dilatancy model is that developed by Rowe (1962), which has been further simplified by Bolton (1986) as follows:

$$\psi = 1.25(\phi - \phi_{cv}) \quad (5.35)$$

where  $\phi_{cv}$  is the angle of friction at the critical state. The above assumption implies a non-associated flow rule as the angles of friction and dilation are not the same.

The differentiation of the yield function and plastic potential with respect to stress can be evaluated by the chain rule

$$\frac{\partial f}{\partial \sigma_{ij}} = \frac{\partial f}{\partial I_1} \frac{\partial I_1}{\partial \sigma_{ij}} + \frac{\partial f}{\partial J_2} \frac{\partial J_2}{\partial \sigma_{ij}} + \frac{\partial f}{\partial \theta_b} \frac{\partial \theta_b}{\partial \sigma_{ij}} \quad (5.36)$$

$$\frac{\partial g}{\partial \sigma_{ij}} = \frac{\partial g}{\partial I_1} \frac{\partial I_1}{\partial \sigma_{ij}} + \frac{\partial g}{\partial J_2} \frac{\partial J_2}{\partial \sigma_{ij}} + \frac{\partial g}{\partial \theta_b} \frac{\partial \theta_b}{\partial \sigma_{ij}} \quad (5.37)$$

### Stress states on a single yield surface

For illustration, let us take tensile stresses as positive and the three principal stresses are in the order  $\sigma_1 < \sigma_2 < \sigma_3$ . If the stress state lies on a single yield surface, then the Mohr-Coulomb yield function is defined as:

$$f = \sigma_3 - \sigma_1 + (\sigma_3 + \sigma_1) \sin \phi - 2c \cos \phi = 0 \quad (5.38)$$

where  $c$  and  $\phi$  are soil cohesion and friction angle respectively. A plastic potential is generally obtained by using a dilation angle  $\psi$ :

$$g = \sigma_3 - \sigma_1 + (\sigma_3 + \sigma_1) \sin \psi = \text{constant} \quad (5.39)$$

With the above assumptions, the elastic-plastic stiffness matrix defined by equation (3.57) can be shown to be (Yu, 1994):

$$\mathbf{D}^{ep} = C_2 \begin{bmatrix} (K + \frac{G}{3})(1 + s)(1 + n) & (K - \frac{2G}{3})(1 + s) & (K + \frac{G}{3})(1 + s)(1 - n) \\ (K - \frac{2G}{3})(1 + n) & K(1 + 3sn) + \frac{4G}{3} & (K - \frac{2G}{3})(1 - n) \\ (K + \frac{G}{3})(1 - s)(1 + n) & (K - \frac{2G}{3})(1 - s) & (K + \frac{G}{3})(1 - s)(1 - n) \end{bmatrix} \quad (5.40)$$

where  $s = \sin \phi$  and  $n = \sin \psi$ ;  $K$  and  $G$  are bulk and shear moduli; and

$$C_2 = \frac{G}{G + (K + \frac{G}{3})sn} \quad (5.41)$$

#### *Stress states on the intersection of two yield surfaces*

If the stress state lies on the intersection of any two yield functions, for example, those defined by:

$$f_1 = \sigma_3 - \sigma_1 + (\sigma_3 + \sigma_1) \sin \phi - 2c \cos \phi = 0 \quad (5.42)$$

$$f_2 = \sigma_2 - \sigma_1 + (\sigma_2 + \sigma_1) \sin \phi - 2c \cos \phi = 0 \quad (5.43)$$

the corresponding plastic potentials may be written as:

$$g_1 = \sigma_3 - \sigma_1 + (\sigma_1 + \sigma_3) \sin \psi = \text{constant} \quad (5.44)$$

$$g_2 = \sigma_2 - \sigma_1 + (\sigma_2 + \sigma_1) \sin \psi = \text{constant} \quad (5.45)$$

By using Prager's consistency condition and the following flow rule for deriving plastic strain rates for corners

$$d\boldsymbol{\varepsilon}_{ij}^p = d\lambda_1 \frac{\partial g_1}{\partial \sigma_{ij}} + d\lambda_2 \frac{\partial g_2}{\partial \sigma_{ij}} \quad (5.46)$$

the elastic-plastic stiffness matrix has been derived by Yu (1994) as follows:

$$\mathbf{D}^{ep} = C_3 \begin{bmatrix} (1 + s)(1 + n) & (1 - n)(1 + s) & (1 + s)(1 - n) \\ (1 - s)(1 + n) & (1 - n)(1 - s) & (1 - s)(1 - n) \\ (1 - s)(1 + n) & (1 - n)(1 - s) & (1 - s)(1 - n) \end{bmatrix} \quad (5.47)$$

where

$$C_3 = \frac{9GK}{12Ksn + G(3-s)(3-n)} \quad (5.48)$$

Similar matrices can be obtained for other combinations of stress magnitudes. The elastic-plastic stiffness matrices for the Tresca model can be obtained from the solution for the Mohr-Coulomb model simply by setting  $\phi = 0$  and  $\psi = 0$ .

### 5.4.2 Drucker-Prager model

The von Mises yield criterion is not suitable for modelling the yielding of frictional material as it does not include the effect of mean stress as observed in experiments. To overcome this limitation of the von Mises yield function, Drucker and Prager (1952) proposed the following revised function for frictional soils

$$f = \sqrt{J_2} - \alpha I_1 - k = 0 \quad (5.49)$$

where  $\alpha$  and  $k$  are material constants. On a deviatoric plane, equation (5.49) plots as a circle (Figure 5.3) as for the von Mises yield surface. However in principal stress space, the Drucker-Prager yield surface is a cone whilst the von Mises yield surface is an infinitely long cylinder.

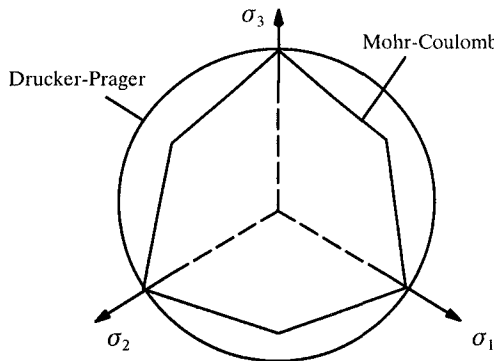


Figure 5.3: Mohr-Coulomb and Drucker-Prager's yield surfaces on a deviatoric plane

To select the material constants  $\alpha$  and  $k$  for use in analysis, the Drucker-Prager yield surface is often matched with the Mohr-Coulomb yield surface using a certain criterion. Figure 5.3 shows such a match at major vertices. Mathematically, this condition demands the following relations

$$\alpha = \frac{2 \sin \phi}{\sqrt{3}(3 - \sin \phi)} \quad (5.50)$$

$$k = \frac{6c \cos \phi}{\sqrt{3}(3 - \sin \phi)} \quad (5.51)$$

As another example, if the Drucker-Prager and Mohr-Coulomb criteria are made to give an identical limit load for a plane strain problem, then the following relationships must hold (Drucker and Prager, 1952; Chen and Saleeb, 1982)

$$\alpha = \frac{\tan \phi}{\sqrt{9 + 12 \tan^2 \phi}} \quad (5.52)$$

$$k = \frac{3c}{\sqrt{9 + 12 \tan^2 \phi}} \quad (5.53)$$

Because of its simplicity, the Drucker-Prager yield criterion has been used quite widely in geotechnical analysis. However experimental research suggests that its circular shape on a deviatoric plane does not agree well with experimental data. For this reason care is needed when the Drucker-Prager plasticity model is used in geotechnical analysis.

To complete the formulation of the Drucker-Prager plasticity model, we need to define a plastic potential. As for the case of the Mohr-Coulomb plasticity model, we may adopt a plastic potential that is in the same form as the yield function, namely

$$g = \sqrt{J_2} - \alpha' I_1 = \text{constant} \quad (5.54)$$

where the angle of friction needed to be replaced by the angle of dilation, and

$$\alpha' = \frac{2 \sin \psi}{\sqrt{3} (3 - \sin \psi)} \quad (5.55)$$

in which  $\psi$  denotes the angle of dilation.

The differentiation of the yield function and plastic potential with respect to stress can be evaluated by the chain rule

$$\begin{aligned} \frac{\partial f}{\partial \sigma_{ij}} &= \frac{\partial f}{\partial I_1} \frac{\partial I_1}{\partial \sigma_{ij}} + \frac{\partial f}{\partial J_2} \frac{\partial J_2}{\partial \sigma_{ij}} \\ &= -\alpha \frac{\partial I_1}{\partial \sigma_{ij}} + \frac{1}{2\sqrt{J_2}} \frac{\partial J_2}{\partial \sigma_{ij}} \end{aligned} \quad (5.56)$$

$$\begin{aligned} \frac{\partial g}{\partial \sigma_{ij}} &= \frac{\partial g}{\partial I_1} \frac{\partial I_1}{\partial \sigma_{ij}} + \frac{\partial g}{\partial J_2} \frac{\partial J_2}{\partial \sigma_{ij}} \\ &= -\alpha' \frac{\partial I_1}{\partial \sigma_{ij}} + \frac{1}{2\sqrt{J_2}} \frac{\partial J_2}{\partial \sigma_{ij}} \end{aligned} \quad (5.57)$$

### 5.4.3 Lade-Duncan and Matsuoka-Nakai models

A major disadvantage of the Mohr-Coulomb model is that it contains corners which require some special numerical treatments. From a computational point of view, it

would therefore be more advantageous to have a yield surface that is smooth. For this reason, the yield surfaces proposed by Lade and Duncan (1975) and Matsuoka and Nakai (1974, 1982) have also been used in geotechnical analysis.

The yield criterion proposed by Lade and Duncan (1975) can be written in terms of the first and third stress invariants as follows

$$f = \frac{I_1^3}{I_3} - k_1 = 0 \quad (5.58)$$

where  $k_1$  is a soil constant depending on density. Figure 5.4 shows its comparison with the Mohr-Coulomb surface on the deviatoric plane.

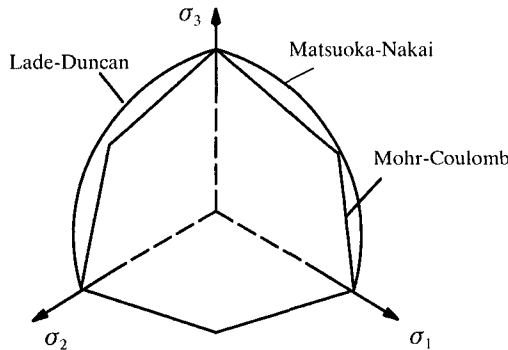


Figure 5.4: Mohr-Coulomb, Lade-Duncan and Matsuoka-Nakai's yield surfaces on a deviatoric plane

On the other hand, the yield criterion proposed by Matsuoka and Nakai (1974) is normally written in the following elegant form in terms of the three stress invariants:

$$f = \frac{I_1 I_2}{I_3} - (9 + 8 \tan^2 \phi) = 0 \quad (5.59)$$

where  $I_1$ ,  $I_2$  and  $I_3$  are the first, second and third invariants of the effective stress tensor respectively, and  $\phi$  denotes the mobilized friction angle under triaxial loading conditions.

To derive the plastic strain rates, Yu (1990) proposed the use of the following plastic potential

$$g = \frac{I_1^* I_2^*}{I_3^*} - (9 + 8 \tan^2 \psi) = 0 \quad (5.60)$$

where  $\psi$  denotes the mobilized dilation angle under triaxial loading conditions and  $I_1^*$ ,  $I_2^*$  and  $I_3^*$  are the first, second and third invariants of a modified stress tensor which is defined by

$$\sigma_{ij}^* = \sigma_{ij} + l\delta_{ij} \quad (5.61)$$

in which  $\delta_{ij}$  is the Kronecker delta. This plastic potential function is of a similar form to the Matsuoka-Nakai yield function, but the friction angle is replaced by the dilation angle, and the apex of the surface is moved from the origin to the point in principal stress space with the coordinates  $(-l, -l, -l)$ . The parameter  $l$  is calculated on the basis that the plastic potential and the yield function must coincide at the current stress state. As shown by Yu (1990), this condition can be successfully used to derive a cubic equation in  $l$  from which the required root may be selected.

The plastic potential (5.60) can only be used for initially dense sand where dilation angle is positive. In order to model the behaviour of an initially loose sand whose dilation angle becomes negative, a plastic potential that takes the same form as the Mohr-Coulomb yield function, but uses dilation angle instead of friction angle can be adopted.

The differentiation of the yield function and plastic potential with respect to stress can be evaluated by the chain rule

$$\frac{\partial f}{\partial \sigma_{ij}} = \frac{\partial f}{\partial I_1} \frac{\partial I_1}{\partial \sigma_{ij}} + \frac{\partial f}{\partial I_2} \frac{\partial I_2}{\partial \sigma_{ij}} + \frac{\partial f}{\partial I_3} \frac{\partial I_3}{\partial \sigma_{ij}} \quad (5.62)$$

$$\frac{\partial g}{\partial \sigma_{ij}} = \frac{\partial g}{\partial I_1} \frac{\partial I_1}{\partial \sigma_{ij}} + \frac{\partial g}{\partial I_2} \frac{\partial I_2}{\partial \sigma_{ij}} + \frac{\partial g}{\partial I_3} \frac{\partial I_3}{\partial \sigma_{ij}} \quad (5.63)$$

#### 5.4.4 Hoek-Brown model

In addition to the linear Mohr-Coulomb yield criterion, a number of researchers have also used non-linear yield criteria to analyse rock mechanics problems. A most popular development has been the empirical non-linear criterion proposed by Hoek and Brown (1980) to describe the yield and failure behaviour of rock masses.

The yield of rock is assumed to be governed by the Hoek and Brown criterion in the following form:

$$f = \sigma_1 - \sigma_3 - \sqrt{mY\sigma_3 + sY^2} = 0 \quad (5.64)$$

where  $\sigma_1$  and  $\sigma_3$  are the major and minor principal stresses;  $Y$  is the uniaxial compressive strength of the intact rock material; and  $m$  and  $s$  are constants depending on the nature of the rock mass and the extent to which it is broken prior to being subjected to the principal stresses  $\sigma_1$  and  $\sigma_3$ .

The Hoek-Brown criterion offers some advantages over other approaches in determining the overall strength of in-situ rock masses because it is based on one simple material property,  $Y$ , and rock mass quality data that may be systematically collected and evaluated during site investigation.

For the convenience of numerical applications, the Hoek-Brown criterion may also be expressed in terms of stress invariants by the following equation

$$f = 4J_2 \cos^2 \theta_l + g(\theta_l) \sqrt{J_2} - aI_1 - k = 0 \quad (5.65)$$

where

$$g(\theta_l) = mY \left( \cos \theta_l + \frac{\sin \theta_l}{\sqrt{3}} \right) \quad (5.66)$$

$$k = sY^2 \quad (5.67)$$

The non-associated flow rule can be obtained by adopting a simplified Hoek-Brown criterion as the plastic potential (Pan and Hudson, 1988)

$$g = 3J_2 + \frac{\sqrt{3}m'Y}{2} \sqrt{J_2} - \frac{m'Y}{3} I_1 = 0 \quad (5.68)$$

where  $m'$  is a reduced Hoek-Brown parameter  $m$ . Since the plastic potential is not a function of Lode's angle, it plots as a circle on a deviatoric plane.

The differentiation of the yield function and plastic potential with respect to stress can be evaluated by the chain rule

$$\frac{\partial f}{\partial \sigma_{ij}} = \frac{\partial f}{\partial I_1} \frac{\partial I_1}{\partial \sigma_{ij}} + \frac{\partial f}{\partial J_2} \frac{\partial J_2}{\partial \sigma_{ij}} + \frac{\partial f}{\partial \theta_l} \frac{\partial \theta_l}{\partial \sigma_{ij}} \quad (5.69)$$

$$\frac{\partial g}{\partial \sigma_{ij}} = \frac{\partial g}{\partial I_1} \frac{\partial I_1}{\partial \sigma_{ij}} + \frac{\partial g}{\partial J_2} \frac{\partial J_2}{\partial \sigma_{ij}} \quad (5.70)$$

## REFERENCES

Bolton, M.D. (1986). The strength and dilatancy of sands, *Geotechnique*, Vol 36, 65-78.

Borja, R., Tamagnini, C. and Amorosi, A. (1997). Coupling plasticity and energy conserving elasticity models for clays. *J. Geotech. Geoenviron. Eng.*, ASCE, Vol 123, 948-957.

Chen, W.F. and Saleeb, A.F. (1982). *Constitutive Equations for Engineering Materials: Vol 1 – Elasticity and Modelling*, Wiley, New York.

Coulomb, C.A. (1773). Essai sur une application des règles des maximis et minimis à quelques problèmes de statique relatifs à l'architecture, *Mem. pres. par div. savants*, Vol 7, 343-382.

de Saint-Venant, B (1870). Memoire sur l'établissement des équations différentielles des mouvements intérieurs opérés dans les corps solides ductiles au delà des limites où l'élasticité pourrait les ramener à leur premier état, *C.R. Acad. Sci. (Paris)*, Vol 70, 473-480.

Drucker, D.C. and Prager, W. (1952). Soil mechanics and plastic analysis for limit design, *Quart. Appl. Math.*, Vol 10, 157-165.

Drucker, D.C., Prager, W. and Greenberg, H.J. (1952). Extended limit design theorems for continuous media, *Quart. Appl. Math.*, Vol 9, 381-389.

Hill, R. (1950). *The Mathematical Theory of Plasticity*, Clarendon Press, Oxford.

Hill, R. (1951). On the state of stress in a plastic-rigid body at the yield point, *Phil. Mag.*, Vol 42, 868-875.

Hoek, E. and Brown, E.T. (1980). *Underground Excavation in Rock*, The Institution of Mining and Metallurgy, London.

Houlsby, G.T. (1985). The use of a variable shear modulus in elastic-plastic models of clays. *Comput. Geotech.*, Vol 1, 3-13.

Lade, P.V. and Duncan, J.M. (1975). Elastoplastic stress strain theory for cohesionless soil. *J. Geotech. Eng. Div.*, ASCE, Vol 101, 1037-1053.

Levy, M. (1870). Memoire sur les équations générales des mouvements intérieurs des corps solides ductiles au delà des limites où l'élasticité pourrait les ramener à leur premier état, *C.R. Acad. Sci. (Paris)*, Vol 70, 1323-1325.

Matsuoka, H. and Nakai, T. (1974). Stress deformation and strength characteristics of soil under three different principal stresses, *Proc. Japan. Soc. Civil Engineers*, Vol 232, 59.

Matsuoka, H. and Nakai, T. (1982). A new failure criterion for soils in three-dimensional stresses, *Proc. IUTAM Symp. on Deformation and Failure of Granular Materials*, (Editors: P.A. Vermeer and H.J. Luger), 253-263.

Nayak, G.C. and Zienkiewicz, O.C. (1972). Elasto-plastic stress analysis: a generalization for various constitutive relations including strain softening. *Int. J. Num. Meth. Eng.*, Vol 5, 113-135.

Pan, X.D. and Hudson, J.A. (1988). Plane strain analysis in modelling three-dimensional tunnel excavations. *Int. J. Rock Mech. Min. Sci.*, Vol 25, 331-337.

Prager, W (1955). The theory of plasticity - a survey of recent achievements, *Proc. Inst. Mech. Eng.*, London, 3-19.

Rankine, W.J. (1857). On the stability of loose earth. *Phil. Trans. R. Soc.*, Vol 147, 9-27.

Rowe, P.W. (1962). The stress-dilatancy relation for static equilibrium of an assembly of particles in contact. *Proc. R. Soc. A*, Vol 267, 500-527.

Sloan, S.W. and Booker, J.R. (1984). Removal of singularities in Tresca and Mohr-Coulomb yield functions. *Commun. Appl. Num. Meth.*, Vol 2, 173-179.

Tresca, H. (1864). Sur l'écoulement des corps solides soumis à de fortes pressions, *C.R. Acad. Sci. (Paris)*, Vol 59, 754.

Tresca, H. (1868). Mémoire sur l'écoulement des corps solides, *Mem. pres. par div. savants*, Vol 18, 733-799.

von Mises, R. (1913). Mechanik der festen Körper im plastisch deformation, *Zustand. Nachr. Ges. Wiss. Gottingen*, 582.

Wroth, C.P. (1973). A brief review of the application of plasticity to soil mechanics, In: *Plasticity and Soil Mechanics*, (Editor: A.C. Palmer), 1-11.

Yu, H.S. (1990). *Cavity Expansion Theory and Its Application to the Analysis of Pressuremeters*, DPhil Thesis, University of Oxford.

Yu, H.S. (1994). A closed form solution of stiffness matrix for Tresca and Mohr-Coulomb plasticity models. *Comput. Struct.*, Vol 53, 755-757.

Zytynski, M., Randolph, M.F., Nova, R. and Wroth, C.P. (1978). On modelling the unloading-reloading behaviour of soils. *Int. J. Num. Analy. Meth. Geomech.*, Vol 2, 87-93.

## CHAPTER 6

### ISOTROPIC HARDENING AND CRITICAL STATE THEORY

#### 6.1 INTRODUCTION

To begin this chapter on work-hardening and critical state theory, it would be instructive to recall the Synopsis of a classic paper ‘Soil Mechanics and Work-Hardening Theories of Plasticity’ by Drucker *et al.* (1957):

*“Soils having cohesion and internal friction are often considered to be perfectly plastic solids. A consistent approach has been proposed on the basis of the mathematical theory of perfect plasticity, and several interesting results were obtained. However, such an idealized treatment will often result in a marked difference between prediction and experimental fact. In particular, the strong dependence of the volume change under shearing action on the prior history of the soil cannot be properly taken into account. It is suggested herein that soil be treated as a work-hardening material which may reach the perfectly plastic state. A remarkable qualitative agreement is then obtained with the known behaviour of soils in triaxial tests; additional study along similar lines appears most promising.”*

Here these authors not only pointed out the limitations of perfect plasticity for soil modelling but also demonstrated the real potential for using a work-hardening approach to describe soil behaviour.

This paper is highly original at least in three aspects:

- (1) It includes, for the first time, the effect of both shear and consolidation loading on the yielding of soils (i.e. the proposed yield surface includes a Mohr-Coulomb surface plus a cap and this idea was later used by DiMaggio and Sandler (1971) to develop their so-called Cap model).
- (2) It uses the current plastic compaction (or density) as a hardening parameter to determine the evolution of cap surfaces.
- (3) It anticipates that an ultimate, perfectly plastic state (such as the critical state) will be reached after large deformation.

As pointed out by Wroth (1973), the introduction of work-hardening into soil mechanics led in turn to the generalization of the family of soil models developed at Cambridge. Many more of these models have been proposed since then. A key feature of all these models has been the *concept of critical states* proposed independently by Roscoe *et al.* (1958) and Parry (1956, 1958).

## 6.2 THE CONCEPT OF CRITICAL STATES

On page 19 of their book 'Critical State Soil Mechanics', Schofield and Wroth (1968) describe the concept of critical states in the following way:

*"The kernel of our idea is the concept that soil and other granular materials, if continuously distorted until they flow as a frictional fluid, will come into a well-defined critical state determined by two equations"*

$$q = Mp \quad (6.1)$$

$$\Gamma = v + \lambda \ln p \quad (6.2)$$

*The constants  $M$ ,  $\Gamma$ , and  $\lambda$  represent basic soil material properties and the parameters  $q$ ,  $v$ , and  $p$  are defined in due course."*

As a result the critical states depend on the mean effective stress  $p$ , shear stress  $q$  and soil specific volume  $v$  and are shown graphically in Figure 6.1 as two straight lines (now known as the critical state lines CSL), where  $e$  denotes the void ratio.

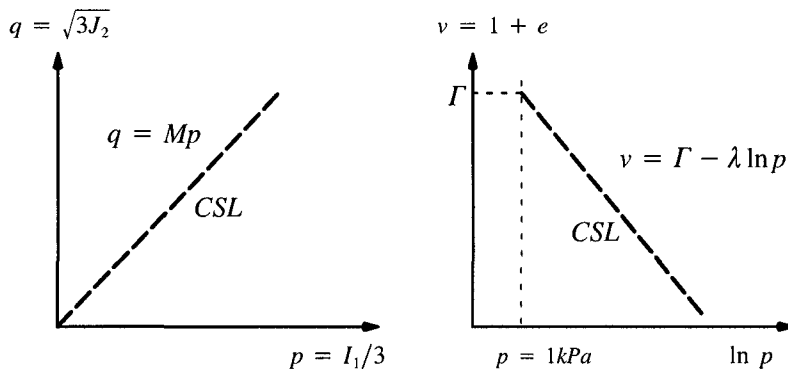


Figure 6.1: The concept of critical states

On pages 107 and 108 of Schofield and Wroth (1968), it was further explained that at the critical state, soils behave as a *frictional fluid* so that yielding occurs at constant volume and constant stresses. In other words, the plastic volumetric strain increment is zero at the critical state, since elastic strain increments will be zero due to the constant stress condition at the critical state. Also it was assumed that the critical state lines are unique for a given soil regardless of stress paths used to bring them about from any initial conditions.

In many ways, the critical states defined or assumed above may be regarded as the ultimate states anticipated by Drucker *et al.* (1957). It is also noted that the con-

cept of steady states proposed later by Poulos (1981) is also similar to the concept of critical states. In addition, Desai and Toth (1996) and Desai (2001) proposed a concept of disturbed states for use in constitutive modelling. In effect, the critical states correspond to Desai's fully disturbed states. Given the uniqueness of the critical state lines, they are used as a convenient base of reference in formulating a strain hardening/softening plasticity model to describe the measured behaviour of soil and other granular materials (Yu, 1998).

The concept of critical states was initially developed based on limited triaxial test data obtained on reconstituted clay (Roscoe *et al.*, 1958; Parry, 1958; Schofield and Wroth, 1968; Roscoe and Burland, 1968). However over the last forty years, a lot of additional experimental data for many other types of soil and granular material (e.g. sand, rock, natural clay, unsaturated soil and sugar) have been obtained which seems to support, at least to a very large extent, the general concept of critical states (e.g. Atkinson and Bransby, 1978; Brown and Yu, 1988; Been *et al.*, 1991; Muir Wood, 1990; Atkinson and Allman, 1992; Novello and Johnston, 1995).

### 6.3 CAM CLAY AND MODIFIED CAM CLAY

After describing the concept of critical states, we are now in the position to detail how a critical state-based, strain hardening plasticity model can be formulated. In doing so, we will use the standard critical state models, Cam clay and modified Cam clay, as examples.

For simplicity, we shall start our development for the case of a triaxial test, that is, when two effective principal stresses are equal and the directions of principal stresses are fixed with respect to the material element. The generalization to a general three-dimensional case will follow afterwards. Assuming compressive stresses and strains as positive, the two effective stress variables normally used in critical state soil mechanics are

$$p = \frac{1}{3}(\sigma_1' + 2\sigma_3') \quad ; \quad q = \sigma_1' - \sigma_3' \quad (6.3)$$

where  $\sigma_1'$ ,  $\sigma_3'$  denote effective vertical and radial stresses respectively. The corresponding strains are

$$\varepsilon_p = \varepsilon_1 + 2\varepsilon_3 \quad ; \quad \varepsilon_q = \frac{2}{3}(\varepsilon_1 - \varepsilon_3) \quad (6.4)$$

#### 6.3.1 Cam clay model

As the earliest elastic-plastic critical state model, Cam clay was developed by Roscoe and Schofield (1963) and Schofield and Wroth (1968).

### (a) Work equation and plastic potential

The plastic work per unit volume of a triaxial sample with the externally applied mean and shear stresses  $p$  and  $q$  is

$$dW_{in} = p \, d\varepsilon_p^p + q \, d\varepsilon_q^p \quad (6.5)$$

where  $\varepsilon_p^p$  and  $\varepsilon_q^p$  are volumetric and shear plastic strains respectively.

To determine how this plastic energy is dissipated, Schofield and Wroth (1968) follow the simple analysis of Taylor (1948) on shear box test results. On page 346 of his book, Taylor assumed that all the plastic work, defined by (6.5), is dissipated entirely in friction, namely

$$dW_{dis} = Mp \, d\varepsilon_q^p \quad (6.6)$$

where  $M$  is the ratio of  $q/p$  at the critical state. The energy conservation then requires

$$dW_{in} = dW_{dis} \quad (6.7)$$

which leads to the following work equation for the Cam clay model

$$p \, d\varepsilon_p^p + q \, d\varepsilon_q^p = Mp \, d\varepsilon_q^p \quad (6.8)$$

The above work equation can be further rearranged as follows

$$\frac{q}{p} + \frac{d\varepsilon_p^p}{d\varepsilon_q^p} = M \quad (6.9)$$

Now let us assume that there exists a plastic potential for the soil that depends on both the mean and shear stresses

$$g = g(p, q) = 0 \quad (6.10)$$

from which we can write the following

$$d\varepsilon_p^p = d\lambda \frac{\partial g}{\partial p} \quad \text{and} \quad d\varepsilon_q^p = d\lambda \frac{\partial g}{\partial q} \quad (6.11)$$

By noting that the plastic strain is normal to the plastic potential, it can be shown that

$$\frac{d\varepsilon_p^p}{d\varepsilon_q^p} = - \frac{dq}{dp} \quad (6.12)$$

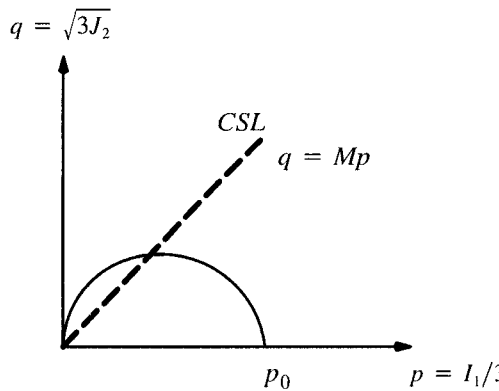
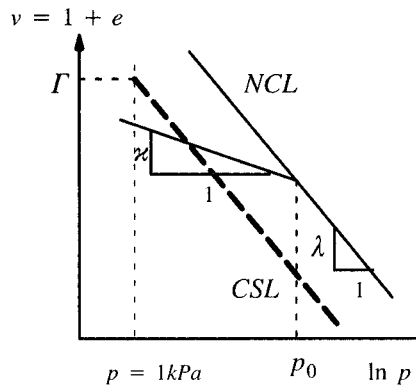


Figure 6.2: The normal consolidation line (NCL), critical state lines (CSL) and yield surface (plastic potential)

By substituting equation (6.12) into equation (6.9), we obtain

$$\frac{q}{p} - \frac{dq}{dp} = M \quad (6.13)$$

which may be integrated to give an equation for the plastic potential

$$g = g(p, q) = \frac{q}{pM} + \ln\left(\frac{p}{p_0}\right) = 0 \quad (6.14)$$

where  $p_0$  is a constant which indicates the size of the plastic potential. Physically it represents the mean stress when  $q/p = 0$  (Figure 6.2).

**(b) Associated plastic flow rule and yield criterion**

In developing the Cam clay model, it was assumed that the soil obeys an associated flow rule so that the yield function is identical to the plastic potential. Hence

$$f = f(p, q, p_0) = \frac{q}{pM} + \ln\left(\frac{p}{p_0}\right) = 0 \quad (6.15)$$

where  $p_0$  is the preconsolidation pressure (Figure 6.2) served as the hardening parameter that changes with the plastic strain.

**(c) Plastic hardening law – volumetric hardening**

It is clear from equation (6.15) that the size of the yield surface is represented by the preconsolidation pressure  $p_0$  (Figure 6.2). In Cam clay,  $p_0$  is assumed to change with the plastic volumetric strain in the following manner

$$dp_0 = \frac{\nu p_0}{\lambda - \nu} d\varepsilon_p^p \quad (6.16)$$

where  $\nu$  is a material constant that represents the slope of elastic loading and unloading lines in a  $v$ - $lnp$  plot (see Figure 6.2).

**(d) Elastic component of the model**

In Cam clay, it was assumed that the bulk modulus is proportional to the mean pressure  $p$

$$K = \frac{\nu p}{\nu} \quad (6.17)$$

The second elastic constant can be chosen by using either an assumed constant value of Poisson's ratio  $\nu$  or an assumed constant value of shear modulus  $G$ . As it is usually more convenient to specify a value of Poisson's ratio, the shear modulus may therefore be assumed to vary with stress level in the same form as  $K$

$$G = \frac{3(1 - 2\nu)}{2(1 + \nu)} K \quad (6.18)$$

From a theoretical point of view, it would be preferable to assume a constant value of shear modulus, as Zytynski *et al.* (1978) showed that the use of a constant Poisson's ratio would lead to a non-conservative model in the sense that it may not conserve energy during closed stress cycles.

**(e) The complete stress-strain relation**

By combining equations (6.11) and (3.29) and noting that the hardening parameter  $\alpha = p_0$  in Cam clay is assumed to depend only on the plastic volumetric strain, we obtain the following equation

$$f_p dp + f_q dq + f_{p_0} p_{0,\varepsilon_p^p} d\lambda g_p = 0 \quad (6.19)$$

where  $f_p = \partial f / \partial p$  and  $f_q = \partial f / \partial q$  etc. The above equation gives the expression for the non-negative plastic multiplier

$$d\lambda = - \frac{f_p dp + f_q dq}{f_{p_0} p_{0,\varepsilon_p^p} g_p} = \frac{1}{K_p} (f_p dp + f_q dq) \quad (6.20)$$

where  $K_p$  is defined as

$$K_p = - f_{p_0} p_{0,\varepsilon_p^p} g_p \quad (6.21)$$

Equation (6.20) can be substituted into equation (6.11) to give the expression for the plastic strain increments

$$d\varepsilon_p^p = d\lambda g_p = \frac{g_p}{K_p} (f_p dp + f_q dq) \quad (6.22)$$

$$d\varepsilon_q^p = d\lambda g_q = \frac{g_q}{K_p} (f_p dp + f_q dq) \quad (6.23)$$

By adding the elastic strain increments, we can obtain the following elastic-plastic relations between stress increments and strain increments

$$d\varepsilon_p = d\varepsilon_p^e + d\varepsilon_p^p = \frac{1}{K} dp + \frac{g_p}{K_p} (f_p dp + f_q dq) \quad (6.24)$$

$$d\varepsilon_q = d\varepsilon_q^e + d\varepsilon_q^p = \frac{1}{3G} dq + \frac{g_q}{K_p} (f_p dp + f_q dq) \quad (6.25)$$

For Cam clay, all the differentiations needed to define the incremental stress-strain relations (6.24) and (6.25) are given as follows

$$f_p = g_p = \frac{\partial f}{\partial p} = - \frac{q}{Mp^2} + \frac{1}{p} \quad (6.26)$$

$$f_q = g_q = \frac{\partial f}{\partial q} = \frac{1}{Mp} \quad (6.27)$$

$$f_{p_0} = \frac{\partial f}{\partial p_0} = - \frac{1}{p_0} \quad (6.28)$$

$$p_{0,\varepsilon_p^p} = \frac{\partial p_0}{\partial \varepsilon_p^p} = \frac{\lambda - \varkappa}{vp_0} \quad (6.29)$$

### 6.3.2 Modified Cam clay model

Modified Cam clay was developed by Roscoe and Burland (1968) and represents a slight extension of Cam clay by adopting a revised work equation to derive the yield function and plastic potential.

Instead of the work equation (6.8) used in Cam clay, modified Cam clay assumes the following work equation

$$p \, d\varepsilon_p^p + q \, d\varepsilon_q^p = p \sqrt{(d\varepsilon_p^p)^2 + (M d\varepsilon_q^p)^2} \quad (6.30)$$

By following the same procedure used above, the yield function and therefore plastic potential can be derived as

$$f = f(p, q, p_0) = \left(\frac{q}{pM}\right)^2 - \frac{p_0}{p} + 1 = 0 \quad (6.31)$$

which is of an elliptical shape in  $q$ - $p$  space.

For modified Cam clay, the incremental stress-strain relations are also defined by equations (6.24) and (6.25). The only difference is that the three differentiations of the yield function (i.e. the plastic potential) with respect to stresses and the hardening parameter needed to be changed due to a different yield function used for modified Cam clay. Hence

$$f_p = g_{,p} = \frac{\partial f}{\partial p} = -\frac{2q^2}{M^2 p^3} + \frac{p_0}{p^2} \quad (6.32)$$

$$f_q = g_{,q} = \frac{\partial f}{\partial q} = \frac{2q}{M^2 p^2} \quad (6.33)$$

$$f_{p_0} = \frac{\partial f}{\partial p_0} = -\frac{1}{p} \quad (6.34)$$

### 6.3.3 Limitations of Cam clay and modified Cam clay

To achieve a better agreement between predicted and observed soil behaviour, a large number of modifications have been proposed to the standard Cam-clay models over the last two decades. A brief review of some of the most important modifications may be found in Gens and Potts (1988). Examples of these modifications include research on the following topics: (a) yield surface for heavily overconsolidated clays (e.g. Zienkiewicz and Naylor, 1973; Atkinson and Bransby, 1978); (b) critical state modelling of sand behaviour (e.g. Nova and Wood, 1979; Pastor *et al.*, 1985); (c) anisotropic yield surfaces for one-dimensionally consolidated soils (e.g. Ohta and Wroth, 1976; Whittle, 1993); (d) inclusion of plastic deformation within

the main yield surface for soils subject to cyclic loading (e.g. Pender, 1978; Dafalias and Herrmann, 1980; Carter *et al.*, 1982 and Naylor, 1985); (e) 3D critical state formulations (e.g. Roscoe and Burland, 1968; Zienkiewicz and Pande, 1977); and (f) modelling of rate-dependent behaviour of clays (e.g. Borja and Kavazanjian, 1985; Kutter and Sathialingam, 1992; Yin and Graham, 1999).

Despite some successes in modifying the standard Cam-clay models in the 1980s, Yu (1995, 1998) identified the following limitations:

- (1) The yield surfaces adopted in many critical state models significantly overestimate failure stresses on the 'dry side'. To overcome this limitation, the Hvorslev surface is often used as the yield function in this region (e.g. Zienkiewicz and Naylor, 1973). The problem with this treatment is that there will be two separate yield surfaces for hardening and softening, and this discontinuity in the yield surface may cause significant numerical difficulties (Naylor, 1985). This is probably why the Hvorslev surface is seldom implemented in geotechnical computer softwares (Gens and Potts, 1988).
- (2) Most critical state soil models assumed an associated flow rule and therefore were unable to predict an important feature of behaviour that is commonly observed in undrained tests on loose sand and normally consolidated undisturbed clays, and that is a peak in the deviatoric stress before the critical state is approached (e.g. Bishop, 1972; Sladen *et al.*, 1985; Pastor *et al.*, 1985; Been and Jefferies, 1985). Furthermore, as shown by Vermeer, 1982, no bifurcation is possible in the hardening regime if an associated flow rule is used, and this contradicts experimental observations (e.g. Nova, 1985).
- (3) The critical state concept had been much less successful for modelling granular materials (e.g. Wroth and Bassett, 1965; Schofield and Wroth, 1968; Nova and Wood, 1979; Saada and Bianchini, 1988; Jefferies, 1993). The main problem lies in the fact that existing Cam-clay models fail to predict observed softening and dilatancy of dense sands and the undrained response of very loose sands. The lack of success in developing a critical state model for sand is also due to the experimental difficulties in obtaining critical state and normal consolidation lines (Atkinson and Bransby, 1978). Until recently, little data for the critical state and normal consolidation lines of sands was available. In addition, experimental data for sands seems to support a different picture of yield surfaces from that seen for clays (e.g. Nova and Wood, 1978; Tatsuoka and Ishihara, 1974; Muir Wood, 1990).

The above observation was confirmed by Gens and Potts (1988) in their state of the art review on the application of critical state models in computational geomechanics, where they noted:

- (1) The materials modelled by critical state models appeared to be mostly limited to saturated clays and silts, and stiff overconsolidated clays did not appear to

be generally modelled with critical state formulations. This fact was probably related to the poor performance of critical state models for soils on the 'dry side'.

(2) Granular materials were rarely modelled by critical state models. In spite of the fact that a number of 'double hardening' sand models (e.g. Nova and Wood, 1979; Vermeer, 1978; Lade, 1977) had been available for many years they did not appear to have been widely used in numerical analyses. This was partially due to the fact that two separate yield surfaces are used in these models for modelling hardening and softening, which may cause significant numerical difficulties. Another reason may be that a large number of constants (some of these constants have no clear physical meaning) need to be determined before these sand models can be applied.

## 6.4 THE STATE PARAMETER INTERPRETATION

### 6.4.1 The state parameter concept

The state parameter is defined by Been and Jefferies (1985) as the difference between specific volume (or void ratio) and the specific volume (or void ratio) at the critical state at the same mean effective stress, see Figure 6.3. This parameter was first used by Wroth and Bassett (1965) in the development of a stress-strain relation for sand.

The experimental research on clay and dense sands by Roscoe and Poorooshagh (1963), Cole (1967) and Stroud (1971) suggests that any two samples of a soil will behave in a similar manner regardless of their stress-strain history provided the state parameter is the same for each sample. Recent work on dense and loose sands by Been and Jefferies (1985), Sladen *et al.* (1985) and Sladen and Ossewell (1989) confirms this observation and suggests that the state parameter can be confidently used to describe much of the behaviour of granular materials over a wide range of stresses and densities. This is because the state parameter does not eliminate the influence of either density or confining pressure on the behaviour of sands, and rather it properly places emphasis on the fact that it is a combination of these parameters that is relevant to the description of granular materials. It has also been demonstrated by Been and his co-workers that many commonly used sand properties, such as angles of friction and dilation, normalize quite well to the state parameter, and this is the utility of the concept to practising engineers.

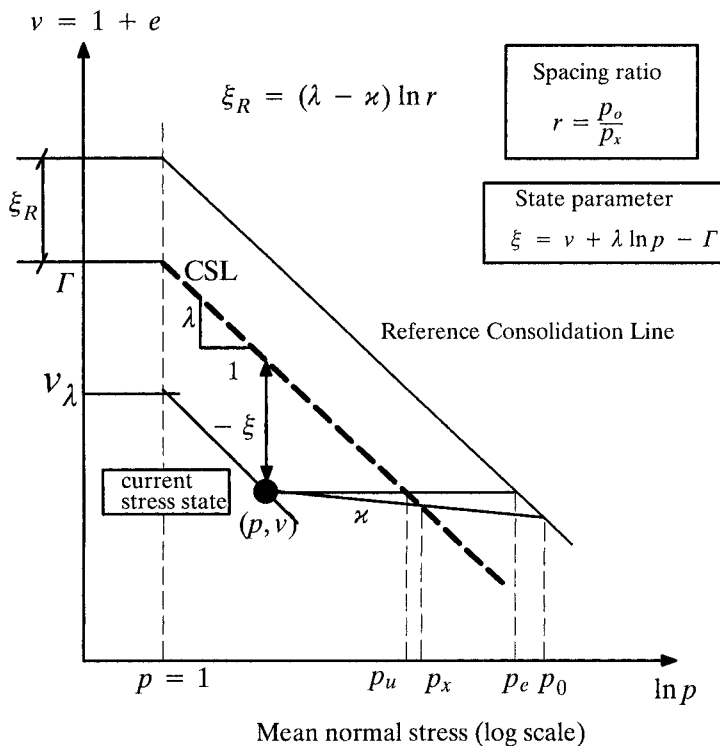


Figure 6.3: The state parameter concept (after Yu, 1995, 1998)

It is well established that most sands behave rather like a clay at high OCR - on shearing they tend to dilate, although some sand deposits may be sufficiently loose to compress on shearing like a clay at low OCR. As a direct relationship between the OCR and the state parameter can be generally established (e.g. Been and Jefferies, 1993), it is expected that the state parameter for sand will play a similar role to the overconsolidation ratio (OCR) for clay. In clays, the OCR has been used as the main quantity to describe the character of clay response under given loading conditions. By comparison, the role of the OCR in sands is less clear, mainly because the preconsolidation pressure can only be determined accurately at high pressures. As an alternative, Stroud (1971) shows that a similar type of information is available if the density and the current pressure are known (i.e. the state parameter). Because the state parameter may be determined easily for both clay and sand, it may be regarded as a better quantity than OCR for describing soil response under various loading conditions.

### 6.4.2 Cam clay and modified Cam clay in terms of the state parameter

Yu (1995, 1998) shows for the first time that Cam clay and modified Cam clay take a simpler form if formulated in terms of the state parameter.

#### (a) Cam clay

As discussed before, the material behaviour prior to the achievement of the critical state is assumed to be controlled by the state parameter which is defined by:

$$\xi = v + \lambda \ln p - \Gamma \quad (6.35)$$

where  $v = (1 + e)$  is known as specific volume and  $e$  is void ratio. It is noted that the state parameter  $\xi$  is zero at the critical state, positive on the 'wet' side and negative on the 'dry' side.

The state boundary surface of the original Cam-clay model is presented by Schofield and Wroth (1968) as follows:

$$\frac{q}{Mp} = \frac{\Gamma + \lambda - \varkappa - v - \lambda \ln p}{\lambda - \varkappa} \quad (6.36)$$

In the original Cam-clay model, equation (6.36) is used as a yield function. In addition, the consistency requirement that the differential of the yield function is zero is used to define a hardening law.

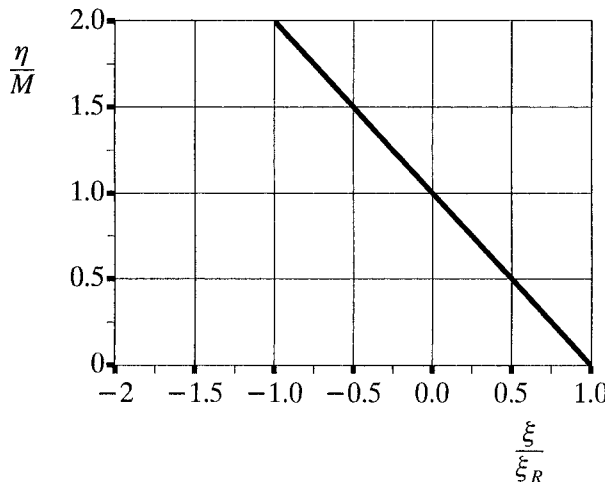


Figure 6.4: Stress-state relation for the original Cam-clay model with  
 $\xi_R = (\lambda - \varkappa) \ln e = \lambda - \varkappa$

By using equation (6.35), the state boundary surface (6.36) may be expressed as a relationship between stress ratio and the state parameter namely :

$$\frac{\eta}{M} = 1 - \frac{\xi}{\xi_R} \quad (6.37)$$

where  $\eta = q/p$  is known as stress ratio, and  $\xi_R$  is a positive reference state parameter which denotes the vertical distance between the CSL and a reference consolidation line. As shown in Figure 6.3, the reference consolidation line is assumed to be parallel to CSL. For clays, NCL should be used as the reference consolidation line. In the original Cam-clay model, the reference state parameter is assumed to be  $\xi_R = (\lambda - \alpha) \ln r = (\lambda - \alpha) \ln e = \lambda - \alpha$ , where  $r$  is known as the spacing ratio. For some sands, information about the NCL may not be accurately known and in this case the reference state parameter may be chosen for a state beyond which the soil is unlikely to reach in practice. The stress-state relation (6.37) implies that when a soil is yielding, the stress ratio  $\eta$  increases linearly with a decrease in the state parameter, see Figure 6.4.

### (b) Modified Cam clay

The state boundary surface of the modified Cam-clay model was presented by Roscoe and Burland (1968) and can be represented as follows :

$$\left(\frac{q}{Mp}\right)^2 = \exp\left(\frac{N - v - \lambda \ln p}{\lambda - \alpha}\right) - 1 \quad (6.38)$$

Equation (6.38) is used as a yield function in the modified Cam-clay model. Using the state parameter definition, the state boundary surface (6.38) can be expressed as a modified stress-state relation, namely

$$\left(\frac{\eta}{M}\right)^2 = 2^{(1 - \frac{\xi}{\xi_R})} - 1 \quad (6.39)$$

In the modified Cam-clay model,  $\xi_R = (\lambda - \alpha) \ln r = (\lambda - \alpha) \ln 2$ . Unlike the linear stress-state relation suggested by the original Cam-clay model, the modified stress-state relation (6.39) is nonlinear, see Figure 6.5.

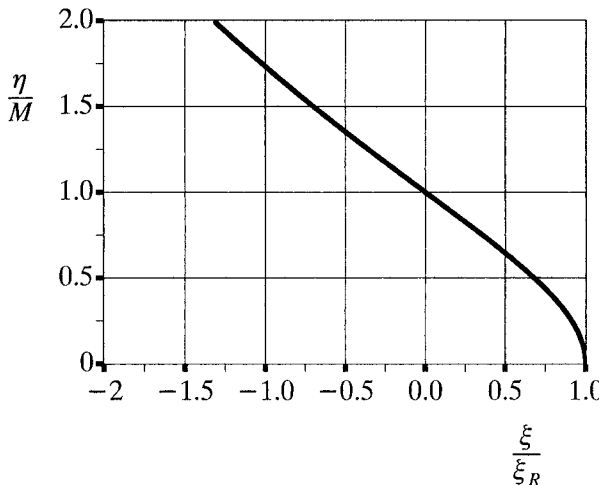


Figure 6.5: Stress-state relation for the modified Cam-clay model with  
 $\xi_R = (\lambda - \alpha) \ln 2$

## 6.5 YU'S UNIFIED CRITICAL STATE MODEL

As noted by Scott (1988), there has been an undesirable trend in recent years in the area of constitutive modelling of soils to increase the number of constitutive constants (some models now use as many as 40 material constants). Apart from the drawback that many of the material constants offer no clear physical meaning, there is a difficulty that representation of a specific phenomenon is governed by a number of constants. Hence the values of certain constants cannot be determined independently of the others. Even if some of these models are considered to be very successful in modelling soil behaviour, the large number of material constants required will make them very hard to apply to practical problems. In contrast, the philosophy adopted by Yu (1998) in choosing the structure of the model, is that simplicity should be paramount and that the material constants required by the model should be related to easily measurable, possibly, conventional constants. In the spirit of the hierarchical approach of Desai *et al.* (1987), the model proposed by Yu (1998) is formulated in such a way that the standard Cam-clay models can be recovered (or approximated) simply by choosing certain values of the material constants. Contrary to many existing critical state models that use distinctively different yield functions and plastic potentials for clay and sand, a single yield function and plastic potential are used here for both clay and sand. As will be shown, this can be

achieved by using a general stress-state relation to derive a unified state boundary surface.

### 6.5.1 A general stress-state relation for clay and sand

After a detailed study of the experimental state boundary surfaces reported by Stroud (1971), Lee and Seed (1967), Schofield and Wroth (1968), Sladen *et al.* (1990) and Coop and Lee (1993), Yu (1995, 1998) proposed the following general stress-state relation for describing the state boundary surface for a variety of soils and other granular materials:

$$\left(\frac{\eta}{M}\right)^n = 1 - \frac{\xi}{\xi_R} \quad (6.40)$$

where  $n$  is a new material constant which typically ranges between 1.0-5.0 and the reference state parameter is  $\xi_R = (\lambda - \alpha) \ln r$ .

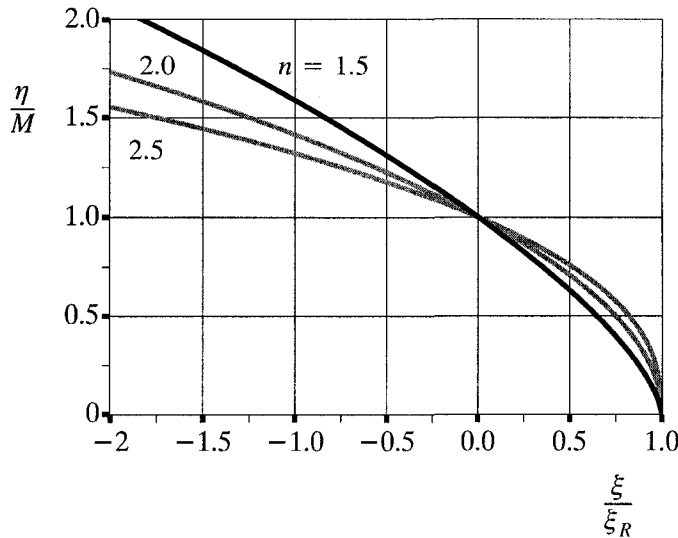


Figure 6.6: General stress-state relations with  $\xi_R = (\lambda - \alpha) \ln r$

For simplicity, the original and modified Cam-clay models use the same  $r$  value for all soil types although in reality this is not the case. In particular, recent experimental data suggests that the values of the spacing ratio for sand are generally much higher than those for clay (Coop and Lee, 1993). In Yu (1998), the spacing ratio  $r$  is allowed to vary with material types. As will be shown later, this assumption

tion can go a long way to overcome some of the most important drawbacks of the standard Cam-clay models mentioned earlier in this chapter.

It is interesting to note that the stress-state relation (6.37) of the original Cam-clay model can be recovered from Equation (6.40) by choosing  $n=1$  and  $r=2.7183$ . Figure 6.6 shows the stress-state relations for three different  $n$  values. In addition, the 'wet' side of the stress-state relation (6.39) for modified Cam-clay can also be matched accurately with Equation (6.40) by choosing  $r=2.0$  in conjunction with a suitable  $n$  value (typically around 1.5-2.0).

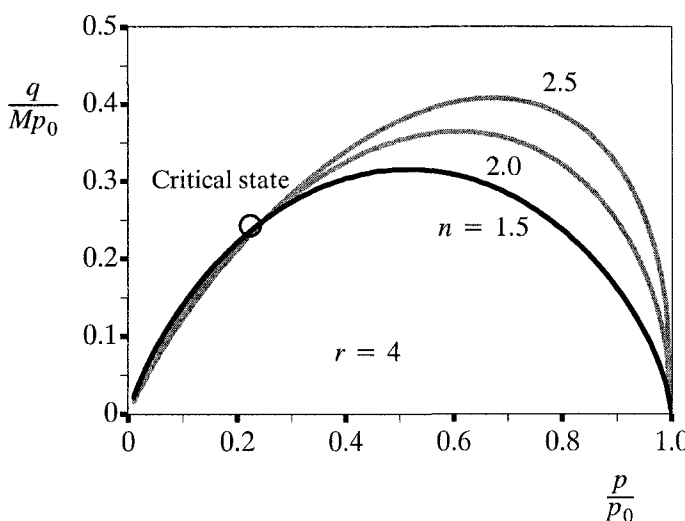


Figure 6.7: State boundary surfaces normalized by preconsolidation pressure

Based on Been and Jefferies's experimental correlations between the peak friction angle and the initial state parameter (Been and Jefferies, 1985), Collins *et al.* (1992) and Yu (1994,1996) have proposed various plasticity models for sand in which the angles of friction and dilation are assumed to be an exponential function of the state parameter. While these existing state parameter models are very successful in modelling dense sands, they may not be valid for very loose granular materials as the plastic deformation of the soil during consolidation cannot be realistically taken into account. Recently, Jefferies (1993) has used a linear relationship between the peak stress ratio (i.e. the peak friction angle) and the state parameter in developing sand models, which may be regarded as special cases of the general stress-state relation (6.40). While the simple rigid state parameter model, Nor-Sand, proposed by Jefferies (1993) proves to be satisfactory for modelling sand be-

haviour under drained loading conditions, it may not be able to model the behaviour of sand under undrained loading conditions.

From Figure 6.3, it can be shown that:

$$\frac{\xi}{\xi_R} = \frac{-(\lambda - \alpha) \ln \frac{p_x}{p}}{(\lambda - \alpha) \ln r} = 1 + \frac{\ln \frac{p}{p_0}}{\ln r} \quad (6.41)$$

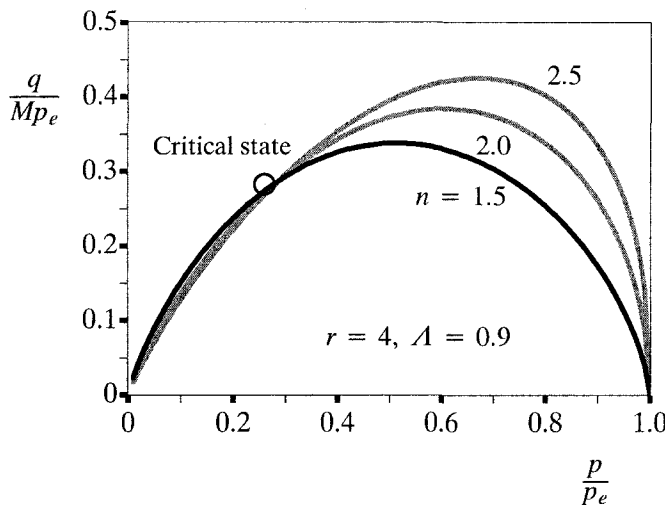


Figure 6.8: State boundary surfaces normalized by equivalent consolidation pressure

Substituting the above equation into the general stress-state relation (6.40) leads to a generalized yield surface in terms of preconsolidation pressure  $p_0$  (i.e. the state boundary surface along the elastic wall) as follows:

$$\left(\frac{\eta}{M}\right)^n = - \frac{\ln \frac{p}{p_0}}{\ln r} \quad (6.42)$$

The state boundary surface (6.42) for  $r=4$  is plotted in Figure 6.7 for three different  $n$  values. It is observed that they look very similar to experimental yielding surfaces for sands reported by Nova and Wood (1978), Tatsuoka and Ishihara (1974), Sladen *et al.* (1985), and Coop and Lee (1993). Figure 6.7 is able to reproduce an important feature of the observed yield surface for sand and that is the deviatoric stress often reaches a local peak before approaching the critical state. This feature

has been theoretically predicted by Chandler (1985) using an energy-based plasticity theory which allowed for volume changes due to particle deformation and particle rearrangement.

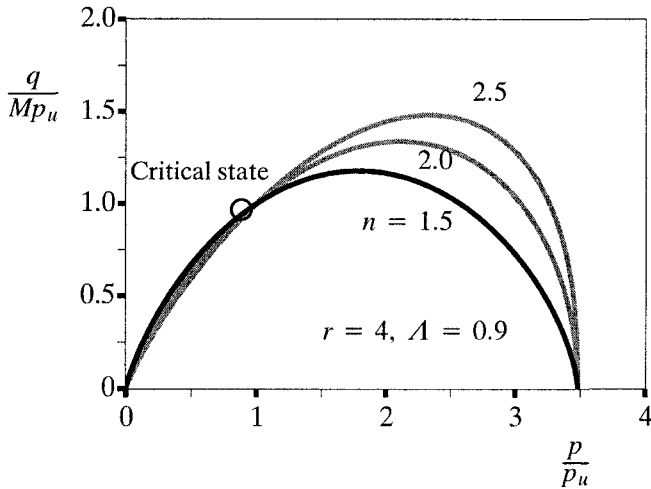


Figure 6.9: State boundary surfaces normalized by equivalent critical state pressure

Following similar procedures to those used before, the stress-state relation (6.40) can also be expressed as the state boundary surface normalized by equivalent critical state  $p_u$  and consolidation pressures  $p_e$  (i.e. the state boundary surfaces at constant  $v$ ) :

$$\left(\frac{\eta}{M}\right)^n = 1 - \frac{\ln \frac{p}{p_u}}{A \ln r} \quad (6.43)$$

$$\left(\frac{\eta}{M}\right)^n = - \frac{\ln \frac{p}{p_e}}{A \ln r} \quad (6.44)$$

where  $A = (\lambda - \nu)/\lambda$  is known as the plastic volumetric strain ratio (Schofield and Wroth, 1968). The state boundary surfaces (6.44) and (6.43) for  $r=4$  and  $A = 0.9$  are plotted in Figure 6.8 and Figure 6.9 respectively for three different  $n$  values.

### 6.5.2 Incremental stress-strain relation for state parameter models

The basic assumption of the state parameter model is the existence of a critical (or steady) state at which the soil deforms without any plastic volume change. The material behavior prior to the achievement of the critical state is assumed to be controlled by the state parameter.

The state parameter model presented by Yu (1995, 1998) is an elastic-plastic strain hardening (or softening) model, that postulates that a soil specimen can be considered as an isotropic continuum. It is assumed that the strain rate tensor is the sum of an elastic, reversible component and of a plastic, irreversible part.

It is noted that the void ratio  $v$  can be eliminated from equation (6.35) using the following expression:

$$\frac{\dot{v}}{v} = -\dot{\varepsilon}_p \quad (6.45)$$

where  $v$  is known as specific volume and  $\varepsilon_p$  denotes volumetric strain. The above equation can be integrated to express the state parameter as a function of the mean stress and plastic volumetric strain:

$$\xi = v_0 \exp(-\varepsilon_p^e - \varepsilon_p^p) + \lambda \ln p - \Gamma \quad (6.46)$$

Suppose now that the plastic behaviour of the materials can be modelled by a yield function depending on stresses and state parameter:

$$f(p, q, \xi) = 0 \quad (6.47)$$

a corresponding plastic potential is defined by:

$$g(p, q, \beta) = 0 \quad (6.48)$$

where  $\beta$  is a parameter controlling the size of the plastic potential which passes through the current stress state.

Following the usual procedure, a complete elastic-plastic stress-strain relationship can be obtained as follows :

$$d\varepsilon_p = \frac{dp}{K} + \frac{g_p}{H} \times [(f_p + f_{,\xi}\xi_p) dp + f_q dq] \quad (6.49)$$

$$d\varepsilon_q = \frac{dq}{3G} + \frac{g_p}{H} \times [(f_p + f_{,\xi}\xi_p) dp + f_q dq] \quad (6.50)$$

where  $H$  is the plastic hardening modulus defined as

$$H = -f_{,\xi}\xi_{,\varepsilon_p^p} g_p \quad (6.51)$$

and  $g_{,p} = \partial g / \partial p$  and  $g_{,q} = \partial g / \partial q$ ;  $K$  and  $G$  are used to denote the bulk and shear moduli of the soils.

Like the standard Cam-clay models, the state parameter theory outlined here is a volumetric strain hardening plasticity model. While the use of both volumetric and deviatoric plastic strain hardening (e.g. Wilde, 1977; Nova, 1977) may be able to capture the strong dilation during hardening prior to failure in dense sands, it leads to a failure state for drained stress paths at which a continuous plastic volume change occurs, and this is contrary to the well established concept of the critical state. Another drawback of this hybrid hardening approach is that a few additional material constants, whose physical meaning is less clear, will need to be introduced into the model. On the other hand, Lade (1977) showed that the behaviour of sand can be modelled successfully by a work hardening plasticity model. Recently, Bar-det (1986) and Crouch *et al.* (1994) demonstrated that volumetric plastic strain hardening models can also be used successfully to model sand behaviour in a wide stress region. Since the primary aim of Yu (1998) was to present a simple unified critical state theory for both clay and sand, the volumetric plastic strain hardening of the standard Cam-clay models has been preserved.

### 6.5.3 A unified state parameter model – CASM

Based on the general incremental stress-strain relation developed in the previous section, this section describes a simple, unified constitutive model for both clay and sand. This simple model is referred to as CASM (standing for **C**lay and **S**and **M**odel).

#### (a) Elastic moduli

As in the standard Cam-clay models, the present state parameter model assumes that the bulk modulus is proportional to the mean effective pressure  $p'$  :

$$K = \frac{\nu p}{\chi} \quad (6.52)$$

The second independent elastic constant is chosen by using either an assumed constant value of Poisson's ratio  $\mu$  or an assumed constant value of shear modulus  $G$ . As it is usually more convenient to specify a value of Poisson's ratio, the shear modulus may therefore be assumed to vary with stress level in the same way as  $K$

$$G = \frac{3(1 - 2\mu)}{2(1 + \mu)} K \quad (6.53)$$

From a theoretical point of view, it would be preferable to assume a constant value of shear modulus, as Zytnski *et al.* (1978) showed that the use of a constant Poisson's ratio would lead to a non-conservative model in the sense that it may not conserve energy during closed stress cycles. It should be noted that this effect may not be so important for static problems since the artificial energy dissipation caused

by the constant Poisson's ratio model is very small compared with the energy dissipation by plastic strains. Furthermore, Gens and Potts (1988) pointed out that a constant  $G$  does not agree well with experimental observations and may imply negative values of Poisson's ratio at low stresses, which is physically unreasonable.

### (b) Stress-state relation and yield function

The choice of the constitutive functions for plastic potential and yield function is an important step in constitutive modelling, since strain rates depend essentially on their derivatives with respective to stresses.

In this subsection, the general stress-state relation (6.40) proposed in a previous section has been adopted to describe the behaviour of soil yielding. In terms of effective mean and deviatoric stresses, and state parameter, the yield function takes the following form :

$$f(p, q, \xi) = \left(\frac{q}{Mp}\right)^n + \frac{\xi}{\xi_R} - 1 = 0 \quad (6.54)$$

or in terms of the preconsolidation pressure it reads

$$f(p, q, p_0) = \left(\frac{q}{Mp}\right)^n + \frac{\ln \frac{p}{p_0}}{\ln r} = 0 \quad (6.55)$$

It is noted that when  $n=1$  and  $\xi_R = (\lambda - \alpha)$ , the above yield function reduces to the original Cam-clay yield surface. In addition, the modified Cam-clay yield surface can also be matched by the above yield function by choosing a certain value of  $n$  (which depends on the plastic volumetric strain ratio of the soil) in conjunction with  $\xi_R = (\lambda - \alpha) \ln 2$ .

As discussed previously, the use of the above stress-state relation to describe yielding of sand is supported by observations of experimentally determined yield surfaces for clays and sands. The above stress-state relation indicates that it is the normalized state parameter (i.e. the state parameter divided by a reference state parameter) rather than the state parameter itself that controls the size of the yield surface. As a result, the present model provides a rational framework for modelling the behaviour of sands with different mineralogy, angularity and particle size.

The need for some form of normalization of the state parameter was also recognized by Desai and co-workers in their development of the disturbed state concept for constitutive modelling (e.g. Desai and Toth, 1996). They used the relative intact (RI) state and the fully adjusted (FA) state to define a disturbance function which is then assumed to control the soil behaviour. In this section, we follow more closely the critical state concept and use the isotropic normal consolidation line (NCL)

and critical state line (CSL) as two reference states in defining the normalized state parameter. It is interesting to note that the disturbance function used by Desai and Toth (1996) is similar, in concept, to the normalized state parameter used in (6.54). The difference is that the present section considers void ratios of various states at the same mean effective stress while void ratios of different states at the same strain level were used in Desai and Toth (1996).

### *Work equation and energy considerations*

It is worth noting that the yield equation (6.55) can also be obtained by assuming an associated flow rule and the following stress-dilatancy relation

$$\frac{d\varepsilon_p^p}{d\varepsilon_q^p} = \frac{M^n - m \eta^n}{m \eta^{n-1}} \quad (6.56)$$

where  $m = n \ln r$ . The above flow rule implies that the work equation is given in the following form

$$p d\varepsilon_p^p + q d\varepsilon_q^p = Mp d\varepsilon_q^p + [\frac{1}{m} (\frac{M}{\eta})^{n-1} - 1] \times Mp d\varepsilon_q^p \quad (6.57)$$

in which the first term of the right-hand side is the power dissipation through friction and the second term represents the power dissipation through other mechanisms such as particle fracture (McDowell and Bolton, 1996) and possible *locked-in energy* (Collins and Kelly, 2002).

### **(c) Stress-dilatancy relation and plastic potential**

#### *Rowe's stress-dilatancy relation*

To define a plastic potential, it is necessary to use a stress-dilatancy relation which defines the relationship between stress ratio and dilatancy rate. Perhaps the most successful stress-dilatancy relation, which may now be considered to be one of the milestones in soil mechanics, is due to Rowe (1962, 1972):

$$\frac{d\varepsilon_p^p}{d\varepsilon_q^p} = \frac{9(M - \eta)}{9 + 3M - 2M\eta} \quad (6.58)$$

Rowe's stress-dilatancy relation, originally developed from minimum energy considerations of particle sliding, has met with great success in describing the deformation of sands and other granular media. As Rowe's stress-dilatancy relation is very similar to the flow rule of the original Cam-clay model, it may also be used to describe the experimental stress-dilatancy data for clays.

Although much effort was devoted in the past to developing an even better stress-dilatancy relation for soils, little progress seems to have been made on this front.

On the other hand, Rowe's stress-dilatancy relation (either in its original or modified forms), which provides satisfactory results for most practical problems, has been widely accepted by the geotechnical community (e.g. Bolton, 1986; Housby, 1991; Jefferies, 1993). Excessive attention to the fine details of the stress-dilatancy relation (or flow rule) for a soil may not be warranted, since, as rightly pointed out by Wroth and Housby (1985), it is invariably much easier to predict the ratios between strains rather than their absolute magnitudes. It is for this reason that Rowe's stress-dilatancy relation will be used to derive a unified plastic potential for both clay and sand.

Following the usual procedure, Rowe's stress-dilatancy relation (6.58) may be integrated to give the following plastic potential:

$$g(p, q) = 3M \ln \frac{p}{C} + (3 + 2M) \ln \left( \frac{2q}{p} + 3 \right) - (3 - M) \ln \left( 3 - \frac{q}{p} \right) = 0 \quad (6.59)$$

where the size parameter  $C$  can be determined easily for any given stress state  $(p, q)$  by solving equation (6.59). Note that the plastic flow rule adopted in CASM is non-associated, as the plastic potential is not identical to the yield surface.

#### *A general stress-dilatancy relation*

Although Rowe's stress-dilatancy relation is accurate for high stress ratios, it is not particularly realistic for stress paths with low stress ratios (such as isotropic consolidation and 1D consolidation). To overcome this limitation, we can adopt a plastic potential that is in a similar form to the yield function in CASM but gives zero plastic volumetric strain increment at critical states. A slight modification of the stress-dilatancy equation (6.56) may be used

$$\frac{de_p^p}{de_q^p} = \frac{M^n - \eta^n}{m \eta^{n-1}} \quad (6.60)$$

where  $n$  is a material constant defined previously in CASM and  $m$  may be treated as a material constant independent of  $n$  and  $r$ . For  $n=1$ , the above stress-dilatancy reduces to the well-known plastic flow rule of Cam clay. By setting  $n=2$  and  $m=1$ , the plastic flow rule of modified Cam clay is recovered. By setting  $m=1$ , equation (6.60) reduces to the expression of McDowell (2002).

One possible approach is to choose  $m$  so that equation (6.60) can accurately model one-dimensional consolidation (Ohmaki, 1982; Alonso *et al.*, 1990; McDowell and Hau, 2003). In other words,  $m$  is selected to ensure that the flow rule predicts zero lateral strain for stress states corresponding to Jaky's (1948)  $K_0$  condition

$$K_0 = 1 - \sin \phi_{cv} = \frac{6 - 2M}{6 + M} \quad (6.61)$$

Therefore at the  $K_0$  condition, the stress ratio takes the following value

$$\eta_{K_0} = \frac{3(1 - K_0)}{1 + 2K_0} = \frac{3M}{6 - M} \quad (6.62)$$

On the other hand, by noting the lateral strain is zero, we have

$$\frac{d\epsilon_p^p + d\epsilon_p^e}{d\epsilon_q^p + d\epsilon_q^e} = = \frac{d\epsilon_1}{\frac{3}{2}d\epsilon_1} = \frac{3}{2} \quad (6.63)$$

If the relative value of the elastic shear strain to the plastic shear strain can be ignored, then equation (6.63) gives

$$\frac{d\epsilon_p^p}{d\epsilon_q^p} = \frac{3}{2} \frac{\lambda - \kappa}{\lambda} = \frac{3}{2}A \quad (6.64)$$

By putting the stress ratio defined by (6.62) into the flow rule (6.60), then equating to (6.64) will lead the following expression for  $m$

$$m = \frac{2}{3} \times \frac{[M(6 - M)]^n - (3M)^n}{A(6 - M) (3M)^{n-1}} \quad (6.65)$$

Following the usual procedure, the general stress-dilatancy relation (6.60) may be integrated to give the following plastic potential:

$$g(p, q) = m \ln[ 1 + (m - 1)(\frac{\eta}{M})^n ] + n(m - 1) \ln \frac{p}{C} \quad (6.66)$$

where  $C$  indicates the size of the plastic potential surface, which can be determined by solving the above equation with current stress values.

#### (d) Hardening law

As discussed earlier, the hardening law used in this model is basically of the isotropic volumetric plastic strain hardening type. In particular, the size of yield surface is controlled by the state parameter which depends on plastic volumetric strains. Using equations (6.35) and (6.46), the volumetric plastic strain hardening law is shown to be :

$$\xi_{,\epsilon_p^p} = -\nu \quad (6.67)$$

The plastic hardening modulus defined by (6.51) can be derived as follows :

$$H = \frac{\nu}{\xi_R} \left[ \frac{9 + 6M}{2q + 3p} - \frac{9 - 3M}{3p - q} \right] \quad (6.68)$$

where  $\xi_R = (\lambda - \alpha) \ln r$ .

#### 6.5.4 Model constants and their identification

There are a total of seven material constants required in CASM. In the following sections, the role of each of these seven constants and the possible methods for determining them are briefly discussed.

##### *Elastic constants – $\alpha$ and $\nu$*

The elastic behaviour is modelled by the slope of the swell line  $\alpha$  and Poisson's ratio  $\nu$ . A typical value of  $\alpha$  for sands is 0.005 and its value is generally much higher for clays, ranging between 0.01 to 0.06. Poisson's ratio  $\nu$  is typically in the range of 0.15-0.35 for clay and sand.

##### *Critical state constants – $\lambda$ , $\Gamma$ and $M$*

The critical state line for a soil is fully defined by constants  $\lambda$ ,  $\Gamma$  and  $M$ . Measurement of these critical state constants is straightforward for clay soil, but for sand it proves to be much more difficult and special care needs to be exercised in determining them using triaxial testing (e.g. Been *et al.*, 1991). Typical values of  $\lambda$  for sands at a relatively low pressure level (say less than 1000 kPa) are between 0.01-0.05 and for some soils its value may be larger in a high pressure region. The  $\lambda$  value for clay is usually in the range of 0.1-0.2.  $\Gamma$  is typically between 1.8-4.0 for various soils. Triaxial tests (drained and undrained with pore pressure measurement) on isotropically consolidated samples can be used to obtain the frictional constant  $M$ . It is necessary to continue these tests to large strains to ensure that the samples are close to the critical state.  $M$  is normally between 0.8-1.0 for clays, and 1.1-1.4 for sands.

##### *Spacing ratio (or Reference state parameter) – $r$ (or $\xi_R$ )*

The spacing ratio  $r$  is used, in one way or another, to define the shape of the yield surface by all critical state constitutive models as well as many bounding surface plasticity models. In Yu (1998), the spacing ratio is used to estimate the reference state parameter which corresponds to the loosest state a soil is likely to reach in practice. For the sake of simplicity, the standard Cam-clay models assume a single constant spacing ratio  $r$  for all soil types. In the original and modified Cam-clay models,  $r$  is fixed at 2.718 and 2.0 respectively. Although reasonable for clays, this simplification is found to be less successful for sands. In CASM, the assumption of a fixed space ratio for all soil types is abandoned and  $r$  is allowed to vary from 1 to  $\infty$ . Experimental data indicates that for clays  $r$  typically lies in the range of 1.5-3.0 and for sands the value of  $r$  is generally much larger (e.g. Coop and Lee, 1993; Crouch *et al.*, 1994).

For most applications, it is satisfactory to treat the NCL as the reference consolidation line, and therefore the measurement of  $r$  for clays does not impose any difficulties as the NCL can be easily located. In contrast, locating the NCL for sands seems to be more difficult as a test device able to supply very high pressure is required (e.g. Atkinson and Bransby, 1978). However, as noted by Crouch *et al.* (1994), existing experimental evidence indicates that many quartz-based sands seem to share essentially the same NCL. If the NCL for a given sand can not be measured, it is acceptable to choose a positive state parameter (typically ranging between 0.05-0.2) that is unlikely to be encountered in practice as the reference state parameter.

#### *Stress-state coefficient – $n$*

The stress-state coefficient  $n$  used in the general stress-state relation (6.40) is a new material constant introduced by Yu (1995, 1998). As discussed before, the value of  $n$  is typically between 1.0-5.0. To determine  $n$  for a given soil, it is necessary to plot the stress paths of a few triaxial tests (both drained and undrained) on soils of different initial conditions in terms of stress ratio  $\eta$  against the state parameter  $\xi$ .

Using the general stress-state relation (6.40), experimental state boundary surfaces should be regarded as a straight line in the plot of  $\ln(1 - \xi/\xi_R)$  against  $\ln(\eta/M)$ . The stress-state coefficient  $n$  is the slope of the state boundary surface in this particular log-log plot.

#### **6.5.5 Prediction and validation**

This section describes an application of CASM to predict the measured behaviour of clay and sand under both drained and undrained loading conditions. For comparison, the original Cam-clay model has also been used to predict the measured stress-strain behaviour for both normally and overconsolidated clays.

#### *Influence of initial conditions on computed stress-strain behaviour*

Before using the CASM model to predict stress-strain behaviour of individual stress-strain curves, it is instructive to investigate the influence of initial conditions on the computed stress-strain relations for both clay and sand under drained and undrained loading conditions.

Figure 6.10 and Figure 6.11 show some aspects of the pattern of computed clay response during triaxial compression tests under drained and undrained conditions. The effects of different values of OCR on the stress-strain relationship shown in these figures are generally in accordance with experimental observation. In this set of simulations, the material constants similar to those of London clay are used, and they are:

$$\lambda = 0.161, \Gamma = 2.759, \nu = 0.3, \kappa = 0.062, M = 0.888, r = 3.0, n = 2.0$$

Plotted in Figure 6.12 and Figure 6.13 are the computed stress-strain response of sand during triaxial compression tests under drained and undrained conditions. The effect of different initial state parameters  $\xi_0$  on the stress-strain relationship are shown. The material constants used are similar to those of Ticino sand which are given below:

$$\lambda = 0.024, \Gamma = 1.986, \nu = 0.3, \kappa = 0.008, M = 1.29, \xi_R = 0.075, n = 2.0$$

To achieve better agreement with experimental data for undrained compression tests on sand at a state looser than critical, it is recommended that the initial state parameter of the sample be taken as the reference state parameter (i.e.  $\xi_R = \xi_0$ ). The effect of model constants  $r$  and  $n$  on computed softening behaviour of sand is illustrated in Figure 6.14. It is clear that by varying the values of  $r$  and  $n$ , CASM can be used to satisfactorily model materials with different softening responses.

It can be seen from Figure 6.10 to Figure 6.14 that CASM is capable of reproducing much of clay and sand stress-strain behaviour observed in the laboratory. Perhaps the only exception is for undrained tests on sand at a state denser than critical where it is often observed that the mean effective stress tends to decrease a bit before increasing to the critical state. As shown in Figure 6.13, CASM does not predict such a pattern of change in the mean effective stress. This is a limitation associated with volumetric strain hardening. As will be shown in the next section, this limitation can be removed by adopting a combined volumetric and shear strain hardening in the formulation (Yu *et al.*, 2005).

To check how well CASM can predict individual stress-strain curves, some experimental data will be used to compare with CASM predictions.

#### *Drained and undrained behaviour of normally and overconsolidated clays*

To assess the performance of CASM for clay, test data from the classic series of tests performed on remoulded Weald clay at Imperial College, London (Bishop and Henkel, 1957) is used. Two of the four tests discussed are drained and two are undrained, while two of the tests are performed on normally consolidated samples with OCR of 1.0 and two on heavily overconsolidated samples with OCR of 24.

The material constants used in the predictions for both CASM and Cam clay are as follows:

#### CASM:

$$\lambda = 0.093, \Gamma = 2.06, \nu = 0.3, \kappa = 0.025, M = 0.9, \xi_R = 0.0679, n = 4.5$$

#### Cam clay:

$$\lambda = 0.093, \Gamma = 2.06, \nu = 0.3, \kappa = 0.025, M = 0.9, r = 2.718, n = 1.0$$

Note the NCL has been used as the reference consolidation line, and therefore the reference state parameter  $\xi_R$  is equal to the initial state parameter of the normally consolidated sample. The critical state constants for Weald clay are from Parry (1956). As accurate elastic constants are not known, some typical values are used in the prediction.

Figure 6.15 to Figure 6.18 present comparisons of the model predictions and the measured behaviour for both drained and undrained compression of normally and overconsolidated Weald clays. It is found that while Cam clay is reasonable for modelling normally consolidated clays, it is not good for modelling overconsolidated clays. For the drained testing of the overconsolidated clay, Figure 6.16 suggests that Cam clay gives a significant over-prediction of the peak deviatoric stress and soil dilatancy. As for the undrained testing, it is evident from Figure 6.18 that Cam clay under-predicts the shear strain at peak strength and over-predicts the negative excess pore pressure. In contrast, Figure 6.15 to Figure 6.18 indicate that the predictions of CASM are consistently better than those of Cam clay for both normally and overconsolidated clays. In particular, CASM is found to be able to capture reasonably well the overall behaviour of the overconsolidated clay observed in the laboratory.

It should also be pointed out that for undrained testing of a normally consolidated clay, Figure 6.17 shows that CASM predicts a strain softening towards the critical state after a peak strength has been reached. Although this behaviour is not apparent in the results of the undrained test of the remoulded Weald clay, compelling evidence has however led Bishop (1972) to conclude that the soil reaches a peak strength before approaching to the critical state is a well established behaviour for undrained tests on normally consolidated samples of many undisturbed cohesive soils. A similar behaviour was also observed by Allman and Atkinson (1992) in their results of undrained testing of reconstituted Bothkennar soil. As will be discussed later, this is also a well known result from the undrained testing of a very loose sand.

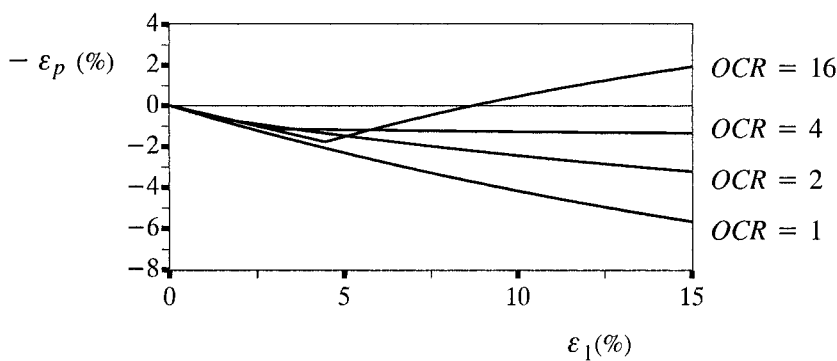
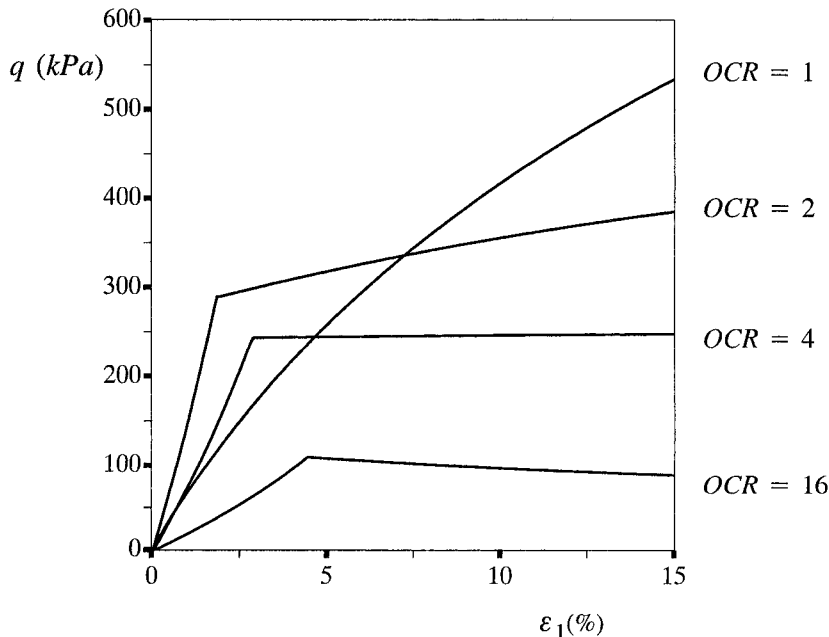


Figure 6.10: Effect of OCR on computed behaviour of drained triaxial compression tests on clay

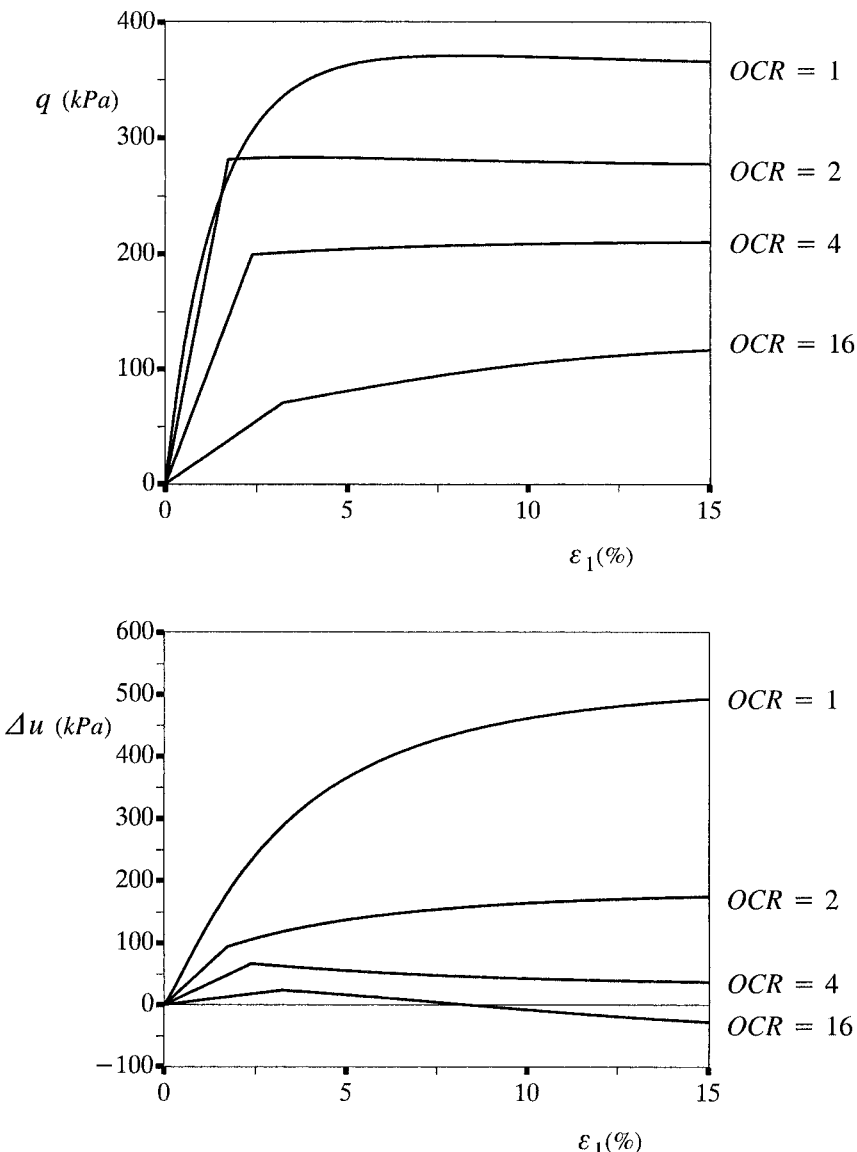


Figure 6.11: Effect of OCR on computed behaviour of undrained triaxial compression tests on clay

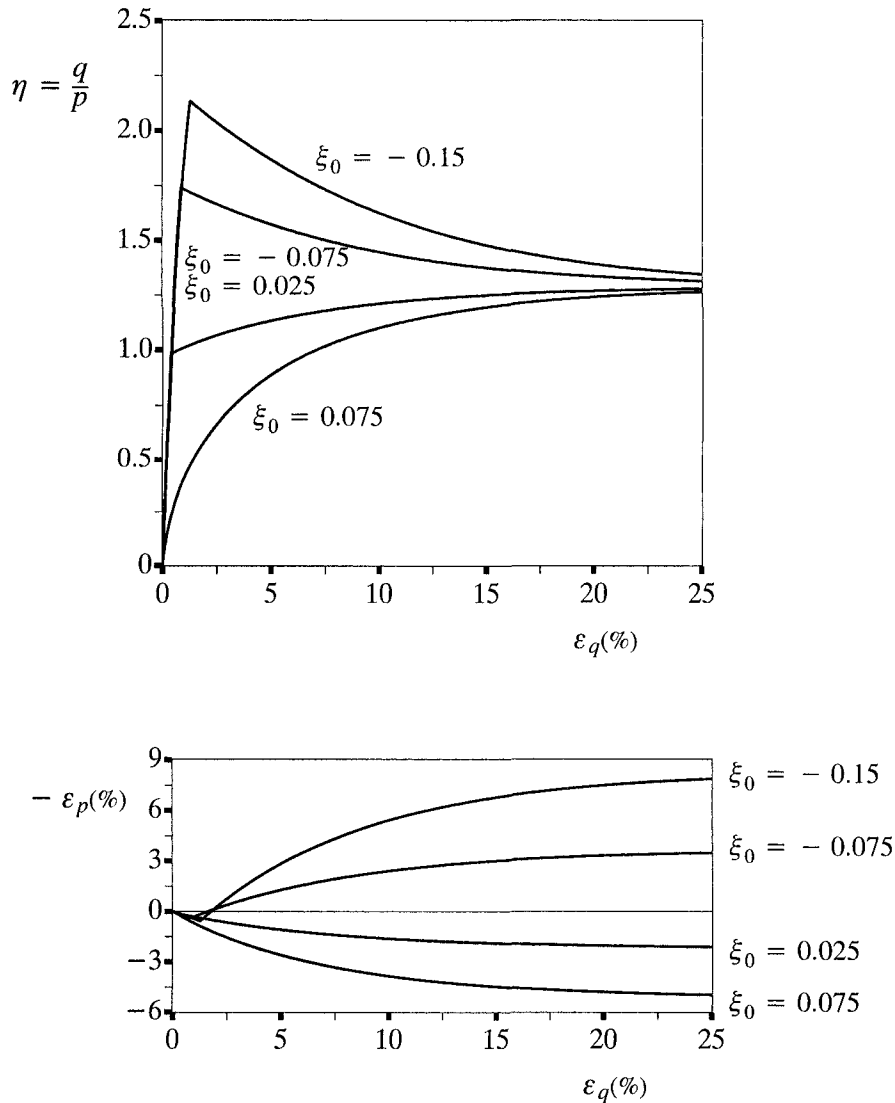


Figure 6.12: Effect of initial state parameter on computed behaviour of drained triaxial compression tests on sand

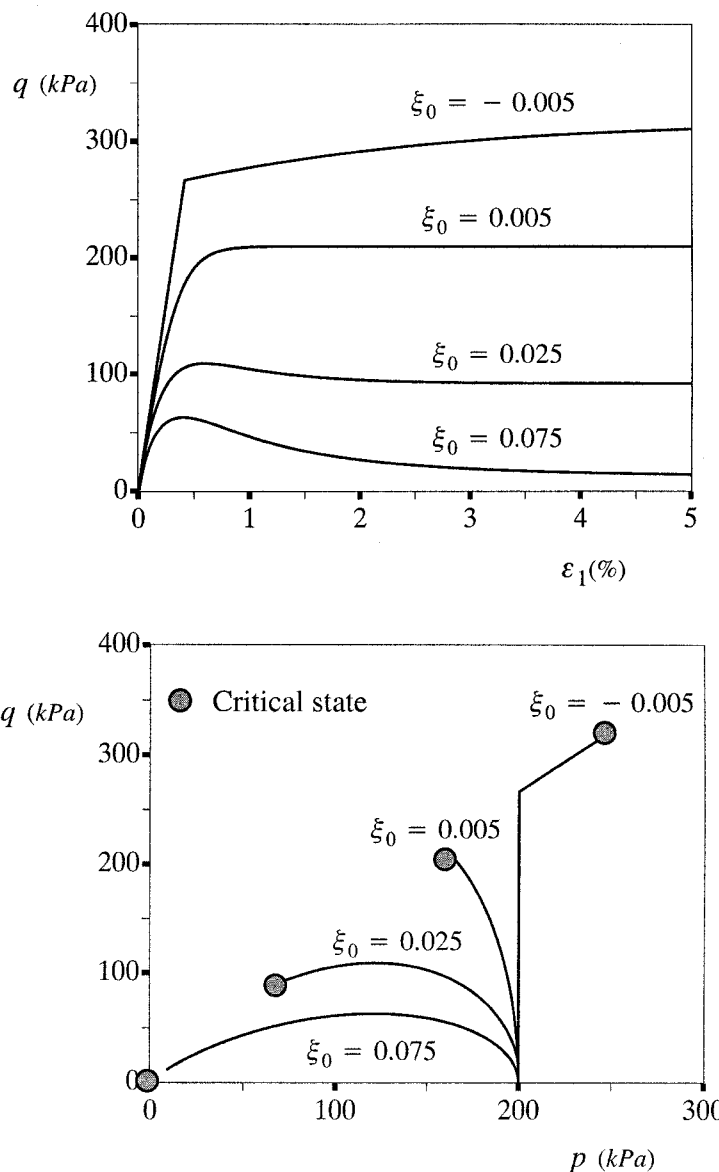


Figure 6.13: Effect of initial state parameter on computed behaviour of undrained triaxial compression tests on sand

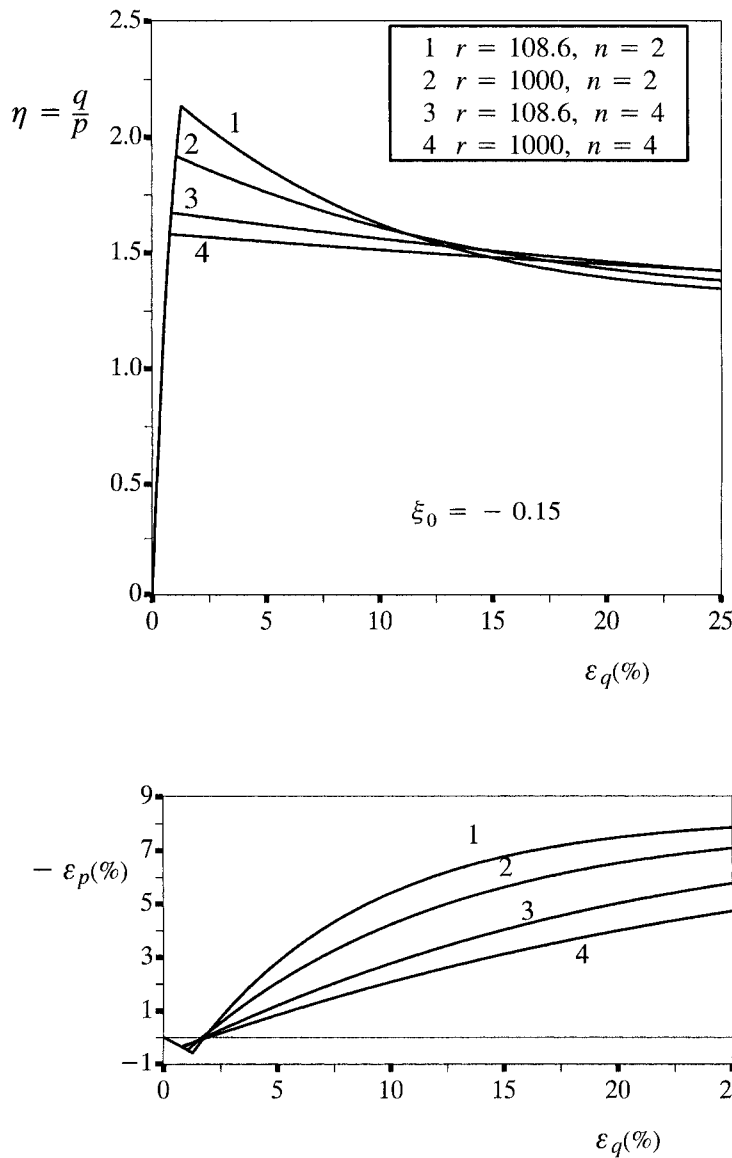


Figure 6.14: Effect of model constants  $r$  and  $n$  on computed behaviour of drained triaxial compression tests on sand

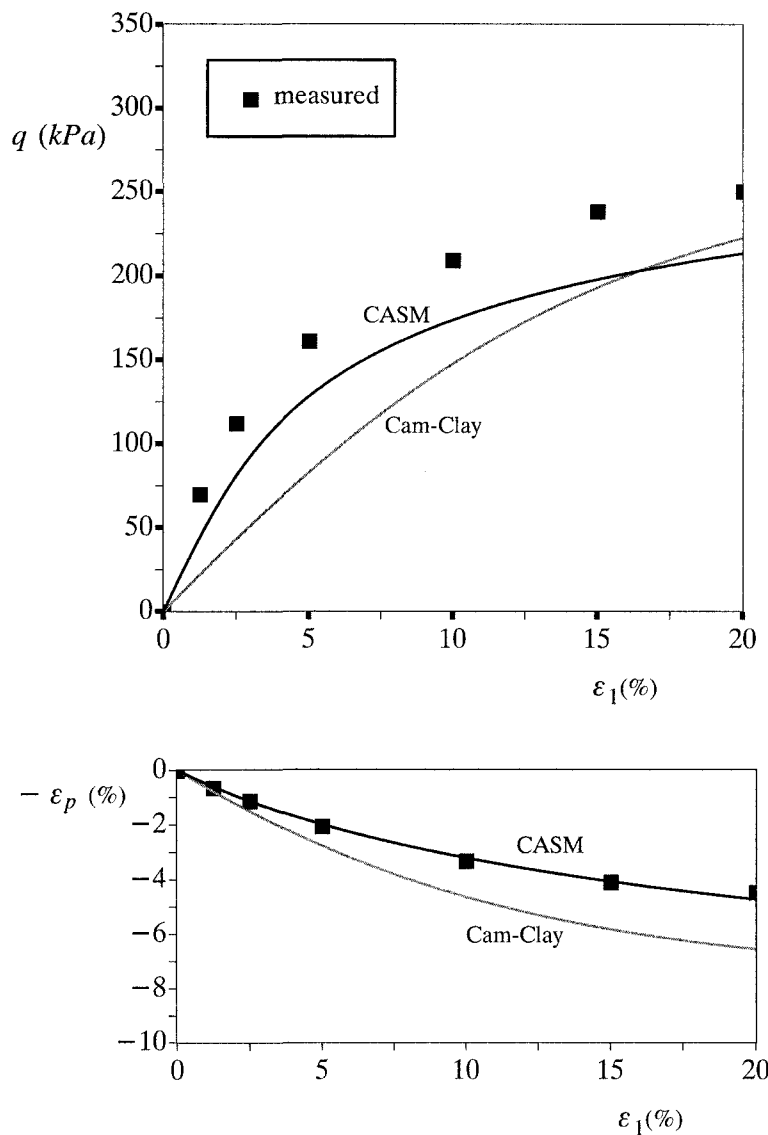


Figure 6.15: Model prediction for drained compression of a normally consolidated sample of Weald clay (OCR=1,  $v_0 = 1.632$ ,  $p_0 = 207\text{kPa}$ )

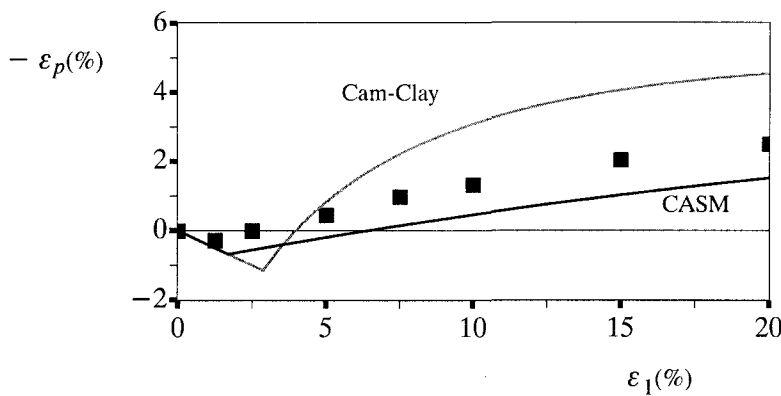
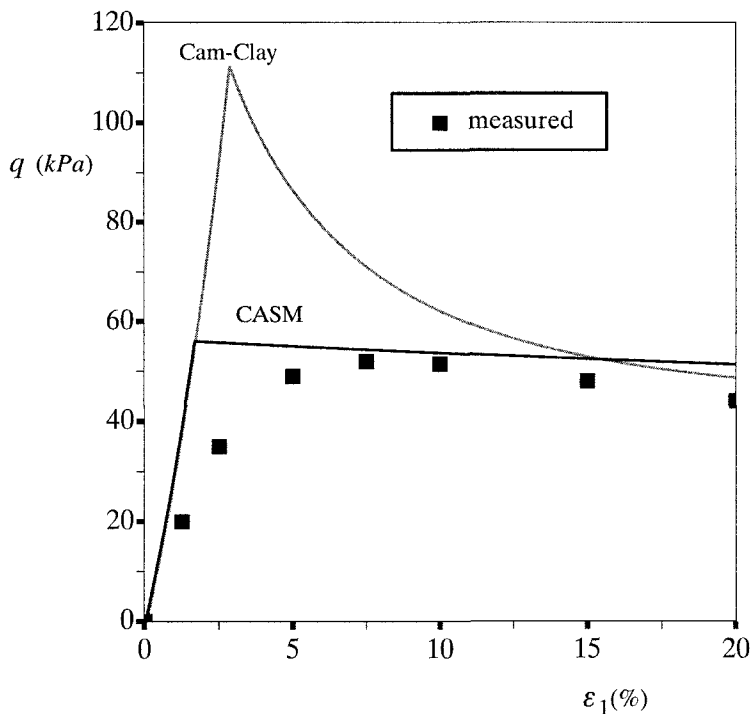


Figure 6.16: Model prediction for drained compression of a heavily overconsolidated sample of Weald clay (OCR=24,  $v_0 = 1.617$ ,  $p_0 = 34.5 kPa$ )

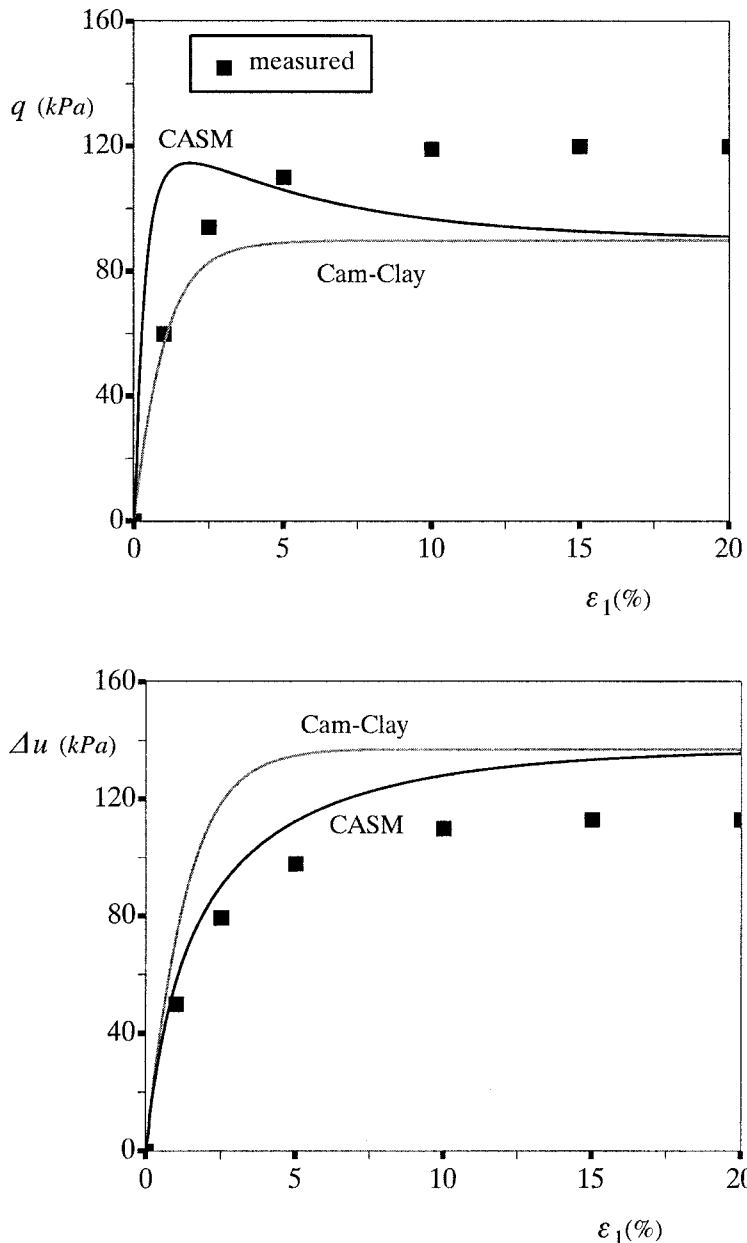


Figure 6.17: Model prediction for undrained compression of a normally consolidated sample of Weald clay ( $OCR=1$ ,  $v_0 = 1.632$ ,  $p_0 = 207kPa$ )

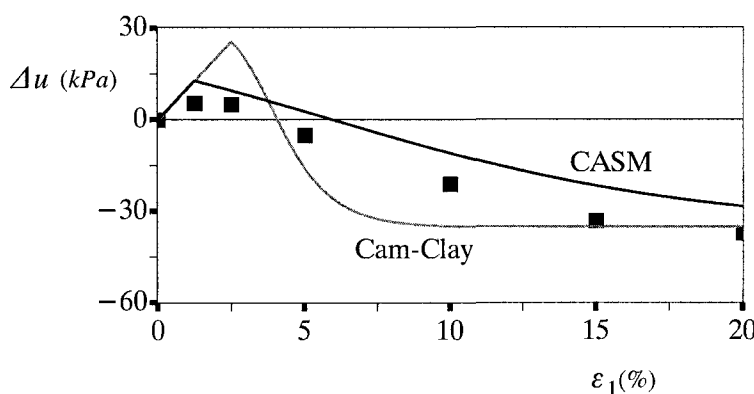
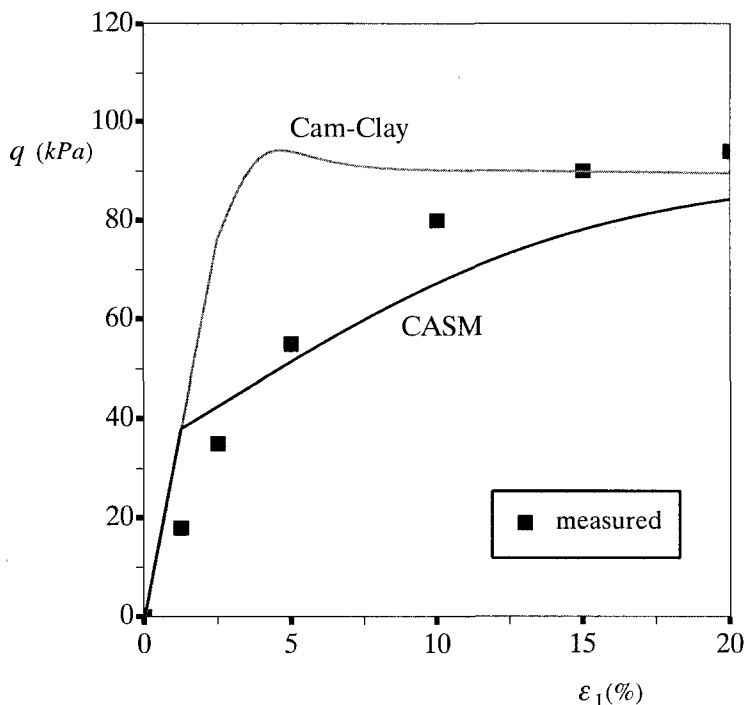


Figure 6.18: Model prediction for undrained compression of a heavily overconsolidated sample of Weald clay (OCR=24,  $v_0 = 1.617$ ,  $p_0 = 34.5kPa$ )

### *Drained behaviour of loose, medium and dense Sands*

To check the performance of CASM for sand, test data reported by Been *et al.* (1991) and Jefferies (1993) on a predominantly quartz sand with a trace of silt known as Erksak 330/0.7 will be used. Three tests are selected to compare with CASM. These tests are on the densest sample D667 (with a relative density of 70%), the loosest sample D684 (with a relative density of 5%) and a medium dense sample D662.

The material constants used in the CASM predictions are as follows:

$$\lambda = 0.0135, \Gamma = 1.8167, \nu = 0.3, \alpha = 0.005, M = 1.2, \xi_R = 0.075, n = 4.0$$

In order to allow for the prediction for sands from the loosest to the densest states, the reference state parameter  $\xi_R$  for CASM is assumed to be equal to the initial state parameter of the loosest sample D684. The critical state constants for Erksak sand are from Been *et al.* (1991) and Jefferies (1993). As for Weald clay, accurate elastic constants are not known for Erksak sand and some typical values are used in the prediction.

Figure 6.19 to Figure 6.21 present comparisons of the predictions and the measured behaviour for tests on samples D667, D662 and D684 respectively. It is clear from these figures that overall CASM is quite satisfactory for predicting measured behaviour on loose, medium and dense sands. It is noted that one obvious deficiency with CASM is that it tends to under-predict the shear strain at peak strength. This is mainly due to the fact that, like Cam clay, CASM does not allow any plastic deformation to develop within the state boundary surface. As will be discussed later, CASM can be readily modified to include some additional strain within the main yield surface, which should lead to an even better agreement between the predicted and the measured stress-strain behaviour.

### *Undrained behaviour of very loose sand*

The term 'very loose' is used here to describe sand in a state which is much looser than its critical state. It is well known that very loose sands can collapse and strain soften during monotonic undrained loading and ultimately reach a critical (or steady) state. During monotonic undrained loading loose sand reaches a peak resistance and then rapidly strain softens to a steady state, and this is a condition necessary for liquefaction to occur. As discussed in the introduction, most existing critical state models, such as Cam clay and Nor-Sand, are unable to model this behaviour.

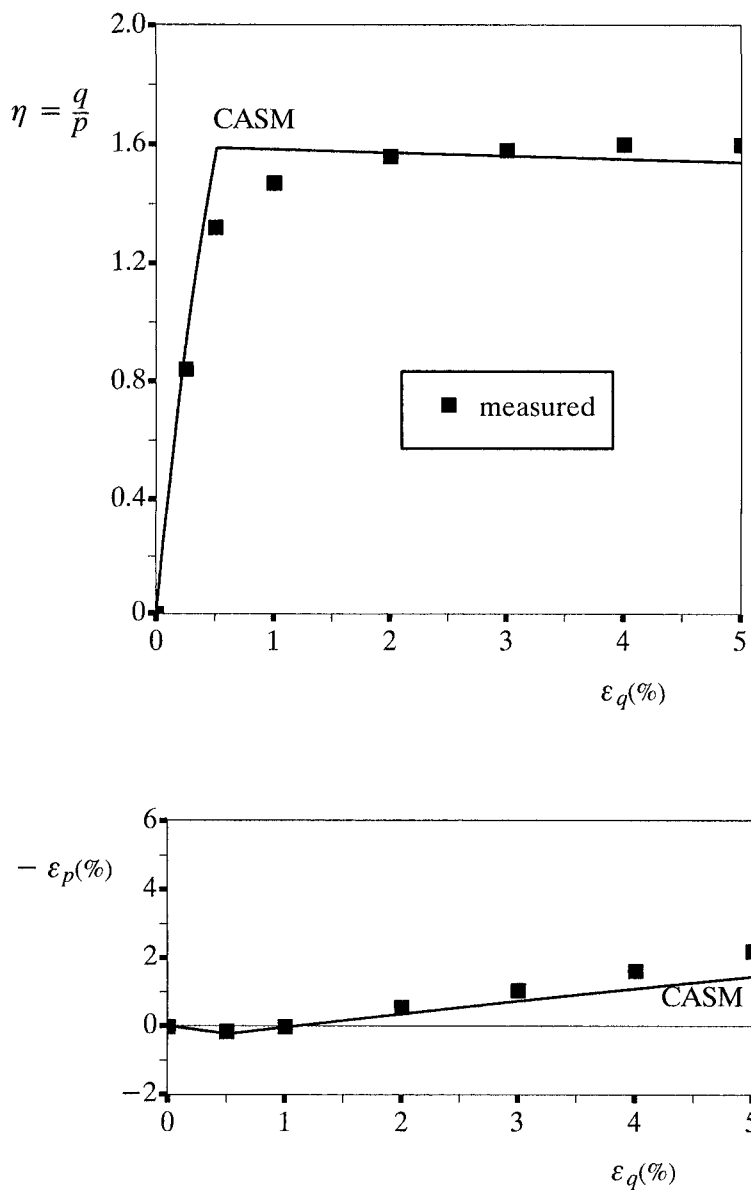


Figure 6.19: Model prediction for drained compression of a very dense sample of Erksak 330/0.7 sand (D667:  $v_0 = 1.59$ ,  $p_0 = 130kPa$ )

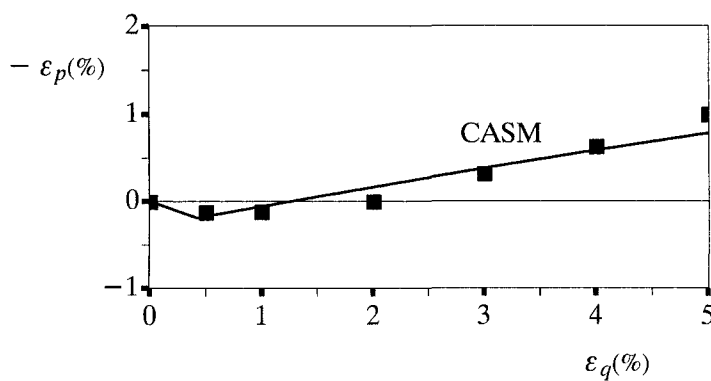
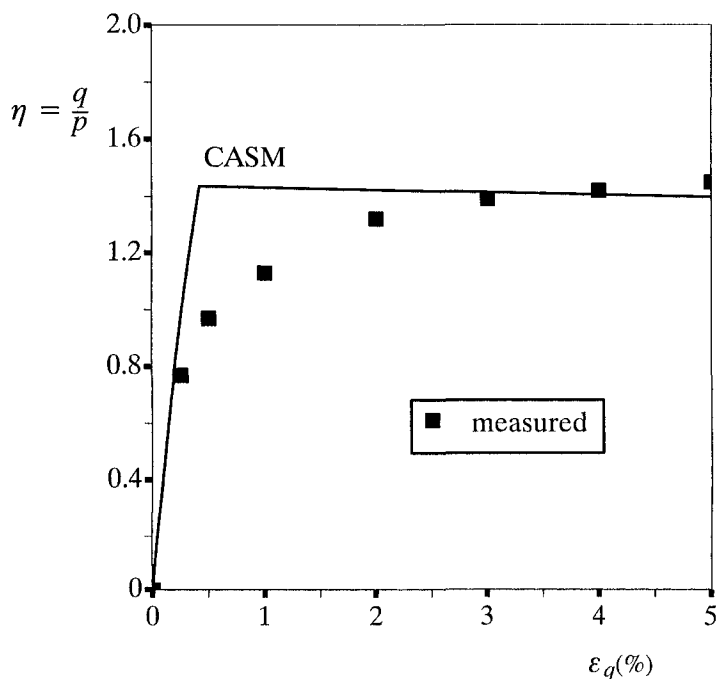


Figure 6.20: Model prediction for drained compression of a medium dense sample of Erksak 330/0.7 sand (D662:  $v_0 = 1.677$ ,  $p_0 = 60kPa$ )

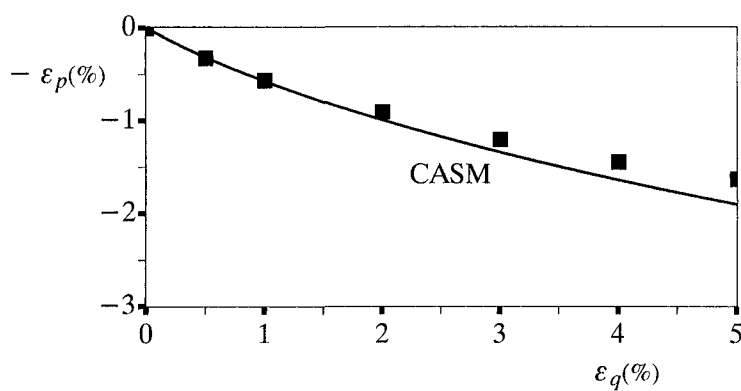
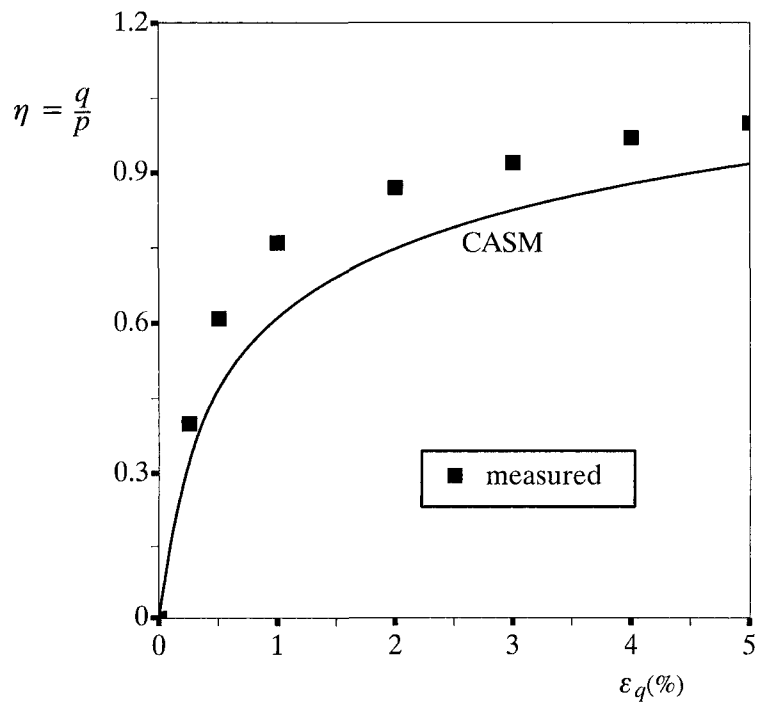


Figure 6.21: Model prediction for drained compression of a very loose sample of Erksak 330/0.7 sand (D684:  $v_0 = 1.82$ ,  $p_0 = 200kPa$ )

To demonstrate the applicability of CASM for modelling undrained behaviour of a very loose sand, test data obtained by Sasitharan *et al.* (1994) on Ottawa sand is used. Four tests have been selected by Yu (1998) to compare with CASM. These tests are on samples with initial void ratios of 0.793 and 0.804. Different initial mean effective stresses were used in these tests.

The material constants used in the CASM predictions are as follows:

$$\lambda = 0.0168, \Gamma = 1.864, \nu = 0.3, \kappa = 0.005, M = 1.19, \xi_R = \xi_0, n = 3.0$$

The critical state constants for Ottawa sand are from Sasitharan *et al.* (1994). Again accurate elastic constants are not known for this sand and some typical values have to be used in the prediction. When CASM is used to model the undrained behaviour of a very loose sand, the reference state parameter  $\xi_R$  can be assumed to be equal to the initial state parameter of each sample. As will be shown below, this assumption proves to be very satisfactory for predicting undrained behaviour of very loose sands.

Figure 6.22 shows a comparison of the CASM prediction and the measured behaviour for undrained tests on one of these four very loose samples ( $\nu_0 = 1.793$ ,  $p_0 = 475kPa$ ). It is evident that CASM can be satisfactorily used to predict the measured behaviour of undrained tests on very loose sands. In particular, CASM predicts that the peak strength is developed at a very small axial strain and afterwards the response shows a marked strain softening with increase in axial strain before approaching the critical state.

### 6.5.6 Remarks

This section presents a simple and unified formulation of the constitutive equations for both clay and sand. From a practical point of view, this is particularly advantageous since when applied in the numerical analysis of a boundary value problem, only different material constants need to be incorporated either for clay or sand, and the form of the constitutive equations remains the same. The present model, CASM, has been developed by using a general stress ratio-state parameter relation as the yield surface. Rowe's stress-dilatancy relation is used as the plastic potential and the resulting plastic flow rule is therefore non-associated. Compared with Cam clay, only one new material constant has been introduced in CASM. In addition, the original Cam-clay yield surface has been shown to be a special case of the yield locus assumed in CASM. Comparisons with experimental data suggest that CASM is able to capture the overall behaviour of clay and sand observed under both drained and undrained loading conditions, and therefore represents a useful extension of Cam clay that is known to be only valid for normally consolidated clays.

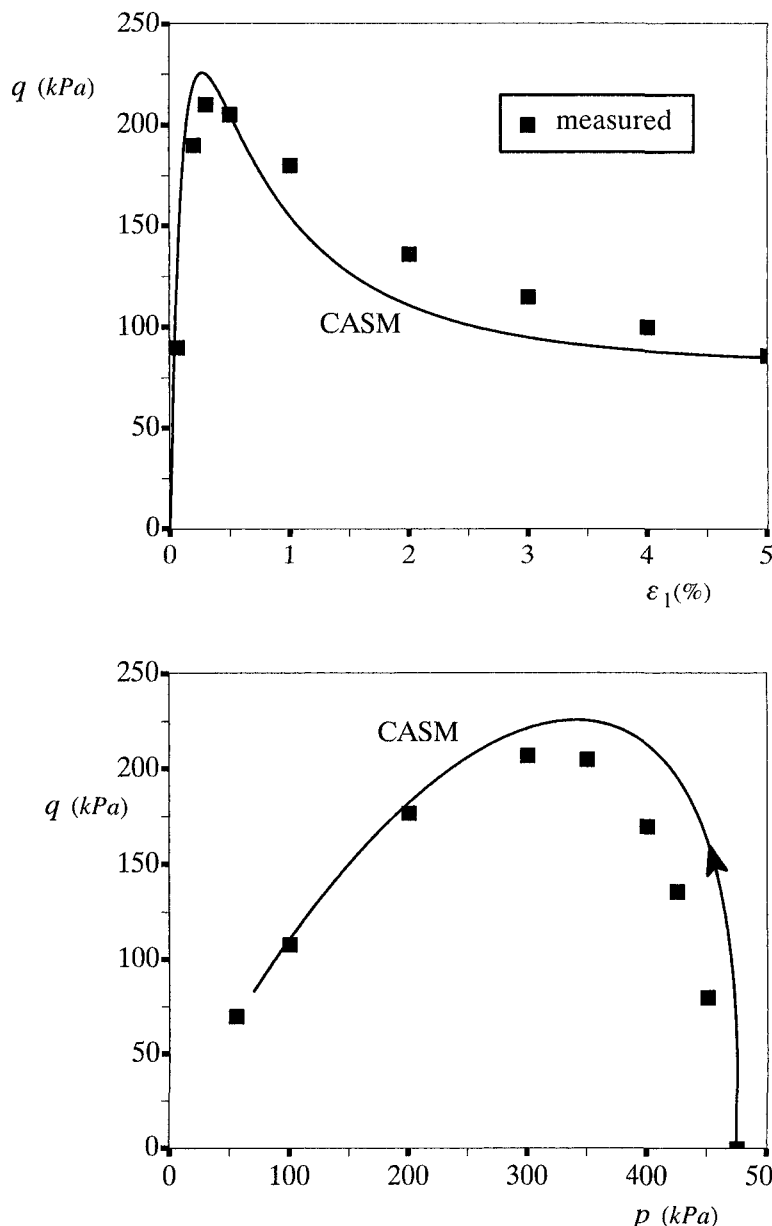


Figure 6.22: Model prediction for undrained compression of a very loose Ottawa sand ( $v_0 = 1.793$ ,  $p_0 = 475kPa$ )

Like Cam clay, CASM assumes that no plastic deformation is allowed to occur within the state boundary surface (or the yield surface). As shown in the previous section, this idealization tends to under-predict the shear strain at peak strength for both sand and overconsolidated clays. This fact is particularly important if the model is applied to the behaviour of soils subjected to cyclic loading. This limitation can, however, be overcome by allowing plastic strains to develop within the main yield or bounding surface (e.g. Pender, 1978; Dafalias and Herrmann, 1980; Carter *et al.*, 1982; Bardet, 1986; and Naylor, 1985). In particular, Zienkiewicz *et al.* (1985) showed that the bounding surface plasticity concept can be easily used to modify the standard critical state plasticity models for modelling cyclic loading problems. On the other hand, Naylor (1985) proposed a simple 'continuous plasticity' model to include some additional strains within the state boundary surface. If required, some of these more complex features can be easily introduced into CASM to improve the model prediction. This will be discussed in Chapter 7.

## 6.6 EXTENSION OF CASM TO INCLUDE SHEAR HARDENING

The formulation of the unified model CASM, presented so far, is based on the volumetric hardening law used in critical state soil mechanics. For some situations, however, volumetric hardening alone cannot predict measured behaviour. A particular example is that for loose sand under undrained shear conditions the shear stress tends to reach a peak followed by a softening process before increasing again. This well-known behaviour may not be predicted using the model with a volumetric hardening.

One effective approach to the modelling of this type of behaviour is to adopt a combined volumetric and shear hardening in the formulation (e.g. Wilde, 1977; Nova and Wood, 1979). Here it is shown that such a combined hardening law can be easily incorporated into the unified critical state model CASM. Instead of the volumetric hardening law, we use the following combined hardening law

$$dp_0 = \frac{\nu p_0}{\lambda - \kappa} (d\epsilon_p^p + \omega d\epsilon_q^p) \quad (6.69)$$

where  $\omega$  is a model constant. It is obvious that when  $\omega = 0$  the above equation reduces to the usual volumetric hardening law.

By using a stress-dilatancy relation such as Rowe's equation, equation (6.69) becomes

$$dp_0 = \frac{\nu p_0}{\lambda - \kappa} d\epsilon_p^p \left( 1 + \frac{9 + 3M - 2M\eta}{9(M - \eta)} \omega \right) \quad (6.70)$$

which means that the size of the yield surface varies not only with plastic volumetric strain but also with the stress ratio  $\eta$ .

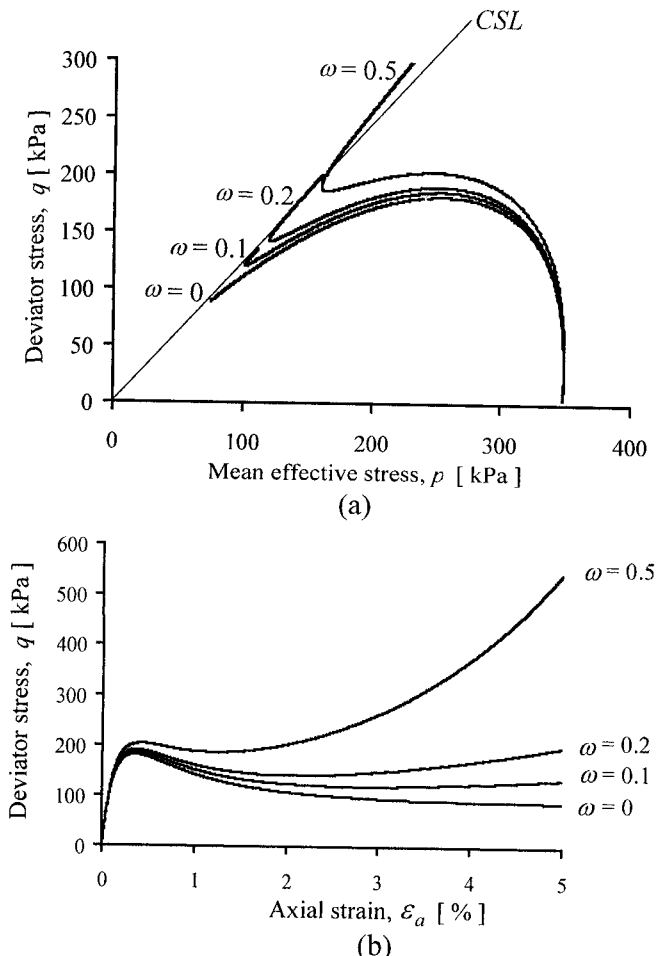


Figure 6.23: Effect of combined hardening on the predicated undrained triaxial stress paths and stress-strain response of a loose sand (after Yu *et al.*, 2005)

By following the usual procedure, the plastic modulus can be derived as

$$H = - \frac{\partial f}{\partial p_0} \frac{\partial p_0}{\partial \varepsilon_p^p} \frac{\partial g}{\partial p} \quad (6.71)$$

$$= \frac{\nu}{(\lambda - \nu) \ln r} \left( 1 + \frac{9 + 3M - 2M\eta}{9(M - \eta)} \omega \right) \frac{\partial g}{\partial p} \quad (6.72)$$

The term  $\partial g / \partial p$  is readily determined as long as the plastic potential is chosen. The incremental stress-strain relations are then written as follows

$$d\epsilon_p = \frac{dp}{K} + \frac{g_p}{H} \times [(f_p + f_{,\xi} \xi_p) dp + f_{,q} dq] \quad (6.73)$$

$$d\epsilon_q = \frac{dq}{3G} + \frac{g_p}{H} \times [(f_p + f_{,\xi} \xi_p) dp + f_{,q} dq] \quad (6.74)$$

This slightly revised CASM model has been termed by Yu *et al.* (2005) and Khong (2004) as CASM-d.

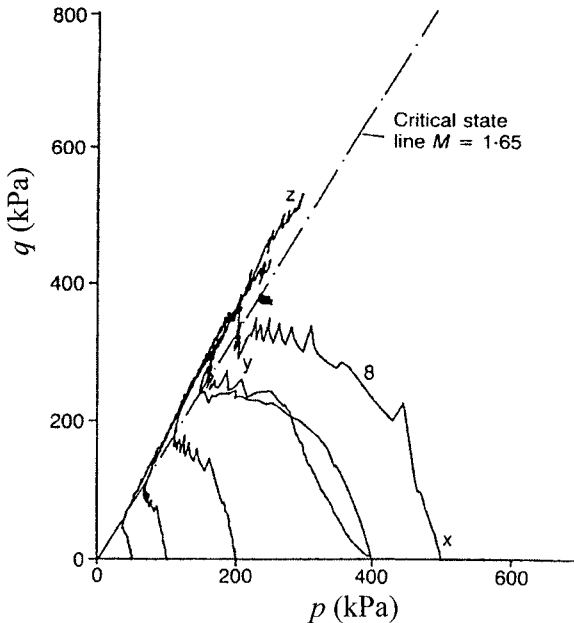


Figure 6.24: Undrained triaxial stress paths of a loose Dogs Bay sand (after Coop, 2000)

The effect of the additional model constant  $\omega$  on predicted stress paths and stress-strain response is shown in Figure 6.23. It is clear from this figure that CASM-d is able to predict the measured behaviour of undrained compression of a very loose sand reported by many researchers. An example of such experimental

data is plotted in Figure 6.24 for loose Dogs Bay sand (Coop, 2000). More experimental results were given by Yu *et al.* (2005) and Wang (2005) for other sands.

## 6.7 EXTENSION OF CASM TO INCLUDE VISCOPLASTICITY

As discussed by Oka (2005), several attempts have also been made to extend critical state models to simulate time-dependent stress-strain behaviour of soils, particularly in clays. Notable examples are Adachi and Oka (1982), Borja and Kavazanjian (1985), Kutter and Sathialingam (1992) and Yin and Graham (1999). These studies are based on the early work on creep of clay by Bjerrum (1967) and the fundamental viscoplasticity concepts developed by Perzyna (1963, 1966).

In this section, the approach proposed by Yin and Graham (1999) is used to extend the unified critical state model CASM to model time-dependent stress-strain behaviour.

We start off by following Perzyna (1963, 1966) to assume that the total strain rate  $\dot{\varepsilon}_{ij}$  is the sum of the elastic strain rate  $\dot{\varepsilon}_{ij}^e$  and visco-plastic (or creep) strain rate  $\dot{\varepsilon}_{ij}^{vp}$ , namely

$$\dot{\varepsilon}_{ij} = \dot{\varepsilon}_{ij}^e + \dot{\varepsilon}_{ij}^{vp} \quad (6.75)$$

The elastic strain rate tensor is linked to the stress rate tensor in the usual manner, which will not be repeated here. Following Perzyna (1963, 1966) and Yin and Graham (1999), we assume that the visco-plastic strain rate tensor is defined by the following associated flow rule:

$$\dot{\varepsilon}_{ij}^{vp} = A \frac{\partial f}{\partial \sigma_{ij}} \quad (6.76)$$

where  $A$  is a scaling function and  $f$  is referred to as a flow surface function which may be assumed to be the same as the yield function.

As shown by Yin and Graham (1999), the elastic visco-plastic constitutive relationship under an isotropic loading condition ( $q = 0, p = p_0$ ) can be expressed as follows

$$\dot{\varepsilon}_{pm} = \dot{\varepsilon}_{pm}^e + \dot{\varepsilon}_{pm}^{vp} = \frac{\varkappa/v}{p_0} \dot{p}_0 + \frac{\psi/v}{t_0} \exp[-(\varepsilon_{pm} - \varepsilon_{pm0}^{ep}) \frac{v}{\psi}] \left( \frac{p_0}{p_{0i}} \right)^{\lambda/\psi} \quad (6.77)$$

where  $v$  is the specific volume of the soil, and  $\varkappa, \psi, t_0, \lambda, p_{0i}$  and  $\varepsilon_{pm0}^{ep}$  are five material constants. The definitions and experimental determination of these constants can be found in Yin and Graham (1999). In particular,  $\psi$  and  $t_0$  are linked by an ex-

pression for creep strains under an isotropic effective stress starting from a reference time line:

$$\varepsilon_{pm}^{vp} = \frac{\psi}{\nu} \ln\left(\frac{t_0 + t_e}{t_0}\right) \quad (6.78)$$

where the reference time  $t_e$  is a creep load duration measured from the reference time line.

In equation (6.77), the visco-plastic strain rate is for soils under isotropic effective stress  $p_0$ , which can be further written as follows

$$\dot{\varepsilon}_{pm}^{vp} = \frac{\psi/\nu}{t_0} \exp\left\{[-(\varepsilon_{pm} - \varepsilon_{pm0}^{ep}) + \frac{\lambda}{\nu} \ln(\frac{p_0}{p_{0i}})] \frac{\nu}{\psi}\right\} \quad (6.79)$$

Now if the yield surface of CASM is selected as a flow function in equation (6.76), we have

$$f(p, q, p_0) = \left(\frac{q}{Mp}\right)^n + \frac{\ln \frac{p}{p_0}}{\ln r} = 0 \quad (6.80)$$

The volumetric and deviatoric visco-plastic strain rates can then be written as follows

$$\dot{\varepsilon}_p^{vp} = A \frac{\partial f}{\partial p} = A \left[ \frac{1 - \ln(\frac{p_0}{p})^n}{p \ln r} \right] \quad (6.81)$$

$$\dot{\varepsilon}_q^{vp} = A \frac{\partial f}{\partial q} = A \left[ \frac{nq^{n-1}}{M^n p^n} \right] \quad (6.82)$$

A further assumption made by Yin and Graham (1999) is that the visco-plastic volumetric strain rate for any stress point on a yield surface is equal to the volumetric visco-plastic strain under the corresponding isotropic loading condition. Therefore equating (6.79) and (6.81) leads to the scaling function  $A$

$$A = \frac{\psi/\nu}{t_0} \exp\left\{[-(\varepsilon_{pm} - \varepsilon_{pm0}^{ep}) + \frac{\lambda}{\nu} \ln(\frac{p_0}{p_{0i}})] \frac{\nu}{\psi}\right\} \times \frac{p \ln r}{1 - \ln(\frac{p_0}{p})^n} \quad (6.83)$$

with which the visco-plastic strain rates at any stress state on the yield surface are fully determined by equations (6.81) and (6.82).

## 6.8 EXTENSION OF CASM FOR UNSATURATED SOILS

The study of stress-strain behaviour of partially saturated soils has been an important subject for many years. Important early contributions include those by Bishop

and Donald (1961), Coleman (1962), and Fredlund and Morgenstern (1977), which led to a conclusion that any pair of stress fields among the following three stress states

$$(\sigma_{ij} - u_a \delta_{ij}) , \quad (\sigma_{ij} - u_w \delta_{ij}) , \quad (u_a - u_w) \delta_{ij}$$

as a suitable stress framework to describe the stress-strain behaviour of partially saturated soils. In these expressions,  $u_a$  and  $u_w$  denote the air and water pressure and  $\delta_{ij}$  is the Kronecker delta (which is equal to 1 when  $i=j$  and 0 otherwise). Here let us consider use the following two stress variables in our development:

$$\sigma_{ij}' = \sigma_{ij} - u_a \delta_{ij} \quad (6.84)$$

$$s = u_a - u_w > 0 \quad (6.85)$$

which are known to be the net stresses and suction respectively.

Although many constitutive models have been proposed over the years for partially saturated soils, perhaps the most influential one has been the critical state model developed by Alonso *et al.* (1990). This model has been used as the basis for several later extensions (e.g. Wheeler and Sivakumar, 1995; Cui and Delage, 1996). To extend CASM to partially saturated soils, we will also largely follow the framework proposed by Alonso *et al.* (1990).

### 6.8.1 Elastic strains

It is assumed that changes of both stress and suction within the yield surfaces are accompanied by recoverable deformations. For simplicity, the soil is regarded an isotropic, elastic material before reaching the yield surfaces. As shown in Figure 6.25, the elastic volumetric strain increment includes contributions from both stress change and suction change, namely

$$d\epsilon_p^e = \frac{\varkappa}{v} \frac{dp}{p} + \frac{\varkappa_s}{v} \frac{ds}{s} \quad (6.86)$$

where  $\varkappa$  and  $\varkappa_s$  are defined in Figure 6.25.

On the other hand, the elastic deviatoric strain increment is the same as the fully saturated soils

$$d\epsilon_q^e = \frac{dq}{3G} \quad (6.87)$$

where  $G$  is the soil shear modulus.

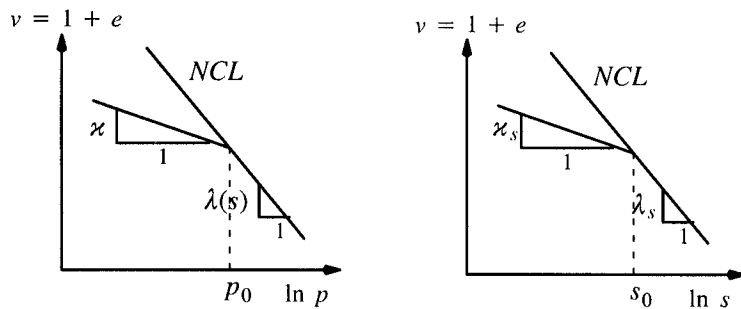


Figure 6.25: Normal consolidation and swelling lines for both net stress and suction

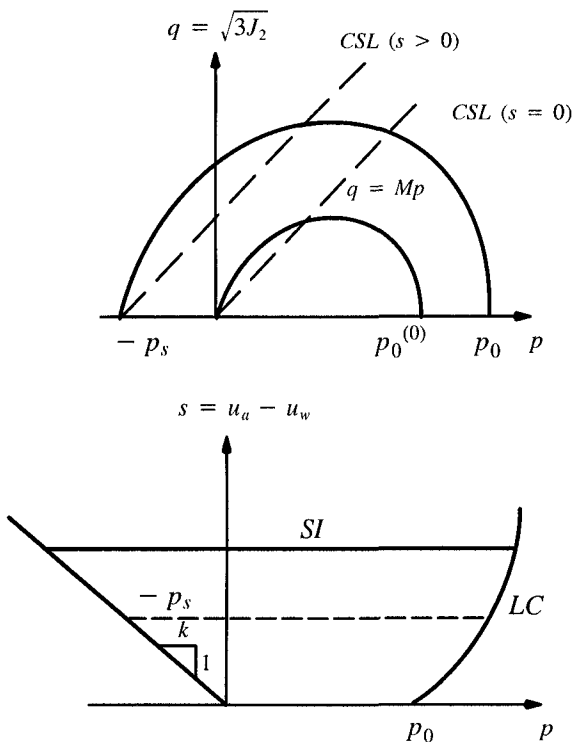


Figure 6.26: Yield surfaces for partially saturated soils

### 6.8.2 Yield surfaces

Due to the effects of both pressure and suction in partially saturated soils, it proves to be convenient to define two separate yield surfaces. The first, known as the loading collapse (LC) yield surface is related to the plastic compression that can occur on increase of stresses or decrease of suction (wetting)

$$f_1 = f(p, q, s, p_0) = \left[ \frac{q}{M(p + ks)} \right]^n + \frac{1}{\ln r} \ln \frac{p + ks}{p_0 + ks} = 0 \quad (6.88)$$

where  $M$  is the slope of the critical state line in a  $q$ - $p$  space, and  $k$  is defined in Figure 6.26. Following Alonso *et al.* (1990), we further assume that the LC in a  $p$ - $s$  space takes the following form

$$\frac{p_0}{p^c} = \left( \frac{p_0^{(0)}}{p^c} \right)^\omega \quad (6.89)$$

where  $p^c$  is a reference stress and  $\omega$  is given by

$$\omega = \frac{\lambda(0) - \kappa}{\lambda(s) - \kappa} \quad (6.90)$$

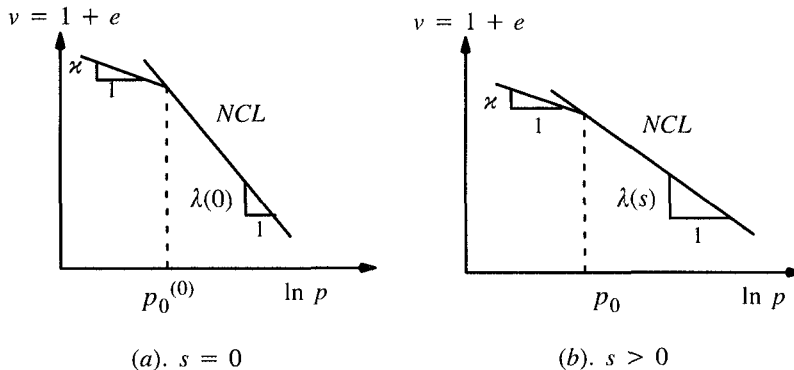


Figure 6.27: Normal consolidation and swelling lines for (a) zero suction and (b) positive suction

As shown in Figure 6.27, the slope of the normal consolidation line varies with suction. Experimental work suggests that the variation may be expressed by the following equation

$$\frac{\lambda(s)}{\lambda(0)} = (1 - \alpha) \exp(\beta s) + \alpha \quad (6.91)$$

in which  $\alpha$  and  $\beta$  are two additional material constants that can be determined experimentally.

The second yield surface, known as the suction increase (SI) yield surface (see Figure 6.26), is related to the plastic compression that can occur on increase of suction  $s$  (drying)

$$f_2 = f(s, s_0) = s - s_0 = 0 \quad (6.92)$$

where  $s_0$  is the maximum previously attained value of the suction.

### 6.8.3 Stress-dilatancy relation and plastic potentials

#### *Loading collapse plastic potential*

To determine the plastic strains, we may specify a plastic potential associated with each yield surface. Associated with the first yield surface, we adopt a plastic potential that is in a similar form to our yield function but that must give zero plastic volumetric strain increment at critical states. One such form is a slight modification of the stress-dilatancy equation (6.56)

$$\frac{d\epsilon_p^p}{d\epsilon_q^p} = \frac{M^n - \eta^n}{m \eta^{n-1}} \quad (6.93)$$

where

$$\eta = \frac{q}{p + ks} \quad (6.94)$$

and  $n$  is a material constant defined previously in Yu's unified critical state model CASM. For zero suction and  $n=2$ ,  $m=1$ , the above stress-dilatancy relation (6.93) reduces to the well-known plastic flow rule of modified Cam clay.

A useful approach is to choose  $m$  so that equation (6.93) can accurately model one-dimensional consolidation. Following the procedure used by Ohmaki (1982) and Alonso *et al.* (1990), we obtain

$$m = \frac{2}{3} \times \frac{\lambda}{\lambda(0) - \alpha} \times \frac{[M(6 - M)]^n - (3M)^n}{(6 - M)(3M)^{n-1}} \quad (6.95)$$

which includes the expression used by Alonso *et al.* (1990) and McDowell and Hau (2003) as a special case when  $n=2$ .

The plastic flow rule defined in (6.93) can be used to derive the plastic potential given below

$$g_1 = m \ln[1 + (m - 1)(\frac{\eta_s}{M})^n] + n(m - 1) \ln \frac{p + ks}{C} \quad (6.96)$$

where C is a size parameter that can be evaluated by solving equation (6.96) from a given state of stresses and suction and

$$\eta_s = \frac{q}{p + ks} \quad (6.97)$$

### *Suction increase plastic potential*

For determining suction induced plastic strains, we assume that an associated plastic flow rule is adequate, namely

$$g_2 = f_2 = g(s, s_0) = s - s_0 = 0 \quad (6.98)$$

#### 6.8.4 Plastic strains

If the stress state is on the LC yield surface, both volumetric and shear plastic strains will be induced,

$$d\epsilon_p^p = d\lambda_1 \frac{\partial g_1}{\partial p} \quad (6.99)$$

$$d\epsilon_q^p = d\lambda_1 \frac{\partial g_1}{\partial q} \quad (6.100)$$

If the stress state is on the SI yield surface, then only volumetric plastic strains will be induced,

$$d\epsilon_p^p = d\lambda_2 \frac{\partial g_2}{\partial s} \quad (6.101)$$

$$d\epsilon_q^p = 0 \quad (6.102)$$

If the stress state lies on both LC and SI yield surfaces (corners), then the assumption made by Koiter (1953) will be used,

$$d\epsilon_p^p = d\lambda_1 \frac{\partial g_1}{\partial p} + d\lambda_2 \frac{\partial g_2}{\partial s} \quad (6.103)$$

$$d\epsilon_q^p = d\lambda_1 \frac{\partial g_1}{\partial q} \quad (6.104)$$

where  $d\lambda_1$  and  $d\lambda_2$  are positive multipliers that can be determined using Prager's consistency condition.

#### 6.8.5 Hardening Laws

Similar to other critical state models for saturated soils, the following hardening laws are assumed for partially saturated soils

$$dp_0^{(0)} = \frac{\nu p_0^{(0)}}{\lambda(0) - \kappa} d\epsilon_p^p \quad (6.105)$$

$$ds_0 = \frac{\nu s_0}{\lambda_s - \kappa_s} d\epsilon_p^p \quad (6.106)$$

## 6.9 EXTENSION OF CASM FOR BONDED GEOMATERIALS

The study of stress-strain behaviour of bonded or cemented soils and weak rock has been an important subject for the last fifteen years. Notable contributions include those by Leroueil and Vaughan (1990), Burland (1990), Elliot and Brown (1985), Gens and Nova (1993), Coop and Atkinson (1993), Huang and Airey (1993), Liu and Carter (1999), Schnaid *et al.* (2001) and Jiang *et al.* (2006) among others.

Leroueil and Vaughan (1990) demonstrate the importance of comparing the observed behaviour of a bonded or structured material with that of the equivalent unbonded one. In terms of theoretical developments, the work of Gens and Nova (1993) is particularly significant as it proposes a sound theoretical framework for developing useful critical state models for bonded materials. In particular this framework accounts for the important effects of bonding on yield surfaces and degradation of bonding during loading processes.

In this section, the formulation of the critical state model CASM is extended to simulate the behaviour of bonded materials. The basic framework of Gens and Nova (1993) is further developed by adopting a general cohesive-frictional plastic flow rule that is able to account for the observed delayed dilation due to the presence of bonding (Schnaid *et al.*, 2001; Coop and Atkinson, 1993).

### *Yield surface for bonded materials*

Following Gens and Nova (1993), the yield surface is assumed to enlarge with increasing amount of bonding in the soil. For simplicity and also to be conservative, we neglect any tensile strength that the soil may have due to the presence of bonding in selecting a yield surface (i.e. the yield surface passes through the origin). If needed, however, this tensile strength can be readily included (e.g. Tan, 2006).

Figure 6.28 shows the normal consolidation lines and yield surfaces for both unbonded material and bonded materials with various amounts of bonding. Mathematically, the yield surface for a bonded material with a given amount of bonding can be expressed as follows:

$$f(p, q, p_c) = \left(\frac{q}{Mp}\right)^n + \frac{\ln \frac{p}{p_c}}{\ln r} = 0 \quad \text{and} \quad p_c = p_0 + p_b \quad (6.107)$$

where  $p_b$  is a material parameter representing the increased size of the yield surface due to soil bonding. It is noted that this quantity will decrease with loading when bonding is gradually damaged. When all bonding is broken,  $p_b$  should be zero.

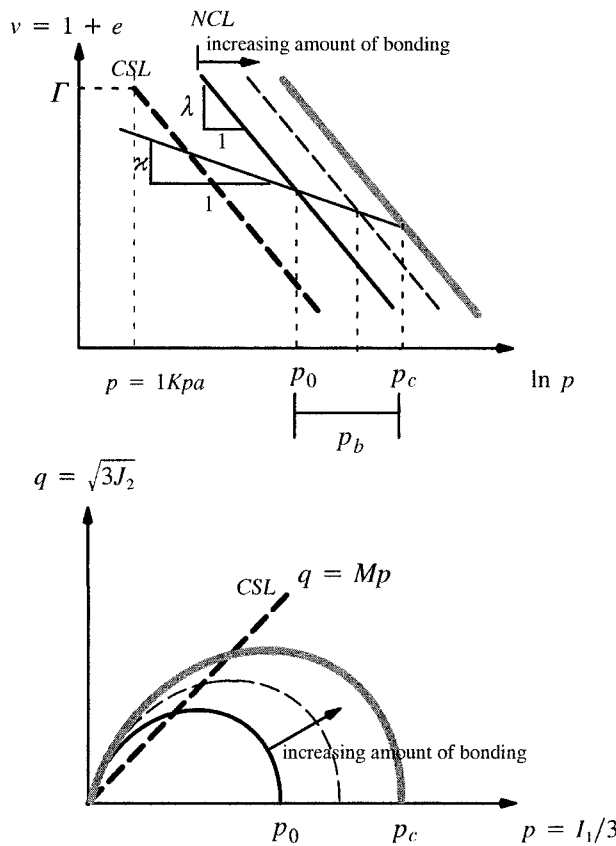


Figure 6.28: The normal consolidation lines (NCL), critical state lines (CSL) and yield surfaces for both unbonded and bonded materials

#### *Plastic flow rule and plastic potential for bonded materials*

As discussed by Gens and Nova (1993), the presence of bonding tends to generate a cohesion  $c$  in the soil. Whilst this cohesion increases the size of the yield surface, it also inhibits the dilation of soil (e.g. Coop and Atkinson, 1993; Schnaid *et al.*, 2001). In terms of energy this is because the total work done by the stresses at the boundary of an element is partly dissipated in friction and partly in disrupting the

bonding. In fact, Rowe (1963) proposes a stress-dilatancy relation that takes into account the effect of soil cohesion on dilation.

Rowe's general cohesive-frictional stress-dilatancy relation may be integrated to give the following plastic potential:

$$g(p, q) = 3M \ln\left(\frac{p - k}{C}\right) + (3 + 2M) \ln\left[\frac{2(q - h)}{p - k} + 3\right] - (3 - M) \ln\left[3 - \frac{q - h}{p - k}\right] = 0 \quad (6.108)$$

where  $k$  and  $h$  are related to soil cohesion  $c$  by the following expressions

$$k = \frac{\sqrt{(3 + 2M)(3 - M)} (36 - 12M)c}{18M^2 - 27M - 81} \quad (6.109)$$

$$h = \frac{\sqrt{(3 + 2M)(3 - M)} (-54 + 18M)c}{18M^2 - 27M - 81} \quad (6.110)$$

and the size parameter  $C$  can be determined for any given stress state  $(p, q)$  by solving equation (6.108) in the usual manner.

#### *Plastic hardening and bonding degradation laws*

During the loading of a bonded material, the bonding is gradually damaged. As a result, the cohesion  $c$  and the increased size of the yield surface  $p_b$  will also reduce. The yield surface for an unbonded material will change with plastic strains in the usual manner. Either a volumetric hardening law or a combined volumetric and shear hardening law can be used for this purpose. If a combined hardening is adopted, then we have

$$\frac{dp_0}{p_0} = \frac{\nu}{\lambda - \nu} [d\varepsilon_p^p + \omega d\varepsilon_q^p] \quad (6.111)$$

which reduces to the usual volumetric hardening law if we set  $\omega = 0$ .

The reduction of both soil cohesion  $c$  and the increased size of the yield surface  $p_b$  is assumed to depend on both the volumetric and deviatoric plastic strains. Hence

$$\frac{dp_b}{p_b} = -D_b \sqrt{[\omega_d (d\varepsilon_p^p)^2 + (d\varepsilon_q^p)^2]} \quad (6.112)$$

$$\frac{dc}{c} = -D_c \sqrt{[\omega_d (d\varepsilon_p^p)^2 + (d\varepsilon_q^p)^2]} \quad (6.113)$$

where  $\omega_d, D_b$  and  $D_c$  are three additional model constants for bonded geomaterials when compared with the unbonded CASM model. If, for simplicity, we can assume

that the degradation of bonding is brought about purely by plastic shear strains, then  $\omega_d$  can be set to zero. In this case, only two new model constants need to be determined for modelling bonded materials. Of course, the initial values of soil cohesion and  $p_b$  will have to be estimated for a given bonded geomaterial.

## 6.10 FORMULATIONS FOR GENERAL STRESS STATES

The generalization of the triaxial plasticity formulations given in the previous sections to a general three-dimensional stress state is presented in this section. Our presentation is based on the work of Yu and Khong (2002) and Khong and Yu (2002). For a general three-dimensional stress state, a suitable pair of stress variables is

$$p = \frac{1}{3}(\sigma_{xx} + \sigma_{yy} + \sigma_{zz}) \quad (6.114)$$

$$q = \left\{ \frac{1}{2}[(\sigma_{xx} - \sigma_{yy})^2 + (\sigma_{yy} - \sigma_{zz})^2 + (\sigma_{zz} - \sigma_{xx})^2] + 3(\sigma_{xy}^2 + \sigma_{yz}^2 + \sigma_{zx}^2) \right\}^{\frac{1}{2}} \quad (6.115)$$

where  $\sigma_{xx}$ ,  $\sigma_{yy}$ ,  $\sigma_{zz}$  denote effective stresses in three directions, and  $\sigma_{xy}$ ,  $\sigma_{yz}$ ,  $\sigma_{zx}$  are shear stresses. The corresponding strains are

$$\varepsilon_p = \varepsilon_{xx} + \varepsilon_{yy} + \varepsilon_{zz} \quad (6.116)$$

$$\varepsilon_q = \frac{1}{3} \left\{ 2[(\varepsilon_{xx} - \varepsilon_{yy})^2 + (\varepsilon_{yy} - \varepsilon_{zz})^2 + (\varepsilon_{zz} - \varepsilon_{xx})^2] + 3(\varepsilon_{xy}^2 + \varepsilon_{yz}^2 + \varepsilon_{zx}^2) \right\}^{\frac{1}{2}} \quad (6.117)$$

As discussed earlier in the book, to define a yield function and a plastic potential in three dimensions, we also need to use Lode's angle defined below

$$\theta_l = -\frac{1}{3} \sin^{-1} \left( \frac{27}{2} \times \frac{\det S}{q^3} \right) \quad (6.118)$$

where

$$\det S = \begin{vmatrix} s_{xx} & \sigma_{xy} & \sigma_{xz} \\ \sigma_{xy} & s_{yy} & \sigma_{yz} \\ \sigma_{zx} & \sigma_{zy} & s_{zz} \end{vmatrix} \quad (6.119)$$

in which the deviatoric stresses are

$$s_{ii} = \sigma_{ii} - p \quad (6.120)$$

The yield function of CASM will therefore become

$$f(p, q, p_0) = \left(\frac{q}{M_\theta p}\right)^n + \frac{\ln \frac{p}{p_0}}{\ln r} = 0 \quad (6.121)$$

where  $M_\theta$  is regarded as a function of Lode's angle  $\theta_l$ . However if  $M_\theta$  is assumed to be a constant (i.e. independent of Lode's angle) then the yield surface will plot as a circle on a deviatoric plane as in Roscoe and Burland (1968). However, the following relationship, proposed by Sheng *et al.* (2000), proves to be much more realistic when compared with experimental data

$$M_\theta = M_{tc} \left\{ \frac{2 l^4}{1 + l^4 + (1 - l^4) \sin(3\theta_l)} \right\}^{\frac{1}{4}} \quad (6.122)$$

in which

$$l = \frac{3 - \sin \phi_{cv}}{3 + \sin \phi_{cv}} \quad (6.123)$$

$$M_{tc} = \frac{6 \sin \phi_{cv}}{3 + \sin \phi_{cv}} \quad (6.124)$$

It is noted that with the  $M$  value varying with Lode's angle according to (6.122), the yield surface of CASM plots much like that of Matosuka-Nakai's yield surface on a deviatoric plane, Figure 6.29.

If Rowe's stress-dilatancy relation is used, the plastic potential takes the following form

$$g(p, q) = 3M_\theta \ln \frac{p}{C} + (3 + 2M_\theta) \ln \left( \frac{2q}{p} + 3 \right) - (3 - M_\theta) \ln \left( 3 - \frac{q}{p} \right) = 0 \quad (6.125)$$

On the other hand, if the general stress-dilatancy relation (6.60) is used, the plastic potential will become

$$g(p, q) = m \ln \left[ 1 + (m - 1) \left( \frac{\eta}{M_\theta} \right)^n \right] + n(m - 1) \ln \frac{p}{C} \quad (6.126)$$

in which  $n$  is a known yield function parameter and  $m$  is calculated by

$$m = \frac{2}{3} \times \frac{[M_\theta(6 - M_\theta)]^n - (3M_\theta)^n}{A(6 - M_\theta)(3M_\theta)^{n-1}} \quad (6.127)$$

Here care is needed for determining  $M_\theta$ . For a given stress state on the yield surface, we can determine the  $M_\theta$  value using equation (6.122). Then by solving either equation (6.125) or (6.126) with the current stress values, we can obtain the size parameter  $C$ . In this way, all the necessary differentiations of the plastic potential with respect to stresses can be evaluated. In other words, the value of  $M_\theta$  is regarded as a constant for a given stress state because the plastic potential must pass through the current stress point in the yield surface. Therefore the plastic potential plots as a circle passing the current stress state on a deviatoric plane.

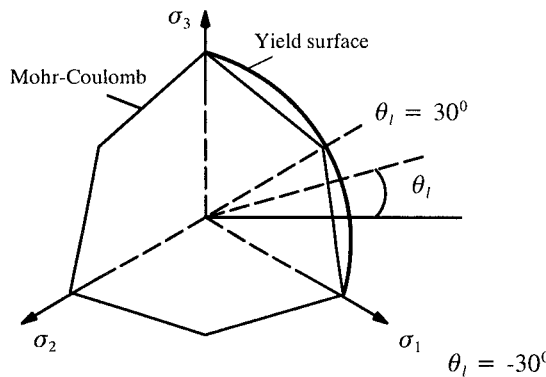


Figure 6.29: Yield surface and plastic potential on a deviatoric plane

Mathematically, we have

$$\frac{\partial f}{\partial \sigma_{ij}} = f,_{\sigma_{ij}} = f,_{p} p,_{\sigma_{ij}} + f,_{q} q,_{\sigma_{ij}} + f,_{M_\theta} M_\theta \theta_{l, \sigma_{ij}} \quad (6.128)$$

$$\frac{\partial g}{\partial \sigma_{ij}} = g,_{\sigma_{ij}} = g,_{p} p,_{\sigma_{ij}} + g,_{q} q,_{\sigma_{ij}} \quad (6.129)$$

With the yield function of CASM, we can obtain

$$f,_{p} = \frac{1}{p \ln r} - \frac{nq^n}{M^n p^{n+1}} \quad (6.130)$$

$$f,_{q} = \frac{nq^{n-1}}{M^n p^n} \quad (6.131)$$

$$f,_{M_\theta} = - \frac{nq^n}{M^n p^{n+1}} \quad (6.132)$$

$$M_{\theta, \theta_l} = \frac{3 \times (2)^{1/4} M_{tc}}{4} \times \frac{(l^4 - 1) \cos(3\theta_l)}{\left[1 + l^4 + (1 - l^4) \sin(3\theta_l)\right]^{5/4}} \quad (6.133)$$

## REFERENCES

Adachi, T. and Oka, F. (1982). Constitutive equations for normally consolidated clay based on elasto-viscoplasticity. *Soils and Foundations*, Vol 22, 55-70.

Allman, M.A. and Atkinson, J.H. (1992). Mechanical properties of reconstituted Bothkennar soil. *Geotechnique*, Vol 42, 289-301.

Alonso, E.E., Gens, A. and Josa, A. (1990). A constitutive model for partially saturated soils. *Geotechnique*, Vol 40, 405-430.

Atkinson, J.H. and Bransby, P.L. (1978). *The Mechanics of Soils*, McGraw-Hill.

Bardet, J.P. (1986). Bounding surface plasticity model for sands. *J. Eng. Mech.*, ASCE, Vol 112, 1198-1217.

Been, K. and Jefferies, M.G. (1985). A state parameter for sands. *Geotechnique*, Vol 35, 99-112.

Been, K. and Jefferies, M.G. (1986). Reply: A state parameter for sands. *Geotechnique*, London, England, Vol 36, 127-132.

Been, K. and Jefferies, M.G. (1993). Towards systematic CPT interpretation. *Predictive Soil Mechanics*, Wroth Memorial Symposium, Thomas Telford, London, 121-134.

Been, K., Crooks, J.H.A., Becker, D.E. and Jefferies, M.G. (1986). The cone penetration test in sands: I, state parameter interpretation. *Geotechnique*, Vol 36, 239-249.

Been, K., Crooks, J.H.A., Becker, D.E. and Jefferies, M.G. (1987). The cone penetration test in sands: II, general inference of state. *Geotechnique*, Vol 37, 285-299.

Been, K., Jefferies, M.G. and Hachey, J.E. (1991). The critical state of sands. *Geotechnique*, Vol 37, 285-299.

Bishop, A.W. (1972). Shear strength parameters for undisturbed and remoulded soil specimens. In: *Stress Strain Behaviour of Soils*, The Roscoe Memorial Symposium, Foulis, 3-58.

Bishop, A.W. and Donald, I.B. (1961). The experimental study of partly saturated soils in the triaxial apparatus. *Proc. 5th Conf. ISSMFES*, Vol 1, 13-21.

Bishop, A.W. and Henkel, D.J. (1957). *The Measurement of Soil Properties in the Triaxial Test*, London, Edward Arnold Publishers Ltd.

Bjerrum, L. (1967). Engineering geology of Norwegian normally consolidated marine clays as related to the settlements of buildings. *Geotechnique*, Vol 17, 83-118.

Bolton, M. D. (1986). The strength and dilatancy of sands. *Geotechnique*, Vol 36, 65-78.

Borjia, R.I. and Kavazanjian, E. Jr (1985). A constitutive model for the stress-strain-time behaviour of wet clays. *Geotechnique*, Vol 35, 283-298.

Brown, E.T. and Yu, H.S. (1988). A model for the ductile yield of porous rock. *Int. J. Num. Anal. Meth. Geomech.*, Vol 12, 679-688.

Burland, J.B. (1990). On the compressibility and shear strength of natural clays. *Geotechnique*, Vol 40, 329-378.

Carter, J.P., Booker, J.R. and Wroth, C.P. (1982). A critical state model for cyclic loading. *Soil Mechanics – Transient and Cyclic Loads*, Wiley, 219-252.

Chandler, H.W. (1985). A plasticity theory without Drucker's postulate for granular materials. *J Mech. Phys. of Solids*, Vol 33, 215-226.

Cole, E.R.L. (1967). *The Behavior of Soils in the Simple Shear Apparatus*. PhD Thesis, Department of Engineering, University of Cambridge, England.

Coleman, J.D. (1962). Discussion: Stress strain relations for partly saturated soil. *Geotechnique*, Vol 12, 348-350.

Collins, I.F. (1991). On the mechanics of state parameter models for sands. *Computer Methods and Advances in Geomechanics* (Editors: G. Beer, J.R. Booker and J.P. Carter), Vol 1, 593-599.

Collins, I.F. and Kelly, P.A. (2002). A thermomechanical analysis of a family of soil models, *Geotechnique*, Vol 48, 507-518.

Collins, I.F., Pender, M.J. and Wan, Y. (1992). Cavity expansion in sands under drained loading conditions. *Int. J. Num. Anal. Meth. Geomech.*, Vol 16, 3-23.

Coop, M.R. (1990). The mechanics of uncemented carbonate sands. *Geotechnique*, Vol 40, 607-626.

Coop, M.R. and Atkinson, J. (1993). The mechanics of cemented carbonate sands. *Geotechnique*, Vol 43, 53-67.

Coop, M.R. and Lee, I.K. (1993). The behavior of granular soils at elevated stresses. *Predictive Soil Mechanics*, Wroth Memorial Symposium, Thomas Telford, London, 186-198.

Crouch R.S., Wolf, J.P. and Dafalias, Y.F. (1994). Unified critical state bounding surface plasticity model for soil. *J. Eng Mech. ASCE*, Vol 120, 2251-2270.

Cui, Y.J. and Delage, P. (1996). Yielding and plastic behaviour of an unsaturated compacted silt. *Geotechnique*, Vol 46, 405-430.

Dafalias, Y.F. and Herrmann, L.R. (1980). Bounding surface formulation of soil plasticity. *Soil Mechanics – Transient and Cyclic Loads*, Wiley, Chapter 10, 253-282.

Desai, C.S. (2001). *Mechanics of Materials and Interfaces: The Disturbed State Concept*, CRC Press, Boca Raton.

Desai, C.S. and Toth, J. (1996). Disturbed state constitutive modelling based on stress strain and nondestructive behaviour. *Int. J. Solids and Structures*, Vol 33, 1619-1650.

Desai, C.S., Galagoda, H.M. and Wathugala, G.W. (1987). Hierarchical modelling for geological materials and discontinuities – joints, interfaces. *Constitutive Laws for Engineering Materials: Theory and Applications*, Elsevier Science Publishing Co. Inc., Vol 1, 81-94.

DiMaggio, F.L. and Sandler, I.S. (1971). Material models for granular soils. *J. Eng. Mech., ASCE*, Vol 97, 935-950.

Drucker, D.C. (1956). On uniqueness in the theory of plasticity. *Quart. J. Appl. Math.*, Vol 14, 35-42.

Drucker, D.C. (1959). A definition of stable inelastic material. *J. Appl. Mech.*, Vol 26, 101-106.

Drucker, D.C., Gibson, R.E. and Henkel, D.J. (1957). Soil mechanics and working hardening theories of plasticity, *Trans. ASCE*, Vol 122, 338-346.

Elliot, G.H. and Brown, E.T. (1985). Yield of a soft and high porosity rock. *Geotechnique*, Vol 35, 413-423.

Fredlund, D.G. and Morgenstern, N.R. (1977). Stress state variables for unsaturated soils. *J. Geotech. Eng. Div., ASCE*, Vol 103, 437-446.

Gens, A. and Nova, R. (1993). Conceptual bases for a constitutive model for bonded soils and weak rocks. *Geotechnical Engineering of Hard Soils - Soft Rocks*, Balkema, 485-494.

Gens, A. and Potts, D.M. (1988). Critical state models in computational geomechanics. *Eng. Comput.*, Vol 5, 178-197.

Hill, R (1950). *The Mathematical Theory of Plasticity*, Clarendon Press, Oxford.

Hird, C.C. and Hassona, F. (1986). Discussion: A state parameter for sands. *Geotechnique*, Vol 36, 124-127.

Houlsby, G.T. (1991). How the dilatancy of soils affects their behaviour. *Proc. 10th Eur. Conference on Soil Mechanics and Foundation Engineering*, Florence.

Huang, J.T. and Airey, D.W. (1993). Conceptual bases for a constitutive model for bonded soils and weak rocks. *Geotechnical Engineering of Hard Soils - Soft Rocks*, Balkema, 553-460.

Jefferies, M.G. (1993). Nor-Sand: a simple critical state model for sand. *Geotechnique*, Vol 43, 91-103.

Jiang, M.J., Yu, H.S. and Harris, D. (2006). Bond rolling resistance and its effects on yielding of bonded granulates by DEM analyses. *Int. J. Num. Anal. Meth. Geomech.* (in press).

Khong, C.D. and Yu, H.S. (2002). Computational aspects of a unified critical state model for clay and sand, *Proc. of 8th NUMOG*, Rome, 271-277.

Koiter, W.T. (1953). Stress-strain relations, uniqueness and variational theorems for elastic-plastic materials with a singular yield surface, *Quart. Appl. Math.*, Vol 11, 350-354.

Kutter, B.L. and Sathialingam, N. (1992). Elastic-viscoplastic modelling of the rate-dependent behaviour of clays. *Geotechnique*, Vol 42, 427-441.

Lade, P. V. (1972). *The Stress-Strain and Strength Characteristics of Cohesionless Soils*. PhD thesis, University of California.

Lade, P. V. (1977). Elasto-plastic stress strain theory for cohesionless soil with curved yield surfaces. *Int. J. Solids and Structures*, Vol 13, 1019-1035.

Lee, K.L. and Seed, H.B. (1967). Drained strength characteristics of sands. *Proc. ASCE, Soil Mechanics and Foundations Division*, Vol 93, 117-141.

Leroueil, S. and Vaughan, P.R. (1990). The general and congruent effects of structure in natural soils and weak rocks. *Geotechnique*, Vol 40, 467-488.

Liu, M.D. and Carter, J.P. (1999). Virgin compression of structured soils. *Geotechnique*, Vol 49, 43-57.

McDowell, G.R. (2002). A simple non-associated flow model for sand, *Granular Matter*, Vol 4, 65-69.

McDowell, G.R. and Bolton, M.D. (1998). On the micromechanics of crushable aggregates, *Geotechnique*, Vol 48, 667-679.

McDowell, G.R. and Hau, K.W. (2003). A simple non-associated three surface kinematic hardening model. *Geotechnique*, Vol 53, 433-437.

Mroz, Z. (1963). Non-associated flow laws in plasticity. *J. de Mecanique*, Vol 2, 21-42.

Muir Wood, D. (1990). *Soil Behaviour and Critical State Soil Mechanics*, Cambridge University Press.

Naylor, D.J. (1985). A continuous plasticity version of the critical state model. *Int. J. Num. Meth. Eng.*, Vol 21, 1187-1204.

Nova, R. (1977). On the hardening of soils. *Archiwum Mechaniki Stosowanej*, Vol 29, 445-458.

Nova, R. (1985). An engineering approach to shear band formation in geological media. *Proc. 5th Int. Conf. on Num. Meth. Geomech*, Nagoya, 509-516.

Nova, R. and Wood, D.M. (1978). An experimental program to define yield function for sand. *Soils and Foundations*, Vol 18, 77-86.

Nova, R. and Wood, D.M. (1979). A constitutive model for sand. *Int. J. Num. Anal. Meth. Geomech.*, Vol 3, 255-278.

Novello, E.A. and Johnston, I.W. (1995). Geotechnical materials and the critical state, *Geotechnique*, Vol 45, 223-235.

Ohmaki, S. (1982). Stress strain behaviour of anisotropically, normally consolidated cohesive soil. *Proc. 1st Int. Symp. of NUMOG*, Zurich, 250-269.

Ohta, H. and Wroth, C.P. (1976). Anisotropy and stress reorientation in clay under load. *Proc. 2nd Int. Conf. on Num. Meth. Geomech.*, Blacksburg, Vol 1, 319-328.

Oka, F. (2005). Computational modelling of large deformation and the failure of geomaterials. *Theme Lecture, Proc. 16th Conf. of ISSMGE*, Japan., Vol 1, 47-94.

Parry, R.H.G. (1956). *Strength and Deformation of Clay*. PhD Thesis, University of London.

Parry, R.H.G. (1958). Correspondence on 'On yielding of soils', *Geotechnique*, Vol 8, 183-186.

Pastor, M., Zienkiewicz, O.C. and Leung, K.H. (1985). Simple model for transient soil loading in earthquake analysis. Part 2: Non-associative models for sands. *Int. J. Num. Anal. Meth. Geomech.*, Vol 9, 477-498.

Pender, M.J. (1978). A model for the behaviour of overconsolidated soil. *Geotechnique*, Vol 28, 1-25.

Perzyna, P. (1963). The constitutive equations for working hardening and rate sensitive plastic materials, *Proc. Vibration Problems, Warsaw.*, Vol 4, 281-290.

Perzyna, P. (1966). Fundamental problems in viscoplasticity, *Advances in Applied Mechanics*, No 4, 244-368.

Pietruszczak, S. and Stolle, D.F.E. (1985). Deformation of strain softening materials : Part 1. objectivity of finite element solutions based on conventional strain softening formulations. *Comput. Geotech.*, Vol 1, 99-115.

Pietruszczak, S. and Mroz, Z. (1980). Numerical analysis of elastic-plastic compression of pillars accounting for material hardening and softening. *Int. J. Rock Mech. Min. Sci.*, Vol 17, 199-207.

Pietruszczak, S. and Mroz, Z. (1981). Finite element analysis of deformation of strain softening materials. *Int. J. Num. Meth. Eng.*, Vol 17, 327-334.

Poulos, S.J. (1981). The steady state of deformation. *J. Geotech. Eng. Div.*, Vol 107, 553-562.

Prevost, J.H. and Hoeg, K. (1975). Soil mechanics and plasticity analysis of strain softening. *Geotechnique*, Vol 25, 279-297.

Roscoe, K.H. and Burland, J.B. (1968). On generalised stress strain behaviour of wet clay. In: *Engineering Plasticity* (edited by Heyman and Leckie), 535-609.

Roscoe, K.H. and Poorooshashb, H.B. (1963). A fundamental principle of similarity in model tests for earth pressure problems. *Proc. 2nd Asian Conference on Soil Mechanics*, Vol 1, 134-140.

Roscoe, K.H. and Schofield, A.N. (1963). Mechanical behaviour of an idealized wet clay. *Proc. European Conf. on Soil Mechanics and Foundation Eng.*, Vol 1, 47-54.

Roscoe, K.H., Schofield, A.N. and Thurairajah, A. (1963). Yielding of clays in states wetter than critical. *Geotechnique*, Vol 13, 211-240.

Roscoe, K.H., Schofield, A.N. and Wroth, C.P. (1958). On the yielding of soils. *Geotechnique*, Vol 8, 22-52.

Rowe, P. W. (1962). The stress-dilatancy relation for static equilibrium of an assembly of particles in contact. *Proc. Roy. Soc. A.* Vol 267, 500-527.

Rowe, P.W. (1963). Stress-dilatancy, earth pressure and slopes. *Proc. ASCE, Soil Mechanics and Foundations Division*, Vol 89, 37-61.

Rowe, P.W. (1972). Theoretical meaning and observed values of deformation parameters for soil. In: *Stress-Strain Behaviour of Soils*, Roscoe Memorial Symposium, Foulis, 143-194.

Saada, A.S. and Bianchini, G. (1988). *Constitutive Equations for Granular Non-Cohesive Soils*. Balkema.

Sasitharan, S., Robertson, P.K., Sego, D.C. and Morgenstern, N.R. (1994). State boundary surface for very loose sand and its practical applications. *Can. Geotech. J.*, Vol 31, 321-334.

Schnaid, F., Prietto, P.D.M. and Consoli, N.C.. (2001). Characterization of cemented sand in triaxial compression. *J. Geotech. Geoenviron. Eng.*, ASCE, Vol 127, 857-868.

Schofield, A.N. and Wroth, C.P. (1968). *Critical State Soil Mechanics*, McGraw-Hill, London.

Scott, R.F. (1988). Constitutive relations for soil: Present and future. In : *Constitutive Equations for Granular Non-cohesive Soils* (Eds, Saada and Bianchini), Balkema, 723-725.

Sheng, D., Sloan, S.W. and Yu, H.S. (2000). Aspects of finite element implementation of critical state models. *Comput. Mech.*, Vol 26, 185-196.

Sladen, J.A., D'Hollander, R.D.D. and Krahn, J. (1985). The liquefaction of sands, a collapse surface approach. *Canadian Geotechnical Journal*, Vol 22, 564-578.

Sladen, J.A. and Osowell, J.M. (1989). The behaviour of very loose sand in the triaxial compression test. *Canadian Geotechnical Journal*, Vol 26, 103-113.

Stroud, M.A. (1971). *The Behavior of Sand at Low Stress Levels in the Simple Shear Apparatus*. PhD Thesis, Department of Engineering, University of Cambridge, England.

Tan, S.M. (2006). *Constitutive and Numerical Modelling of Bonded Geomaterials*, Forthcoming PhD Thesis, University of Nottingham, UK.

Tatsuoka, F. and Ishihara, K. (1974). Yielding of sand in triaxial compression. *Soils and Foundations*, Vol 14, 6-76.

Taylor, D.W. (1948). *Fundamentals of Soil Mechanics*, Wiley, New York.

Vermeer, P.A. (1978). A double hardening model for sand. *Geotechnique*, Vol 28, 413-433.

Vermeer, P.A. (1982). A simple shear band analysis using compliances. *Proc. IUTAM Conf. on Deformation and Failure of Granular Materials*, Delft, 493-499.

Wang, J. (2005). *The Stress-Strain and Strength Characteristics of Portaway Sand*, PhD Thesis, University of Nottingham, UK.

Wheeler, S.J. and Sivakumar, V. (1995). An elasto-plastic critical state framework for unsaturated soil. *Geotechnique*, Vol 45, 35-53.

Whittle, A.J. (1993). Evaluation of a constitutive model for overconsolidated clays. *Geotechnique*, Vol 43, 289-313.

Wilde, P. (1977). Two-invariants dependent model of granular media. *Archives Mech*, Vol 29, 799-809.

William, K., Pramono, E. and Sture, S. (1987). Uniqueness and stability issues of strain softening computations. *Constitutive Laws for Engineering Materials: Theory and Applications*, Elsevier Science Publishing Co. Inc., Vol 1, 249-260.

Wroth, C.P. (1973). A brief review of the application of plasticity to soil mechanics, In: *Plasticity and Soil Mechanics*, (Editor: A.C. Palmer), 1-11.

Wroth, C.P. and Bassett, N. (1965). A stress-strain relationship for the shearing behavior of a sand. *Geotechnique*, Vol 15, 32-56.

Wroth, C.P. and Housby, G.T. (1985). Soil mechanics – property characterization and analysis procedures. *Proc. 11th ICSMFE*, San Francisco, Vol 1, 1-57.

Yin, J.H. and Graham, J. (1999). Elastic visco-plastic modelling of the time dependent stress-strain behaviour of soils. *Can. Geotech. J.*, Vol 36, 736-745.

Yu, H.S. (1994). State parameter from self-boring pressuremeter tests in sand. *J. Geotech. Eng.*, ASCE, Vol. 120, No. 12, 2118-2135.

Yu, H.S. (1995). A unified critical state model for clay and sand. *Civil Engineering Research Report No 112.08.1995*, University of Newcastle, NSW.

Yu, H.S. (1996). Interpretation of pressuremeter unloading tests in sands. *Geotechnique*, Vol 46, 17-34.

Yu, H.S. (1998). CASM: A unified state parameter model for clay and sand. *Int. J. Num. Anal. Meth. Geomech.*, Vol 22, 621-653.

Yu, H.S. and Khong, C.D. (2002). Application of a unified critical state model in finite element analysis, *Proc. 3rd Conf. on 3D Finite Elements for Pavement Analysis Design and Research*, Amsterdam, 253-267.

Yu, H.S., Khong, C.D., Wang, J. and Zhang, G. (2005). Experimental evaluation and extension of a simple critical state model for sand. *Granular Matter*, Vol 7, 213-225.

Zienkiewicz, O.C. and Naylor, D.J. (1973). Finite element studies of soils and porous media. *Lectures on Finite Elements in Continuum Mechanics* (Editors: J.T. Oden and E.R. de Arantes), UAH Press, 459-493.

Zienkiewicz, O.C. and Pande, G.N. (1977). Some useful forms of isotropic yield surfaces for soil and rock mechanics. *Finite Elements in Geomechanics*, (Editor: G. Gudehus), Chapter 5, 179-198.

Zienkiewicz, O.C., Leung, K.H. and Pastor, M. (1985). Simple model for transient soil loading in earthquake analysis. Part 1: Basic model and its application. *Int. J. Num. Anal. Meth. Geomech.*, Vol 9, 453-476.

Zytynski, M., Randolph, M.F., Nova, R. and Wroth, C.P. (1978). On modelling the unloading-reloading behaviour of soils. *Int. J. Num. Anal. Meth. Geomech.*, Vol 2, 87-93.

## CHAPTER 7

# MULTI-SURFACE AND BOUNDING SURFACE PLASTICITY

### 7.1 INTRODUCTION

The mathematical theory of plasticity described so far in this book is based on the concept of a single yield surface. This single yield surface is used to separate the domains of elastic and plastic states. As demonstrated in Chapter 6, single yield surface plasticity offers a reasonable explanation of the overall stress-strain behaviour of soils for the case of proportional loading where the load increases monotonically and no unloading occurs. However further application of the single yield surface plasticity theory indicates that it suffers from the following main shortcomings:

- (1) The elastic domain assumed is often too large when compared with experimental data. In addition, the sudden change from elastic to plastic domains predicted by the single yield surface theory is also in contrast to the gradual change in stiffness from elastic to plastic states observed in experiments.
- (2) The isotropic hardening and Prager's or Ziegler's kinematic hardening (Prager, 1955; Ziegler, 1959) cannot generally model the complex behaviour of soils observed in experiments under cyclic or repeated loading conditions where stress reversals occur frequently.

These limitations of the classical theory of plasticity provided a strong incentive for extensive research from the 1960s to search for better hardening rules for modelling both smooth elastic-plastic transition and cyclic behaviour. Although several approaches have been proposed, the two most successful and widely used theories for this purpose are: (a) The theory of multi-surface plasticity due to Mroz (1967) and Iwan (1967); and (b) The theory of bounding surface (or two surface) plasticity due to Dafalias and Popov (1975) and Krieg (1975). Both of these concepts were initially developed for metals, but quickly found applications in modelling geomaterials (e.g. Prevost, 1977, 1978; Mroz *et al.*, 1978, 1979, 1981; Dafalias and Herrmann, 1982).

This chapter aims to present the concepts of the multi-surface and bounding surface plasticity and demonstrate how these concepts can be used to develop more accurate constitutive models for describing soil behaviour under both monotonic and cyclic loading conditions. Our presentation is limited to formulations in stress space, although multi-surface plasticity models can also be formulated in strain space (e.g. Yoder and Iwan, 1981; Zheng *et al.*, 1986; Simpson, 1992).

## 7.2 THE MULTI-SURFACE CONCEPT

### 7.2.1 One-dimensional loading and unloading

Consider a soil element subject to one-dimensional compressive loading and unloading. A typical stress-strain curve is given in Figure 7.1(a). After the soil starts to become plastic (i.e., after transition into the plastic region, that is the point  $a$  in Figure 7.1(b)), the tangential stiffness or modulus will reduce. The basic idea of Mroz's multi-surface plasticity (Mroz, 1967) is to approximate the actual stress-strain curve by  $n$  linear segments of constant tangential moduli as shown in Figure 7.1(b). In stress space, this approximation can be represented by  $n$  hypersurfaces  $f_1, f_2, f_3, \dots f_{n+1}$  where  $f_1$  is the yield surface and  $f_2, f_3, \dots f_{n+1}$  define regions of constant plastic work hardening moduli.

Now let us discuss the process of one-dimensional loading. For simplicity we assume that initially all the surfaces are circular and concentric enclosing the origin  $o$ , Figure 7.1(c). When the stress point moves from the origin  $o$  along the vertical axis, it first reaches the elastic limit corresponding to the stress-strain point  $a$  and the yield surface  $f_1$  moves along this axis with the stress point until it contacts the surface  $f_2$  corresponding to the stress-strain point  $b$ . Up to now all other surfaces remain fixed. Now the stress point will take the surfaces  $f_1$  and  $f_2$  and move along the vertical axis until it reaches the surface  $f_3$  corresponding to the stress-strain point  $c$ . If the stress point moves further, then it will touch the surface  $f_4$  which is the end of the loading programme indicated in Figure 7.1(e). Now consider the process of unloading from the stress-strain point  $d$ . Obviously if the stress point moves along the vertical axis back towards the origin  $o$ , it will first reach the lower side of the yield surface  $f_1$  when reverse plasticity occurs (i.e. the stress-strain point  $e$ ). If the unloading continues, then both the stress point and the yield surface  $f_1$  will touch the lower side of the surface  $f_2$  at the stress-strain point  $f$ , as shown in Figure 7.1(f).

### 7.2.2 General loading

In order to extend the above one-dimensional model to general three-dimensional stress states, it is necessary to make an assumption about how the loading surface should translate upon loading. In this respect, two proposals have been made, one due to Mroz (1967) and another by Iwan (1967). It is noted that due to its simplicity, Mroz's proposal has been almost universally adopted by later researchers in using multi-surface plasticity models.

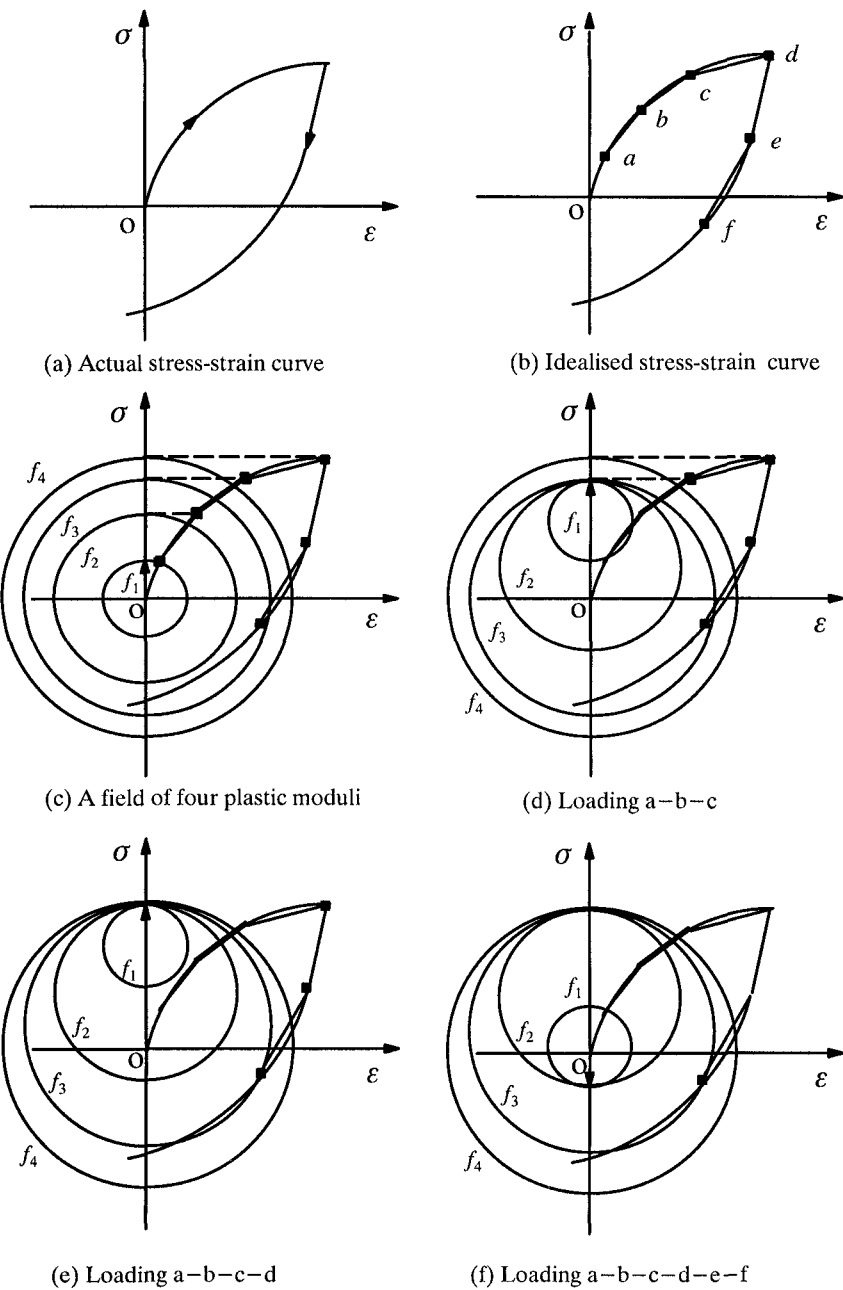


Figure 7.1: Idealised stress-strain behaviour with multi-surface plasticity

### (a) Mroz's translation rule

Mroz (1967) assumed that the loading surfaces cannot intersect but consecutively contact and push each other. To explain this, let us consider Figure 7.2. Assume that the current stress point lies on the loading surface  $f_i$  and is denoted by P. The question is under a given stress increment how the current loading surface  $f_i$  should translate and move towards the next loading surface  $f_{i+1}$ , which is of the same shape as  $f_i$ . With Mroz's rule, we need to find a conjugate point R on the next loading surface  $f_{i+1}$  for the current stress point P. The conjugate point R is the point on  $f_{i+1}$  that has the same direction of outward normal as the current stress point. A easy way to locate the point R is to note that the straight line  $Ro_{i+1}$  is parallel with  $Po_i$ , where  $o_i$ ,  $o_{i+1}$  are the centres of the current and next loading surfaces respectively. Once the point R is located, then Mroz's translation rule suggest that the centre of the current loading surface should move along the vector PR. This rule ensures that, as the surfaces are dragged by the current stress point, they never intersect and it makes the surfaces align gradually along the current stress path direction, see Figure 7.2.

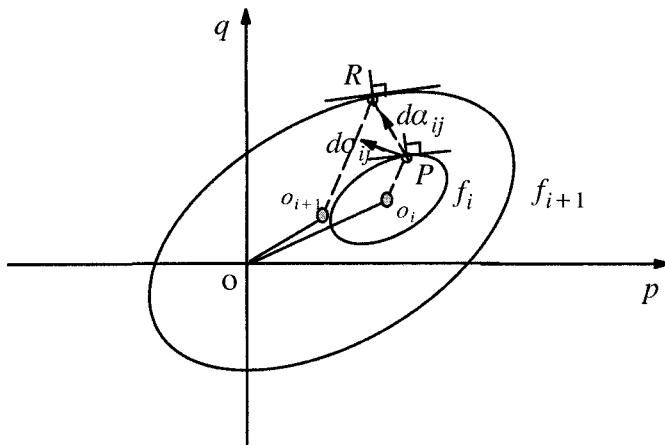


Figure 7.2: Mroz's translation of the loading surface  $f_i$

To describe the motion of loading surfaces of constant plastic moduli, let us consider a typical situation shown in Figure 7.2. Assume the two loading surfaces  $f_i$  and  $f_{i+1}$  are mathematically expressed by

$$f_i = f(\sigma_{ij} - \alpha_{ij}^i) - R_0^i = 0 \quad (7.1)$$

$$f_{i+1} = f(\sigma_{ij} - \alpha_{ij}^{i+1}) - R_0^{i+1} = 0 \quad (7.2)$$

where the position vectors  $\alpha_{ij}^i$  and  $\alpha_{ij}^{i+1}$  define the coordinates of the centres of the surfaces  $f_i$  and  $f_{i+1}$  respectively.  $R_0^i$  and  $R_0^{i+1}$  indicate the sizes of the loading surfaces  $f_i$  and  $f_{i+1}$ .

Now if the current stress state  $\sigma_{ij}$  lies on the surface  $f_i$  and is denoted by point P, Mroz's translation rule suggests that the instantaneous translation of  $f_i$  upon loading will occur along PR, where R is a point on the next loading surface  $f_{i+1}$  corresponding to the same direction of outward normal. Inspection of geometry gives

$$\frac{\sigma_{ij}^R - \alpha_{ij}^{i+1}}{\sigma_{ij}^P - \alpha_{ij}^i} = \frac{R_0^{i+1}}{R_0^i} \quad (7.3)$$

in which  $\sigma_{ij}^P$  and  $\sigma_{ij}^R$  denote stresses at points P and R respectively.

Since the centre of the surface  $f_i$  moves along PR, we can write

$$d\alpha_{ij}^i = d\mu (\sigma_{ij}^R - \sigma_{ij}^P) \quad (7.4)$$

where  $d\mu$  is a positive constant to be determined. Substituting the expression for  $\sigma_{ij}^R$  from equation (7.3) into equation (7.4) leads to

$$d\alpha_{ij}^i = \frac{d\mu}{R_0^i} \left[ (R_0^{i+1} - R_0^i) \sigma_{ij}^P - (\alpha_{ij}^i R_0^{i+1} - \alpha_{ij}^{i+1} R_0^i) \right] \quad (7.5)$$

It is noted that for a special case when the centres of the two surfaces coincide (i.e.,  $\alpha_{ij}^i = \alpha_{ij}^{i+1}$ ), the above equation reduces to

$$d\alpha_{ij}^i = d\mu \frac{R_0^{i+1} - R_0^i}{R_0^i} \left( \sigma_{ij}^P - \alpha_{ij}^i \right) \quad (7.6)$$

which is the same as the kinematic hardening rule of Ziegler (1959) for the single surface plasticity.

To fully define the movement rule for the surface  $f_i$  upon loading, the constant  $d\mu$  remains to be determined. This constant can be calculated using the condition that the current stress point, upon loading, remains on the yield surface  $f_i$ , namely

$$df_i = \frac{\partial f_i}{\partial \sigma_{ij}} d\sigma_{ij} + \frac{\partial f_i}{\partial \alpha_{ij}^i} d\alpha_{ij}^i = 0 \quad (7.7)$$

Given the form of loading surfaces assumed, we have

$$\frac{\partial f_i}{\partial \sigma_{ij}} = - \frac{\partial f_i}{\partial \alpha_{ij}} \quad (7.8)$$

Hence equation (7.7) can be rewritten as

$$\frac{\partial f_i}{\partial \sigma_{ij}} d\sigma_{ij} - \frac{\partial f_i}{\partial \alpha_{ij}} d\alpha_{ij}^i = 0 \quad (7.9)$$

which can be further reduced to

$$d\mu = \frac{\frac{\partial f_i}{\partial \sigma_{ij}} d\sigma_{ij}}{\frac{\partial f_i}{\partial \sigma_{kl}} (\sigma_{kl}^R - \sigma_{kl}^P)} \quad (7.10)$$

### Combined kinematic and isotropic hardening

So far we have assumed that the sizes of loading surfaces are constant throughout the loading process. However apart from translation, the loading surface may also expand or contract during the loading process. To include this isotropic hardening we may assume that the sizes of the loading surfaces are a function of some measure of plastic strain,  $\alpha$ . Therefore the two loading surfaces  $f_i$  and  $f_{i+1}$  are expressed by

$$f_i = f(\sigma_{ij} - \alpha_{ij}^i) - R_0^i(\alpha) = 0 \quad (7.11)$$

$$f_{i+1} = f(\sigma_{ij} - \alpha_{ij}^{i+1}) - R_0^{i+1}(\alpha) = 0 \quad (7.12)$$

Then instead of equation (7.9), the following consistency condition holds for the current stress state

$$\frac{\partial f_i}{\partial \sigma_{ij}} d\sigma_{ij} - \frac{\partial f_i}{\partial \alpha_{ij}} d\alpha_{ij}^i + \frac{\partial f_i}{\partial R_0^i} \frac{\partial R_0^i}{\partial \alpha} d\alpha = 0 \quad (7.13)$$

which gives

$$d\mu = \frac{\frac{\partial f_i}{\partial \sigma_{ij}} d\sigma_{ij} + \frac{\partial f_i}{\partial R_0^i} \frac{\partial R_0^i}{\partial \alpha} d\alpha}{\frac{\partial f_i}{\partial \sigma_{kl}} (\sigma_{kl}^R - \sigma_{kl}^P)} \quad (7.14)$$

Therefore all loading surfaces that are not reached by the current stress point expand or contract uniformly (isotropic hardening) while the remaining surfaces which are in mutual contact at the current stress point undergo both translation (kinematic hardening) and expansion/contraction (isotropic hardening).

**(b) Iwan's translation rule**

As an alternative to Mroz's translation rule, Iwan (1967) assumed that the current loading surface translates in a direction parallel to the increment of plastic strain at any point in the stress history of the material. To explain this, let us consider Figure 7.3. Assume that the current stress point lies on the loading surface  $f_i$  and is denoted by  $P$ . With Iwan's rule, we need to determine the direction of the plastic strain rates at the current stress point  $P$ . If the associated plastic flow rule is assumed, then the plastic strain rate will be normal to the current loading surface, as shown by the vector  $PQ$  in Figure 7.3. Hence Iwan's translation rule suggests that the centre of the current loading surface should move along the vector  $PQ$ . This translation rule may result in intersections between loading surfaces.

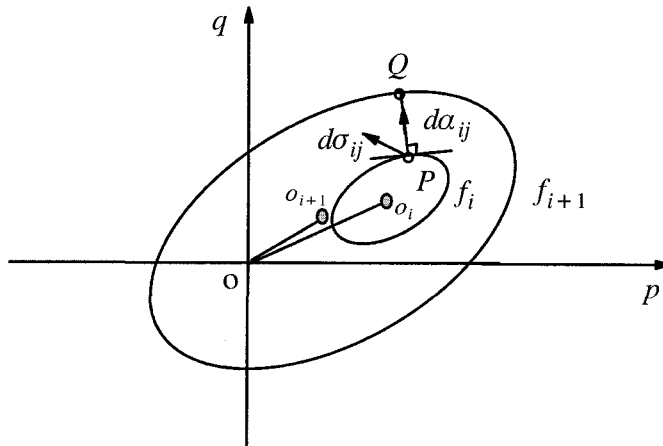


Figure 7.3: Iwan's translation of the loading surface  $f_i$

If the associated flow rule is assumed then Iwan's translation rule is the same as the kinematic hardening rule of Prager (1955) for single surface plasticity. In mathematical terms, we have

$$da_{ij}^i = d\mu \frac{\partial f_i}{\partial \sigma_{ij}} \quad (7.15)$$

where  $d\mu$  is a constant, which can be determined from the condition that the current stress point lies on the loading surface, namely

$$\frac{\partial f_i}{\partial \sigma_{ij}} d\sigma_{ij} - \frac{\partial f_i}{\partial \sigma_{ij}} da_{ij}^i = 0 \quad (7.16)$$

which can be further reduced to

$$d\mu = \frac{\frac{\partial f_i}{\partial \sigma_{ij}} d\sigma_{ij}}{\frac{\partial f_i}{\partial \sigma_{kl}} \times \frac{\partial f_i}{\partial \sigma_{kl}}} \quad (7.17)$$

For combined kinematic and isotropic hardening, the above equation needs to be replaced by

$$d\mu = \frac{\frac{\partial f_i}{\partial \sigma_{ij}} d\sigma_{ij} + \frac{\partial f_i}{\partial R_0^i} \frac{\partial R_0^i}{\partial \alpha} d\alpha}{\frac{\partial f_i}{\partial \sigma_{kl}} \times \frac{\partial f_i}{\partial \sigma_{kl}}} \quad (7.18)$$

### 7.3 MULTI-SURFACE PLASTICITY MODELS FOR SOILS

This section describes how the concept of multi-surface plasticity of Mroz (1967) and Iwan (1967) can be used to develop constitutive models for soils. The notable work carried out in this area includes models given by Prevost (1977, 1978) and Mroz *et al.* (1978) for clay and those by Prevost (1985) and Lacy and Prevost (1987) for sand.

#### 7.3.1 Total stress multi-surface modelling of undrained clay

Prevost (1977, 1978) was the first to apply Mroz's multi-surface plasticity concept to soil stress-strain modelling. His attention was on developing a multi-surface model for predicting accurately the observed stress-strain-strength of undrained clay. For undrained clay, a simpler total stress, rather than effective stress, analysis may be used. Of course with the total stress formulation, the effect of stress history (i.e. OCR) cannot be included in the analysis. For simplicity, Prevost used the von Mises yield function as the basis for his development of a total stress, multi-surface plasticity model for undrained clays.

##### *Volumetric and deviatoric behaviour*

For total stress undrained analysis, it is particularly advantageous to divide the stresses and strains into volumetric and deviatoric components, with the deviatoric aspects defined as

$$s_{ij} = \sigma_{ij} - \frac{1}{3}\sigma_{kk}\delta_{ij} \quad (7.19)$$

$$e_{ij} = \varepsilon_{ij} - \frac{1}{3}\varepsilon_{kk}\delta_{ij} \quad (7.20)$$

where  $\delta_{ij}$  is the Kronecker delta.

For elastic behaviour, the stress-strain relations can be written in the following familiar form

$$d\varepsilon_{kk} = \frac{d\sigma_{kk}}{3K} \quad (7.21)$$

$$de_{ij} = \frac{ds_{ij}}{2G} \quad (7.22)$$

where K and G are elastic bulk and shear moduli. It is noted that for undrained loading, a rather high value should be used for the bulk modulus.

#### *Elastic and plastic deviatoric strains*

It is assumed that the total deviatoric strain is the sum of elastic and plastic components, namely

$$de_{ij} = de_{ij}^e + de_{ij}^p \quad (7.23)$$

where the elastic strain rate  $de_{ij}^e$  is determined from equation (7.22) and the plastic strain rate  $de_{ij}^p$  is determined from a plasticity theory.

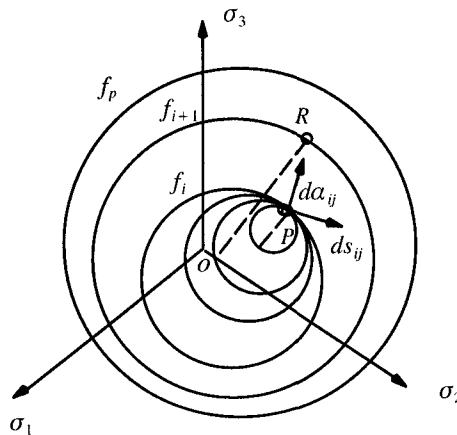


Figure 7.4: Field of loading surfaces in a deviatoric plane

#### *Field of loading surface for undrained clay*

The field of constant plastic moduli, introduced by Mroz (1967), is defined in stress space by the collection of nested loading surfaces,  $f_1, f_2, f_3, \dots, f_p$  with respec-

tive sizes  $k^{(1)} < k^{(2)} < k^{(3)} < \dots < k^{(p)}$ , Figure 7.4. During undrained loading, the yielding of clay is independent of the mean total stress and only deviatoric stresses  $s_{ij}$  appear in the yield or loading functions. For mathematical simplicity, the simple von Mises function was used by Prevost (1977, 1978). The loading functions,  $f_i$ , are then represented by equations of the following form

$$f_i = \left\{ \frac{3}{2} [s_{ij} - \alpha_{ij}^{(i)}] [s_{ij} - \alpha_{ij}^{(i)}] \right\}^{1/2} - k^{(i)} = 0 \quad (7.24)$$

where  $i = 1, 2, \dots, p$  and  $\alpha_{ij}^{(i)}$  represent the coordinates of the centre of the yield surface,  $f_i$ , in the deviatoric stress space. For the special case of  $\alpha_{ij}^{(i)} = 0$ , the above equation reduces to

$$f_i = \sqrt{3J_2} - k^{(i)} = 0 \quad (7.25)$$

Since the  $\alpha_{ij}^{(i)}$  are not necessarily all equal to zero, the yielding of soils is thus generally anisotropic. A plastic modulus,  $K_p^{(i)}$ , is associated with each of the yield surfaces. It was assumed that the plastic potential is identical to the loading surface and therefore the associated flow rule is obtained.

It is noted that the outmost yield surface,  $f_p$ , represents a failure surface, beyond which any stress states and inner yield surfaces cannot go.

According to Mroz's translation rule, all yield surfaces may be translated in stress space by the stress point without changing in form nor orientation, and they consecutively touch and push each other but cannot intersect. Consider a situation shown in Figure 7.4, when, after moving along a stress path, the stress point reaches the yield surface  $f_i$ . All the smaller yield surfaces,  $f_1, f_2, \dots, f_{i-1}$ , have been translated to become tangential to each other and to  $f_i$  at the common contact point P. From similarity, we have

$$\frac{s_{ij} - \alpha_{ij}^{(1)}}{k^{(1)}} = \frac{s_{ij} - \alpha_{ij}^{(2)}}{k^{(2)}} = \dots = \frac{s_{ij} - \alpha_{ij}^{(i-1)}}{k^{(i-1)}} = \frac{s_{ij} - \alpha_{ij}^{(i)}}{k^{(i)}} \quad (7.26)$$

#### Plastic flow rule

The plastic strain rate is the sum of the elastic and plastic components. The plastic strain rate is assumed to be normal to the yield surface at the stress point. In tensor notation, it can be written as follows (Prevost, 1978)

$$de_{ij} = \frac{ds_{ij}}{2G} + \frac{3}{2K_p^{(i)}} \frac{[s_{ij} - \alpha_{ij}^{(i)}]}{[k^{(i)}]^2} [s_{kl} - \alpha_{kl}^{(i)}] ds_{kl} \quad (7.27)$$

which can also be inverted to give

$$ds_{ij} = 2Gde_{ij} - \frac{3[2G - K_t^{(i)}]}{2} \frac{[s_{ij} - \alpha_{ij}^{(i)}]}{[k^{(i)}]^2} [s_{kl} - \alpha_{kl}^{(i)}]de_{kl} \quad (7.28)$$

The plastic shear modulus  $K_p^{(i)}$  in equation (7.27) can be obtained by the following equation

$$\frac{1}{K_p^{(i)}} = \frac{1}{K_t^{(i)}} - \frac{1}{2G} \quad (7.29)$$

in which the total modulus  $K_t^{(i)}$  can be obtained from a triaxial stress-strain curve as shown in Figure 7.5.

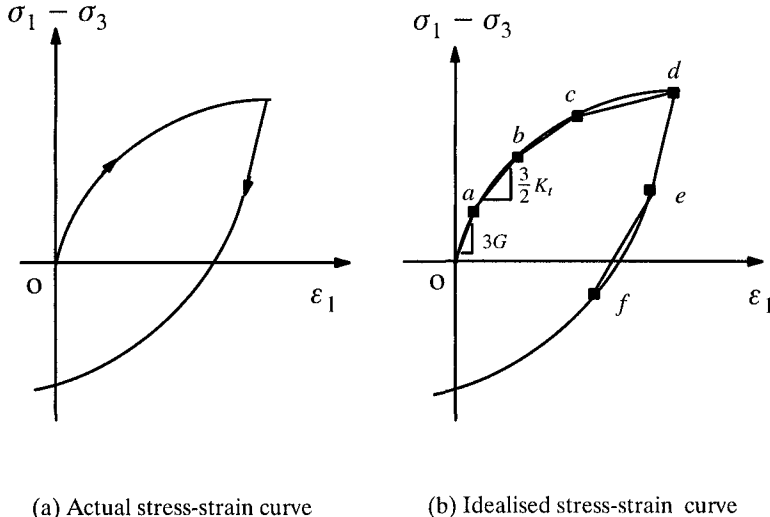


Figure 7.5: Determination of the plastic shear moduli from triaxial test results

#### Hardening rule

When the current stress point lies on the yield surface,  $f_i$ , and moves towards the next yield surface,  $f_{i+1}$ , the instantaneous translation of the yield surface  $f_i$  is

$$d\alpha_{ij}^{(i)} = d\mu \overline{PR}_{ij} \quad (7.30)$$

where

$$\overline{PR}_{ij} = \frac{k^{(i+1)}}{k^{(i)}} [s_{ij} - \alpha_{ij}^{(i)}] - [s_{ij} - \alpha_{ij}^{(i+1)}] \quad (7.31)$$

and  $k^{(i)}$  and  $k^{(i+1)}$  are the instantaneous sizes of the yield surfaces  $f_i$  and  $f_{i+1}$  respectively, for a given plastic strain level,  $\alpha$ . In other words, the yield surfaces are also allowed to expand or contract apart from translation.

The constant  $d\mu$  can be determined from the condition that the current stress point remains on the yield surface (i.e. Prager's consistency condition) as follows

$$d\mu = \frac{b}{a} \left( 1 - \sqrt{1 - \frac{2ac}{b^2}} \right) \quad (7.32)$$

where

$$a = [k^{(i+1)}]^2 + \frac{3}{2}[s_{ij} - \alpha_{ij}^{(i+1)}][s_{ij} - \alpha_{ij}^{(i+1)}] - 2d\frac{k^{(i+1)}}{k^{(i)}} \quad (7.33)$$

$$b = k^{(i+1)}k^{(i)} + \frac{3}{2}\overline{PR}_{ij} ds_{ij} - d \quad (7.34)$$

$$c = \frac{3}{2}[s_{ij} - \alpha_{ij}^{(i+1)}]ds_{ij} + \frac{3}{4}ds_{ij}ds_{ij} - k^{(i)}dk^{(i)} - \frac{1}{2}[dk^{(i)}]^2 \quad (7.35)$$

$$d = \frac{3}{2}[s_{ij} - \alpha_{ij}^{(i)}][s_{ij} - \alpha_{ij}^{(i+1)}] \quad (7.36)$$

If the stress increment  $ds_{ij}$  and yield surface expansion  $dk^{(i)}$  are relatively small, then equation (7.32) can be simplified to

$$d\mu = \frac{\frac{3}{2}[s_{ij} - \alpha_{ij}^{(i)}] ds_{ij} - k^{(i)}dk^{(i)}}{k^{(i)}k^{(i+1)} - \frac{3}{2}[s_{ij} - \alpha_{ij}^{(i+1)}][s_{ij} - \alpha_{ij}^{(i)}]} \quad (7.37)$$

The multi-surface plasticity model described in this section has been used successfully by Prevost *et al.* (1981) in a finite element modelling of centrifuge soil-structure interaction models under both monotonic and cyclic loadings.

It is worth mentioning that a simplified version of Prevost's model (i.e. without softening and using Iwan's translation rule instead of Mroz's translation rule) was used by Housby (1999) for finite element analysis of three-dimensional tunnel problems in undrained clay.

### 7.3.2 Multi-surface modelling of frictional soils

An extension of the above multi-surface plasticity model for undrained clay has been made by Prevost (1985) and Lacy and Prevost (1987) to simulate the stress-strain behaviour of cohesive-frictional soils. A key difference between the behaviours of undrained and frictional soils is that the yielding of frictional soil depends on mean effective stress.

### (a) Formulation for triaxial stress states

For triaxial loading, we have the following effective stress variables

$$p = \frac{1}{3}(\sigma_1' + 2\sigma_3') \quad ; \quad q = \sigma_1' - \sigma_3' \quad (7.38)$$

The yield function is chosen to be of the following form

$$f_i = (q - \bar{p}\alpha^i)^2 - (\bar{p}M^i)^2 = 0 \quad (7.39)$$

where

$$\bar{p} = p - a \quad (7.40)$$

and the yield surfaces and the meaning of  $M$ ,  $\beta$  and  $a$  are shown in Figure 7.6 in both two and three dimensions. For  $a = 0$ , the soil becomes purely frictional.

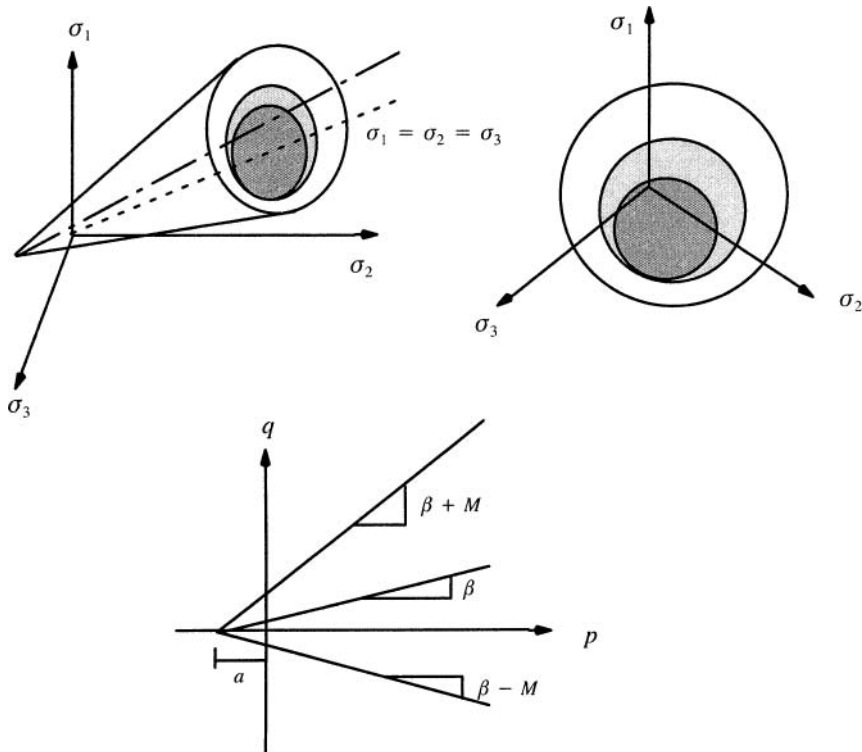


Figure 7.6: Multi-surface model for frictional soils

To ensure that the loading surfaces do not insect, the following condition must be satisfied

$$M^{i+1} + \alpha^{i+1} \geq M^i + \alpha^i \quad (7.41)$$

### (b) Formulation for general stress states

#### *Yield/loading function*

In terms of deviatoric stress and mean stress tensor, the yield function takes the following form

$$f_i = \frac{3}{2}(s_{ij} - \bar{p}\alpha_{ij}^i)(s_{ij} - \bar{p}\alpha_{ij}^i) - (\bar{p}M^i)^2 = 0 \quad (7.42)$$

where the deviatoric stress tensor is defined by

$$s_{ij} = \sigma_{ij} - p\delta_{ij} \quad (7.43)$$

#### *Plastic flow rule*

The plastic strain is assumed to be the sum of two components

$$d\epsilon_{ij}^p = d\lambda \frac{\partial(g_1^i + g_2^i)}{\partial\sigma_{ij}} \quad (7.44)$$

where the two plastic potential functions are

$$g_1^i = \frac{3}{2}(s_{ij} - \bar{p}\alpha_{ij}^i)(s_{ij} - \bar{p}\alpha_{ij}^i) \quad (7.45)$$

$$g_2^i = \frac{(\eta/\bar{\eta})^2 - 1}{(\eta/\bar{\eta})^2 + 1} \delta_{ij} \quad (7.46)$$

in which

$$\eta = \frac{\sqrt{\frac{3}{2}s_{ij}s_{ij}}}{\bar{p}} \quad (7.47)$$

and  $\bar{\eta}$  is a material constant, and if  $\eta/\bar{\eta} < 1$ ,  $g_2^i < 0$ , then plastic compression will occur; otherwise if  $\eta/\bar{\eta} > 1$ ,  $g_2^i > 0$  then plastic dilation will occur. In other words, the case  $\eta = \bar{\eta}$  corresponds to no plastic volumetric strains which is known be the critical state.

#### *Kinematic translation rule*

Like in undrained clay, Mroz's translation rule is used. Thus the centre of the yield cone will move along the direction that is along the vector linking the current stress point P and its conjugate point R in the next yield surface in the deviatoric plane,

$$\bar{p}da_{ij} = d\mu \bar{PR}_{ij} \quad (7.48)$$

where we can easily obtain

$$\bar{PR}_{ij} = \frac{M^{i+1}}{M^i} (s_{ij} - \bar{p}\alpha_{ij}^i) - (s_{ij} - \bar{p}\alpha_{ij}^{i+1}) \quad (7.49)$$

and  $d\mu$  can be determined from the consistency condition that the stress point remains on the current yield surface.

For each yield surface, it is assumed that the plastic modulus can be calculated by

$$K_p = K_p' (p/p_1)^n \quad (7.50)$$

where  $n$  is a material constant,  $p_1$  a reference pressure, and

$$K_p' = \frac{K_c - K_e}{2} \theta + \frac{K_c + K_e}{2} \quad (7.51)$$

in which the plastic moduli  $K_c$  and  $K_e$  are measured from triaxial compression and tension tests; and also we have

$$\theta = \frac{\bar{J}_3}{M\bar{p}\bar{J}_2} \quad (7.52)$$

and

$$\bar{J}_2 = \bar{s}_{ij}\bar{s}_{ij} \quad (7.53)$$

$$\bar{J}_3 = \det(\bar{s}_{ij}) \quad (7.54)$$

$$\bar{s}_{ij} = s_{ij} - \bar{p}\alpha_{ij}^i \quad (7.55)$$

### Model constant identification from triaxial tests

For simplicity, we will consider the model formulation for the purely frictional case to illustrate how the model constants can be identified from triaxial tests. In triaxial stress space, the stress-strain relations are given by Prevost (1985):

$$d\epsilon_q = \frac{dq}{3G} + \frac{2}{3K_p} \times \frac{dq - \eta dp}{1 + \frac{2}{9}\eta^2} \quad (7.56)$$

$$d\epsilon_p = \frac{dp}{K} + \frac{2}{\sqrt{6}K_p} \times \frac{1 - (\eta/\bar{\eta})^2}{1 + (\eta/\bar{\eta})^2} \times \frac{dq - \eta dp}{\sqrt{1 + \frac{2}{9}\eta^2}} \quad (7.57)$$

where  $\eta = \eta_c = \beta + M$ ;  $\bar{\eta} = \bar{\eta}_c$  for yielding caused by loading in compression and  $\eta = \eta_e = \beta - M$ ;  $\bar{\eta} = \bar{\eta}_e$  for yielding due to loading in extension.

The identification of the model constants associated with any yield surface  $f$  is made as follows. The smooth experimental shear stress-strain curves are approximated by linear segments along which the tangent (or secant) modulus is constant. It is obvious that the accuracy achieved by this linear approximation is directly dependent upon the number of linear segments used. The yield surface  $f$  is identified by the condition that the slope  $dq/d\epsilon_q$  be the same in compression and extension. This is shown in Figure 7.7. The model constants are then simply derived from the use of equations (7.56) and (7.57) and the known stress paths used in the triaxial tests. Once the elastic moduli  $G$  and  $K$  are known, the identification procedure has been shown to be straightforward (Prevost, 1985).

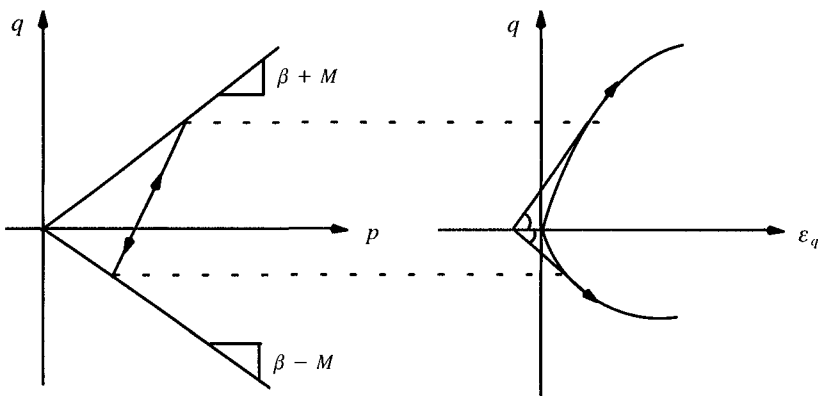


Figure 7.7: Identification of multi-surfaces for frictional soils (after Prevost, 1985)

#### 7.4 THE BOUNDING SURFACE CONCEPT

By assuming a piecewise linear stress-strain behaviour, the theory of multi-surface plasticity described in the previous sections cannot predict the smooth transition from elastic to fully plastic state for general loading which is observed experimentally on most materials. The theory of bounding surface (or two surface) plasticity has been developed to overcome this limitation of multi-surface plasticity.

The concept of a bounding (or limit) surface was first proposed by Krieg (1975) and Dafalias and Popov (1975) independently for modelling cyclic behaviour of metals. As shown in Figure 7.8, this theory makes use of two surfaces, an inner loading/yield surface ( $f=0$ ) and an outer bounding/limit surface ( $F=0$ ). As stated by Krieg (1975), the theory of bounding surface plasticity is best described as Mroz's multi-surface theory with a continuum of intermediate loading surfaces where the

distribution of these surfaces is analytically described *a priori*. The location of the inner and outer surfaces completely describes the distribution of all intermediate surfaces so reference to them is not necessary.

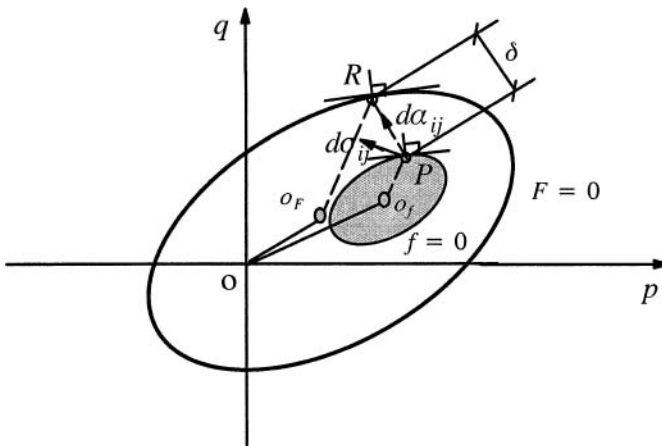


Figure 7.8: Theory of bounding surface plasticity

The key feature of the bounding surface concept is that the hardening of the loading surface (i.e. plastic modulus) depends on a distance vector from the current stress state to the bounding surface (i.e.  $\delta$  in Figure 7.8). Therefore when the stress state is remote from the bounding surface, the material is stiff. On the other hand, if the stress state is near the bounding surface, the material adopts a stiffness that is similar to that of the bounding surface. In this way, a smooth transition from a high to a low stiffness is achieved during a plastic loading process. A detailed outline of the mathematical foundation of the bounding surface plasticity is given by Dafalias (1986).

Since its development, the concept of bounding surface plasticity has been used widely by many researchers as the basis for developing numerous plasticity models for clay (Mroz *et al.*, 1978, 1979; Dafalias and Herrmann, 1982; Al Tabbaa and Wood, 1989; Whittle, 1993; Li and Meissner, 2002) and sand (Bardet, 1987). Yu and Khong (2003) recently proposed a unified bounding surface model for clay and sand.

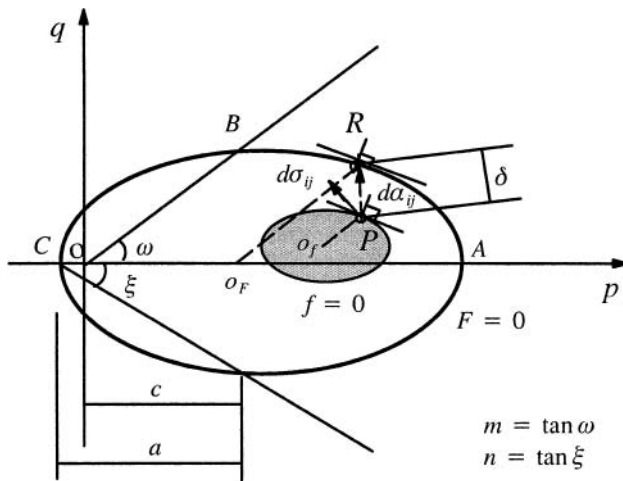


Figure 7.9: Mroz's two-surface formulation

## 7.5 BOUNDING SURFACE MODELS FOR SOILS

### 7.5.1 Two surface kinematic hardening formulation for clay

Following the formulation of Krieg (1975) and Dafalias and Popov (1975), Mroz *et al.* (1979) presented a general effective stress formulation for bounding surface plasticity of clay soils. The formulation makes use of a yield surface and a bounding surface and kinematic hardening for the yield surface. Mroz's formulation for clay was based on the critical state theory and was later followed and further evaluated by Al-Tabbaa and Wood (1989) for cyclic behaviour of clay soils.

#### (a) Yield and bounding surface equations

In the formulation of Mroz *et al.* (1979), the state boundary surface (or consolidation surface) in the critical state theory is regarded as the bounding surface. The surface is assumed to be in a general elliptic form

$$F(p, q, \epsilon_p^p) = (p - c)^2 + \frac{q^2}{n^2} - a^2 = 0 \quad (7.58)$$

where  $c$  and  $a$  are shown in Figure 7.9 and also we have

$$m = \tan \omega ; \quad n = \tan \xi ; \quad \frac{n}{m} = \frac{c}{a} \quad (7.59)$$

The inner yield surface is assumed to be of a same form expressed by

$$f(p, q, \varepsilon_p^p) = (p - \alpha_p)^2 + \frac{(q - \alpha_q)^2}{n^2} - a_0^2 = 0 \quad (7.60)$$

where  $(\alpha_p, \alpha_q)$  are the coordinates of the centre of the yield surface. The yield surface may translate within the domain enclosed by the boundary surface.

### (b) Associated flow rule

If the associated flow rule is assumed for the yield surface, we can follow the usual procedure to obtain the plastic strain rates as follows

$$d\varepsilon_p^p = \frac{1}{H} \frac{\partial f}{\partial p} df = \frac{2}{H} (p - \alpha_p) df \quad (7.61)$$

$$d\varepsilon_q^p = \frac{1}{H} \frac{\partial f}{\partial q} df = \frac{2}{H} \frac{q - \alpha_q}{n^2} df \quad (7.62)$$

in which  $H$  is a hardening parameter and

$$df = \frac{\partial f}{\partial p} dp + \frac{\partial f}{\partial q} dq = 2(p - \alpha_p) dp + 2 \frac{q - \alpha_q}{n^2} dq \quad (7.63)$$

The above plastic strain rates can also be written in the following form

$$d\varepsilon_p^p = \frac{1}{K_p} n_p d\sigma_n \quad (7.64)$$

$$d\varepsilon_q^p = \frac{1}{K_p} n_q d\sigma_n \quad (7.65)$$

where  $K_p$  is an alternative plastic hardening modulus which is equal to the ratio of the stress increment along the normal to the yield surface to the magnitude of the plastic strain increments; and  $n_p$  and  $n_q$  are components of the unit normal to the yield surface, namely

$$n_p = \frac{\frac{\partial f}{\partial p}}{\sqrt{\left(\frac{\partial f}{\partial p}\right)^2 + \left(\frac{\partial f}{\partial q}\right)^2}} = \frac{p - \alpha_p}{G_f} \quad (7.66)$$

$$n_q = \frac{\frac{\partial f}{\partial q}}{\sqrt{\left(\frac{\partial f}{\partial p}\right)^2 + \left(\frac{\partial f}{\partial q}\right)^2}} = \frac{q - \alpha_q}{n^2 G_f} \quad (7.67)$$

and

$$G_f = \sqrt{(p - \alpha_p)^2 + \frac{(q - \alpha_q)^2}{n^4}} \quad (7.68)$$

$$d\sigma_n = \frac{1}{G_f} \left[ (p - \alpha_p)dp + \frac{q - \alpha_q}{n^2}dq \right] \quad (7.69)$$

**(c) Rules of translation and expansion/contraction of yield and bounding surfaces**

We now formulate the rules of translation and expansion or contraction of the yield and bounding surfaces. For simplicity, the yield surface is allowed to translate and expand or contract during plastic loading, but the bounding surface only undergoes expansion or contraction during the loading process.

For the translation of the yield surface within the bounding surface, the rule of Mroz (1967) is used to ensure that both surfaces do not overlap at any time. This means that the centre of the yield surface will move along the direction PR as shown in Figure 7.9. Note that the coordinates of the centres of the yield and bounding surfaces are denoted by  $(\alpha_p, \alpha_q)$  and  $(\frac{n}{m}a, 0)$  respectively. If we also allow the variation of the yield and bounding surface (i.e.,  $a$  and  $a_0$ ), it can be shown (Mroz *et al.*, 1979) that the change of the centre of the yield surface is defined by

$$da_q = d\mu[-q_p + \frac{a}{a_0}(q_p - \alpha_q)] + \frac{da - da_0}{a_0}(q_p - \alpha_q) \quad (7.70)$$

$$da_p = d\mu[c - p_p + \frac{a}{a_0}(p_p - \alpha_p)] + \frac{da - da_0}{a_0}(p_p - \alpha_p) + \frac{n}{m}da \quad (7.71)$$

where  $(p_p, q_p)$  denote the current stress state at point P. The use of the condition that the stress point remains on the yield surface leads to

$$f_p dp + f_{,q} dq - f_p da_p - f_{,q} da_q + f_{,a_0} da_0 = 0 \quad (7.72)$$

By substituting equations (7.70) and (7.71) into (7.72),  $d\mu$  can be determined.

We now remain to specify how expansion/contraction of the yield and bounding surfaces would depend on the plastic strain. As in the critical state theory, we assume that the size of the yield and bounding surface evolve with plastic volumetric strain, thus

$$da = \frac{\partial a}{\partial \epsilon_p^p} d\epsilon_p^p = \frac{1}{K_p} \frac{\partial a}{\partial \epsilon_p^p} n_p d\sigma_b \quad (7.73)$$

If the ratio of the sizes of the yield and bounding surfaces is assumed to be a constant, then we have

$$da_0 = \frac{a_0}{a} da \quad (7.74)$$

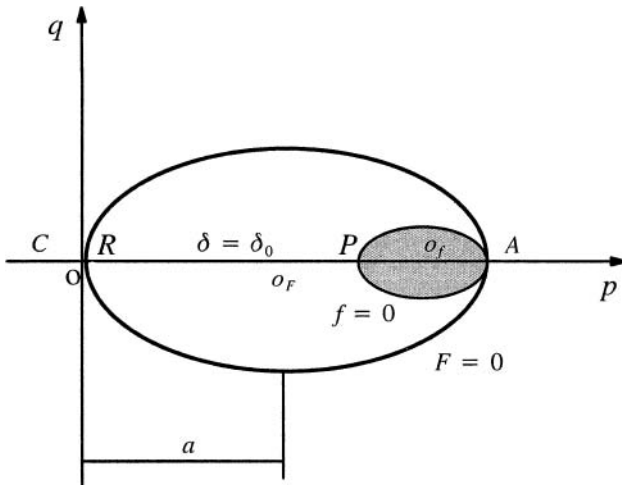


Figure 7.10: Situation with a maximum distance PR

**(d) Variation of plastic modulus – a mapping rule**

To complete the model we still need to assume how the plastic modulus changes in the domain between the yield and bounding surfaces. We can assume that the plastic modulus (either  $H$  or  $K_p$ ) varies continuously from its initial value  $K_p^P$  on the yield surface at point P to the value  $K_p^R$  on the bounding surface at R. To determine  $K_p^R$ , we can consider the case when both the yield and bounding surface are in contact. Since the plastic deformation is now determined by the bounding surface, we have

$$d\varepsilon_p^p = \frac{1}{K_p^R} n_p d\sigma_n \quad (7.75)$$

$$d\varepsilon_q^p = \frac{1}{K_p^R} n_q d\sigma_n \quad (7.76)$$

in which the plastic modulus  $K_p^R$  is derived from the consistency condition

$$\frac{\partial F}{\partial p} dp + \frac{\partial F}{\partial q} dq + \frac{\partial F}{\partial \varepsilon_p^p} d\varepsilon_p^p = 0 \quad (7.77)$$

as follows

$$K_p^R = -\frac{\partial F}{\partial \varepsilon_p^R} n_p \frac{1}{2G_F} \quad (7.78)$$

$$= \frac{1}{G_F^2} \left[ (p - \frac{n}{m}a) \frac{n}{m} + a \right] (p - \frac{n}{m}a) \frac{\partial a}{\partial \varepsilon_p^R} \quad (7.79)$$

where

$$G_F = \left[ (p - c)^2 + \frac{q^2}{n^4} \right]^{\frac{1}{2}} \quad (7.80)$$

It is interesting to note that for points A, B and C shown in Figure 7.9, equation(7.79) reduces to

$$K_p^A = (1 - \frac{n}{m}) \frac{\partial a}{\partial \varepsilon_p^A} \quad (7.81)$$

$$K_p^B = 0 \quad (7.82)$$

$$K_p^C = - (1 - \frac{n}{m}) \frac{\partial a}{\partial \varepsilon_p^C} \quad (7.83)$$

It is further noted that for modified Cam clay (when  $n=m$ ), the plastic moduli for points A, B and C are all equal to zero.

An analytical expression is normally assumed to determine the plastic modulus at point P as a function of the plastic modulus at R from (7.79) and the distance between points P and R. The distance between P and R can be determined as

$$\delta = \left[ \left( \frac{q_R - q_p}{n} \right)^2 + (p_R - p_p)^2 \right]^{\frac{1}{2}} \quad (7.84)$$

and the maximum distance is denoted by

$$\delta_0 = \max(\delta) \quad (7.85)$$

one such case with a maximum distance between P and R is shown in Figure 7.10 for the case when  $n=m$ . Now we have two boundary values:

$$K_p = K_{p0} \quad \text{when} \quad \delta = \delta_0 = \max(\delta) \quad (7.86)$$

$$K_p = K_p^R \quad \text{when} \quad \delta = 0 \quad (7.87)$$

For cases in between, we can determine the plastic modulus as

$$K_p^P = K_p^R + (K_{p0} - K_p^R) \left( 1 - \frac{\delta}{\delta_0} \right)^\gamma \quad (7.88)$$

in which  $\gamma$  is a material constant.

**(e) Complete incremental stress-strain relations**

Assuming the elastic stress-strain relation used in the critical state theory, the complete elastic-plastic stress-strain relations can now be determined as follows

$$d\epsilon_q = C_{11}dq + C_{12}dp \quad (7.89)$$

$$d\epsilon_q = C_{21}dq + C_{22}dp \quad (7.90)$$

where

$$C_{11} = \frac{1}{3G} + \frac{1}{K_p} \times \frac{(q - \alpha_q)^2}{n^4 G_f^2} \quad (7.91)$$

$$C_{12} = C_{21} = \frac{1}{K_p} \times \frac{(q - \alpha_q)(p - \alpha_p)}{n^2 G_f^2} \quad (7.92)$$

$$C_{22} = \frac{1}{K} + \frac{1}{K_p} \times \frac{(p - \alpha_p)^2}{G_f^2} \quad (7.93)$$

**(f) A special case: the bubble model of Al-Tabbaa and Wood (1989)**

The so-called bubble model proposed by Al-Tabbaa (1987) and Al-Tabbaa and Wood (1989) is an example of the two surface formulation of bounding surface plasticity presented above.

*Bounding/yield surfaces*

The model of Al-Tabbaa and Wood (1989) is based on the assumption that both the yield surface and bounding surface are of the same shape as for modified Cam clay (Roscoe and Burland, 1968). In other words, they are derived from the above formulation of Mroz *et al.* (1979) by setting  $m = n = M$ . It is noted that the parameter  $a$  used in Mroz *et al.* (1979) is equal to half of the preconsolidation pressure, namely

$$2a = p_0 \quad (7.94)$$

For simplicity, the ratio of the size of the bounding surface to that of the yield surface is regarded as a constant, thus

$$\frac{a_0}{a} = R \quad (7.95)$$

*Hardening rule*

The model of Al-Tabbaa and Wood (1989) is based on the assumption that the normal consolidation line is linear in the space of  $\ln v - \ln p$  rather than in the usual space of  $v - \ln p$ . This results in the following hardening rule

$$\frac{dp_0}{d\epsilon_p^p} = \frac{p_0}{\lambda^* - \kappa^*} \quad (7.96)$$

in which  $\lambda^*$  and  $\kappa^*$  are the slopes of the normal consolidation line and elastic swelling line in the space of  $\ln v$ - $\ln p$ .

### Translation rule

With the above assumptions, the change of the centre of the yield surface is simplified to

$$d\alpha_p = \frac{dp_0}{p_0} \alpha_p + d\mu \left( \frac{p - \alpha_p}{R} - (p - p_0/2) \right) \quad (7.97)$$

$$d\alpha_q = \frac{dp_0}{p_0} \alpha_q + d\mu \left( \frac{q - \alpha_q}{R} - q \right) \quad (7.98)$$

where the constant  $d\mu$  is derived from the consistency condition for the yield surface as follows

$$d\mu = \frac{(p - \alpha_p) \left( dp - p \frac{dp_0}{p_0} \right) + \frac{(q - \alpha_q)}{M^2} \left( dq - q \frac{dp_0}{p_0} \right)}{(p - \alpha_p) \left( \frac{p - \alpha_p}{R} - (p - p_0/2) \right) + \frac{q - \alpha_q}{M^2} \left( \frac{q - \alpha_q}{R} - q \right)} \quad (7.99)$$

### Plastic strain rates

Assuming an associated flow rule, the plastic strain rates can be derived from the yield function as follows

$$d\epsilon_p^p = \frac{1}{H} \left( (p - \alpha_p)^2 dp + \frac{1}{M^2} (p - \alpha_p)(q - \alpha_q) dq \right) \quad (7.100)$$

$$d\epsilon_q^p = \frac{1}{H} \left( \frac{1}{M^2} (p - \alpha_p)(q - \alpha_q) dp + \frac{(q - \alpha_q)^2}{M^2} dq \right) \quad (7.101)$$

The plastic modulus  $H$  is assumed to be a function of its value at the bounding surface  $H_p$  and the distance between the current stress point and its conjugate point on the bounding surface.  $H_p$  is obtained for the case when the yield surface and bounding surface are in contact, therefore

$$H_p = \frac{(p - \alpha_p)}{\lambda^* - \kappa^*} \left( p(p - \alpha_p) + \frac{q(q - \alpha_q)}{M^2} \right) \quad (7.102)$$

For the cases when the yield surface is not in contact with the bounding surface, the following simple equation is used to determine the plastic modulus

$$H = H_p + \frac{p_0^3}{\lambda^* - \varkappa^*} \left( \frac{b}{b_{\max}} \right)^\psi \quad (7.103)$$

where  $b$  is defined as the component of the distance between the current stress point and its conjugate point in the direction of the normal to the yield surface (Hashiguchi, 1985). Thus

$$b = \frac{p - \alpha_p}{p_0/2} \left( \frac{p - \alpha_p}{R} - (p - p_0/2) \right) + \frac{q - \alpha_q}{p_0 M^2} \left( \frac{q - \alpha_q}{R} - q \right) \quad (7.104)$$

and  $b_{\max}$  is a maximum reference value for  $b$  chosen when the relative position of the yield and bounding surfaces are as shown in Figure 7.10. In this case, we have

$$b_{\max} = (1 - R)p_0 \quad (7.105)$$

### 7.5.2 Radial mapping formulation of bounding surface plasticity

Another well known bounding surface formulation for clay was due to Dafalias and Herrmann (1982). This formulation was later adopted by Bardet (1986) to develop a bounding surface model for sand.

The basic idea of Dafalias and Herrmann's formulation is that an isotropically expanding or contracting loading surface, rather than a yield surface, is used in the model. In addition, a radial mapping is used to determine a unique 'image point' on the bounding surface that corresponds to the current stress point on the loading surface. This approach is considerably simpler than Mroz's two-surface kinematic hardening formulation, but at least in its original form is less suitable for modelling cyclic behaviour because it does not account for stress-induced anisotropy (Dafalias and Herrmann, 1982). As will be shown in the next section, however, a simple extension of Dafalias and Herrmann's formulation can be made to improve its accuracy in modelling soils under cyclic loads.

To describe this formulation, we will again consider a bounding surface  $F=0$  which may take the same form as modified Cam clay. It is also assumed that a loading surface  $f=0$ , which always passes the current stress point and the origin, is of the same form as that of the bounding surface, as shown in Figure 7.11. For simplicity, we assume that the elastic domain reduces to a point. In other words, plastic deformation occurs as soon as loading commences in stress space.

Let us consider a volumetric hardening bounding surface in a general form

$$F(\bar{p}, \bar{q}, \varepsilon_p^p) = 0 \quad (7.106)$$

where  $(\bar{p}, \bar{q})$  denotes the stress state on the bounding surface,  $\varepsilon_p^p$  is assumed to be the hardening parameter. Assume the loading surface is of the same form

$$f(p, q, \varepsilon_p^p) = 0 \quad (7.107)$$

The plastic strain increments are assumed to be governed by a plastic potential in a general form

$$g(q, p) = g(\bar{q}, \bar{p}) = 0 \quad (7.108)$$

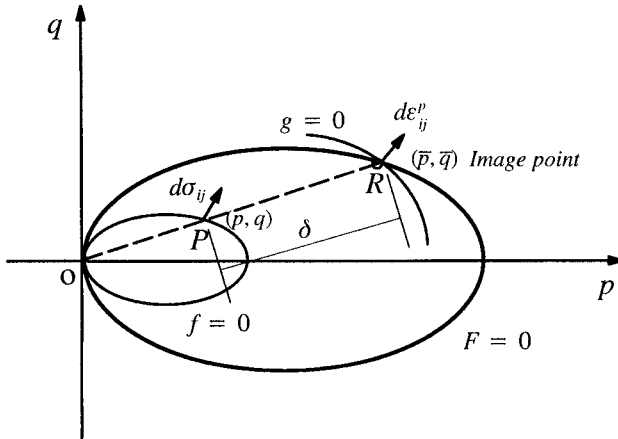


Figure 7.11: Bounding surface formulation with radial mapping

As stated in Dafalias and Herrmann (1982) and Dafalias (1986), the following three key equations complete the bounding surface formulation:

(1) It is assumed that stress increments at stress point  $(dp, dq)$ , and at image point  $(d\bar{p}, d\bar{q})$ , give the same plastic strain increment, therefore

$$\frac{1}{H} \left( \frac{\partial f}{\partial p} dp + \frac{\partial f}{\partial q} dq \right) \frac{\partial g}{\partial p} = \frac{1}{H} \left( \frac{\partial F}{\partial \bar{p}} d\bar{p} + \frac{\partial F}{\partial \bar{q}} d\bar{q} \right) \frac{\partial g}{\partial \bar{p}} \quad (7.109)$$

$$\frac{1}{H} \left( \frac{\partial f}{\partial p} dp + \frac{\partial f}{\partial q} dq \right) \frac{\partial g}{\partial q} = \frac{1}{H} \left( \frac{\partial F}{\partial \bar{p}} d\bar{p} + \frac{\partial F}{\partial \bar{q}} d\bar{q} \right) \frac{\partial g}{\partial \bar{q}} \quad (7.110)$$

If we introduce the following

$$n_p = \frac{1}{a_f} \frac{\partial f}{\partial p} \quad ; \quad n_q = \frac{1}{a_f} \frac{\partial f}{\partial q} \quad (7.111)$$

with

$$a_f = \sqrt{\left( \frac{\partial f}{\partial p} \right)^2 + \left( \frac{\partial f}{\partial q} \right)^2} \quad (7.112)$$

so that

$$(n_p)^2 + (n_q)^2 = 1 \quad (7.113)$$

In this way, we can easily show that  $(n_p, n_q)$  are the same for the stress point on the loading surface and the image point on the bounding surface as long as they are of the same form. In addition the same can be defined for a plastic potential

$$m_p = \frac{1}{a_g} \frac{\partial g}{\partial p} \quad ; \quad m_q = \frac{1}{a_g} \frac{\partial g}{\partial q} \quad (7.114)$$

with

$$a_g = \sqrt{\left(\frac{\partial g}{\partial p}\right)^2 + \left(\frac{\partial g}{\partial q}\right)^2} \quad (7.115)$$

With the above definitions, equations (7.109) and (7.110) reduce to

$$\frac{1}{K_p} (n_p dp + n_q dq) = \frac{1}{\bar{K}_p} (n_p d\bar{p} + n_q d\bar{q}) \quad (7.116)$$

in which the new plastic modulus  $K_p$  is linked to  $H$  by

$$K_p = \frac{H}{a_f a_g} \quad (7.117)$$

In terms of the plastic modulus  $K_p$ , the plastic strain rates are

$$d\varepsilon_p^p = \frac{1}{K_p} (n_p dp + n_q dq) m_p \quad (7.118)$$

$$d\varepsilon_q^p = \frac{1}{K_p} (n_p dp + n_q dq) m_q \quad (7.119)$$

(2) The bounding surface plastic modulus  $\bar{K}_p$  is obtained from the consistency condition  $dF = 0$ , namely

$$dF = \frac{\partial F}{\partial \bar{p}} d\bar{p} + \frac{\partial F}{\partial \bar{q}} d\bar{q} + \frac{\partial F}{\partial \varepsilon_p^p} d\varepsilon_p^p = 0 \quad (7.120)$$

with the aid of equations (7.116) and (7.118), the above equation becomes

$$\bar{K}_p = - \frac{1}{a_f a_g} \frac{\partial F}{\partial \varepsilon_p^p} \frac{\partial g}{\partial \bar{p}} \quad (7.121)$$

It is noted that all terms in equation (7.121) should be evaluated using stress states at the image point.

(3) The plastic modulus  $K_p$  needed to determine the plastic strain rates at the current stress point from equations (7.118) and (7.119) is assumed to be a function of

the distance between the current point  $(p, q)$  and its image point  $(\bar{p}, \bar{q})$  and the bounding surface plastic modulus  $\bar{K}_p$  derived from equation (7.121). Dafalias and Herrmann (1982) assumed that a possible function could be written as follows

$$K_p = \bar{K}_p + S(p, q, \varepsilon_p^p) \times \frac{\delta}{\delta_0 - \delta} \quad (7.122)$$

where  $S$  is an experimentally determined, positive shape hardening function of the state and the distance  $\delta$  is defined by

$$\delta = \sqrt{(\bar{p} - p)^2 + (\bar{q} - q)^2} \quad (7.123)$$

and  $\delta_0$  is a properly chosen reference distance such that  $\delta_0 - \delta \geq 0$ .

### 7.5.3 Bounding surface formulation for clay with three surfaces

Hashiguchi (1981) and Mroz *et al.* (1981) were among the first to suggest the use of three surfaces in a bounding surface formulation. The reason for Hashiguchi (1981) to use a third surface was to provide a smoother elastic-plastic transition than the theory of two surface plasticity. On the other hand, Mroz *et al.* (1981) used a third surface (termed intermediate surface), apart from the yield and bounding surface, to describe the progressive material degradation.

Based on experimental observation that the stress-strain behaviour of overconsolidated clays depends both on its current stress state and on the loading history, Stallebrass (1990) introduced a third surface (called history surface) into the theory of bounding surface plasticity. The 3-SKH model presented by Stallebrass (1990) and Stallebrass and Taylor (1997) is a simple extension of the two surface bubble model of Al-Tabbaa and Wood (1989). Most recently, further improvements on Stallebrass's model have been made by Hau (2003) and Hau and McDowell (2003) by using a non-associated flow rule.

#### *Bounding, history and yield surfaces*

The model of Stallebrass (1990) consists of three surfaces that are of the same form as that of modified Cam clay, namely

$$F(p, q, \varepsilon_p^p) = (p - p_0/2)^2 + \frac{(q)^2}{M^2} - \left(\frac{p_0}{2}\right)^2 = 0 \quad (7.124)$$

$$f_2(p, q, \varepsilon_p^p) = (p - p_a)^2 + \frac{(q - q_a)^2}{M^2} - \left(\frac{Tp_0}{2}\right)^2 = 0 \quad (7.125)$$

$$f_1(p, q, \varepsilon_p^p) = (p - p_b)^2 + \frac{(q - q_b)^2}{M^2} - \left(\frac{TS p_0}{2}\right)^2 = 0 \quad (7.126)$$

where  $F$  is the bounding surface and  $f_2$  and  $f_1$  are the history and yield surfaces respectively, Figure 7.12.  $(p_a, q_a)$  are the coordinates of the centre of the history surface and  $(p_b, q_b)$  are the coordinates of the centre of the yield surface.  $T$  is the ratio of the size of the history surface to that of the bounding surface.  $S$  is the ratio of the size of the yield surface to that of the history surface.

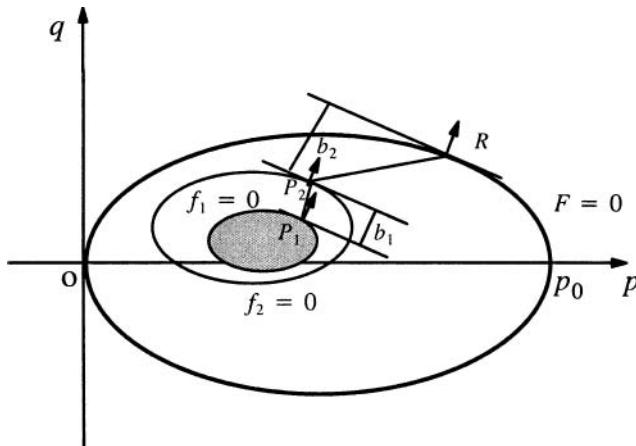


Figure 7.12: Bounding surface formulation with three surfaces

#### *Elastic stress-strain relations*

The model of Stallebrass (1990) has the same elastic stress-strain relations as that of Al-Tabbaa and Wood (1989), namely

$$d\epsilon_p^e = \frac{\kappa^*}{p} dp \quad (7.127)$$

$$d\epsilon_q^e = \frac{1}{3G} dp \quad (7.128)$$

#### *Plastic stress-strain relations*

The three surface model of Stallebrass (1990) has the same form of plastic stress-strain relations as that of Al-Tabbaa and Wood (1989) derived from an associated flow rule and the yield function,

$$d\epsilon_p^p = \frac{1}{H} \left( (p - p_b)^2 dp + \frac{1}{M^2} (p - p_b)(q - q_b) dq \right) \quad (7.129)$$

$$d\epsilon_q^p = \frac{1}{H} \left( \frac{1}{M^2} (p - p_b)(q - q_b) dp + \left( \frac{q - q_b}{M^2} \right)^2 dq \right) \quad (7.130)$$

The plastic modulus  $H$  is assumed to be a function of its value at the bounding surface  $H_p$  and the distance between the current stress point and its conjugate points on both the history surface and the bounding surface.  $H_p$  is obtained for the case when the yield surface, history surface and bounding surface are in contact, therefore

$$H_p = \frac{(p - p_b)}{\lambda^* - \kappa^*} \left( p(p - p_b) + \frac{q(q - q_b)}{M^2} \right) \quad (7.131)$$

For the cases when the yield surface is not in contact with the history and bounding surfaces, the following simple equation is used to determine the plastic modulus

$$H = H_p + \frac{p_0^3}{\lambda^* - \kappa^*} \left( \frac{b_2}{b_{2max}} \right)^\psi + \frac{S^2 p_0^3}{\lambda^* - \kappa^*} \left( \frac{b_1}{b_{1max}} \right)^\psi \quad (7.132)$$

where, as in the Al-Tabbaa and Wood two surface model,  $b_1$  is defined as the component of the distance between the current stress point  $P_1$  and its conjugate point on the history surface  $P_2$  in the direction of the normal to the yield surface. In the same way,  $b_2$  is defined as the component of the distance between the conjugate point on the history surface  $P_2$  and the conjugate point on the bounding surface  $R$  in the direction of the normal to the history surface, see Figure 7.12.

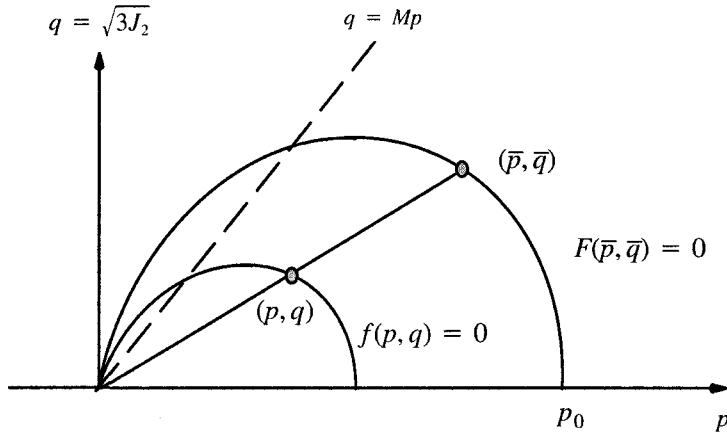


Figure 7.13: Bounding surface formulation CASM-b

## 7.6 UNIFIED BOUNDING SURFACE MODEL

In Chapter 6, a unified critical state model for clay and sand, CASM, developed by Yu (1995, 1998) has been presented. Its various extensions to include plastic strains

within the main yield surface (i.e. bounding surface) and also for accurately modelling cyclic behaviour have been given by Yu and Khong (2003), Khong (2004) and Yu *et al.* (2006). These extensions follow the general idea of the bounding surface concept and are therefore briefly described here.

### 7.6.1 Bounding surface formulation for monotonic loading – CASM-b

The extension of the basic unified clay and sand model CASM developed by Yu (1998) to include plastic strains within the main yield surface has been given by Yu and Khong (2003). This extended CASM model, termed CASM-b, is based on the radial mapping formulation of bounding surface plasticity, which is similar to those of Dafalias and Herrmann (1982) and Bardet (1986).

#### *Bounding/loading surfaces*

The bounding and loading surfaces in CASM-b are shown in Figure 7.13 which are the same as its parent model CASM, namely

$$F(\bar{p}, \bar{q}, \varepsilon_p^p) = \left( \frac{\bar{q}}{M\bar{p}} \right)^n + \frac{1}{\ln r} \ln\left(\frac{\bar{p}}{p_0}\right) = 0 \quad (7.133)$$

$$f(p, q, \varepsilon_p^p) = \left( \frac{q}{Mp} \right)^n + \frac{1}{\ln r} \ln\left(\frac{p}{\beta p_0}\right) = 0 \quad (7.134)$$

where  $\beta = q/\bar{q} = p/\bar{p}$  is the ratio of the size of the loading surface to that of the bounding surface, which is 0 at the origin and 1 at the image point on the bounding surface.

#### *Plastic potentials and flow rule*

To define a plastic potential, it is often necessary to use a stress-dilatancy relation between stress ratio and dilatancy rate. A most successful stress-dilatancy relation, which may now be considered to be one of the milestones in soil mechanics, is due to Rowe (1962):

$$\frac{d\varepsilon_p^p}{d\varepsilon_p^q} = \frac{9(M - \eta)}{9 + 3M - 2M\eta} \quad (7.135)$$

Rowe's stress-dilatancy relation, originally developed from minimum energy considerations of particle sliding, has met with greatest success in describing the deformation of sands and other granular media. Following the usual procedure, Rowe's stress-dilatancy relation (7.135) may be integrated to give the following plastic potential

$$g(p, q) = 3M \ln \frac{p}{C} + (3 + 2M) \ln \left( \frac{2q}{p} + 3 \right) - (3 - M) \ln (3 - \frac{q}{p}) = 0 \quad (7.136)$$

where the size parameter  $C$  can be determined easily for any given stress state  $(p, q)$  by solving equation (7.136). Note that the plastic flow rule adopted in CASM is non-associated, as the plastic potential is not identical to the yield surface.

Although Rowe's stress-dilatancy relation is accurate for high stress ratios, it is not particularly realistic for stress paths with low stress ratios (such as isotropic consolidation and 1D consolidation). To overcome this limitation, we can alternatively adopt a plastic potential that is in a similar form as the yield function in CASM but gives zero plastic volumetric strain increment at critical states. A slight modification of the stress-dilatancy equation (6.56) may be used

$$\frac{d\epsilon_p^p}{d\epsilon_q^p} = \frac{M^n - \eta^n}{m \eta^{n-1}} \quad (7.137)$$

where  $n$  is a material constant defined previously in CASM and  $m$  may be treated as a material constant independent of  $n$  and  $r$ . For  $n=1$ , the above stress-dilatancy reduces to the well-known plastic flow rule of Cam clay. By setting  $n=2$  and  $m=1$ , the plastic flow rule of modified Cam clay is recovered. By setting  $m=1$ , equation (7.137) reduces to the expression of McDowell (2002).

One possible approach is to choose  $m$  so that equation (7.137) can accurately model one-dimensional consolidation (Ohmaki, 1982; Alonso *et al.*, 1990; McDowell and Hau, 2003). In other words,  $m$  is selected to ensure that the flow rule predicts zero lateral strain for stress states corresponding to Jaky's (1948)  $K_0$  condition. As noted in Chapter 6,  $m$  can be shown to be related to the critical state constants in the following way

$$m = \frac{2}{3} \times \frac{[M(6 - M)]^n - (3M)^n}{A(6 - M) (3M)^{n-1}} \quad (7.138)$$

where  $\Gamma = (\lambda - \alpha)/\lambda$ .

Following the usual procedure, the general stress-dilatancy relation (7.137) may be integrated to give the following plastic potential:

$$g(p, q) = m \ln \left( 1 + (m - 1) \left( \frac{\eta}{M} \right)^n \right) + n(m - 1) \ln \frac{p}{C} \quad (7.139)$$

where  $C$  indicates the size of the plastic potential surface, which can be determined by solving the above equation with current stress values.

### *The plastic modulus at the image point of the bounding surface*

Following Dafalias and Herrmann (1982) and Bardet (1986), it is assumed that stress increments at stress point  $(dp, dq)$ , and at image point  $(d\bar{p}, d\bar{q})$ , give the same plastic strain increment, therefore the plastic volumetric strain rate at the current stress state can be expressed as

$$de_p^p = \frac{1}{H} \left( \frac{\partial f}{\partial p} dp + \frac{\partial f}{\partial q} dq \right) \frac{\partial g}{\partial p} = \frac{1}{H_b} \left( \frac{\partial F}{\partial \bar{p}} d\bar{p} + \frac{\partial F}{\partial \bar{q}} d\bar{q} \right) \frac{\partial g}{\partial \bar{p}} \quad (7.140)$$

where  $H$  and  $H_b$  are the plastic moduli at the current stress point and image point respectively.

The use of the consistency condition for the bounding surface requires

$$dF = \frac{\partial F}{\partial \bar{p}} d\bar{p} + \frac{\partial F}{\partial \bar{q}} d\bar{q} + \frac{\partial F}{\partial e_p^p} de_p^p = 0 \quad (7.141)$$

with the aid of equation (7.140), the above equation becomes

$$H_b = - \frac{\partial F}{\partial e_p^p} \frac{\partial g}{\partial \bar{p}} = - \frac{\partial F}{\partial p_0} \frac{\partial p_0}{\partial e_p^p} \frac{\partial g}{\partial \bar{p}} \quad (7.142)$$

It is noted that all terms in equation (7.142) can be determined. The hardening rule is specified and should be evaluated using stress states at the image point.

The expression for the bounding surface plastic modulus (7.142) is valid for any plastic potentials and volumetric laws. If we use the plastic potential derived from Rowe's stress-dilatancy relation and the usual hardening law given below

$$dp_0 = \frac{\nu p_0}{\lambda - \nu} de_p^p \quad (7.143)$$

then the bounding surface plastic modulus can be derived as follows

$$H_b = \frac{3\nu}{(\lambda - \nu)\bar{p} \ln r} \left( \frac{3 + 2M}{3 + 2\eta} - \frac{3 - M}{3 - \eta} \right) \quad (7.144)$$

If, however, the general plastic potential (7.139) is used, then the following expression for the bounding surface plastic modulus can be obtained

$$H_b = \frac{n(m-1)\nu}{(\lambda - \nu)\bar{p} \ln r} \left( 1 - \frac{m(\frac{\eta}{M})^n}{1 + (m-1)(\frac{\eta}{M})^n} \right) \quad (7.145)$$

### *The plastic modulus at the current stress point*

In bounding surface plasticity, the plastic modulus at the current stress point is assumed to be a function of the plastic modulus at its image point and how far it is

from the image point (i.e. the value of  $\beta$ ). In CASM-b, we use the following mapping function to derive the plastic modulus at the current stress point

$$H = H_b + \frac{h}{p} \times \frac{(1 - \beta)^\psi}{\beta} \quad (7.146)$$

which satisfies two boundary conditions

$$H = H_b \text{ when } \beta = 1 \quad (7.147)$$

$$H = +\infty \text{ when } \beta = 0 \quad (7.148)$$

where  $h$  and  $\psi$  are two additional material constants.

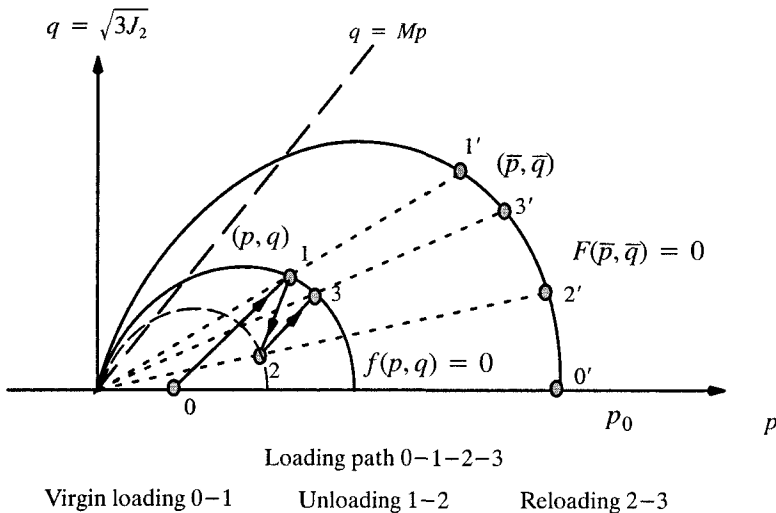


Figure 7.14: Bounding surface cyclic formulation CASM-c

### 7.6.2 Bounding surface formulation for cyclic loading – CASM-c

The radial mapping bounding surface formulation of CASM presented in the previous section is suitable for modelling monotonic loading of clay and sand. However the model is less accurate for predicting the stress-strain behaviour of soils under cyclic loading. This is mainly due to its isotropic hardening nature. In particular unloading is regarded as purely elastic in CASM-b and this is not consistent with observed cyclic behaviour of soils (Wood, 1982). In this regard, a two or three surface bounding surface model or a multi-surface plasticity formulation will have a better prediction capability for cyclic soil behaviour.

In this section, Yu and Khong's bounding surface model CASM-b is further developed with the aim of improving its accuracy in modelling cyclic behaviour (Yu *et al.*, 2006). This new cyclic soil model, termed CASM-c, has certain features that are similar to the model of McVay and Taesiri (1985).

The new model CASM-c divides a general loading path into three distinct types: virgin shear loading (the stress path 0–1), unloading (the stress path 1–2) and reloading (the stress path 2–3), as shown in Figure 7.14. For each type of loading, a different expression is used to determine the plastic modulus.

### *Virgin shear loading*

For virgin shear loading such as the stress path 0–1, it is natural to assume that the plastic modulus is calculated in the same way as in the model CASM-b, namely

$$H = H_b + \frac{h}{p} \times \frac{(1 - \beta)^\psi}{\beta} \quad (7.149)$$

where  $H_b$  is the plastic modulus at the image point on the bounding surface, which can be obtained from either (7.144) or (7.145).

### *Unloading*

For unloading (e.g. the stress path 1–2), the plastic modulus is determined by the following equation

$$H = \frac{H_u}{1 - \beta} \quad (7.150)$$

where  $H_u$  is a model constant. The above equation was also used by McVay and Taesiri (1985). With the above equation, the unloading behaviour is purely elastic if the stress point lies on the bounding surface ( $\beta = 1$ ). As the stress point moves away from the bounding surface ( $0 < \beta < 1$ ), the soil becomes less stiff and behaviour is elastic-plastic. Finally when the stress point is close to the origin (far from the bounding surface,  $\beta = 0$ ), the unloading plastic modulus reaches a minimum value  $H_u$ .

### *Reloading*

For reloading (e.g. the stress path 2–3), the plastic modulus is assumed to be governed by the following equation

$$H = H_b + H_R \times \left( \frac{1 - \beta}{\beta} \right) \times (1 + \varepsilon_q^p)^k \quad (7.151)$$

where  $H_R$  and  $k$  are two additional material constants and  $\varepsilon_q^p$  is the accumulated plastic shear strain. The soil behaviour under reloading is the reverse of the unload-

ing process. In other words, when the stress point is far away from the bounding surface ( $\beta = 0$ ), the plastic modulus is very large and the behaviour is almost purely elastic. The soil behaviour is elastic-plastic when the stress point is moving towards the bounding surface. But when the stress point lies on the bounding surface ( $\beta = 1$ ), the plastic modulus  $H = H_b$ , which can be readily calculated in the same way as in the model CASM-b.

### 7.6.3 Performance of CASM-c for simulating cyclic triaxial tests

#### (a) Cyclic triaxial tests on sand

A comprehensive triaxial testing programme on a granular soil called Portaway sand has been carried out by Wang (2005) at Nottingham. The main purpose of this laboratory study was to provide a valuable database for validating recently developed critical state models (Yu, 1998; Khong, 2004; Yu *et al.*, 2005; Yu *et al.*, 2006).

Yu *et al.* (2006) present a detailed comparison between measured cyclic soil behaviour and CASM-c simulations for various loading conditions. In the study, all the model constants for Portaway sand have been determined using conventional laboratory tests (Wang, 2005; Yu *et al.*, 2005). The values for the main model constants for Portaway sand are determined as follows:

$$\lambda = 0.025, \quad \varkappa = 0.005, \quad \mu = 0.16, \quad \Gamma = 1.796, \quad M = 1.190,$$

$$n = 3.5, \quad r = 19.2, \quad h = 5.0, \quad \psi = 1.0$$

#### *One-way undrained loading in compression or extension*

Figure 7.15 and Figure 7.16 show the experimental data (the left column) and CASM-c simulations (the right column) of one-way undrained cyclic loading in compression and extension respectively on very loose sand specimens. It is evident that the numerically simulated stress paths, stress-strain relationships and excess pore pressure developments are in general agreement with the experimental results. Three distinct stages of the tests are discussed and only the first two stages are modelled by CASM-c with the following observations:

- (1) Virgin loading: CASM-c captures two important features for tests in compression during this stage, which are occurrences of significant effective stress reduction and pore pressure increase at the first cycle. The tendency of pore pressure increase is not obvious in extension and this is also predicted by the model CASM-c.

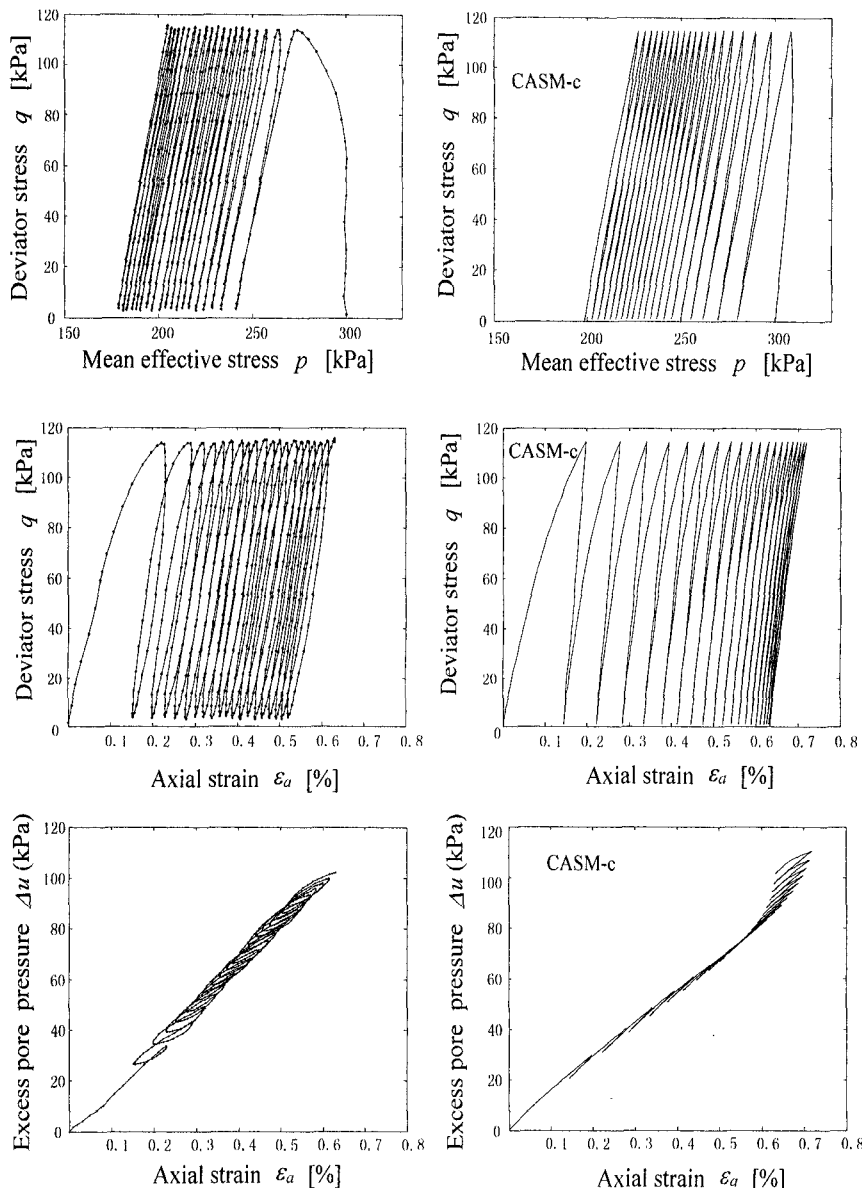


Figure 7.15: CASM-c simulations of measured undrained cyclic compression test

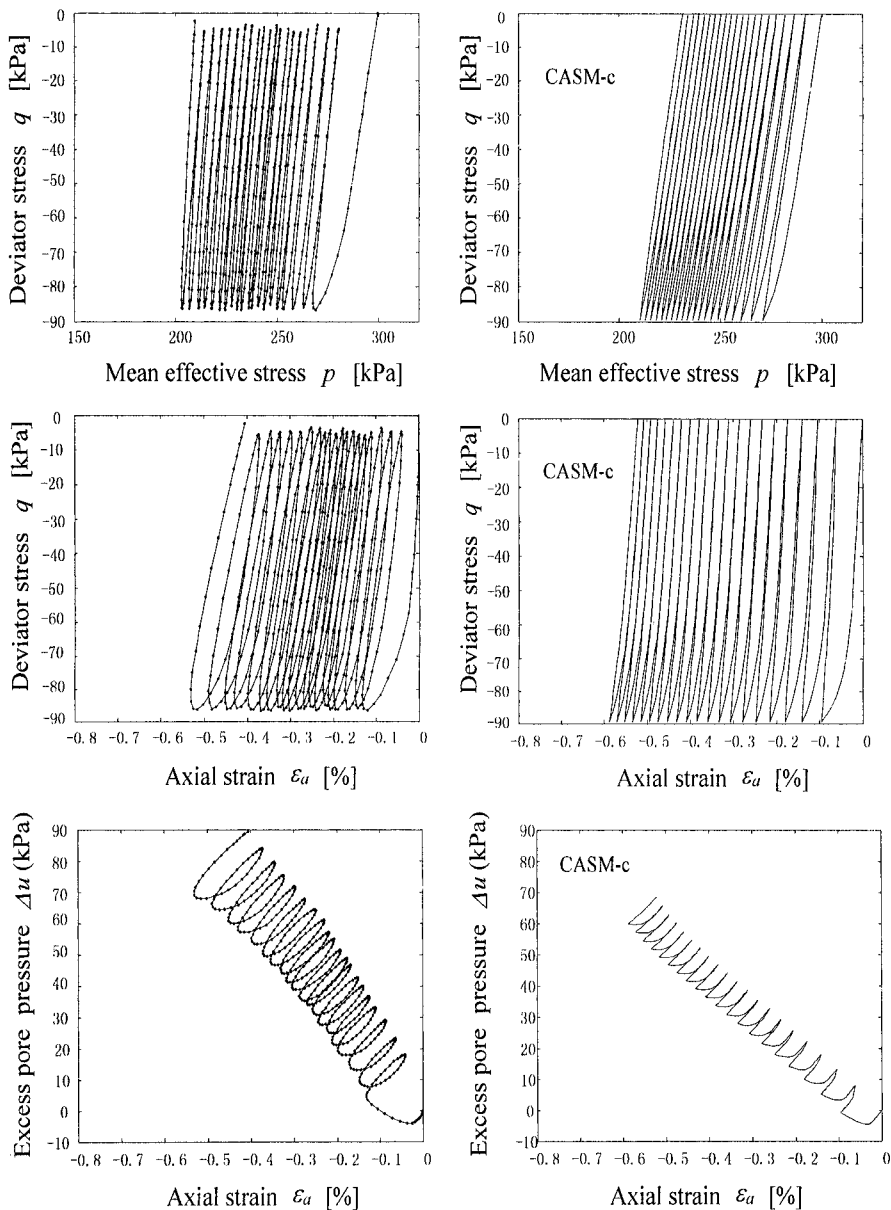


Figure 7.16: CASM-c simulations of measured undrained cyclic extension test

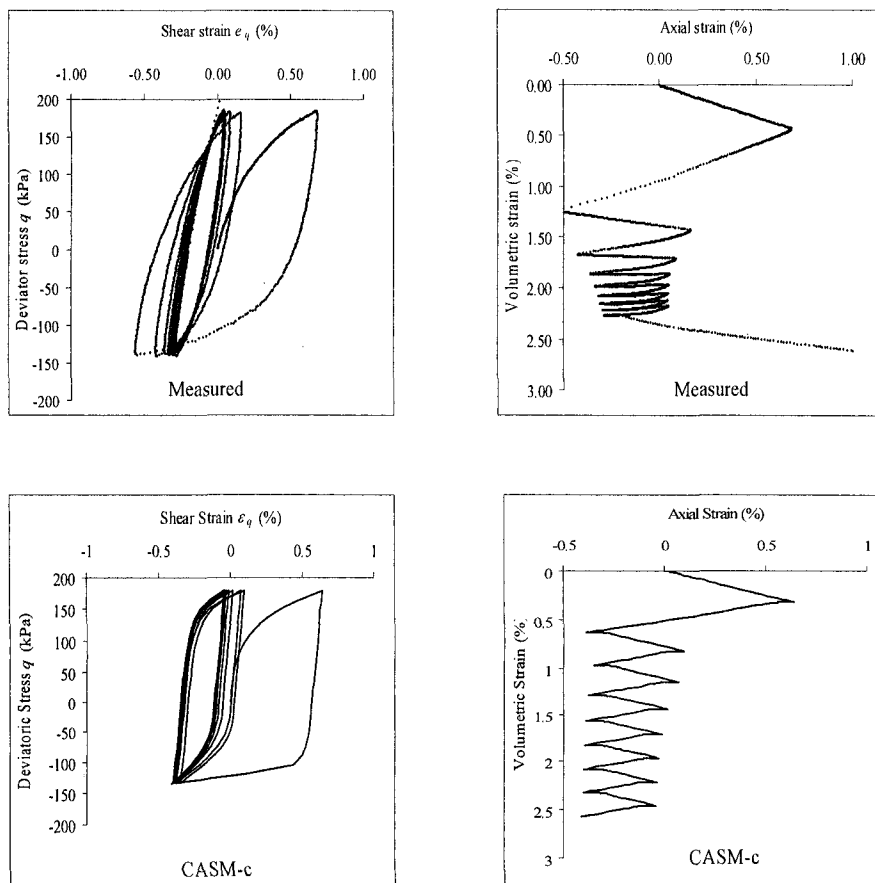


Figure 7.17: CASM-c simulations of measured two-way drained cyclic test

(2) Before liquefaction: 20 cycles are simulated by CASM-c. A striking feature of the effective stress path at this stage is that a significant reduction of mean effective stress occurs in the unloading segment, which is in agreement with many other independent experimental observations. A slight increase of mean effective stress is observed in the reloading segment. It can be seen that CASM-c simulations follow closely the trends of the experimental stress paths, but the hysteretic loops are not captured in the simulations.

(3) After liquefaction: This stage is characterized by a rapid change in plastic deformation, shear strength and excess pore pressure. The measured pore pressure is considered unreliable due to dynamic effects. Hence no attempts are made to model this unstable behaviour using CASM-c.

*Two-way drained loading with constant mean effective stress*

The results of CASM-c simulations and experimental data for a two-way drained cyclic loading test of a very loose Portaway sand are shown in Figure 7.17. A constant mean effective stress is maintained throughout the test. It can be seen that the size of stress-strain hysteretic loops decreases and the specimen undergoes densification continuously with cyclic loading. It is evident that the specimen has reached a 'shakedown' state after 8 cycles, at which the elastic behaviour becomes dominant. The CASM-c simulations broadly match the experimental results although the agreement for volumetric strains is not as good as that of stress-strain relationships. It is also clear that the observed hysteretic loops in this test can be modelled reasonably well by CASM-c.

**(b) Cyclic triaxial tests on clay**

As mentioned earlier, two of the recently developed cyclic models for clay are the two-surface bubble model by Al-Tabbaa (1987) and the three-surface 3-SKH model by Stallebrass (1990). These models have been used with some success to simulate the cyclic behaviour of clay. In this section, CASM-c will be compared with these two models to predict the behaviour of Speswhite kaolin under cyclic loading conditions.

Figure 7.18(a) shows the results of cyclic tests on normally consolidated Speswhite kaolin conducted by Al-Tabbaa (1987) where the stress ratio ( $\eta = q/p$ ) is plotted against the deviatoric and volumetric strains. The soil was isotropically consolidated to  $p = 300\text{kPa}$  and then loaded cyclically between a stress ratio of 0 and 0.34 at a constant cell pressure.

The tests carried out by Al-Tabbaa (1987) were simulated by Hau (2003) using both the Bubble and 3-SKH models. His results are plotted in Figure 7.18(b) and (c) respectively. It is clear that both of these models predict the right trend for shear strain and volumetric strain but the shear strain was greatly over-predicted after four cycles. The experimental results indicate that the shear strain stabilized but neither of these models can predict this behaviour. On the other hand, the volumetric strains predicted by these models are reasonable.

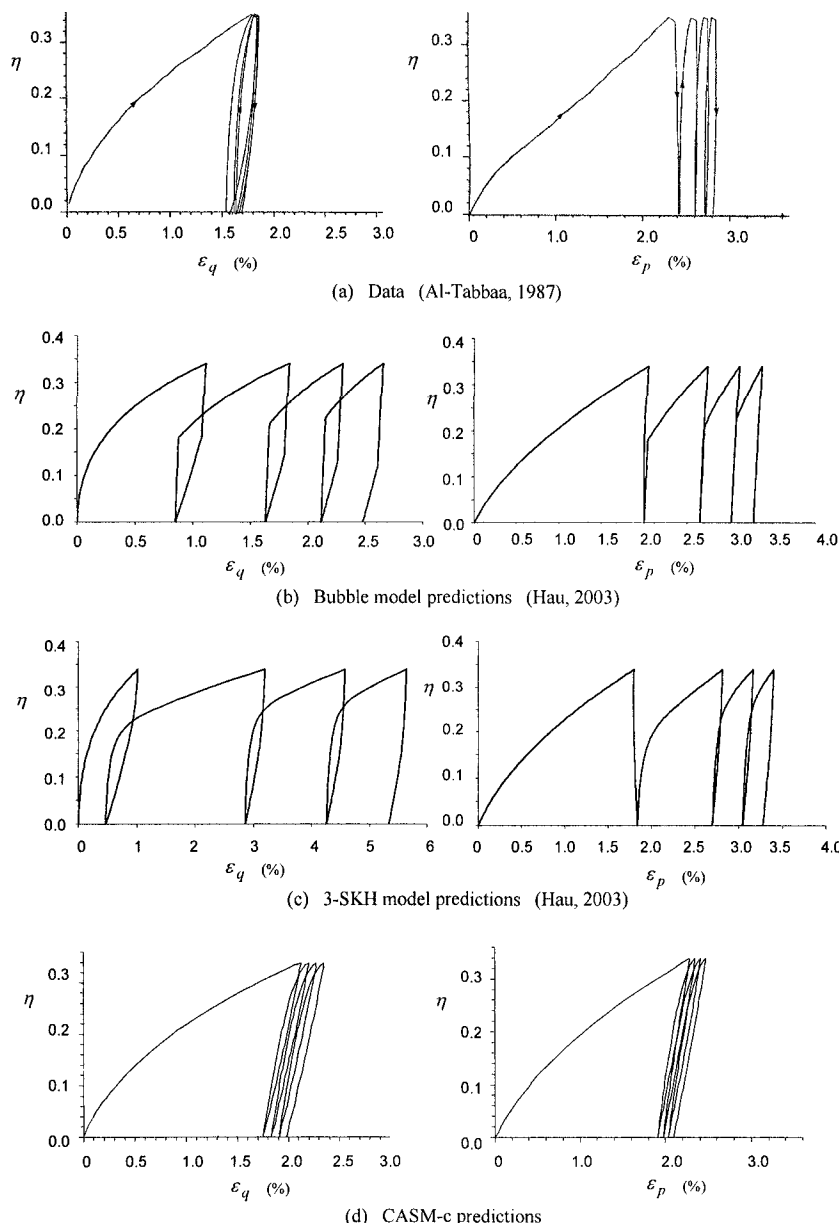


Figure 7.18: Measured and predicted clay behaviour under one-way drained cyclic loading (after Yu *et al.*, 2006)

Yu *et al.* (2006) present CASM-c simulations for this test. In the study, all the model constants for Speswhite kaolin are taken from Hau (2003). The values for the main model constants for Speswhite kaolin are determined as follows:

$$\lambda = 0.19, \quad \kappa = 0.03, \quad \mu = 0.3, \quad \Gamma = 3.056, \quad M = 0.86,$$

$$n = 2.0, \quad r = 2.718, \quad h = 5.0, \quad \psi = 1.0, \quad H_u = 0.15, \quad H_R = 0.5, \quad k = 30$$

The simulated responses by CASM-c are shown in Figure 7.18(d). It is evident that CASM-c gives a better prediction for the overall cyclic behaviour of the soil when compared with the Bubble and 3-SKH models. This is very encouraging given that the formulation for CASM-c is much easier to implement in finite element analysis (Khong, 2004).

## REFERENCES

Al-Tabbaa, A. (1987). *Permeability and Stress-Strain Response of Speswhite Kaolin*, PhD Thesis, Cambridge University.

Al-Tabbaa, A. and Wood, D.M. (1989). An experimentally based 'bubble' model for clay. *Proc. of NUMOG3*, 91-99.

Bardet, J.F. (1986). Bounding surface plasticity model for sand, *J. Eng. Mech.*, Vol 112, 1198-1217.

Dafalias, Y.F. (1986). Bounding surface plasticity. I: mathematical foundation and hypo-plasticity, *J. Eng. Mech.*, Vol 112, 966-987.

Dafalias, Y.F. and Herrmann, L.R. (1982). Bounding surface formulation of plasticity, *Soil Mechanics – Transient and Cyclic Loads*, (Editors: G.N. Pande and O.C. Zienkiewicz), 253-282.

Dafalias, Y.F. and Popov, E.P. (1975). A model of nonlinearly hardening materials for complex loadings, *Acta. Mech.*, Vol 21, 173-192.

Hashiguchi, K. (1981). Constitutive equations of elastoplastic materials with anisotropic hardening and elastic-plastic transition, *J. Appl. Mech.*, ASME, Vol 48, 297-301.

Hashiguchi, K. (1985). Two and three surface models of plasticity, *Proc. 5th Int. Conf. Numerical Methods in Geomechanics*, Nagoya, 125-134.

Hau, K.W. (2003). *Application of a Three surface kinematic Hardening Model to the Repeated Loading of Thinly Surfaced Pavements*, PhD Thesis, University of Nottingham, UK.

Hill, R (1950). *The Mathematical Theory of Plasticity*, Clarendon Press, Oxford.

Houlsby, G.T. (1999). A model for the variable stiffness of undrained clay. *Proc. Int. Symp. on Pre-failure Deformation of Soils*, Torino, Vol 1, 443-450.

Iwan, W.D. (1967). On a class of models for the yielding behaviour of continuous and composite systems, *J. Appl. Mech.*, Vol 34, 612-617.

Khong, C.D. (2004). *Development and Numerical Evaluation of Unified Critical State Models*, PhD Thesis, University of Nottingham, UK.

Khong, C.D. and Yu, H.S. (2002). Computational aspects of a unified critical state model for clay and sand, *Proc. 8th NUMOG*, Rome, 271-277.

Krieg, R.D. (1975). A practical two-surface plasticity theory, *J. Appl. Mech.*, Vol 42, 641-646.

Lacy, S.J. and Prevost, J.H. (1987). Constitutive model for geomaterials, *Proc. 2nd Int. Conf. on Constitutive Laws for Eng. Materials*, Elsevier, Vol 1, 149-160.

McDowell, G.R. (2002). A simple non-associated flow model for sand, *Granular Matter*, Vol 4, 65-69.

McVay, M. and Taesiri, Y. (1985). Cyclic behaviour of pavement base materials, *J. Geotech. Eng.*, ASCE, Vol 111, 1-17.

Mroz, Z. (1967). On the description of anisotropic hardening, *J. Mech. Phys. Solids*, Vol 15, 163-175.

Mroz, Z., Norris, V.A. and Zienkiewicz, O.C. (1978). An anisotropic hardening model for soils and its application to cyclic loading, *Int. J. Num. Anal. Meth. Geomech.*, Vol 2, 203-221.

Mroz, Z., Norris, V.A. and Zienkiewicz, O.C. (1979). Application of an anisotropic hardening model in the analysis of elasto-plastic deformation of soils, *Geotechnique*, Vol 29, 1-34.

Mroz, Z., Norris, V.A. and Zienkiewicz, O.C. (1981). An anisotropic critical state model for soils subject to cyclic loading, *Geotechnique*, Vol 31, 451-469.

Prager, W (1955). The theory of plasticity – a survey of recent achievements, *Proc. Inst. Mech. Eng.*, London, 3-19.

Prevost, J.H. (1977). Mathematical modelling of monotonic and cyclic undrained clay behaviour, *Int. J. Num. Anal. Meth. Geomech.*, Vol 1, 195-216.

Prevost, J.H. (1978). Plasticity theory for soil stress-strain behaviour, *J. Eng. Mech. Div.*, ASCE, Vol 104, 1117-1194.

Prevost, J.H. (1985). A simple plasticity theory for frictional cohesionless soils. *Soil Dynamics Earthquake Eng.*, Vol 4, 9-17.

Prevost, J.H., Cunny, B., Hughes, T.J.R. and Scott, R.F. (1981). Offshore gravity structures: analysis. *J. Geotech. Eng. Div.*, Vol 107, 143-165.

Roscoe, K.H. and Burland, J.B. (1968). On the generalised behaviour of wet clay. In: *Engineering Plasticity* (editors: J. Heyman and F.A. Leckie), Cambridge University Press, 535-609.

Rowe, P. W. (1962). The stress-dilatancy relation for static equilibrium of an assembly of particles in contact. *Proc. R. Soc. A.*, Vol 267, 500-527.

Schofield, A.N. and Wroth, C.P. (1968). *Critical State Soil Mechanics*, McGraw-Hill, London.

Simpson, B. (1992). Retaining structure: displacement and design, *Geotechnique*, Vol 42, 539-576.

Stallebrass, S.E. (1990). *The Effect of Recent Stress History on the Deformation of Over-consolidated Soils*, PhD Thesis, City University, UK.

Stallebrass, S.E. and Taylor, R.N. (1997). The development and evaluation of a constitutive model for the prediction of ground movements in overconsolidated clay. *Geotechnique*, Vol 47, 235-253.

Wang, J. (2005). *The Stress-Strain and Strength Characteristics of Portaway Sand*, PhD Thesis, University of Nottingham, UK.

Whittle, A.J. (1993). Evaluation of a constitutive model for overconsolidated clays. *Geotechnique*, Vol 43, 289-313.

Yoder, P.J. and Iwan, W.D. (1981). On the formulation of strain-space plasticity with multiple loading surfaces. *J. Appl. Mech.*, Vol 48, 773-778.

Yu, H.S. (1995). A unified critical state model for clay and sand. *Civil Engineering Research Report No 112.08.1995*, University of Newcastle, NSW.

Yu, H.S. (1998). CASM: A unified state parameter model for clay and sand. *Int. J. Num. Analy. Meth. Geomech.*, Vol 22, 621-653.

Yu, H.S. and Khong, C.D. (2003). Bounding surface formulation of a unified critical state model for clay and sand, *Proc. 3rd Int. Conf. Deformation Characteristics of Geomaterials*, Lyon, 1111-1118.

Yu, H.S., Khong, C.D. and Wang, J. (2006). A unified plasticity model for cyclic behaviour of clay and sand, *Mech. Res. Commun.* (in press).

Yu, H.S., Khong, C.D., Wang, J. and Zhang, G. (2005). Experimental evaluation and extension of a simple critical state model for sand. *Granular Matter*, Vol 7, 213-225.

Zheng, Y., Chu, J. and Xu, Z. (1986). Strain space formulation of the elasto-plastic theory and its finite element implementation. *Comput. Geotech.* Vol 2, 373-388.

Ziegler, H. (1959). A modification of Prager's hardening rule. *Quart. Appl. Math.* Vol 17, 55.

## CHAPTER 8

### NON-COAXIAL PLASTICITY

#### 8.1 INTRODUCTION

The plastic potential theory described so far in this book is by far the most popular theory used by geotechnical engineers to develop soil plasticity models. A major deficiency of the models based on plastic potential theory is that the principal axes of stress and plastic strain-rate are generally coincident (i.e. coaxiality). This assumption was first made by de Saint-Venant in 1870 with great physical insight (Hill, 1950). A theory of plasticity based on this fundamental coaxial assumption is termed as coaxial plasticity.

However, there is strong experimental and micromechanics-based evidence to suggest that in real granular materials these principal axes often do not coincide (Roscoe *et al.*, 1967; Drescher and de Jong, 1972; Drescher, 1976; Arthur *et al.*, 1977, 1980; Christofferson *et al.*, 1981; Zhang, 2003; Jiang *et al.*, 2005; Jiang and Yu, 2006). Experiments performed on granular materials (e.g. Roscoe, 1970; Arthur *et al.*, 1980; Ishihara and Towhata, 1983) show the effect of principal stress rotations on material response. Test results from torsional experiments in the hollow cylinder apparatus show that the assumption of coaxiality is generally valid when the principal stress directions are fixed during loading. However a significant deviation between principal stress and principal plastic strain rate directions occurs during the rotation of principal stress directions. Generally this deviation decreases with increasing shear stress level (Gutierrez *et al.*, 1991).

It is also noted that the classical potential theory may also predict a non-coaxial behaviour if the plastic potential is assumed to be an anisotropic function of the stress tensor. However this approach is unable to model the dependence of plastic strain rates on the stress rate that is tangential to the yield surface. This important feature has been observed in many soil experiments for many years (e.g. Tsutsumi and Hashiguchi, 2005).

The purpose of this chapter is to present some of the most recent developments of plasticity theories that are able to predict the observed non-coaxial behaviour.

#### 8.2 EVIDENCE OF NON-COAXIAL SOIL BEHAVIOUR

The non-coaxiality of the principal axes of stress and plastic strain rate tensors has been observed in the soil laboratory for many years (Roscoe, 1970; Drescher and

de Josselin de Jong, 1971; Arthur *et al.*, 1980; Gutierrez *et al.*, 1991; Joer *et al.*, 1998). This was achieved in the testing of soil elements where the axes of principal stress vary and the direction of principal plastic strain rates (or total strain rates) were measured. The tests that permit some control of the rotation of the principal axes of stresses include the simple shear test (Roscoe, 1953; Airey *et al.*, 1985), the directional cell test (Arthur *et al.*, 1977), and the torsional hollow cylinder test (Saad and Baah, 1967; Lade, 1975; Hight *et al.*, 1983).

### 8.2.1 Simple shear

The simple shear test is one of the earliest methods for laboratory testing of soils. In fact much of the initial work on the development of critical state soil mechanics at Cambridge rests on the results of simple shear experiments (Roscoe *et al.*, 1958; Roscoe, 1970; Stroud, 1971). A good review of simple shear testing of soils has been given by Airey *et al.* (1985) where both advantages and limitations of the test are highlighted. A major limitation of the test appears to be the practical difficulty of imposing a uniform normal and shear stress field on the shearing plane. In particular, the simple shear devices developed at both Cambridge (Roscoe, 1953) and NGI (Bjerrum and Landva, 1966) do not allow for the development of complementary shear stresses on the vertical sides normal to the plane of deformation. As a result the shear and normal stresses must be non-uniform along the plane of deformation (Airey *et al.* 1985). Nevertheless certain middle sections of the sample have been shown to deform uniformly in the Cambridge simple shear apparatus (Stroud, 1971; Budhu and Britto, 1987; Airey *et al.*, 1985).

Roscoe *et al.* (1967) appears to be the first to report the results from simple shear tests in sand concerning the non-coaxiality of the principal axes of stress and strain rate tensors. Shown in Figure 8.1 are typical measured directions of the principal axes of stress and strain rate tensors as reported by Roscoe *et al.* (1967). Plotted in the horizontal axis is the shear strain and in the vertical axis the angles of the minor principal stress and corresponding strain rate from the horizontal direction. It must be pointed out that for sand the difference between the total strain increment and plastic strain increment is rather small and therefore for the purpose of our discussion there is no need to distinguish between them (Gutierrez *et al.*, 1991). It is evident that in a test when the direction of the principal stress rotates, the corresponding direction of the principal strain rate does not coincide with that of the principal stress. The difference is very significant at a small shear strain and then gradually reduces with an increasing shear strain. A similar non-coaxial behaviour has also been reported by other researchers (e.g. Airey *et al.*, 1985).

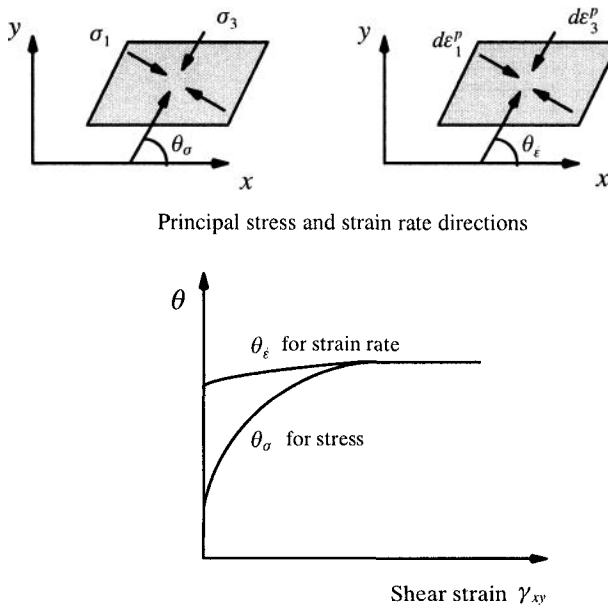


Figure 8.1: Typical non-coaxial behaviour in simple shear tests (Roscoe *et al.* 1967)

To improve the Cambridge simple shear device, Arthur *et al.* (1977) later developed a directional shear cell that is able to control the normal and shear stresses on the plane of deformation but also on the plane that is normal to the shearing plane. A similar apparatus (termed a general stress apparatus) has also been used by Matsuo *et al.* (1986) to test granular materials. The results from the studies by Matsuo *et al.* (1988) and Arthur *et al.* (1977, 1980) using the improved simple shear test devices have confirmed the results obtained earlier by Roscoe *et al.* (1967) in that the behaviour of granular material is generally non-coaxial.

### 8.2.2 Torsional shear using a hollow cylinder apparatus

Another widely used device that can be used to test soils subject to stress rotation is the hollow cylinder apparatus (Saada and Baah, 1967; Lade, 1975; Ishihara *et al.*, 1980), a brief review of which can be found in Hight *et al.* (1983). In particular, Gutierrez *et al.* (1991) used the hollow cylinder apparatus to study the effect of principal stress rotation on the plastic behaviour of sand. The hollow cylinder apparatus allows the independent control of the axial force  $F$ , torque  $T$ , inner and outer cell pressures  $p_i$  and  $p_o$  as shown in Figure 8.2. Application of these loads permits the control of four stress components on an element along the wall of the hollow

cylindrical soil. These stresses are the axial stress, radial stress, hoop stress and shear stress.

By controlling the four stress components, different tests can be performed on soils using the hollow cylinder apparatus. For example, a pure stress rotation test is accomplished by changing only  $\alpha$  while keeping the other parameters constant. The stress paths used in the tests by Gutierrez *et al.* (1991) were for a constant mean pressure  $p = (\sigma_1 + \sigma_3)/2 = (\sigma_z + \sigma_\theta)/2$ , which can therefore be represented in X-Y stress space with the following definitions:

$$X = \frac{1}{2}(\sigma_z - \sigma_\theta) \quad (8.1)$$

$$Y = \sigma_{z\theta} \quad (8.2)$$

In X-Y space, a vector from the origin has a distance equal to the radius of the Mohr's circle for stress

$$\tau_{\max} = \frac{1}{2}(\sigma_1 - \sigma_3) = \sqrt{\left(\frac{\sigma_z - \sigma_\theta}{2}\right)^2 + \sigma_{z\theta}^2} \quad (8.3)$$

and makes an angle of  $2\alpha$  from the X-axis.

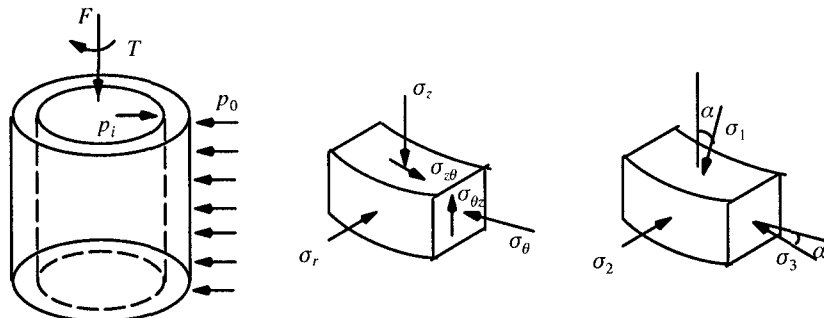


Figure 8.2: Stress components in a hollow cylinder test

As presented in Gutierrez *et al.* (1991), three types of test employing different stress paths in X-Y stress space were performed to investigate the effects of principal stress rotation on the plastic flow of sand. The first series involved monotonic loading tests along various fixed principal stress directions. The stress paths for these tests are straight radial lines in X-Y space. The second group of tests is concerned with pure rotation of principal stress directions at various constant mobilized angles of friction (i.e. at constant stress ratios). The stress paths of these tests

are circular segments in X-Y stress space. The third type of test involved simultaneous increase in shear stress level and rotation of principal stress direction. These combined stress paths plot as spirals in X-Y stress space.

The plastic strain rate vectors from the above three types of tests are plotted by Gutierrez *et al.* (1991) together with the stress paths in X-Y stress space. They are shown in Figure 8.3 for the cases of pure rotation of principal stress directions and combined shear loading and stress rotation. In this figure, the strain rate vectors are plotted for both total strains and plastic strains. It is evident that the difference is rather small indicating that elastic components of strain rates are much smaller than the plastic components.

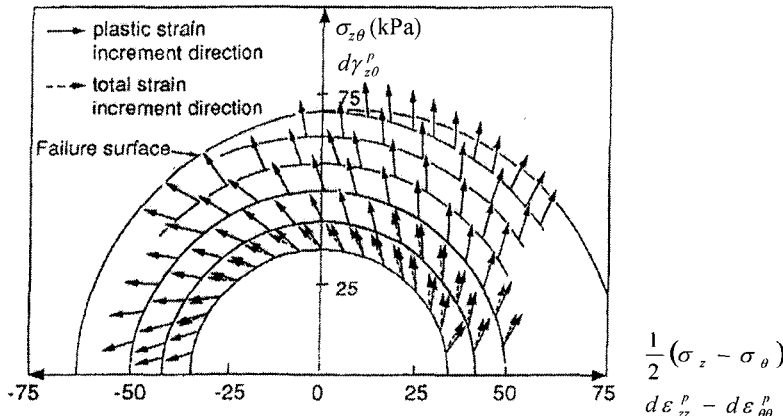


Figure 8.3: Non-coaxial behaviour from torsional shear (after Gutierrez *et al.*, 1991)

Some important remarks can be drawn from the results presented in Figure 8.3. For tests with fixed directions of principal stresses, the principal axes of stress and plastic strain rate tensors are practically identical. However for tests involving stress rotation, the direction of principal stress is significantly different from that of the principal plastic strain increments. This difference tends to reduce with increasing shear strain or stress level.

### 8.2.3 DEM simulations of simple shear of a granular assembly

Zhang (2003) and Thornton and Zhang (2005) presented a numerical simulation of simple shear of a granular assembly using the discrete element method (DEM). Particles were assumed to be spherical in shape and this is a simple idealization of real sand.

The orientations of the major principal stress and principal strain rate to the horizontal direction during the DEM simulations were presented by Zhang (2003) for three different initial stress states. For the case of an isotropic initial stress state (the initial horizontal stress is equal to the vertical stress), the behaviour is almost coaxial as the direction of the principal stress matches that of the principal strain rate. However for cases with an anisotropic initial stress state, the behaviour is non-coaxial as the direction of the principal stress is significantly different from that of the principal strain rate (see Figure 8.4). In agreement with the simple shear tests by Roscoe *et al.* (1967), the difference reduces with increasing shear strain level. In particular this difference becomes very small at failure and the behaviour may be regarded as coaxial.

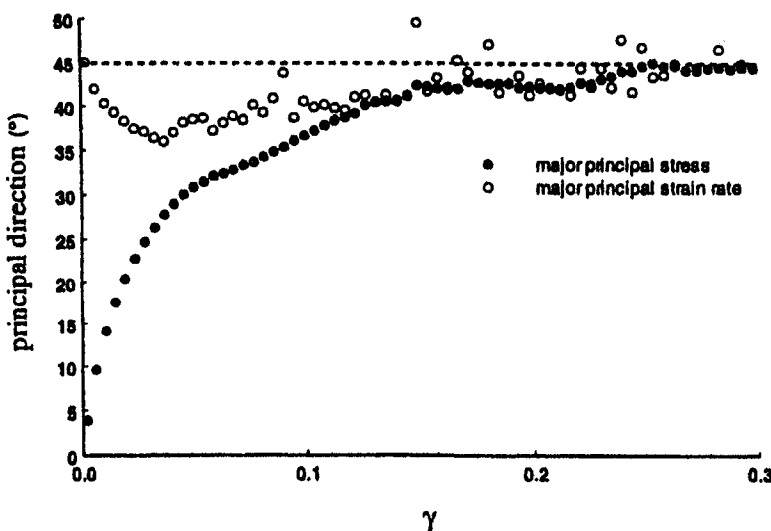


Figure 8.4: Non-coaxial behaviour from DEM simulation (after Zhang, 2003)

### 8.3 A YIELD VERTEX NON-COAXIAL THEORY

In the development of a more accurate plastic flow rule for modelling fissured rock, Rudnicki and Rice (1975) argue that the conventional plastic potential theory over-estimates the stiffness of response to stress increments directed tangential to what is taken as the current yield surface. In the fissure model, such stressing at a pointed vertex will initiate or cause continued plastic loading for some orientations. Hence,

the response is not purely elastic as predicted by the conventional plastic potential theory. Rather, it is intermediate between the soft plastic response to 'straight stressing' and the stiff elastic response governed by elastic moduli.

To take this into account, Rudnicki and Rice (1975) introduced, in addition to the plastic hardening modulus governing 'straight ahead' stressing, a second hardening modulus which governs the response to that part of a stress increment directed tangentially to what is taken as the yield surface. Since it has been argued that no vertex is associated with hydrostatic stress increments, these tangential increments are taken as purely deviatoric.

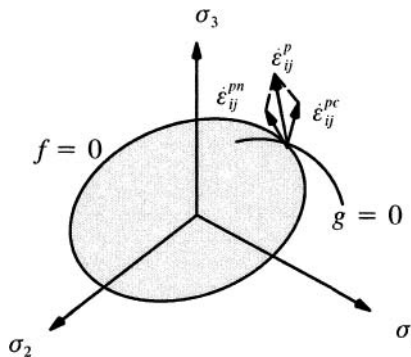


Figure 8.5: The non-coaxial plastic flow rule defined by equation (8.4)

Until most recently the application of the Rudnicki and Rice's non-coaxial plasticity theory had been restricted to several analytical treatments (e.g. Rudnicki and Rice, 1975; Papamichos and Vardoulakis, 1995). This non-coaxial plasticity theory is very well known in theoretical mechanics but less well known in the soil mechanics community. In fact, there was no major work in developing finite element procedures and formulations based on this theory for applications to soil-structure interaction analysis.

Most recently Yang and Yu (2006a,b) have developed a general elastic-plastic finite element formulation for implementing the non-coaxial theory of Rudnicki and Rice (1975). Yang and Yu (2006a,b) assumed that the total strain rate is the sum of elastic strain and plastic strain components. While the plastic strain rate is assumed to be defined by a non-coaxial theory, the classical Hooke's law is used to derive the elastic strain rate. According to Rudnicki and Rice's non-coaxial theory shown in Figure 8.5, the plastic strain rate  $\dot{\epsilon}_{ij}^P$  is split into two parts: the coaxial plastic strain rate  $\dot{\epsilon}_{ij}^{pc}$  and non-coaxial strain rate  $\dot{\epsilon}_{ij}^{pn}$ :

$$\dot{\varepsilon}_{ij}^p = \dot{\varepsilon}_{ij}^{pc} + \dot{\varepsilon}_{ij}^{pn} = \lambda \frac{\partial g}{\partial \sigma_{ij}} + \frac{1}{h_1} \dot{s}_{ij}^t \quad \text{if } f = 0 \quad (8.4)$$

where  $f$  and  $g$  are the yield function and plastic potential respectively,  $\lambda$  is a scalar function and  $h_1$  is a new plastic modulus which governs the response to that part of a stress increment directed tangentially to the yield surface. The stress tensor  $\dot{s}_{ij}^t$  is assumed to be purely deviatoric (Rudnicki and Rice, 1975) as it has been argued that non-coaxial plastic deformation is not associated with hydrostatic stress increments.

If the yield surface is circular on a deviatoric plane such as the case for the Drucker-Prager criterion, the stress tensor  $\dot{s}_{ij}^t$  is shown by Rudnicki and Rice (1975) as

$$\dot{s}_{ij}^t = \dot{s}_{ij} - \frac{s_{ij} s_{kl}}{2\tau^2} \dot{s}_{kl} \quad (8.5)$$

where  $\tau = \sqrt{(s_{ij} s_{ij})/2}$  and  $s_{ij}$  is the deviatoric stress tensor. This constitutive equation reduces to the classical, coaxial plastic potential theory when  $h_1 = \infty$ . In the case that  $h_1$  is a finite value, the strain rate  $\dot{\varepsilon}_{ij}^p$  and stress  $\sigma_{ij}$  are not coaxial.

As shown by Tsutsumi and Hashiguchi (2005) and Yang and Yu (2006b), a more general expression for the stress tensor  $\dot{s}_{ij}^t$  with a non-circular yield surface on the deviatoric plane is defined by

$$\dot{s}_{ij}^t = \dot{s}_{ij} - (\dot{s}_{kl} : n_{kl}) n_{ij} \quad (8.6)$$

where  $n_{ij}$  denotes the normal to the yield surface on the deviatoric plane, normalised by the magnitude of the tensor. For a circular yield surface, it can be shown that  $n_{ij} = s_{ij}/(\sqrt{2}\tau)$  and therefore equation (8.6) reduces to Rudnicki and Rice's equation (8.5).

Equation (8.4) together with elasticity theory and the consistency condition (i.e.  $\dot{f} = 0$  at yield) will allow a complete incremental stress-strain relationship to be derived so that the plastic deformation is governed by the non-coaxial plastic theory. As shown by Yang and Yu (2006a,b) and Papamichos and Vardoulakis (1995), the non-coaxial component of the plastic strain rate can be further written as follows:

$$\dot{\varepsilon}_{ij}^{pn} = \frac{1}{h_1} N_{ijkl} \dot{\sigma}_{kl} \quad (8.7)$$

where

$$N_{ijkl} = \frac{1}{2} (\delta_{ik} \delta_{jl} + \delta_{il} \delta_{jk} - \frac{2}{3} \delta_{ij} \delta_{kl} - n_{ij} n_{kl}) \quad (8.8)$$

which takes the following form with a circular yield surface:

$$N_{ijkl} = \frac{1}{2}(\delta_{ik}\delta_{jl} + \delta_{il}\delta_{jk} - \frac{2}{3}\delta_{ij}\delta_{kl} - \frac{s_{ij}s_{kl}}{\tau^2}) \quad (8.9)$$

By combining equations (8.4) and (8.7), we may obtain the following relationship between total stress rate and total strain rate:

$$\dot{\sigma}_{ij} = D_{ijkl}^{ep} \dot{\varepsilon}_{kl} \quad (8.10)$$

where

$$D_{ijkl}^{ep} = D_{ijkl}^e - \frac{D_{ijpq}^e \frac{\partial g}{\partial \sigma_{pq}} D_{klmn}^e \frac{\partial f}{\partial \sigma_{mn}}}{K_p + \frac{\partial f}{\partial \sigma_{uv}} D_{uvst}^e \frac{\partial g}{\partial \sigma_{st}}} - \frac{4G^2}{h_1 + 2G} N_{ijkl} \quad (8.11)$$

where the first two terms are the usual expressions for stiffness from a standard coaxial plasticity model. The third term is a new contribution due to the effect of the non-coaxial behaviour in which  $G$  denotes the shear modulus.

The non-coaxial stress-strain relationship (8.10) has been successfully applied to the Drucker-Prager plasticity model by Yang and Yu (2006a) and Yu *et al.* (2005) as well as to the critical state model CASM (Yu, 1998) by Yang and Yu (2006b).

#### 8.4 NON-COAXIAL THEORY BASED ON DOUBLE SHEARING

Non-coaxiality has been studied theoretically within the context of fully developed flows in perfectly plastic granular materials. An early kinematic model for granular flow was developed by de Josselin de Jong (1958, 1971). His so-called ‘double sliding, free rotating model’ for planar flow was based on the assumption of shear flow occurring along two surfaces where the available shear resistance has been exhausted. Using the same concept of double shearing, Spencer (1964) established a set of kinematic equations termed the ‘double shearing model’ but with a different rotation term from that of de Josselin de Jong (1971). Although these two models have a common basis, they are slightly different in nature (Mandl and Luque, 1970; Spencer, 1982; Harris, 1993, 1995; Savage and Lockner, 1997). In particular, the ‘double sliding, free rotating model’ of de Josselin de Jong is indeterminate in nature and therefore additional assumptions are required before it can be used to solve boundary value problems (Teunissen and Vermeer, 1988).

The validity of any proposed non-coaxial, elastic plastic models will have to be assessed by comparing their predicted behaviour with experimental data. Yu and Yuan (2006) recently developed the theory of a class of non-coaxial, elastic-plastic

soil models with its links established with the plastic potential theory and the double shearing theory. The theory was implemented into a finite element program for validation purposes using experimental results from the simple shear test. In contrast to the approach used in the double shearing model, which is based on kinematic assumptions, Yu and Yuan (2006) set out to establish a general non-coaxial flow rule by extending the conventional potential theory to account for non-coaxiality. Moreover, the scope of the modelling in the paper includes the range of pre-failure deformation and therefore represents an extension to the original double shearing models that were proposed for describing fully plastic flow (Spencer, 1964, 1982; Mehrabadi and Cowin, 1978).

In agreement with Anand (1983) and Savage and Lockner (1997), the study presented by Yu and Yuan (2006) suggested that it is necessary to relax the original kinematic hypothesis of the coincidence of stress and velocity characteristics in order to allow the double shearing concept to be used more successfully in the range of pre-failure deformation.

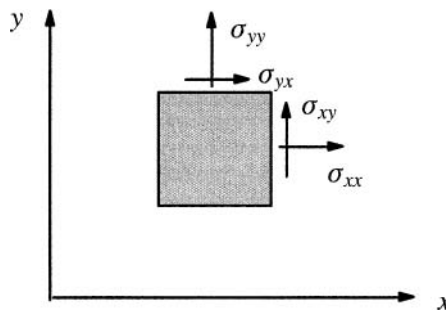


Figure 8.6: The coordinate system for plane strain problems

#### 8.4.1 A class of non-coaxial plasticity theories in plane strain

For simplicity, granular material is often modelled as an elastic perfectly plastic material. Given that the double shearing theory of Spencer (1964, 1982) has been developed and discussed in the context of perfect plasticity and plane strain conditions, this section will also focus on a perfectly plastic formulation under plane strain conditions. However, the formulation can be readily extended to consider hardening plasticity and non-plane strain cases (Yuan, 2005).

With a tension positive notation (Figure 8.6), a stress-strain relationship for an elastic-plastic material in plane strain can be written as follows:

$$\dot{\sigma}_{ij} = D_{ijkl}^e (\dot{\epsilon}_{kl} - \dot{\epsilon}_{kl}^p) \quad (8.12)$$

where  $\dot{\sigma}_{ij} = (\dot{\sigma}_{xx}, \dot{\sigma}_{yy}, \dot{\sigma}_{xy})^T$  and  $\dot{\epsilon}_{ij} = (\dot{\epsilon}_{xx}, \dot{\epsilon}_{yy}, \dot{\epsilon}_{xy})^T$ . Under the conditions of plane strain, the elastic stiffness matrix is given by

$$D_{ijkl}^e = \frac{E}{(1 + \nu)(1 - 2\nu)} \begin{bmatrix} 1 - \nu & \nu & 0 \\ \nu & 1 - \nu & 0 \\ 0 & 0 & 0.5 - \nu \end{bmatrix} \quad (8.13)$$

in which  $E$  and  $\nu$  are Young's modulus and Poisson's ratio.

To synthesize the double shearing theory and the plastic potential models, Yu and Yuan (2006) have followed Spencer (1982) and Harris (1993, 1995) in proposing the formulation of a class of non-coaxial models that take the following general form in terms of plastic strain rates

$$\dot{\epsilon}_{ij}^p = \dot{\epsilon}_{ij}^{pc} + \dot{\epsilon}_{ij}^{pn} = \lambda \frac{\partial g}{\partial \sigma_{ij}} + A \ t_{ij} \quad \text{if } f = 0 \quad (8.14)$$

where  $f$  and  $g$  are the yield function and plastic potential respectively,  $\lambda$  and  $A$  are scalar functions and  $A$  is dimensionless. The vector  $t_{ij}$  is defined as

$$t_{ij} = [\cos 2\theta_\sigma, -\cos 2\theta_\sigma, 2 \sin 2\theta_\sigma]^T \quad (8.15)$$

where  $\theta_\sigma$  is defined as the angle between the direction of the minor principal compressive stress direction and the x-axis that is expressed by

$$\cos 2\theta_\sigma = \frac{\sigma_{xx} - \sigma_{yy}}{\sqrt{(\sigma_{xx} - \sigma_{yy})^2 + 4\sigma_{xy}^2}} \quad (8.16)$$

$$\sin 2\theta_\sigma = \frac{2\sigma_{xy}}{\sqrt{(\sigma_{xx} - \sigma_{yy})^2 + 4\sigma_{xy}^2}} \quad (8.17)$$

Equation (8.14) is a generalization of the double shearing model and classical potential theory, to which it reduces when  $A = 0$ . In the case when  $A$  is not equal to zero, the plastic strain rate tensor  $\dot{\epsilon}_{ij}^p$  and stress tensor  $\sigma_{ij}$  are not coaxial.

As shown in Figure 8.7 with a Mohr-Coulomb criterion, the plastic strain rate given by the first term of Equation (8.14) is the same as that from the conventional, coaxial plastic potential theory, which is normal to a plastic potential surface. The second term is the non-coaxial, stress rate dependent plastic strain rate component that is tangential to the yield locus in the deviatoric plane. This non-coaxial model is different from the elastic-plastic version of de Josselin de Jong's double sliding free rotating model proposed by Teunissen and Vermeer (1988), in which non-coaxial plastic strain rates are not directly related to rotation of principal stresses.

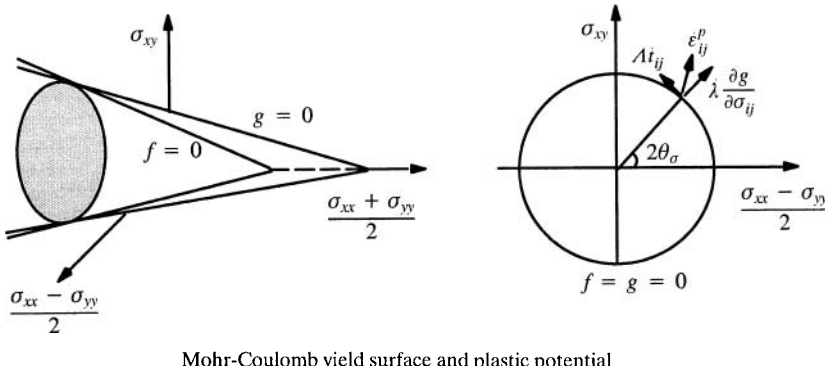


Figure 8.7: The non-coaxial plastic flow rule defined by equation (8.14)

In the original double shearing theory of Spencer (1964, 1982) and Mehrabadi and Cowin (1978), the stress and velocity characteristic directions are known to coincide. It can be shown (Harris, 1993) that this property leads to the following expression for  $\Lambda$

$$\Lambda = -\frac{\sin \phi - \sin \psi}{2(1 - \sin \phi \sin \psi)} \quad (8.18)$$

where  $\phi$  and  $\psi$  are the angles of friction and dilation respectively. Therefore the double shearing models of Spencer (1964) and Mehrabadi and Cowin (1978) can be recovered from equation (8.14) by using equation (8.18) to determine  $\Lambda$ .

#### 8.4.2 Incremental non-coaxial stress-strain relationship

Equation (8.14) represents a general plane strain, non-coaxial theory that combines the double shearing theory with the conventional plastic potential theory. It is obvious from equation (8.14) that the non-coaxial plastic strain components are controlled by the value of  $\Lambda$  and stress rate  $\dot{\sigma}_{ij}$  (as  $t_{ij}$  can be expressed in terms of stress rate  $\dot{\sigma}_{ij}$ ). In order to implement the non-coaxial theory into a finite element code for use in solving boundary value problems in geotechnical engineering, it is necessary to derive a general incremental stress-strain relationship.

By combining equations (8.15), (8.16) and (8.17), we obtain

$$t_{ij} = \frac{1}{\Lambda} H_{ijkl} \dot{\sigma}_{kl} \quad (8.19)$$

where

$$H_{ijkl} = \begin{bmatrix} a_1 & -a_1 & a_2 \\ -a_1 & a_1 & -a_2 \\ a_2 & -a_2 & a_3 \end{bmatrix} \quad (8.20)$$

in which

$$a_1 = \frac{4A\sigma_{xy}^2}{\sqrt{(\sigma_{xx} - \sigma_{yy})^2 + 4\sigma_{xy}^2}} \quad (8.21)$$

$$a_2 = -\frac{4A\sigma_{xy}(\sigma_{xx} - \sigma_{yy})}{\sqrt{(\sigma_{xx} - \sigma_{yy})^2 + 4\sigma_{xy}^2}} \quad (8.22)$$

$$a_3 = \frac{4A(\sigma_{xx} - \sigma_{yy})^2}{\sqrt{(\sigma_{xx} - \sigma_{yy})^2 + 4\sigma_{xy}^2}} \quad (8.23)$$

By following the usual procedure, we may obtain the following relationship between total stress rate and total strain rate for perfect plasticity:

$$\dot{\sigma}_{ij} = D_{ijkl}^{ep} \dot{\epsilon}_{kl} \quad (8.24)$$

where

$$D_{ijkl}^{ep} = \bar{D}_{ijkl}^e - \frac{\bar{D}_{ijpq}^e \frac{\partial g}{\partial \sigma_{pq}} \bar{D}_{klmn}^e \frac{\partial f}{\partial \sigma_{mn}}}{\frac{\partial f}{\partial \sigma_{uv}} \bar{D}_{uvst}^e \frac{\partial g}{\partial \sigma_{st}}} \quad (8.25)$$

in which the modified elastic matrix  $\bar{D}_{ijkl}^e$  is linked to the conventional elastic matrix as follows

$$\bar{D}_{ijkl}^e = S_{ijkl}^{-1} \times D_{ijkl}^e \quad (8.26)$$

and

$$S_{ijkl} = I_{ijkl} + D_{ijkl}^e \times H_{ijkl} \quad (8.27)$$

where  $I_{ijkl}$  is the identity matrix.

### 8.4.3 Extension of non-coaxial plasticity theories to axisymmetry

The previous sections present a class of non-coaxial relationships for plane strain problems. As shown in Yuan (2005), the theory can also be extended to axisymmetric problems for which the stresses are shown in Figure 8.8.

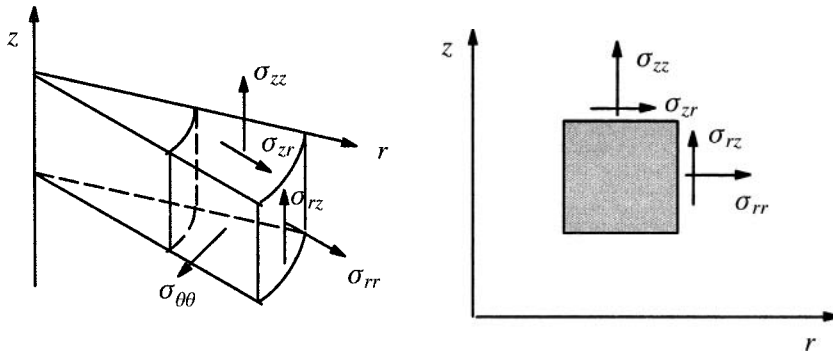


Figure 8.8: The coordinate system for axisymmetric problems

The key idea is to treat all the stress and strain variables on the r-z plane in axisymmetry as those acting on the x-y plane in plane strain. For axisymmetric problems, we have the following stress and strain rates:

$$\dot{\sigma}_{ij} = (\dot{\sigma}_{rr}, \dot{\sigma}_{zz}, \dot{\sigma}_{\theta\theta}, \dot{\sigma}_{rz})^T \quad (8.28)$$

$$\dot{\varepsilon}_{ij} = (\dot{\varepsilon}_{rr}, \dot{\varepsilon}_{zz}, \dot{\varepsilon}_{\theta\theta}, \dot{\gamma}_{rz})^T \quad (8.29)$$

As in plane strain, the plastic strain rates in axisymmetry are assumed to be defined by

$$\dot{\varepsilon}_{ij}^p = \dot{\varepsilon}_{ij}^{pc} + \dot{\varepsilon}_{ij}^{pn} = \lambda \frac{\partial g}{\partial \sigma_{ij}} + \Lambda \dot{t}_{ij} \quad \text{if } f = 0 \quad (8.30)$$

where  $f$  and  $g$  are yield function and plastic potential respectively,  $\lambda$  and  $\Lambda$  are scalar functions and  $\Lambda$  is dimensionless. The vector  $t_{ij}$  is defined as

$$t_{ij} = [\cos 2\theta_\sigma, -\cos 2\theta_\sigma, 0, 2 \sin 2\theta_\sigma]^T \quad (8.31)$$

where  $\theta_\sigma$  is defined as the angle between the direction of the minor principal compressive stress direction and the r-axis.

By combining equations (8.31), (8.16) and (8.17), we obtain

$$t_{ij} = \frac{1}{\Lambda} H_{ijkl} \dot{\sigma}_{kl} \quad (8.32)$$

where

$$H_{ijkl} = \begin{bmatrix} a_1 & -a_1 & 0 & a_2 \\ -a_1 & a_1 & 0 & -a_2 \\ 0 & 0 & 0 & 0 \\ a_2 & -a_2 & 0 & a_3 \end{bmatrix} \quad (8.33)$$

in which

$$\begin{aligned} a_1 &= \frac{4A\sigma_{xy}^2}{\sqrt{(\sigma_{xx} - \sigma_{yy})^2 + 4\sigma_{xy}^2}} \\ a_2 &= -\frac{4A\sigma_{xy}(\sigma_{xx} - \sigma_{yy})}{\sqrt{(\sigma_{xx} - \sigma_{yy})^2 + 4\sigma_{xy}^2}} \\ a_3 &= \frac{4A(\sigma_{xx} - \sigma_{yy})^2}{\sqrt{(\sigma_{xx} - \sigma_{yy})^2 + 4\sigma_{xy}^2}} \end{aligned}$$

We then obtain the following relationship between the stress rates and strain rates for axisymmetric problems:

$$\dot{\sigma}_{ij} = D_{ijkl}^{ep} \dot{\epsilon}_{kl} \quad (8.34)$$

where

$$D_{ijkl}^{ep} = \bar{D}_{ijkl}^e - \frac{\bar{D}_{ijpq}^e \frac{\partial g}{\partial \sigma_{pq}} \bar{D}_{klmn}^e \frac{\partial f}{\partial \sigma_{mn}}}{\frac{\partial f}{\partial \sigma_{uv}} \bar{D}_{uvst}^e \frac{\partial g}{\partial \sigma_{st}}} \quad (8.35)$$

in which the modified elastic matrix  $\bar{D}_{ijkl}^e$  is linked to the conventional elastic matrix  $D_{ijkl}^e$  as follows

$$\bar{D}_{ijkl}^e = S_{ijkl}^{-1} \times D_{ijkl}^e \quad (8.36)$$

and

$$S_{ijkl} = I_{ijkl} + D_{ijkl}^e \times H_{ijkl} \quad (8.37)$$

where  $I_{ijkl}$  is the identity matrix.

## 8.5 COMPARISON OF VERTEX AND DOUBLE SHEARING THEORIES

In this section, we present a brief comparison made by Yang and Yu (2005) between the two non-coaxial theories that were presented in the previous two sections. In particular, we consider the non-coaxial plastic strain rate tensors defined by (8.4) and (8.14) under the conditions of plane strain.

In the yield vertex theory with a circular yield surface on the deviatoric plane, the non-coaxial plastic strain rates are assumed to be governed by the following equation

$$\dot{\varepsilon}_{ij}^{pn} = \frac{1}{h_1} \dot{s}_{ij}^t \quad \text{if } f = 0 \quad (8.38)$$

The tensor  $\dot{s}_{ij}^t$  is assumed to be purely deviatoric (Rudnicki and Rice, 1975):

$$\dot{s}_{ij}^t = \dot{s}_{ij} - \frac{s_{ij} s_{kl}}{2\tau^2} \dot{s}_{kl} \quad (8.39)$$

In plane strain, we can show that

$$s_{xx} = \frac{\sigma_{xx} - \sigma_{yy}}{2} \quad (8.40)$$

$$s_{yy} = \frac{\sigma_{yy} - \sigma_{xx}}{2} \quad (8.41)$$

$$s_{xy} = \sigma_{xy} \quad (8.42)$$

$$\tau = \sqrt{\frac{1}{4}(\sigma_{xx} - \sigma_{yy})^2 + \sigma_{xy}^2} \quad (8.43)$$

Therefore we can obtain

$$\dot{s}_{ij}^t = \begin{bmatrix} \dot{s}_{xx} \\ -\dot{s}_{xx} \\ \dot{s}_{xy} \end{bmatrix} - \frac{s_{xx}\dot{s}_{xx} + s_{xy}\dot{s}_{xy}}{\tau^2} \begin{bmatrix} s_{xx} \\ -s_{xx} \\ s_{xy} \end{bmatrix} \quad (8.44)$$

On the other hand, the theory followed by Spencer (1982), Harris (1993) and Yu and Yuan (2006) assumes that the non-coaxial plastic strain rates are defined by

$$\dot{\varepsilon}_{ij}^{pn} = A \dot{t}_{ij} \quad \text{if } f = 0 \quad (8.45)$$

and in plane strain we can show that

$$\dot{t}_{ij} = \frac{1}{\tau} \begin{bmatrix} \dot{s}_{xx} \\ -\dot{s}_{xx} \\ \dot{s}_{xy} \end{bmatrix} - \frac{s_{xx}\dot{s}_{xx} + s_{xy}\dot{s}_{xy}}{\tau^3} \begin{bmatrix} s_{xx} \\ -s_{xx} \\ s_{xy} \end{bmatrix} \quad (8.46)$$

By comparing equations (8.44) and (8.46), we have

$$\dot{s}_{ij}^t = \tau \dot{t}_{ij} \quad (8.47)$$

It is therefore evident that the use of the double shearing based non-coaxial theory is similar in form to the yield vertex theory. In addition the double shearing theory with a constant non-coaxial coefficient  $A$  may be made equivalent, at least in form, to the yield vertex theory with a pressure dependent plastic modulus defined by

$$h_1 = \frac{\tau}{A} \quad (8.48)$$

Alternatively the yield vertex theory with a constant plastic modulus  $h_1$  may also be regarded as similar to the double shearing based theory with a pressure dependent non-coaxial coefficient

$$A = \frac{\tau}{h_1} \quad (8.49)$$

## 8.6 NUMERICAL SIMULATION OF SIMPLE SHEAR

As stated earlier, there is much experimental data on the stress-strain relationship for simple shear tests of soil, which indicates the non-coaxial nature of soil behaviour. Before any non-coaxial models can be applied in practice, they must be shown to be able to model some of the observed non-coaxial behaviour in the laboratory. The validation of the two non-coaxial models presented in this chapter using the simple shear test has been made by Yu and Yuan (2006) and Yang and Yu (2006a,b) by implementing the non-coaxial plasticity models into the finite element code ABAQUS. In addition, the non-coaxial models have also been applied to analyse soil-structure interaction problems (Yu and Yuan, 2005; Yuan, 2005).

### 8.6.1 Mohr-Coulomb model with the generalised double shear theory

Using the Mohr-Coulomb criterion with the generalised non-coaxial double shear flow rule (8.14), Yu and Yuan (2006) studied the effect of non-coaxial behaviour on the behaviour of soils under simple shear. The key factors that are investigated include non-associated flow rules, non-coaxial flow rules and initial stress ratios (i.e. the ratio of initial horizontal stress to the vertical stress denoted by  $K_0$ ).

*Simple shear on a normally consolidated sample ( $K_0 < 1$ )*

Presented in Figure 8.9 to Figure 8.11 are the numerical results for the ratio of shear stress to normal stress against shear strain and volumetric strain against shear strain for three different dilation angles ( $\psi = 0^0, 5^0, 35^0$ ) with  $K_0 = 0.43$  (i.e. a normally consolidated sample) and the friction angle of  $\phi = 35^0$ . For each analysis, three different values of the non-coaxial coefficient of  $A = 0.0, 0.02, 0.05$  are used to investigate the effect of non-coaxial behaviour. As expected, an increase in dilation angle makes the soil response more dilatant and therefore leads to a higher limiting ratio of shear stress to normal stress at large shear strain. It is interesting to note that an increasing value of non-coaxial coefficient leads to a softer stress-strain response and a slightly smaller dilation. For simple shear, however, the ultimate ratio of shear stress to normal stress for a non-coaxial flow rule tends to approach the limiting value of the coaxial plasticity although this may occur at a very large shear strain.

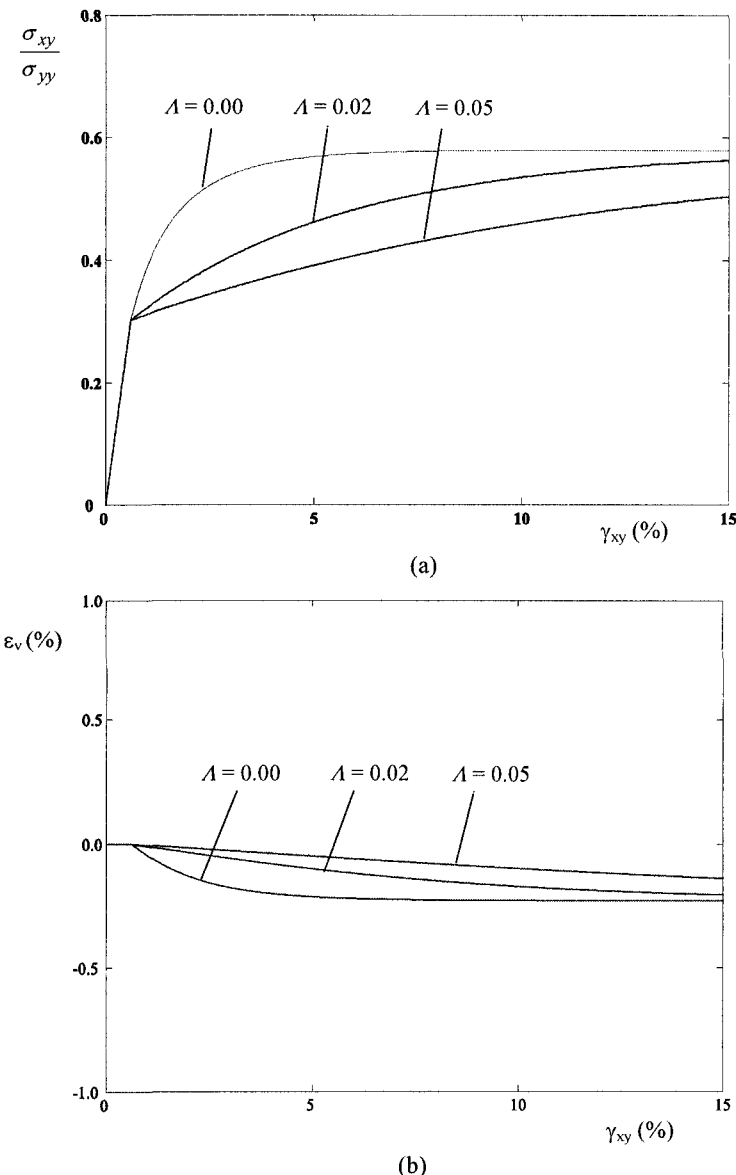


Figure 8.9: Simple shear results for  $K_0 = 0.43, \phi = 35^\circ, \psi = 0^\circ$

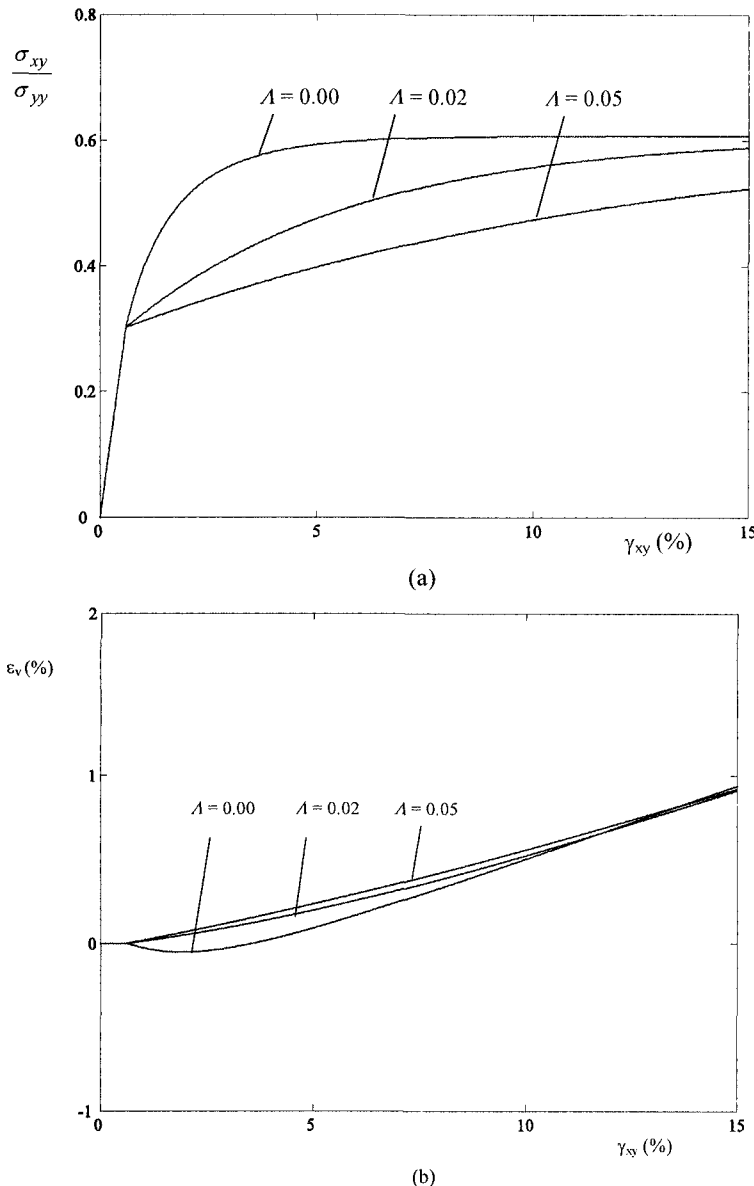


Figure 8.10: Simple shear results for  $K_0 = 0.43, \phi = 35^\circ, \psi = 5^\circ$

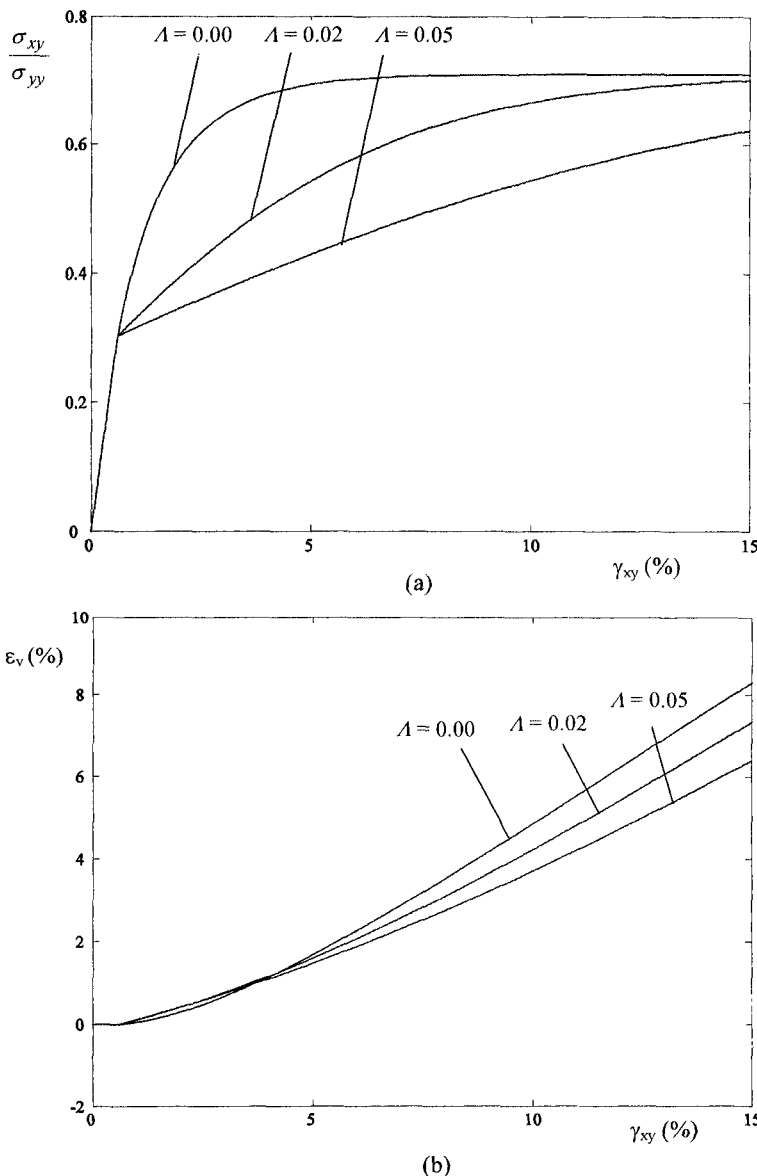


Figure 8.11: Simple shear results for  $K_0 = 0.43, \phi = 35^\circ, \psi = 35^\circ$

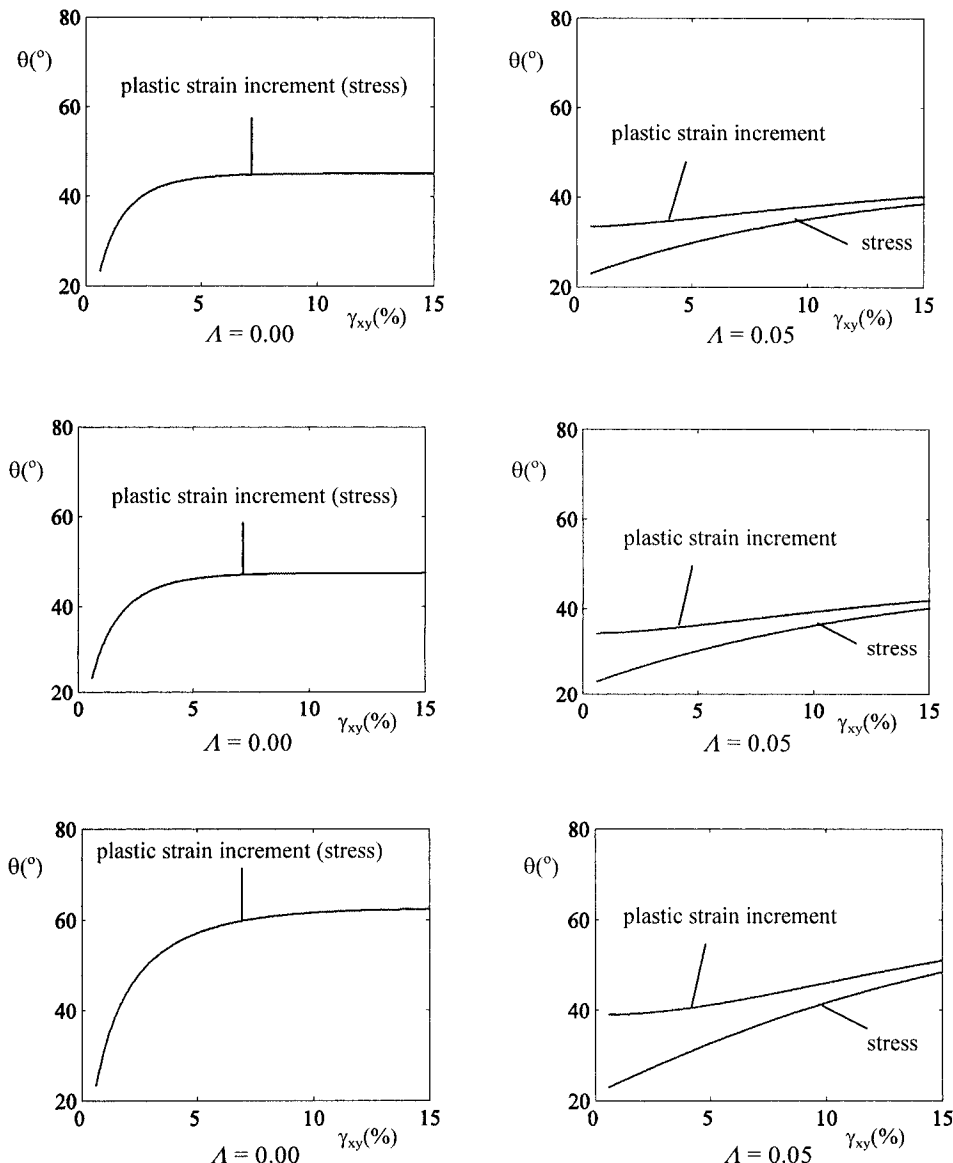


Figure 8.12: Numerical results of non-coaxiality for  $K_0 = 0.43$

With coaxial plasticity, the directions of principal stress and principal plastic strain are coincident. At the ultimate failure when the deformation is plastic, the horizontal plane is a velocity characteristic and is therefore inclined at  $45^\circ + \psi/2$  to the direction of the major principal stress (Davis, 1968). The changes of direction for principal stresses and principal plastic strain rates for various values of dilation angle and non-coaxial coefficient are shown in Figure 8.12. When  $A = 0$  (i.e. coaxial plasticity), the ultimate value is  $45^\circ$  for the dilation angle of  $\psi = 0^\circ$ ,  $47.5^\circ$  for the dilation angle of  $\psi = 5^\circ$ , and  $62.5^\circ$  for the dilation angle of  $\psi = 35^\circ$ . These numerical values agree well with the theoretical predictions as shown in Davis (1968).

For non-coaxial plasticity, however, Figure 8.12 shows clearly that the difference between orientations of principal stresses and principal plastic strain rates enlarges as the non-coaxial coefficient increases, and decreases with increasing shear strains. In general, the pattern of this predicted non-coaxial behaviour is consistent with simple shear experimental data as reported by Roscoe (1970) and plotted in Figure 8.1.

#### *Simple shear on an overconsolidated sample ( $K_0 > 1$ )*

Presented in Figure 8.13 to Figure 8.15 are the numerical results for the ratio of shear stress to normal stress against shear strain and the volumetric strain against shear strain for three different dilation angles ( $\psi = 0^\circ, 5^\circ, 35^\circ$ ) with  $K_0 = 3$  (i.e. an overconsolidated sample) and a friction angle of  $\phi = 35^\circ$ . For each analysis, three different values of the non-coaxial coefficient of  $A = 0.0, 0.02, 0.05$  are used to investigate the effect of non-coaxial behaviour.

For a non-associated flow rule with  $\psi = 0^\circ, 5^\circ$  and  $K_0 = 3$ , a strain softening response is observed. As discussed by Vermeer (1990) for a coaxial model, this softening is not due to the material strength reduction but comes entirely from the decrease of the horizontal compressive stress in the soil when a non-associated flow rule is used. This strain softening phenomenon is absent as long as an associated flow rule is employed. However, in all the cases the ultimate ratios of shear stress to normal stress appear to approach the coaxial value at large shear strains. In addition, the inclusion of non-coaxial behaviour tends to delay the onset of this non-associated softening and make the rate of softening slower. From these results, it can be concluded that the non-associated softening effect depends on initial stress states and the flow rule as well as the degree of non-coaxiality of the soil.

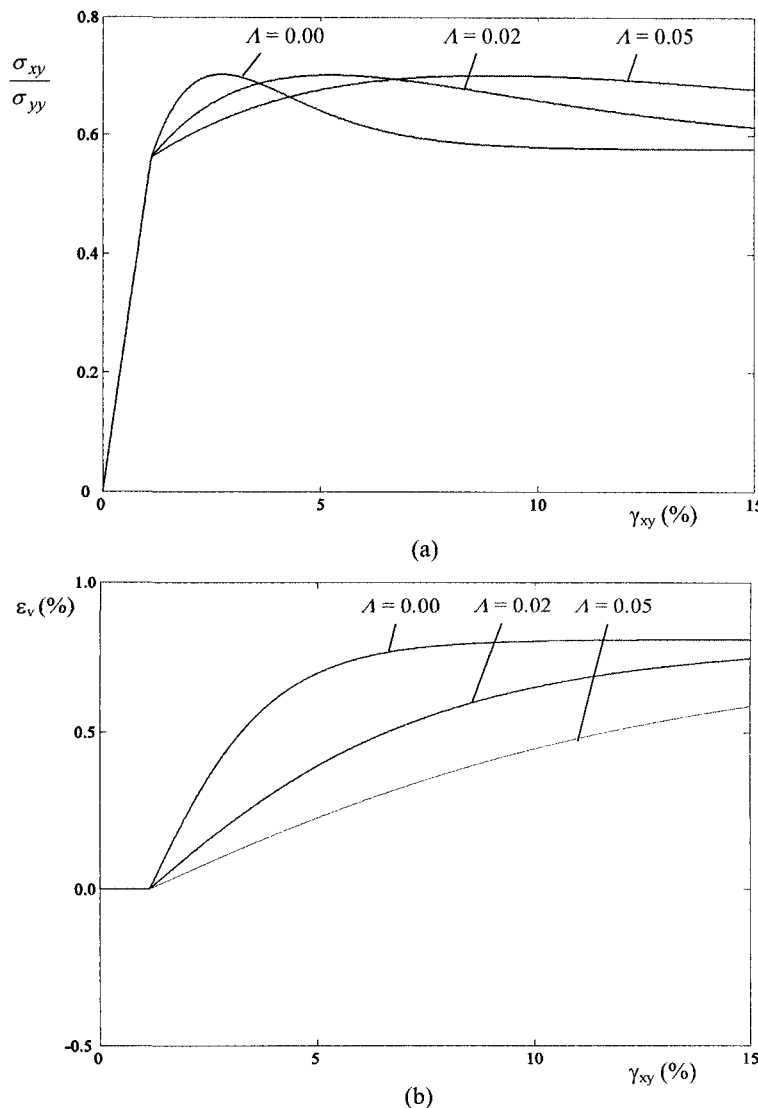


Figure 8.13: Simple shear results for  $K_0 = 3, \phi = 35^\circ, \psi = 0^\circ$

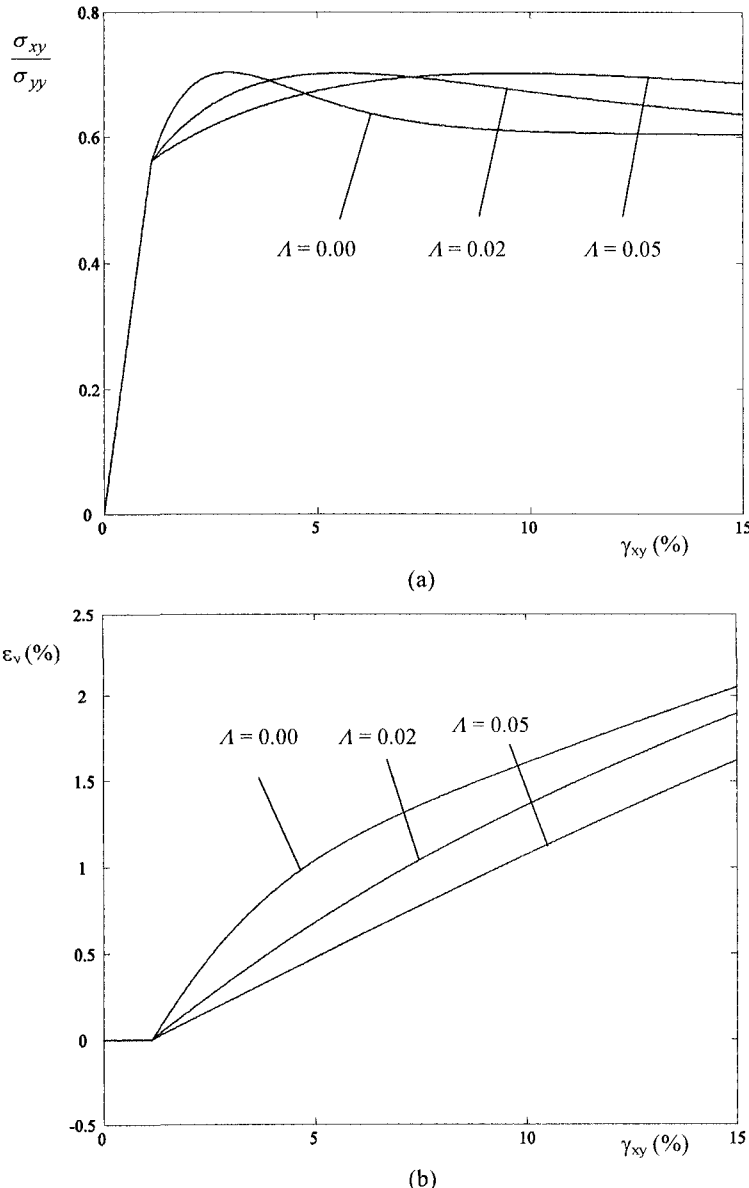


Figure 8.14: Simple shear results for  $K_0 = 3, \phi = 35^\circ, \psi = 5^\circ$

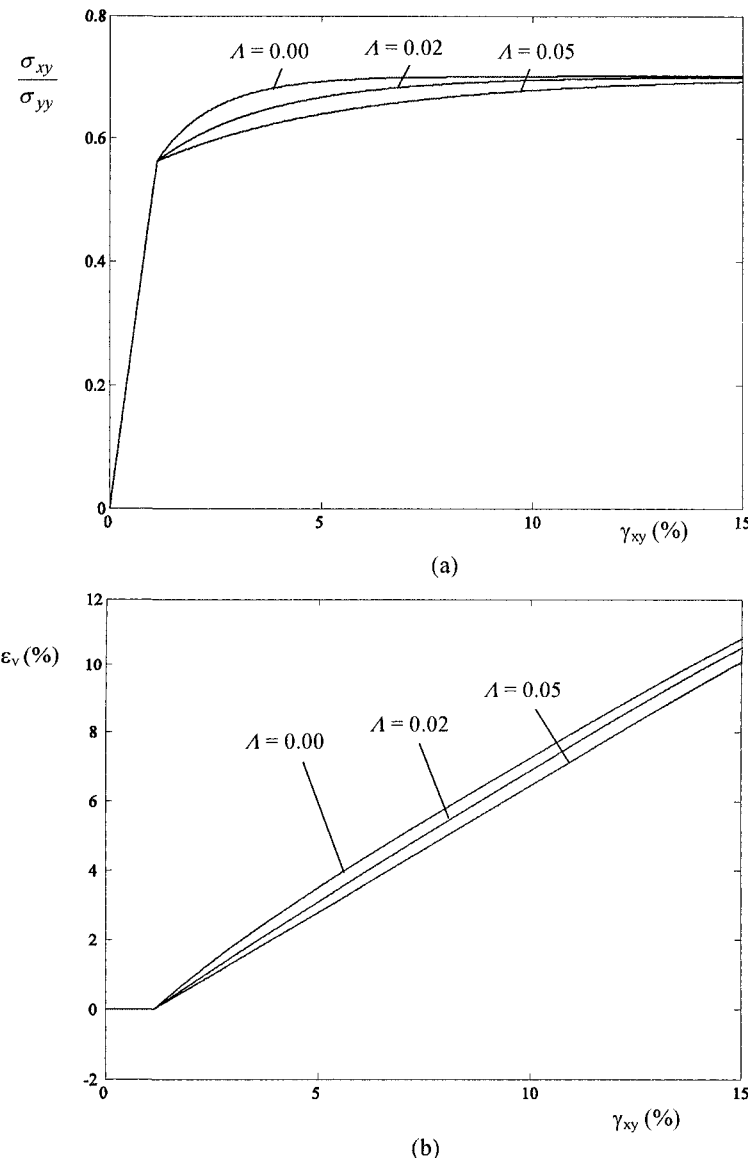


Figure 8.15: Simple shear results for  $K_0 = 3, \phi = 35^\circ, \psi = 35^\circ$

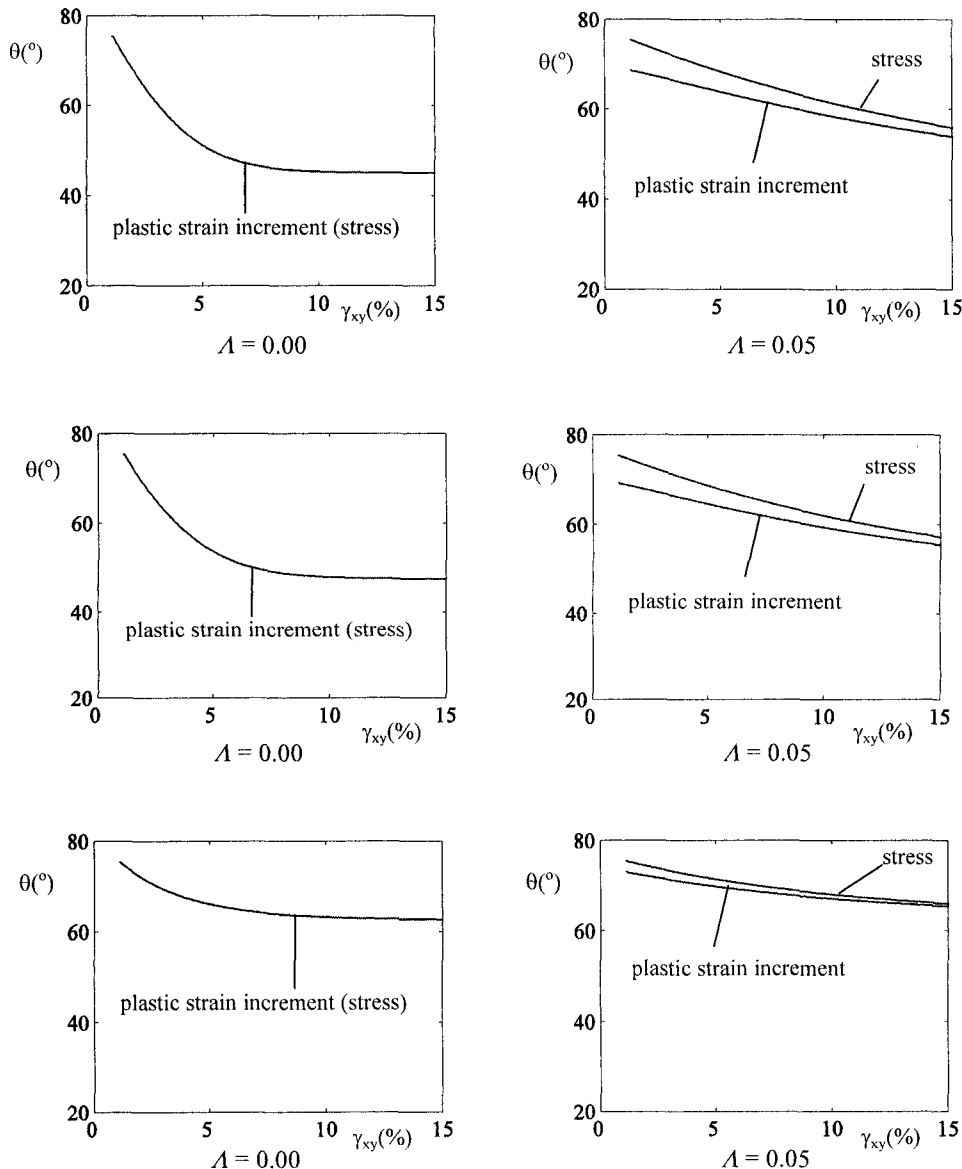


Figure 8.16: Numerical results of non-coaxiality for  $K_0 = 3$

The changes of principal stress and principal plastic strain rate direction for various values of dilation angle and non-coaxial coefficient are shown in Figure 8.16. When  $\lambda = 0$  (i.e. coaxial plasticity), the ultimate value is  $45^\circ$  for the dilation angle of  $\psi = 0^\circ$ ,  $47.5^\circ$  for the dilation angle of  $\psi = 5^\circ$ , and  $62.5^\circ$  for the dilation angle of  $\psi = 35^\circ$ . These numerical values agree well with the theoretical predictions as shown in Davis (1968).

For non-coaxial plasticity, however, Figure 8.16 shows clearly that the difference between orientations of principal stresses and principal plastic strain rates enlarges as the non-coaxial coefficient increases, and decreases with increasing shear strains. Another important finding from the numerical results plotted in Figure 8.16 and Figure 8.12 is that the direction of principal plastic strain rate is always ‘in advance’ of that of principal stress. This phenomenon has been observed in experiments and reported by many researchers (e.g. Gutierrez *et al.*, 1991; Joer *et al.*, 1998).

### 8.6.2 The critical state model CASM with the yield vertex flow rule

The yield vertex non-coaxial plastic flow rule defined by equation (8.4) has been implemented into the Drucker-Prager yield surface (Yang and Yu, 2006a) and the critical state model CASM (Yang and Yu, 2006b). Both of these non-coaxial models have been applied to simulate simple shear and soil-structure interaction problems. In this section, we only present selected results for the numerical simulation of simple shear in clay and sand using the non-coaxial CASM model. Full details can be found in Yang and Yu (2006b).

#### *Simple shear in sand*

In using the non-coaxial CASM model to simulate simple shear of sand, Yang and Yu (2006b) use the model constants that are relevant for Erksak sand (Yu, 1998):

$$\lambda = 0.0135, \Gamma = 1.8167, \nu = 0.3, \kappa = 0.005, M = 1.2, \xi_R = 0.075, n = 4.0$$

Using the yield vertex non-coaxial flow rule, the degree of non-coaxiality is controlled by the plastic modulus  $h_1$ . It is better to normalise this plastic modulus by an elastic modulus say the shear modulus so that  $h_1/G$  can be used to indicate the degree of non-coaxiality of soils. Figure 8.17 and Figure 8.18 present the numerical results for stress-strain relations and the non-coaxial response of simple shear of a normally consolidated sand ( $K_0 < 1$ ) and an overconsolidated sand ( $K_0 > 1$ ) respectively. In general the inclusion of non-coaxial behaviour tends to make the stress-strain response softer. It is evident that the predicted non-coaxial behaviour is consistent with the experimental observations (Roscoe, 1970) and DEM simulations (Zhang, 2003) for granular materials.

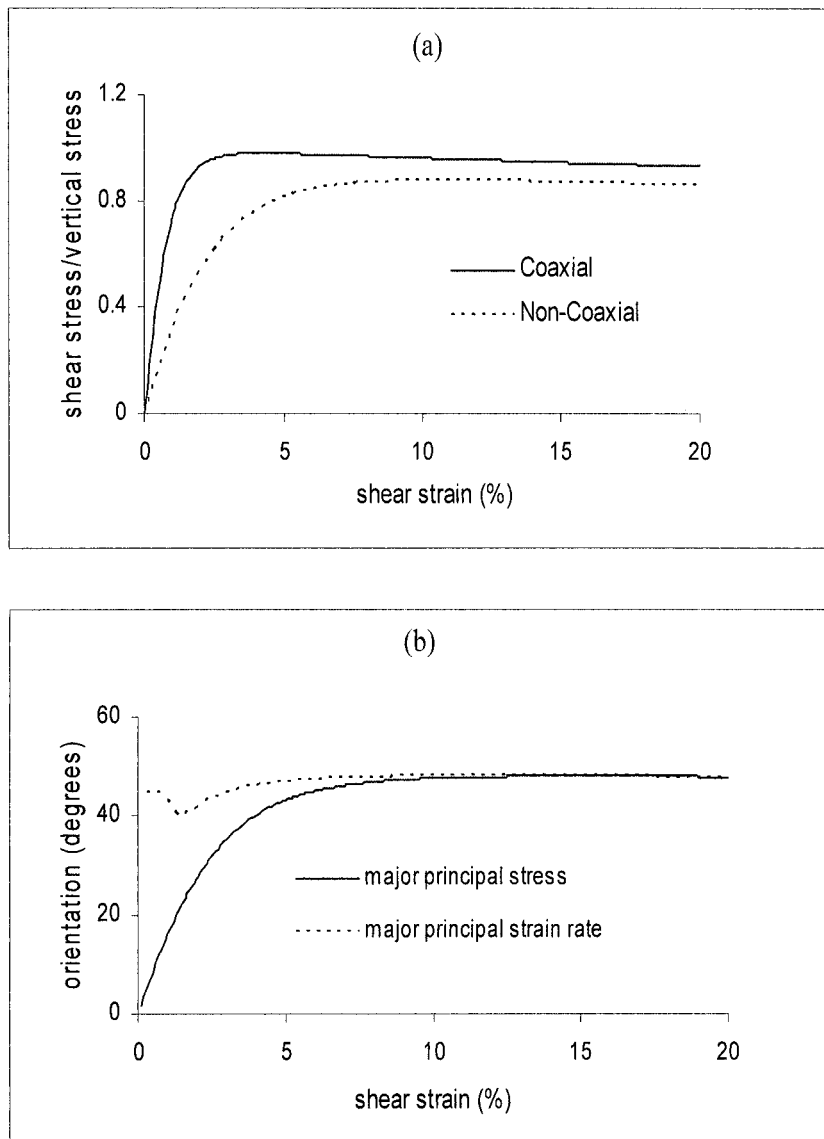


Figure 8.17: Results of simple shear of dense Erksak sand with  $K_0 = 0.23$

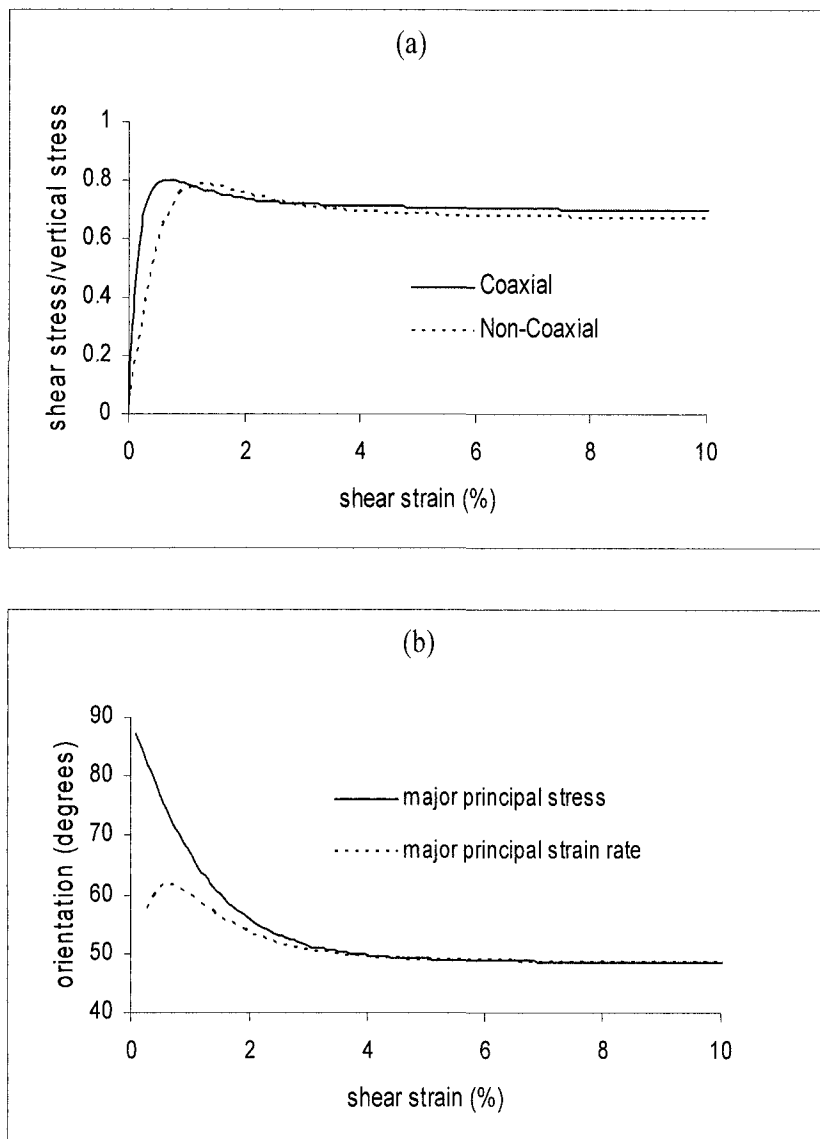


Figure 8.18: Results of simple shear of dense Erksak sand with  $K_0 = 4.0$

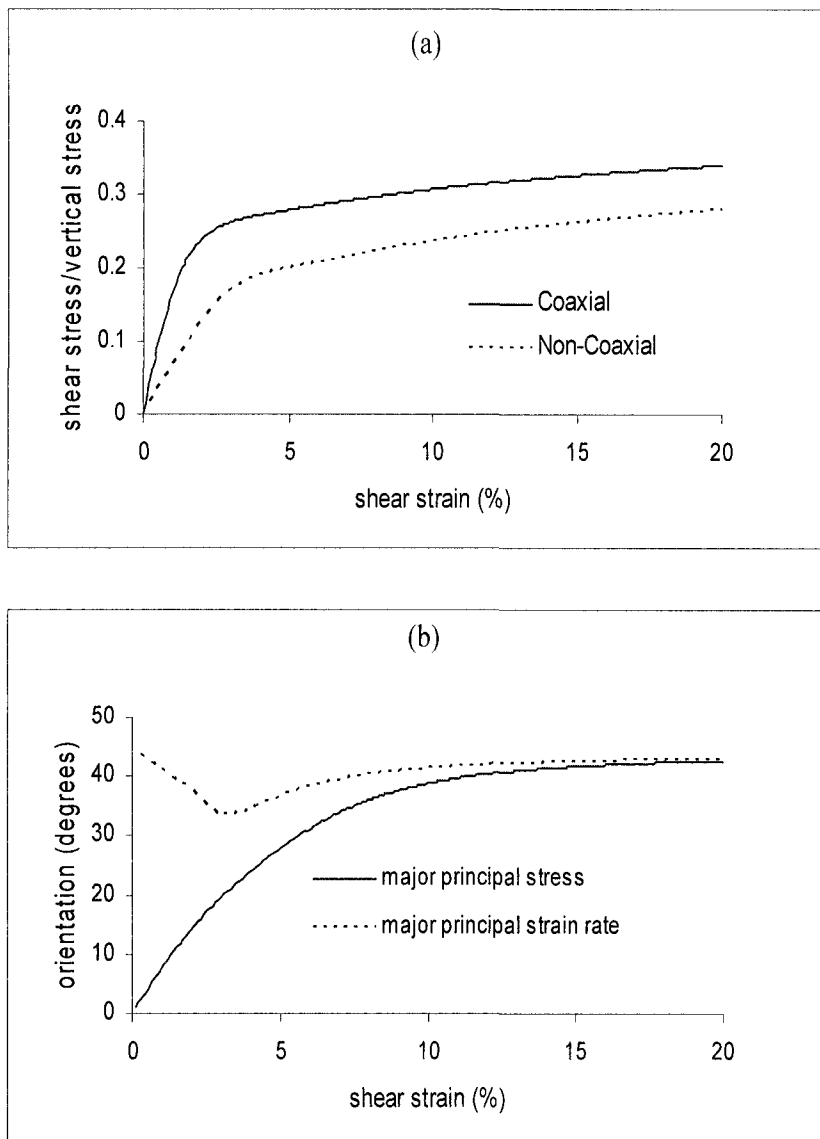


Figure 8.19: Results of simple shear of a normally consolidated Weald clay with  $OCR = 1$  and  $K_0 = 0.5$

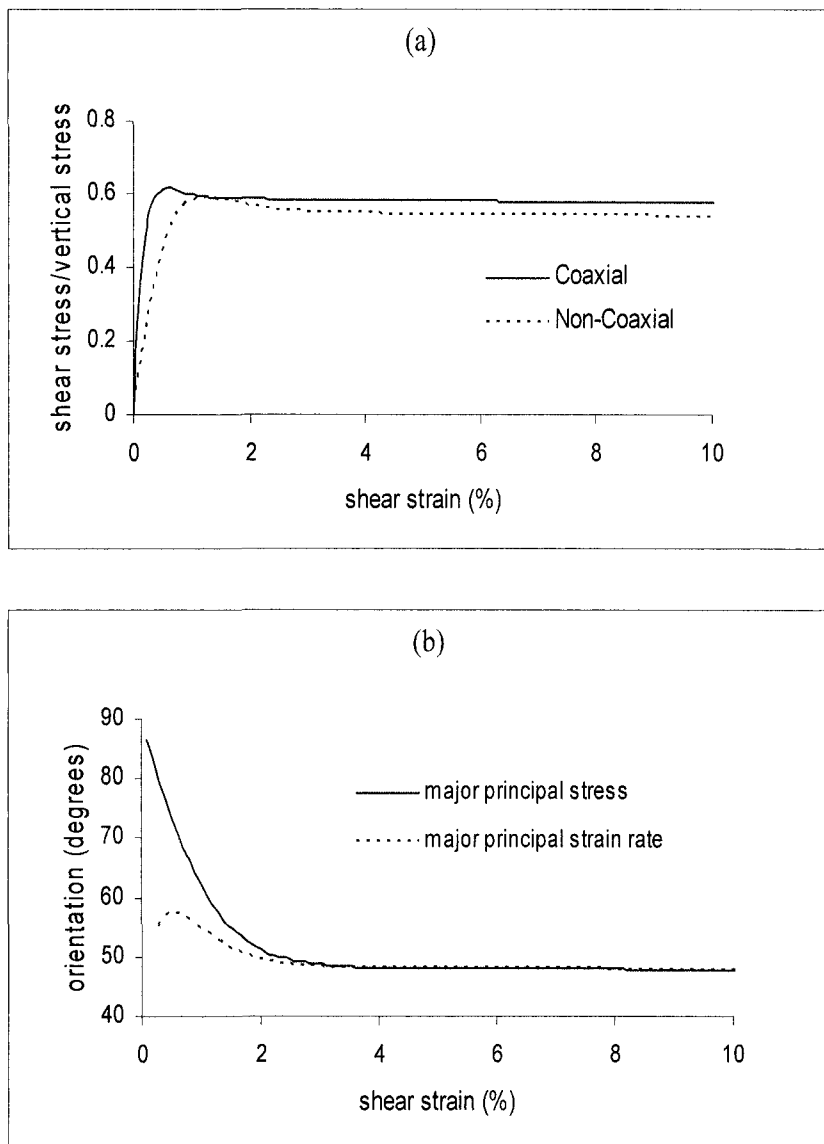


Figure 8.20: Results of simple shear of an overconsolidated Weald clay with  $OCR = 24$  and  $K_0 = 2.81$

### Simple shear in clay

To use the non-coaxial CASM model to simulate simple shear of clay, the model constants that are relevant for Weald clay may be used (Yu, 1998):

$$\lambda = 0.093, \Gamma = 2.06, \nu = 0.3, \varkappa = 0.025, M = 0.9, \xi_R = 0.0679, n = 4.5$$

Using the yield vertex non-coaxial flow rule, the degree of non-coaxiality is controlled by the normalised plastic modulus  $h_1/G$ . Figure 8.19 and Figure 8.20 present the numerical results for stress-strain relations and the non-coaxial response of simple shear of a normally consolidated sand ( $OCR = 1, K_0 = 0.5$ ) and an over-consolidated sand ( $OCR = 24, K_0 = 2.81$ ) respectively. In these results,  $h_1/G = 1$  was used, although results for other  $h_1/G$  values can be found in Yang and Yu (2006b). In general the inclusion of non-coaxial behaviour tends to make the stress-strain response softer. It is evident that the predicted non-coaxial behaviour is consistent with the experimental observations (Roscoe, 1970) and DEM simulations (Zhang, 2003) for granular materials.

### REFERENCES

Airey, D.W., Budhu, M. and Wood, D.M. (1985). Some aspects of the behaviour of soils in simple shear, In: *Development in Soil Mechanics and Foundation Engineering*, (Editors: P K Banerjee and R Butterfield), Elsevier, Vol 2, 185-213.

Allersma, H.G.B. (1982). Photo-elastic stress analysis and strain in simple shear, In: *Proc. IUTAM Conf. Deformation and Failure of Granular Materials*, Delft, 345-353.

Anand, L. (1983). Plane deformations of ideal granular materials, *J. Mech. Phys. Solids.*, Vol 33, 215-226.

Arthur, J.R.F., Chua, K.S., Dunstan, T. (1977). Induced anisotropy in a sand, *Geotechnique*, Vol 27, 13-30.

Arthur, J.R.F., Chua, K.S., Dunstan, T. and Rodriguez, C.J. I. (1980). Principal stress rotation: a missing parameter, *J. Geotech. Eng.*, ASCE, Vol 106, 419-433.

Bjerrum, L. and Landva, A. (1966). Direct simple shear tests on a Norwegian quick clay, *Geotechnique*, Vol 16, 1-20.

Budhu, M. and Britto, A. (1987). Numerical analysis of soils in simple shear devices, *Soils and Foundations*, Vol 27, 31-41.

Christoffersen, J., Mehrabadi, M.M. and Nemat-Nasser, S. (1981). A micromechanical description of granular material behaviour, *J. Appl. Mech.*, Vol 48, 339-344.

Cundall, P.A. and Strack, O.D.L. (1979). A discrete numerical model for granular assemblies, *Geotechnique*, Vol 29, 47-65.

Davis, E.H. (1968). Theories of plasticity and the failure of soil masses, In: *Soil Mechanics: Selected Topics*, (Editor: I. K. Lee), Butterworths, London, 341-380.

de Josselin de Jong, G. (1958). The undefiniteness in kinematics for friction materials, *Proc. Conf. Earth Pressure Problems*, Brussels, Vol 1, 55-70.

de Josselin de Jong, G. (1971). The double sliding, free rotating model for granular assemblies, *Geotechnique*, Vol 21, 155-162.

Drescher, A. (1976). An experimental investigation of flow rules for granular materials using optically sensitive glass particles, *Geotechnique*, Vol 26, 591-601.

Drescher, A. and de Josselin de Jong, G. (1972). Photoelastic verification of a mechanical model for the flow of a granular material, *J. Mech. Phys. Solids*, Vol 20, 337-351.

Gutierrez, M., Ishihara, K. (2000). Non-coaxiality and energy dissipation in granular material, *Soils and Foundations*, Vol 40, 49-59.

Gutierrez, M., Ishihara, K. and Towhata, I. (1991). Flow theory for sand during rotation of principal stress direction, *Soils and Foundations*, Vol 31, 121-132.

Harris, D. (1993). Constitutive equations for planar deformation of rigid plastic materials, *J. Mech. Phys. Solids*, Vol 41, 1515-1531.

Harris, D. (1995). A unified formulation for plasticity models of granular and other materials, *Proc. R. Soc. A.*, Vol 450, 37-49.

Hight, D.W., Gens, A. and Symes, M.J. (1983). The development of a new hollow cylinder apparatus for investigating the effects of principal stress rotation in soils, *Geotechnique*, Vol 33, 355-383.

Hill, R (1950). *The Mathematical Theory of Plasticity*, Clarendon Press, Oxford.

Jiang, M.J., Harris, D. and Yu, H.S. (2005). Kinematic models for non-coaxial granular materials: Part I and Part II, *Int. J. Num. Anal. Meth. Geomech.*, Vol 29, 643-689.

Jiang, M.J. and Yu, H.S. (2006). Application of the discrete element method to modern geomechanics, In: *Modern Trends in Geomechanics*, (Editors: W. Wu and H.S. Yu), Springer.

Joer, H.A., Lanier, J. and Fahey, M. (1998). Deformation of granular materials due to rotation of principal axes, *Geotechnique*, Vol 48, 605-619.

Kjellman, W. (1951). Testing the shear strength of clay in Sweden, *Geotechnique*, Vol 2, 225-232.

Kolymbas, D. (1991). An outline of hypoplasticity, *Arch. Appl. Mech.*, Vol 61, 143-151.

Mandl, G. and Luque, R.F. (1970). Fully developed plastic flow of granular materials, *Geotechnique*, Vol 20, 277-307.

Matsuoka, H. (1974). A microscopic study on shear mechanism of granular materials, *Soils and Foundations*, Vol 14, 29-43.

Matsuoka, H., Iwata, Y. and Sakakibara, K. (1986). A constitutive model of sands and clays for evaluating the influence of rotation of principal stress axes, *Proc. of NUMOG2*, Ghent, 67-78.

Mehrabadi, M.M. and Cowin, S.C. (1978). Initial planar deformation of dilatant granular materials, *J. Mech. Phys. Solids.*, Vol 26, 269-284.

Oda, M. and Konishi, J. (1974). Microscopic deformation mechanism of granular material in simple shear, *Soils and Foundations*, Vol 14, 25-38.

Owen, D.R.J. and Hinton, E. (1980). *Finite Elements in Plasticity: Theory and Practice*, Pineridge Press, Swansea.

Lade, P.V. (1975). Torsion shear tests on cohesionless soil, *Proc. 5th Pan Am. Conf. Soil Mech.*, Buenos Aires, Vol 1, 117-127.

Papamichos, E. and Vardoulakis, I. (1995). Shear band formation in sand according to non-coaxial plasticity model, *Geotechnique*, Vol 45, 649-661.

Roscoe, K.H. (1970). The influence of strains in soil mechanics, *Geotechnique*, Vol 20, 129-170.

Roscoe, K.H., Bassett, R.H. and Cole, E.R. (1967). Principal axes observed during simple shear of a sand, *Proc. Conf.*, Oslo, Vol 1, 231-237.

Rudnicki, J.W. and Rice, J.R. (1975). Conditions for the localisation of deformation in pressure-sensitive dilatant materials, *J. Mech. Phys. Solids.*, Vol 23, 371-394.

Saada, A.S. and Baah, A.K. (1967). Deformation and failure of a cross anisotropic clay under combined stresses, *Proc. 3rd Pan Am. Conf. Soil Mech.*, Caracas, Vol 1, 67-88.

Savage, J.C. and Lockner, D.A. (1997). A test of the double-shearing model of flow for granular materials, *J. Geophys. Res.*, Vol 102(B6), 12287-12294.

Schofield, A.N. and Wroth, C.P. (1968). *Critical State Soil Mechanics*, McGraw-Hill, London.

Spencer, A.J.M. (1964). A theory of the kinematics of ideal soils under plane strain conditions, *J. Mech. Phys. Solids.*, Vol 12, 337-351.

Spencer, A.J.M. (1982). Deformation of ideal granular materials. In: *Mechanics of Solids*, (Editors: H G Hopkins and M J Sewell), 607-652.

Stroud, M.A. (1971). *The Behavior of Sand at Low Stress Levels in the Simple Shear Apparatus*. PhD Thesis, Department of Engineering, University of Cambridge, England.

Teunissen, J.A.M. and Vermeer, P.A. (1988). Analysis of double shearing in frictional materials, *Int. J. Num. Analy. Meth. Geomech.*, Vol 12, 323-340.

Thornton, C. and Zhang, L. (2005). A numerical examination of shear banding and simple shear non-coaxial flow rules, *Phil. Mag.* (in press).

Tsutsumi, S. and Hashiguchi, K. (2005). General non-proportional loading behaviour of soils, *Int. J. Plasticity*, Vol 21, 1941-1969.

Vermeer, P.A. (1990). The orientation of shear bands in biaxial tests, *Geotechnique*, Vol 40, 323-336.

Yang, Y. and Yu, H.S. (2005). A comparison of two classes of non-coaxial plasticity models in plane strain, *Unpublished Note*, University of Nottingham.

Yang, Y. and Yu, H.S. (2006a). Numerical simulations of simple shear with non-coaxial soil models, *Int. J. Num. Anal. Meth. Geomech.*, Vol 30, 1-19.

Yang, Y. and Yu, H.S. (2006b). A non-coaxial critical state soil model and its application to simple shear simulations, *Int. J. Num. Anal. Meth. Geomech.* (in press).

Yu, H.S. (1995). A unified critical state model for clay and sand. *Civil Engineering Research Report No 112.08.1995*, University of Newcastle, NSW.

Yu, H.S. (1998). CASM: A unified state parameter model for clay and sand. *Int. J. Num. Anal. Meth. Geomech.*, Vol 22, 621-653.

Yu, H.S. and Yuan, X. (2005). The importance of accounting for non-coaxial behaviour in modelling soil-structure interaction, *Proc. 11th Int Conf. of IACMAG*, (Editors: G Barla and M. Barla), Patron Editore, Invited Issue Paper, Vol 4, 709-718.

Yu, H.S. and Yuan, X. (2006). On a class of non-coaxial plasticity models for granular soils, *Proc. R. Soc. A.*, Vol 462, 725-748.

Yu, H.S., Yang, Y. and Yuan, X. (2005). Application of non-coaxial plasticity models in geotechnical analysis. *Proc. of 16th Int. Conf. of ISSMGE.*, Osaka, Vol. 2, 993-996.

Yuan, X. (2005). *Non-Coaxial Plasticity for Granular Soils*, PhD Thesis, University of Nottingham, UK.

Zhang, L. (2003). *The Behaviour of Granular Material in Pure Shear, Direct Shear and Simple Shear*, PhD Thesis, Aston University, UK.

## CHAPTER 9

# PLASTICITY WITHOUT A PRIOR YIELD CRITERION

### 9.1 INTRODUCTION

All the theories of plasticity presented so far in this book have one thing in common and that is they all rely on a prior assumption of a yield criterion with either a single yield surface or multiple yield surfaces. These theories have been developed largely by using or modifying the main concepts of the classical theory of plasticity developed and matured before the 1950s. They are still the theories that are most widely used in soil mechanics and geotechnical engineering. Over the last two decades, however, there have also been some developments on the use of alternative approaches to constructing plastic soil stress-strain relations. These relatively modern, alternative approaches include:

- (1) The mathematical theory of envelopes (e.g. Chandler, 1985, 1988, 1990);
- (2) The endochronic theory based on intrinsic time (e.g. Valanis, 1971, 1980, 1984; Valanis and Read, 1982);
- (3) The incremental or hypoplastic theory (e.g. Kolymbas, 1977, 1991, 2000; Gudehus, 1996; Darve and Labanieh, 1982; Desrues and Chambon, 1993);
- (4) The thermomechanical or hyperplastic approach (e.g. Ziegler, 1977; Ziegler and Wehrli, 1987; Houlsby, 1981, 1982; Collins and Houlsby, 1997; Houlsby and Puzrin, 2000, 2006; Collins and Kelly, 2002).

All the four approaches mentioned above also have one thing in common and that is they do not need to assume a yield criterion at the beginning. Rather, the yield (or failure in the case of hypoplasticity) criterion and plastic flow rules are products of the formulations. The purpose of this chapter is to provide a brief description for each of these four alternative approaches to plasticity. The interested reader is directed to relevant references for further details. It is anticipated that further new insights may be obtained by following these new approaches, which could serve as a useful guide for further refinement of classical theories of plasticity.

### 9.2 THE MATHEMATICAL THEORY OF ENVELOPES

In an important paper, Chandler (1985) presented a plasticity theory which starts with a dilatancy rule and a function of plastic strain rates which represents the en-

ergy dissipated during plastic deformation. Yield functions and flow rules are then derived from energy conservation and the mathematical theory of envelopes. To some extent, this approach is an extension of the energy approach adopted in critical state soil mechanics. In particular, unlike the critical state soil mechanics approach, the method proposed by Chandler does not assume the universal validity of the associated flow rule. The following presentation is based on the work of Chandler (1985).

### 9.2.1 Stress and strain variables

It is often convenient to divide stresses into the mean and deviatoric components, namely

$$\sigma_{ij} = s_{ij} + p\delta_{ij} \quad (9.1)$$

where  $p = \sigma_{kk}/3$  is the mean pressure and  $s_{ij}$  is the deviatoric stress tensor.  $\delta_{ij}$  is the Kronecker delta (equal to 1 when  $i=j$ , or 0 otherwise). Similarly the strain rates can be divided into the mean and deviatoric components. For plastic strain rates, this means

$$\dot{\epsilon}_{ij}^p = \dot{\epsilon}_{ij}^p + \frac{1}{3}\dot{\epsilon}_{kk}^p\delta_{ij} \quad (9.2)$$

where  $\dot{\epsilon}_{ij}^p$  denotes the deviatoric plastic strain rate tensor.

For a granular material, the plastic strain rates may be further divided into those caused by the rearrangement of the particles ( $\dot{\epsilon}_{ij}^R, \dot{\epsilon}_{kk}^R$ ) and those resulting from the permanent deformation of the particles ( $\dot{\epsilon}_{ij}^D, \dot{\epsilon}_{kk}^D$ ) (Chandler, 1985). That is

$$\dot{\epsilon}_{ij}^p = \dot{\epsilon}_{ij}^R + \dot{\epsilon}_{ij}^D \quad (9.3)$$

$$\dot{\epsilon}_{kk}^p = \dot{\epsilon}_{kk}^R + \dot{\epsilon}_{kk}^D \quad (9.4)$$

for the deviatoric and volumetric strain rates respectively.

Experimental results with rigid particles seem to support the assumption that for small amounts of plane deformation, the rate of volume change resulting from particle rearrangement is proportional to the shear strain rate. If we generalise this hypothesis into a three-dimensional stress state, we have

$$d = \frac{\dot{\epsilon}_{kk}^R}{\sqrt{\dot{\epsilon}_{ij}^R \dot{\epsilon}_{ij}^R}} \quad (9.5)$$

where the constant  $d$  plays a role similar to that of the angle of dilation as used by Davis (1968) and Roscoe (1970).

### 9.2.2 Energy balance, yield function and flow rule

It is assumed that the energy input in a system can be stored as an increase in elastic energy or dissipated. The energy dissipated or the dissipation function can be written as follows (Martin, 1975):

$$\dot{D} = \sigma_{ij} \dot{\varepsilon}_{ij}^P = \sigma_{ij} (\dot{\varepsilon}_{ij}^R + \dot{\varepsilon}_{ij}^D) \quad (9.6)$$

which can be further expressed in terms of the mean and deviatoric stresses and their corresponding plastic strain rates in the following way

$$\dot{D} = s_{ij} (\dot{e}_{ij}^R + \dot{e}_{ij}^D) + p(\dot{e}_{kk}^R + \dot{e}_{kk}^D) \quad (9.7)$$

with equation (9.5), the above dissipation function can be written as

$$\dot{D} = s_{ij} (\dot{e}_{ij}^R + \dot{e}_{ij}^D) + p \left( \dot{e}_{kk}^D + d \sqrt{\dot{e}_{ij}^R \dot{e}_{ij}^R} \right) \quad (9.8)$$

As stated by Chandler (1985), if any particular combination of strain rates is specified in (9.8), the stresses must lie on a surface in the stress space. An infinite number of other surfaces can be obtained by choosing other combinations of strain rates. By assuming a suitable dissipation function  $\dot{D}$ , these surfaces will form an envelope enclosing a region in the stress space where no surfaces enter (Courant, 1956). Plastic flow cannot occur inside this region. This envelope may be termed as a yield surface as in the classical theory of plasticity. When the stress state touches this envelope, plastic flow occurs in the direction in  $(\dot{\varepsilon}_{ij}^R, \dot{\varepsilon}_{ij}^D)$  space determined by which surface is touched. This defines a plastic flow rule.

Chandler (1985) pointed out that this procedure is directly analogous to that used to obtain an interaction diagram for a steel frame structure (Baker *et al.*, 1965). The failure mechanism has become the combination of strain rates, the loading parameters have become the stresses and the work dissipated at the plastic hinges has become the dissipation function.

### 9.2.3 Examples

The theory outlined above can be applied to a range of dissipation functions. Some examples are given to illustrate its application to soil modelling.

#### (a) Deformation without particle rearrangement

It is instructive to consider a simple case where soil plastic deformation is purely due to particle deformation. In other words, the plastic strain due to particle rearrangement is zero. In this case, we may assume the following dissipation function

$$\dot{D}_1 = \sqrt{k^2 \dot{e}_{ij}^D \dot{e}_{ij}^D + l^2 (\dot{\epsilon}_{kk}^D)^2} \quad (9.9)$$

where  $k$  and  $l$  are material constants with dimension of pressure.

The energy balance equation (9.8) for the case without particle rearrangement can be written as

$$\Phi = s_{ij} \dot{e}_{ij}^D + p \dot{\epsilon}_{kk}^D - \dot{D}_1 = 0 \quad (9.10)$$

By following the procedure used in the theory of envelopes, we have

$$\frac{\partial \Phi}{\partial \dot{e}_{ij}^D} = s_{ij} - \frac{k^2 \dot{e}_{ij}^D}{\dot{D}_1} = 0 \quad (9.11)$$

$$\frac{\partial \Phi}{\partial \dot{\epsilon}_{kk}^D} = p - \frac{l^2 \dot{\epsilon}_{kk}^D}{\dot{D}_1} = 0 \quad (9.12)$$

These two equations provide a plastic flow rule

$$\frac{\dot{\epsilon}_{kk}^D}{\dot{e}_{ij}^D} = \left(\frac{k}{l}\right)^2 \frac{s_{ij}}{p} \quad (9.13)$$

They can also be used in conjunction with equation (9.10) to eliminate the strain rates to give the yield function

$$f = \frac{s_{ij} s_{ij}}{k^2} + \left(\frac{p}{l}\right)^2 - 1 = 0 \quad (9.14)$$

which reduces to the von Mises yield surface if  $l$  is much larger than  $k$ . Also the flow rule (9.13) reduces to the incompressibility condition for this case.

### (b) Deformation without particle distortion

Here we consider soils with effectively rigid particles so that any deformation can only be due to a rearrangement of the particles. Energy is assumed to be dissipated by friction alone. In this case, we may assume the following dissipation function

$$\dot{D}_2 = Mp \sqrt{\dot{e}_{ij}^R \dot{e}_{ij}^R} \quad (9.15)$$

where  $M$  is a dimensionless parameter similar to a coefficient of friction. With equation (9.5) and energy balance (9.8), we have

$$\Phi = s_{ij} \dot{e}_{ij}^R + p \dot{\epsilon}_{kk}^R - \dot{D}_2 = 0 \quad (9.16)$$

$$= s_{ij} \dot{e}_{ij}^R + p(d - M) \sqrt{\dot{e}_{ij}^R \dot{e}_{ij}^R} = 0 \quad (9.17)$$

The partial differentiation of  $\Phi$  with respect to  $\dot{e}_{ij}^R$  gives

$$\frac{\partial \Phi}{\partial \dot{e}_{ij}^R} = s_{ij} + p(d - M) \frac{\dot{e}_{ij}^R}{\sqrt{\dot{e}_{ij}^R \dot{e}_{ij}^R}} = 0 \quad (9.18)$$

This equation, together with equation (9.5), fully defines the plastic flow rule. By combining equations (9.5), (9.17) and (9.18) to eliminate the strain rate, the yield function can be obtained as follows

$$f = \sqrt{s_{ij} s_{ij}} + p(d - M) = 0 \quad (9.19)$$

which is equivalent to the yield function proposed by Drucker and Prager (1952). However the flow rule obtained here is generally of a non-associated type.

### (c) Deformation due to particle distortion and rearrangement

For real granular materials, observed deformation would be due to both particle distortion and rearrangement. Their relative contributions depend on soil particle properties and applied stress conditions such as the ratio of shear stress to the mean stress. If we focus on cohesionless soils, then the following dissipation function, which combines the cases (a) and (b) discussed before, may be assumed to include the effects of particle distortion and rearrangement

$$\dot{D}_3 = \sqrt{k^2 \dot{e}_{ij}^D \dot{e}_{ij}^D + l^2 (\dot{\varepsilon}_{kk}^D)^2 + M p \dot{e}_{ij}^R \dot{e}_{ij}^R} \quad (9.20)$$

The energy balance is

$$\Phi = s_{ij}(\dot{e}_{ij}^R + \dot{e}_{ij}^D) + p \left( \dot{\varepsilon}_{kk}^D + d \sqrt{\dot{e}_{ij}^R \dot{e}_{ij}^R} \right) - \dot{D}_3 = 0 \quad (9.21)$$

As usual, we have

$$\frac{\partial \Phi}{\partial \dot{\varepsilon}_{kk}^D} = p - \frac{l^2 \dot{\varepsilon}_{kk}^D}{\dot{D}_3} = 0 \quad (9.22)$$

$$\frac{\partial \Phi}{\partial \dot{e}_{ij}^D} = s_{ij} - \frac{k^2 \dot{e}_{ij}^D}{\dot{D}_3} = 0 \quad (9.23)$$

$$\frac{\partial \Phi}{\partial \dot{e}_{ij}^R} = s_{ij} + \dot{e}_{ij}^R \times \left( \frac{pd - M^2 p^2 g}{g \dot{D}_3} \right) = 0 \quad (9.24)$$

where  $g$  is defined by

$$g = \frac{\sqrt{\dot{e}_{ij}^R \dot{e}_{ij}^R}}{D_3} \quad (9.25)$$

Substitution of these equations into the energy balance equation (9.21) gives the yield function

$$f = s_{ij} s_{ij} \left( \frac{1}{k^2} - \frac{g}{pd - M^2 p^2 g} \right) + pgd + \left( \frac{p}{l} \right)^2 - 1 = 0 \quad (9.26)$$

After some rearrangement,  $g$  defined in equation (9.25) can also be expressed as a function of stresses

$$g = \frac{1}{Mp} \left( 1 - \frac{s_{ij} s_{ij}}{k^2} - \frac{p^2}{l^2} \right)^{\frac{1}{2}} \quad (9.27)$$

As noted by Chandler (1985), the above yield function can be simplified by using the following dimensionless stress variables

$$\bar{p} = \frac{p}{l} \quad ; \quad \bar{s} = \frac{\sqrt{s_{ij} s_{ij}}}{k} \quad (9.28)$$

and the dimensionless numbers

$$\bar{M} = \frac{l}{k} M \quad ; \quad N = \frac{l}{k} d \quad (9.29)$$

With the above new variables, the yield function (9.26) can be rewritten as

$$f = \bar{s} - \frac{\bar{M}^2 \bar{p}}{1 + \bar{M}^2 \bar{p}^2} \left( \frac{N}{\bar{M}^2} + \sqrt{\frac{1}{\bar{M}^2} - \left[ \frac{N^2}{\bar{M}^2} + \frac{1}{\bar{M}^2} - 1 \right] \bar{p}^2 - \bar{p}^4} \right) = 0 \quad (9.30)$$

which is only valid provided

$$\bar{s}^2 + \bar{p}^2 \leq 1 \quad (9.31)$$

otherwise the term  $g$  becomes imaginary. If this occurs, the yield function is assumed to be given by

$$f = \bar{s}^2 + \bar{p}^2 - 1 = 0 \quad (9.32)$$

### 9.3 THE ENDOCHRONIC THEORY

The endochronic theory of plasticity is a special case of the theory of viscoplasticity originated by Valanis (1971, 1980, 1984) based on the concept of intrinsic time. When describing its initial development, Valanis and Read (1982) state:

*“In the late 1960s, the formulation of constitutive theories of viscoelastic materials from concepts of irreversible thermodynamics and internal state variables reached an advanced level of development (Valanis, 1968). On the basis of this success, it was natural to inquire if a similar approach could be used to establish a theory of plasticity, and the attempt by Valanis to explore this question led to the development of the endochronic theory in 1971.”*

It is therefore clear that the endochronic theory builds on the principle of thermodynamics and internal variables and is a direct extension of viscoelastic theories. Like many other theories of plasticity, the endochronic theory was initially developed for modelling metals where the volumetric behaviour was assumed to be purely elastic. This model may be used to model undrained clay in terms of total stress. Due to its initial success in modelling metal behaviour (Valanis, 1971, 1980), the theory has undergone development and modification with the aim of modelling soil stress-strain behaviour (e.g. Dungar and Nuh, 1980; Valanis and Reed, 1982).

It is shown by Valanis (1971, 1980) and Watanabe and Atluri (1986) that the endochronic theory is *unifying* in the sense that many existing theories of viscoelasticity, plasticity (e.g. perfect plasticity, theories with isotropic hardening, kinematic hardening, or combined hardening, bounding surface plasticity with two-surface or multi-surface plasticity) can be obtained from it as special cases by imposing suitable constraints on the material parameters involved. In addition, it does not make use of the idea of a yield surface to start off the model formulation.

### 9.3.1 General formulation for cohesive soils under undrained conditions

In this case, the plastic strain is of deviatoric nature so it is convenient to divide stresses into the mean and deviatoric components, namely

$$\sigma_{ij} = s_{ij} + p\delta_{ij} \quad (9.33)$$

where  $p = \sigma_{kk}/3$  is the mean pressure and  $s_{ij}$  is the deviatoric stress tensor.  $\delta_{ij}$  is the Kronecker delta (equal to 1 when  $i=j$ , or 0 otherwise). Similarly the strain rates can be divided into the mean and deviatoric components. For plastic strain rates, this means

$$\dot{\epsilon}_{ij}^p = \dot{e}_{ij}^p + \frac{1}{3}\dot{\epsilon}_{kk}^p\delta_{ij} \quad (9.34)$$

where  $\dot{e}_{ij}^p$  denotes the deviatoric plastic strain rate tensor. If the volumetric behaviour is assumed to be purely elastic then we have

$$\dot{\epsilon}_{ij}^p = \dot{e}_{ij}^p \quad (9.35)$$

The endochronic theory of plasticity as derived by Valanis (1971, 1980) based on the irreversible thermodynamics consideration is

$$s_{ij} = 2G \int_0^z \varrho(z - z') \frac{de_{ij}^P}{dz'} dz' \quad (9.36)$$

where  $G$  is shear modulus and the kernel  $\varrho(z)$  is a material function and  $z$  is the intrinsic time scale which is linked to the intrinsic time measure  $\xi$  by

$$dz = \frac{d\xi}{f(\xi)} \quad \text{or} \quad z = \int \frac{d\xi}{f(\xi)} \quad (9.37)$$

where  $f$  is a function of the history of plastic strain, which is of thermodynamic origin and is related proportionally to the degree of internal friction in a material. If a material hardens,  $f(\xi)$  increases with  $\xi$ . If a material softens,  $f(\xi)$  decreases with  $\xi$ . Otherwise if a material is a perfectly plastic then  $f(\xi)$  is a constant.

For the deviatoric stress-strain relation (9.36), the intrinsic time measure may be defined as follows

$$d\xi = (de_{ij}^P de_{ij}^P)^{1/2} \quad (9.38)$$

Valanis (1971, 1980) proves that the kernel can be written in the following form

$$\varrho(z) = \varrho_0 \delta(z) + \varrho_1(z) \quad (9.39)$$

in which  $\varrho_0$  is a material constant,  $\delta(z)$  is a Dirac delta function, and  $\varrho_1(z)$  is a non-singular function. The use of equation (9.39) in equation (9.36) leads to

$$s_{ij} = S_y^0 \frac{de_{ij}^P}{dz} + 2G \int_0^z \varrho_1(z - z') \frac{de_{ij}^P}{dz'} dz' \quad (9.40)$$

where

$$S_y^0 = 2G\varrho_0 \quad (9.41)$$

If we set

$$\alpha_{ij} = 2G \int_0^z \varrho_1(z - z') \frac{de_{ij}^P}{dz'} dz' \quad (9.42)$$

then equation (9.40) can be written as

$$s_{ij} - \alpha_{ij} = S_y^0 \frac{de_{ij}^P}{dz} \quad (9.43)$$

*The case of  $f(\xi) = 1$*

In this case, we have

$$dz = d\xi \quad (9.44)$$

then equation (9.43) can be used to give

$$(s_{ij} - \alpha_{ij})(s_{ij} - \alpha_{ij}) = (S_y^0)^2 \quad (9.45)$$

and

$$de_{ij}^P = (s_{ij} - \alpha_{ij}) \frac{d\xi}{S_y^0} \quad (9.46)$$

If the kernel is chosen so that  $\alpha_{ij} = 0$ , then the above equation reduces to

$$de_{ij}^P = \frac{d\xi}{S_y^0} s_{ij} \quad (9.47)$$

which is the flow rule for an elastic perfectly plastic material obeying a von Mises yield criterion. However, if  $\alpha_{ij}$  is nonzero, then equation (9.46) represents a flow rule of a perfectly plastic material with kinematic hardening. The translation rule for the yield surface is governed by equations (9.39) and (9.42).

It can be easily shown (Valanis, 1980) that Prager's rule of kinematic hardening is a particular case of the endochronic theory by setting  $\varrho_1(z) = \text{constant}$  in equation (9.39). By setting a different  $\varrho_1(z)$  function, a different translation rule of kinematic hardening is obtained. It is of particular interest to note that Watanabe and Atluri (1986) demonstrate that both the theories of multi-surface and bounding surface plasticity can also be obtained as special cases of the endochronic theory by choosing suitable kernel functions.

*The case when  $f(\xi)$  is monotonically increasing*

In this case, we can obtain

$$(s_{ij} - \alpha_{ij})(s_{ij} - \alpha_{ij}) = (f(\xi) S_y^0)^2 \quad (9.48)$$

and

$$de_{ij}^P = (s_{ij} - \alpha_{ij}) \frac{d\xi}{f(\xi) S_y^0} \quad (9.49)$$

Thus the yield surface defined by equation (9.48) can translate as well as expand at the same time (i.e. combined isotropic and kinematic hardening).

If the kernel is chosen so that  $\alpha_{ij} = 0$ , then the above equations reduce to

$$s_{ij} s_{ij} = (f(\xi) S_y^0)^2 \quad (9.50)$$

$$d\epsilon_{ij}^p = \frac{d\xi}{f(\xi) S_y^0} s_{ij} \quad (9.51)$$

which corresponds to the flow rule for purely isotropic hardening plastic material obeying a von Mises yield criterion.

### 9.3.2 Formulation for cohesionless soils

For soils in general the volumetric behaviour is not entirely elastic. Also plastic deformation may occur once the load is applied on soils. To account for these two observed effects, Valanis and Reed (1982) present a modified endochronic theory. This new theory can be described as follows.

The intrinsic time measures for deviatoric and volumetric behaviours may be defined as follows

$$d\xi_D = (d\epsilon_{ij}^p d\epsilon_{ij}^p)^{1/2} \quad (9.52)$$

$$d\xi_H = |d\epsilon_{kk}^p| \quad (9.53)$$

and a general intrinsic time scale  $z$  may be assumed to be linked to the intrinsic time measures  $\xi_D$  and  $\xi_H$  by

$$dz = \sqrt{k_{00}(d\xi_D)^2 + k_{01}(d\xi_H)^2} \quad (9.54)$$

where  $k_{00}$  and  $k_{01}$  are constants. The endochronic theory of plasticity as derived by Valanis and Reed (1982) is expressed by

$$s_{ij} = \int_0^z \varrho(z - z') \frac{d\epsilon_{ij}^p}{dz'} dz' \quad (9.55)$$

$$\sigma_{kk} = \int_0^z K(z - z') \frac{d\epsilon_{kk}^p}{dz'} dz' \quad (9.56)$$

where the kernel functions  $\varrho(0) = K(0) = \infty$ .

#### *Modelling of cohesionless soils under simple shear*

The behaviour of sand under simple shear may be described by the endochronic theory. To illustrate this, consider equation (9.55)

$$s_{ij} = \int_0^z \varrho(z - z') \frac{d\epsilon_{ij}^p}{dz'} dz'$$

In order to account for the hardening-softening behaviour exhibited by dense cohesionless soils, we assume the following intrinsic time scale

$$dz = \frac{d\xi_D}{f(z)} \quad (9.57)$$

Then the stress-strain relation (9.55) can be written as

$$s_{ij} = \int_0^z \varrho(z - z') f(z') \frac{de_{ij}^p}{d\xi_D} dz' \quad (9.58)$$

It is found (Valanis and Reed, 1982) that the response of soils to simple shear can be described very well by the following forms of functions

$$\varrho(z) = \varrho_0 \frac{e^{-kz}}{z^\alpha} \quad (9.59)$$

$$f(z) = 1 + \beta * e^{-k_1 z} \quad (9.60)$$

where  $\varrho_0, \alpha, \beta$ ,  $k$  and  $k_1$  are constants. The theory is found to be very capable of simulating unloading-reloading behaviour of soils.

## 9.4 HYPOPLASTICITY

Hypoplasticity is a term used to describe a class of incremental (or rate) approach to stress-strain relations originated by Green (1956a,b) and further developed in Germany (Kolymbas, 1991, Gudehus, 1996) and in France (Darve and Labanieh, 1982; Desrues and Chambon, 1993). A comparative review of the German and French approaches was given by Tamagnini *et al.* (1999). The hypoplastic theory has its root in the hypoelasticity of Truesdell (1955) and assumes an incremental relation between stress and strain tensors. The theory does not distinguish between elastic and plastic strains. Whilst the literature on this type of theory is large (e.g. Kolymbas, 2000; Gudehus, 1996; Wu and Kolymbas, 2000), the following brief description is based on the work of Kolymbas (1994).

### 9.4.1 The basic hypoplastic equation

The hypoplasticity approach is to propose a rate equation between stress and strain. Such an approach generally requires trial and error procedures (e.g. Kolymbas, 1991). The first useful rate equation was proposed by Kolymbas (1985) and has four terms

$$\begin{aligned} \dot{\sigma}_{ij} = & C_1(\sigma_{ik}\dot{\epsilon}_{kj} + \epsilon_{ik}\dot{\sigma}_{kj}) + C_2\sigma_{kl}\dot{\epsilon}_{kl}\delta_{ij} \\ & + \left( C_3\sigma_{ij} + C_4 \frac{\sigma_{ik}\sigma_{kj}}{\sigma_{ll}} \right) \sqrt{\dot{\epsilon}_{pq}\dot{\epsilon}_{pq}} \end{aligned} \quad (9.61)$$

where  $\delta_{ij}$  is the Kronecker delta (equal to 1 when  $i=j$ , or 0 otherwise). It is clear that the above equation is of a nonlinear nature. For application in numerical methods, it is often convenient to write equation (9.61) in the following form

$$\dot{\sigma}_{ij} = D_{ijkl}\dot{\varepsilon}_{kl} \quad (9.62)$$

where

$$D_{ijkl} = C_1(\sigma_{ik}\delta_{jl} + \delta_{il}\dot{\sigma}_{kj}) + C_2\sigma_{kl}\delta_{ij} + \left( C_3\sigma_{ij} + C_4\frac{\sigma_{im}\sigma_{mj}}{\sigma_{nn}} \right) \frac{\dot{\varepsilon}_{kl}}{\sqrt{\dot{\varepsilon}_{pq}\dot{\varepsilon}_{pq}}} \quad (9.63)$$

It is noted that in this stress-strain relation the stiffness matrix depends on four material constants, stresses, stress rates as well as the direction of strain rates.

#### 9.4.2 Determination of model constants

The four constants,  $C_1, C_2, C_3, C_4$ , used in the stress-strain rate equation can be obtained from the results of a standard triaxial test, as shown in Figure 9.1. From the figure, we can obtain the following four parameters:

- (1) The initial slope of the stress strain curve,  $E_0$
- (2) The angle of initial dilatancy,  $\beta_0$
- (3) The angle of friction at the limit state,  $\phi$
- (4) The angle of dilatancy at the limit state,  $\beta$

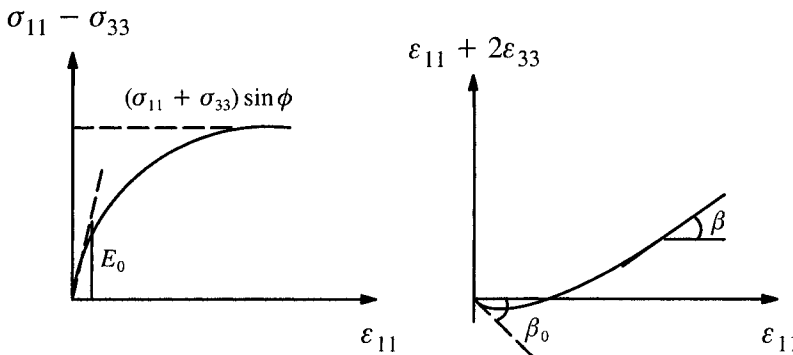


Figure 9.1: Results of a standard triaxial test

If we then define the following quantities

$$a = \frac{1 + \sin\phi}{1 - \sin\phi} \quad (9.64)$$

$$b_0 = \frac{1 + \tan\beta_0}{2} \quad (9.65)$$

$$b = \frac{1 + \tan\beta}{2} \quad (9.66)$$

$$c_0 = \sqrt{1 + 2b_0^2} \quad (9.67)$$

$$c = \sqrt{1 + 2b^2} \quad (9.68)$$

$$d = \frac{a - 1}{a + 2} [2b - a)(2a + 1) + 3ac] \quad (9.69)$$

$$f = \frac{2b - a}{1 - 2b_0} \quad (9.70)$$

the model coefficients can be obtained from the following equations

$$C_1 = \frac{E_0}{\sigma_{33}(1 + b_0)} \quad (9.71)$$

$$\frac{C_4}{C_1} = \frac{\frac{b + fb_0}{c + fc_0} - \frac{b + a}{c(1 - a)}}{\frac{a + 1}{a + 2} - \frac{fc_0/3 + c/(a + 2)}{c + fc_0}} \quad (9.72)$$

$$C_3 = -\frac{1}{c + fc_0} \left[ (b + fb_0)C_1 + \left(\frac{fc_0}{3} + \frac{c}{a + 2}\right)C_4 \right] \quad (9.73)$$

$$C_2 = \frac{1}{1 - 2b_0} \left( b_0 C_1 + c_0 C_3 + \frac{c_0 C_4}{3} \right) \quad (9.74)$$

#### 9.4.3 Improved hypoplastic equations

The application of the rate equation (9.61) suggests that the following equation proposed by Wu (1992) may give better prediction of soil behaviour

$$\begin{aligned} \dot{\sigma}_{ij} = & C_1 \sigma_{kk} \dot{\epsilon}_{ij} + C_2 \frac{\sigma_{kl} \dot{\epsilon}_{kl}}{\sigma_{mm}} \sigma_{ij} \\ & + \left( C_3 \frac{\sigma_{ik} \sigma_{kj}}{\sigma_{mm}} + C_4 \frac{s_{ik} s_{kj}}{\sigma_{mm}} \right) \sqrt{\dot{\epsilon}_{pq} \dot{\epsilon}_{pq}} \end{aligned} \quad (9.75)$$

where  $s_{ij}$  is the deviatoric stress tensor and  $\delta_{ij}$  is the Kronecker delta (equal to 1 when  $i=j$ , or 0 otherwise).

Wu (1992) further showed that by slightly modifying equation (9.75), the feature of critical states may also be included. One example is given below

$$\begin{aligned}\dot{\sigma}_{ij} = & C_1 \sigma_{kk} \dot{\varepsilon}_{ij} + C_2 \frac{\sigma_{kl} \dot{\varepsilon}_{kl}}{\sigma_{mm}} \sigma_{ij} \\ & + I_e \left( C_3 \frac{\sigma_{ik} \sigma_{kj}}{\sigma_{mm}} + C_4 \frac{s_{ik} \delta_{kj}}{\sigma_{mm}} \right) \sqrt{\dot{\varepsilon}_{pq} \dot{\varepsilon}_{pq}}\end{aligned}\quad (9.76)$$

where

$$I_e = (1 - a_1) \frac{e - e_{\min}}{e_{\text{cri}} - e_{\min}} + a_1$$

$$a_1 = q_1 + q_2 \exp(-q_3 \sigma_{kk})$$

$$e_{\text{cri}} = p_1 + p_2 \exp(-p_3 \sigma_{kk})$$

and  $e_{\min}, q_1, q_2, q_3, p_1, p_2, p_3$  are an additional seven model parameters. In total, the model requires 11 material constants.

Many further developments have been made which include the work of Gudehus (1996). Interested readers are referred to the book edited by Kolymbas (2000) for further details.

## 9.5 HYPERPLASTICITY

Hyperplasticity is a term sometime used to describe the class of plasticity theory derived from both specific free energy and specific dissipation function (e.g. Ziegler, 1977; Houlsby, 1982; Maugin, 1992; Collins and Houlsby, 1997; Collins and Kelly, 2002). This theory may be regarded as an extension of the method of deriving elastic behaviour from an elastic potential (i.e. hyperelasticity). The specific free energy  $\Psi$  is a function of state (i.e. of the kinematic variables) and the specific dissipation function  $\Phi$  is a non-negative function of the state and rate of change of the state (i.e. of the kinematic variables and their time derivatives). Therefore

$$\Psi = \Psi(\varepsilon_{ij}, \alpha_{kl}^{(n)}) \quad (9.77)$$

$$\Phi = \Phi(\varepsilon_{ij}, \alpha_{kl}^{(n)}, \dot{\varepsilon}_{mn}, \dot{\alpha}_{pq}^{(n)}) \quad (9.78)$$

where  $\alpha_{kl}^{(n)}$  are a set of internal kinematic variables (such as plastic strains). The significance of these functions is fully explained in Ziegler (1977). To put it simply,

equation (9.77) ensures that the first law of thermodynamics is obeyed, and the positive dissipation function (9.78) ensures that the material complies with the second law.

By using the orthogonality principle of Ziegler (1977), it can be shown that for a rate-independent material the following two equations are valid (Houlsby, 1982)

$$\sigma_{ij} = \varrho \frac{\partial \Psi}{\partial \varepsilon_{ij}} + \varrho \frac{\partial \Phi}{\partial \dot{\varepsilon}_{ij}} \quad (9.79)$$

$$0 = \varrho \frac{\partial \Psi}{\partial \alpha_{kl}} + \varrho \frac{\partial \Phi}{\partial \dot{\alpha}_{kl}} \quad (9.80)$$

where  $\varrho$  is the density. The above two equations are sufficient to determine the behaviour of a material once the functions  $\Psi$  and  $\Phi$  are given.

### 9.5.1 Derivation of von Mises plasticity

Houlsby (1982) shows that the formulation of an elastic-perfectly plastic material with a von Mises yield criterion and an associated flow rule can be derived by assuming the following free energy expression and dissipation function

$$\varrho \Psi = \left( \frac{\lambda}{2} + \frac{\mu}{3} \right) \varepsilon_{ii} \varepsilon_{jj} + \mu (e_{ij} - e_{ij}^p) (e_{ij} - e_{ij}^p) \quad (9.81)$$

$$\varrho \Phi = \sqrt{2} k (\dot{\varepsilon}_{ij}^p \dot{\varepsilon}_{ij}^p)^{1/2} \quad (9.82)$$

where  $\lambda$  and  $\mu$  are Lame's constants and  $k$  shear strength in pure shear. Here the role of kinematic internal variables is taken by the deviatoric plastic strain. By applying equations (9.79) and (9.80), we obtain

$$\sigma_{ij} = \left( \lambda + \frac{2\mu}{3} \right) \varepsilon_{kk} \delta_{ij} + 2\mu (e_{ij} - e_{ij}^p) \quad (9.83)$$

$$0 = -2\mu (e_{ij} - e_{ij}^p) + \frac{\sqrt{2} k \dot{\varepsilon}_{ij}^p}{(\dot{\varepsilon}_{ij}^p \dot{\varepsilon}_{ij}^p)^{1/2}} \quad (9.84)$$

It can be shown from equation (9.83) that the volumetric stress-strain relation is purely elastic

$$\frac{\sigma_{kk}}{3} = \left( \lambda + \frac{2\mu}{3} \right) \varepsilon_{kk} \quad (9.85)$$

and the deviatoric stress-strain relation is

$$s_{ij} = 2\mu (e_{ij} - e_{ij}^p) \quad (9.86)$$

The combination of equations (9.83) and (9.84) leads to the following well known plastic flow rule

$$\dot{\varepsilon}_{ij}^p = \frac{(\dot{\varepsilon}_{kl}^p \dot{\varepsilon}_{kl}^p)^{1/2}}{\sqrt{2} k} s_{ij} \quad (9.87)$$

Furthermore, if the plastic strain rate is non-zero, then the above equation can be squared to give the von Mises yield function

$$s_{ij} s_{ij} = 2k^2 \quad (9.88)$$

The above formulation is for an elastic-perfectly plastic model with the von Mises yield function. It is noted that the effect of work hardening may also be included by introducing an additional term into the free energy expression

$$\varrho\Psi = \left(\frac{\lambda}{2} + \frac{\mu}{3}\right)\varepsilon_{ii}\varepsilon_{jj} + \mu(e_{ij} - e_{ij}^p)(e_{ij} - e_{ij}^p) + h e_{ij}^p e_{ij}^p \quad (9.89)$$

which yields a new yield function

$$(s_{ij} - 2h e_{ij}^p)(s_{ij} - 2h e_{ij}^p) = 2k^2 \quad (9.90)$$

This resulting yield function represents kinematic hardening with a hardening modulus  $h$ . As pointed out by Houlsby (1982), isotropic hardening may also be achieved by replacing the shear strength  $k$  in the dissipation function by a positive function of the plastic strain.

### 9.5.2 Derivation of Cam clay plasticity

Houlsby (1981) was the first to show that it is possible to derive critical state models using the thermo-mechanical approach, although a more general and extensive treatment has been recently given by Collins and Kelly (2002). For example, a critical state model, almost identical to modified Cam clay, can be obtained by assuming the following specific free energy and dissipation functions:

$$\begin{aligned} \varrho\Psi = p_r \varkappa^* \exp \frac{(\varepsilon_p - \varepsilon_p^p)}{\varkappa^*} + \frac{3}{2} G(\varepsilon_q - \varepsilon_q^p)^2 \\ + p_r(\lambda^* - \varkappa^*) \exp \frac{\ln(\Gamma/V_0) + \varepsilon_p^p}{\lambda^* - \varkappa^*} \end{aligned} \quad (9.91)$$

$$\varrho\Phi = [p_r(\lambda^* - \varkappa^*) \exp \frac{\ln(\Gamma/V_0) + \varepsilon_p^p}{\lambda^* - \varkappa^*}] [(\dot{\varepsilon}_p^p)^2 + M^2(\dot{\varepsilon}_q^p)^2]^{\frac{1}{2}} \quad (9.92)$$

where  $p_r$  is a reference pressure (often taken as 1kPa), that is necessary to establish dimensional consistency. A slight difference from the conventional Cam clay formulations is that  $\lambda^*$  and  $\varkappa^*$  used here are slopes of the critical state line and elastic swelling line in the  $(\ln V, \ln p)$  space.

Application of equation (9.79) to these specific free energy and dissipation functions gives the equations for stresses:

$$p = \varrho \frac{\partial \Psi}{\partial \varepsilon_p} + \varrho \frac{\partial \Phi}{\partial \dot{\varepsilon}_p} = p_r \exp \frac{\varepsilon_p - \varepsilon_p^p}{\kappa^*} \quad (9.93)$$

$$q = \varrho \frac{\partial \Psi}{\partial \varepsilon_q} + \varrho \frac{\partial \Phi}{\partial \dot{\varepsilon}_q} = 3G(\varepsilon_q - \varepsilon_q^p) \quad (9.94)$$

whose rate forms may be shown to be the same as the following incremental elastic laws:

$$\dot{\varepsilon}_p = \frac{\kappa^* \dot{p}}{p} + \dot{\varepsilon}_p^p \quad (9.95)$$

$$\dot{\varepsilon}_q = \frac{\dot{q}}{3G} + \dot{\varepsilon}_q^p \quad (9.96)$$

On the other hand, application of equation (9.80) would lead to the following yield function and plastic flow rule:

$$(p - p_x)^2 + \left(\frac{q}{M}\right)^2 = p_x^2 \quad (9.97)$$

$$\frac{\dot{\varepsilon}_q^p}{\dot{\varepsilon}_p^p} = \frac{q}{M^2(p - p_x)} \quad (9.98)$$

where

$$p_x = p_r(\lambda^* - \kappa^*) \exp \frac{\ln(\Gamma/V_0) + \varepsilon_p^p}{\lambda^* - \kappa^*} \quad (9.99)$$

It is readily shown that the flow rule defined by (9.98) is associated as the plastic strains are normal to the yield surface given by (9.97). It should be noted that the use of the consistency condition with the yield function (9.97) together with the flow rule (9.98) will fully define the plastic strains.

### 9.5.3 Remarks

Whilst having some important advantages the thermo-mechanical approach appears to be indirect in the sense that for a given material appropriate specific free energy and dissipation functions may be more difficult to determine than appropriate yield surfaces. Houlsby (1981) noted that for simple models the thermo-mechanical approach may not offer any significant advantages over the conventional plasticity of assuming yield functions.

## REFERENCES

Baker, J., Horne, M.R. and Heyman, J. (1965). *The Steel Skeleton*, Vol II. Cambridge University Press.

Chandler, H.W. (1985). A plasticity theory without Drucker's postulate, suitable for granular materials, *J. Mech. Phys. Solids.*, Vol 33, 215-226.

Chandler, H.W. (1988). A variational principle for granular materials, *Int. J. Num. Anal. Meth. Geomech.*, Vol 12, 371-378.

Chandler, H.W. (1990). A model for the deformation and flow of granular materials undergoing monotonic shear loading, *Geotechnique*, Vol 40, 379-388.

Collins, I.F. and Houlsby, G.T. (1997). Application of thermomechanical principles to the modelling of geotechnical materials, *Proc. R. Soc. A.*, Vol 453, 1975-2001.

Collins, I.F. and Kelly, P.A. (2002). A thermomechanical analysis of a family of soil models, *Geotechnique*, Vol 52, 507-518.

Darve, F. and Labanieh, S. (1982). Incremental constitutive law for sands and clays. *Int. J. Num. Anal. Meth. Geomech.*, Vol 6, 243-275.

Desrues, J. and Chambon, R. (1993). A new rate type constitutive model for geomaterials: CLoE. In: *Modern Approaches to Plasticity*, (Editor: D Kolymbas), Elsevier, 309-324.

Drucker, D.C. and Prager, W. (1952). Soil mechanics and plastic analysis for limit design, *Quart. Appl. Math.*, Vol 10, 157-165.

Dungar, R. and Nuh, S. (1980). Endochronic-critical state models for sand, *J. Eng. Mech. Div.*, ASCE, Vol 106, 951-967.

Green, A.E. (1956a). Hypo-elasticity and plasticity, *Proc. R. Soc. A.*, Vol 234, 46-59.

Green, A.E. (1956b). Hypo-elasticity and plasticity: II, *J. Rat. Mech. Anal.*, Vol 5, 725-734.

Gudehus, G. (1996). A comprehensive constitutive equation for granular material, *Soils and Foundations*, Vol 36, 1-12.

Hill, R (1950). *The Mathematical Theory of Plasticity*, Clarendon Press, Oxford.

Houlsby, G.T. (1981). *A Study of Plasticity Theories and Their Applicability to Soils*, PhD Thesis, Cambridge University.

Houlsby, G.T. (1982). A derivation of the small-strain incremental theory of plasticity from thermodynamics, In: *Proc. IUTAM Conf. Deformation and Failure of Granular Materials*, Delft, 109-118.

Houlsby, G.T. and Puzrin, A.M. (2000). A thermomechanical framework for constitutive models for rate independent dissipative materials, *Int. J. Plasticity*, Vol 16, 1017-1047.

Houlsby, G.T. and Puzrin, A.M. (2006). *Principles of Hyperplasticity*, Springer, London.

Kolymbas, D. (1977). A rate dependent constitutive equation for soils. *Mech. Resear. Comm.*, Vol 4, 367-372.

Kolymbas, D. (1991). An outline of hypoplasticity, *Arch. Appl. Mech.*, Vol 61, 143-151.

Kolymbas, D. (1994). Hypoplasticity as a constitutive framework for granular materials. In: *Computer Methods and Advances in Geomechanics*, (Editors: Siriwardane and Zaman), Balkema, 197-208.

Kolymbas, D. (Editor) (2000). *Constitutive Modelling of Granular Materials*, Springer.

Martin, J.B. (1975). *Plasticity: Fundamentals and General Results*, MIT Press, Cambridge.

Maugin, G.A. (1992). *The Thermomechanics of Plasticity and Fracture*, Cambridge University Press.

Tamagnini, C., Viggiani, G. and Chambon, R. (2000). A review of two different approaches to hypoplasticity, In: *Constitutive Modelling of Granular Materials*, (Editor: D Kolymbas), Springer, 107-146.

Truesdell, C. (1955). Hypo-elasticity, *J. Rat. Mech. Anal.*, Vol 4, 83-133.

Valanis, K.C. (1971). A theory of viscoplasticity without a yield surface, *Arch. Mech.*, Vol 23, 517-534.

Valanis, K.C. (1980). Fundamental consequences of a new intrinsic time measure plasticity as a limit of the endochronic theory, *Arch. Mech.*, Vol 32, 171.

Valanis, K.C. (1984). Continuum foundations of endochronic plasticity, *J. Eng. Mater. Tech.*, Vol 106, 367.

Valanis, K.C. and Read, H.E. (1982). A new endochronic plasticity model for soils, In: *Soil Mechanics – Transient and Cyclic Loads*, Wiley, 375-417.

Watanabe, O. and Atluri, S.N. (1986). Internal time, general internal variable, and multi-yield surface theories of plasticity and creep: a unification of concepts, *Int. J. Plasticity*, Vol 2, 37.

Wu, W. (1992). *Hypoplastizität als Mathematisches Modell zum mechanischen Verhalten granularer Stoffe*, PhD Thesis, Karlsruhe University, Germany.

Wu, W. and Kolymbas, D. (2000). Hypoplasticity then and now, In: *Constitutive Modelling of Granular Materials*, (Editor: D. Kolymbas), Springer, 57-106.

Ziegler, H. (1977). *An Introduction to Thermodynamics*, North Holland, Amsterdam.

Ziegler, H. and Wehrli, C. (1987). The derivation of constitutive relations from the free energy and the dissipation function, *Adv. Appl. Mech.*, Vol 25, 183-238.

## CHAPTER 10

# RIGOROUS ANALYSIS OF ELASTIC-PLASTIC PROBLEMS

### 10.1 INTRODUCTION

This chapter presents rigorous analytical solutions for a number of simple elastic-plastic boundary value problems that may be relevant in geotechnical engineering. These selected problems include the expansion of cylindrical and spherical cavities in elastic-plastic soils, the two-dimensional loading of a plane strain elastic-plastic wedge, and the two-dimensional penetration of a cone into rigid plastic soils.

The main purpose of this chapter is to use a few examples to illustrate various procedures for deriving rigorous solutions of stress and strain for elastic-plastic problems. Further analytical solutions of interest may be found in Hill (1950), Gibson and Anderson (1961), Salencon (1969), Carter *et al.* (1986), Sagaseta (1987), Norbury and Wheeler (1987), Bigoni and Laudiero (1989), Yu (1992, 1993, 2000), Durban and Fleck (1991), Yu and Housby (1995), Collins and Yu (1996), Yu and Rowe (1999) and Hill (2000) for a variety of plasticity models.

### 10.2 EXPANSION OF CAVITIES IN AN INFINITE MEDIUM

This section is concerned with the expansion of cavities in an infinite soil mass. The solution presented here was derived by Yu (1990) and also presented by Yu and Housby (1991). A tension positive notation is adopted in this chapter.

The soil properties are defined by Young's modulus  $E$  and Poisson's ratio  $\nu$ , cohesion  $C$ , angles of friction and dilation  $\phi$  and  $\psi$ . The initial stress (assumed to be isotropic) is  $p_0$ . To simplify the presentation, it is possible to combine both the cylindrical and spherical analyses. The parameter  $k$  can be used to indicate cylindrical analysis ( $k=1$ ) or spherical analysis ( $k=2$ ). To abbreviate the mathematics we define the following quantities, all of which are constants in any given analysis:

$$G = \frac{E}{2(1 + \nu)} \quad (10.1)$$

$$M = \frac{E}{1 - \nu^2(2 - k)} \quad (10.2)$$

$$Y = \frac{2C \cos \phi}{1 - \sin \phi} \quad (10.3)$$

$$\alpha = \frac{1 + \sin \phi}{1 - \sin \phi} \quad (10.4)$$

$$\beta = \frac{1 + \sin \psi}{1 - \sin \psi} \quad (10.5)$$

$$\gamma = \frac{\alpha(\beta + k)}{k(a-1)\beta} \quad (10.6)$$

$$\delta = \frac{Y + (a-1)p_0}{2(k + \alpha)G} \quad (10.7)$$

$$\mu = \frac{(1 + k)\delta[1 - \nu^2(2 - k)]}{(1 + \nu)(\alpha - 1)\beta} \times [a\beta + k(1 - 2\nu) + 2\nu - \frac{k\nu(\alpha + \beta)}{1 - \nu(2 - k)}] \quad (10.8)$$

$$\chi = \exp \left\{ \frac{(\beta + k)(1 - 2\nu)(1 + (2 - k)\nu)[Y + (a - 1)p_0]}{E(\alpha - 1)\beta} \right\} \quad (10.9)$$

At any time in any position in the soil around the cavity with cavity radius of  $a$ , the stresses must satisfy the following equation of equilibrium:

$$(\sigma_\theta - \sigma_r) = \frac{r}{k} \frac{\partial \sigma_r}{\partial r} \quad (10.10)$$

which is subject to two boundary conditions:

$$\sigma_r|_{r=a} = -p \quad (10.11)$$

$$\sigma_r|_{r=\infty} = -p_0 \quad (10.12)$$

With a tension positive notation, the Mohr-Coulomb yield condition is given by

$$\alpha\sigma_\theta - \sigma_r = Y \quad (10.13)$$

### (a) Elastic solution

As the cavity pressure increases from its initial value, the deformation of the soil is at first purely elastic. Under conditions of radial symmetry, the elastic stress-strain relationship can be expressed as:

$$\dot{\epsilon}_r = \frac{\partial \dot{u}}{\partial r} = \frac{1}{M} [\dot{\sigma}_r - \frac{kv}{1 - \nu(2 - k)} \dot{\sigma}_\theta] \quad (10.14)$$

$$\dot{\epsilon}_\theta = \frac{\dot{u}}{r} = \frac{1}{M} [-\frac{\nu}{1 - \nu(2 - k)} \dot{\sigma}_r + [1 - \nu(k - 1)] \dot{\sigma}_\theta] \quad (10.15)$$

The solution of equations (10.10), (10.14) and (10.15), subject to the stress boundary conditions (10.11) and (10.12), is shown to be:

$$\sigma_r = -p_0 - (p - p_0) \left(\frac{a}{r}\right)^{1+k} \quad (10.16)$$

$$\sigma_\theta = -p_0 + \frac{p - p_0}{k} \left(\frac{a}{r}\right)^{1+k} \quad (10.17)$$

$$u = \frac{p - p_0}{2kG} \left(\frac{a}{r}\right)^{1+k} r \quad (10.18)$$

The initial yielding occurs at the inner cavity wall when the stresses satisfy the yield condition (10.13) and that happens when the cavity pressure reaches the following value:

$$p = p_{1y} = \frac{k[Y + (\alpha - 1)p_0]}{k + \alpha} + p_0 = 2kG\delta + p_0 \quad (10.19)$$

### (b) Elastic-plastic stress analysis

After initial yielding takes place at the cavity wall, a plastic zone will form around the inner cavity wall with an increase in the applied cavity pressure  $p$ . The outer radius of the plastic zone is denoted by  $c$ .

#### *Stresses in the plastic region*

The stress components in the plastic zone must satisfy the equilibrium equation and the yield condition, and are shown to be in the form:

$$\sigma_r = \frac{Y}{\alpha - 1} + Ar^{-\frac{k(\alpha - 1)}{\alpha}} \quad (10.20)$$

$$\sigma_\theta = \frac{Y}{\alpha - 1} + \frac{A}{\alpha} r^{-\frac{k(\alpha - 1)}{\alpha}} \quad (10.21)$$

where  $A$  is a constant of integration.

*Stresses in the elastic region*

The stress components in the elastic region can be obtained from the equilibrium equation and elastic stress-strain equations as follows:

$$\sigma_r = -p_0 - Br^{-(1+k)} \quad (10.22)$$

$$\sigma_\theta = -p_0 + \frac{B}{k}r^{-(1+k)} \quad (10.23)$$

where B is the second integration constant.

The continuity of stress components at the elastic-plastic interface can be used to determine the constants A and B:

$$A = -\frac{(1+k)\alpha[Y + (\alpha-1)p_0]}{(\alpha-1)(k+\alpha)} c^{\frac{k(\alpha-1)}{\alpha}} \quad (10.24)$$

$$B = \frac{k[Y + (\alpha-1)p_0]}{k + \alpha} c^{1+k} \quad (10.25)$$

At the cavity wall  $\sigma_r|_{r=a} = -p$  and this condition can be used, in conjunction with (10.20) and (10.24), to express the plastic radius  $c$  in terms of the current cavity radius and applied pressure

$$\frac{c}{a} = \left\{ \frac{(k+\alpha)[Y + (\alpha-1)p]}{\alpha(1+k)[Y + (\alpha-1)p_0]} \right\}^{\frac{a}{k(\alpha-1)}} \quad (10.26)$$

The stresses are now established in terms of a single unknown  $c$ . In the next subsection the displacements are examined, allowing for the determination of  $c$  and therefore the complete pressure-expansion relationship.

**(c) Elastic-plastic displacement analysis**

Substituting equations (10.22) and (10.23) into (10.15) gives the displacement in the elastic zone:

$$u = \delta \left( \frac{c}{r} \right)^{1+k} r \quad (10.27)$$

where  $\delta$  is defined at the beginning of this section. The determination of the displacement field in the plastic zone requires the use of a plastic flow rule which indicates the relative magnitude of plastic strains in different directions.

For the expansion of cylindrical and spherical cavities, the non-associated Mohr-Coulomb flow rule can be expressed as:

$$\frac{\dot{\varepsilon}_r^p}{\dot{\varepsilon}_\theta^p} = \frac{\dot{\varepsilon}_r - \dot{\varepsilon}_r^e}{\dot{\varepsilon}_\theta - \dot{\varepsilon}_\theta^e} = -\frac{k}{\beta} \quad (10.28)$$

where  $\beta$  is a simple function of dilation angle given before. If  $\beta = \alpha$  then the flow rule for the soil is said to be fully associated.

Substituting elastic stress equations (10.14) and (10.15) into the plastic flow rule (10.28) results in:

$$\begin{aligned} \beta \dot{\varepsilon}_r + k \dot{\varepsilon}_\theta &= \frac{1}{M} [\beta - \frac{k\nu}{1 - \nu(2 - k)}] \dot{\sigma}_r \\ &+ \frac{1}{M} [k(1 - 2\nu) + 2\nu - \frac{k\beta\nu}{1 - \nu(2 - k)}] \dot{\sigma}_\theta \end{aligned} \quad (10.29)$$

where  $M$  is defined at the beginning of this subsection. The distributions of stress and strain in the soil at the initiation of plastic yield are obtained from equations (10.14)-(10.18) by putting  $p = p_{1y}$  defined in equation (10.19). The integral of equation (10.29) subject to this initial condition is found to be:

$$\begin{aligned} \beta \varepsilon_r + k \varepsilon_\theta &= \frac{1}{M} [\beta - \frac{k\nu}{1 - \nu(2 - k)}] \sigma_r \\ &+ \frac{1}{M} [k(1 - 2\nu) + 2\nu - \frac{k\beta\nu}{1 - \nu(2 - k)}] \sigma_\theta \\ &+ \frac{1}{M} [\beta + k(1 - 2\nu) + 2\nu - \frac{k\nu(1 + \beta)}{1 - \nu(2 - k)}] p_0 \end{aligned} \quad (10.30)$$

To account for effects of large strain in the plastic zone the logarithmic strains are adopted, namely

$$\varepsilon_r = \ln\left(\frac{dr}{dr_0}\right)$$

$$\varepsilon_\theta = \ln\frac{r}{r_0}$$

Substituting the above large strain definitions and plastic stresses (10.20) and (10.21) into equation (10.30) leads to:

$$\ln\left[\left(\frac{r}{r_0}\right)^\frac{k}{\beta} \frac{dr}{dr_0}\right] = \ln\chi - \mu\left(\frac{r}{r_0}\right)^{\frac{k(a-1)}{a}} \quad (10.31)$$

where  $\chi$  and  $\mu$  are defined at the start of this section.

By means of transformation:

$$\varrho = \left(\frac{c}{r}\right)^{\frac{k(\alpha-1)}{\alpha}} \quad (10.32)$$

$$\xi = \left(\frac{r_0}{c}\right)^{\frac{\beta+k}{\beta}} \quad (10.33)$$

and use of equation (10.27), equation (10.31) can be integrated over the interval  $[c, r]$ , leading to:

$$\frac{\chi}{\gamma} \left\{ (1-\delta)^{\frac{\beta+k}{\beta}} - \left(\frac{r_0}{c}\right)^{\frac{\beta+k}{\beta}} \right\} = \int_1^R \exp(\mu\varrho) \varrho^{-\gamma-1} d\varrho \quad (10.34)$$

By putting  $r = r_0$  and  $r_0 = a_0$  and making use of equation (10.26), we find:

$$\frac{\chi}{\gamma} \left\{ (1-\delta)^{\frac{\beta+k}{\beta}} - R^{-\gamma} \left(\frac{a_0}{a}\right)^{\frac{\beta+k}{\beta}} \right\} = \int_1^R \exp(\mu\varrho) \varrho^{-\gamma-1} d\varrho \quad (10.35)$$

in which  $R$  is a function of the current cavity pressure given by:

$$R = \frac{(k+\alpha)[Y + (\alpha-1)p]}{\alpha(1+k)[Y + (\alpha-1)p_0]} \quad (10.36)$$

For the special case of a spherical cavity in Mohr-Coulomb materials with an associated flow rule (i.e.  $k = 2$  and  $\beta = \alpha$ ), equation (10.35) reduces to the solution derived by Chadwick (1959).

With the aid of the series expansion:

$$\exp(\mu\varrho) = \sum_{n=0}^{\infty} \frac{(\mu\varrho)^n}{n!} \quad (10.37)$$

the following explicit expression for the pressure-expansion relationship is obtained:

$$\left(\frac{a}{a_0}\right)^{\frac{\beta+k}{\beta}} = \frac{R^{-\gamma}}{(1-\delta)^{\frac{\beta+k}{\beta}} - \frac{\gamma}{\chi} \sum_{n=0}^{\infty} A_n(R, \mu)} \quad (10.38)$$

in which  $A_n$  is defined by:

$$A_n(R, \mu) = \begin{cases} \frac{\mu^n}{n!} \ln R & \text{if } n = \gamma \\ \frac{\mu^n}{n!(n-\gamma)} (R^{n-\gamma} - 1) & \text{otherwise} \end{cases} \quad (10.39)$$

#### (d) Special cases

##### *Limit pressure*

When a cavity is expanded in a plastically deforming material the cavity pressure does not increase indefinitely, but a limit pressure is approached. By putting  $a/a_0 \rightarrow \infty$  in equation (10.38), the limit cavity pressure  $p_{\lim}$  can be obtained by finding  $R_{\lim}$  from the following equation:

$$\sum_{n=0}^{\infty} A_n(R_{\lim}, \mu) = \frac{\chi}{\gamma} (1-\delta)^{\frac{\beta+k}{\beta}} \quad (10.40)$$

where  $A_n$  is related to  $R_{\lim}$  by equation (10.39). Once  $R_{\lim}$  is obtained, the limit cavity pressure  $p_{\lim}$  can be readily derived from the following equation:

$$R_{\lim} = \frac{(k + \alpha)[Y + (\alpha-1)p_{\lim}]}{\alpha(1 + k)[Y + (\alpha-1)p_0]} \quad (10.41)$$

It is found that the cavity limit pressure depends strongly on the angles of friction and dilation, as well as the stiffness properties of the soil.

##### *Frictionless case*

The solution presented here can be applied to soils with friction and dilation. It does not reduce to the solution for a frictionless soil (i.e. Tresca soil) when friction angle  $\phi = 0$ . This is because in this case  $\alpha = 1$  and the terms in  $\alpha - 1$  which frequently appear in the denominator make the expressions indeterminate. However, it can be confirmed that at very small  $\phi$  values the solution presented in this section approaches the solution for Tresca materials.

##### *Small strain case*

Large strain theory is complex and wherever possible, small strain theory is used to model cavity expansion. In small strain theory the fact that displacements modify the position of material points is ignored, so the theory is only valid for small expansions. In particular, prediction of limit pressure is not possible with small strain assumptions. It can be shown that if the small strain assumption is made it is possible to obtain the following closed form expression for displacement in the plastic zone:

$$\begin{aligned}
 u = & [\delta + \frac{\alpha\beta\mu}{k(\alpha + \beta) + \alpha\beta(1-k)} - \frac{\beta \ln \chi}{\beta + k}] (\frac{c}{r})^{\frac{k}{\beta}} c \\
 & + \frac{\beta \ln \chi}{\beta + k} r - \frac{\alpha\beta\mu}{k(\alpha + \beta) + \alpha\beta(1-k)} (\frac{c}{r})^{\frac{k(a-1)}{\alpha}} r
 \end{aligned} \quad (10.42)$$

Equation (10.42) is only applicable to the situation in which the maximum value of the cavity pressure is sufficiently small for the squares and higher powers of strains included in the large strain definitions to be negligible. This small strain solution is also given by Carter *et al.* (1986). For the special case of spherical and cylindrical cavities with an associated flow rule, the solution (10.42) reduces to the small strain equations obtained by Chadwick (1959) and Florence and Schwer (1978) respectively.

#### *Neglecting elastic strain in the plastic zone*

A common assumption which considerably simplifies the analysis of plastic cavity expansion is to ignore the contribution of elastic strain within the plastic zone (e.g. Hughes *et al.*, 1977). While this may at first seem to be a reasonable assumption, as the elastic strains are much smaller than the plastic strains, it does have a significant effect on the predicted results.

Neglecting the elastic deformation in the plastically deforming region results in a relatively simple expression for the relationship between the cavity pressure and cavity displacement:

$$\frac{(k + \alpha)[Y + (a-1)p]}{\alpha(1 + k)[Y + (a-1)p_0]} = \left\{ \frac{1 - (\frac{a_0}{a})^{1 + \frac{k}{\beta}}}{1 - (1 - \delta)^{1 + \frac{k}{\beta}}} \right\}^{\frac{1}{\gamma}} \quad (10.43)$$

A comparison between the approximate large strain solution (10.43) and the exact large strain solution (10.38) indicates that the effects of elastic strain in the plastic zone are more important for soils with high friction and dilation angles and low elastic stiffness. By putting  $a/a_0 \rightarrow \infty$  and  $\psi = 0$  and assuming  $\delta = 0$ , equation (10.43) reduces to the limit solution derived by Vesic (1972).

### 10.3 CAVITY EXPANSION SOLUTION FOR TRESCA MATERIALS

Before a closed form similarity solution is presented for cavity expansion in Mohr-Coulomb materials, it is instructive to review the cavity expansion solution for Tresca materials obtained using Hill's incremental velocity method.

### 10.3.1 Expansion of a spherical cavity in a finite medium

The large strain solution of stresses and displacements for the expansion of a spherical cavity in a Tresca material has been presented by Hill (1950). The following presentation includes non-zero external pressures (i.e. non-zero initial stresses before expansion) and therefore is a generalization of Hill's solution which was presented for zero initial stress conditions.

#### Stress analysis

Assume the current internal and external radii of a shell are denoted by  $a$  and  $b$  (see Figure 1). Initially the radii of the internal and external boundaries are  $a_0$  and  $b_0$ , and a hydrostatic pressure  $p_0$  acts throughout the soil. An internal pressure is increased monotonically from its initial value  $p_0$  on the internal surface. An essential task of the analysis is to determine the variation of internal and external radii with the internal pressure  $p$ . As the internal pressure increases from  $p_0$  the material will behave elastically, and the elastic solutions for both stresses and displacements can be shown to be:

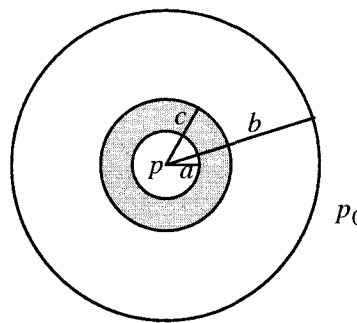


Figure 10.1: Expansion of a cavity in an elastic-plastic material

$$\sigma_r = -p_0 - (p - p_0) \frac{\left(\frac{b_0}{r}\right)^3 - 1}{\left(\frac{b_0}{a_0}\right)^3 - 1} \quad (10.44)$$

$$\sigma_\theta = \sigma_\phi = -p_0 + (p - p_0) \frac{\frac{1}{2} \left(\frac{b_0}{r}\right)^3 + 1}{\left(\frac{b_0}{a_0}\right)^3 - 1} \quad (10.45)$$

The radial displacement is

$$u = r - r_0 = \frac{(p - p_0)}{E} \frac{(1-2\nu)r + \frac{(1+\nu)b_0^3}{2r^2}}{\left(\frac{b_0}{a_0}\right)^3 - 1} \quad (10.46)$$

The Tresca yield criterion is expressed by maximum and minimum principal stresses as follows:

$$\sigma_1 - \sigma_3 = Y \quad (10.47)$$

where  $Y = 2S_u$  and  $S_u$  is known as the undrained shear strength.

It is easily seen that the yield condition (10.47) is first satisfied at the internal boundary. Substituting the elastic stress equations (10.44) and (10.45) into equation (10.47) and knowing that  $\sigma_1 = \sigma_\theta$  and  $\sigma_3 = \sigma_r$ , the internal pressure required to cause yielding at the internal boundary is:

$$p = p_{1y} = p_0 + \frac{2Y}{3} \left[ 1 - \left( \frac{a_0}{b_0} \right)^3 \right] \quad (10.48)$$

The displacements at both internal and external boundaries when plastic yielding commences at the internal boundary are:

$$u|_{r=a_0} = \frac{Ya_0}{E} \left[ \frac{2(1-2\nu)a_0^3}{3b_0^3} + \frac{1+\nu}{3} \right] \quad (10.49)$$

$$u|_{r=b_0} = \frac{Y(1-\nu)a_0}{Eb_0^2} \quad (10.50)$$

If the internal pressure is further increased, a plastic region will spread into the shell; the radius of the plastic region at any moment is denoted by  $c$ . In the outer elastic region, the stresses are still of the form:

$$\sigma_r = -A \left[ \left( \frac{b_0}{r} \right)^3 - 1 \right] - p_0 \quad (10.51)$$

$$\sigma_\theta = \sigma_\phi = A \left[ \frac{1}{2} \left( \frac{b_0}{r} \right)^3 + 1 \right] - p_0 \quad (10.52)$$

where  $A$  is a constant that can be determined by the condition that the material just on the elastic side of the plastic boundary must be on the point of yielding. Substitution of equations (10.51) and (10.52) in equation (10.47),  $A$  is found to be:

$$A = \frac{2Yc^3}{3b_0^3} \quad (10.53)$$

The elastic stress distribution is therefore obtained by substituting (10.53) into (10.51) and (10.52):

$$\sigma_r = -\frac{2Yc^3}{3b_0^3} \left[ \left( \frac{b_0}{r} \right)^3 - 1 \right] - p_0 \quad (10.54)$$

$$\sigma_\theta = \sigma_\phi = \frac{2Yc^3}{3b_0^3} \left[ \frac{1}{2} \left( \frac{b_0}{r} \right)^3 + 1 \right] - p_0 \quad (10.55)$$

The displacement in the elastic region is given by:

$$u = \frac{2Yc^3}{3Eb_0^3} \left[ (1-2\nu)r + \frac{(1+\nu)b_0^3}{2r^2} \right] \quad (10.56)$$

From equations (10.54) to (10.56), it is seen that the solution in the elastic region is dependent only on the radius of the elastic-plastic boundary  $c$ . In the plastic region, we have the equilibrium equation:

$$\frac{\partial \sigma_r}{\partial r} = \frac{2(\sigma_\theta - \sigma_r)}{r} \quad (10.57)$$

Substituting the yield condition (10.47) into the equilibrium equation (10.57) results in:

$$\sigma_r = 2Y \ln r + B \quad (10.58)$$

where  $B$  is another constant that can be determined using the condition that the radial stress must be continuous across the elastic-plastic boundary. Equating (10.54) and (10.58) at  $r = c$  leads to:

$$B = -2Y \ln c - \frac{2Y}{3} \left[ 1 - \left( \frac{c}{b_0} \right)^3 \right] - p_0 \quad (10.59)$$

By substituting (10.59) into (10.58) and (10.47), the following solution for stresses in the plastic region can be obtained:

$$\sigma_r = -2Y \ln \left( \frac{c}{r} \right) - \frac{2Y}{3} \left[ 1 - \left( \frac{c}{b_0} \right)^3 \right] - p_0 \quad (10.60)$$

$$\sigma_\theta = Y - 2Y \ln \left( \frac{c}{r} \right) - \frac{2Y}{3} \left[ 1 - \left( \frac{c}{b_0} \right)^3 \right] - p_0 \quad (10.61)$$

By substituting  $r = a$  in equation (10.60), the internal pressure needed to produce plastic flow to a radius  $c$  is found to be

$$p = 2Y \ln \left( \frac{c}{a} \right) + \frac{2Y}{3} \left[ 1 - \left( \frac{c}{b_0} \right)^3 \right] + p_0 \quad (10.62)$$

#### *Displacement analysis*

In calculating the displacement of any individual particle it is convenient to take the movement of the plastic boundary as the scale of 'time' or progress of the expan-

sion, since the parameter  $c$  appears in the formulae for the stresses. We can speak of the velocity  $V$  of a particle, meaning that the particle is displaced by an amount  $Vdc$  when the plastic boundary moves outwards a further distance  $dc$ .  $V$  can be expressed directly in terms of the total displacement  $u$ , which is a function of both the current radius  $r$  and plastic radius  $c$  so that:

$$du = \frac{\partial u}{\partial c} dc + \frac{\partial u}{\partial r} dr = \left( \frac{\partial u}{\partial c} + V \frac{\partial u}{\partial r} \right) dc \quad (10.63)$$

where  $r$  and  $c$  are taken as the independent variables. Equating the above equation to  $Vdc$  we obtain the expression for the particle velocity:

$$V = \frac{\frac{\partial u}{\partial c}}{1 - \frac{\partial u}{\partial r}} \quad (10.64)$$

Now the compressibility equation in the plastic region is:

$$d\varepsilon_r + d\varepsilon_\theta + d\varepsilon_\phi = \frac{1-2\nu}{E} (d\sigma_r + d\sigma_\theta + d\sigma_\phi) \quad (10.65)$$

To evaluate the increments of stress and strain, we must follow a given element. Thus:

$$d\varepsilon_r = \frac{\partial(du)}{\partial r} = \frac{\partial V}{\partial r} dc \quad (10.66)$$

$$d\varepsilon_\theta = d\varepsilon_\phi = \frac{du}{r} = \frac{Vdc}{r} \quad (10.67)$$

$$d\sigma_r = \left( \frac{\partial \sigma_r}{\partial c} + V \frac{\partial \sigma_r}{\partial r} \right) dc \quad (10.68)$$

$$d\sigma_\theta = d\sigma_\phi = \left( \frac{\partial \sigma_\theta}{\partial c} + V \frac{\partial \sigma_\theta}{\partial r} \right) dc \quad (10.69)$$

Hence the compressibility condition can be written as follows:

$$\frac{\partial V}{\partial r} + \frac{2V}{r} = \frac{1-2\nu}{E} \left( \frac{\partial}{\partial c} + V \frac{\partial}{\partial r} \right) (\sigma_r + 2\sigma_\theta) \quad (10.70)$$

Substituting the expressions for stresses in the plastic region (10.60) and (10.61) into (10.70) leads to

$$\frac{\partial V}{\partial r} + \frac{2V}{r} = 6(1-2\nu) \frac{Y}{E} \left[ \frac{V}{r} - \frac{1}{c} \left( 1 - \frac{c^3}{b_0^3} \right) \right] \quad (10.71)$$

It is noted that the velocity is known on the plastic boundary from the solution for the displacement in the elastic region. Thus from (10.56) and (10.64) we obtain

$$V_{r=c} = \frac{Y}{E} \left[ 2(1-2\nu) \frac{c^3}{b_0^3} + (1 + \nu) \right] \quad (10.72)$$

With the above boundary condition, equation (10.71) can be integrated to give the following solution for the velocity  $V$ :

$$V = \frac{3(1-\nu)Yc^2}{Er^2} - \frac{2(2-2\nu)Y}{E} \left(1 - \frac{c^3}{b_0^3}\right) \frac{r}{c} \quad (10.73)$$

It should be noted that the above solution was obtained after second and higher powers of  $Y/E$  (which is typically very small for realistic values of  $Y$  and  $E$ ) were ignored. For the cavity wall  $r=a$ , we have  $V=da/dc$ , so that

$$\frac{da}{dc} = \frac{3(1-\nu)Yc^2}{Ea^2} - \frac{2(2-2\nu)Y}{E} \left(1 - \frac{c^3}{b_0^3}\right) \frac{a}{c} \quad (10.74)$$

After integration, we can express the cavity expansion in terms of the radius of the plastic boundary:

$$\begin{aligned} \left(\frac{a}{a_0}\right)^3 = 1 + \frac{3(1-\nu)Yc^3}{Ea_0^3} - \frac{2(1-2\nu)Y}{E} \\ \times \left[3 \ln\left(\frac{c}{a_0}\right) + 1 - \left(\frac{c}{b_0}\right)^3\right] \end{aligned} \quad (10.75)$$

### 10.3.2 Similarity solutions for cavity expansion in an infinite medium

For the special case when a spherical cavity is expanded from zero radius in an infinite medium, the stresses are functions of  $r/a$  only, and the ratio of plastic radius to the current cavity radius remains constant (Hill, 1950). As a result, equation (10.74) can be directly used to give the plastic radius:

$$\frac{c}{a} = \left[\frac{E}{3(1-\nu)Y}\right]^{1/3} \quad (10.76)$$

Substituting the above solution into equation (10.62) leads to the following solution for the constant internal cavity pressure:

$$p_{\text{lim}} = \frac{2Y}{3} \left[1 + \ln\left(\frac{E}{3(1-\nu)Y}\right)\right] + p_0 \quad (10.77)$$

## 10.4 SIMILARITY SOLUTIONS FOR MOHR-COULOMB MATERIALS

This section deals with the special case of cavity expansion from zero initial radius in an infinite soil mass. As noted by Hill (1950), this problem has no characteristic length and hence will possess a similarity solution, in which the cavity pressure is constant and the continuing deformation is geometrically self-similar. As a result, the incremental velocity approach used by Hill (1950) to analyse cavity expansion

in Tresca materials may also be used to obtain a solution for limiting pressures of the cavity expansion in Mohr-Coulomb materials. One of the first attempts in obtaining an analytical solution for cavity limit pressure in Mohr-Coulomb materials was made by Carter *et al.* (1986). However, the solution of Carter *et al.* (1986) is approximate only, as the convected part of the stress rate was ignored in their derivation. Later, by including the convected part of the stress rate, Collins and Wang (1990) derived rigorous solutions for purely frictional soils. The solution of Collins and Wang (1990) was however obtained by using numerical integration as their solution was not expressed in closed-form.

By following Hill's solution procedure described in the previous section, a complete analytical solution for the expansion of cavities from zero initial radius in an infinite cohesive-frictional soil mass is derived by Yu (2000) and Yu and Carter (2002). The solution procedure adopted by Yu and Carter (2002) is different from that used by Collins and Wang (1990) as the plastic radius  $c$  is used here as the time scale, and it is shown that by using a series expansion the solution can be expressed in closed form.

#### 10.4.1 Soil properties

The soil properties are defined by Young's modulus  $E$  and Poisson's ratio  $\nu$ , and the cohesion  $C$ , and angles of friction and dilation  $\phi$  and  $\psi$ . The initial stress (assumed to be isotropic) is  $p_0$ . To simplify the presentation, the parameter  $k$  is used to distinguish between cylindrical analysis ( $k=1$ ) and spherical analysis ( $k=2$ ). The analysis presented here is for cohesive-frictional soils under fully drained conditions. All stress quantities are effective stresses.

To abbreviate the mathematics, it is convenient to define the following quantities, all of which are constants in any given analysis.

$$G = \frac{E}{2(1 + \nu)}$$

$$M = \frac{E}{1 - \nu^2(2 - k)}$$

$$Y = \frac{2C \cos \phi}{1 - \sin \phi}$$

$$\alpha = \frac{1 + \sin \phi}{1 - \sin \phi}$$

$$\beta = \frac{1 + \sin \psi}{1 - \sin \psi}$$

$$\delta = \frac{Y + (\alpha-1)p_0}{2(k + \alpha)G}$$

At any time in any position in the soil around the cavity with radius of  $a$ , the stresses must satisfy the following equation of equilibrium:

$$(\sigma_\theta - \sigma_r) = \frac{r}{k} \frac{\partial \sigma_r}{\partial r} \quad (10.78)$$

subject to the following two boundary conditions:

$$\sigma_r|_{r=a} = -p \quad (10.79)$$

$$\sigma_r|_{r=\infty} = -p_0 \quad (10.80)$$

The Mohr-Coulomb yield condition during cavity expansion is as follows:

$$\alpha\sigma_\theta - \sigma_r = Y \quad (10.81)$$

#### 10.4.2 Elastic solution in the outer elastic zone

The stress-strain relations for soils in the outer elastic zone can be expressed as:

$$d\epsilon_r = \frac{\partial(du)}{\partial r} = \frac{1}{M} [d\sigma_r - \frac{kv}{1 - \nu(2 - k)} d\sigma_\theta] \quad (10.82)$$

$$d\epsilon_\theta = \frac{du}{r} = \frac{1}{M} [-\frac{\nu}{1 - \nu(2 - k)} d\sigma_r + [1 - \nu(k - 1)] d\sigma_\theta] \quad (10.83)$$

The solution for the stresses and radial displacement can be shown to be:

$$\sigma_r = -p_0 - (p_{1y} - p_0) \left(\frac{c}{r}\right)^{1+k} \quad (10.84)$$

$$\sigma_\theta = -p_0 + \frac{p_{1y} - p_0}{k} \left(\frac{c}{r}\right)^{1+k} \quad (10.85)$$

$$u = \frac{p_{1y} - p_0}{2kG} r \left(\frac{c}{r}\right)^{1+k} \quad (10.86)$$

where

$$p_{1y} = \frac{k[Y + (\alpha-1)p_0]}{k + \alpha} + p_0 = 2kG\delta + p_0 \quad (10.87)$$

is the cavity pressure at first yield.

#### 10.4.3 Stress solution in the plastic zone

*Stresses in the plastic region*

The stress components which satisfy the equilibrium equation (10.78) and the yield condition (10.81) are found to be:

$$\sigma_r = \frac{Y}{a-1} + Ar^{-\frac{k(a-1)}{a}} \quad (10.88)$$

$$\sigma_\theta = \frac{Y}{a-1} + \frac{A}{a}r^{-\frac{k(a-1)}{a}} \quad (10.89)$$

where A is a constant of integration.

#### *Stresses in the elastic region*

The stress components in the elastic region can be obtained from the equilibrium equation and elastic stress-strain equations as follows:

$$\sigma_r = -p_0 - Br^{-(1+k)} \quad (10.90)$$

$$\sigma_\theta = -p_0 + \frac{B}{k}r^{-(1+k)} \quad (10.91)$$

where B is the second constant of integration.

The continuity of stress components at the elastic-plastic interface can be used to determine the constants A and B:

$$A = -\frac{(1+k)\alpha[Y + (a-1)p_0]}{(a-1)(k+\alpha)}c^{\frac{k(a-1)}{a}} \quad (10.92)$$

$$B = \frac{k[Y + (a-1)p_0]}{k+\alpha}c^{1+k} \quad (10.93)$$

At the cavity wall we have  $\sigma_r|_{r=a} = -p$  and this condition can be used to express the plastic radius  $c$  in terms of the current cavity radius and applied pressure

$$\frac{c}{a} = \left\{ \frac{(k+\alpha)[Y + (a-1)p]}{\alpha(1+k)[Y + (a-1)p_0]} \right\}^{\frac{a}{k(a-1)}} \quad (10.94)$$

The stresses are now established in terms of a single unknown  $c$ . In the next subsection the displacements are examined, allowing determination of  $c$  and therefore the cavity pressure.

#### **10.4.4 Elastic-plastic displacement analysis**

Substituting equations (10.87) into (10.86) gives the displacement in the elastic zone:

$$u = \delta r \left( \frac{c}{r} \right)^{1+k} \quad (10.95)$$

with  $\delta$  as defined earlier in this section. The determination of the displacement field in the plastic zone requires the use of a plastic flow rule which indicates the relative magnitude of plastic strains in different directions.

For the expansion of cavities, the non-associated Mohr-Coulomb flow rule can be expressed as:

$$\frac{\dot{\varepsilon}_r^p}{\dot{\varepsilon}_\theta^p} = \frac{\dot{\varepsilon}_r - \dot{\varepsilon}_r^e}{\dot{\varepsilon}_\theta - \dot{\varepsilon}_\theta^e} = -\frac{k}{\beta} \quad (10.96)$$

where  $\beta$  is a simple function of dilation angle, defined previously. If  $\beta = \alpha$  then the flow rule for the soil is associated.

Substituting the elastic strain rate equations (10.82) and (10.83) into (10.96) the plastic flow rule results in:

$$\begin{aligned} \beta d\varepsilon_r + k d\varepsilon_\theta &= \frac{1}{M} \left[ \beta - \frac{kv}{1 - \nu(2 - k)} \right] d\sigma_r \\ &+ \frac{1}{M} \left[ k(1 - 2\nu) + 2\nu - \frac{k\beta\nu}{1 - \nu(2 - k)} \right] d\sigma_\theta \end{aligned} \quad (10.97)$$

with  $M$  as defined at the beginning of this section. In the plastic zone, from the yield equation we have  $d\sigma_\theta = \frac{1}{\alpha} d\sigma_r$ , and as a result equation (10.97) reduces to:

$$d\varepsilon_r + \frac{k}{\beta} d\varepsilon_\theta = \frac{\chi}{\beta} d\sigma_r \quad (10.98)$$

where

$$\begin{aligned} \chi &= \frac{1}{M} \left[ \beta - \frac{kv}{1 - \nu(2 - k)} \right] \\ &+ \frac{1}{M\alpha} \left[ k(1 - 2\nu) + 2\nu - \frac{k\beta\nu}{1 - \nu(2 - k)} \right] \end{aligned} \quad (10.99)$$

In calculating the displacement of any individual particle it is convenient to take the movement of the plastic boundary as the scale of 'time' or progress of the expansion, since the parameter  $c$  appears in the formulae for the stresses. We can speak of the velocity  $V$  of a particle, meaning that the particle is displaced by an amount  $Vdc$  when the plastic boundary moves outwards a further distance  $dc$ .  $V$  can be expressed directly in terms of the total displacement  $u$ , which is a function of both the current radius  $r$  and plastic radius  $c$  so that:

$$du = \frac{\partial u}{\partial c} dc + \frac{\partial u}{\partial r} dr = \left( \frac{\partial u}{\partial c} + V \frac{\partial u}{\partial r} \right) dc \quad (10.100)$$

where  $r$  and  $c$  are taken as the independent variables. Equating  $du$  to  $Vdc$  we obtain the expression for the particle velocity:

$$V = \frac{\frac{\partial u}{\partial c}}{1 - \frac{\partial u}{\partial r}} \quad (10.101)$$

To evaluate the increments of stress and strain, we should follow a given material element and therefore:

$$d\varepsilon_r = \frac{\partial(du)}{\partial r} = \frac{\partial V}{\partial r} dc \quad (10.102)$$

$$d\varepsilon_\theta = \frac{du}{r} = \frac{Vdc}{r} \quad (10.103)$$

$$d\sigma_r = \left( \frac{\partial \sigma_r}{\partial c} + V \frac{\partial \sigma_r}{\partial r} \right) dc \quad (10.104)$$

Equation (10.98) can therefore be written in terms of velocity:

$$\frac{\partial V}{\partial r} + \frac{k}{\beta} \frac{V}{r} = \frac{\chi}{\beta} \left( \frac{\partial \sigma_r}{\partial c} + V \frac{\partial \sigma_r}{\partial r} \right) \quad (10.105)$$

Substituting the expressions for radial stress in the plastic zone (10.88) and (10.92) into equation (10.105) gives the following differential equation for the velocity:

$$\frac{\partial V}{\partial r} + P(r)V = Q(r) \quad (10.106)$$

in which

$$P(r) = \frac{k}{\beta r} - \frac{\chi q k(\alpha-1)}{\alpha \beta} \left( \frac{c}{r} \right)^{\frac{k(\alpha-1)}{\alpha}} \frac{1}{r} \quad (10.107)$$

$$Q(r) = \frac{s}{c} \left( \frac{c}{r} \right)^{\frac{k(\alpha-1)}{\alpha}} \quad (10.108)$$

and  $q$  and  $s$  are defined by:

$$q = \frac{(1+k)\alpha[Y + (\alpha-1)p_0]}{(\alpha-1)(k+\alpha)} \quad (10.109)$$

$$s = -\frac{\chi q k(\alpha-1)}{\alpha \beta} \quad (10.110)$$

It is noted that the velocity is known on the plastic boundary from the solution for the displacement in the elastic region. Thus from (10.95) we have:

$$V_{r=c} = \delta(1 + k) \quad (10.111)$$

With the above boundary condition, equation (10.106) can be integrated to give the following solution for the velocity  $V$ :

$$V = \exp\left[-\frac{\chi q}{\beta}\left(\frac{c}{r}\right)^{\frac{k(\alpha-1)}{\alpha}}\right] \left\{ \sum_{n=0}^{\infty} A_n \left(\frac{c}{r}\right)^{\frac{k(\alpha-1)(1+n)}{\alpha}} 1 + [\delta(1 + k) \exp\left(\frac{\chi q}{\beta}\right) - \sum_{n=0}^{\infty} A_n] \left(\frac{c}{r}\right)^{\frac{k}{\beta}} \right\} \quad (10.112)$$

in which  $A_n$  is defined by:

$$A_n = \frac{1}{n!} \left(\frac{\chi q}{\beta}\right)^n \frac{a\beta s}{ka - k\beta(\alpha-1)(1+n) + \alpha\beta} \quad (10.113)$$

and  $n$  is an integer ranging from 0 to infinity.

At the cavity wall  $r=a$ , we have  $V=da/dc$ , so that

$$\frac{da}{dc} = \exp\left[-\frac{\chi q}{\beta}\left(\frac{c}{a}\right)^{\frac{k(\alpha-1)}{\alpha}}\right] \left\{ \sum_{n=0}^{\infty} A_n \left(\frac{c}{a}\right)^{\frac{k(\alpha-1)(1+n)}{\alpha}} 1 + [\delta(1 + k) \exp\left(\frac{\chi q}{\beta}\right) - \sum_{n=0}^{\infty} A_n] \left(\frac{c}{a}\right)^{\frac{k}{\beta}} \right\} \quad (10.114)$$

For the problem of cavity expansion from zero initial radius, the deformation can be assumed to be geometrically similar in the plastic zone so that the ratio of the radius of the elastic-plastic boundary to that of the cavity wall is a constant. Hence:

$$\frac{da}{dc} = \frac{a}{c} \quad (10.115)$$

with the above relation, equation (10.114) reduces to a nonlinear equation in  $c/a$ :

$$\frac{a}{c} = \exp\left[-\frac{\chi q}{\beta}\left(\frac{c}{a}\right)^{\frac{k(\alpha-1)}{\alpha}}\right] \left\{ \sum_{n=0}^{\infty} A_n \left(\frac{c}{a}\right)^{\frac{k(\alpha-1)(1+n)}{\alpha}} 1 + [\delta(1 + k) \exp\left(\frac{\chi q}{\beta}\right) - \sum_{n=0}^{\infty} A_n] \left(\frac{c}{a}\right)^{\frac{k}{\beta}} \right\} \quad (10.116)$$

which can be easily solved for the value of  $c/a$ . Once  $c/a$  is determined, equation (10.94) can be used to calculate the limit pressure  $p$ .

### 10.4.5 Neglecting the convected part of stress rate

If the convected part of the stress rate,  $V \frac{\partial \sigma_r}{\partial r}$ , is ignored, the governing equation can be considerably simplified to:

$$\frac{\partial V}{\partial r} + \frac{k}{\beta} \frac{V}{r} = \frac{\chi}{\beta} \frac{\partial \sigma_r}{\partial c} \quad (10.117)$$

which can be further reduced to:

$$\frac{\partial V}{\partial r} + \frac{k}{\beta} \frac{V}{r} = Q(r) \quad (10.118)$$

in which  $Q(r)$  is given by equation (10.108). With the boundary condition (10.111), the above equation can be solved to give the following solution for velocity  $V$ :

$$V = \gamma \left( \frac{C}{r} \right)^{\frac{k(a-1)}{\alpha} - 1} + [\delta(1+k) - \gamma] \left( \frac{C}{r} \right)^{\frac{k}{\beta}} \quad (10.119)$$

where

$$\gamma = \frac{\alpha \beta s}{k \alpha - k \beta (a-1) + \alpha \beta} \quad (10.120)$$

Following the same argument as used before, equation (10.119) can be applied at the cavity wall  $r=a$  to obtain a nonlinear equation on  $c/a$ :

$$1 = \gamma \left( \frac{C}{a} \right)^{\frac{k(a-1)}{\alpha} - 1} + [\delta(1+k) - \gamma] \left( \frac{C}{a} \right)^{1 + \frac{k}{\beta}} \quad (10.121)$$

The above equation is the same as that obtained by Carter *et al.* (1986).

### 10.4.6 Results and discussion

Numerical results for both plastic radius and cavity limit pressure have been presented in Yu and Carter (2002). Here only selected results on limit pressures are given to compare the complete rigorous similarity solutions, defined by equation (10.116) with the approximate solution of Carter *et al.* (1986), as defined by equation (10.121). The results from Chadwick's total strain method are also compared with those from Hill's incremental velocity approach.

Soil properties are defined by five parameters: Young's modulus  $E$ , Poisson's ratio  $\nu$ , cohesion  $C$ , and angles of friction and dilation  $\phi$  and  $\psi$ . To cover a wide range of possible cases, the friction angle is varied from 20 to 50 degrees in Yu and Carter (2002), and the dilation angle is varied from zero to the value of the friction angle. A constant value of 0.3 is used for Poisson's ratio.  $E/p_0$  varies between 26 and 2600 (i.e.  $2G/p_0$  is between 20 and 2000).

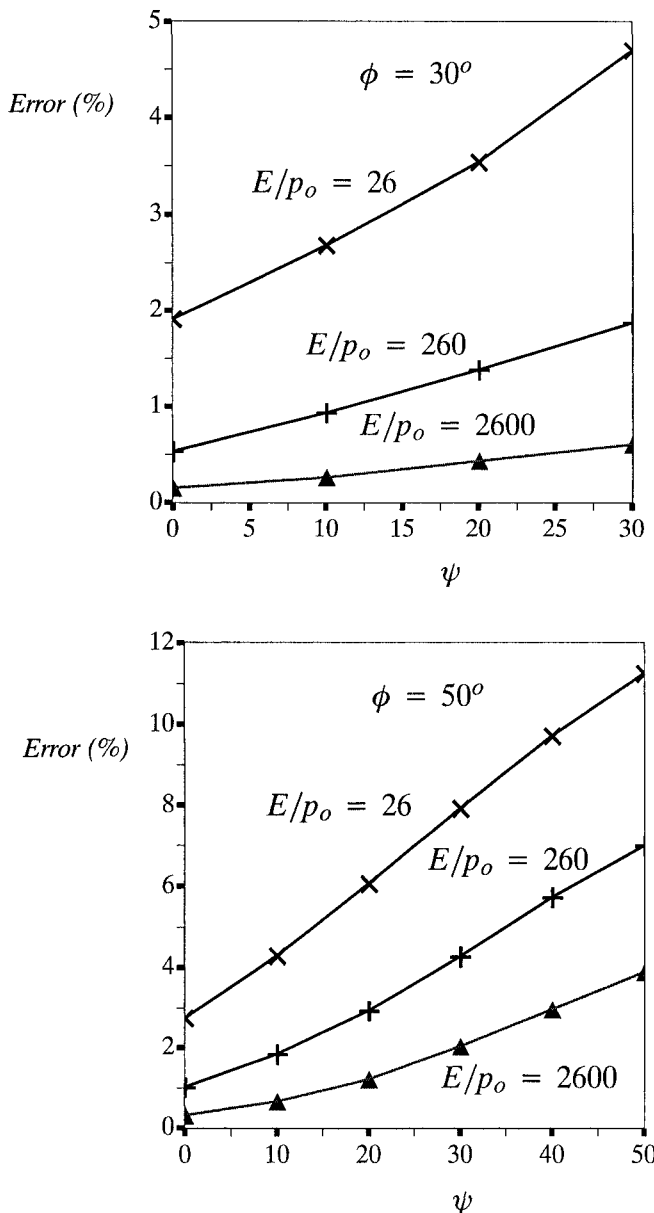


Figure 10.2: Errors of limit pressure caused by ignoring the convected part of stress rate for cylindrical cavity expansion in purely frictional soils

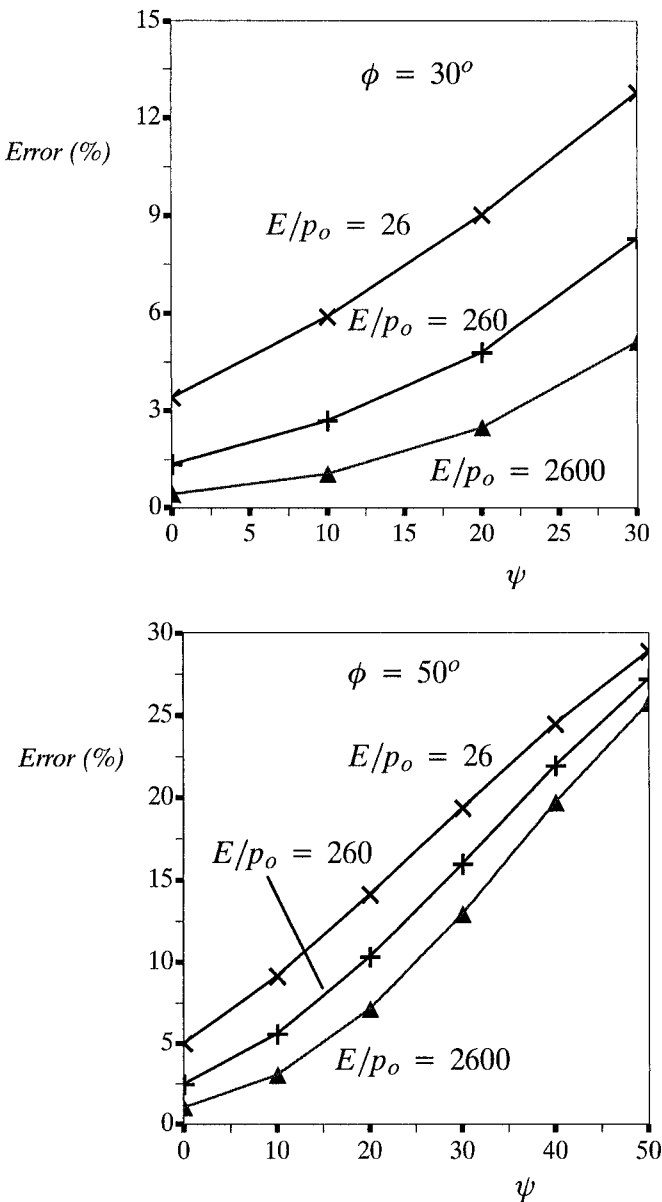


Figure 10.3: Errors of limit pressure caused by ignoring the convected part of stress rate for spherical cavity expansion in purely frictional soils

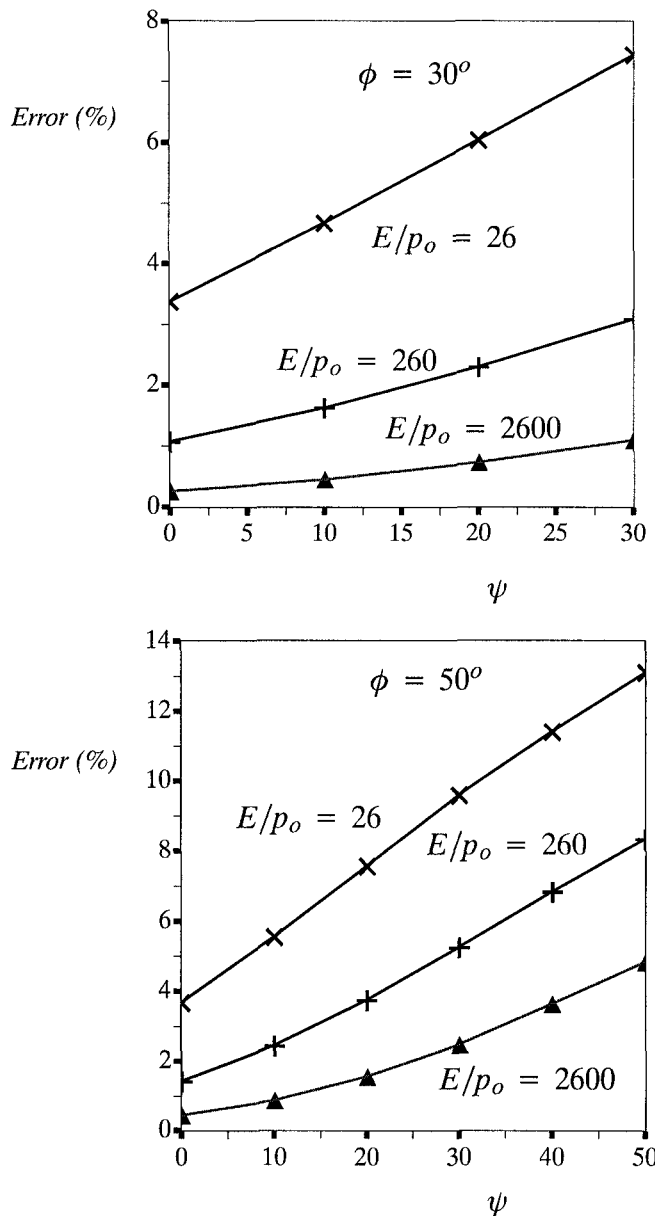


Figure 10.4: Errors of limit pressure due to ignoring the convected part of stress rate for cylindrical cavity expansion in cohesive-frictional soils ( $C/p_0 = 1$ )

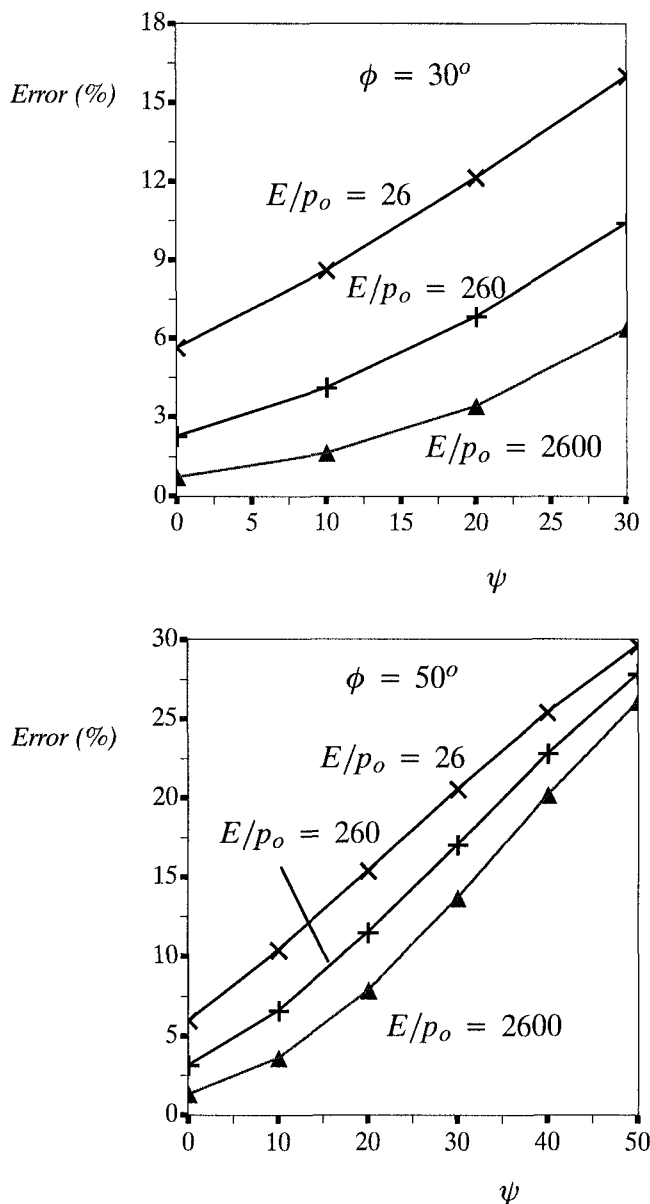


Figure 10.5: Errors of limit pressure due to ignoring the convected part of stress rate for spherical cavity expansion in cohesive-frictional soils ( $C/p_0 = 1$ )

First of all, we will focus on cavity expansion in purely frictional soils when soil cohesion  $C=0$ . For Tresca materials, Chadwick (1959) showed that the solution from his approach was identical to that obtained by Hill (1950) using an incremental velocity approach. However if the convected part of stress rate is neglected when following Hill's solution method (as is the case in Carter *et al.*, 1986), errors would be introduced into the final cavity limit pressure solutions. The errors introduced on cavity limit pressures using this assumption are presented in Figure 10.2 and Figure 10.3 for both cylindrical and spherical cavities. It is clear that the resulting errors depend on the angles of friction and dilation as well as soil stiffness properties. While the resulting error increases with increasing angles of friction and dilation, it tends to decrease with the soil stiffness. It is also noted that the error introduced by neglecting the convected part of the stress rate for a spherical cavity is significantly larger than that for a cylindrical cavity. For example, for all the soil properties considered, the maximum error is 11.25% for a cylindrical cavity and 28.89% for a spherical cavity.

In order to investigate the possible effect of soil cohesion on the similarity solutions, Figure 10.4 and Figure 10.5 present results for the case of cohesive-frictional soils with  $C/p_0=1$ . Inspection of the results suggests that the general conclusions made earlier for purely frictional soils are also valid for cohesive-frictional soils. It is noted that the resulting errors for a cohesive-frictional soil are generally larger than those for a purely frictional soil. The difference is more significant for soils with low values of friction angle. When the friction angle is very large, the effect of cohesion on the resulting errors becomes very small.

The following conclusions can be drawn from the results presented:

- (1) Cavity expansion from zero initial radius in an infinite Mohr-Coulomb material possesses a similarity solution, in which the cavity pressure remains a constant and the continuing deformation is geometrically self-similar. This constant cavity pressure is equal to the limiting pressure achieved at very large strains for the expansion of a finite cavity. By following Hill's incremental velocity approach, a rigorous closed form similarity solution for cavity expansion from zero radius in cohesive frictional soils has been derived in this section.
- (2) The errors introduced by neglecting the convected part of the stress rate are small for low values of frictional and dilation angles but will increase to as much as 30% when friction and dilation angles become large. This difference is also dependent on cavity type and stiffness properties of the soil. It is important however to note that neglecting the convected part of the stress rate tends to give lower values of cavity limit pressures, and therefore would be conservative if used to estimate bearing capacity of deep foundations in practice.

(3) Numerical results suggest that the cavity limit solutions obtained by Yu (1990) and Yu and Housby (1991) using Chadwick's total strain method are practically identical to the solutions obtained in this book by following Hill's incremental velocity approach. However, the main advantage of Chadwick's total strain method is that it can be used to derive analytical solutions for cavity expansion curves, as shown in Yu and Housby (1991).

## 10.5 ELASTIC-PLASTIC LOADING OF A PLANE STRAIN WEDGE

Analytical solutions for two-dimensional problems considering elastic-plastic deformation are very difficult to obtain. A rare example is the loading of a plane strain wedge modelled by an elastic-perfectly plastic model obeying von Mises' criterion, for which the exact solution of stresses and displacements was derived by Naghdi (1957). The small strain formulation was used in this solution.

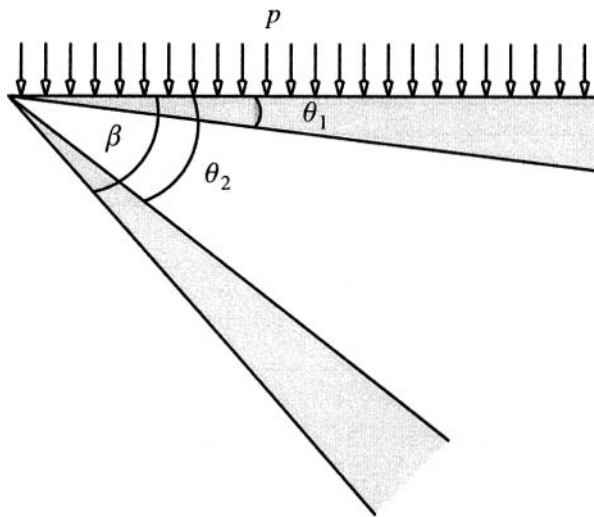


Figure 10.6: Elastic-plastic solution of a plane strain wedge

### 10.5.1 The wedge problem and governing equations

This section is concerned with the elastic, perfectly plastic solution of an incompressible isotropic wedge in the state of plane strain, subjected to a uniform normal pressure on one boundary only (shown in Figure 10.6). The present analysis is mainly for the case when the wedge angle  $\beta$  is less than 90 degrees. For this problem, Naghdi (1957) derived a complete solution for stresses and displacements for

a wedge region defined by  $0 \leq \beta \leq \frac{\pi}{2}$  (also see Maugin, 1992). Shown in Figure 10.6 is the wedge and boundary conditions.

It is more convenient to use cylindrical coordinates  $(r, \theta, z)$  for the wedge problem. The radial and tangential displacements  $u_r$  and  $u_\theta$  are independent of  $z$  which is normal to the the cross section of the wedge. In plane strain, we have  $u_z = 0$ . The strains are given by

$$\varepsilon_r = \frac{\partial u_r}{\partial r} \quad (10.122)$$

$$\varepsilon_\theta = \frac{u_r}{r} + \frac{1}{r} \frac{\partial u_\theta}{\partial \theta} \quad (10.123)$$

$$2\varepsilon_{r\theta} = \frac{1}{r} \frac{\partial u_r}{\partial \theta} + \frac{\partial u_\theta}{\partial r} - \frac{u_\theta}{r} \quad (10.124)$$

and the condition of incompressibility and the plane strain condition in the  $z$  direction give

$$\varepsilon_r = -\varepsilon_\theta \quad (10.125)$$

In the absence of body forces, the equations of equilibrium are

$$\frac{\partial s_r}{\partial r} + \frac{1}{r} \frac{\partial \sigma_{r\theta}}{\partial \theta} + \frac{s_r - s_\theta}{r} + \frac{\partial \sigma_m}{\partial r} = 0 \quad (10.126)$$

$$\frac{\partial \sigma_{r\theta}}{\partial r} + \frac{1}{r} \frac{\partial s_\theta}{\partial \theta} + 2 \frac{\sigma_{r\theta}}{r} + \frac{1}{r} \frac{\partial \sigma_m}{\partial \theta} = 0 \quad (10.127)$$

where the deviator stresses are linked to the mean stress  $\sigma_m$  as follows

$$s_r = \sigma_r - \sigma_m \quad (10.128)$$

$$s_\theta = \sigma_\theta - \sigma_m \quad (10.129)$$

$$s_z = \sigma_z - \sigma_m = -(s_r + s_\theta) \quad (10.130)$$

The von Mises criterion in plane strain takes the following form:

$$s_r^2 + s_r s_\theta + s_\theta^2 + \sigma_{r\theta}^2 = k_0^2 \quad (10.131)$$

where  $k_0$  is the yield stress in pure shear. The elastic-plastic stress-strain relationship based on von Mises' condition can be shown to be as follows (Prager and Hodge, 1951):

$$2G[\dot{\varepsilon}_r, \dot{\varepsilon}_\theta, \dot{\varepsilon}_z, \dot{\varepsilon}_{r\theta}] = [s_r, s_\theta, s_z, \dot{\sigma}_{r\theta}] + \lambda[s_r, s_\theta, s_z, \sigma_{r\theta}] \quad (10.132)$$

in which  $G$  is shear modulus and  $\lambda$  is a scalar factor.

### 10.5.2 The fully elastic solutions

The displacement field for an elastic, incompressible isotropic material in plane strain is governed by the following equations:

$$G[\nabla^2 u_r - \frac{1}{r}(\frac{\partial u_r}{\partial r} + \frac{2}{r}\frac{\partial u_\theta}{\partial \theta})] + \frac{\partial \sigma_m}{\partial r} = 0 \quad (10.133)$$

$$G[\nabla^2 u_\theta + \frac{1}{r}(-\frac{\partial u_\theta}{\partial r} + \frac{2}{r}\frac{\partial u_r}{\partial \theta})] + \frac{1}{r}\frac{\partial \sigma_m}{\partial r} = 0 \quad (10.134)$$

$$(\frac{\partial}{\partial r} + \frac{1}{r})u_r + \frac{1}{r}\frac{\partial u_\theta}{\partial \theta} = 0 \quad (10.135)$$

where

$$\nabla^2 = \frac{\partial^2}{\partial r^2} + \frac{1}{r}\frac{\partial}{\partial r} + \frac{1}{r^2}\frac{\partial^2}{\partial \theta^2} \quad (10.136)$$

The solution of the above equations for a plane strain wedge subjected to uniform tractions can be shown to be of the following form:

$$Gu_r = -r(a \cos 2\theta + c \sin 2\theta) \quad (10.137)$$

$$Gu_\theta = r(a \sin 2\theta - c \cos 2\theta) - dr \log r \quad (10.138)$$

$$\sigma_m = 2(b + d\theta) \quad (10.139)$$

where  $a, b, c$  and  $d$  are constants of integration. The corresponding stresses are obtained from the linear elastic Hooke's law as follows:

$$s_r = -s_\theta = -2(a \cos 2\theta + c \sin 2\theta) \quad (10.140)$$

$$\sigma_{r\theta} = -d + 2(a \sin 2\theta - c \cos 2\theta) \quad (10.141)$$

$$s_z = 0 \quad (10.142)$$

Consider the boundary conditions that are defined as follows:

$$\sigma_\theta = -p, \quad \sigma_r = \sigma_{r\theta} = 0; \quad \text{at } \theta = 0 \quad (10.143)$$

$$\sigma_\theta = \sigma_r = \sigma_{r\theta} = 0; \quad \text{at } \theta = \beta \quad (10.144)$$

The constants of integration for the above boundary conditions can be shown to be

$$a = -p \frac{\tan \beta}{4\alpha} \quad (10.145)$$

$$b = -p(\frac{1}{2} + \frac{\tan \beta}{4\alpha}) \quad (10.146)$$

$$c = \frac{p}{4\alpha} \quad (10.147)$$

$$d = -\frac{p}{2\alpha} \quad (10.148)$$

in which

$$\alpha = \tan\beta - \beta \quad (10.149)$$

### 10.5.3 The initial yield and the elastic-plastic boundary

Since  $s_r = -s_\theta$ , the von Mises yield condition takes the following form

$$s_\theta^2 + \sigma_{r\theta}^2 = k_0^2 \quad (10.150)$$

which can be rewritten as follows from the elastic stress expressions:

$$\left(\frac{p}{2\alpha}\right)^2 f(\theta) = k_0^2 \quad (10.151)$$

in which

$$f(\theta) = \tan^2\beta + 2(1 - \cos 2\theta) - 2\tan\beta \sin 2\theta \quad (10.152)$$

Therefore yielding begins at the values of  $\theta$  for which the function  $f(\theta)$  attains its maximum value. For the range of  $0 < \beta < \pi/2$  considered here, it can be shown that the function  $f(\theta)$  is a minimum at  $\theta = \beta/2$ , and will reach its maximum simultaneously at  $\theta = 0$  and  $\theta = \beta$ . In other words, when the pressure  $p$  is gradually increased, yielding will occur first on the outside boundaries when the pressure has reached the value

$$p^* = \frac{2k_0\alpha}{(\tan\beta)^2} \quad (10.153)$$

For a pressure  $p > p^*$ , a portion of the wedge becomes plastic, and since the yield condition does not depend on the radius  $r$ , the elastic-plastic boundary should be a wedge bounded by  $\theta = \theta_1$  and  $\theta = \theta_2$  shown in Figure 10.6.

### 10.5.4 Elastic-plastic solutions

The solution is still of the same form as before in the elastic region defined by  $\theta_1 \leq \theta \leq \theta_2$ . However on the elastic-plastic boundaries, the stresses just satisfy the yield condition, namely

$$s_\theta^2(\theta_1) + \sigma_{r\theta}^2(\theta_1) = k_0^2 \quad (10.154)$$

$$s_\theta^2(\theta_2) + \sigma_{r\theta}^2(\theta_2) = k_0^2 \quad (10.155)$$

As shown before, the elastic stress solution does not involve the radius  $r$ . Therefore continuity of stresses across the elastic-plastic boundaries demands that these

stresses remain independent of  $r$  throughout the wedge. It then follows that the equations of equilibrium can be written as follows:

$$\frac{\partial \sigma_{r\theta}}{\partial \theta} + (s_r - s_\theta) = 0 \quad (10.156)$$

$$\frac{\partial s_\theta}{\partial \theta} + 2\sigma_{r\theta} + \frac{\partial \sigma_m}{\partial \theta} = 0 \quad (10.157)$$

which are valid in both elastic and plastic regions.

Differentiating the first equilibrium equation, multiplying the result by  $\lambda$  and making use of the elastic-plastic stress-strain relations, the following differential equation for the radial displacement in the plastic region may be derived

$$\frac{1}{r} \frac{\partial^2 \dot{u}_r}{\partial \theta^2} - r \frac{\partial^2 \dot{u}_r}{\partial r^2} + 3 \frac{\partial \dot{u}_r}{\partial r} + \frac{\dot{u}_r}{r} = \frac{\sigma_{r\theta} \partial \lambda}{G \partial \theta} \quad (10.158)$$

Since no radial slip can occur along the elastic-plastic boundaries,  $u_r$  must also be a linear function of  $r$  in the plastic domain. In other words, we can write

$$u_r = r \varepsilon_r(\theta, \phi) \quad (10.159)$$

with  $\phi$  as an indication of time that could be identified as either  $\theta_1$  or  $\theta_2$ .

Using the above equation, the differential equation of the radial displacement can be written as follows after integration

$$\frac{\partial^2 \varepsilon_r}{\partial \theta^2} + 4\varepsilon_r = \int \frac{\sigma_{r\theta} \partial \lambda}{G \partial \theta} d\phi \quad (10.160)$$

where, without loss of generality, an arbitrary function of  $\theta$  has been set equal to zero.  $\lambda$  is proportional to the rate of performed work, which is given by

$$\lambda = \frac{1}{2k_0^2} (s_r \dot{\varepsilon}_r + s_\theta \dot{\varepsilon}_\theta + 2\sigma_{r\theta} \dot{\varepsilon}_{r\theta}) \quad (10.161)$$

Invoking now the continuity of stresses at  $\theta = \theta_1$  and  $\theta = \theta_2$  it can be shown that  $s_r = -s_\theta$  at all points in the plastic regions. Therefore the first equation of equilibrium and the von Mises yield condition are combined to give

$$\frac{\partial \sigma_{r\theta}}{\partial \theta} = \pm 2 \sqrt{k_0^2 - \sigma_{r\theta}^2} \quad (10.162)$$

which can be integrated to conform to the following boundary conditions:

$$\sigma_\theta = -p, \quad \sigma_{r\theta} = 0 \quad \text{for } \theta = 0 \text{ and } \phi = \theta_1 \quad (10.163)$$

$$\sigma_\theta = \sigma_{r\theta} = 0 \quad \text{for } \theta = \beta \text{ and } \phi = \theta_2 \quad (10.164)$$

The solution of stresses in the plastic regions can be derived as follows:

$$s_r = -s_\theta = k_0 \cos 2\theta, \quad s_z = 0 \quad (10.165)$$

$$\sigma_{r\theta} = -k_0 \sin 2\theta \quad (10.166)$$

$$\sigma_m = k_0 - p \quad (10.167)$$

for the plastic region defined by  $0 \leq \theta \leq \theta_1$  and

$$s_r = -s_\theta = -k_0 \cos 2(\theta - \beta), \quad s_z = 0 \quad (10.168)$$

$$\sigma_{r\theta} = k_0 \sin 2(\theta - \beta) \quad (10.169)$$

$$\sigma_m = -k_0 \quad (10.170)$$

for the plastic region defined by  $\theta_2 \leq \theta \leq \beta$ .

Now with the stress solution, the differential equation of radial displacement can be rewritten as

$$\frac{\partial^2 \varepsilon_r}{\partial \theta^2} + 2 \tan 2\theta \frac{\partial \varepsilon_r}{\partial \theta} + 4(\sec^2 2\theta) \varepsilon_r = 0 \quad (10.171)$$

which can be combined with the condition of incompressibility to produce the displacement solution in the plastic region. It can also be shown that

$$\theta_1 + \theta_2 = \beta \quad (10.172)$$

When the wedge becomes completely plastic, then we have

$$\theta_1 = \theta_2 = \beta/2 \quad (10.173)$$

In this special case, the stress solutions obtained here reduce to those of the rigid perfectly plastic solutions presented in Prager and Hodge (1951) using slip line analysis.

## 10.6 PLASTIC FLOW PAST A SMOOTH CONE

Spencer (1984) published an exact solution of the equations that govern the axially symmetric plastic flow, in the kinematically determined regime, of a rigid-perfectly plastic material obeying both Tresca and Mohr-Coulomb yield conditions. The solution was also applied to the problem of flow of an infinite medium past a smooth rigid infinite cone. By the superposition of an axial velocity, the solution also describes the penetration of an infinite body by a cone.

The rigid-perfectly plastic solutions of axisymmetric stress and deformation have been obtained by Shield (1955) for Tresca's yield condition and Cox *et al.*

(1961) for Mohr-Coulomb's yield condition using slip line field theory. Various possibilities arise depending on the relative magnitude of the hoop stress  $\sigma_\phi$  (which is a principal stress component) and the principal stresses  $\sigma_1$  and  $\sigma_2$  that lie in the meridional planes. Most of these slip line solutions are for the Haar-von Karman states, in which  $\sigma_\phi$  is assumed to be equal to either  $\sigma_1$  or  $\sigma_2$ . In contrast, less attention has been given to other regimes. Lippmann (1962, 1965) studied the case when  $\sigma_\phi$  is either the greatest or the least of the principal stresses. These states have been termed 'kinematically determined', since for them the velocity equations are uncoupled from the stress equations. In addition to the two exact solutions obtained by Lippmann for these situations, Spencer (1984) derived another large strain analytical solution which has application to cone penetration in soils.

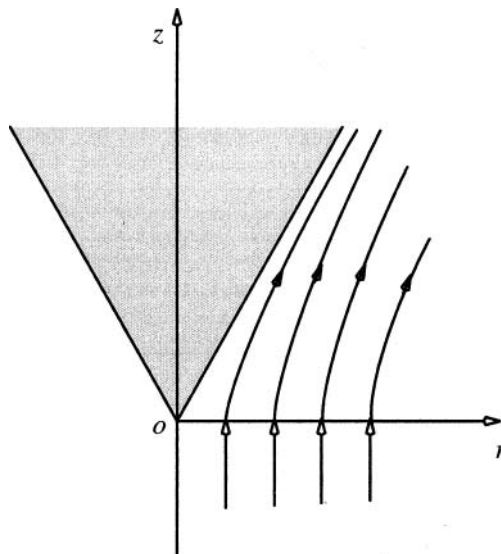


Figure 10.7: Streamlines for plastic flow past a rigid cone (after Spencer, 1984)

#### 10.6.1 Kinematically determined axially symmetric stress and deformation fields

The stress and velocity fields are referred initially to cylindrical polar coordinates  $r, \phi, z$ . For axially symmetric deformations, the velocity component in the hoop ( $\phi$ ) direction is zero. The velocity components in  $r$  and  $z$  directions, termed as  $v_r$  and  $v_z$  respectively, are functions of the coordinates  $r$  and  $z$ . Therefore the strain rates are expressed as follows:

$$\dot{\varepsilon}_r = \frac{\partial v_r}{\partial r} \quad (10.174)$$

$$\dot{\varepsilon}_\phi = \frac{v_r}{r} \quad (10.175)$$

$$\dot{\varepsilon}_z = \frac{\partial v_z}{\partial z} \quad (10.176)$$

$$\dot{\varepsilon}_{rz} = \frac{1}{2} \left[ \frac{\partial v_r}{\partial z} + \frac{\partial v_z}{\partial r} \right] \quad (10.177)$$

The incompressibility condition takes the form

$$\dot{\varepsilon}_r + \dot{\varepsilon}_\phi + \dot{\varepsilon}_z = 0; \quad \text{or} \quad \frac{\partial v_r}{\partial r} + \frac{v_r}{r} + \frac{\partial v_z}{\partial z} = 0 \quad (10.178)$$

The corresponding stress components are  $\sigma_r$ ,  $\sigma_\phi$ ,  $\sigma_z$  and  $\sigma_{rz}$  which are functions of the coordinates  $r$  and  $z$ . The stresses  $\sigma_r$ ,  $\sigma_z$  and  $\sigma_{rz}$  are acting on the same plane. On this plane, the principal stresses can be calculated by the following well-known equations

$$\sigma_1 = \frac{1}{2}(\sigma_r + \sigma_z) + \sqrt{\sigma_{rz}^2 + \frac{1}{4}(\sigma_r - \sigma_z)^2} \quad (10.179)$$

$$\sigma_2 = \frac{1}{2}(\sigma_r + \sigma_z) - \sqrt{\sigma_{rz}^2 + \frac{1}{4}(\sigma_r - \sigma_z)^2} \quad (10.180)$$

Therefore  $\sigma_1$ ,  $\sigma_2$  and  $\sigma_\phi$  form the three principal stresses. Which one is the major or minor principal stress depends on their relative values. For convenience let us denote the principal stresses by  $\sigma_I$ ,  $\sigma_{II}$  and  $\sigma_{III}$  in which  $\sigma_I > \sigma_{II} > \sigma_{III}$ .

In the plastically deforming region, the stresses must satisfy both yield condition and equations of equilibrium. Without body forces, the equations of equilibrium are

$$\frac{\partial \sigma_r}{\partial r} + \frac{\partial \sigma_{rz}}{\partial z} + \frac{\sigma_r - \sigma_\phi}{r} = 0 \quad (10.181)$$

$$\frac{\partial \sigma_{rz}}{\partial r} + \frac{\partial \sigma_{zz}}{\partial z} + \frac{\sigma_{rz}}{r} = 0 \quad (10.182)$$

For purely cohesive material, Tresca's yield condition is widely used. In terms of principal stresses, it takes the following simple form

$$\sigma_I - \sigma_{III} = 2S_u \quad (10.183)$$

where  $S_u$  is the undrained shear strength under the triaxial loading condition. In the solution derived by Spencer (1984), the hoop stress  $\sigma_\phi$  was assumed to be either the greatest or least, namely

$$\sigma_\phi > \sigma_1 > \sigma_2; \quad \sigma_\phi - \sigma_2 = 2S_u \quad (10.184)$$

$$\sigma_1 > \sigma_2 > \sigma_\phi; \quad \sigma_1 - \sigma_\phi = 2S_u \quad (10.185)$$

The flow rule associated with Tresca's yield condition requires that the strain rate corresponding to the intermediate principal stress component is equal to zero. This gives

$$\frac{1}{2}(\dot{\varepsilon}_r + \dot{\varepsilon}_z) + l \sqrt{\dot{\varepsilon}_{rz}^2 + \frac{1}{4}(\dot{\varepsilon}_r - \dot{\varepsilon}_z)^2} = 0 \quad (10.186)$$

or

$$\frac{\partial v_r}{\partial r} + \frac{\partial v_z}{\partial z} + l \sqrt{\left(\frac{\partial v_r}{\partial z} + \frac{\partial v_z}{\partial r}\right)^2 + \left(\frac{\partial v_r}{\partial r} - \frac{\partial v_z}{\partial z}\right)^2} = 0 \quad (10.187)$$

where  $l = +1$  for the case when  $\sigma_\phi$  is the greatest principal stress and  $l = -1$  for the case when  $\sigma_\phi$  is the least principal stress.

The above equation together with the incompressibility condition form two equations for the two velocities  $v_r$  and  $v_z$ , which do not involve the stress. It is in this sense that the problem analysed is said to be kinematically determined. These two equations of velocities can be more easily solved by using an additional variable,  $\psi$ , which is the angle the principal stress  $\sigma_1$  makes with the radial direction defined by

$$\tan 2\psi = \frac{2\sigma_{rz}}{\sigma_r - \sigma_z} \quad (10.188)$$

For coaxial plasticity, we also have

$$\tan 2\psi = \frac{\frac{\partial v_r}{\partial z} + \frac{\partial v_z}{\partial r}}{\frac{\partial v_r}{\partial r} - \frac{\partial v_z}{\partial z}} \quad (10.189)$$

The condition of zero strain rate associated with the intermediate principal stress can then be rewritten as follows

$$\frac{\partial v_r}{\partial r} + \frac{\partial v_z}{\partial z} + l \left\{ \left( \frac{\partial v_r}{\partial z} + \frac{\partial v_z}{\partial r} \right) \sin 2\psi + \left( \frac{\partial v_r}{\partial r} - \frac{\partial v_z}{\partial z} \right) \cos 2\psi \right\} = 0 \quad (10.190)$$

Now the velocity equations can be replaced by the following simpler equivalent system in terms of  $v_r, v_z, \psi$

$$\frac{\partial v_r}{\partial r} + \frac{1}{2}(1 - l \cos 2\psi) \frac{v_r}{r} = 0 \quad (10.191)$$

$$\frac{\partial v_z}{\partial z} + \frac{1}{2}(1 + l \cos 2\psi) \frac{v_r}{r} = 0 \quad (10.192)$$

$$\frac{\partial v_r}{\partial z} + \frac{\partial v_z}{\partial r} - l \sin 2\psi \frac{v_r}{r} = 0 \quad (10.193)$$

When the angle  $\psi$  is determined then the stresses can be calculated by combining the yield condition, equations of equilibrium and the definition of the angle  $\psi$  in terms of stresses, which provide four equations for four stress components.

For an ideal granular material we can assume the Mohr-Coulomb yield criterion in the following form:

$$\sigma_I - \sigma_{III} = 2C \cos \varphi - (\sigma_I + \sigma_{III}) \sin \varphi \quad (10.194)$$

where the cohesion  $C$  and the angle of internal friction  $\varphi$  are constants. It is clear that Tresca's yield condition corresponds to the special case  $\varphi = 0$  and  $C = S_u$ . Here we consider the following two possible cases:

$$\sigma_\phi > \sigma_1 > \sigma_2; \quad \sigma_\phi(1 + \sin \varphi) = 2C \cos \varphi + \sigma_2(1 - \sin \varphi) \quad (10.195)$$

$$\sigma_1 > \sigma_2 > \sigma_\phi; \quad \sigma_1(1 + \sin \varphi) = 2C \cos \varphi + \sigma_\phi(1 - \sin \varphi) \quad (10.196)$$

The flow rule used by Spencer (1984) is for incompressible granular material derived from his double shear theory, which turns out to be the same as those from the Tresca yield criterion.

### 10.6.2 Governing equations in spherical polar coordinates

In this section we express the equations derived in the previous section in terms of spherical polar coordinates  $R, \theta, \phi$ , where

$$r = R \sin \theta, \quad z = R \cos \theta \quad (10.197)$$

In these coordinates we denote the the strain rates and stress components as

$$\dot{\varepsilon}_{ij} = \begin{bmatrix} \dot{\varepsilon}_R & \dot{\varepsilon}_{R\theta} & 0 \\ \dot{\varepsilon}_{R\theta} & \dot{\varepsilon}_\theta & 0 \\ 0 & 0 & \dot{\varepsilon}_\phi \end{bmatrix} \quad (10.198)$$

$$\sigma_{ij} = \begin{bmatrix} \sigma_R & \sigma_{R\theta} & 0 \\ \sigma_{R\theta} & \sigma_\theta & 0 \\ 0 & 0 & \sigma_\phi \end{bmatrix} \quad (10.199)$$

where

$$\dot{\varepsilon}_R = \frac{\partial v_R}{\partial R} \quad (10.200)$$

$$\dot{\varepsilon}_\theta = \frac{1}{R} \frac{\partial v_\theta}{\partial \theta} + \frac{v_R}{R} \quad (10.201)$$

$$\dot{\varepsilon}_\phi = \frac{v_R}{R} + \cot \theta \frac{v_\theta}{R} \quad (10.202)$$

$$\dot{\varepsilon}_{R\theta} = \frac{1}{2} \left[ \frac{1}{R} \frac{\partial v_R}{\partial \theta} + \frac{\partial v_\theta}{\partial r} - \frac{v_\theta}{R} \right] \quad (10.203)$$

where  $v_R, v_\theta$  are velocity components in the R and  $\theta$  directions. The incompressibility condition is

$$\dot{\varepsilon}_R + \dot{\varepsilon}_\theta + \dot{\varepsilon}_\phi = 0 \quad (10.204)$$

The principal stress components are given by

$$\sigma_1 = \frac{1}{2}(\sigma_R + \sigma_\theta) + \sqrt{\sigma_{r\theta}^2 + \frac{1}{4}(\sigma_R - \sigma_\theta)^2} \quad (10.205)$$

$$\sigma_2 = \frac{1}{2}(\sigma_R + \sigma_\theta) - \sqrt{\sigma_{r\theta}^2 + \frac{1}{4}(\sigma_R - \sigma_\theta)^2} \quad (10.206)$$

and the equations of equilibrium reduce to

$$\frac{\partial \sigma_R}{\partial R} + \frac{1}{R} \frac{\partial \sigma_{R\theta}}{\partial \theta} + \frac{2\sigma_R - \sigma_\theta - \sigma_\phi}{R} = 0 \quad (10.207)$$

$$\frac{\partial \sigma_{R\theta}}{\partial R} + \frac{1}{R} \frac{\partial \sigma_\theta}{\partial \theta} + \frac{\sigma_\theta - \sigma_\phi}{R} \cot \theta + \frac{3\sigma_{R\theta}}{R} = 0 \quad (10.208)$$

We denote by  $\eta$  the angle between the direction of the principal axis of stress associated with  $\sigma_1$  and the radial direction, measured in the direction of increasing  $\theta$ . Thus

$$\eta = \frac{1}{2}\pi - \theta - \psi \quad (10.209)$$

Then

$$\tan 2\eta = \frac{2\sigma_{R\theta}}{\sigma_R - \sigma_\theta} = \frac{2\dot{\varepsilon}_{R\theta}}{\dot{\varepsilon}_R - \dot{\varepsilon}_\theta} \quad (10.210)$$

The plastic flow rule becomes

$$\frac{1}{2}(\dot{\varepsilon}_R + \dot{\varepsilon}_\theta) + l \sqrt{\dot{\varepsilon}_{R\theta}^2 + \frac{1}{4}(\dot{\varepsilon}_R - \dot{\varepsilon}_\theta)^2} = 0 \quad (10.211)$$

Therefore the incompressibility condition, the plastic flow rule and the definition of angle  $\eta$  form three equations in terms of  $v_R, v_\theta$  and  $\eta$ :

$$\frac{\partial v_R}{\partial R} + \frac{1}{2}(1 - l \cos 2\eta) \left[ \frac{v_R}{R} + \cot \theta \frac{v_\theta}{R} \right] = 0 \quad (10.212)$$

$$\frac{1}{R} \frac{\partial v_\theta}{\partial \theta} + \frac{v_R}{R} + \frac{1}{2}(1 + l \cos 2\eta) \left[ \frac{v_R}{R} + \cot \theta \frac{v_\theta}{R} \right] = 0 \quad (10.213)$$

$$\frac{1}{R} \frac{\partial v_R}{\partial \theta} + \frac{\partial v_\theta}{\partial R} - \frac{v_\theta}{R} - l \sin 2\eta \left[ \frac{v_R}{R} + \cot \theta \frac{v_\theta}{R} \right] = 0 \quad (10.214)$$

### 10.6.3 A class of exact solutions

The above equations have solutions of the form

$$v_R = R^p F_p(\theta); \quad v_\theta = R^p G_p(\theta); \quad \eta = H_p(\theta) \quad (10.215)$$

where  $p$  is a number. As pointed out by Spencer (1984), except for a few special cases, the resulting ordinary differential equations for  $F_p$ ,  $G_p$  and  $H_p$  do not appear to have simple solutions.

Spencer (1984) considered a class of solutions for which

$$1 - l \cos 2\eta = 0 \quad (10.216)$$

so that  $\eta = 0$  for the case when  $l = 1$  and  $\eta = \pi/2$  for the case when  $l = -1$ . In either case the principal axes of stress coincide with the radial ( $R$ ) and tangential ( $\theta$ ) directions. For this special case, the governing equations of velocity components take the following simple form

$$\frac{\partial v_R}{\partial R} = 0 \quad (10.217)$$

$$\frac{\partial v_\theta}{\partial \theta} + 2v_R + v_\theta \cot \theta = 0 \quad (10.218)$$

$$\frac{1}{R} \frac{\partial v_R}{\partial \theta} + \frac{\partial v_\theta}{\partial R} - \frac{v_\theta}{R} = 0 \quad (10.219)$$

which can be solved to give the following solutions

$$v_R = A(1 + \cos \theta \log \tan \frac{1}{2}\theta) + D \cos \theta \quad (10.220)$$

$$v_\theta = BR \operatorname{cosec} \theta + A(\cot \theta - \sin \theta \log \tan \frac{1}{2}\theta) - D \sin \theta \quad (10.221)$$

and alternatively we have

$$v_r = BR \cot \theta + A \operatorname{cosec} \theta \quad (10.222)$$

$$v_z = -BR + A \log \tan \frac{1}{2}\theta + D \quad (10.223)$$

where  $A$ ,  $B$ ,  $D$  are integration constants.

We now consider the stress. Since for either  $\eta = 0$  or  $\eta = \pi/2$ ,  $\sigma_R$  and  $\sigma_\theta$  are principal stress components,  $\sigma_{R\theta} = 0$ , and so Tresca's yield condition reduces to

$$\sigma_\phi - \sigma_\theta = 2lS_u \quad (10.224)$$

The second equation of equilibrium then gives

$$\sigma_\theta = 2lS_u \log \sin \theta + \frac{1}{R} p'(R) \quad (10.225)$$

where the arbitrary function  $p'(R)/R$  is expressed in this form for convenience. The first equation of equilibrium is then used to determine  $\sigma_R$  and then the complete solution for stresses is as follows

$$\sigma_R = lS_u(1 + 2 \log \sin \theta) + 2p'(R)/R^2 + q(\theta)/R^2 \quad (10.226)$$

$$\sigma_\theta = 2lS_u \log \sin \theta + \frac{1}{R} p'(R) \quad (10.227)$$

$$\sigma_\phi = lS_u(1 + \log \sin \theta) + p'(R)/R \quad (10.228)$$

The functions  $p'(R)$  and  $q(\theta)$  are not completely arbitrary but must be such that  $\sigma_R$  is the intermediate principal stress in the deforming region. It is noted that this condition is satisfied if we set  $p'(R) = ER^2$  and  $q(\theta) = 0$ , for any constant  $E$ . The condition for the rate of plastic work to be positive is

$$(B \cos \theta + R^{-1}C)lS_u > 0 \quad (10.229)$$

For a granular material obeying the Mohr-Coulomb yield criterion, which takes the following form

$$\sigma_\phi(1 + l \sin \varrho) - \sigma_\theta(1 - l \sin \varrho) = 2lC \cos \varrho \quad (10.230)$$

then from the second equation of equilibrium, we have

$$\sigma_\theta = C \cot \varrho + \frac{p'(R)}{R(1 - l \sin \varrho)} \sin^n \theta \quad (10.231)$$

and

$$\sigma_\phi = C \cot \varrho + \frac{p'(R)}{R(1 + l \sin \varrho)} \sin^n \theta \quad (10.232)$$

in which

$$n = -2l \sin \varrho / (1 + l \sin \varrho) \quad (10.233)$$

Finally the first equation of equilibrium gives

$$\sigma_R = C \cot \varrho + \frac{2p'(R)}{R^2 \cos^2 \varrho} \sin^n \theta + \frac{q(\theta)}{R^2} \quad (10.234)$$

Once again the functions  $p'(R)$  and  $q(\theta)$  are such that  $\sigma_R$  is the intermediate principal stress component. The condition for positive plastic work-rate is

$$-(B \cos \theta + R^{-1}A)lp'(R) > 0 \quad (10.235)$$

#### 10.6.4 Plastic flow past an infinite cone

As an application of the solution given in equations (10.220) and (10.221), we consider the problem of flow past the cone  $\theta = \alpha$  ( $\alpha < \pi/2$ ). The region  $z < 0$  is assumed to move as a rigid body with speed  $V$  in the positive  $z$  direction. On the surface of the cone, the normal velocity component  $v_\theta$  is zero. Hence the velocity boundary conditions for the region  $\alpha < \theta < \pi/2$  are

$$v_\theta = 0, \quad \theta = \alpha \quad (10.236)$$

$$v_\theta = -V, \quad \theta = \frac{\pi}{2} \quad (10.237)$$

The solution (10.220) and (10.221) which satisfies these conditions is

$$v_R = V \frac{\sin \alpha (1 + \cos \theta \log \tan \frac{\theta}{2})}{\cot \alpha - \sin \alpha \log \tan \frac{\alpha}{2}} + V \cos \theta \quad (10.238)$$

$$v_\theta = V \frac{\sin \alpha (\cot \theta - \sin \theta \log \tan \frac{\theta}{2})}{\cot \alpha - \sin \alpha \log \tan \frac{\alpha}{2}} - V \sin \theta \quad (10.239)$$

By superimposing on this solution a rigid body speed  $V$  in the negative  $z$ -direction, we obtain the solution to the problem of a rigid cone moving through an infinite rigid-plastic medium with speed  $V$  in the negative  $z$ -direction. This solution may have applications in penetration mechanics.

If we introduce the stream function  $\Psi$  such that

$$v_R = -\frac{1}{R^2 \sin \theta} \frac{\partial \Psi}{\partial \theta} \quad (10.240)$$

$$v_\theta = \frac{1}{R \sin \theta} \frac{\partial \Psi}{\partial \theta} \quad (10.241)$$

For the velocity solutions, we can determine the stream function as follows

$$\begin{aligned} \Psi &= \frac{1}{2} R^2 v_\theta \sin \theta \\ &= \frac{1}{2} R^2 V \left\{ \sin^2 \alpha \frac{\cos \theta - \sin^2 \theta \log \tan \frac{\theta}{2}}{\cos \alpha - \sin^2 \alpha \log \tan \frac{\alpha}{2}} - \sin^2 \theta \right\} \end{aligned} \quad (10.242)$$

The streamlines are the curves defined by  $\Psi = \text{constant}$ . Some typical streamlines for  $\alpha = 30^\circ$  are shown in Figure 10.7. The streamlines are all similar curves with the origin as the centre of similarity.

To determine the stress for a frictionless (or purely cohesive) material, we note that if  $V$  is positive, then  $A$  is positive and since  $B=0$ , the condition of positive plastic work-rate requires  $l = +1$ . Now let's assume the stress component  $\sigma_z = -P$  for  $z<0$ . In other words we have the following boundary conditions on  $z=0$

$$\sigma_\theta = -P, \quad \sigma_{R\theta} = 0, \quad \theta = \frac{\pi}{2} \quad (10.243)$$

The second condition is satisfied automatically. The first condition demands

$$p'(R) = -RP \quad (10.244)$$

There we have the complete stress solution

$$\sigma_R = -P + S_u(1 + 2 \log \sin \theta) \quad (10.245)$$

$$\sigma_\theta = -P + 2S_u \log \sin \theta \quad (10.246)$$

$$\sigma_\phi = -P + 2S_u(1 + \log \sin \theta) \quad (10.247)$$

where the function  $q(\theta)$  was set to zero to ensure that  $\sigma_R$  is the intermediate principal stress. The normal pressure on the cone is

$$P - 2S_u \log \sin \alpha$$

Similarly, for a frictional material, with the boundary conditions mentioned for the purely cohesive material, we can show that the stress solutions are

$$\sigma_R = C \cot \varrho - \frac{1 - \sin \varrho}{\cos^2 \varrho} (P + C \cot \varrho) \sin^n \theta \quad (10.248)$$

$$\sigma_\theta = C \cot \varrho - (P + C \cot \varrho) \sin^n \theta \quad (10.249)$$

$$\sigma_\phi = C \cot \varrho - \frac{1 - \sin \varrho}{1 + \sin \varrho} (P + C \cot \varrho) \sin^n \theta \quad (10.250)$$

where

$$n = -\frac{2 \sin \varrho}{1 + \sin \varrho} \quad (10.251)$$

The pressure on the surface of the cone is now

$$P \sin^n \alpha - C \cot \varrho (1 - \sin^n \alpha)$$

It can be shown that for a special case of  $\varrho = 0$ , the above solutions of a frictional material tend to the solution obtained before for a purely cohesive material.

## REFERENCES

Bigoni, D. and Laudiero, F. (1989). The quasi-static finite cavity expansion in a non-standard elasto-plastic medium. *Int. J. Mech. Sci.*, Vol 31, 825-837.

Carter, J.P., Booker, J.R. and Yeung, S.K. (1986). Cavity expansion in cohesive frictional soils. *Geotechnique*, Vol 36, 349-353.

Chadwick, P. (1959). The quasi-static expansion of a spherical cavity in metals and ideal soils. *Quart. J. Mech. Appl. Math.*, Vol 12, 52-71.

Collins, I.F. and Wang, Y. (1990). Similarity solutions for the quasi-static expansion of cavities in frictional materials. *Research Report No. 489*, Department of Engineering Science, University of Auckland, New Zealand.

Collins, I.F. and Yu, H.S. (1996). Undrained cavity expansions in critical state soils. *Int. J. Num. Anal. Meth. Geomech.*, Vol 20, 485-516.

Cox, A.D., Eason, G. and Hopkins, H.G. (1961). Axially symmetric plastic deformation of soils, *Phil. Trans. Roy. Soc. A.*, Vol 254, 1-45.

Davis, E.H. (1968). Theories of plasticity and the failure of soil masses. In: *Soil Mechanics* (edited by I.K. Lee). London, Butterworths.

Durban, D. and Fleck, N.A. (1991). Singular plastic fields in steady penetration of a rigid cone. *J. Appl. Mech.*, ASME, Vol 59, 706-710.

Florence, A.L. and Schwer, L.E. (1978). Axisymmetric compression of a Mohr-Coulomb medium around a circular hole. *Int. J. Num. Analy. Meth. Geomech.*, Vol 2, 367-379.

Gibson, R.E. and Anderson, W.F. (1961). In situ measurement of soil properties with the pressuremeter. *Civil Engineering and Public Works Review*, Vol 56, 615-618.

Hill, J.M. (2000). Some symmetric cavity problems for a hypoplastic granular material. *Quart. J. Mech. Appl. Math.*, Vol 53, 111-135.

Hill, R. (1950). *The Mathematical Theory of Plasticity*. Oxford University Press.

Hughes, J.M.O., Wroth, C.P. and Windle, D. (1977). Pressuremeter tests in sands. *Geotechnique*, Vol 27, 455-477.

Lippmann, H. (1962). Principal line theory of axially symmetric plastic deformation. *J. Mech. Phys. Solids*, Vol 10, 111-122.

Lippmann, H. (1965). Statics and dynamics of axially symmetric flow. *J. Mech. Phys. Solids*, Vol 13, 29-39.

Maugin, G.A. (1992). *The Thermomechanics of Plasticity and Fracture*, Cambridge University Press.

Naghdi, P.M. (1957). Stresses and displacements in an elastic-plastic wedge, *J. Appl. Mech.*, ASME, Vol 24, 98-104.

Norbury, J. and Wheeler, A.A. (1987). On the penetration of an elastic-plastic material by a slender body, *Quart. J. Mech. Appl. Math.*, Vol 40, 477-491.

Prager, W. and Hodge, P.G. (1951). *The Theory of Perfectly Plastic Solids*, John Wiley and Sons, New York.

Sagasetu, C. (1987). Analysis of undrained soil deformation due to ground loss. *Geotechnique*, Vol 37, 301-320.

Salencon, J. (1969). Contraction quasi-statique d'une cavite a symetrie spherique ou cylindrique dans un milieu elastoplastique. *Annales des Ponts et Chaussees*, Vol 4, 231-236.

Shield, R.T. (1955). On the plastic flow of metals under conditions of axial symmetry, *Proc. R. Soc. A.*, Vol 233, 267-287.

Spencer, A.J.M. (1984). Plastic flow past a smooth cone. *Acta Mechanica*, Vol 54, 63-74.

Vesic, A.S. (1972). Expansion of cavities in infinite soil mass. *J. Soil Mechanics and Foundations Div.*, ASCE, Vol 98, 265-290.

Yu, H.S. (1990). *Cavity Expansion Theory and Its Application to the Analysis of Pressure-meters*, DPhil Thesis, Oxford University, UK.

Yu, H.S. (1992). Expansion of a thick cylinder of soils. *Comput. Geotech.*, Vol 14, 21-41.

Yu, H.S. (1993). Finite elastoplastic deformation of an internally pressurized hollow sphere. *Acta Mechanica Solida Sinica*, Vol 6, 81-97.

Yu, H.S. (2000). *Cavity Expansion Methods in Geomechanics*, Kluwer Academic Publishers.

Yu, H.S. and Carter, J.P. (2002). Rigorous similarity solutions for cavity expansion in cohesive frictional soils, *Int. J. Geomech.*, Vol 2, 233-258.

Yu, H.S. and Houlsby, G.T. (1991). Finite cavity expansion in dilatant soil: loading analysis. *Geotechnique*, Vol 41, 173-183.

Yu, H.S. and Houlsby, G.T. (1995). A large strain analytical solution for cavity contraction in dilatant soils. *Int. J. Num. Anal. Meth. Geomech.*, Vol 19, 793-811.

Yu, H.S. and Rowe, R.K. (1999). Plasticity solutions for soil behaviour around contracting cavities and tunnels, *Int. J. Num. Anal. Meth. Geomech.*, Vol 23, 1245-1279.

## CHAPTER 11

### SLIP LINE ANALYSIS

#### 11.1 INTRODUCTION

A complete analysis of elastic-plastic problems is only possible for simple cases where loading and geometry are simple. Some of these examples (such as cavity expansion problems) are given in the previous chapter, where a complete elastic-plastic solution can be derived. In reality, however, most practical problems are such that a complete elastic-plastic treatment is very complex. There are a class of problems of great practical interest for which the failure load is not very sensitive to the elastic component of strain (i.e. unrestricted plastic flow). Therefore the elastic strain in the plastically deforming region may be disregarded. For consistency, we would also need to ignore the elastic strain in the non-plastic zone. In effect we are concerned with a rigid-plastic material that is rigid when the stress is below the yield stress and perfectly plastic when the stress reaches the yield stress. For rigid-plastic materials, great simplicity may be achieved in solving both stress and velocity governing equations for plane strain problems. In essence, the problem of plane strain plastic flow becomes statically determined in the sense that there will be three stress equations for three unknown stress components provided that the stresses are prescribed on the boundary. Once the solution of stress is obtained, the coaxiality assumption can be readily used to determine all the velocity components. In particular it turns out that the simplest way of solving these stress equations is to express them in terms of a coordinate system that is along potential slip (or failure) surfaces. It is for this reason that this type of analysis is termed *slip line analysis* or the theory of slip line fields in the literature (Hill, 1950).

This chapter gives a brief presentation of slip line analysis and its application to geotechnical engineering. The theory of slip line fields is best explained and understood for materials obeying an isotropic, mean pressure-independent yield condition (e.g. Tresca's yield criterion) for which simple slip lines exist. As a result, we will first present slip line analysis of cohesive materials. Its extension to frictional materials will be discussed later. While slip line analysis is more rigorous for plane strain problems, a similar treatment is possible for axisymmetric problems provided some additional assumptions about the magnitude of the hoop stress are made (Shield, 1955; Cox *et al.*, 1961). Therefore the use and application of slip line analysis to axisymmetric problems will also be addressed.

## 11.2 STRESS FIELDS IN PLASTIC REGIONS

In this section, we will present equations that stress fields must satisfy in the plastic region of a rigid plastic body that is modelled by the Mohr-Coulomb failure criterion (that is suitable for modelling cohesive-frictional soils). The equations for the Tresca criterion (that is often used to model clay soils under undrained conditions) can be recovered simply by setting the angle of friction to zero.

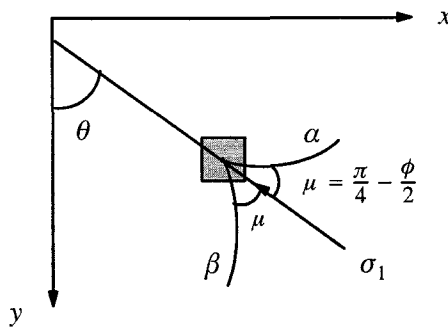


Figure 11.1: The coordinate system and stress characteristics for plane strain problems

### 11.2.1 Basic equations in terms of stresses

#### *Equilibrium equations*

Referring to the coordinate system shown in Figure 11.1, we have the following two equations of equilibrium under conditions of plane strain:

$$\frac{\partial \sigma_x}{\partial x} + \frac{\partial \sigma_{xy}}{\partial y} = 0 \quad (11.1)$$

$$\frac{\partial \sigma_{xy}}{\partial x} + \frac{\partial \sigma_y}{\partial y} = \gamma \quad (11.2)$$

where  $\gamma$  is the unit weight of the material in the  $y$  direction.

#### *The Mohr-Coulomb failure criterion*

If a point is in the plastic state, then the stress Mohr circle touches the failure envelope as shown in Figure 11.2. This means that the stresses can be expressed as follows:

$$\sigma_x = p - R \cos 2\theta \quad (11.3)$$

$$\sigma_y = p + R \cos 2\theta \quad (11.4)$$

$$\sigma_{xy} = R \sin 2\theta \quad (11.5)$$

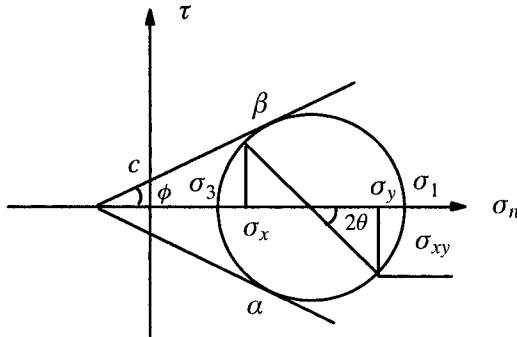


Figure 11.2: Stress states at failure

where  $p$  and  $R$  are the mean stress and the radius of the Mohr stress circle, namely

$$p = \frac{1}{2}(\sigma_x + \sigma_y) = \frac{1}{2}(\sigma_1 + \sigma_3) \quad (11.6)$$

$$R = (p + c \cot \phi) \sin \phi \quad (11.7)$$

Therefore at the state of failure the stress components can be expressed as a function of the mean stress and the angle  $\theta$ .

By substituting equations (11.3)-(11.5) into equilibrium equations (11.1)-(11.2), we obtain the following governing equations

$$\begin{aligned} \frac{\partial p}{\partial y} (1 + \sin \phi \cos 2\theta) + \frac{\partial p}{\partial x} \sin \phi \sin 2\theta \\ + 2R \left( -\frac{\partial \theta}{\partial y} \sin 2\theta + \frac{\partial \theta}{\partial x} \cos 2\theta \right) = 0 \end{aligned} \quad (11.8)$$

$$\begin{aligned} \frac{\partial p}{\partial y} \sin \phi \sin 2\theta + \frac{\partial p}{\partial x} (1 - \sin \phi \cos 2\theta) \\ + 2R \left( \frac{\partial \theta}{\partial y} \cos 2\theta + \frac{\partial \theta}{\partial x} \sin 2\theta \right) = \gamma \end{aligned} \quad (11.9)$$

These are two simultaneous first order partial differential equations governing the variation of the stress state in terms of  $(p, \theta)$ . For problems with stress boundary conditions, the above two equations can be used to determine two unknowns  $(p, \theta)$ ,

which can then be used to derive the stress components ( $\sigma_x, \sigma_y, \sigma_{xy}$ ) using equations (11.3)-(11.5).

### 11.2.2 Solution using the method of characteristics

It is not difficult to note that the best way of solving the governing equations (11.8)-(11.9) is using the so-called method of characteristics (Hill, 1950). This is because the equations are hyperbolic. In this method, the equations are re-expressed along two characteristic directions so that integration can be readily carried out. Following the method outlined in Hill (1950) and Kachanov (1974), it can be shown that the two characteristics ( $\alpha, \beta$ ) for the two equations (11.8)-(11.9) are defined by

$$\frac{dx}{dy} = \tan(\theta \pm \mu) \quad (11.10)$$

where  $\mu = \pi/4 - \phi/2$  as shown in Figure 11.1. It can be shown from Figure 11.2 that the two characteristics defined in (11.10) represent the two failure planes on which the failure criterion is satisfied. This is why they are also termed *slip lines* or shear lines which refer to two dimensions.

Along the directions of ( $\alpha, \beta$ ), the variation of stress state in a plastic region can be shown to be as follows:

$$dp + 2(p + c \cot \phi) \tan \phi d\theta = - \frac{\gamma \sin(\theta - \mu)}{\cos \phi \cos(\theta + \mu)} dy \quad (11.11)$$

$$dp - 2(p + c \cot \phi) \tan \phi d\theta = \frac{\gamma \sin(\theta + \mu)}{\cos \phi \cos(\theta - \mu)} dy \quad (11.12)$$

### 11.2.3 Slip line solutions for simple cases

In a general case, the solution of the governing equations (11.12)-(11.11) under certain stress boundary conditions requires numerical methods (e.g. finite difference approach). For some simple cases, however, the solution takes a very simple form and can be obtained analytically.

*Cohesive soils with self-weight ( $\phi = 0$ )*

For a cohesive soil, the angle of friction is zero. In this case, the equations (11.12) and (11.11) reduce to the following simple form:

$$dp + 2cd\theta = - \gamma dy \quad \text{along an } \alpha\text{-line} \quad (11.13)$$

$$dp - 2cd\theta = \gamma dy \quad \text{along a } \beta\text{-line} \quad (11.14)$$

The two slip lines are defined by

$$\frac{dx}{dy} = \tan(\theta \pm \frac{\pi}{4}) \quad (11.15)$$

from which it is clear that for cohesive soils the  $(\alpha, \beta)$  lines are normal to each other.

*Cohesive soils with no self-weight ( $\phi = 0, \gamma = 0$ )*

For a cohesive soil with no self-weight, the equations (11.12) and (11.11) reduce to an even simpler form given below:

$$dp + 2cd\theta = 0 \quad \text{along an } \alpha\text{-line} \quad (11.16)$$

$$dp - 2cd\theta = 0 \quad \text{along a } \beta\text{-line} \quad (11.17)$$

which, through integration, give

$$p + 2c\theta = C_\alpha \quad \text{along an } \alpha\text{-line} \quad (11.18)$$

$$p - 2c\theta = C_\beta \quad \text{along a } \beta\text{-line} \quad (11.19)$$

where  $C_\alpha$  and  $C_\beta$  are integration constants along  $(\alpha, \beta)$  lines. The above two equations are also known as the Hencky equations, which have been widely used to determine plastic stress fields in metal plasticity as described in Hill (1950), Prager and Hodge (1951) and Kachanov (1974).

*Cohesive-frictional soils with no self-weight ( $\gamma = 0$ )*

For a cohesive-frictional soil with no self-weight, the equations (11.12) and (11.11) reduce to the following:

$$dp + 2(p \tan \phi + c)d\theta = 0 \quad \text{along an } \alpha\text{-line} \quad (11.20)$$

$$dp - 2(p \tan \phi + c)d\theta = 0 \quad \text{along a } \beta\text{-line} \quad (11.21)$$

which, after integration, lead to

$$p = C_\alpha e^{-2\theta \tan \phi} - c \cot \phi \quad \text{along an } \alpha\text{-line} \quad (11.22)$$

$$p = C_\beta e^{2\theta \tan \phi} - c \cot \phi \quad \text{along a } \beta\text{-line} \quad (11.23)$$

where  $C_\alpha$  and  $C_\beta$  are integration constants along  $(\alpha, \beta)$  lines. In other words, the two stress variables  $(p_1, \theta_1)$  and  $(p_2, \theta_2)$  at two points along the same stress characteristic are linked by the following equations

$$\ln \frac{p_2 + c \cot \phi}{p_1 + c \cot \phi} = -2(\theta_2 - \theta_1) \tan \phi \quad \text{along an } \alpha\text{-line} \quad (11.24)$$

$$\ln \frac{p_2 + c \cot \phi}{p_1 + c \cot \phi} = 2(\theta_2 - \theta_1) \tan \phi \quad \text{along a } \beta\text{-line} \quad (11.25)$$

### 11.2.4 Stress boundary conditions

The solution to the governing stress equations (11.12)-(11.11) requires sufficient stress boundary conditions in terms of the mean stress and the direction of the principal stress ( $p, \theta$ ). As shown in Figure 11.3, consider a boundary  $\Gamma$  whose normal forms an angle of  $\delta$  from the  $y$  direction. On the boundary, the normal and shear stresses are known as  $\sigma_n$  and  $\sigma_{nt}$ . What we need to do is to determine the values of  $(p, \theta)$  from given values of  $(\sigma_n, \sigma_{nt})$ .

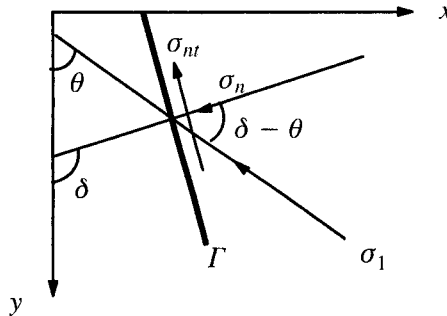


Figure 11.3: The stress conditions on a boundary

Given that the stresses at the boundary must be on the Mohr circle that touches the failure envelope as shown in Figure 11.4, from the geometry of the Mohr circle or equations (11.4)-(11.5), we have

$$\sigma_n = p + R \cos 2(\delta - \theta) \quad (11.26)$$

$$\sigma_{nt} = R \sin 2(\delta - \theta) \quad (11.27)$$

where as before  $p$  is the mean stress and  $R$  is the radius of the Mohr circle defined by  $R = (p + \cot \phi) \sin \phi$ .

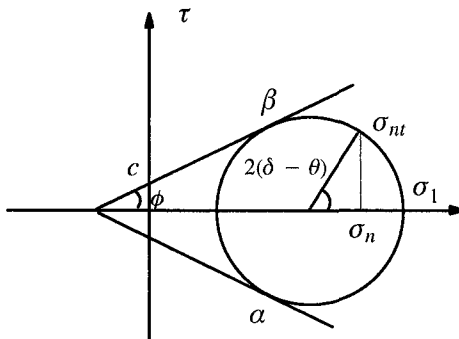


Figure 11.4: Stress states at failure

From the above equations, we can solve  $(p, \theta)$  in terms of the given values of  $(\sigma_n, \sigma_{nt})$  and the direction of the boundary  $\delta$ . It can be shown that the mean stress  $p$  can be solved from the following equation

$$(\sigma_n - p)^2 + \sigma_{nt}^2 = (p + c \cot \phi)^2 \sin^2 \phi \quad (11.28)$$

once the mean stress is determined, either of equations (11.26) or (11.27) can be used to obtain the value of  $\theta$ .

An important special case is that the shear stress acting on the boundary is zero. In this case, equation (11.27) can be used to give the angle of  $\theta$  as follows:

$$\theta = (-1)^n n \frac{\pi}{2} + \delta \quad (11.29)$$

where  $n$  is either 1 or 2 depending on a given problem (determining whether  $\sigma_n$  is the major principal stress). As for the mean stress, equation (11.28) can be used to give

$$p = \frac{\sigma_n \mp c \cos \phi}{1 \pm \sin \phi} \quad (11.30)$$

with the first sign for the case when  $\sigma_n$  is the major principal stress and the second for the case when  $\sigma_n$  is the minor principal stress.

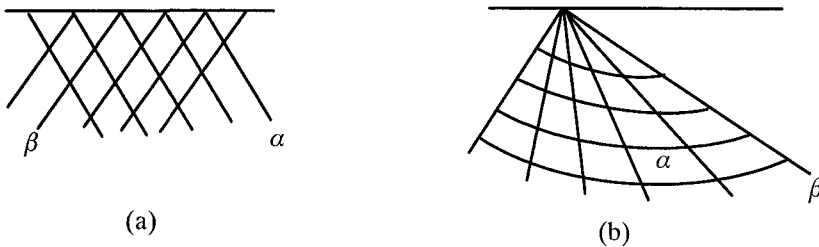


Figure 11.5: Slip line fields containing straight slip lines

### 11.2.5 Simple slip line fields

For the most general case (i.e. cohesive-frictional soils with self-weight), a rigorous solution of a practical problem using the slip line theory would require numerical construction of slip line fields and this will be covered in the next section. This section gives some simple slip line fields that have proved to be very useful in giving solutions for many simplified practical problems of great interest. In particular there is a class of slip line fields that contain straight slip lines. It can be shown easily that if one slip line of a given family is straight, then all slip lines of that family must be straight.

As shown in Figure 11.5, there are two most common stress fields that contain straight slip (or shear) lines and they are (a) constant stress states where slip lines are parallel to each other (b) transitional stress states where one family of slip lines meet at a point.

#### *Constant stress states*

If all the slip lines of one family are straight and parallel, then those of the other family must be likewise, as shown Figure 11.5(a). Since the value of  $\theta$  is constant it follows from equations (11.16)-(11.17) or (11.20)-(11.21) that for weightless soils the mean stress  $p$  is also constant. Therefore the stress field  $(\sigma_x, \sigma_y, \sigma_{xy})$  remains constant.

#### *Transitional stress states*

If the slip lines of one family are straight and meet at a point, those of the other family should be logarithmic arcs as shown in Figure 11.5(b). This system of slip lines is also called a centred fan. It will be shown later in this chapter that a number of

important problems can be solved by inserting a centred fan between two constant stress regions.

### 11.2.6 Boundary value problems and construction of slip line fields

The process of solving a boundary value problem using slip line analysis involves the construction of a complete slip line field from known boundary conditions for the stresses. For the case when soil self-weight can be ignored, analytical methods are possible in such a process. However, a numerical method (such as the finite difference method) would need to be used in order to include the effect of gravity (Booker and Davis, 1977; Walker, 2004; Martin, 2005). Collins (1982) presented a detailed description of alternative numerical methods of solution.

As discussed by Hill (1950), Booker (1970) and Booker and Davis (1977), several distinct types of slip line field construction are found to occur repeatedly in the problem solving process, often in the same problem in different parts of the plastic regions. Given below are the three most widely used boundary value problems.

#### *Initial characteristics or Riemann problem*

If two intersecting characteristics are known, then the slip line field between them is determined uniquely. Refer to Figure 11.6(a), the slip line field can be determined once we know the position and stress variables for OA and OB. The same procedure applies if the radius of curvature of one of the given slip lines, say OB, is allowed to become indefinitely small. In this special case, O is a singularity through which all  $\alpha$  lines pass, Figure 11.6(b).

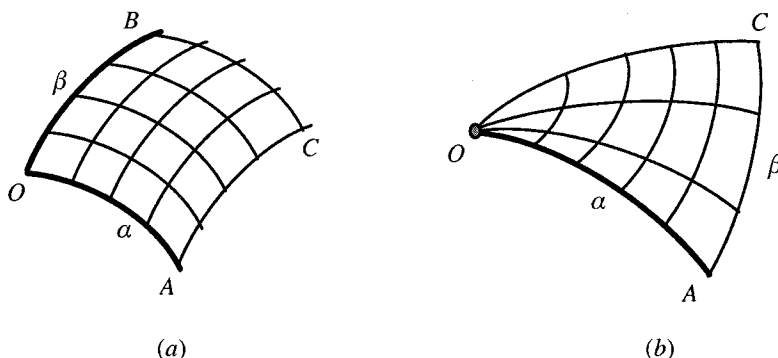


Figure 11.6: Initial characteristics or Riemann problem

#### *Cauchy problem*

If two stresses are known on an arc AC of a non-characteristic curve, then the slip line field is determined in the influence domain between the intersecting characteristics through A and C. A common example is when AB is a stress-free surface. Refer to Figure 11.7, the slip line field can be determined once we know the normal and shear stresses acting on OC.

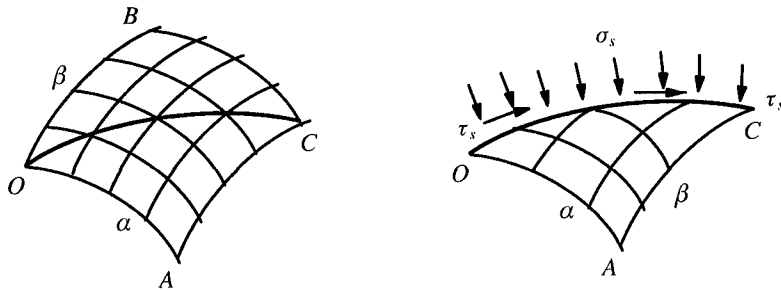


Figure 11.7: Cauchy problem

#### *Mixed or Goursat problem*

If one characteristic is given and one condition of stress (such as the direction of principal stress,  $\theta$ ) is specified on a non-characteristic curve, then the slip line field between these two curves is determined uniquely. A common example is the construction of the slip line field between a given slip line and a frictionless rigid boundary. Refer to Figure 11.8, the slip line field can be determined once we know the slip line OA and the direction of the principal stress on OC (i.e. the  $\theta$  value is given).

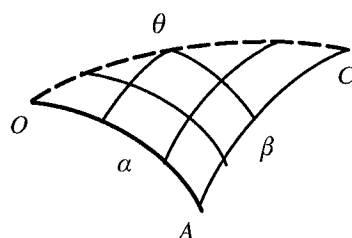


Figure 11.8: Mixed or Goursat problem

### 11.3 VELOCITY FIELDS IN PLASTIC REGIONS

For a rigid plastic material, there will be a constant distribution of velocities in the plastic regions at the onset of plastic collapse or failure. It is therefore necessary to determine such velocity fields for an exact solution to a given problem as it must also satisfy displacement boundary conditions apart from stress boundary conditions. Published slip line solutions of problems of interest to geomechanics have been almost exclusively for material obeying an associated flow rule, with an important exception in Cox (1963) where the effect of non-associated flow rules on failure loads was studied. For clarity, the governing equations of velocity fields for associated and non-associated flow rules will be presented separately.

#### 11.3.1 Velocity fields for associated flow rules

##### *Governing equations of velocity fields*

Let  $u_x$  and  $u_y$  be the velocity components in the  $x$  and  $y$  directions. The strain rates will be given by

$$\dot{\varepsilon}_x = \frac{\partial u_x}{\partial x} = \lambda \frac{\partial f}{\partial \sigma_x} \quad (11.31)$$

$$\dot{\varepsilon}_y = \frac{\partial u_y}{\partial y} = \lambda \frac{\partial f}{\partial \sigma_y} \quad (11.32)$$

$$\dot{\gamma}_{xy} = \frac{\partial u_x}{\partial y} + \frac{\partial u_y}{\partial x} = \lambda \frac{\partial f}{\partial \sigma_{xy}} \quad (11.33)$$

where  $\lambda$  is a positive plastic scalar and  $f$  denotes a yield function.

The Mohr-Coulomb yield function takes the following form

$$f = \sqrt{\frac{1}{4}(\sigma_y - \sigma_x)^2 + \sigma_{xy}^2} - \frac{1}{2}(\sigma_x + \sigma_y) \sin \phi - c \cos \phi = 0 \quad (11.34)$$

which can be substituted into equations (11.31)-(11.33) to give

$$\dot{\varepsilon}_x = -\frac{1}{2}\lambda(\sin \phi + \cos 2\theta) \quad (11.35)$$

$$\dot{\varepsilon}_y = -\frac{1}{2}\lambda(\sin \phi - \cos 2\theta) \quad (11.36)$$

$$\dot{\gamma}_{xy} = \pm \lambda \sin 2\theta \quad (11.37)$$

By adding equations (11.35) and (11.36), we obtain the following expression for the volumetric strain rate

$$\dot{\varepsilon}_v = \dot{\varepsilon}_x + \dot{\varepsilon}_y = -\lambda \sin \phi \quad (11.38)$$

from which it can be seen that for any friction angle greater than zero the plastic volumetric strain rate will be negative and therefore leads to dilation. Evidence suggests that the dilation predicted using this equation based on an associated flow rule is excessive. This is why we will study in the next section the velocity fields derived from the use of a non-associated flow rule.

The equations (11.35)-(11.37) can also be used to derive

$$\dot{\varepsilon}_x + \dot{\varepsilon}_y = -\dot{\gamma}_{xy} \sin \phi \operatorname{cosec} 2\theta \quad (11.39)$$

$$\dot{\varepsilon}_y - \dot{\varepsilon}_x = \dot{\gamma}_{xy} \cot 2\theta \quad (11.40)$$

Then by the use of equations (11.31)-(11.33), we obtain the following governing equations for velocities:

$$\frac{\partial u_x}{\partial x} + \cot 2\theta \frac{\partial u_y}{\partial y} + \cot 2\theta \frac{\partial u_x}{\partial x} - \frac{\partial u_y}{\partial y} = 0 \quad (11.41)$$

$$\frac{\partial u_x}{\partial x} + \sin \phi \operatorname{cosec} 2\theta \frac{\partial u_y}{\partial y} + \sin \phi \operatorname{cosec} 2\theta \frac{\partial u_x}{\partial x} + \frac{\partial u_y}{\partial y} = 0 \quad (11.42)$$

### *Solutions by the method of characteristics*

As for the stress field equations (11.8)-(11.9), the above equations governing the velocity fields cannot be solved easily without changing the coordinate system. Since they are hyperbolic, the best approach to solution is again by the use of the method of characteristics. Following a standard procedure it can be shown that the characteristics of the velocity equations are the same as those for stress equations. The slopes of the velocity characteristics are defined by

$$\frac{dx}{dy} = \tan(\theta \pm \mu) \quad (11.43)$$

where  $\mu = \pi/4 - \phi/2$ . As shown in Figure 11.1, the velocity (or stress) characteristics are equally disposed about the major principal stress direction.

To obtain the equations governing the variation in velocity along a velocity characteristic, we find it convenient to define two new velocities  $u_\alpha, u_\beta$  which are the components of the sum velocity projected along the two characteristics:

$$u_x = \frac{u_\beta \cos(\theta + \mu) - u_\alpha \cos(\theta - \mu)}{-\sin 2\mu} \quad (11.44)$$

$$u_y = \frac{u_\beta \sin(\theta + \mu) - u_\alpha \sin(\theta - \mu)}{\sin 2\mu} \quad (11.45)$$

By substituting the above equations into (11.41)-(11.42), we can obtain the following equations giving variation of velocity along velocity characteristics  $(\alpha, \beta)$

$$\cos \phi du_\alpha + (u_\beta - u_\alpha \sin \phi) d\theta = 0 \quad \text{along an } \alpha\text{-line} \quad (11.46)$$

$$\cos \phi du_\beta + (u_\beta \sin \phi - u_\alpha) d\theta = 0 \quad \text{along a } \beta\text{-line} \quad (11.47)$$

For a cohesive soil, the above velocity equations reduce to Geiringer's (1930) equations in metal plasticity

$$du_\alpha + u_\beta d\theta = 0 \quad \text{along an } \alpha\text{-line} \quad (11.48)$$

$$du_\beta - u_\alpha d\theta = 0 \quad \text{along a } \beta\text{-line} \quad (11.49)$$

that implies that the rate of extension along any slip line is zero.

It is instructive to compare the nature of the velocity equations with that of stress equations. With the stress equations, we have two equations and two stress variables  $p$  and  $\theta$ . So the system is statically determinate in the sense that the stress fields in the plastic region can be determined as long as the stress boundary conditions are known. The velocity equations, as defined in (11.46) and (11.47), are different. Now we have two equations but with three variables  $u_\alpha$ ,  $u_\beta$  and  $\theta$ . Therefore in general the velocity solutions are possible only after the stress solutions (and therefore  $\theta$ ) are determined.

### 11.3.2 Velocity fields for non-associated flow rules

#### *Governing equations of velocity fields*

Let  $u_x$  and  $u_y$  be the velocity components in the  $x$  and  $y$  directions. The strain rates will be given by

$$\dot{\varepsilon}_x = \frac{\partial u_x}{\partial x} = \lambda \frac{\partial g}{\partial \sigma_x} \quad (11.50)$$

$$\dot{\varepsilon}_y = \frac{\partial u_y}{\partial y} = \lambda \frac{\partial g}{\partial \sigma_y} \quad (11.51)$$

$$\dot{\gamma}_{xy} = \frac{\partial u_x}{\partial y} + \frac{\partial u_y}{\partial x} = \lambda \frac{\partial g}{\partial \sigma_{xy}} \quad (11.52)$$

where  $\lambda$  is a positive plastic scalar and  $g$  denotes a plastic potential which is different from the yield function.

For the non-associated Mohr-Coulomb plasticity, we often assume a plastic potential in the following form

$$g = \sqrt{\frac{1}{4}(\sigma_y - \sigma_x)^2 + \sigma_{xy}^2} - \frac{1}{2}(\sigma_x + \sigma_y) \sin \psi = \text{constant} \quad (11.53)$$

where  $\psi$  is the angle of dilation that ranges between zero and the angle of friction. By substituting the above plastic potential into equations (11.50)-(11.52) we have

$$\dot{\varepsilon}_x = -\frac{1}{2}\lambda(\sin \psi + \cos 2\theta) \quad (11.54)$$

$$\dot{\varepsilon}_y = -\frac{1}{2}\lambda(\sin \psi - \cos 2\theta) \quad (11.55)$$

$$\dot{\gamma}_{xy} = \pm \lambda \sin 2\theta \quad (11.56)$$

By adding equations (11.54) and (11.55), we obtain the following expression for the volumetric strain rate

$$\dot{\varepsilon}_v = \dot{\varepsilon}_x + \dot{\varepsilon}_y = -\lambda \sin \psi \quad (11.57)$$

from which it can be seen that for any dilation angle greater than zero the plastic volumetric strain rate will be negative and therefore lead to dilation. By setting a suitable dilation angle, the above equation can give prediction that is consistent with measurement. This is why the non-associated Mohr-Coulomb plasticity has found a wide application in geomechanics (Davis, 1968).

The equations (11.54)-(11.56) can also be used to derive

$$\dot{\varepsilon}_x + \dot{\varepsilon}_y = -\dot{\gamma}_{xy} \sin \psi \operatorname{cosec} 2\theta \quad (11.58)$$

$$\dot{\varepsilon}_y - \dot{\varepsilon}_x = \dot{\gamma}_{xy} \cot 2\theta \quad (11.59)$$

Then by the use of equations (11.50)-(11.52), we obtain the following governing equations for velocities:

$$\frac{\partial u_x}{\partial x} + \cot 2\theta \frac{\partial u_y}{\partial y} + \cot 2\theta \frac{\partial u_x}{\partial x} - \frac{\partial u_y}{\partial y} = 0 \quad (11.60)$$

$$\frac{\partial u_x}{\partial x} + \sin \psi \operatorname{cosec} 2\theta \frac{\partial u_y}{\partial y} + \sin \psi \operatorname{cosec} 2\theta \frac{\partial u_x}{\partial x} + \frac{\partial u_y}{\partial y} = 0 \quad (11.61)$$

### *Solutions by the method of characteristics*

As for the stress field equations (11.8)-(11.9), the above equations governing the velocity fields cannot be solved easily without changing the coordinate system. Since they are hyperbolic, the best approach to solution is again by the use of the method of characteristics. Following a standard procedure it can be shown that the characteristics of the velocity equations are not the same as those for stress equations. The slopes of the velocity characteristics are defined by

$$\frac{dx}{dy} = \tan(\theta \pm \mu') \quad (11.62)$$

where  $\mu' = \pi/4 - \psi/2$ . As shown in Figure 11.9, the velocity characteristics are equally disposed about the major principal stress direction.

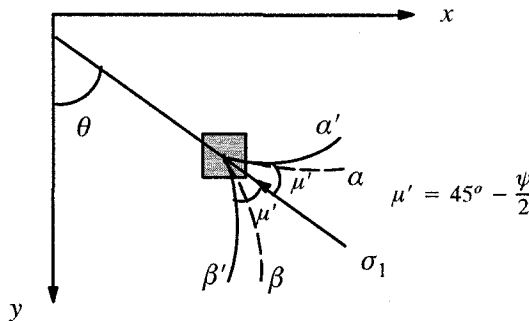


Figure 11.9: The velocity characteristics for non-associated flow rules

To obtain the equations governing the variation in velocity along a velocity characteristic, we find it convenient to define two new velocities  $u_{\alpha'}$ ,  $u_{\beta'}$  which are the components of the sum velocity projected along the two characteristics  $\alpha'$  and  $\beta'$

$$u_x = \frac{u_{\beta'} \cos(\theta + \mu') - u_{\alpha'} \cos(\theta - \mu')}{-\sin 2\mu'} \quad (11.63)$$

$$u_y = \frac{u_{\beta'} \sin(\theta + \mu') - u_{\alpha'} \sin(\theta - \mu')}{\sin 2\mu'} \quad (11.64)$$

By substituting the above equations into (11.41)-(11.42), we can obtain the following equations giving variation of velocity along velocity characteristics  $(\alpha', \beta')$

$$\cos \psi du_{\alpha'} + (u_{\beta'} - u_{\alpha'} \sin \psi) d\theta = 0 \quad \text{along an } \alpha'\text{-line} \quad (11.65)$$

$$\cos \psi du_{\beta'} + (u_{\beta'} \sin \psi - u_{\alpha'} d\theta) = 0 \quad \text{along a } \beta'\text{-line} \quad (11.66)$$

### 11.3.3 Discontinuities in velocity

A line across which there is a change in velocity field is termed a velocity discontinuity. In treating specific plastic problems, it proves essential to use the fact that the line separating a region in which plastic flow occurs from a region which remains at rest must be a velocity characteristic. Prager and Hodge (1951) prove this

for a cohesive material. We now follow Davis (1968) in proving that this is indeed the case for a general cohesive-frictional material.

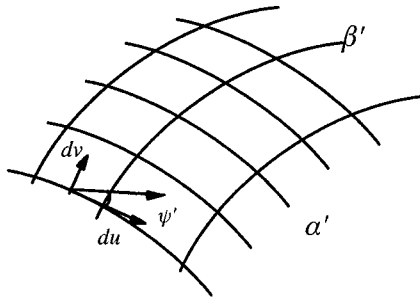


Figure 11.10: Velocity discontinuity for non-associated flow rules

For simplicity, we assume that the change (or jump) in normal and tangential velocities across a velocity discontinuity be  $du$  and  $dv$ . Without losing generality, we take the  $x$  direction tangential to the discontinuity and the  $y$  direction normal to it. Given the velocities on the rigid side of the discontinuity are zero, it then follows that the velocities on the plastically deforming side should be  $du$  and  $dv$ . We now use equations (11.60) and (11.61) to obtain the following two equations

$$du \cot 2\theta - dv = 0 \quad (11.67)$$

$$du \sin \psi \cosec 2\theta + dv = 0 \quad (11.68)$$

which can be combined to give

$$\theta = \pm \left( \frac{\pi}{4} + \frac{\psi}{2} \right) \quad (11.69)$$

$$\frac{dv}{du} = \mp \tan \psi \quad (11.70)$$

From the above two equations, it is an easy matter to conclude that the discontinuity must be a velocity characteristic and the resultant jump in velocity must be in a direction at  $\psi$  to the discontinuity. This is shown in Figure 11.10. It should be mentioned that the above discussion is for a non-associated flow rule. In the case of an associated flow rule, the conclusion should be modified as: the discontinuity must be a velocity characteristic and the resultant jump in velocity must be in a direction that forms an angle of  $\phi$  to the discontinuity.

### 11.3.4 Stress conditions on velocity characteristics

It should be noted that only velocity characteristics can be termed 'slip lines' as velocity discontinuities can occur across them. For materials with an associated flow rule, the stress and velocity characteristics are the same so the stress characteristics may also be termed 'slip lines'. However this is not the case with materials with a non-associated flow rule where the velocity characteristics are different from the stress characteristics. In other words, the stress characteristics for a non-associated material cannot be termed 'slip line'.

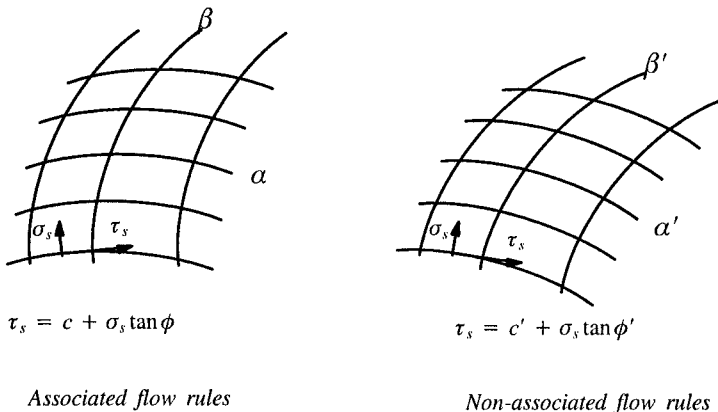


Figure 11.11: Stress conditions on velocity characteristics (i.e. slip lines)

Now let us consider the stress condition along velocity characteristics, Figure 11.11. We assume the shear and normal stresses acting on a velocity characteristic (i.e. a slip line) be denoted by  $\tau_s$  and  $\sigma_s$ . If the material obeys an associated flow rule, then the velocity characteristic or a slip line is also a stress characteristic on which by definition the stresses satisfy the Mohr-Coulomb yield criterion, namely

$$\tau_s = c + \sigma_s \tan \phi \quad (11.71)$$

where  $c$  and  $\phi$  are soil cohesion and friction angle. If the material obeys a non-associated flow rule, however, we know from a simple Mohr circle construction that the stresses on a velocity characteristic or a slip line do not satisfy the yield criterion, but are linked by the following equation

$$\tau_s = c' + \sigma_s \tan \phi' \quad (11.72)$$

in which

$$c' = \frac{c \cos \psi \cos \phi}{1 - \sin \psi \sin \phi} \quad (11.73)$$

$$\tan \phi' = \frac{\cos \psi \sin \phi}{1 - \sin \psi \sin \phi} \quad (11.74)$$

Therefore we should use  $c'$  and  $\phi'$  as measures of ‘cohesion’ and ‘friction angle’ on slip lines (Davis, 1968; Drescher and Detournay, 1993).

## 11.4 GEOTECHNICAL STABILITY EXAMPLES

In this section we present a few important examples that allow for analytical solutions of both stress and velocity fields at the state of plastic failure. In an analytical treatment, the effect of self-weight of soil has to be ignored. However the self-weight can be taken into account easily using a numerical integration method (e.g. Sokolovskii, 1965; Booker and Davis, 1977; Salencon, 1977).

### 11.4.1 Bearing capacity of embankments – stress fields

Figure 11.12 shows an embankment of cohesive-frictional soil subjected to a uniform surcharge on the slope. The slope makes an angle of  $\omega$  from the vertical direction. We are interested in the bearing capacity of the embankment if it is subjected to an uniform vertical load as shown in the figure.

Due to the symmetrical nature of the problem, we only need to consider half of the embankment. An inspection of the boundary conditions suggests that the slip line fields for this problem can be divided into three distinct zones:

#### *Zone I –Passive zone ACD*

Within zone ACD, the stress state is uniform. The boundary stress (surcharge  $q$ ) must be the minor principal stress due to its passive nature. Therefore the direction of the major principal stress is tangential to AD and this gives

$$\theta = \omega \quad (11.75)$$

Then from equation (11.30) we obtain the mean stress within Zone I as

$$p = \frac{q + c \cos \phi}{1 - \sin \phi} \quad (11.76)$$

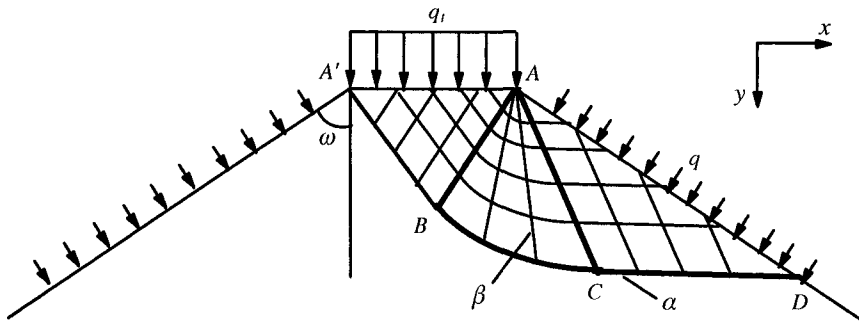


Figure 11.12: Plastic stress fields of embankments with surcharge on the slope

#### Zone III –Active zone AA'B

Within zone AA'B, the stress state is uniform. The boundary stress (the applied vertical load) must be the major principal stress. Therefore the direction of the major principal stress is tangential to the vertical (y) direction and this gives

$$\theta = 0 \quad (11.77)$$

Again from equation (11.30) we obtain the mean stress within Zone III as

$$p = \frac{q_t - c \cos \phi}{1 + \sin \phi} \quad (11.78)$$

#### Zone II –Transitional zone ABC

Within zone II, the stress state is not uniform but varies from the uniform zone III to zone I. The nature of this variation, for example, along the  $\alpha$  line is governed by equation (11.24). By substituting the values of  $(p, \theta)$  for zones I and III into equation (11.24), we readily obtain the value of vertical load at plastic collapse

$$q_t = (q + c \cot \phi) \tan^2 \left( \frac{\pi}{4} + \frac{\phi}{2} \right) e^{2\omega \tan \phi} - c \cot \phi \quad (11.79)$$

#### 11.4.2 Bearing capacity of embankments – velocity fields

Before the stress field obtained can be acceptable, we need to derive a kinematically admissible velocity field.

#### Zone III –Active zone AA'B

Now let us consider the velocity fields in the plastic zone, Figure 11.13. In the active zone AA'B, assume the vertical velocity is  $u_y = u_o$ . It is therefore easy to derive that within this zone the velocities along  $\alpha$  and  $\beta$  lines should be

$$u_\alpha = u_\beta = u_o \sin\left(\frac{\pi}{4} + \frac{\phi}{2}\right) \quad (11.80)$$

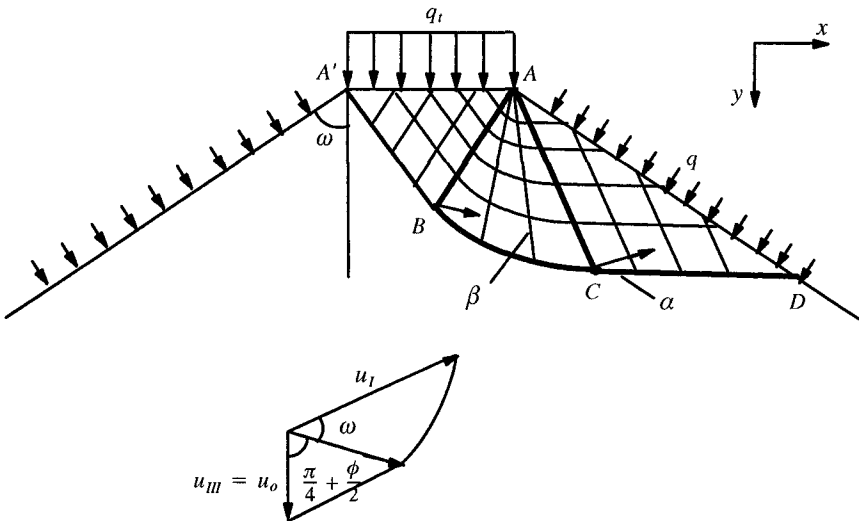


Figure 11.13: Velocity fields of embankments with surcharge on the slope

#### Zone II – Transitional zone ABC

Within the transitional zone, we know that at point B, the velocity along the  $\alpha$  line should be

$$u_\alpha = u_o \sin\left(\frac{\pi}{4} + \frac{\phi}{2}\right) \quad (11.81)$$

If we consider the  $\alpha$  line, BC, that separates the plastic zone from the rigid one. The velocity along the  $\beta$  line must be zero. Therefore from equation (11.46), we obtain

$$du_\alpha = u_\alpha \tan \phi d\theta \quad (11.82)$$

which can be integrated to give

$$u_\alpha = C_\alpha e^{\theta \tan \phi} \quad (11.83)$$

the integration constant  $C_\alpha$  can be determined from the boundary condition at point B where

$$u_a|_B = u_o \sin\left(\frac{\pi}{4} + \frac{\phi}{2}\right) \quad \text{for } \theta = 0 \quad (11.84)$$

The constant  $C_a$  is found to be

$$C_a = u_o \sin\left(\frac{\pi}{4} + \frac{\phi}{2}\right) \quad (11.85)$$

As a result the velocity variation along BC is governed by

$$u_a = u_o \sin\left(\frac{\pi}{4} + \frac{\phi}{2}\right) e^{\theta \tan \phi} \quad (11.86)$$

### *Zone I – Passive zone ACD*

Within zone ACD, the stress state is uniform and so is the velocity field. From the velocity variation along BC derived above we know that at point C the velocity along the  $\alpha$  line can be obtained by using  $\theta = \omega$

$$u_a|_C = u_o \sin\left(\frac{\pi}{4} + \frac{\phi}{2}\right) e^{\omega \tan \phi} \quad (11.87)$$

From the discussion previously on discontinuities in velocity we know that CD must be a discontinuity in velocity. The actual resultant velocity along CD forms an angle of  $\phi$  from CD. The magnitude can be derived from the following expression:

$$u_I = \frac{u_a|_C}{\cos \phi} = u_o \frac{\sin\left(\frac{\pi}{4} + \frac{\phi}{2}\right)}{\cos \phi} e^{\omega \tan \phi} \quad (11.88)$$

### **11.4.3 Bearing capacity of embankments – Hill's mechanism**

The stress and velocity solutions presented above are based on Prandtl's failure mechanism. Now we will study the same problem but by using a different failure mechanism as suggested by Hill (1950).

#### *Plastic stress fields*

The stress characteristics network for an embankment based on Hill's mechanism is shown in Figure 11.14. It is then an easy matter to show that the bearing capacity for the embankment using Hill's mechanism is the same as that derived previously using Prandtl's mechanism.

#### *Plastic velocity fields*

Although Hill's mechanism gives the same collapse load as that by Prandtl's mechanism, they lead to very different velocity fields. The velocity field from

Prandtl's mechanism has been described previously. Now we consider in detail the velocity field with Hill's failure mechanism.

### Zone III – Active zone AOB

Now let us consider the velocity fields in the plastic zone, Figure 11.14. Assume the vertical velocity of OA with loading  $q_t$  is  $u_y = u_o$ . It is therefore easy to derive that within this zone the total velocity within the active zone AOB should be

$$u_{III} = u_o / \cos(\frac{\pi}{4} + \frac{\phi}{2}) = u_o \sec(\frac{\pi}{4} + \frac{\phi}{2}) \quad (11.89)$$

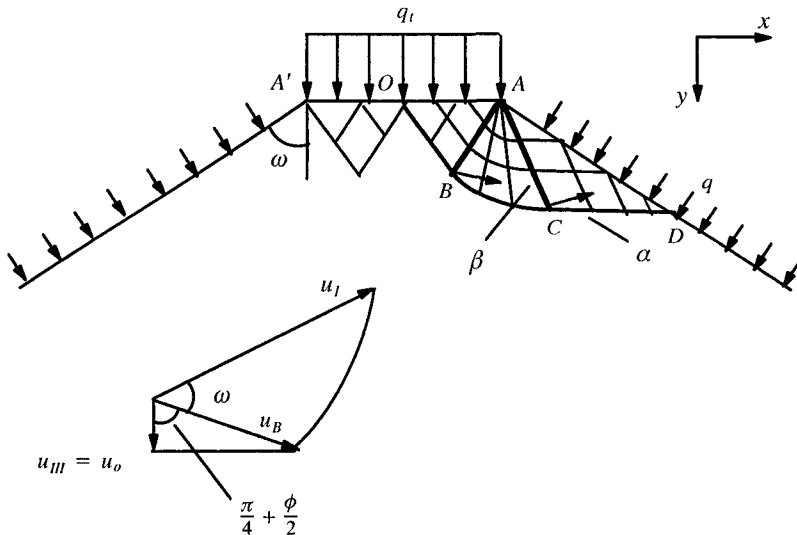


Figure 11.14: Stress and velocity fields of embankments based on Hill's mechanism

### Zone II – Transitional zone ABC

Within the transitional zone, we know that at point B, the velocity along the  $\alpha$  line should be

$$u_\alpha|_B = u_{III} \cos \phi = u_o \cos \phi \sec(\frac{\pi}{4} + \frac{\phi}{2}) \quad (11.90)$$

If we consider the  $\alpha$  line, BC, that separates the plastic zone from the rigid one. The velocity along the  $\beta$  line must be zero. Therefore from equation (11.46), we obtain

$$du_\alpha = u_\alpha \tan \phi d\theta \quad (11.91)$$

which can be integrated to give

$$u_\alpha = C_\alpha e^{\theta \tan \phi} \quad (11.92)$$

the integration constant  $C_\alpha$  can be determined from the boundary condition at point B where

$$u_\alpha|_B = u_o \cos \phi \sec\left(\frac{\pi}{4} + \frac{\phi}{2}\right) \quad \text{for } \theta = 0 \quad (11.93)$$

The constant  $C_\alpha$  is found to be

$$C_\alpha = u_o \cos \phi \sec\left(\frac{\pi}{4} + \frac{\phi}{2}\right) \quad (11.94)$$

As a result the velocity variation along BC is governed by

$$u_\alpha = u_o \cos \phi \sec\left(\frac{\pi}{4} + \frac{\phi}{2}\right) e^{\theta \tan \phi} \quad (11.95)$$

### Zone I –Passive zone ACD

Within zone ACD, the stress state is uniform and so is the velocity field. From the velocity variation along BC derived above we know that at point C the velocity along the  $\alpha$  line can be obtained by using  $\theta = \omega$

$$u_\alpha|_C = u_o \cos \phi \sec\left(\frac{\pi}{4} + \frac{\phi}{2}\right) e^{\omega \tan \phi} \quad (11.96)$$

From the discussion previously on discontinuities in velocity we know that CD must be a discontinuity in velocity. The actual resultant velocity along CD forms an angle of  $\phi$  from CD. The magnitude can be derived from the following expression:

$$u_I = \frac{u_\alpha|_C}{\cos \phi} = u_o \sec\left(\frac{\pi}{4} + \frac{\phi}{2}\right) e^{\omega \tan \phi} \quad (11.97)$$

This suggests that Hill's mechanism gives a different value for velocity fields from that predicted using Prandtl's mechanism.

#### 11.4.4 Shallow foundations on a cohesive-frictional soil

When the angle  $\omega = \pi/2$ , the embankment problem we have just considered becomes a shallow foundation problem. This is shown in Figure 11.15.

##### Plastic stress fields in the plastic zone

The bearing capacity of a surface footing with a surcharge can then be obtained from equation (11.79) by using  $\omega = \pi/2$

$$q_t = (q + c \cot \phi) \tan^2 \left( \frac{\pi}{4} + \frac{\phi}{2} \right) e^{\pi \tan \phi} - c \cot \phi \quad (11.98)$$

This solution for a surface footing is known as Prandtl's solution. The above solution can be further expressed in terms of contributions from cohesion and surcharge as follows

$$q_t = N_c c + N_q q \quad (11.99)$$

where

$$N_q = \tan^2 \left( \frac{\pi}{4} + \frac{\phi}{2} \right) e^{\pi \tan \phi} \quad (11.100)$$

$$N_c = (N_q - 1) \cot \phi \quad (11.101)$$

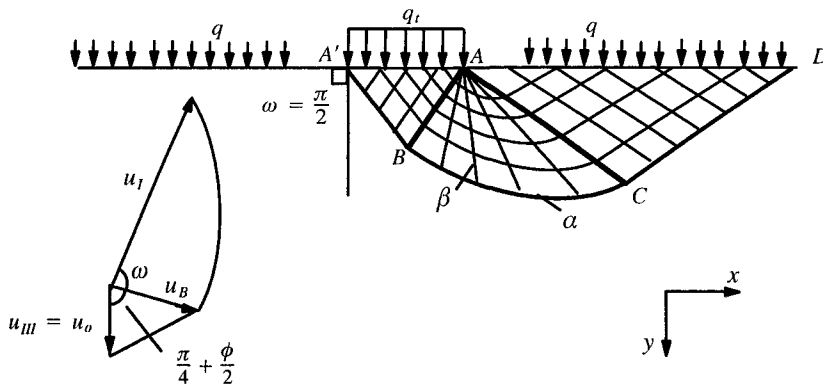


Figure 11.15: Bearing capacity of surface foundations with surcharge

#### Velocity fields in the plastic zone

The velocity fields in the plastic zone for a shallow foundation based on Prandtl's mechanism are derived from the solutions for the embankment by putting  $\omega = \pi/2$ . The velocity diagram is shown in Figure 11.15.

#### Complete solution by extending stresses into the rigid region

The plastic stress solutions obtained so far may not be regarded as an exact (or complete) solution (Bishop, 1953). This is because these stresses have only been shown to satisfy the yield condition and equilibrium equations in the plastic zone. Nothing has been said as to whether such a stress field can be extended into the rigid region without violating the yield condition.

In the terminology of Bishop (1953), these stresses are termed a partial stress field or an incomplete solution. In addition to meeting the equilibrium equations and yield condition, if a satisfactory velocity field can be found that is associated with such a stress field and also satisfies the displacement boundary conditions, then such an incomplete solution may be regarded as an upper bound solution.

Suppose, however, that the partial stress field can be extended to the entire body, satisfying the equilibrium equations, yield criterion and the stress boundary conditions. It can be regarded as a lower bound solution. The solution obtained should then be treated as an exact or actual solution since it is proved to be both an upper bound and a lower bound solution. The uniqueness of the stress field is confirmed by Hill (1951) who proved that where deformation is actually occurring in any mode, the stress found is the actual state.

Shield (1954) first extended the incomplete stress solution into the rigid region in a statically admissible manner for cohesive-frictional materials, and as a result the collapse load defined by (11.99) is also a lower bound and therefore the true value of the average pressure at failure. Details of such a stress extension procedure can be found in Phillips (1956) and Randolph and Housby (1984).

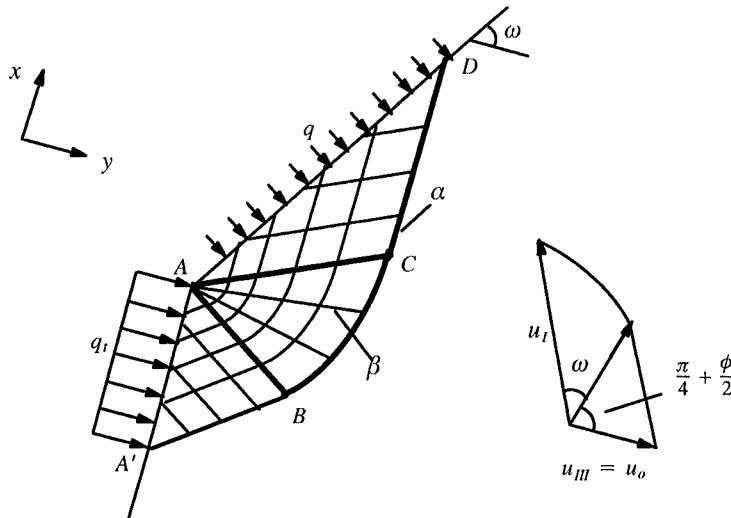


Figure 11.16: Plastic stress fields of passive loading of a retaining wall

#### 11.4.5 Retaining walls on a cohesive-frictional soil

It is worth noting that the solution derived earlier for the vertical loading of an embankment on a cohesive-frictional soil can also be used to give solutions for prob-

lems of retaining walls such as that shown in Figure 11.16. For example the pressure for passive loading of a retaining wall is

$$q_t = (q + c \cot \phi) \tan^2 \left( \frac{\pi}{4} + \frac{\phi}{2} \right) e^{2\omega \tan \phi} - c \cot \phi \quad (11.102)$$

where  $\omega$  is defined in Figure 11.16.

#### 11.4.6 Pseudo-steady wedge penetration into a cohesive-frictional soil

We now consider a pseudo-steady wedge penetration into a semi-infinite mass of cohesive-frictional soil, Figure 11.17. With pseudo-steady plastic flow, the slip line pattern, while not remaining fixed as in the problem of steady flow, retains its shape and changes only in size. The solution for this problem in a purely cohesive soil with the Tresca model was first derived by Hill *et al.* (1947). The extension to a cohesive-frictional soil was later made by Shield (1953). In this section we will follow Shield closely and present the cohesive-frictional solution. The solution for the special case of a purely cohesive soil, as described by Hill (1950) and Prager and Hodge (1951), will be given briefly in a later section.

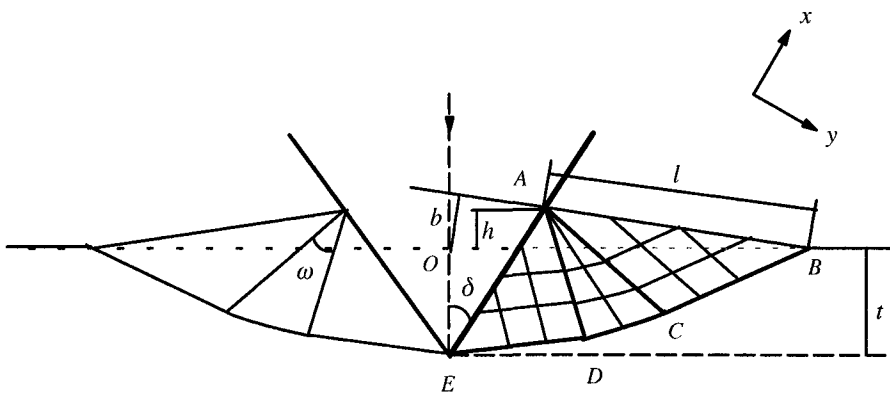


Figure 11.17: Steady wedge penetration into cohesive-frictional soils

As the wedge is pushed into the soil, the displaced soil will form a raised lip at each side of the wedge, and the shape of the lip has to be determined as part of the solution to the problem. Following Hill (1950), Shield (1953) assumes that the surfaces of the lips are straight and shows a solution exists that satisfies this assumption. The pattern of the stress characteristics, and therefore slip lines for associated flow rules, are plotted in Figure 11.17.

We denote by  $l$  the length AB of the lip, by  $b$  the distance of O from AB, and by  $h$  the elevation of A above OB. The depth of the penetration of the wedge is denoted by  $t$  and if the downward velocity of the wedge is assumed as the unit of velocity, we may take  $t$  to be the time variable. The lip AB makes an angle of  $\delta - \omega$  with the undisturbed level OB and it is easily shown that we have the following expressions for  $l$ ,  $b$ ,  $h$  in terms of  $t$ ,  $\delta$ ,  $\omega$ :

$$l = \frac{t}{e^{-\omega \tan \phi} \tan(\frac{\pi}{4} - \frac{\phi}{2}) \cos \delta - \sin(\delta - \omega)} \quad (11.103)$$

$$h = \frac{t \sin(\delta - \omega)}{e^{-\omega \tan \phi} \tan(\frac{\pi}{4} - \frac{\phi}{2}) \cos \delta - \sin(\delta - \omega)} \quad (11.104)$$

$$b = \frac{t \sin(\delta - \omega) [e^{-\omega \tan \phi} \tan(\frac{\pi}{4} - \frac{\phi}{2}) \sin \delta + \cos(\delta - \omega)]}{e^{-\omega \tan \phi} \tan(\frac{\pi}{4} - \frac{\phi}{2}) \cos \delta - \sin(\delta - \omega)} \quad (11.105)$$

In the active zone of ADE,  $u_\alpha$  is a constant and is linked to the the velocity of ADE

$$u_\alpha = u_{ADE} \cos \phi \quad (11.106)$$

The boundary condition along AE requires that the velocity of the wedge and that of the soil in contact with it must have the same projection on the normal to AE, and based on this we can obtain

$$u_{ADE} = \sin \delta \sec(\frac{\pi}{4} + \frac{\phi}{2}) \quad (11.107)$$

noting the downward velocity of the wedge is assumed to be a unit.

In the zone of radial shear, the velocity increases exponentially along each  $\alpha$  line. It can be shown that along AC the velocity vector has the constant value

$$u_{AC} = \sin \delta \sec(\frac{\pi}{4} + \frac{\phi}{2}) e^{\omega \tan \phi} \quad (11.108)$$

Given the passive zone ABC has a state of uniform stress and is therefore moving as a rigid body with velocity  $u_{AC}$  in the direction that is normal to AC, the projection of the velocity of the lip AB on the normal to AB is

$$u_{AC} \cos(\frac{\pi}{4} - \frac{\phi}{2}) = \sin \delta \tan(\frac{\pi}{4} + \frac{\phi}{2}) e^{\omega \tan \phi} \quad (11.109)$$

while the projection of the velocity of the vertex E, that is moving downward with unit velocity, on the normal to AB is  $\cos(\delta - \omega)$ . Hence the distance of E from AB

increases at a constant rate which is the sum of these two projections. At a time  $t$ , the distance of E from AB has therefore reached the following value

$$t[\sin \delta \tan(\frac{\pi}{4} + \frac{\phi}{2})e^{\omega \tan \phi} + \cos(\delta - \omega)] \quad (11.110)$$

From the geometry of Figure 11.17, we can see that this distance is also equal to

$$b + t \cos(\delta - \omega) \quad (11.111)$$

By equating expressions (11.110) and (11.111), we have

$$b = t \sin \delta \tan(\frac{\pi}{4} + \frac{\phi}{2})e^{\omega \tan \phi} \quad (11.112)$$

By substituting equation (11.112) into equation (11.105), we can obtain

$$\cos(2\delta - \omega) = \frac{\cos \omega [e^{\omega \tan \phi} \tan(\frac{\pi}{4} + \frac{\phi}{2}) + e^{-\omega \tan \phi} \tan(\frac{\pi}{4} - \frac{\phi}{2})]}{2 \sin \omega + e^{\omega \tan \phi} \tan(\frac{\pi}{4} + \frac{\phi}{2}) + e^{-\omega \tan \phi} \tan(\frac{\pi}{4} - \frac{\phi}{2})} \quad (11.113)$$

which determines how the angle of  $\omega$  would vary with the wedge half angle  $\delta$  and the angle of friction  $\phi$ .

Once the slip line network ( $\omega$ ) is determined, it is a relatively easy matter to derive the vertical pressure acting on the wedge. This is found to be

$$q_t = c \cot \phi [e^{2\omega \tan \phi} \tan^2(\frac{\pi}{4} + \frac{\phi}{2}) - 1] \quad (11.114)$$

#### 11.4.7 Solutions accounting for non-associated flow rules

For all the solutions presented so far, we assume that the soil obeys an associated flow rule. In this case, the stress characteristics coincide with the velocity characteristics. However in reality the flow rule of a cohesive-frictional material is non-associated which means that the angle of dilation is not the same but much less than the angle of friction. In this case, the velocity characteristics are governed by equation (11.62), and are different from the stress characteristics defined by equation (11.43).

Cox (1963) appears to have been the first to study the velocity characteristics of a non-associated flow rule by considering the angle of dilation as zero. In this special case (which is reasonable for loose frictional soils), the plastic volumetric strain is zero according equation (11.57).

For zero dilation ( $\psi = 0$ ), the velocity equations are

$$\frac{\partial u_x}{\partial x} + \cot 2\theta \frac{\partial u_y}{\partial y} + \cot 2\theta \frac{\partial u_x}{\partial x} - \frac{\partial u_y}{\partial y} = 0 \quad (11.115)$$

$$\frac{\partial u_x}{\partial x} + \frac{\partial u_y}{\partial y} = 0 \quad (11.116)$$

for which there are the following two velocity characteristics,  $\alpha'$  and  $\beta'$  lines, as defined below

$$\frac{dx}{dy} = \tan(\theta \pm \frac{\pi}{4}) \quad (11.117)$$

which are now orthogonal, depending only on the direction of the major principal stress, which is known from the solution for the stress field.

In the usual way, we can obtain the following equations giving variation of velocity along velocity characteristics ( $\alpha', \beta'$ )

$$du_{\alpha'} + u_{\beta'} d\theta = 0 \quad \text{along an } \alpha'\text{-line} \quad (11.118)$$

$$du_{\beta'} - u_{\alpha'} d\theta = 0 \quad \text{along a } \beta'\text{-line} \quad (11.119)$$

Following the study of Cox (1963), we can plot for the case of zero dilation angle both the stress characteristics and velocity characteristics for a footing with Hill's failure mechanism in Figure 11.18. It can be seen that the velocity characteristics are more complex than the stress characteristics.

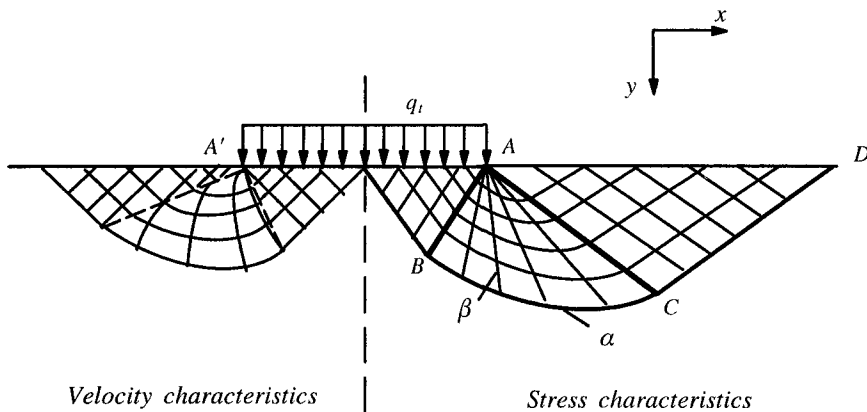


Figure 11.18: Velocity characteristics for a non-associated flow rule  
(adopted from Cox, 1963)

For the case of Prandtl's failure mechanism, the slip line network is similar to that shown in Figure 11.18. Examples are also given in Davis (1968) and Salencon (1977).

### 11.4.8 Special solutions for a purely cohesive soil

For purely cohesive soils where the angle of friction is zero, the solutions are well known as they are the same as those obtained in metal plasticity by Hill (1950), Prager and Hodge (1951) and Bishop (1953). In this case, the slip line field is simpler as in Zones I and III, the  $\alpha$  and  $\beta$  lines are normal to each other. In the transitional zone II, the  $\alpha$  line is part of a circle.

#### *Embankment made of cohesive soils*

The solution for the vertical load on an embankment with a surcharge can be shown to be

$$q_t = q + 2(1 + \omega)c \quad (11.120)$$

#### *Shallow foundations on cohesive soils*

The bearing capacity of a shallow foundation can be obtained from equation (11.120) and  $\omega = \pi/2$ . The solution is well-known

$$q_t = q + (2 + \pi)c \quad (11.121)$$

It should be noted that it was Bishop (1953) who first extended the stress field into the rigid region in a statically admissible manner for cohesive materials and therefore established the solution (11.121) as the exact solution for foundation problems in cohesive materials.

#### *Wedge penetration into cohesive soils*

The solution for this problem was derived by Hill *et al.* (1947) and also presented in detail by Prager and Hodge (1951). The procedure used was the same as that used earlier for solving the same problem in cohesive-frictional soils. It is found that the angle  $\omega$  is linked to the wedge angle  $\delta$

$$2\delta = \omega + \cos^{-1} \tan\left(\frac{\pi}{4} - \frac{\omega}{2}\right) \quad (11.122)$$

Once the angle  $\omega$  is determined the pressure acting on the wedge can be calculated by

$$q_t = 2c(1 + \omega) \quad (11.123)$$

## 11.5 PLASTIC ANISOTROPY

The governing equations and plastic solutions described so far are only valid for an isotropic yield criterion. The Mohr-Coulomb yield function is defined as follows

$$f(\sigma_x, \sigma_y, \sigma_{xy}) = R - (p + c \cot \phi) \sin \phi = 0 \quad (11.124)$$

where

$$R = \sqrt{\left(\frac{\sigma_x - \sigma_y}{2}\right)^2 + \sigma_{xy}^2} \quad (11.125)$$

$$p = \frac{\sigma_x + \sigma_y}{2} \quad (11.126)$$

The cross section of the yield criterion (11.124) with a constant  $Z$  is a circle in the space of  $(X, Y, Z)$  with  $X = (\sigma_x - \sigma_y)/2$ ,  $Y = \sigma_{xy}$  and  $Z = (\sigma_x + \sigma_y)/2 = p$ . This is because the yield criterion can also be expressed in the following form:

$$X^2 + Y^2 = [(Z + c \cot \phi) \sin \phi]^2 \quad (11.127)$$

which is plotted in Figure 11.19, where the radius of the circle depends on the value of mean pressure  $Z$ .

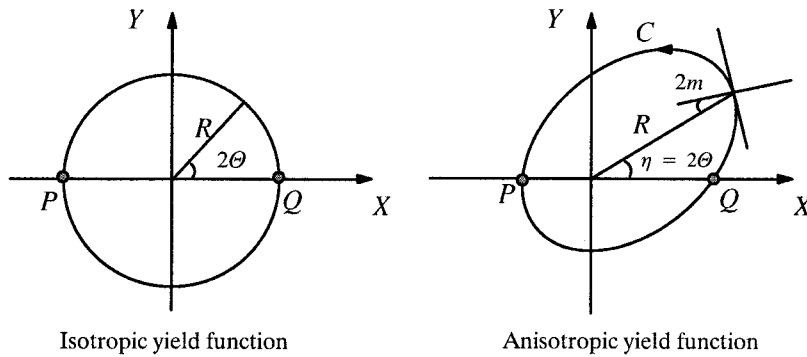


Figure 11.19: The isotropic and anisotropic Mohr-Coulomb yield surfaces in X-Y stress space

### 11.5.1 Solution for a general anisotropic cohesive-frictional material

In a significant paper, Booker and Davis (1972) presented an extension of the slip line equations for the isotropic Mohr-Coulomb condition to a general anisotropic criterion, which contains Hill's (1950) earlier treatment as a special case. In Booker and Davis (1972), the yield condition considered is of the following general form:

$$f(\sigma_x, \sigma_y, \sigma_{xy}) = R - F(p, \Theta) = 0 \quad (11.128)$$

or in terms of  $X, Y, Z$  it takes the form

$$X^2 + Y^2 = (F(Z, \Theta))^2 \quad (11.129)$$

where  $F$  is a known function of the mean pressure  $Z$  and the direction of principal stress

$$\tan(2\Theta) = \frac{2\sigma_{xy}}{\sigma_x - \sigma_y} \quad (11.130)$$

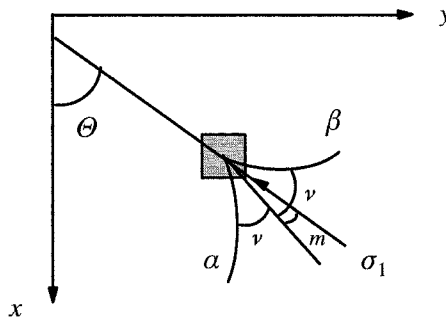


Figure 11.20: The coordinate system and stress characteristics for anisotropic plasticity

Referring to the coordinate system shown in Figure 11.20, the equations of equilibrium are

$$\frac{\partial\sigma_x}{\partial x} + \frac{\partial\sigma_{xy}}{\partial y} = \gamma \quad (11.131)$$

$$\frac{\partial\sigma_{xy}}{\partial x} + \frac{\partial\sigma_y}{\partial y} = 0 \quad (11.132)$$

Note that  $x$  is used to denote the direction of gravity. It proves useful to use Mohr's stress representation

$$\sigma_x = p + R \cos 2\Theta \quad (11.133)$$

$$\sigma_y = p - R \cos 2\Theta \quad (11.134)$$

$$\sigma_{xy} = R \sin 2\Theta \quad (11.135)$$

If we substitute the above three equations into the equations of equilibrium (11.131) and (11.132), it is found that the resultant equations are hyperbolic. To simplify the mathematics, we now introduce the following variables  $m$  and  $\nu$  defined by

$$\tan(2m) = \frac{1}{2F} \frac{\partial F}{\partial \Theta} \quad (11.136)$$

$$\cos(2\nu) = \cos(2m) \frac{\partial F}{\partial p} \quad (11.137)$$

Booker and Davis (1972) show that the characteristics of (11.131)-(11.135) are

$$\frac{dy}{dx} = \tan(\xi_\alpha) = \tan(\Theta - m - \nu) \quad (11.138)$$

$$\frac{dy}{dx} = \tan(\xi_\beta) = \tan(\Theta - m + \nu) \quad (11.139)$$

Integrals of (11.138) and (11.139) are called  $\alpha$  and  $\beta$  lines. The equilibrium equations may be written as follows

$$\sin[2(m - \nu)] \frac{\partial p}{\partial \alpha} + 2F \frac{\partial \Theta}{\partial \alpha} + \gamma \cos(2m) [\sin(2\nu) \frac{\partial x}{\partial \alpha} + \cos(2\nu) \frac{\partial y}{\partial \alpha}] = 0 \quad (11.140)$$

$$\sin[2(m + \nu)] \frac{\partial p}{\partial \beta} + 2F \frac{\partial \Theta}{\partial \beta} + \gamma \cos(2m) [-\sin(2\nu) \frac{\partial x}{\partial \beta} + \cos(2\nu) \frac{\partial y}{\partial \beta}] = 0 \quad (11.141)$$

which are hyperbolic if the characteristics (11.138) and (11.139) are real and distinct. It is noted that the angle  $m$  defined by (11.136) has a simple geometric interpretation, which is shown in Figure 11.19, where C is the intersection of the three-dimensional yield surface with the plane  $Z=p=\text{constant}$ .

### 11.5.2 Solution for a purely cohesive material

If the yield function is independent of mean pressure, that is  $F = F(\Theta)$ , therefore from equations (11.136) and (11.137), we have  $m = m(\Theta)$  and  $\nu = \pi/4$ . Equations (11.140) and (11.141) can be reduced to

$$-\frac{\partial \bar{p}}{\partial \alpha} + 2F \sec(2m) \frac{\partial \Theta}{\partial \alpha} = 0 \quad (11.142)$$

$$\frac{\partial \bar{p}}{\partial \beta} + 2F \sec(2m) \frac{\partial \Theta}{\partial \beta} = 0 \quad (11.143)$$

where  $\bar{p} = p - \gamma x$ . Referring to Figure 11.19, we denote by  $S(\eta)$  the arc length of the curve C starting from point Q. It can be shown that

$$\frac{dS}{d\eta} = R \sec(2m) \quad (11.144)$$

with which equations (11.142) and (11.143) can be rewritten as follows

$$-\frac{\partial \bar{p}}{\partial \alpha} + \frac{\partial S}{\partial \alpha} = 0 \quad (11.145)$$

$$\frac{\partial \bar{p}}{\partial \beta} + \frac{\partial S}{\partial \beta} = 0 \quad (11.146)$$

and therefore

$$\bar{p} - S(2\Theta) = \text{constant} \quad \text{on an } \alpha\text{-line} \quad (11.147)$$

$$\bar{p} + S(2\Theta) = \text{constant} \quad \text{on a } \beta\text{-line} \quad (11.148)$$

It is noted that the solutions (11.147) and (11.148) have also been derived by Rice (1972) independently.

Both Booker and Davis (1972) and Rice (1972) have applied the above solutions to derive the bearing capacity of a smooth strip footing in clay modelled by a general anisotropic yield surface. The bearing capacity solution is simply expressed as follows

$$q = \bar{PQ} + S \quad (11.149)$$

where  $S$  is the minimum arc length between points  $P$  and  $Q$ , shown in Figure 11.19. This solution reduces to the special solutions of Hill (1950) and Davis and Christian (1971) when their special yield surfaces are used. In addition, for the special case of an isotropic Tresca model, the solution (11.149) leads to the following well-known solution

$$q = \bar{PQ} + S = 2c + \pi c = (2 + \pi)c \quad (11.150)$$

## 11.6 AXISYMMETRIC PROBLEMS

Slip line analysis was initially developed for plane strain problems. Its successful application to the analysis of axisymmetric problems was made by Shield (1955) for Tresca materials and later by Cox *et al.* (1961) for Mohr-Coulomb materials. For axisymmetric problems, there is a need to make the assumption (Haar and von Karman, 1909) that the hoop stress is either the major or minor principal stress.

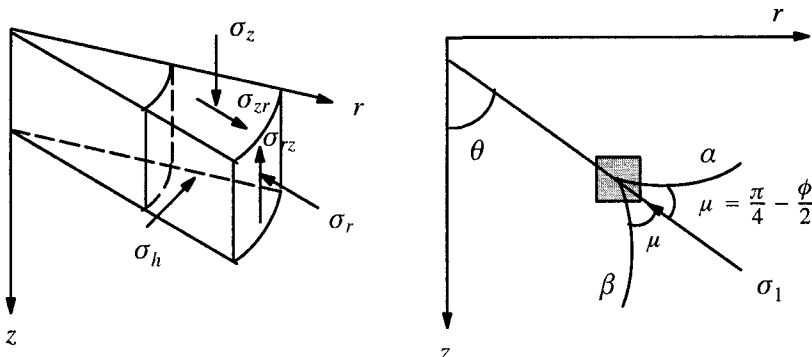


Figure 11.21: The coordinate system and stress characteristics for axisymmetric problems

### 11.6.1 Basic equations in terms of stresses

#### *Equilibrium equations*

Referring to the axisymmetric coordinate system shown in Figure 11.21, we have the following two equations of equilibrium under axisymmetric conditions:

$$\frac{\partial \sigma_r}{\partial r} + \frac{\partial \sigma_{rz}}{\partial z} = -\frac{\sigma_r - \sigma_h}{r} \quad (11.151)$$

$$\frac{\partial \sigma_{rz}}{\partial r} + \frac{\partial \sigma_z}{\partial z} = \gamma - \frac{\sigma_{rz}}{r} \quad (11.152)$$

where  $\gamma$  is the unit weight of the material in the  $z$  direction and  $\sigma_h$  is the hoop stress (which is assumed to be equal to either the major or minor principal stress).

By substituting equations (11.3)-(11.5) into equilibrium equations (11.151)-(11.152), we obtain the following governing equations

$$\begin{aligned} \frac{\partial p}{\partial z} (1 + \sin \phi \cos 2\theta) + \frac{\partial p}{\partial r} \sin \phi \sin 2\theta \\ + 2R(-\frac{\partial \theta}{\partial z} \sin 2\theta + \frac{\partial \theta}{\partial r} \cos 2\theta) = \gamma' \sin \alpha \end{aligned} \quad (11.153)$$

$$\begin{aligned} \frac{\partial p}{\partial z} \sin \phi \sin 2\theta + \frac{\partial p}{\partial r} (1 - \sin \phi \cos 2\theta) \\ + 2R(\frac{\partial \theta}{\partial z} \cos 2\theta + \frac{\partial \theta}{\partial r} \sin 2\theta) = \gamma' \cos \alpha \end{aligned} \quad (11.154)$$

where  $p$  and  $R$  are mean stress and the radius of the Mohr stress circle, namely

$$p = \frac{1}{2}(\sigma_r + \sigma_z) = \frac{1}{2}(\sigma_1 + \sigma_3) \quad (11.155)$$

$$R = (p + c \cot \phi) \sin \phi \quad (11.156)$$

and  $\gamma'$  is an equivalent bulk unit weight at an orientation  $\alpha$ , which accounts for the effects of the additional terms in the axial symmetry equilibrium equations when compared with plane strain cases (Houlsby and Wroth, 1982). It is easily shown

$$\gamma' \sin \alpha = -\frac{\sigma_r - \sigma_h}{r} \quad (11.157)$$

$$\gamma' \cos \alpha = \gamma - \frac{\sigma_{rz}}{r} \quad (11.158)$$

As noted by Houlsby and Wroth (1982), by setting  $\gamma' = \gamma$ ,  $\alpha = 0$ , the governing equations (11.153) and (11.154) in axisymmetry reduce to those for plane strain problems.

Equations (11.153) and (11.154) are two simultaneous first order partial differential equations governing the variation of the stress state in terms of  $(p, \theta)$ . For prob-

lems with known stress boundary conditions, the above two equations can be used to determine two unknowns  $(p, \theta)$ , which can then be used to derive the stress components  $(\sigma_r, \sigma_z, \sigma_{rz})$ .

### 11.6.2 Solution using the method of characteristics

The best way of solving the governing equations (11.153)-(11.154) is using the so-called method of characteristics (Hill, 1950). This is because the equations are hyperbolic. In this method, the equations are re-expressed along two characteristic directions so that integration can be readily carried out. Following the method outlined in Cox *et al.* (1961) and Kachanov (1974), it can be shown that the two characteristics  $(\alpha, \beta)$  for the two equations (11.153)-(11.154) are defined by

$$\frac{dr}{dz} = \tan(\theta \pm \mu) \quad (11.159)$$

where  $\mu = \pi/4 - \phi/2$  as shown in Figure 11.21. It can be shown that the two characteristics defined in (11.159) represent the two failure planes on which the failure criterion is satisfied. This is why they are also termed *slip lines* or shear lines which refer to two dimensions.

Along the directions of  $(\alpha, \beta)$ , the variation of stress state in a plastic region can be shown to be as follows:

$$dp \cos \phi + 2(c \cos \phi + p \sin \phi)d\theta = \gamma' \sin(\alpha - \phi)dr + \gamma' \cos(\alpha - \phi)dz \quad (11.160)$$

$$dp \cos \phi - 2(c \cos \phi + p \sin \phi)d\theta = \gamma' \sin(\alpha + \phi)dr + \gamma' \cos(\alpha + \phi)dz \quad (11.161)$$

which can be solved for given boundary conditions. Detailed applications can be found in Shield (1955), Cox *et al.* (1961), Lockett (1962), Housby (1982), Bolton and Lau (1993) and Walker (2004) among others.

## REFERENCES

- Bishop, J.F.W. (1953). On the complete solutions of deformation of a plastic rigid material, *J. Mech. Phys. Solids*, Vol 2, 43-53.
- Booker, J.R. (1970). *Applications of Theories of Plasticity to Cohesive Frictional Soils*, PhD Thesis, University of Sydney, NSW.
- Booker, J.R. and Davis, E.H. (1972). A general treatment of plastic anisotropy under conditions of plane strain, *J. Mech. Phys. Solids*, Vol 20, 239-250.
- Booker, J.R. and Davis, E.H. (1977). Stability analysis by plasticity theory, In: *Numerical Methods in Geotechnical Engineering*, (Editors: C. Desai and J. Christian), 719-748.
- Bolton, M.D. and Lau, C.K. (1993). Vertical bearing capacity factors for circular and strip footings on Mohr-Coulomb soil, *Canadian Geotech. J.*, Vol 30, 1024-1033.

Collins, I.F. (1982). Boundary value problems in plane strain plasticity. In: *Mechanics of Solids*, (Editors: H G Hopkins and M J Sewell), 135-184.

Cox, A.D. (1963). The use of non-associated flow rules in soil plasticity, *RARDE Report (b) 2/63*.

Cox, A.D., Eason, G. and Hopkins, H.G. (1961). Axially symmetric plastic deformation of soils, *Phil. Trans. Roy. Soc. A.*, Vol 254, 1-45.

Davis, E.H. (1968). Theories of plasticity and the failure of soil masses, In: *Soil Mechanics: Selected Topics*, (Editor: I. K. Lee), Butterworths, London, 341-380.

Davis, E.H. and Christian, J.T. (1971). Bearing capacity of anisotropic cohesive soils, *J. Soil Mech. Founds. Div.*, ASCE, Vol 97, 753-769.

Drescher, A. and Detournay, E. (1993). Limit load in translational failure mechanisms for associative and non-associative materials. *Geotechnique*, Vol. 43, 443-456.

Haar, A. and Karman, Th. (1909). Zur Theorie der Spannungszustände in plastischen und sandartigen Medien, *Nachr. Ges. Wiss. Gottingen, Math. Phys. Kl.*, 204-218.

Hill, R. (1950). *The Mathematical Theory of Plasticity*, Clarendon Press, Oxford.

Hill, R. (1951). On the state of stress in a plastic-rigid body at the yield point, *Phil. Mag.*, Vol 42, 868-875.

Hill, R., Lee, E.H. and Tupper, S.J. (1947). The theory of wedge indentation of ductile materials, *Proc. R. Soc. A.*, Vol 188, 273-289.

Houlsby, G.T. (1982). Theoretical analysis of the fall cone test, *Geotechnique*, Vol 32, 111-118.

Houlsby, G.T. and Wroth, C.P. (1982). Direct solution of plasticity problems in soils by the method of characteristics, *Proc. 4th Int. Conf. Num. Meth. Geomech.*, Edmonton, Vol 3, 1059-1071.

Kachanov, L.M. (1974). *Fundamentals of the Theory of Plasticity*. Mir Publishers, Moscow.

Lockett, F.J. (1962). Indentation of a rigid/plastic material by a conical indenter. *J. Mech. Phys. Solids*, Vol 11, 345-356.

Martin, C.M. (2005). Exact bearing capacity calculations using the method of characteristics, *Proc. 11th Int. Conf. of IACMAG*, (Editors: G Barla and M. Barla), Patron Editore, Vol 4, 411-450.

Phillips, A. (1956). *Introduction to Plasticity*, Ronald Press, New York.

Prager, W. and Hodge, P.G. (1951). *The Theory of Perfectly Plastic Solids*, John Wiley and Sons, New York.

Randolph, M.F. and Houlsby, G.T. (1984). The limiting pressure on a circular pile loaded laterally in cohesive soil, *Geotechnique*, Vol 34, 613-623.

Rice, J.R. (1972). Plane strain slipline theory for anisotropic rigid/plastic materials, *J. Mech. Phys. Solids*, Vol 21, 63-74.

Salencon, J. (1977). *Applications of the Theory of Plasticity in Soil Mechanics*, Wiley, Chichester.

Shield, R.T. (1953). Mixed boundary value problems in soil mechanics, *Quart. Appl. Math.*, Vol 11, 61-75.

Shield, R.T. (1954). Plastic potential theory and Prandtl bearing capacity solution, *J. Appl. Mech.*, ASME, Vol 21, 193-194.

Shield, R.T. (1955). On the plastic flow of metals under conditions of axial symmetry, *Proc. R. Soc. A.*, Vol 233, 267-287.

Sokolovskii, V.V. (1965). *Statics of Granular Media*, Pergamon, Oxford.

Walker, J. (2004). *Numerical Analysis of Cone Penetration in Soils*, First Year Research Report, University of Nottingham, UK.

## CHAPTER 12

### LIMIT ANALYSIS

#### 12.1 INTRODUCTION

The purpose of stability analysis is to determine the maximum load that a soil structure can sustain before it fails. The soil collapse load is primarily a function of the soil strength which can be measured from either laboratory or in-situ tests. Two main methods can be used to determine the soil collapse load. They are indirect load-path analysis and direct limit analysis.

With load-path analysis, a complete load-displacement response has to be computed before the soil collapse load can be estimated. Examples of this type of procedure, using the finite element method, can be found in Nagtegaal *et al.* (1974), Chen (1975), Sloan and Randolph (1982), Alehossein *et al.* (1992), Yu *et al.* (1993) and Potts and Zdravkovic (1999) among many others. This approach, although powerful, is often too cumbersome to use in practice since it requires a complete specification of the stress-strain relations and material properties for each soil and structural component. This information is not only difficult to measure accurately but also very expensive to obtain.

As an alternative, by assuming that soil strengths are independent of the deformation, it is possible to use the bound theorems of limit analysis to estimate the soil collapse load directly (Chen, 1975; Chen and Liu, 1999). Theoretically, the direct method of limit analysis allows the collapse load of soil structures to be obtained in a relatively simple manner. In practice, however, the application of this direct approach poses a number of challenging computational problems which have only been partially resolved recently. The first major advantage of using the bound theorems for stability analysis is that they automatically provide an upper bound and a lower bound on the true collapse load. This means that the engineer can automatically estimate the accuracy of the solutions obtained. The second advantage is that the bound theorems only require the strength properties for each material concerned. In general these are much easier to measure than the deformation properties which are needed for load-path analysis.

By using finite elements and a suitable linear approximation of the yield surface, the lower and upper bound theorems lead to large linear programming problems (e.g. Lysmer, 1970; Anderheggen and Knopfel, 1972; Bottero *et al.*, 1980; Sloan, 1988a,b, 1989; Sloan and Kleeman, 1995; Yu and Sloan, 1991a,b, 1994a,b,c, 1995;

1997; Yu *et al.*, 1994, 1998; Merifield *et al.*, 1999, 2001; Maier *et al.*, 2000). On the other hand, nonlinear programming problems can be formulated if nonlinear yield functions are not linearized (e.g. Gao, 1988; Zouain *et al.*, 1993; Liu *et al.*, 1995; Lyamin and Sloan, 2002a,b; Li and Yu, 2005, 2006a,b). In addition, an iterative linear matching method has also been used by Ponter and Boulbibane (2006) for limit analysis. A key advantage of using a numerical formulation of the bound theorems is that it can deal with complex loading, complicated geometries and a variety of material failure conditions.

## 12.2 BASIC PROCEDURES OF LIMIT ANALYSIS

In this section, a brief description of the basic procedures for both upper and lower bound limit analysis is given. For this purpose, simple problems are considered so that analytical solutions are possible. Although choices are many, we will use the passive loading of a vertical retaining wall behind a cohesive-frictional soil mass (shown in Figure 12.1) as the example to illustrate the basic steps for performing both upper bound and lower bound limit analysis.

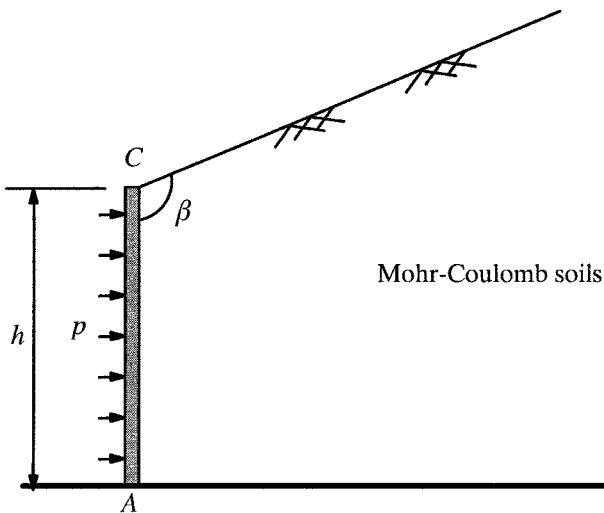


Figure 12.1: Problem of passive loading of a vertical retaining wall

### 12.2.1 Lower bound method of limit analysis

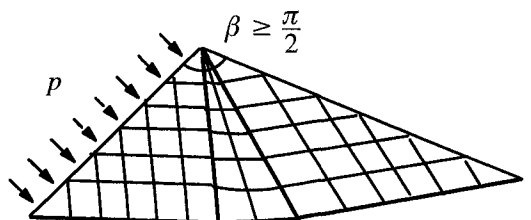
#### *The lower bound theorem*

As stated in Chapter 4, the limit load that is calculated from an equilibrium distribution of stresses that is also everywhere below yield will be lower than the true col-

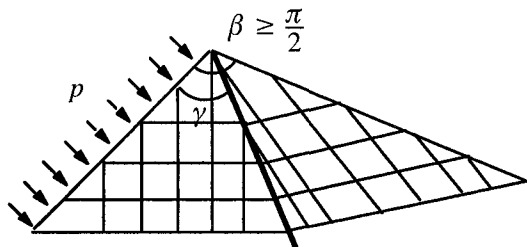
lapse load. This is the so-called lower bound theorem. In lower bound analysis, the main task is to devise a stress field that must satisfy both equilibrium and yield condition. The resulting stress field is also known as a statically admissible stress field. It proves to be useful to employ stress discontinuities in the construction of statically admissible stress fields (Prager and Hodge, 1951; Shield, 1954).

### Stress fields for a loaded wedge

As an example, we now consider a wedge that is under uniform pressure on one of its boundaries, as shown in Figure 12.2.



(a) Slip line field



(b) Stress fields with one discontinuity

Figure 12.2: Statically admissible stress fields for a loaded wedge (after Shield, 1954)

From the discussion in Chapter 11, we can easily show that a slip line network can be drawn for this wedge problem. The pressure  $p$  required to produce plastic flow with this pattern of failure lines is given as a function of friction angle  $\phi$ :

$$p = c \cot \phi \left\{ \exp[(2\beta - \pi) \tan \phi] \tan^2 \left( \frac{\pi}{4} + \frac{\phi}{2} \right) - 1 \right\} \quad (12.1)$$

By using a stress discontinuity, Shield (1954) shows that a statically admissible stress field, as shown in Figure 12.2(b), can be constructed. In particular, we have

$$\gamma = \frac{\beta}{2} + \frac{\mu}{2} \quad (12.2)$$

where  $\mu$  is given by

$$\sin \mu = \sin \phi \sin \beta, \quad 0 \leq \mu \leq \frac{\pi}{2} \quad (12.3)$$

The stress jump condition can also be used to determine the lower bound solution to the pressure,  $p$ , as follows:

$$p = c \cot \phi \left\{ \frac{\sin(\beta - \mu)}{\sin(\beta + \mu)} \tan^2 \left( \frac{\pi}{4} + \frac{\phi}{2} \right) - 1 \right\} \quad (12.4)$$

For the special case of purely cohesive materials with  $\phi = 0$ , we have  $\mu = 0$  and equation (12.4) takes the form

$$p = 2c(1 - \cos \beta) \quad (12.5)$$

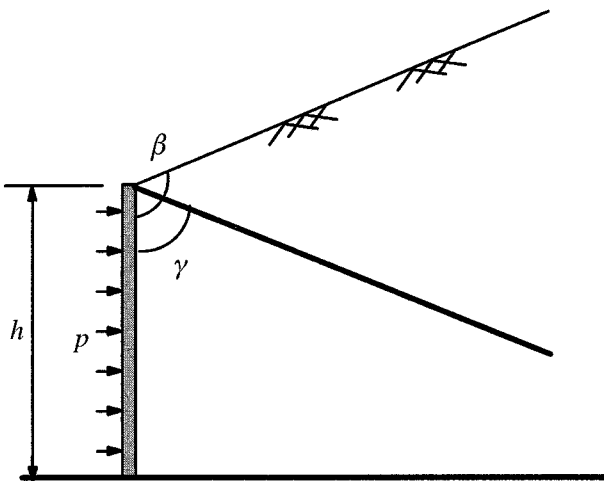


Figure 12.3: A lower bound solution for passive loading of a vertical retaining wall

#### *Lower bound solution for a retaining wall*

For the passive loading of a retaining wall problem shown in Figure 12.3, a lower bound solution to the horizontal pressure using a stress discontinuity can be taken from the lower bound solution (12.4) for a wedge.

For example, let us take  $\beta = 120^\circ$  and  $\phi = 30^\circ$  as used in Davis (1968). We obtain  $\mu = 25.66^\circ$  and  $\gamma = 72.8^\circ$  from equations (12.2) and (12.3). Equation

(12.4) can be used to obtain a lower bound solution  $p = 7.45c$ , which compares very well with the exact solution,  $p = 7.7c$ , derived from slip line analysis (12.1).

### 12.2.2 Upper bound method of limit analysis

#### *The upper bound theorem*

The upper bound theorem has been described and proved in Chapter 4. In simple terms, it means that an upper bound to the true collapse load can be derived from an energy equation between the external work and the internal plastic power dissipation with any kinematically admissible failure mechanism.

#### *An upper bound solution to passive loading of the retaining wall problem*

To use the upper bound theorem to perform limit analysis, a few steps need to be followed. First a kinematic failure mechanism is assumed; second a relevant velocity field diagram is drawn to give the relationship between various velocity components; third, work out external work and internal (or plastic) power dissipation and equate them, which leads to an expression for the upper bound solution.

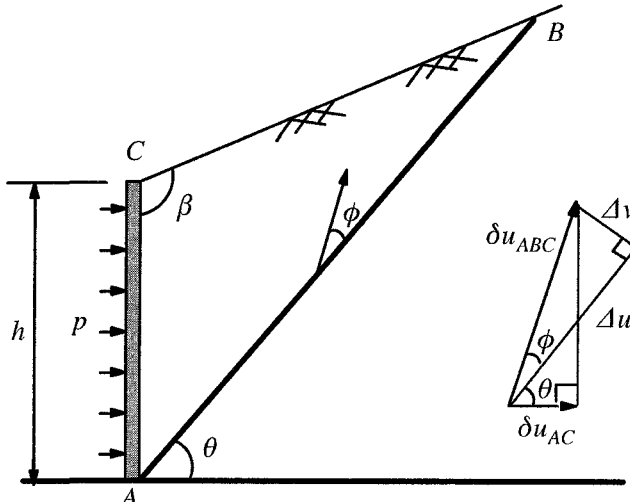


Figure 12.4: A rigid block failure mechanism for passive loading of a retaining wall

In addition, it is a common practice to assume that plastic dissipation occurs entirely in velocity discontinuities. This means that no plastic deformation has taken place in the continuum. This assumption has been used mainly to lend simplicity to the analyses. In this regard, the rate of plastic power dissipation for a velocity discontinuity within the Mohr-Coulomb material can be expressed as the following simple form (Davis, 1968):

$$D = c\Delta u \quad (12.6)$$

where  $c$  is cohesion and  $\Delta u$  is the tangential velocity along a velocity discontinuity.

For the retaining wall example shown in Figure 12.4, we assume that a failure surface is planar plotted as AB in the figure which forms an angle of  $\theta$  from the horizontal direction, so that at failure the soil mass will be assumed to move as a rigid block ABC. Hence plastic power dissipation will occur along AB only. From the velocity diagram shown in Figure 12.4, we have the following relationship between the tangential velocity jump along AB and the horizontal velocity experienced by the retaining wall AB:

$$\Delta u = \frac{\cos \phi}{\cos(\theta + \phi)} \delta u_{AC} \quad (12.7)$$

Hence the energy equation of the upper bound theorem can be written as follows:

$$ph \times \delta u_{AC} = c\Delta u \times \overline{AB} \quad (12.8)$$

The consideration of geometry indicates

$$\overline{AB} = \frac{\sin \beta}{\sin(\frac{\pi}{2} - \beta + \theta)} h \quad (12.9)$$

By substituting equations (12.7) and (12.9) into the work equation (12.8), we obtain a general upper bound expression for horizontal pressure  $p$ :

$$p = \frac{\sin \beta \cos \phi}{\sin(\frac{\pi}{2} - \beta + \theta) \cos(\phi + \theta)} c \quad (12.10)$$

The best upper bound for the assumed failure plane can be obtained by setting

$$\frac{\partial p}{\partial \theta} = 0 \quad (12.11)$$

which gives a critical angle  $\theta$  at which the upper bound becomes the best (i.e. lowest).

For example, let us take  $\beta = 120^\circ$  and  $\phi = 30^\circ$  as used in Davis (1968). It can be shown that the upper bound is the smallest when  $\theta = 45^\circ$ . The best upper bound is obtained by putting  $\theta = 45^\circ$  into equation (12.10). The resulting upper bound value is  $p = 11.2c$ , which is considerably greater than the exact solution.

However this difference can be reduced dramatically by using a two rigid-block failure mechanism, as shown in Figure 12.5. In this two rigid block failure mechanism, the velocity discontinuity BC coincides with the stress discontinuity shown

in Figure 12.3. Also the velocity discontinuities AB and BD follow the direction of slip lines. This revised failure mechanism leads to an upper bound of  $p = 8.02c$  (Davis, 1968), which is much closer to the exact solution of 7.7c.

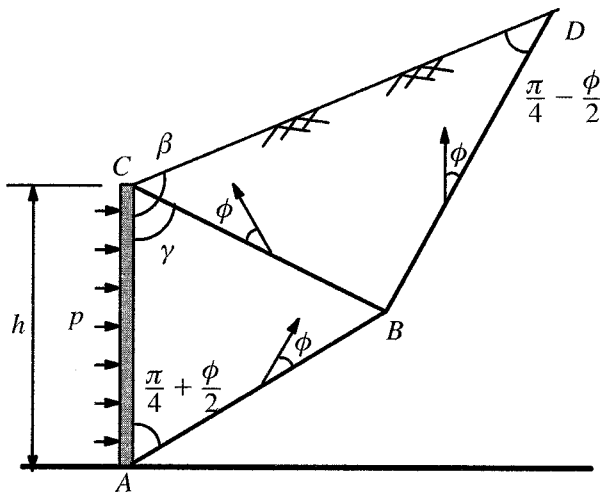


Figure 12.5: Two rigid block failure mechanism for passive loading of a retaining wall (after Davis, 1968)

### 12.2.3 Upper bound limit analysis and limit equilibrium analysis

Coulomb's analysis of retaining wall problems was based on the equilibrium of forces acting on a wedge of soil isolated behind the retaining wall. This method is known as limit equilibrium analysis (Terzaghi, 1943). As noted by Collins (1973), it gives exactly the same result as the energy balance method used in the upper bound limit analysis as long as a rigid failure mechanism is used. This equivalence was proved by Michalowski (1989) and also discussed by Drescher and Detournay (1993) and Davis and Selvadurai (2002).

Following Davis and Selvadurai (2002), we consider a rigid triangular element 1 surrounded by three elements 2, 3, and 4 (see Figure 12.6). The velocities of each element with some common stationary point 0 are denoted as  $v_{01}, v_{02}, v_{03}$  and  $v_{04}$ . The relative velocities as shown in Figure 12.6 are  $v_{12}, v_{13}, v_{14}$ . If we denote the three sides of the element 1 as  $L_{12}, L_{13}, L_{14}$  and the traction vectors which act on those sides as  $\mathbf{T}_{12}, \mathbf{T}_{13}, \mathbf{T}_{14}$ , the work done by the external forces associated with element 1 can be written as follows:

$$W_{ex} = v_{02} \int_{L_{12}} \mathbf{T}_{12} dL + v_{03} \int_{L_{13}} \mathbf{T}_{13} dL + v_{04} \int_{L_{14}} \mathbf{T}_{14} dL - v_{01} \iint_A \mathbf{b} dA \quad (12.12)$$

where  $\mathbf{b}$  is the body force vector and  $A$  is the area of element 1.

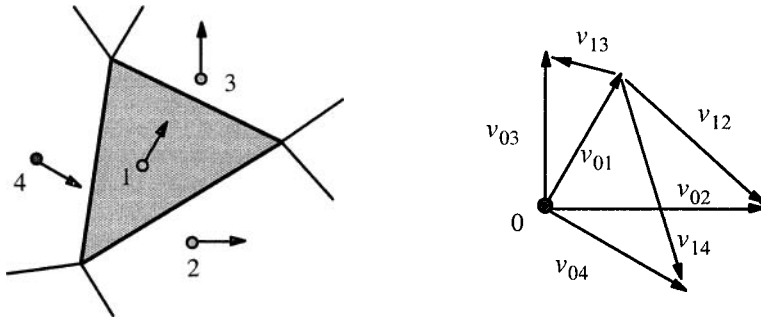


Figure 12.6: A triangular rigid element with velocities of surrounding elements  
(after Davis and Selvadurai, 2002)

On the other hand the power dissipation associated with element 1 in the absence of volume change of the element can be expressed as follows:

$$W_{in} = v_{12} \int_{L_{12}} \mathbf{T}_{12} dL + v_{13} \int_{L_{13}} \mathbf{T}_{13} dL + v_{14} \int_{L_{14}} \mathbf{T}_{14} dL \quad (12.13)$$

The upper bound theorem requires  $W_{ex} = W_{in}$ . In addition we can also obtain the following from Figure 12.6:

$$v_{12} = v_{02} - v_{01}; \quad v_{13} = v_{03} - v_{01}; \quad v_{14} = v_{04} - v_{01} \quad (12.14)$$

The above equations together with the upper bound theorem lead to

$$0 = v_{01} \int_{L_{12}} \mathbf{T}_{12} dL + v_{01} \int_{L_{13}} \mathbf{T}_{13} dL + v_{01} \int_{L_{14}} \mathbf{T}_{14} dL - v_{01} \iint_A \mathbf{b} dA \quad (12.15)$$

which is equivalent to the following given  $v_{01}$  is arbitrary:

$$\int_{L_{12}} \mathbf{T}_{12} dL + \int_{L_{13}} \mathbf{T}_{13} dL + \int_{L_{14}} \mathbf{T}_{14} dL = \iint_A \mathbf{b} dA \quad (12.16)$$

It is evident that the above equation is a statement of equilibrium of forces for the triangular element 1. Hence we have proved that, for a rigid failure mechanism,

the energy balance equation of the upper bound limit analysis is equivalent to the equations of equilibrium used in the limit equilibrium analysis.

#### 12.2.4 General remarks

The discussion presented in the previous subsections indicates that the bound theorems of limit analysis can be very powerful for estimating collapse loads. Their applications by hand are however restricted to simple problems where it is possible to assume good failure mechanisms or stress discontinuities. It is also true that the upper bound method is easier to apply than the lower bound method, as the engineer tends to be less familiar with properties of statically admissible stress fields. More importantly, such simple approaches, as outlined above, may not be possible for most practical problems with complex geometry, loading and material failure conditions.

Therefore there is a need to develop general numerical methods that can be applied by the practising engineer to obtain accurate upper and lower bound solutions for real geotechnical stability problems. As a result, much progress has been made over the last two decades on the development of numerical limit analysis techniques using finite elements and mathematical programming. The remaining sections of this chapter will present some of the key developments in this exciting field.

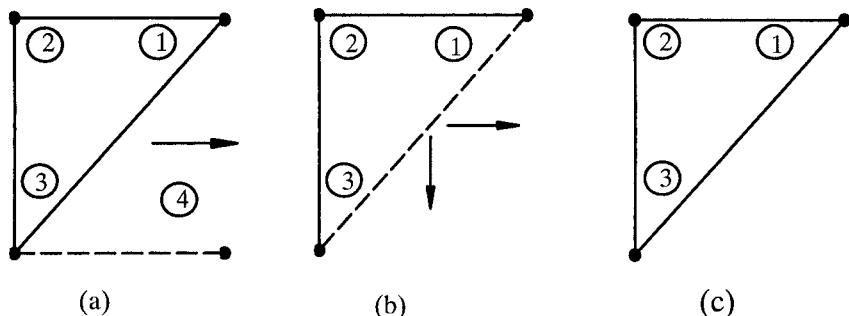


Figure 12.7: Elements used in lower bound analyses. (a) 4-noded rectangular extension element, (b) 3-noded triangular extension element, and (c) 3-noded triangular element

#### 12.3 LOWER BOUND ANALYSIS USING LINEAR PROGRAMMING

The development of finite element formulations of the lower bound theorem for soil mechanics problems appears to be first carried out by Lysmer (1970). In this approach, three-noded triangular stress elements are used to model static stress fields.

The task of finding the best lower bound collapse loads reduces to solving a large linear programming problem. This type of approach has later been followed by many others including Sloan (1988a,b) for plane strain problems and Yu and Sloan (1991a) for axisymmetric problems. The formulations have also been extended to analyse problems related to reinforced soils (Yu and Sloan, 1994b) and jointed rock (Yu and Sloan, 1994c; Sutcliffe *et al.*, 2004).

### 12.3.1 Plane strain finite element formulations

According to the lower bound limit theorem, any statically admissible stress field will result in a lower bound estimate of the true collapse load. A statically admissible stress field is one which satisfies equilibrium and stress boundary conditions and does not violate the yield criterion.

The lower bound finite element formulation to be presented uses three types of elements (as shown in Figure 12.7) (e.g. Bottero *et al.*, 1980 and Sloan, 1995). Each node is associated with three stresses,  $\sigma_x$ ,  $\sigma_y$  and  $\sigma_{xy}$  (Figure 12.8) with the variation of stresses throughout each element assumed to be linear. The inclusion of triangular and rectangular extension elements extends the solution over a semi-infinite domain and therefore provides a complete statically admissible stress field.

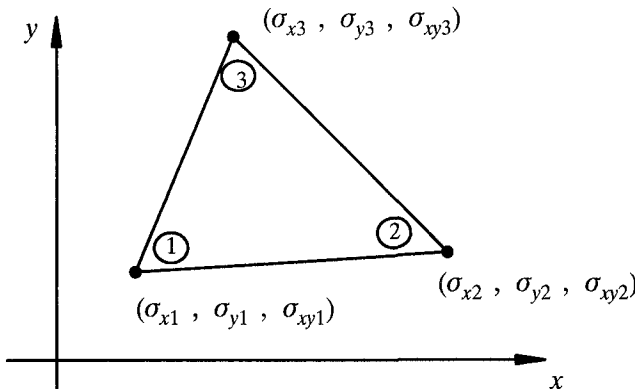


Figure 12.8: Three-noded linear stress triangle with 3 unknown stresses at each node

Unlike the elements used in displacement finite element analysis, several nodes may share the same coordinate and each node is associated with only one element. In this way statically admissible stress discontinuities can occur at all edges between adjoining triangles. By ensuring the equations of equilibrium are satisfied,

and that the stress boundary conditions and the yield criteria are not violated, a rigorous lower bound on the collapse load is obtained.

### Element equilibrium

The stresses throughout each element must satisfy the following two equilibrium equations :

$$\frac{\partial \sigma_x}{\partial x} + \frac{\partial \sigma_{xy}}{\partial y} = 0 \quad (12.17)$$

$$\frac{\partial \sigma_y}{\partial y} + \frac{\partial \sigma_{xy}}{\partial x} = \gamma \quad (12.18)$$

where tensile stresses are taken as positive, a right handed Cartesian coordinate system is adopted and  $\gamma$  is the unit weight of the material. This results in two equality constraints on nodal stresses for each element.

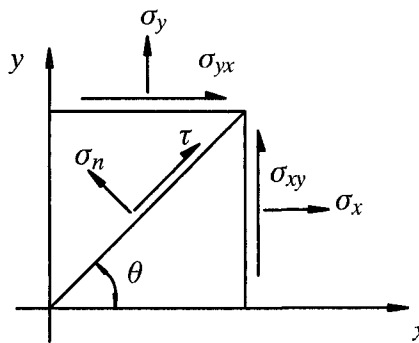


Figure 12.9: Stress transformation for plane strain problems

### Discontinuity equilibrium

It is necessary to impose additional constraints on the nodal stresses at the edges of adjacent triangles in order to permit admissible discontinuities. For a discontinuity to be statically admissible only the normal stress parallel to the discontinuity may be discontinuous, with continuity of the corresponding shear stresses and normal stresses perpendicular to the discontinuity maintained. With reference to Figure 12.9, the normal and shear stresses acting on a plane inclined at angle  $\theta$  to the x-axis (positive anti-clockwise) are given by

$$\sigma_n = \sigma_x \sin^2 \theta + \sigma_y \cos^2 \theta - \sigma_{xy} \sin 2\theta \quad (12.19)$$

$$\tau = -\frac{1}{2}\sigma_x \sin 2\theta + \frac{1}{2}\sigma_y \sin 2\theta + \sigma_{xy} \cos 2\theta \quad (12.20)$$

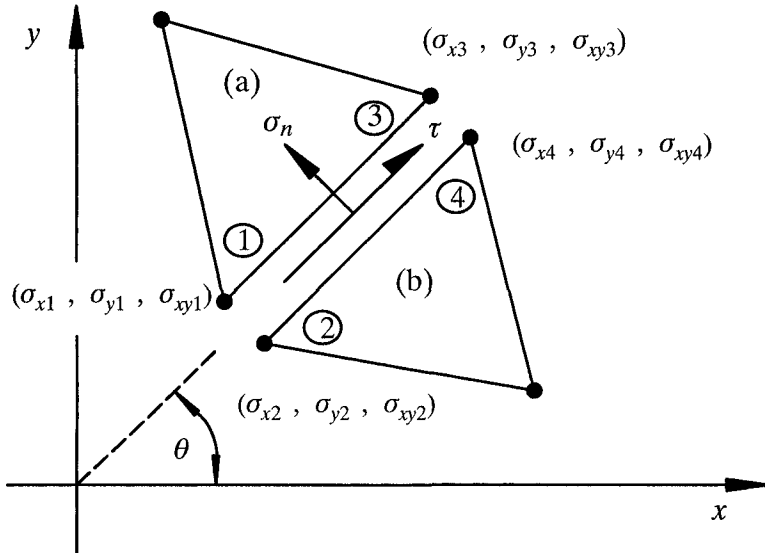


Figure 12.10: Statically admissible stress discontinuity between adjacent triangles

Looking at Figure 12.10, for triangles *a* and *b*, equilibrium along the discontinuity (or common side) requires that at every point along this side:

$$\sigma_n^a = \sigma_n^b; \quad \tau^a = \tau^b \quad (12.21)$$

Since stresses are confined to varying linearly along any element edge, an equivalent condition is achieved by enforcing the constraints:

$$\sigma_{n1}^a = \sigma_{n2}^b; \quad \sigma_{n3}^a = \sigma_{n4}^b; \quad \tau_1^a = \tau_2^b; \quad \tau_3^a = \tau_4^b \quad (12.22)$$

As such, each statically admissible discontinuity along an element edge results in four equality constraints on the nodal stresses.

#### Boundary conditions

In order to enforce prescribed boundary conditions it is necessary to impose additional constraints on the nodal stresses. The problem of the bearing capacity of a footing has boundary conditions in the form of:

$$\sigma_n = q = \text{constant}; \quad \tau = t = \text{constant} \quad (12.23)$$

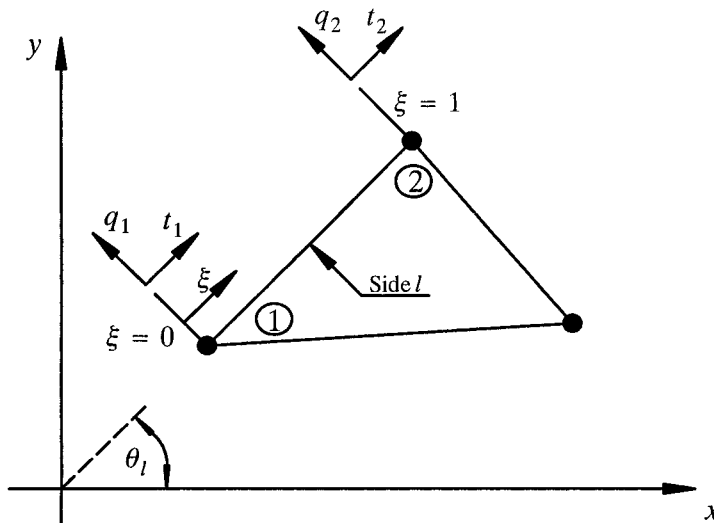


Figure 12.11: Stress boundary conditions

Given a linear variation of the stress components  $\sigma_x$ ,  $\sigma_y$  and  $\sigma_{xy}$  along the edge of each triangle, a more general boundary condition may be imposed, in the form of (see Figure 12.11):

$$\sigma_n^l = q_1 + (q_2 - q_1)\xi ; \quad \tau_n^l = t_1 + (t_2 - t_1)\xi \quad (12.24)$$

where

$l$  = edge of triangle  $e$  where boundary tractions are specified

$\xi$  = local coordinate along  $l$

$q_1, q_2$  = normal stresses specified at nodes 1 and 2 (tension positive)

$t_1, t_2$  = shear stresses specified at nodes 1 and 2 (clockwise shears positive)

The boundary conditions of equation (12.24) are then satisfied by requiring

$$\sigma_{n1}^e = q_1 ; \quad \sigma_{n2}^e = q_2 ; \quad \tau_1^e = t_1 , \quad \tau_2^e = t_2 \quad (12.25)$$

So for each edge where a boundary traction is specified, a maximum of four equality constraints on the nodal stresses are generated.

#### *Yield condition*

Under conditions of plane strain, the Mohr-Coulomb yield criterion may be written as

$$F = (\sigma_x - \sigma_y)^2 + 4\sigma_{xy}^2 - (2c \cos \phi - (\sigma_x + \sigma_y) \sin \phi)^2 = 0 \quad (12.26)$$

where  $c$  is the cohesion and  $\phi$  is the friction angle. In terms of the quantities  $(\sigma_x - \sigma_y)$  and  $2\sigma_{xy}$ , this yield function plots as a circle, as shown in Figure 12.12.

A key feature of formulating limit analysis as a linear programming problem is the use of a linearized yield surface. With reference to Figure 12.12, if  $p$  is the number of sides used to approximate the yield function (12.26), then the linearized yield function can be shown to be (Sloan, 1988b):

$$A_k \sigma_x + B_k \sigma_y + C_k \sigma_{xy} \leq E, \quad k = 1, 2, \dots, p \quad (12.27)$$

where

$$A_k = \cos\left(\frac{2\pi k}{p}\right) + \sin \phi \cos\left(\frac{\pi}{p}\right)$$

$$B_k = -\cos\left(\frac{2\pi k}{p}\right) + \sin \phi \cos\left(\frac{\pi}{p}\right)$$

$$C_k = 2 \sin\left(\frac{2\pi k}{p}\right)$$

$$E = 2c \cos \phi \cos\left(\frac{\pi}{p}\right)$$

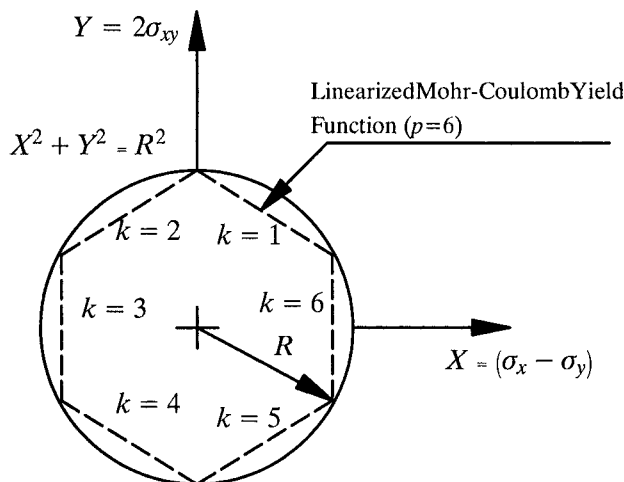


Figure 12.12: Linearized Mohr-Coulomb yield function ( $p=6$ )

Thus the linearized yield condition imposes  $p$  inequality constraints on the stresses at each node.

By using a linearized failure surface it is sufficient to enforce the linear constraint (12.27) at each nodal point to ensure that the stresses satisfy the yield conditions everywhere.

### *Objective function*

For many geotechnical problems, we seek a statically admissible stress field which maximises the integral of the normal stress over some part of the boundary. If the out-of-plane length of the footing is denoted by  $h$ , then the integral to be maximised is in the form of:

$$P = h \int_S \sigma_n \, ds \quad (12.28)$$

where  $P$  represents the collapse load. Due to the linear variation of stresses along any boundary it is possible to perform the integration analytically as:

$$P = \frac{h}{2} \sum_{edges} (\sigma_{n1} + \sigma_{n2}) l_{12} \quad (12.29)$$

where  $l_{12}$  is the length of the segment over which the force is to be optimized, defined by the nodes (1,2) and  $(\sigma_{n1}, \sigma_{n2})$  are the normal stresses at the segment ends.

### *Lower bound linear programming problem*

By assembling the various constraints and objective functions the problem of finding a statically admissible stress field which maximises the collapse load may be written as:

$$\text{Minimize} \quad - \mathbf{C}^T \mathbf{X} \quad (12.30)$$

$$\text{Subject to} \quad \mathbf{A}_1 \mathbf{X} = \mathbf{B}_1$$

$$\mathbf{A}_2 \mathbf{X} \leq \mathbf{B}_2$$

where  $\mathbf{A}_1, \mathbf{B}_1$  represent the coefficients due to equilibrium and stress boundary conditions;  $\mathbf{A}_2, \mathbf{B}_2$  represent the coefficients for the yield conditions;  $\mathbf{C}$  is the vector of objective function coefficients and  $\mathbf{X}$  is the global vector of unknown stresses. An active set algorithm is used to solve the above linear programming problem, the details of which can be found in Sloan (1988a). The solution for the unknown stresses  $\mathbf{X}$  from (12.30) define a statically admissible stress field and, as such, the corresponding collapse load defines a rigorous lower bound on the true collapse load.

### **12.3.2 Axisymmetric finite element formulations**

A finite element formulation of the lower bound theorem for axisymmetric problems has been developed by Yu and Sloan (1991). The axisymmetric formulation

is based on a different set of stress variables to that for plane strain problems as described in the previous section.

### (a) Numerical formulations

#### *The assumed stress fields*

Figure 12.13 shows the three-noded triangular element used for the lower bound limit analysis. The stresses are assumed to vary linearly throughout each triangle according to

$$\sigma_r = c'_1 + c'_2 r + c'_3 z \quad (12.31)$$

$$\sigma_z = c'_4 + c'_5 r + c'_6 z \quad (12.32)$$

$$\sigma_\theta = c'_7 + c'_8 r + c'_9 z \quad (12.33)$$

$$\sigma_{rz} = c'_{10} + c'_{11} r + c'_{12} z \quad (12.34)$$

where  $c'_1, c'_2, c'_3, \dots, c'_{12}$  are constants for the triangular element.

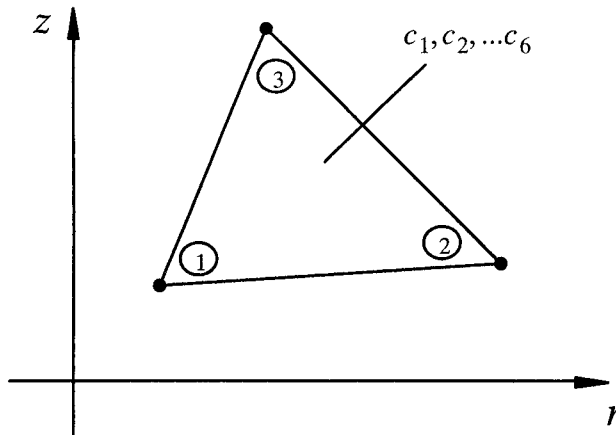


Figure 12.13: Three-noded linear stress triangle with 6 unknown coefficients for each triangular element

In order to use the lower bound theorem, the stress field must satisfy the following equilibrium equations:

$$\frac{\partial \sigma_z}{\partial z} + \frac{\partial \sigma_{rz}}{\partial r} + \frac{\sigma_{rz}}{r} = \gamma \quad (12.35)$$

$$\frac{\partial \sigma_r}{\partial r} + \frac{\partial \sigma_{rz}}{\partial z} + \frac{\sigma_r - \sigma_\theta}{r} = 0 \quad (12.36)$$

where  $\gamma$  denotes the unit-weight of the material. By substituting equations (12.31)-(12.34) into equations (12.35)-(12.36), we obtain a stress field that satisfies equilibrium according to

$$\begin{bmatrix} \sigma_r \\ \sigma_z \\ \sigma_\theta \\ \sigma_{rz} \end{bmatrix} = \begin{bmatrix} 1 & z & r & 0 & 0 & 0 \\ 0 & 0 & 0 & 1 & z & r \\ 1 & z & 2r & 0 & 0 & 0 \\ 0 & 0 & 0 & 0 & -0.5r & 0 \end{bmatrix} \begin{bmatrix} c_1 \\ c_2 \\ c_3 \\ c_4 \\ c_5 \\ c_6 \\ \gamma \end{bmatrix} \quad (12.37)$$

where  $c_1, c_2, c_3, \dots, c_6$  are unknown variables for each triangular element. Note that six unknowns, rather than twelve, are generated for each element. The above equation may also be written in the following compact form

$$\sigma = L \times X^e \quad (12.38)$$

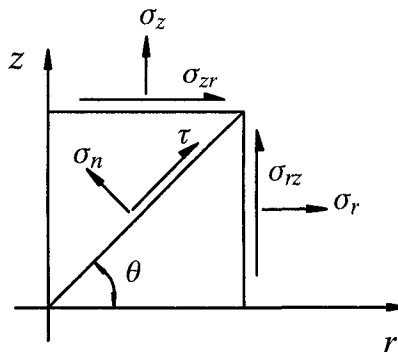


Figure 12.14: Stress transformation for axisymmetric problems

#### Discontinuity equilibrium

In order to permit statically admissible discontinuities at the edges of adjacent triangles, it is necessary to enforce additional constraints on the nodal stresses. A statically admissible discontinuity permits the tangential stress to be discontinuous, but requires that continuity of the corresponding shear and normal components is retained. With reference to Figure 12.14, the normal and shear stresses acting on a plane inclined at an angle of  $\theta$  to the r-axis (measured anticlockwise) are given by

$$\sigma_n = \sigma_r \sin^2 \theta + \sigma_z \cos^2 \theta - \sigma_{rz} \sin 2\theta \quad (12.39)$$

$$\tau = -\frac{1}{2} \sigma_r \sin 2\theta + \frac{1}{2} \sigma_z \sin 2\theta + \sigma_{rz} \cos 2\theta \quad (12.40)$$

Figure 12.15 shows two triangles, (a) and (b), which share a side defined by the nodal pairs (1,2) and (3,4). Equilibrium of the discontinuity requires that at every point along the discontinuity

$$\sigma_n^a = \sigma_n^b; \quad \tau^a = \tau^b \quad (12.41)$$

Since stresses are confined to varying linearly along any element edge, an equivalent condition is achieved by enforcing the constraints:

$$\sigma_{n1}^a = \sigma_{n2}^b; \quad \sigma_{n3}^a = \sigma_{n4}^b; \quad \tau_1^a = \tau_2^b; \quad \tau_3^a = \tau_4^b \quad (12.42)$$

As such, each statically admissible discontinuity along an element edge results in four equality constraints on the unknown element coefficients.

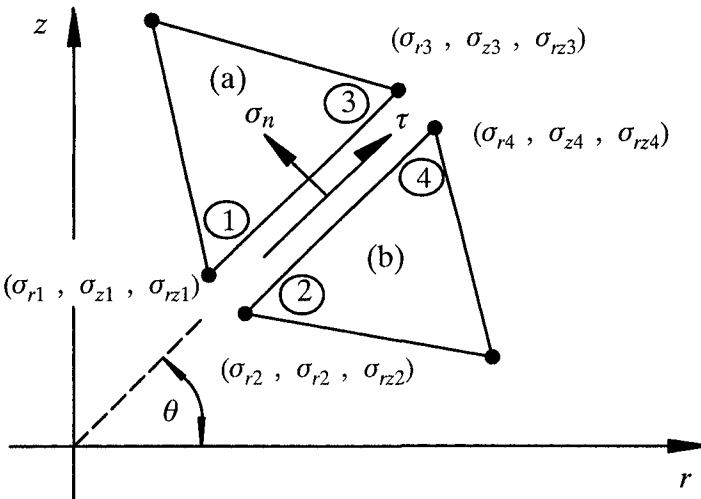


Figure 12.15: Statically admissible stress discontinuity between adjacent triangles

#### Boundary conditions

In order to satisfy the stress boundary conditions, the normal and shear stresses must be equal to their prescribed values on the boundary of the mesh. The general form of this constraint for a particular edge defined by nodes 1 and 2 takes the form

$$\sigma_{n1}^e = q_1; \quad \sigma_{n2}^e = q_2; \quad \tau_1^e = t_1, \quad \tau_2^e = t_2 \quad (12.43)$$

where  $(q_1, t_1)$  and  $(q_2, t_2)$  are the prescribed normal and shear stresses at nodes 1 and 2 respectively. So for each edge where a boundary traction is specified, a maximum of four equality constraints on the element coefficients are generated.

#### Yield condition

Under conditions of axisymmetric loading, the Mohr-Coulomb yield criterion needs to be written in the following three possible cases

$$F_1 = (\sigma_r - \sigma_z)^2 + 4\sigma_{rz}^2 - (2c \cos \phi - (\sigma_r + \sigma_z) \sin \phi)^2 = 0 \quad (12.44)$$

$$F_2 = (\sigma_r - \sigma_z)^2 + 4\sigma_{rz}^2 - \left( \frac{4c \cos \phi}{1 - \sin \phi} + \sigma_r + \sigma_z - 2\sigma_\theta \frac{1 + \sin \phi}{1 - \sin \phi} \right)^2 = 0 \quad (12.45)$$

$$F_3 = (\sigma_r - \sigma_z)^2 + 4\sigma_{rz}^2 - \left( \frac{4c \cos \phi}{1 + \sin \phi} - \sigma_r - \sigma_z - 2\sigma_\theta \frac{1 - \sin \phi}{1 + \sin \phi} \right)^2 = 0 \quad (12.46)$$

where  $c$  is the cohesion and  $\phi$  is the friction angle. To ensure that the stresses do not violate the yield condition, and hence fulfil the requirements of the lower bound theorem, it is necessary that  $F_1 \leq 0$ ,  $F_2 \leq 0$  and  $F_3 \leq 0$  throughout each triangle. To preserve linearity, the yield surfaces are linearized in such a way that the linearized yield surfaces lie inside the Mohr-Coulomb yield surfaces in stress space. This ensures that the solutions obtained are rigorous lower bounds on the true limit load.

The  $p$ -sided linearized yield condition at any point may be expressed as

$$\mathbf{T}_1 \boldsymbol{\sigma} \leq D_1 \quad (12.47)$$

$$\mathbf{T}_2 \boldsymbol{\sigma} \leq D_2 \quad (12.48)$$

$$\mathbf{T}_3 \boldsymbol{\sigma} \leq D_3 \quad (12.49)$$

where

$$\boldsymbol{\sigma} = [\sigma_r, \sigma_z, \sigma_\theta, \sigma_{rz}]^T \quad (12.50)$$

$$\mathbf{T}_1 = [\cos \frac{2\pi k}{p} - \sin \phi \cos \frac{\pi}{p}, -(\cos \frac{2\pi k}{p} + \sin \phi \cos \frac{\pi}{p}), 0, 2 \sin \frac{2\pi k}{p}] \quad (12.51)$$

$$D_1 = 2c \cos \phi \cos \frac{\pi}{p} \quad (12.52)$$

$$\mathbf{T}_2 = [\cos \frac{2\pi k}{p} - \cos \frac{\pi}{p}, -(\cos \frac{2\pi k}{p} + \cos \frac{\pi}{p}), 2 \frac{1 - \sin \phi}{1 + \sin \phi} \cos \frac{\pi}{p}, 2 \sin \frac{2\pi k}{p}] \quad (12.53)$$

$$D_2 = \frac{4c \cos \phi}{1 + \sin \phi} \cos \frac{\pi}{p} \quad (12.54)$$

$$\mathbf{T}_3 = [\cos \frac{2\pi k}{p} + \cos \frac{\pi}{p}, -(\cos \frac{2\pi k}{p} - \cos \frac{\pi}{p}), 2 \frac{\sin \phi - 1}{1 + \sin \phi} \cos \frac{\pi}{p}, 2 \sin \frac{2\pi k}{p}] \quad (12.55)$$

$$D_3 = \frac{4c \cos \phi}{1 - \sin \phi} \cos \frac{\pi}{p} \quad (12.56)$$

in which  $k=1,2,\dots,p$ .

Given that the stresses are assumed to vary linearly across each triangle, it is sufficient to enforce these constraints at each nodal point to ensure they are satisfied throughout the mesh. The constraints (12.47)-(12.49) for a node may also be expressed in the following form in terms of unknown element coefficients

$$(\mathbf{T}_1 \times \mathbf{L})\mathbf{X}^e \leq D_1 \quad (12.57)$$

$$(\mathbf{T}_2 \times \mathbf{L})\mathbf{X}^e \leq D_2 \quad (12.58)$$

$$(\mathbf{T}_3 \times \mathbf{L})\mathbf{X}^e \leq D_3 \quad (12.59)$$

### *Objective function*

For many axisymmetric problems, we seek a statically admissible stress field which maximises the integral of the normal stress over some part of the boundary in the form of:

$$P = 2\pi \int_S \sigma_n r \, ds \quad (12.60)$$

where  $P$  represents the collapse load which is to be maximised to achieve the best lower bound. Due to the linear variation of stresses along any boundary it is possible to perform the integration analytically (Yu and Sloan, 1991a).

### *Lower bound linear programming problem*

By assembling the various constraints and objective functions the problem of finding a statically admissible stress field which maximises the collapse load (12.60) may be written as:

$$\text{Minimize} \quad -\mathbf{C}^T \mathbf{X} \quad (12.61)$$

$$\text{Subject to} \quad \mathbf{A}_1 \mathbf{X} = \mathbf{B}_1$$

$$\mathbf{A}_2 \mathbf{X} \leq \mathbf{B}_2$$

where  $\mathbf{A}_1, \mathbf{B}_1$  represent the coefficients due to equilibrium and stress boundary conditions;  $\mathbf{A}_2, \mathbf{B}_2$  represent the coefficients for the yield conditions;  $\mathbf{C}$  is the vector of objective function coefficients and  $\mathbf{X}$  is the global vector of unknown coefficients. The solution for the unknown vector  $\mathbf{X}$  from (12.61) defines a statically admissible stress field and, as such, the corresponding collapse load defines a rigorous lower bound on the true collapse load.

**(b) Numerical examples**

A numerical analysis of the stability of a vertical cut in both cohesive and cohesive-frictional soils is presented here to demonstrate the application of the proposed numerical procedure.

*Stability of a vertical cut in a purely cohesive soil*

Figure 12.16(a) shows the finite element mesh used in the lower bound calculation for the vertical cut with  $H/a = 1$ . The stability number for an axisymmetric vertical cut may be represented by the quantity  $\gamma H/c$ , where  $H$  is the height of the cut and  $c$  is the undrained shear strength of the cohesive soil.

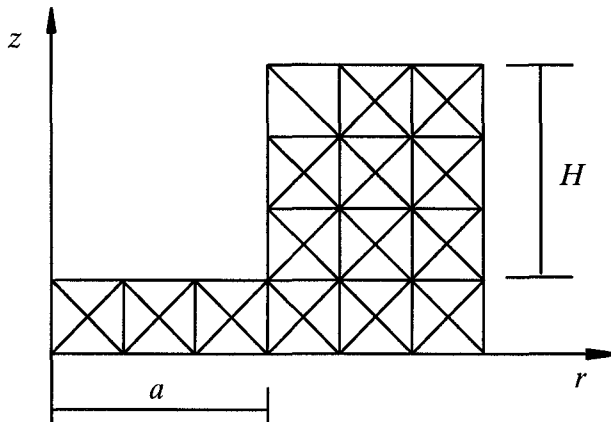
Different values of  $p$  are used in the analysis so that the sensitivity of the results to the linearization of the yield surface can be studied. Figure 12.16(b) summarises the results for the analysis of a vertical cut in undrained soil, where  $n$  and  $m$  represent the numbers of variables and constraints in the linear programming problem respectively. The quantities  $i$  and  $t$  are the number of total iterations required and the CPU time (in seconds) for an Apollo 3500 (Yu and Sloan, 1991a). The results suggest that the lower bound solution is relatively insensitive to the number of sides used in the linearized yield polygon. A 12-sided linearization of the yield surface gives a reasonably good solution for this particular problem.

*Stability of a vertical cut in a cohesive-frictional soil*

The stability of a cohesive-frictional vertical cut is also investigated. In the calculation, the angle of soil friction is assumed to be  $\phi = 30^0$ . The mesh used is the same as for a cohesive soil and the results are given in Figure 12.16(c). The results suggest that the lower bound solution is more sensitive to the number of sides used in the linearized yield polygon. To obtain a good solution for a cohesive-frictional material, at least a 24-sided linearization of the yield surface is necessary.

**12.3.3 Plane strain finite element formulations for jointed media**

It is well recognised that discontinuities in rock masses often have much lower strength properties than the intact material. If the joint sets are reasonably constant in orientation and closely spaced, the rock mass may be considered to be homogeneous but anisotropic. The overall properties of the jointed rock are therefore determined by the strength of intact material and the strength and orientation of rock joints. A finite element formulation for lower bound limit analysis of jointed media has been developed by Yu and Sloan (1994c). Further applications of this formulation to masonry and jointed rock are presented by Sutcliffe *et al.* (2001, 2004).



(a) A lower bound finite element mesh

$p$	$n$	$m$	$i$	$t$	$\gamma H/c$
6	361	3597	73	240	2.83
12	361	6837	112	414	3.12
24	361	13317	130	730	3.20
48	361	26277	219	2049	3.21

(b) Results for a cohesive cut

$p$	$n$	$m$	$i$	$t$	$\gamma H/c$
6	361	3597	38	167	4.08
12	361	6837	48	227	4.85
24	361	13317	53	349	5.05
48	361	26277	60	615	5.11

(c) Results for a cohesive-frictional cut

Figure 12.16: Lower bound mesh and numerical results for stability of a vertical cut

### (a) Numerical formulations

#### *Failure surface for the intact rock material*

For simplicity it is assumed that the intact rock material is isotropic, homogenous and obeys the Mohr-Coulomb failure criterion. If tensile stresses are positive, the Mohr-Coulomb criterion for plane problems may be expressed as:

$$F_r = (\sigma_x - \sigma_y)^2 + (2\sigma_{xy})^2 - (2c \cos \phi - (\sigma_x + \sigma_y) \sin \phi)^2 = 0 \quad (12.62)$$

where  $\sigma_x$ ,  $\sigma_y$  are normal stresses in the horizontal and vertical directions respectively,  $\sigma_{xy}$  is the shear stress, and  $c$ ,  $\phi$  denote the cohesion and friction angle of the intact rock material.

#### *Failure surface for discontinuities*

Following Davis (1980), a cohesive-frictional Mohr-Coulomb failure criterion is also used to describe the limiting strength of the rock joints.

For any joint set  $i$  the linearized Mohr-Coulomb failure surface may be expressed as:

$$F_i = |\tau| - c_i + \sigma_n \tan \phi_i = 0 \quad (12.63)$$

where  $\tau$  is the shear stress and  $\sigma_n$  is the normal stress on the joint. This failure criterion can be expressed in terms of  $\sigma_x$ ,  $\sigma_y$  and  $\sigma_{xy}$  using the following relations:

$$\sigma_n = \sigma_x \sin^2 \theta_i + \sigma_y \cos^2 \theta_i - \sigma_{xy} \sin 2\theta_i \quad (12.64)$$

$$\tau = -\frac{1}{2} \sigma_x \sin 2\theta_i + \frac{1}{2} \sigma_y \sin 2\theta_i + \sigma_{xy} \cos 2\theta_i \quad (12.65)$$

where  $\theta_i$  is the angle of the joint set  $i$  from the horizontal axis (positive anti-clockwise, refer Figure 12.9).

Using the relations (12.64) and (12.65) the failure criterion expressed in (12.63) may be re-written as:

$$\begin{aligned} F_i = \frac{1}{2} & |(\sigma_y - \sigma_x) \sin 2\theta + 2 \sigma_{xy} \cos 2\theta| \\ & - c_i + (\sigma_x \sin^2 \theta + \sigma_y \cos^2 \theta - \sigma_{xy} \sin 2\theta) \tan \phi_i = 0 \end{aligned} \quad (12.66)$$

#### *Linearized yield condition*

As described previously, joints in the rock mass modify the nature of the yield criterion. The effect of discontinuities is incorporated by including distinct failure sur-

faces for the intact rock material and for each of the joint sets. In this fashion the jointed rock mass is represented as a homogeneous but anisotropic material.

For the jointed rock material, the overall failure criterion is expressed by equations (12.62) and (12.66). In order to satisfy the yield conditions it is necessary to impose the constraints  $F_r \leq 0$  and  $F_i \leq 0$ . It is readily seen that for a joint set  $i$  the requirement that  $F_i \leq 0$  results in two linear constraints on the nodal stresses. If however, the inequality constraint  $F_r \leq 0$  is applied directly, non-linear constraints result since  $F_r$  is quadratic in the unknown stresses. Since the lower bound theorem is to be formulated as a linear programming problem, it is necessary to approximate (12.62) using a yield condition which is a linear function of the unknown stress variables. For the solution to be a rigorous lower bound the linear approximation to the failure surface must lie inside the generalized Mohr-Coulomb failure surface.

With reference to Figure 12.12, if  $p$  is the number of sides used to approximate the yield function (12.62), then the linearized yield function can be shown to be:

$$A_k \sigma_x + B_k \sigma_y + C_k \sigma_{xy} \leq E, \quad k = 1, 2, \dots, p \quad (12.67)$$

where

$$A_k = \cos\left(\frac{2\pi k}{p}\right) + \sin \phi \cos\left(\frac{\pi}{p}\right)$$

$$B_k = -\cos\left(\frac{2\pi k}{p}\right) + \sin \phi \cos\left(\frac{\pi}{p}\right)$$

$$C_k = 2 \sin\left(\frac{2\pi k}{p}\right)$$

$$E = 2c \cos \phi \cos\left(\frac{\pi}{p}\right)$$

Thus the linearized yield condition for the intact rock mass imposes  $p$  inequality constraints on the stresses at each node. In addition, the failure condition (12.66) for the joint leads to two linear inequality constraints on the unknown stresses:

$$A_k \sigma_x + B_k \sigma_y + C_k \sigma_{xy} \leq c_i, \quad k = p + 2i - 1, \quad p + 2i \quad (12.68)$$

where

$$A_{p+2i-1} = \sin^2 \theta_i \tan \phi_i - \frac{1}{2} \sin 2\theta_i$$

$$B_{p+2i-1} = \frac{1}{2} \sin 2\theta_i + \cos^2 \theta_i \tan \phi_i$$

$$C_{p+2i-1} = \cos 2\theta_i - \sin 2\theta_i \tan \phi_i$$

$$A_{p+2i} = \sin^2 \theta_i \tan \phi_i + \frac{1}{2} \sin 2\theta_i$$

$$B_{p+2i} = -\frac{1}{2} \sin 2\theta_i + \cos^2 \theta_i \tan \phi_i$$

$$C_{p+2i} = -\cos 2\theta_i - \sin 2\theta_i \tan \phi_i$$

By using a linearized failure surface it is sufficient to enforce the linear constraints (12.67) and (12.68) at each nodal point to ensure that the stresses satisfy the yield conditions everywhere.

### (b) Numerical examples

To illustrate the effectiveness of the procedure described above, a few examples involving rock joints are analysed in this section. The results are compared with available solutions obtained from the literature. Further details can be found in Yu and Sloan (1994c) and Sutcliffe *et al.* (2004).

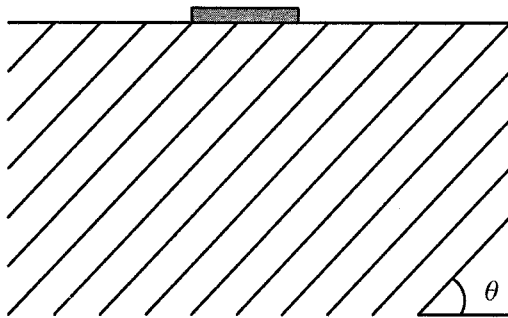


Figure 12.17: A strip footing resting on a rock mass with one joint set

#### *Bearing capacity of a strip footing on rock with one joint set*

The problem of the bearing capacity of a rigid footing on a rock mass with one set of joints (Figure 12.17) was also analysed. The lower bound mesh shown in Figure 12.18 is used. Ignoring the self weight of the material, the bearing capacity of the rock mass depends upon the cohesion and friction angle of the intact material and of the joint interfaces. Further, the orientation of the joint set plays a significant role in the determination of the collapse load.

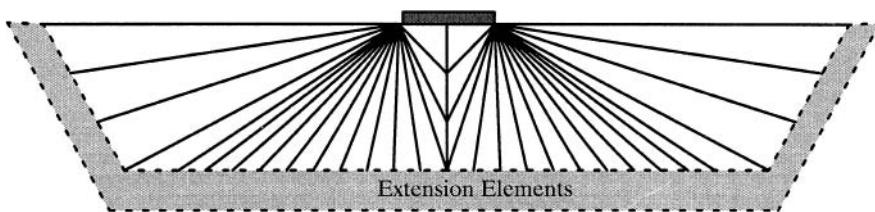


Figure 12.18: Lower bound finite element mesh for a strip footing on a joint rock mass

Figure 12.19 represents a comparison between the numerical lower bound solution and the displacement finite element solution of Alehossein *et al.* (1992) for a perfectly smooth rock-footing interface. The results are presented as normalised bearing capacity against the orientation of the joint set and represent the solution for the case where  $\phi = \phi_i = 35^\circ$  and  $c_i/c = 0.1$ . As expected, the displacement finite element solutions of Alehossein *et al.* (1992) tend to give higher results than those of the numerical lower bound method. The slip-line solution of Davis (1980) also results in a slightly higher result due mainly to the fact that a slip-line solution is not necessarily a rigorous lower bound.

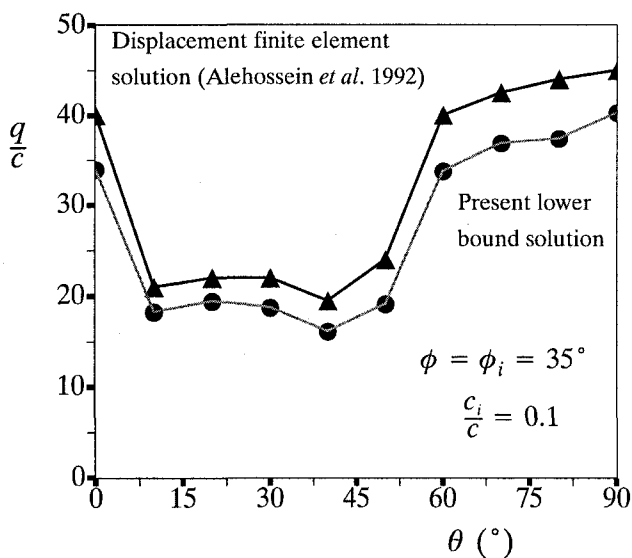


Figure 12.19: Bearing capacity versus angle of rock joints - one joint set

It is noted from Figure 12.19 that the minimum bearing capacity for this particular case occurs in the vicinity of joint orientations of around  $10^\circ$  and  $40^\circ$ . The two minimum bearing capacities are approximately half the maximum bearing capacity which occurs when the joint set is aligned vertically.

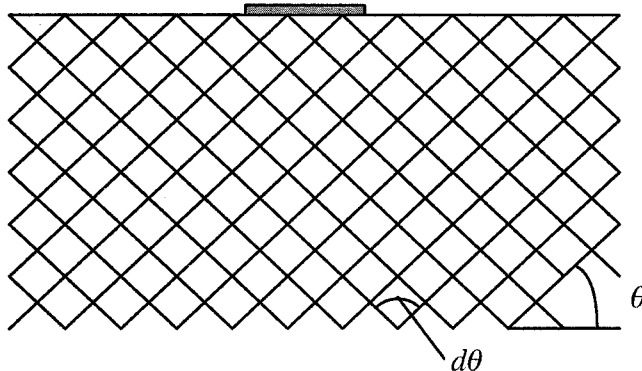


Figure 12.20: A strip footing on a rock mass with two joint sets

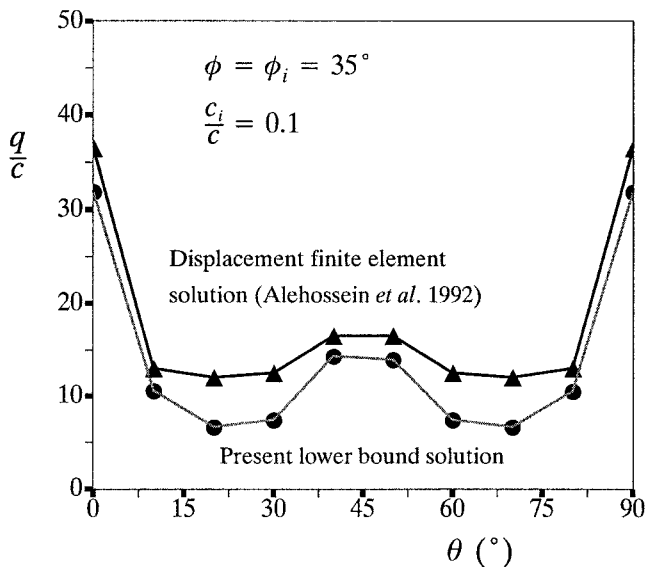


Figure 12.21: Bearing capacity versus angle of rock joints - two normal joint sets  
( $d\theta = 90^\circ$ )

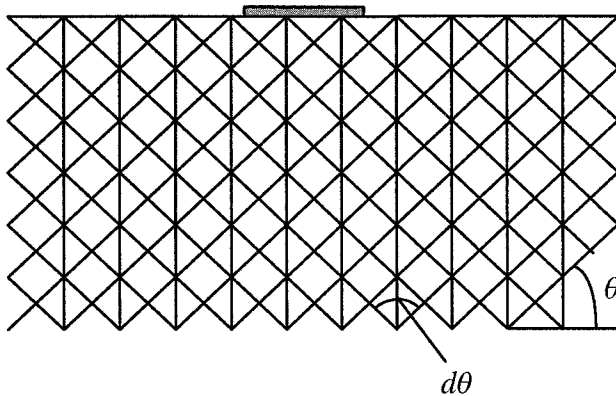


Figure 12.22: A strip footing on a rock mass with three joint sets

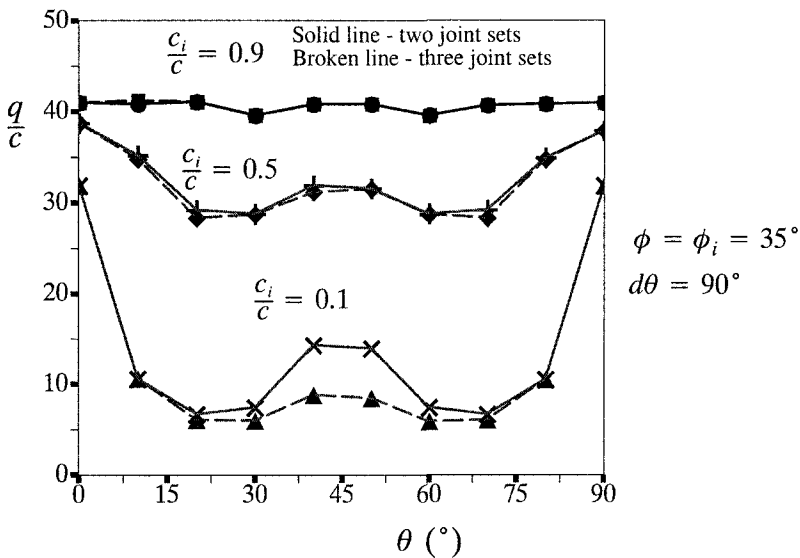


Figure 12.23: Bearing capacity versus angle of rock joints - two normal joint sets plus a vertical joint set

#### *Bearing capacity of a strip footing on rock with two joint sets*

The second problem to be analysed is that of the bearing capacity of a strip footing on a rock mass with two joint sets as shown in Figure 12.20. Figure 16 shows the comparison between the normalised bearing capacity for current lower bound solu-

tion and the displacement finite element solution of Alehossein *et al.* (1992) for the case where the joint sets are orthogonal and  $\phi = \phi_i = 35^\circ$ ,  $c_i/c = 0.1$ . As with the first example, the lower bound solution produces results less than that of the displacement finite element method. It can be seen that the minimum bearing capacities occur in the vicinity of joint orientations of  $20^\circ, 110^\circ$  and  $70^\circ, 160^\circ$ . The maximum bearing capacity is achieved when the joint sets are orientated vertically and horizontally.

*Bearing capacity of a strip footing on rock with three joint sets*

The final example is a simple extension of the second example above. Analyses were performed on a strip footing on a jointed rock mass with two joints sets at varying orientations and a third joint set aligned vertically (Figure 12.22).

Figure 12.23 presents the bearing capacity versus the orientation of joint sets. It is evident from these results that the inclusion of a third, vertically aligned joint set results in a further reduction in overall bearing capacity. The value of this reduction in capacity is again dependant on both the joint orientation and the relative orientation between the joint sets.

#### 12.3.4 Plane strain finite element formulations for anisotropic soils

It is generally accepted that the strength parameters of natural soils are anisotropic. Measurements of the fabric of clays have shown that the particles tend to become orientated in the horizontal direction during one dimensional deposition and subsequent loading. This preferred particle orientation causes an inherent anisotropy which can lead to changes in soil properties as the direction of the major principal stress varies during shear. Yu and Sloan (1995) were among the first to extend the finite element formulation of the collapse bound theorems to account for the anisotropic failure surfaces. The main changes lie in the detailed expression of the anisotropic failure criterion and its linear approximation, which are given below.

*Proposed anisotropic strength theory*

Based on the earlier studies of Lo (1965), the cohesive strength is assumed to vary with direction according to the following equation

$$c_\theta = c_h + (c_v - c_h) \sin^2 \theta \quad (12.69)$$

where  $c_h, c_v$  denote the limiting values of cohesion on the horizontal and vertical planes respectively and  $\theta$  is the angle between the direction of a plane where the limiting cohesion  $c_\theta$  is measured and the horizontal direction.

Because of the anisotropic nature of cohesion, the conventional isotropic Mohr-Coulomb failure criterion is no longer valid. The shear strength that can be developed on a plane that defines an angle of  $\theta$  from the horizontal direction is:

$$s = c_\theta - \sigma_n \tan \phi = c_h + (c_v - c_h) \sin^2 \theta - \sigma_n \tan \phi \quad (12.70)$$

where the normal and shear stress components on the plane are

$$\sigma_n = \sigma_x \sin^2 \theta + \sigma_y \cos^2 \theta - \sigma_{xy} \sin 2\theta \quad (12.71)$$

$$\tau = -\frac{1}{2} \sigma_x \sin 2\theta + \frac{1}{2} \sigma_y \sin 2\theta + \sigma_{xy} \cos 2\theta \quad (12.72)$$

There will be a critical plane on which the available shear strength  $s$  will first be reached as the shear stress increases namely:

$$\tau - s = 0 \quad (12.73)$$

The orientation of this critical plane can be obtained by solving for

$$\frac{\partial(\tau - s)}{\partial \theta} = 0 \quad (12.74)$$

Solving for the critical orientation angle from (12.74) and substituting into (12.73) gives the following anisotropic strength criterion:

$$F = X^2 + Y^2 - R^2 = 0 \quad (12.75)$$

where

$$X = \sigma_y - \sigma_x - 2\sigma_{xy} \tan \phi$$

$$Y = c_v - c_h + 2\sigma_{xy} - \sigma_x \tan \phi + \sigma_y \tan \phi$$

$$R = c_v + c_h - \sigma_x \tan \phi - \sigma_y \tan \phi$$

#### *Internal linearized yield criterion*

If  $p$  is the number of sides used to approximate the yield function (12.75), then the internal linearized yield function can be shown to be (Yu and Sloan, 1995):

$$A_k \sigma_x + B_k \sigma_y + C_k \sigma_{xy} \leq D_k, \quad k = 1, 2, \dots, p \quad (12.76)$$

where

$$A_k = -\cos \frac{2\pi k}{p} - \tan \phi \sin \frac{2\pi k}{p} + \tan \phi \cos \frac{\pi}{p}$$

$$B_k = \cos \frac{2\pi k}{p} + \tan \phi \sin \frac{2\pi k}{p} + \tan \phi \cos \frac{\pi}{p}$$

$$C_k = -2 \tan \phi \cos \frac{2\pi k}{p} + 2 \sin \frac{2\pi k}{p}$$

$$D_k = (c_v + c_h) \cos \frac{\pi}{p} + (c_h - c_v) \sin \frac{2\pi k}{p}$$

### 12.3.5 Plane strain finite element formulations for reinforced soils

The increasing use of reinforced soils in geotechnical engineering requires the development of reliable and practical yield design methods for reinforced earth structures. For this reason, Yu and Sloan (1997) developed a finite element formulation for performing both lower and upper bound limit analyses. In their formulation, the conventional isotropic Mohr-Coulomb yield criterion is modified to include the effect of anisotropy which is caused by the presence of reinforcement. The influence of the soil-reinforcement failure conditions on the overall behaviour is taken into account by assuming that the shear and normal stresses at the interface are governed by a general Mohr-Coulomb criterion.

#### *Failure conditions for reinforced soils*

In Yu and Sloan (1997), the reinforced soil is treated as a macroscopically homogeneous but anisotropic material. The soil is assumed to be reinforced uni-directionally, which is the situation in most practical applications, and three stress tensors are defined at every point in the homogenised continuum as detailed in Yu and Sloan (1994c). The first tensor defines the macrostress,  $\sigma_{ij}$ , while the other tensors,  $\sigma^s_{ij}$  and  $\sigma^r_{ij}$ , describe the microstresses which act on the soil and reinforcement respectively. In the x-y plane, the reinforcement is assumed to be of thickness  $d$  and of equal normal spacing  $h$ . For cases where the proportion of the reinforcement is very small so that  $d/h \ll 1$ , these three stress tensors are related in the following way (e.g. de Buhan *et al.*, 1989):

$$\sigma_x^s = \sigma_x - \sigma^r \cos^2 \theta \quad (12.77)$$

$$\sigma_y^s = \sigma_y - \sigma^r \sin^2 \theta \quad (12.78)$$

$$\sigma_{xy}^s = \sigma_{xy} - \sigma^r \sin \theta \cos \theta \quad (12.79)$$

where  $\sigma^r$  is the actual tensile stress acting in the reinforcement times  $d/h$  and  $\theta$  represents the angle between the direction of the reinforcement and the horizontal x-axis.

Following de Buhan *et al.* (1989), it is assumed that the reinforcing inclusions inside the soil act merely as tensile load carrying elements, and offer no resistance to shear, bending or compression. The constraint

$$0 \leq \sigma^r \leq \sigma_0 \quad (12.80)$$

is therefore imposed on  $\sigma^r$ , where  $\sigma_0 = (d/h)\sigma_{yield}$  and  $\sigma_{yield}$  denotes the actual tensile yield strength of the reinforcement. It should be noted that if required the for-

mulation can be easily modified to permit the reinforcement to carry a finite load in compression.

If the soil mass is assumed to obey the Mohr-Coulomb failure condition, we have

$$F_s = (\sigma_x^s - \sigma_y^s)^2 + (2\sigma_{xy}^s)^2 - (2c \cos \phi - (\sigma_x^s + \sigma_y^s) \sin \phi)^2 = 0 \quad (12.81)$$

which can be written in terms of the microstresses as follows

$$\begin{aligned} F_s = & (\sigma_x - \sigma_y - \sigma^r \cos 2\theta)^2 + (2\sigma_{xy} - \sigma^r \sin 2\theta)^2 \\ & - (2c \cos \phi - (\sigma_x + \sigma_y - \sigma^r) \sin \phi)^2 = 0 \end{aligned} \quad (12.82)$$

Apart from considering the failure condition for the soil mass, we also need to ensure that the soil-reinforcement interface does not violate the yield criterion, namely

$$F_i = |\tau| - c_i + \sigma_n \tan \phi_i = 0 \quad (12.83)$$

where  $\tau$  is the shear stress and  $\sigma_n$  is the normal stress on the interface, and  $c_i$  and  $\phi_i$  denote the interface cohesion and interface friction angle respectively. The above failure condition can be expressed in terms of the macrostress tensor

$$\begin{aligned} F_i = & \frac{1}{2} |\sin 2\theta (\sigma_y - \sigma_x) + 2 \cos 2\theta \sigma_{xy}| \\ & - c_i + (\sin^2 \theta \sigma_x + \cos^2 \theta \sigma_y - \sin 2\theta \sigma_{xy}) \tan \phi_i = 0 \end{aligned} \quad (12.84)$$

#### *Linearization of failure conditions for reinforced soils*

With reference to Figure 12.24, the linearized form of  $F_s$  (equation (12.82)) can be shown to be:

$$A_k \sigma_x + B_k \sigma_y + C_k \sigma_{xy} + D_k \sigma^r \leq 2c \cos \phi \cos \frac{\pi}{p}, \quad k = 1, 2, \dots, p \quad (12.85)$$

where

$$A_k = \cos\left(\frac{2\pi k}{p}\right) + \sin \phi \cos\left(\frac{\pi}{p}\right)$$

$$B_k = -\cos\left(\frac{2\pi k}{p}\right) + \sin \phi \cos\left(\frac{\pi}{p}\right)$$

$$D_k = -\cos 2\theta \cos \frac{2\pi k}{p} - \sin 2\theta \sin \frac{2\pi k}{p} - \sin \phi \cos \frac{\pi}{p}$$

Thus the linearized yield condition for the homogenised soil imposes  $p$  inequality constraints on the macrostresses at any given point. Similarly the failure criterion

for the soil-reinforcement interface (12.84) leads to two linear inequality constraints in the unknown macrostresses:

$$A_k \sigma_x + B_k \sigma_y + C_k \sigma_{xy} \leq c_i, \quad k = p + 1, \quad p + 2 \quad (12.86)$$

where

$$A_{p+1} = \sin^2 \theta \tan \phi_i - \frac{1}{2} \sin 2\theta$$

$$B_{p+1} = \frac{1}{2} \sin 2\theta + \cos^2 \theta \tan \phi_i$$

$$C_{p+1} = \cos 2\theta - \sin 2\theta \tan \phi_i$$

$$A_{p+2} = \sin^2 \theta \tan \phi_i + \frac{1}{2} \sin 2\theta$$

$$B_{p+2} = -\frac{1}{2} \sin 2\theta + \cos^2 \theta \tan \phi_i$$

$$C_{p+2} = -\cos 2\theta - \sin 2\theta \tan \phi_i$$

$$Y = 2\sigma_{xy} - \sigma' \sin 2\theta$$

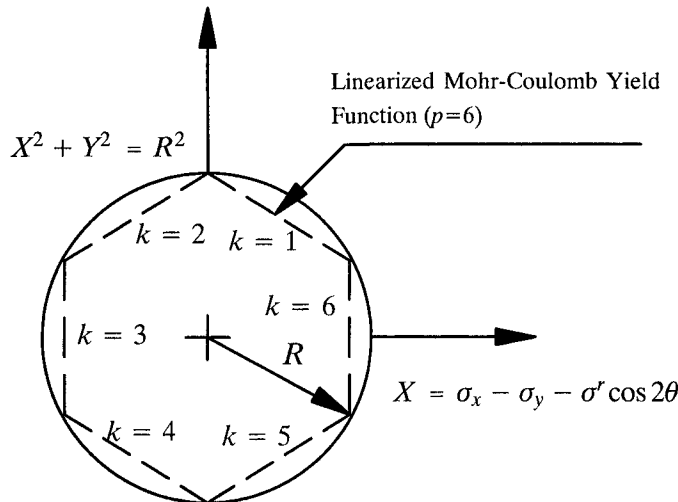


Figure 12.24: Linearized Mohr-Coulomb yield function ( $p=6$ )

Since the reinforcement is assumed to carry negligible load in compression and a finite load in tension, we also need to impose the additional restriction (12.80). It is sufficient to enforce the inequalities (12.80), (12.85) and (12.86) on each set of nodal stresses in order that they are satisfied throughout the mesh.

## 12.4 UPPER BOUND ANALYSIS USING LINEAR PROGRAMMING

## 12.4.1 Formulation based on constant strain finite elements

## (a) Numerical formulation

For upper bound analysis, Sloan and Kleeman (1995) developed an effective finite element formulation that allows for velocity discontinuities everywhere in the mesh. This method is based on the linear three-noded triangle but a velocity discontinuity may occur at any edge that is shared by a pair of adjacent triangles, and the sign of shearing is chosen automatically during the optimisation process to give the least amount of dissipated power.

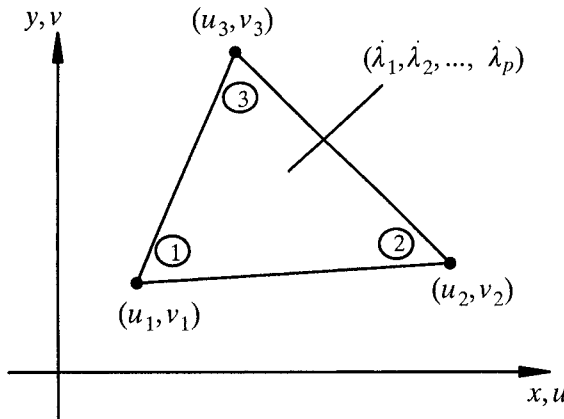


Figure 12.25: Three-noded linear triangle for upper bound analysis

The three-noded triangle used in the upper bound formulation is shown in Figure 12.25. Each node has two velocity components and each element has  $p$  plastic multiplier rates (where  $p$  is the number of planes in the linearized yield criterion). Within a triangle, the velocities are assumed to vary linearly according to

$$u = \sum_{i=1}^{i=3} N_i u_i \quad (12.87)$$

$$v = \sum_{i=1}^{i=3} N_i v_i \quad (12.88)$$

where  $(u_i, v_i)$  are nodal velocities in the  $x$  and  $y$  directions respectively and  $N_i$  are linear shape functions.

### Constraints from plastic flow in continuum

The upper bound theorem demands that the velocity field must satisfy the set of constraints imposed by an associated flow rule. For plane strain deformation, the associated flow rule is of the form

$$\dot{\varepsilon}_x = \frac{\partial u}{\partial x} = \lambda \frac{\partial F}{\partial \sigma_x} \quad (12.89)$$

$$\dot{\varepsilon}_y = \frac{\partial v}{\partial y} = \lambda \frac{\partial F}{\partial \sigma_y} \quad (12.90)$$

$$\dot{\gamma}_{xy} = \frac{\partial v}{\partial x} + \frac{\partial u}{\partial y} = \lambda \frac{\partial F}{\partial \tau_{xy}} \quad (12.91)$$

where  $\lambda \geq 0$  is a plastic multiplier rate and tensile strains are taken as positive.

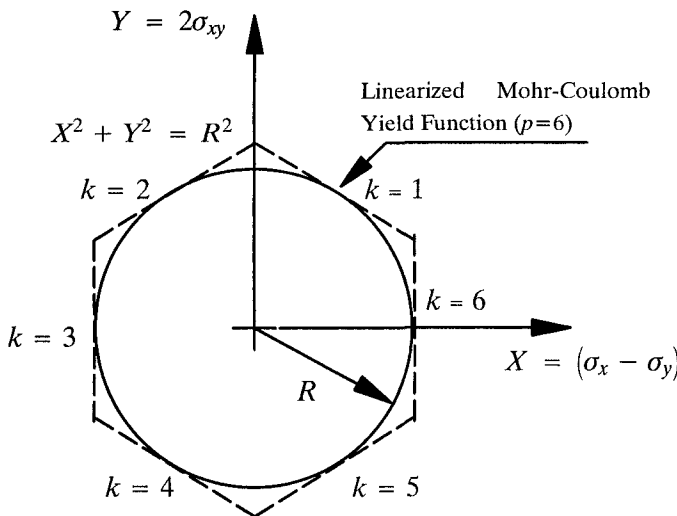


Figure 12.26: Linearized Mohr-Coulomb yield function ( $p=6$ ) for upper bound analysis

To remove the stress terms from the flow rule equations, and thus provide a linear relationship between the unknown velocities and plastic multiplier rates, a linear approximation to the Mohr-Coulomb yield criterion is employed. Unlike a lower bound formulation, an external surface must be used for upper bound analysis to ensure its upper bound nature.

For an external linearisation with  $p$  planes as shown in Figure 12.26, the equations of the  $k$ th plane of the Mohr-Coulomb criterion can be written as follows:

$$F_k = A_k \sigma_x + B_k \sigma_y + C_k \sigma_{xy} - 2c \cos \phi = 0, \quad k = 1, 2, \dots, p \quad (12.92)$$

where

$$A_k = \cos\left(\frac{2\pi k}{p}\right) + \sin \phi$$

$$B_k = -\cos\left(\frac{2\pi k}{p}\right) + \sin \phi$$

$$C_k = 2 \sin\left(\frac{2\pi k}{p}\right)$$

The flow rule imposes three equality constraints on the nodal velocities and plastic multiplier rates for each element. For the linearized yield criterion defined by (12.92), the plastic strain rates are given by

$$\dot{\epsilon}_x = \frac{\partial u}{\partial x} = \sum_{k=1}^{k=p} \dot{\lambda}_k \frac{\partial F_k}{\partial \sigma_x} = \sum_{k=1}^{k=p} \dot{\lambda}_k A_k \quad (12.93)$$

$$\dot{\epsilon}_y = \frac{\partial v}{\partial y} = \sum_{k=1}^{k=p} \dot{\lambda}_k \frac{\partial F_k}{\partial \sigma_y} = \sum_{k=1}^{k=p} \dot{\lambda}_k B_k \quad (12.94)$$

$$\dot{\gamma}_{xy} = \frac{\partial v}{\partial x} + \frac{\partial u}{\partial y} = \sum_{k=1}^{k=p} \dot{\lambda}_k \frac{\partial F_k}{\partial \sigma_{xy}} = \sum_{k=1}^{k=p} \dot{\lambda}_k C_k \quad (12.95)$$

where  $\dot{\lambda}_k \geq 0$  is the plastic multiplier rate associated with the  $k$ th plane of the yield surface.

By using equations (12.87) and (12.88), the flow rule constraints for each triangle may be written as follows

$$\sum_{i=1}^{i=3} \frac{\partial N_i}{\partial x} u_i - \sum_{k=1}^{k=p} \dot{\lambda}_k A_k = 0 \quad (12.96)$$

$$\sum_{i=1}^{i=3} \frac{\partial N_i}{\partial y} v_i - \sum_{k=1}^{k=p} \dot{\lambda}_k B_k = 0 \quad (12.97)$$

$$\sum_{i=1}^{i=3} \frac{\partial N_i}{\partial x} v_i + \sum_{i=1}^{i=3} \frac{\partial N_i}{\partial y} u_i - \sum_{k=1}^{k=p} \dot{\lambda}_k C_k = 0 \quad (12.98)$$

#### *Constraints from plastic shearing in velocity discontinuities*

A typical velocity discontinuity in the upper bound mesh is shown in Figure 12.27. The discontinuity occurs at the common edge between two adjacent triangles, defined by the nodal pairs (1,2) and (3,4) and is of zero thickness.

With the Mohr-Coulomb criterion with the associated flow rule, the normal and tangential velocity jumps across the discontinuity must satisfy the following equation:

$$\frac{\Delta v}{|\Delta u|} = \tan \phi \quad (12.99)$$

where  $\Delta v$  is the normal velocity jump and  $\Delta u$  is the tangential velocity jump. The absolute sign on the tangential velocity jump is consistent with the fact that the dilation occurs regardless of the sign of tangential shearing.

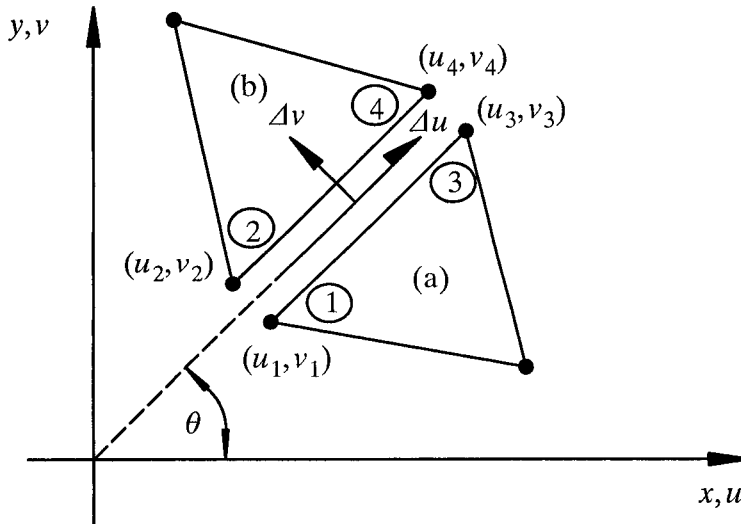


Figure 12.27: A velocity discontinuity between adjacent triangles

For any pair of nodes on the discontinuity (i,j), it can be shown that the tangential and normal velocity jumps can be defined as the velocities of the nodes i and j:

$$\Delta u_{ij} = (u_j - u_i) \cos \theta + (v_j - v_i) \sin \theta \quad (12.100)$$

$$\Delta v_{ij} = (u_i - u_j) \sin \theta + (v_i - v_j) \cos \theta \quad (12.101)$$

where  $\theta$  is the angle of the discontinuity to the x-axis as shown in Figure 12.27.

To cast the upper bound formulation as a linear programming problem, it is necessary to remove the absolute sign in the flow rule (12.99). Bottero *et al.* (1980) and Sloan (1989) specified a sign condition so that  $s\Delta u$  replaces  $|\Delta u|$  where  $s$  is either equal to 1 or -1 (and this needs to be specified for a velocity before the calculation starts). This method enables the linear programming formulation to be preserved, but has the disadvantage that it requires additional constraints of the form

$$s\Delta u_{ij} \geq 0 \quad (12.102)$$

to be imposed at each nodal pair (i,j) on the discontinuity.

In the work of Sloan and Kleeman (1995), a better formulation was developed to permit an arbitrary number of velocity discontinuities with un-prescribed signs. In this formulation, each nodal pair (i,j) on a discontinuity is associated with two nonnegative variables  $u_{ij}^+$  and  $u_{ij}^-$ , which give rise to two additional unknowns. The tangential velocity jump at each nodal pair  $\Delta u_{ij}$  is defined as the difference between these two quantities according to

$$\Delta u_{ij} = u_{ij}^+ - u_{ij}^- \quad (12.103)$$

with

$$u_{ij}^+ \geq 0 \quad (12.104)$$

$$u_{ij}^- \geq 0 \quad (12.105)$$

By comparing equations (12.100) and (12.103), we have

$$u_{ij}^+ - u_{ij}^- = (u_j - u_i) \cos \theta + (v_j - v_i) \sin \theta \quad (12.106)$$

In order to be compatible with the velocity expansions in the triangles, the quantities  $u_{ij}^+$ ,  $u_{ij}^-$  are assumed to vary linearly along the discontinuity.

To avoid the need for absolute value signs in the flow rule relations, Sloan and Kleeman (1995) assumed that  $|u^+ - u^-|$  can be replaced by  $u^+ + u^-$  in equation (12.99) so that the normal velocity jump is given by

$$\Delta v = (u^+ + u^-) \tan \phi \quad (12.107)$$

which needs to be imposed at both nodal pairs on the discontinuity. The above substitution is clearly inexact if  $u^+$  and  $u^-$  are both positive simultaneously. Thus the correct flow rule is satisfied only if either  $u^+$  or  $u^-$  is equal to zero at both nodes of the discontinuity. If this is not the case, Sloan and Kleeman (1995) proved that the discontinuity behaves as though it were in a soil of greater strength. This key result ensures that the formulation of making use of a revised flow rule (12.107) will yield a rigorous upper bound on the true collapse load.

### *Constraints from velocity boundary conditions*

To be kinematically admissible, the velocity field must satisfy the boundary conditions. Consider a node i on a boundary that is inclined at angle of  $\theta$  to the x-axis. For a general case, where the boundary is subject to a prescribed tangential velocity

$u_0$  and a prescribed normal velocity  $v_0$ , the nodal velocity components  $(u_i, v_i)$  must satisfy the following constraints:

$$\begin{bmatrix} \cos \theta & \sin \theta \\ -\sin \theta & \cos \theta \end{bmatrix} \begin{bmatrix} u_i \\ v_i \end{bmatrix} = \begin{bmatrix} u_0 \\ v_0 \end{bmatrix} \quad (12.108)$$

#### *Power dissipation in the continuum*

In the proposed upper bound formulation, plastic flow may occur in both the continuum and the velocity discontinuities. The total power dissipated in these shearing modes forms the objective function and is expressed in terms of the unknowns. Within each triangle, the power dissipation by the stresses is given by

$$P_c = \iint_A (\sigma_x \dot{\epsilon}_x + \sigma_y \dot{\epsilon}_y + \sigma_{xy} \dot{\gamma}_{xy}) dA \quad (12.109)$$

By making use of the flow rules and the yield condition, the above equation reduces to

$$P_c = 2A \cos \phi \sum_{k=1}^{k=p} \lambda_k \iint_A c dA \quad (12.110)$$

It is noted that a linear variation of the cohesion can also be taken into account using the above equation.

#### *Power dissipation in velocity discontinuities*

The power dissipated by plastic shearing along a velocity discontinuity is given by an integral of the form

$$P_d = \int_l c |\Delta u| dl \quad (12.111)$$

As previously discussed it was necessary to replace  $|u^+ - u^-|$  by  $u^+ + u^-$  in the velocity flow rule. Therefore the power dissipation (12.111) should also be replaced by the following equation

$$P_d = \int_l c (u^+ + u^-) dl \quad (12.112)$$

#### *Upper bound linear programming problem*

The objective function coefficients for each triangle and discontinuity, which describe the internal power dissipation, are summarised by equations (12.110) and

(12.112). All of these node and element coefficients may be assembled in the usual manner to give the following linear programming problem

$$\begin{aligned}
 & \text{Minimize} && C_2^T X_2 + C_3^T X_3 && (12.113) \\
 & \text{Subject to} && A_{11} X_1 + A_{12} X_2 & = \mathbf{0} \\
 & && A_{21} X_1 + A_{23} X_3 & = \mathbf{0} \\
 & && A_{31} X_1 & = B_3 \\
 & && A_{41} X_1 & = B_4 \\
 & && A_{51} X_1 & = B_5 \\
 & && X_2 & \geq \mathbf{0} \\
 & && X_3 & \geq \mathbf{0}
 \end{aligned}$$

where  $X_1$  is a global vector of nodal velocities,  $X_2$  is a global vector of element plastic multiplier rates and  $X_3$  is a global vector of discontinuity parameters.

### (b) Numerical application to limit analysis of slopes

we now apply the lower bound formulation presented in Section 12.3 and the upper bound formulation presented in this section to perform stability analysis of slopes. The presentation is based on the work of Yu *et al.* (1998).

#### *Problem of stability of simple slopes*

The slope geometry analysed by Yu *et al.* (1998) is shown in Figure 12.28. Two types of analysis are considered: undrained stability analysis of purely cohesive slopes and drained stability analysis of cohesive-frictional slopes. The purely cohesive soil under undrained loading conditions is modelled by a rigid perfectly-plastic Tresca yield criterion with an associated flow rule. The strength of the cohesive soil is determined by the undrained shear strength  $S_u$  which may increase linearly with depth as is the case in normally consolidated clays (Gibson and Morgenstern, 1962; Hunter and Schuster, 1968). Under drained loading conditions, a perfectly-plastic Mohr-Coulomb model is used to describe the soil behaviour. For this case, the strength parameters are the effective cohesion  $c'$  and the effective friction angle  $\phi'$ . Both of these quantities are assumed to be constant throughout the slope. For simplicity, the effect of seepage (or pore pressures) on the stability of cohesive-frictional slopes has not been included in this study. The solutions obtained are therefore only relevant for fully drained loading conditions where the effect of pore pressures can be neglected. Recent work by Miller and Hamilton (1989) and Micha-

lowski (1994) suggests that it is also possible to incorporate the effect of pore pressures in limit analysis. Such an extension has been made by Kim *et al.* (1999).

The solutions for the simple slopes considered here are relevant to excavations and man-made fills built on soil or rock (Taylor, 1948; Gibson and Morgenstern, 1962; Hunter and Schuster, 1968; Duncan *et al.*, 1987). Duncan *et al.* (1987) have showed that stability charts for simple slopes can also be used to obtain reasonably accurate answers for more complex problems if irregular slopes are approximated by simple slopes and carefully determined averaged values of unit weight, cohesion, and friction angles are used.

In the analyses considered in this section, three-noded stress and velocity triangular elements with stress and velocity discontinuities are used for lower and upper bound analyses respectively. Typical lower bound and upper bound meshes for a simple slope are shown in Figure 12.29(a) and (b). Relevant boundary conditions are also shown in the figures.

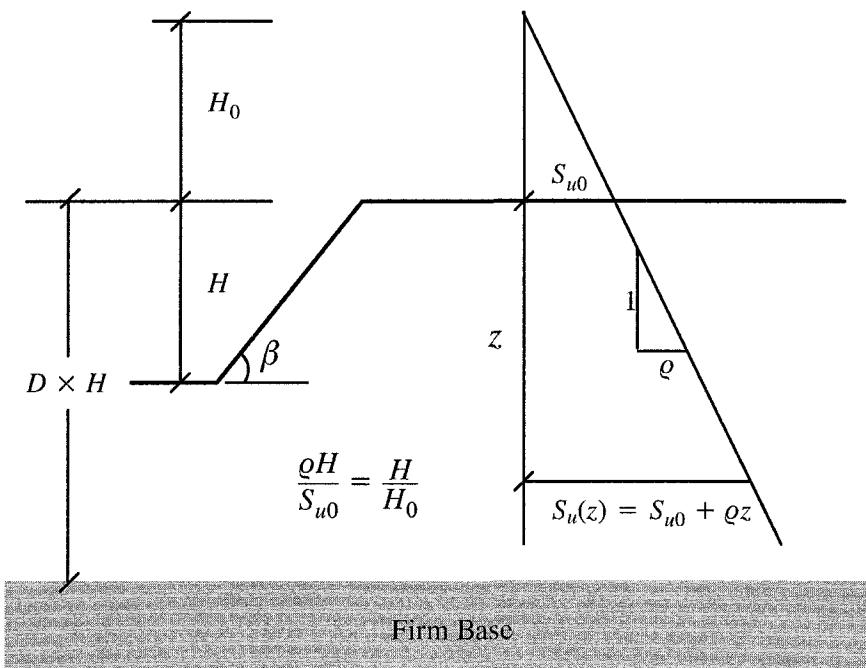
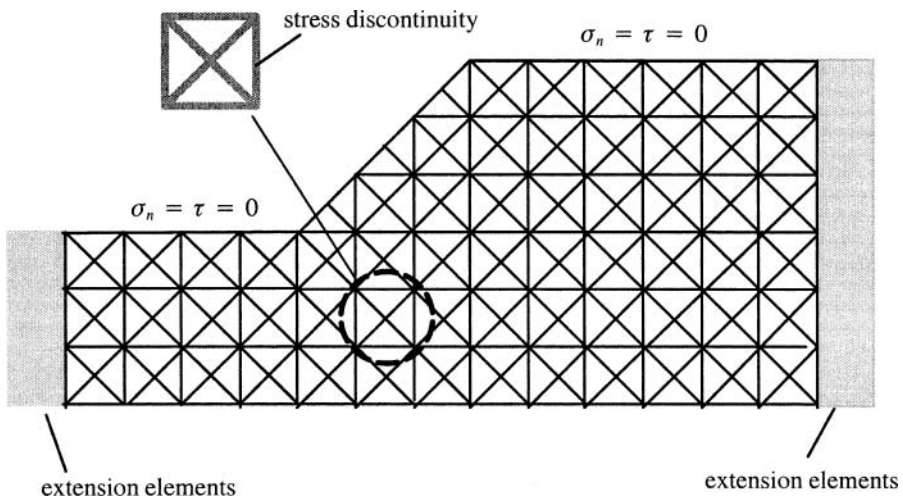
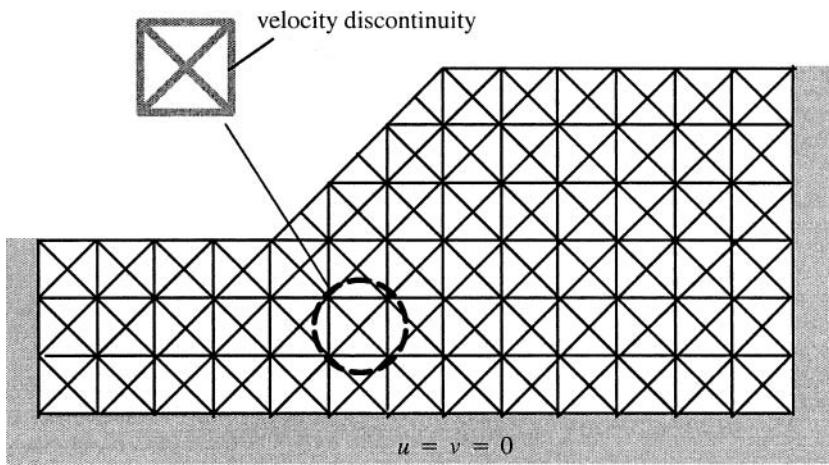


Figure 12.28: Stability of a simple slope



(a) A typical lower bound mesh for slope analysis



(b) A typical upper bound mesh for slope analysis

Figure 12.29: Typical lower and upper bound meshes for slope analysis

### *Results for undrained stability of slopes*

The results of undrained slope stability calculations using the upper and lower bound methods of limit analysis and Bishop's limit equilibrium method are presented in Figure 12.30 to Figure 12.33 for slope angles of  $\beta = 75^0, 60^0, 45^0, 15^0$  respectively. Note that the top and bottom solid lines are used to represent numerical upper and lower bound solutions. The solutions from the limit equilibrium computer code, STABL, are plotted as the dashed lines. For each slope angle, the results for four different depth factors of  $D=1, 1.5, 2, 4$  are given. To account for the effect of increasing strength with depth, the results are presented in terms of the stability number  $N_F = \gamma H/S_{uo}^m = \gamma HF/S_{uo}$  against a dimensionless parameter  $\lambda_{cq} = \varrho H/S_{uo}^m = \varrho HF/S_{uo}$ , where  $\gamma$  is the unit weight of the soil,  $\varrho$  denotes the rate of increase of the undrained shear strength with depth (Figure 12.28), and  $S_{uo}$  and  $S_{uo}^m$  denote, respectively, the actual (or available) shear strength and the mobilized strength of the soil. Note that for undrained cases, the factor of safety is defined as  $F = S_{uo}/S_{uo}^m$ .

In the undrained limit analyses, for given  $\varrho$  and slope geometry parameters of  $H, D, \beta$ , and mobilized shear strength  $S_{uo}^m$ , the upper and lower bound programs are used to obtain the best upper and lower bounds on the unit weight  $\gamma$ . Once this is known, the stability number  $N_F = \gamma H/S_{uo}^m = \gamma HF/S_{uo}$  and the dimensionless parameter  $\lambda_{cq} = \varrho H/S_{uo}^m = (\varrho HF)/S_{uo}$  can be calculated. On the other hand, when the limit equilibrium code is used, we first set the values of  $H, D, \gamma, \beta, S_{uo}$  and  $\varrho$  and then determine the safety factor  $F$ . As a result, the stability number  $N_F = (\gamma HF)/S_{uo}$  and the dimensionless parameter  $\lambda_{cq} = (\varrho HF)/S_{uo}$  can be calculated.

For almost all the cases considered, the exact solutions are bracketed within 5-10% by the upper and lower bound solutions. The comparison of the bounding solutions with the limit equilibrium results can best be considered separately for soils with a constant undrained shear strength profile and those with increasing strength with depth. If the undrained shear strength of the soil is constant ( $\lambda_{cq} = 0$ ), Bishop's limit equilibrium solutions are found to be in good agreement with the rigorous upper and lower bounds. On the other hand, if the undrained shear strength of the soil increases linearly with depth ( $\lambda_{cq} > 0$ ), the limit equilibrium results are generally close to the upper bound solutions for steep slopes. When the slope angle is less than 30 degrees, the limit equilibrium analysis tends to underestimate the true stability number. This underestimation is particularly significant when  $\beta = 15^0$  and  $\lambda_{cq} > 0.5$ . For example, Figure 12.33 shows that when

$D = 4$ ,  $\beta = 15^0$  and  $\lambda_{cq} = 1.0$ , the limit equilibrium method underestimates the true stability number by as much as 35%.

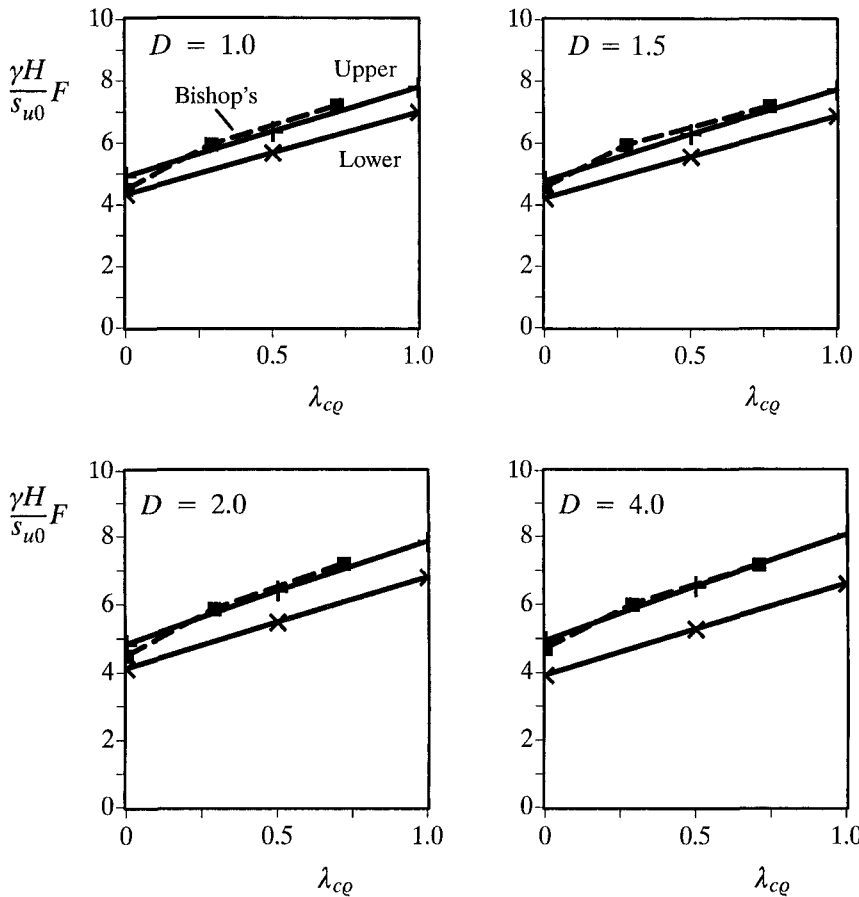


Figure 12.30: Effect of increasing strength with depth on stability number for slope angle of 75 degrees

In summary, the Bishop limit equilibrium method produces reasonably accurate solutions for the stability of homogeneous slopes. For slopes in soils whose strength increases with depth, significant underestimation of the stability number can be obtained from the limit equilibrium analysis for slopes with a low slope angle and a high  $\lambda_{cq}$  value.

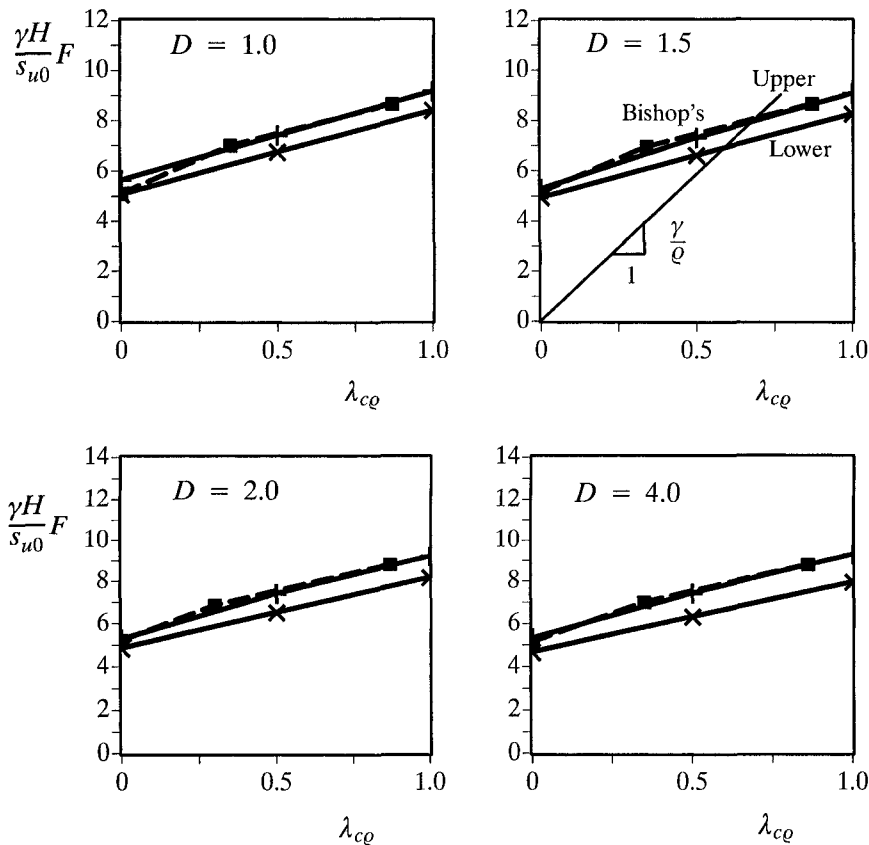


Figure 12.31: Effect of increasing strength with depth on stability number for slope angle of 60 degrees

As far as the effect of increasing strength with depth is concerned, it is most interesting to note that the bounding solutions suggest that the stability number increases approximately linearly with the value of  $\lambda_{cQ}$ . Figure 12.34 presents the effect of slope angle on the stability number for slopes with two different  $\lambda_{cQ}$  values and two different depth factors. As expected, for all the cases considered the stability number decreases with increasing value of the slope angle. The effect of slope angle on the stability number is found to be more significant for the slopes with a low value of depth factor and a high  $\lambda_{cQ}$  value.

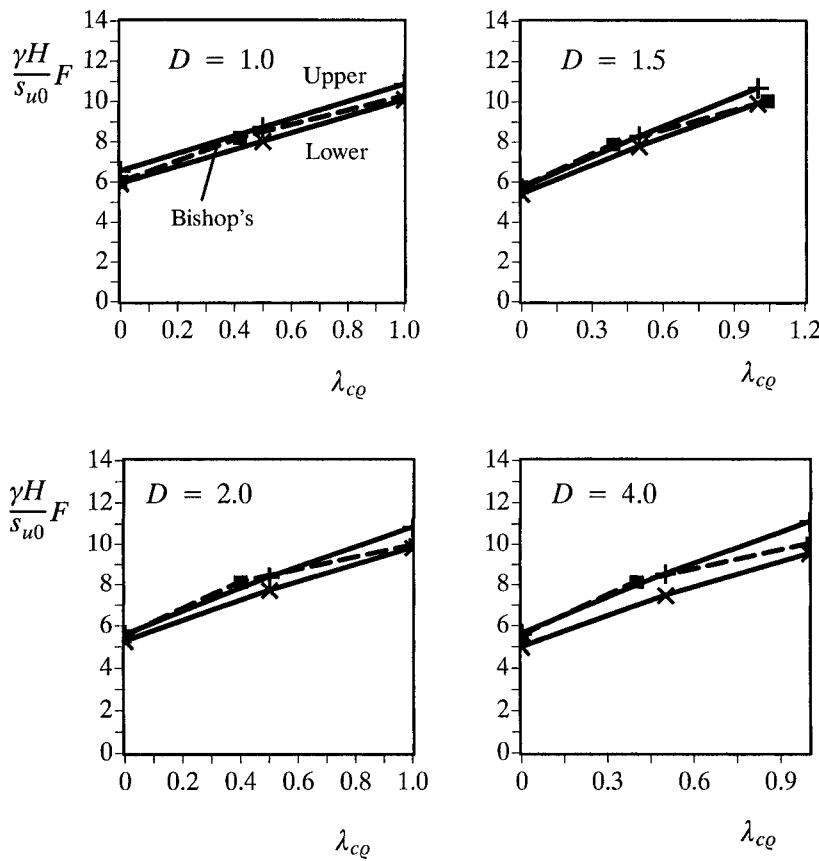


Figure 12.32: Effect of increasing strength with depth on stability number for slope angle of 45 degrees

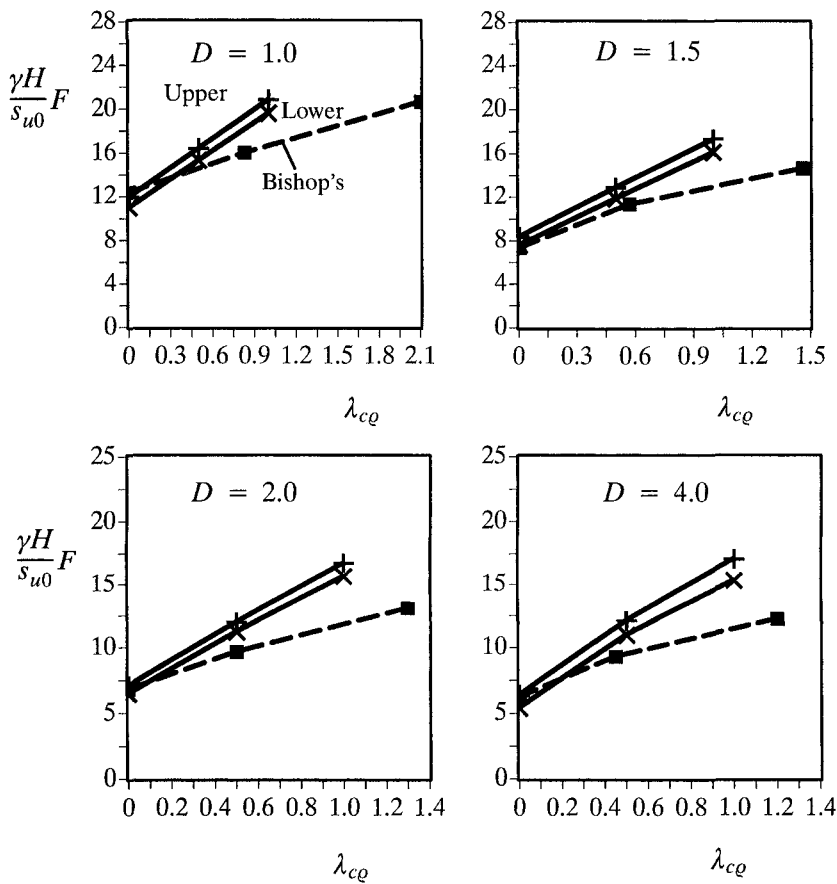


Figure 12.33: Effect of increasing strength with depth on stability number for slope angle of 15 degrees

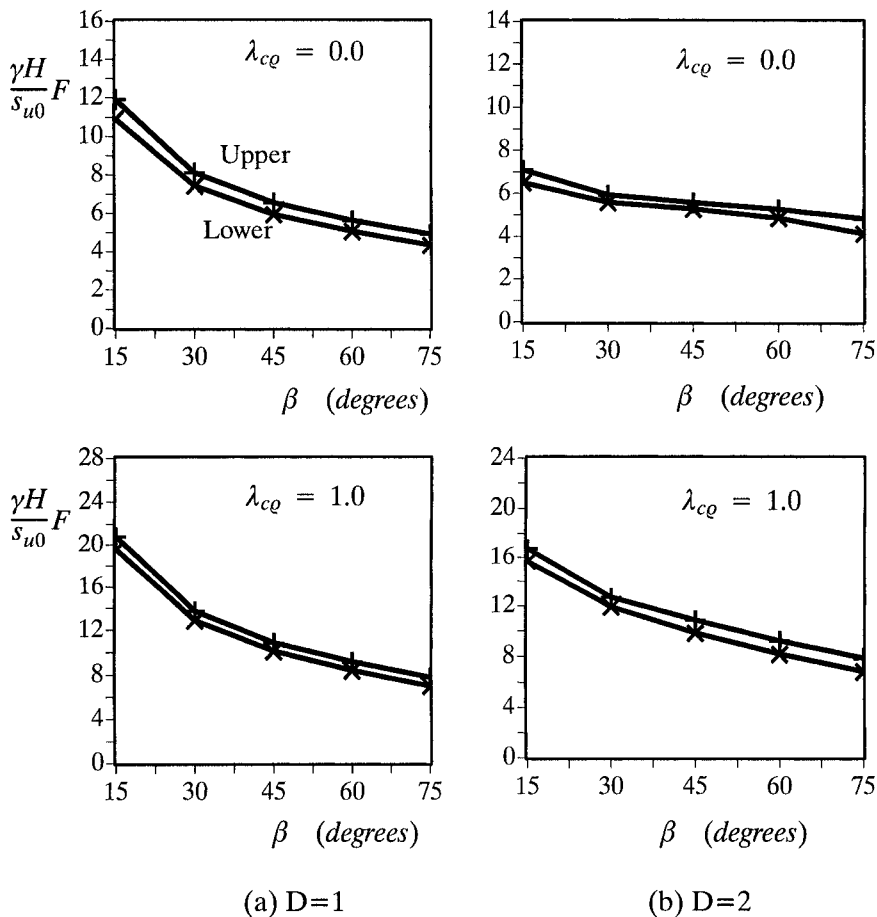


Figure 12.34: Effect of slope angle on stability number

*Example of Application for undrained stability analysis*

We now illustrate how the results presented in Figure 12.30 to Figure 12.33 can be used to determine the factor of safety for a clay slope.

**Problem:** A cut slope is to be excavated in a normally consolidated clay. The slope has the following parameters: the slope angle  $\beta = 60^0$ , the height of the slope is  $H = 12$  m, the depth factor is  $D = 1.5$ , the soil unit weight is  $\gamma = 18.5\text{kN/m}^3$ . The undrained shear strength of the soil on the top of the slope surface is  $s_{u0} = 40\text{kN/m}^2$  and the rate of increase of the undrained shear strength with depth

is estimated as  $\varrho = 1.5 kN/m^3$ . What is the factor of safety of this soil slope against undrained failure?

A procedure for using the results of the present study to solve the above slope stability problem can be summarized as follows:

(1) From the values of  $\gamma$ ,  $H$ ,  $s_{u0}$  and  $\varrho$ , we can calculate the dimensionless parameters:

$$\frac{\gamma H}{s_{u0}} = (18.5 \times 12)/40 = 5.55;$$

(2) Determine the ratio of  $\frac{N_F}{\lambda_{c\varrho}} = (\frac{\gamma H}{s_{u0}} F) / (\frac{\varrho H}{s_{u0}} F) = \frac{\gamma}{\varrho} = \frac{18.5}{1.5} = 12.33$ ;

(3) With  $\beta = 60^\circ$  and  $D = 1.5$ , it follows that the results presented in Figure 12.31 should be used to determine the safety factor;

(4) In Figure 12.31, draw a straight line passing through the origin with a gradient of  $\gamma/\varrho = 12.33$ . This straight line will intersect with the three curves representing the lower bound, upper bound and Bishop's limit equilibrium solutions;

(5) From these three intersection points, we can back-figure the following stability numbers  $N_F = 6.8, 7.8$  and  $8.0$ , from which the lower bound, upper bound and Bishop's limit equilibrium solutions of the factor of safety can be calculated as

$$F = N_F / (\frac{\gamma H}{s_{u0}}) = 1.23, 1.41 \text{ and } 1.44.$$

### *Results for drained stability of slopes*

Drained slope stability calculations using the upper and lower bound methods of limit analysis and Bishop's limit equilibrium method have been carried out with four values of the depth factor  $D=1, 1.5, 2, 4$ . As in the undrained cases, the drained results suggest that the effect of the depth factor on the stability of cohesive-frictional slopes is very small once the depth factor exceeds about 2. This is because for most cases (except for slopes with a very low slope angle and an unrealistically low friction angle) the critical failure surface tends to pass through the toe for cohesive-frictional slopes (Taylor, 1948; Chen, 1975).

In order to compare the present bounding solutions with the limit equilibrium results, the solutions for the drained stability of slopes are presented in terms of the stability number  $N_F = \gamma H/c'_m = (\gamma H F)/c'$  against a dimensionless parameter  $\lambda_{c\phi} = \gamma H \tan \phi'_m / c'_m = (\gamma H \tan \phi')/c'$ , where  $c'$ ,  $\phi'$  and  $c'_m$ ,  $\phi'_m$  denote, respectively, the actual soil cohesion and friction angle and mobilized cohesion and friction angle. For drained stability, the factor of safety is defined as  $F = c'/c'_m = \tan \phi'/\tan \phi'_m$ . The dimensionless parameter  $\lambda_{c\phi}$  was introduced

by Janbu (1954) and later used by Cousins (1978) among many others to develop stability charts for cohesive-frictional slopes. A major advantage of using Janbu's parameter to develop a stability chart is that for a given slope with known soil strength parameters, slope angle, unit weight, slope height and depth factor, the safety factor can be obtained without resorting to an iterative procedure. This is so because, with the assumption of the safety factors for both cohesion and friction angle being equal, the parameter  $\lambda_{c\phi}$  is no longer a function of the safety factor  $F$ .

In the present drained limit analyses, for given values of  $H$ ,  $D$ ,  $\beta$ ,  $c' m$  and  $\phi' m$ , the upper and lower bound programs are used to determine the best upper and lower bound solutions of the unit weight  $\gamma$  from which the stability number  $N_F = \gamma H / c' m = (\gamma HF) / c'$  and Janbu's dimensionless parameter  $\lambda_{c\phi} = \gamma H \tan \phi' m / c' m = (\gamma H \tan \phi') / c'$  can be calculated. In the limit equilibrium analysis, we first set the values of  $H$ ,  $D$ ,  $\gamma$ ,  $\beta$ ,  $c'$  and  $\phi'$  and therefore the dimensionless parameter  $\lambda_{c\phi} = (\gamma H \tan \phi') / c'$ , and then determine the safety factor  $F$  from which the stability number  $N_F = (\gamma HF) / c'$  is calculated.

The results from the upper and lower bound calculations and the limit equilibrium analyses are presented in terms of the stability number  $N_F = (\gamma HF) / c'$  against  $\lambda_{c\phi}$  in Figure 12.35 to Figure 12.38 for four slope angles and four depth factors. The results indicate that the upper and lower bound solutions are generally close together and converge rapidly when the slope angle decreases. Again, it is observed that the difference between the upper and lower bound solutions increases slightly as the depth factor is increased. This is due to the effect of the mesh densities on the results of the numerical limit analyses. When the slope angle  $\beta \leq 45^\circ$ , a remarkably good agreement is observed between the upper and lower bound solutions with a maximum difference being less than 5%. It is evident from these figures that the limit equilibrium analysis produces accurate stability numbers for homogeneous cohesive-frictional slopes, although they are generally closer to the lower bound solutions.

#### *Example of application for drained stability analysis*

We now demonstrate how the results presented in Figure 12.35 to Figure 12.38 can be used to determine the factor of safety for a given soil slope with known geometry and actual soil strength.

**Problem:** A simple soil slope has the following properties: the slope angle  $\beta = 45^\circ$ , the height of the slope is  $H = 9\text{ m}$ , the depth factor is  $D = 2$ , the soil unit weight is  $\gamma = 19\text{kN/m}^3$ , the soil strength is defined by  $c' = 20\text{kN/m}^2$  and  $\phi' = 35^\circ$ . What is the factor of safety of this soil slope against failure?

A simple procedure for using the results of the present study to solve the above slope stability problem may be summarized as follows:

- (1) From the values of  $\gamma$ ,  $H$ ,  $c'$  and  $\phi'$ , we can calculate Janbu's dimensionless parameter:  $\lambda_{c\phi} = (\gamma H \tan \phi')/c' = (19 \times 9 \times \tan 35^0)/20 = 5.99$ ;
- (2) With  $\beta = 45^0$  and  $D = 2$ , it follows that the results presented in Figure 12.37(c) should be used to determine the safety factor;
- (3) From  $\lambda_{c\phi} = 5.99$  as calculated in (1), Figure 12.37(c) can be used to give the stability numbers of  $N_F = \gamma H F / c' = 15.4, 16.3$  and  $17.5$  corresponding to lower bound, limit equilibrium and upper bound solutions respectively;
- (4) With  $\gamma = 19kN/m^3$ ,  $H = 9 m$ ,  $c' = 20kN/m^2$  and the derived values of Janbu's parameter  $N_F = 15.4, 16.3$  and  $17.5$  from (3), the lower bound, limit equilibrium and upper bound solutions of the factor of safety are calculated as  $F = cN_F/(\gamma H) = 1.8, 1.91$  and  $2.05$ .

#### *Concluding remarks*

The following conclusions can be drawn from the results presented in this section:

- (1) For most cases considered in this study, it is found that the exact stability solution for both drained and undrained slopes can be predicted to within 5-10% by the numerical upper and lower bound solutions presented.
- (2) For the special case of homogeneous slopes, the numerical upper bound solutions obtained for slopes with a large depth factor are slightly higher (i.e. worse) than Chen's upper bounds for slopes in an infinitely deep layer with a failure surface passing below the toe (Chen, 1975). The lower bound solutions obtained in this section are most valuable for two reasons: (i) few rigorous lower bound solutions exist for slope stability problems in the literature, and (ii) the lower bound solutions can be used in practice to give a safe design.
- (3) A detailed comparison of the bounding solutions presented with those from the Bishop limit equilibrium method suggests that while the limit equilibrium analysis gives reasonable solutions for homogeneous slopes, it tends to underestimate the true stability solution significantly for inhomogeneous slopes with a low slope angle.
- (4) For undrained slopes, the increasing strength with depth has a significant effect on the stability number. It is interesting to note that the stability number increases approximately linearly with the values of the dimensionless parameter  $\lambda_{c\phi}$ .

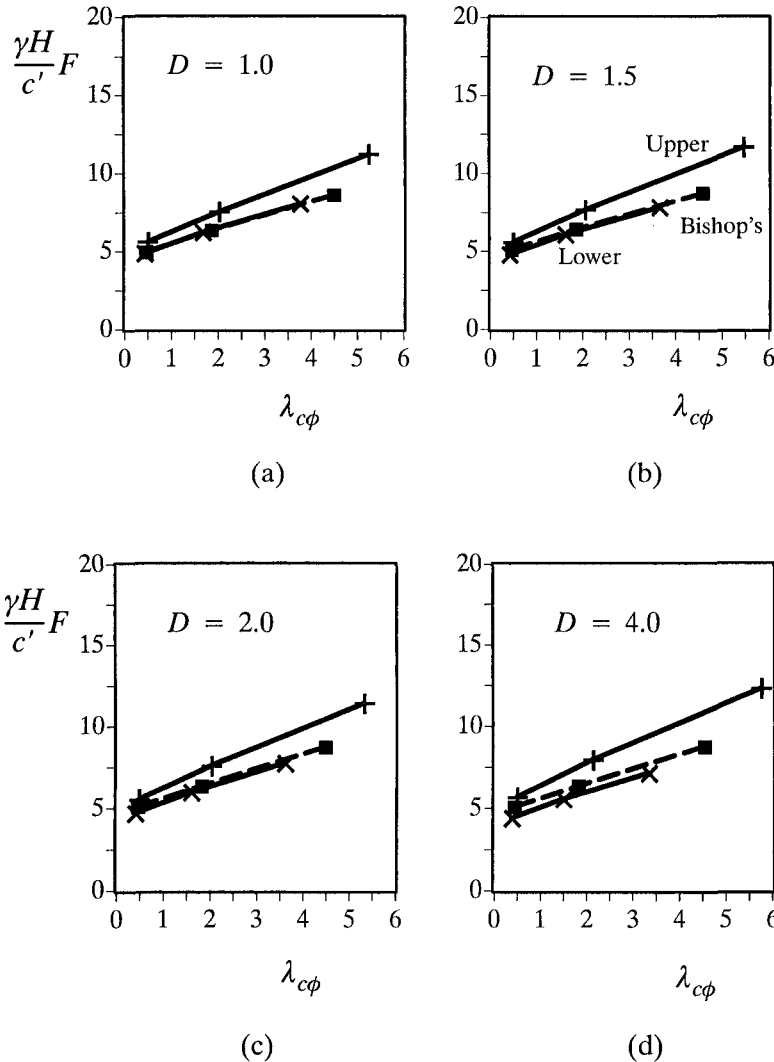


Figure 12.35: Stability number versus  $\lambda_{c\phi}$  for cohesive frictional slopes with slope angle of 75 degrees

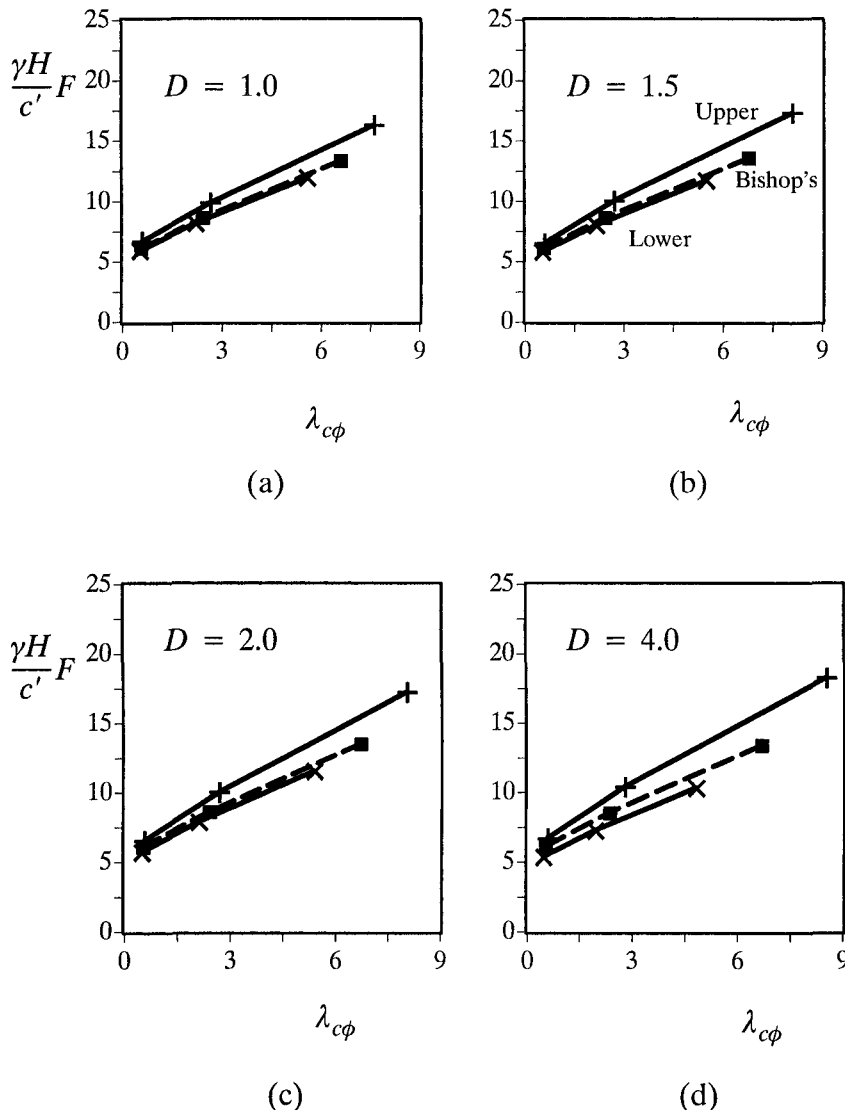


Figure 12.36: Stability number versus  $\lambda_{c\phi}$  for cohesive frictional slopes with slope angle of 60 degrees

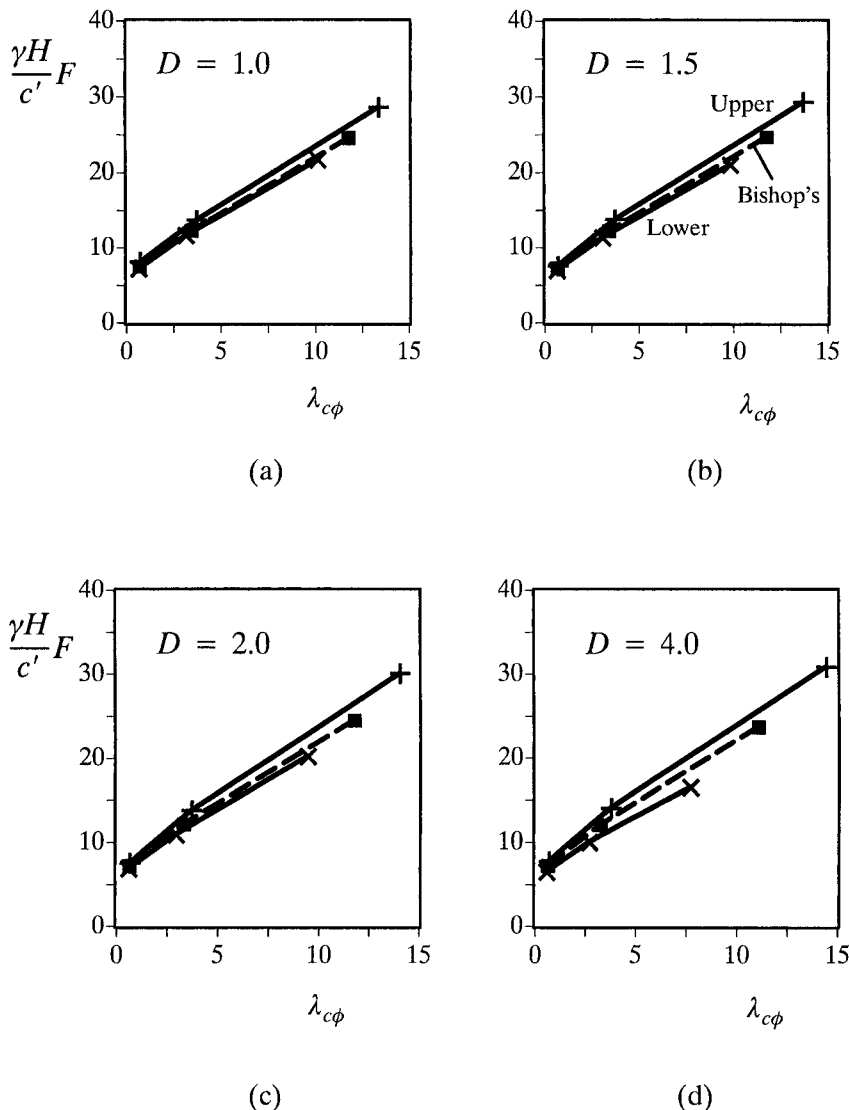


Figure 12.37: Stability number versus  $\lambda_{c\phi}$  for cohesive frictional slopes with slope angle of 45 degrees

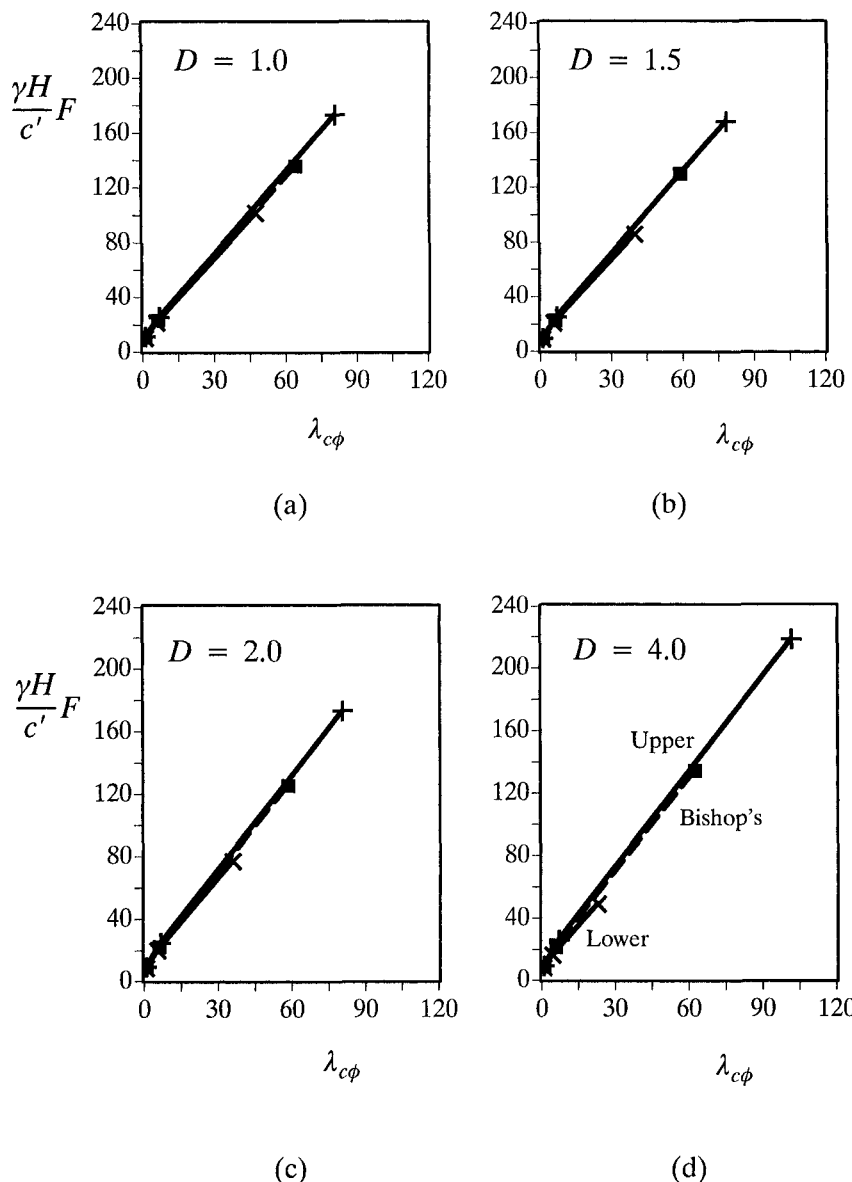


Figure 12.38: Stability number versus  $\lambda_{c\phi}$  for cohesive frictional slopes with slope angle of 30 degrees

### 12.4.2 Formulation based on linear strain finite elements

This section describes an upper bound formulation based on the six-noded triangular elements developed by Yu *et al.* (1994). This quadratic element gives a better performance than the constant strain element particularly when used to carry out limit analysis for incompressible materials.

#### (a) Numerical formulation

##### *The assumed velocity field*

Figure 12.39 shows a quadratic element with six nodes. Each element is associated with 12 nodal velocities and 3p plastic multiplier rates (where p is the number of sides in the linearized yield surface). The velocities are assumed to vary throughout each triangle according to

$$u = \sum_{i=1}^{i=6} N_i u_i \quad (12.114)$$

$$v = \sum_{i=1}^{i=6} N_i v_i \quad (12.115)$$

where  $(u_i, v_i)$  are nodal velocities in the x and y directions respectively and  $N_i$  are quadratic shape functions. The latter are defined as

$$N_1 = \alpha(2\alpha - 1) \quad (12.116)$$

$$N_2 = \beta(2\beta - 1) \quad (12.117)$$

$$N_3 = \gamma(2\gamma - 1) \quad (12.118)$$

$$N_4 = 4\alpha\beta \quad (12.119)$$

$$N_5 = 4\beta\gamma \quad (12.120)$$

$$N_6 = 4\alpha\gamma \quad (12.121)$$

with

$$\begin{pmatrix} \alpha \\ \beta \\ \gamma \end{pmatrix} = \frac{1}{2A} \begin{bmatrix} a_i & b_i & c_i \\ a_j & b_j & c_j \\ a_k & b_k & c_k \end{bmatrix} \begin{pmatrix} 1 \\ x \\ y \end{pmatrix} \quad (12.122)$$

$$a_i = x_2y_3 - x_3y_2; \quad b_i = y_2 - y_3; \quad c_i = x_3 - x_2 \quad (12.123)$$

$$a_j = x_3y_1 - x_1y_3; \quad b_j = y_3 - y_1; \quad c_k = x_1 - x_3 \quad (12.124)$$

$$a_k = x_1y_2 - x_2y_1; \quad b_k = y_1 - y_2; \quad c_k = x_2 - x_1 \quad (12.125)$$

where A is the element area and  $\alpha + \beta + \gamma = 1$ .

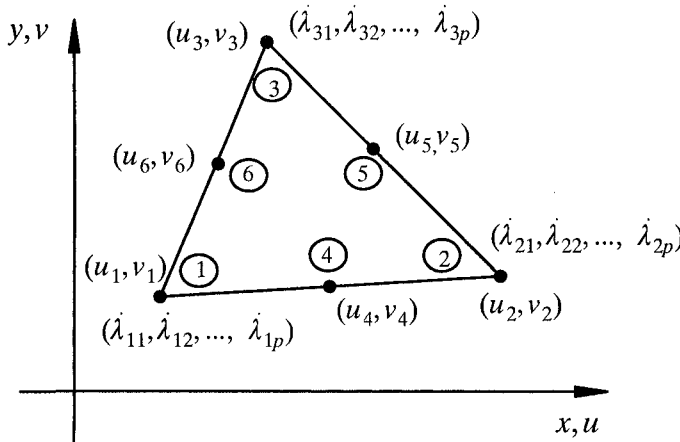


Figure 12.39: Six-noded linear triangle for upper bound analysis

#### Flow rule constraints for triangles

To use the upper bound theorem, a rigid-perfectly plastic material model with an associated flow rule is assumed. The plastic strain rates vary linearly throughout each triangle. For the Tresca criterion, it can be shown that the plastic flow rule will be satisfied everywhere within an element if we impose the flow rule at each corner of the element. The plastic flow rule at each corner node  $i$  can be expressed as follows:

$$\dot{\varepsilon}_{ix} = \left(\frac{\partial u}{\partial x}\right)_i = \lambda_i \left(\frac{\partial F}{\partial \sigma_x}\right)_i \quad (12.126)$$

$$\dot{\varepsilon}_{iy} = \left(\frac{\partial v}{\partial y}\right)_i = \lambda_i \left(\frac{\partial F}{\partial \sigma_y}\right)_i \quad (12.127)$$

$$\dot{\gamma}_{ixy} = \left(\frac{\partial v}{\partial x} + \frac{\partial u}{\partial y}\right)_i = \lambda_i \left(\frac{\partial F}{\partial \sigma_{xy}}\right)_i \quad (12.128)$$

where  $\lambda_i \geq 0$  is a plastic multiplier rate,  $F$  is the yield function and tensile strains are taken as positive.

When a linearization with  $p$  sides is used, each side of the Tresca yield criterion may be expressed as a linear function of the stresses according to

$$F_k = A_k \sigma_x + B_k \sigma_y + C_k \sigma_{xy} - 2c = 0, \quad k = 1, 2, \dots, p \quad (12.129)$$

where  $c$  is the cohesive strength and

$$A_k = \cos\left(\frac{2\pi k}{p}\right)$$

$$B_k = -\cos\left(\frac{2\pi k}{p}\right)$$

$$C_k = 2 \sin\left(\frac{2\pi k}{p}\right)$$

The flow rule imposes three equality constraints on the nodal velocities and plastic multiplier rates for each corner node. For the linearized yield criterion defined by (12.129), the plastic strain rates are given by

$$\dot{\varepsilon}_{ix} = \left(\frac{\partial u}{\partial x}\right)_i = \sum_{k=1}^{k=p} \dot{\lambda}_{ik} \frac{\partial F_k}{\partial \sigma_x} = \sum_{k=1}^{k=p} \dot{\lambda}_{ik} A_k \quad (12.130)$$

$$\dot{\varepsilon}_{iy} = \left(\frac{\partial v}{\partial y}\right)_i = \sum_{k=1}^{k=p} \dot{\lambda}_{ik} \frac{\partial F_k}{\partial \sigma_y} = \sum_{k=1}^{k=p} \dot{\lambda}_{ik} B_k \quad (12.131)$$

$$\dot{\gamma}_{ixy} = \left(\frac{\partial v}{\partial x} + \frac{\partial u}{\partial y}\right)_i = \sum_{k=1}^{k=p} \dot{\lambda}_{ik} \frac{\partial F_k}{\partial \sigma_{xy}} = \sum_{k=1}^{k=p} \dot{\lambda}_{ik} C_k \quad (12.132)$$

where  $i = 1 \rightarrow 3$ ,  $k = 1 \rightarrow p$ .

Thus the flow rule imposes nine equality constraints on the nodal velocities and plastic multiplier rates for each triangle. Each plastic multiplier rate is also subject to a non-negativity constraint.

#### *Flow rule constraints for discontinuities*

In addition to allowing plastic deformation throughout each triangle, the upper bound finite element formulation also permits localised plastic deformation along velocity discontinuities. A typical segment of a velocity discontinuity, defined by the nodal pairs (1,2), (3,4) and (5,6) is shown in Figure 12.40. For this arrangement, the jumps in tangential and normal velocities at the nodal pair (i,j) are given by

$$\Delta u_{ij} = (u_j - u_i) \cos \theta + (v_j - v_i) \sin \theta \quad (12.133)$$

$$\Delta v_{ij} = (u_i - u_j) \sin \theta + (v_i - v_j) \cos \theta \quad (12.134)$$

where  $\theta$  is the angle of the discontinuity to the x-axis as shown in Figure 12.40, and ij stands for (1,2), (3,4) or (5,6).

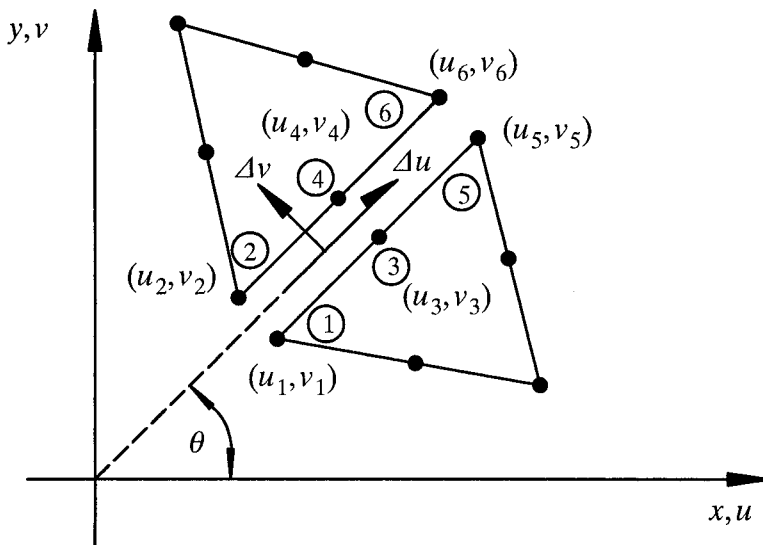


Figure 12.40: A velocity discontinuity between adjacent 6-noded triangles

To preserve a linear constraint matrix in the formulation, it is necessary to specify the sign  $s$  of the tangential velocity jump such that  $|\Delta u| = s\Delta u$  and  $s$  is equal to either 1 or  $-1$ . In order to ensure  $s\Delta u \geq 0$  along the discontinuity, we need to linearize the quadratic curve defined by  $s\Delta u$  so that a linear programming problem can be obtained. If a 5-sided linearization is used (which is sufficiently accurate), it may be shown that the following six linear constraints are optimum in the sense that they constrain the velocity by the least amount:

$$s\Delta u_{12} \geq 0 \quad (12.135)$$

$$s\Delta u_{34} \geq \frac{1}{4}(s\Delta u_{56} - 5s\Delta u_{12}) \quad (12.136)$$

$$s\Delta u_{34} \geq \frac{1}{8}(s\Delta u_{56} - s\Delta u_{12}) \quad (12.137)$$

$$s\Delta u_{34} \geq \frac{1}{8}(s\Delta u_{12} - s\Delta u_{56}) \quad (12.138)$$

$$s\Delta u_{34} \geq \frac{1}{4}(s\Delta u_{12} - 5s\Delta u_{56}) \quad (12.139)$$

$$s\Delta u_{56} \geq 0 \quad (12.140)$$

Also, the assumption of a Tresca yield criterion implies that slip along a velocity discontinuity produces no dilation. This condition is satisfied if we enforce it at each of the three nodal pairs, namely

$$\Delta v_{ij} = (u_i - u_j) \sin \theta + (v_j - v_i) \cos \theta = 0 \quad (12.141)$$

where (i,j) stands for (1,2), (3,4) or (5,6).

### *Velocity boundary condition constraints*

The last type of constraint to be imposed on the unknowns arises from the velocity boundary conditions. Consider a node i on a boundary that is inclined at an angle of  $\theta$  to the x-axis. For a general case, where the boundary is subject to a prescribed tangential velocity  $u_0$  and a prescribed normal velocity  $v_0$ , the nodal velocity components  $(u_i, v_i)$  must satisfy the following constraints:

$$\begin{bmatrix} \cos \theta & \sin \theta \\ -\sin \theta & \cos \theta \end{bmatrix} \begin{bmatrix} u_i \\ v_i \end{bmatrix} = \begin{bmatrix} u_0 \\ v_0 \end{bmatrix} \quad (12.142)$$

### *Power dissipation in the continuum*

The plastic flow may occur in both the continuum and the velocity discontinuities. The total power dissipated in these shearing modes forms the objective function and is expressed in terms of the unknowns. Within each triangle, the power dissipation by the stresses is given by

$$P_c = \iint_A (\sigma_x \dot{\epsilon}_x + \sigma_y \dot{\epsilon}_y + \sigma_{xy} \dot{\gamma}_{xy}) dA \quad (12.143)$$

By making use of the flow rules and the yield condition, the above equation gives

$$P_c = \frac{2Ac}{3} \sum_{k=1}^{k=p} (\lambda_{1k} + \lambda_{2k} + \lambda_{3k}) \quad (12.144)$$

when the cohesion strength  $c$  is uniform across the element.

### *Power dissipation in velocity discontinuities*

The power dissipated by plastic shearing along a velocity discontinuity is given by an integral of the form

$$P_d = \int_l c |\Delta u| dl = sc \int_l \Delta u dl \quad (12.145)$$

where  $s$  is either +1 or -1 according to the specified sign of the discontinuity. For the velocity discontinuity shown in Figure 12.40, the above integration may be performed analytically to give

$$P_d = \frac{sc l}{6} (\Delta u_{12} + 4\Delta u_{34} + \Delta u_{56}) \quad (12.146)$$

*Upper bound linear programming problem*

The objective function coefficients for each triangle and discontinuity, which describe the internal power dissipation, are summarised by equations (12.144) and (12.146). All of these node and element coefficients may be assembled in the usual manner to give the following linear programming problem

$$\text{Minimize} \quad C_1^T X_1 + C_2^T X_2$$

$$\text{Subject to} \quad A_{11} X_1 + A_{12} X_2 = B_1$$

$$A_2 X_1 \leq B_2$$

$$A_3 X_1 = B_3$$

$$A_4 X_1 = B_4$$

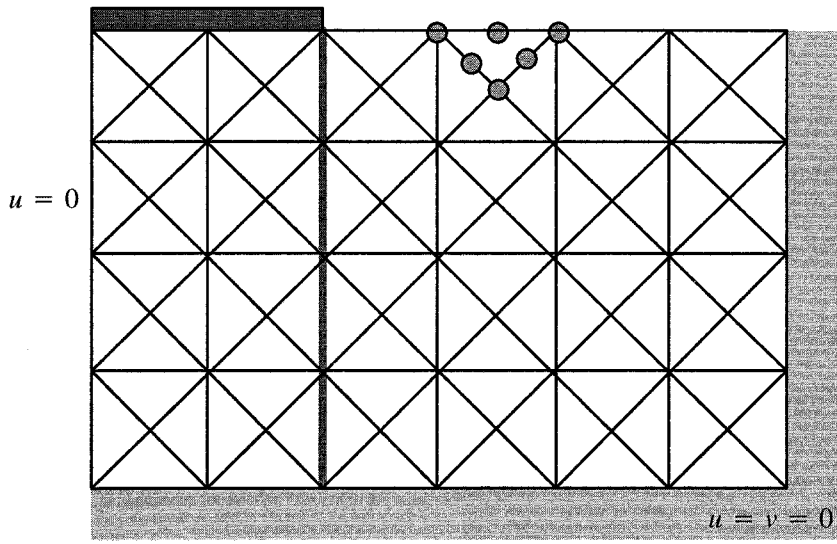
$$X_2 \geq 0$$

where  $X_1$  is a global vector of nodal velocities and  $X_2$  is a global vector of element plastic multiplier rates.

The above linear programming problem can be solved efficiently by adopting an active set algorithm that was developed by Best and Ritter (1985) and later modified by Sloan (1988a).

**(b) Numerical example**

In this section, we present a simple example of upper bound analysis of a smooth strip footing on undrained clay using the numerical formulation that has just been outlined. Figure 12.41(a) shows a relatively coarse upper bound mesh with 6-noded elements. The numerical results are given in Figure 12.41(b), where  $n$  and  $m$  represent the numbers of variables and constraints in the linear programming problem. The quantity  $i$  is the number of total iterations required in solving the linear programming problem. Three different values of  $p$  are used in the analysis so that the sensitivity of the results to the linearization of the yield surface can be studied. It is evident that the upper bound solutions are reasonably sensitive to the number of sides used to linearize the yield surface. It should also be noted that the bearing capacity solution ( $N_c = q/c$ ) will approach the exact solution (i.e.  $N_c = 5.14$ ) when a finer upper bound mesh and a larger  $p$  value are used in the analysis.



(a) Upper bound mesh with 6-noded elements

$p$	$n$	$m$	$i$	$N_c = q/c$
6	951	2193	770	5.49
12	951	3921	1000	5.34
24	951	7377	1650	5.29

(b) Results for a smooth strip footing on clay

Figure 12.41: Upper bound mesh and bearing capacity for a smooth strip footing

## 12.5 LIMIT ANALYSIS USING NONLINEAR PROGRAMMING

Apart from the linear programming techniques presented so far, nonlinear programming has also been used in conjunction with finite elements to perform limit analysis. The advantage of using nonlinear programming is that there will be no need to linearize yield functions which may prove to be difficult for some general yield criteria. In geotechnical engineering, we can use two finite element formulations for nonlinear programming limit analysis. The first procedure was developed by Lyamin and Sloan (2002a,b) whose formulations are based on the original work of Zouain *et al.* (1993). In this approach, the collapse load is determined by solving a nonlinear programming problem subject to a large number of equality and inequality constraints. The formulation is of a mixed nature as it makes use of both stresses and velocities. Application of the formulation is more difficult as it is rather complex and also requires special finite elements. The second nonlinear programming approach has been developed by Li and Yu (2005) by extending the earlier work of Zhang *et al.* (1991) and Liu *et al.* (1995) for metal plasticity. The main advantage of this second approach is that it makes use of the standard displacement-based finite elements and is therefore easier to apply in practice. For this reason, the second approach will be presented in this section.

### 12.5.1 Limit analysis for a general yield criterion

#### *A general yield criterion*

Many widely used yield criteria for cohesive-frictional materials can be expressed in a general form as follows

$$F(\sigma) = \sigma^T P \sigma + \sigma^T Q - 1 = 0 \quad (12.147)$$

where  $\sigma$  is the stress vector,  $P$  and  $Q$  are the coefficient matrix and vector that are related to strength properties of the material (i.e. cohesion and frictional angle).

Equation (12.147) is a general yield function for frictional materials. For example, the Mohr-Coulomb criterion in plane strain can be expressed as

$$F(\sigma_{ij}) = (\sigma_{xx} - \sigma_{yy})^2 + (2\sigma_{xy})^2 - (2c \cos \phi - (\sigma_{xx} + \sigma_{yy}) \sin \phi)^2 = 0 \quad (12.148)$$

where  $c$  and  $\phi$  are cohesion and frictional angle respectively. It can be shown that the above function can be expressed in the form of (12.147) with the following coefficient matrix and vector:

$$\mathbf{P} = \begin{bmatrix} \frac{1}{4c^2} & \frac{-1-\sin^2\phi}{4c^2\cos^2\phi} & 0 \\ \frac{-1-\sin^2\phi}{4c^2\cos^2\phi} & \frac{1}{4c^2} & 0 \\ 0 & 0 & \frac{1}{c^2\cos^2\phi} \end{bmatrix} \quad (12.149)$$

$$\mathbf{Q} = \begin{bmatrix} \sin\phi \\ \frac{\sin\phi}{c\cos\phi} \\ \frac{\sin\phi}{c\cos\phi} \\ 0 \end{bmatrix} \quad (12.150)$$

Taking tensile stresses as positive, the Drucker-Prager criterion is written as follows:

$$F(\sigma_{ij}) = \alpha I_1 + \sqrt{J_2} - k = 0 \quad (12.151)$$

where  $I_1$  is the first invariant of the stress tensor,  $J_2$  is the second invariant of the deviatoric stress tensor,  $\alpha$  and  $k$  are material strength parameters.

It can be shown that for a three-dimensional stress state, the Drucker-Prager yield function (12.151) can also be expressed in the form of (12.147) provided we set

$$\mathbf{P} = \begin{bmatrix} p_1 & p_2 & p_2 & 0 & 0 & 0 \\ p_2 & p_1 & p_2 & 0 & 0 & 0 \\ p_2 & p_2 & p_1 & 0 & 0 & 0 \\ 0 & 0 & 0 & p_3 & 0 & 0 \\ 0 & 0 & 0 & 0 & p_3 & 0 \\ 0 & 0 & 0 & 0 & 0 & p_3 \end{bmatrix} \quad (12.152)$$

$$\mathbf{Q} = \begin{bmatrix} q_0 \\ q_0 \\ q_0 \\ 0 \\ 0 \\ 0 \end{bmatrix} \quad (12.153)$$

where

$$p_1 = \frac{1-3\alpha^2}{3k^2} \quad (12.154)$$

$$p_2 = -\frac{1+6\alpha^2}{6k^2} \quad (12.155)$$

$$p_3 = \frac{1}{k^2} \quad (12.156)$$

$$q_0 = \frac{2\alpha}{k} \quad (12.157)$$

*The kinematic theorem of limit analysis*

In theory, an upper bound to the true collapse load of a structure can be obtained by using the kinematic theorem of limit analysis. As detailed in Chapter 4, the kinematic theorem states: among all kinematically admissible velocity fields, the real one yields the lowest rate of plastic dissipation power. Mathematically, the upper bound theorem can be formulated as follows

$$m \iint_{S_T} T_i u_i \, dS_T \leq \iint_V \iint_V \sigma_{ij} \dot{\varepsilon}_{ij} \, dV - \iint_V \iint_V f_i u_i \, dV \quad (12.158)$$

where  $m$  is the collapse load multiplier,  $T_i$  is the basic load of surface tractions (may be set as a unit value),  $f_i$  is the body force,  $u_i$  and  $\dot{\varepsilon}_{ij}$  are kinematically admissible velocity and strain rate fields,  $S_T$  denotes the traction boundary and  $V$  represents the space domain of the structure.

It is noted that the rate of plastic dissipation power is defined by

$$D(\dot{\varepsilon}_{ij}) = \sigma_{ij} \dot{\varepsilon}_{ij} \quad (12.159)$$

According to the mathematical programming theory, the kinematic theorem (12.158) can be formulated as follows in the absence of body force:

$$m = \min \iint_V \iint_V \sigma_{ij} \dot{\varepsilon}_{ij} \, dV = \min \iint_V \iint_V D(\dot{\varepsilon}_{ij}) \, dV \quad (12.160)$$

$$\text{Subject to } \iint_{S_T} T_i u_i \, dS = 1 \quad (12.161)$$

$$\dot{\varepsilon}_{ij} = \frac{1}{2}(u_{ij} + u_{ji}) \quad \text{in } V \quad (12.162)$$

$$u_i = 0 \quad \text{on } S_U \quad (12.163)$$

where  $S_U$  denotes the displacement boundary. Hence the kinematic limit analysis of a structure has been reduced to the calculation of the smallest limit load multiplier  $m$ , as the collapse load is equal to  $mT_i$ .

*Dissipation power for a general yield criterion*

From equation (12.159), it is clear that the plastic dissipation power depends on both stress and strain fields. It should be noted that the stress field is linked to the strain rate field through the associated plastic flow rule, namely

$$\dot{\varepsilon}_{ij} = \lambda \frac{\partial F(\sigma_{ij})}{\partial \sigma_{ij}} \quad (12.164)$$

which is reduced to the following by using the general yield equation (12.147)

$$\boldsymbol{\varepsilon} = 2\lambda \mathbf{P}\boldsymbol{\sigma} + \lambda \mathbf{Q} \quad (12.165)$$

from which we can express the stress field in terms of strain field

$$\boldsymbol{\sigma} = \frac{1}{2\lambda} \mathbf{P}^{-1} \boldsymbol{\varepsilon} - \frac{1}{2} \mathbf{P}^{-1} \mathbf{Q} \quad (12.166)$$

If the matrix  $\mathbf{P}$  is non-singular,  $\mathbf{P}^{-1}$  can be determined uniquely. However for the case of a singular  $\mathbf{P}$  matrix, we can use  $\mathbf{P} + \gamma$  to replace  $\mathbf{P}$ , where  $\gamma$  is a very small real value.

Given that the stress field is on the yield surface, equations (12.166) and (12.147) can be combined to determine the plastic multiplier rate  $\lambda$ :

$$\lambda = \sqrt{\frac{\boldsymbol{\varepsilon}^T \mathbf{P}^{-1} \boldsymbol{\varepsilon}}{4 + \mathbf{Q}^T \mathbf{P}^{-1} \mathbf{Q}}} \quad (12.167)$$

Now we can express the rate of plastic dissipation power purely in terms of the strain rate field:

$$\begin{aligned} D(\dot{\boldsymbol{\varepsilon}}_{ij}) &= \sigma_{ij} \dot{\varepsilon}_{ij} = \boldsymbol{\sigma}^T \boldsymbol{\varepsilon} \\ &= \frac{1}{2} \sqrt{(\boldsymbol{\varepsilon}^T \mathbf{P}^{-1} \boldsymbol{\varepsilon}) \cdot (4 + \mathbf{Q}^T \mathbf{P}^{-1} \mathbf{Q})} - \frac{1}{2} \boldsymbol{\varepsilon}^T \mathbf{P}^{-1} \mathbf{Q} \end{aligned} \quad (12.168)$$

Therefore once the kinematically admissible velocity field is obtained, the plastic dissipation power can also be calculated. The key result is that there is no need to evaluate stress fields in kinematic limit analysis which simplifies the numerical procedure considerably.

### *The nonlinear programming problem*

Based on the above expression for the rate of plastic dissipation power, the kinematic limit analysis of frictional materials can be formulated as the following mathematical programming problem:

$$m = \min \iint_V \left[ \frac{1}{2} \sqrt{(\boldsymbol{\varepsilon}^T \mathbf{P}^{-1} \boldsymbol{\varepsilon}) \cdot (4 + \mathbf{Q}^T \mathbf{P}^{-1} \mathbf{Q})} - \frac{1}{2} \boldsymbol{\varepsilon}^T \mathbf{P}^{-1} \mathbf{Q} \right] dV \quad (12.169)$$

$$\text{Subject to } \iint_{S_T} \mathbf{T}^T \mathbf{u} dS = 1 \quad (12.170)$$

$$\boldsymbol{\varepsilon} = \frac{1}{2} (\nabla \mathbf{u} + \mathbf{u} \nabla) \quad \text{in } V \quad (12.171)$$

$$\mathbf{u} = 0 \quad \text{on } S_U \quad (12.172)$$

where  $\mathbf{T}$  is the basic load column vector of surface tractions and  $\mathbf{u}$  is the velocity column vector.

### 12.5.2 Finite element approximation of velocity fields

To describe the variation of kinematically admissible velocity fields, the standard displacement-based finite elements are used. In the finite element method, the structure is divided into a large number of small elements, in which the velocity (or displacement increments) is assumed to vary in a certain manner (e.g. linear or quadratic variations).

The velocity field  $\mathbf{u}$  within an element,  $e$ , is linked to its nodal velocity vector  $\delta$  through shape functions  $\mathbf{N}$ , namely

$$\mathbf{u}_e = \mathbf{N}_e \delta_e \quad (12.173)$$

from which we can determine the strain rate field from the velocity field as follows

$$\boldsymbol{\varepsilon}_e = \mathbf{L}\mathbf{u} = \mathbf{L}\mathbf{N}_e \delta_e = \mathbf{B}_e \delta_e \quad (12.174)$$

in which

$$\mathbf{B}_e = [\mathbf{B}_1, \mathbf{B}_2, \dots, \mathbf{B}_n] \quad (12.175)$$

and

$$\mathbf{B}_i = \begin{bmatrix} \frac{\partial N_i}{\partial x} & 0 & 0 \\ 0 & \frac{\partial N_i}{\partial y} & 0 \\ 0 & 0 & \frac{\partial N_i}{\partial z} \\ \frac{\partial N_i}{\partial y} & \frac{\partial N_i}{\partial x} & 0 \\ 0 & \frac{\partial N_i}{\partial z} & \frac{\partial N_i}{\partial y} \\ \frac{\partial N_i}{\partial z} & 0 & \frac{\partial N_i}{\partial x} \end{bmatrix} \quad (i = 1, 2, \dots, n) \quad (12.176)$$

where  $n$  is the number of nodes in each element.

By using the Gaussian integration technique, the objective function in equation (12.169) can be further reduced to

$$\iint_V \left[ \frac{1}{2} \sqrt{(\boldsymbol{\varepsilon}^T \mathbf{P}^{-1} \boldsymbol{\varepsilon}) \cdot (4 + \mathbf{Q}^T \mathbf{P}^{-1} \mathbf{Q})} - \frac{1}{2} \boldsymbol{\varepsilon}^T \mathbf{P}^{-1} \mathbf{Q} \right] dV$$

$$= \sum_{e=1}^N \sum_{i=1}^{NG} (\varrho_e)_i |J|_i \left[ \frac{1}{2} \sqrt{(\delta_e^T (K_e)_i \delta_e) \cdot (4 + Q^T P^{-1} Q)} - \frac{1}{2} \delta_e^T (G_e)_i \right] \quad (12.177)$$

where  $(\varrho_e)_i$  is the Gaussian integral weight at the  $i$ -th Gaussian integration point within the element,  $e$ ,  $|J|_i$  is the determinant of the Jacobian matrix at the  $i$ -th Gaussian integration point, and  $NG$  is the number of integration points within each element. We also have

$$K_e = B_e^T P^{-1} B_e \quad (12.178)$$

$$G_e = B_e^T P^{-1} Q \quad (12.179)$$

If we introduce a transformation matrix for each element,  $C_e$ , then we can express the nodal velocity vector  $\delta_e$  in terms of the global velocity vector,  $\delta$

$$\delta_e = C_e \times \delta \quad (12.180)$$

with which the objective function (12.177) can be further expressed in terms of the global nodal velocity vector

$$\int \int \int_V \left[ \frac{1}{2} \sqrt{(\epsilon^T P^{-1} \epsilon) \cdot (4 + Q^T P^{-1} Q)} - \frac{1}{2} \epsilon^T P^{-1} Q \right] dV \\ = \sum_{e=1}^N \sum_{i=1}^{NG} (\varrho_e)_i |J|_i \left[ \frac{1}{2} \sqrt{(\delta_e^T (K_e)_i \delta_e) \cdot (4 + Q^T P^{-1} Q)} - \frac{1}{2} \delta_e^T (G_e)_i \right] \quad (12.181)$$

$$= \sum_{i=1}^{NG \times e} \varrho_i |J|_i \left[ \frac{1}{2} \sqrt{(\delta^T K_i \delta) \cdot (4 + Q^T P^{-1} Q)} - \frac{1}{2} (\delta^T G_i) \right] \quad (12.182)$$

in which

$$K_i = C_e^T (K_e)_i C_e \quad (12.183)$$

$$G_i = C_e^T (G_e)_i \quad (12.184)$$

In addition, the normalization condition (12.170) can be expressed in terms of the global nodal velocity vector as follows

$$F^T \delta = 1 \quad (12.185)$$

in which  $F$  is the basic column vector of equivalent nodal loads.

After the velocity boundary condition (12.172) is imposed by means of the standard finite element method, the nonlinear programming problem can be solved to obtain the lowest load multiplier  $m$ ,

$$m = \min_{\delta} \sum_{i=1}^{NG \times e} \varrho_i |J|_i \left[ \frac{1}{2} \sqrt{(\delta^T K_i \delta) \cdot (4 + Q^T P^{-1} Q)} - \frac{1}{2} (\delta^T G_i) \right] \quad (12.186)$$

$$\text{Subject to} \quad F^T \delta = 1 \quad (12.187)$$

### 12.5.3 The iterative solution algorithm

The kinematic (i.e. upper bound) limit analysis defined by equations (12.186)-(12.187) is a minimum optimization problem with a single equality constraint. The objective function is nonlinear, continuous but may be nondifferentiable. For a continuous and differentiable quadratic mathematical programming problem under Kuhn-Tucker's conditions, several effective methods can be used to solve it (Himmelblau, 1972).

For the mathematical programming problem (12.186), there is a calculation of square root which could make the objective function unsmooth and nondifferentiable. This would cause difficulties in solving the programming problem. The nonlinear objective function becomes nondifferentiable in rigid areas (where the strain fields are zero) for limit analysis. This difficulty can be overcome by using an iterative algorithm used by Zhang *et al.* (1991) and Liu *et al.* (1995) for purely cohesive materials and by Li and Yu (2005) for cohesive-frictional materials. This technique is concerned with how to distinguish rigid and deforming plastic areas. A similar technique was also used by Huh and Yang (1991) for solving nonlinear programming problems.

By using the Lagrangian method (Himmelblau, 1972), the equality constraint can be removed so that the equations (12.186) and (12.187) can be combined to give an unconstrained minimum optimization problem with the following new objective function:

$$L(\delta, q) = \sum_{i=1}^{NG \times e} \varrho_i |J|_i \left[ \frac{1}{2} \sqrt{(\delta^T K_i \delta) \cdot (4 + Q^T P^{-1} Q)} - \frac{1}{2} (\delta^T G_i) \right] + q(1 - F^T \delta) \quad (12.188)$$

where  $q$  is the Lagrangian multiplier.

In order to perform an iterative technique for solving the nonlinear programming, it is better to re-write the objective function (12.188) in the following form

$$L(\delta, q) = \sum_{i=1}^{NG \times e} \varrho_i |J|_i \left[ \frac{1}{2} \times \frac{(\delta^T K_i \delta) \cdot (4 + Q^T P^{-1} Q)}{\omega^{ICP}} - \frac{1}{2} (\delta^T G_i) \right] + q(1 - F^T \delta) \quad (12.189)$$

in which

$$\omega^{ICP} = \sqrt{(\boldsymbol{\delta}^T \mathbf{K}_i \boldsymbol{\delta}) \cdot (4 + \mathbf{Q}^T \mathbf{P}^{-1} \mathbf{Q})} \quad (12.190)$$

which serves as an iteration control parameter.

To overcome the difficulties which may arise from an unsMOOTH objective function, all the nondifferentiable areas need to be identified where the first part of the objective function becomes zero (i.e.  $\omega^{ICP} = 0$ ). In order to find all nondifferentiable regions, an iterative technique is needed. The iteration begins with the assumption that the strain rate is non-zero everywhere and therefore the nondifferentiable region does not exist at the first iteration step. However from the second step, the strain rate will be updated and the nondifferentiable areas can be identified by checking if  $\omega^{ICP} = 0$ .

Once a nondifferentiable area is identified at an iteration step, the condition  $\omega^{ICP} = 0$  will be introduced as a constraint into the nonlinear programming problem using the penalty method. Hence the objective function will be modified at each iteration step until the limit load multiplier is determined.

In view of the above discussion, an iterative solution algorithm for calculating the limit multiplier is proposed as follows:

*Step 0: initializing the nonlinear objective function*

As shown in Huh and Yang (1991) and Liu *et al.* (1995), the selection of the initial nodal velocity field does not affect the convergence of iteration. It may be proved that from any initial trial solution, the subsequent iterations are locked in a certain convex hull that contains the exact solution of the problem (Huh and Yang, 1991). For simplicity, we can begin the iteration by setting  $\omega^{ICP} = 1$  in the objective function (12.189). Then the initial nodal velocity vector  $\boldsymbol{\delta}_0$  can be estimated by solving the mathematical programming problem with the following objective function:

$$L(\boldsymbol{\delta}, q) = \sum_{i=1}^{NG \times e} \varrho_i |J|_i \left[ \frac{1}{2} (\boldsymbol{\delta}^T \mathbf{K}_i \boldsymbol{\delta}) \cdot (4 + \mathbf{Q}^T \mathbf{P}^{-1} \mathbf{Q}) - \frac{1}{2} (\boldsymbol{\delta}^T \mathbf{G}_i) \right] + q(1 - \mathbf{F}^T \boldsymbol{\delta}) \quad (12.191)$$

Using the minimum optimization theory, a system of linear equations can be obtained by applying

$$\frac{\partial L(\boldsymbol{\delta}, q)}{\partial \boldsymbol{\delta}} = 0; \quad \frac{\partial L(\boldsymbol{\delta}, q)}{\partial q} = 0 \quad (12.192)$$

as follows

$$\sum_{i=1}^{NG \times e} \varrho_i |J|_i \left[ (\mathbf{K}_i \boldsymbol{\delta}) \cdot (4 + \mathbf{Q}^T \mathbf{P}^{-1} \mathbf{Q}) - \frac{1}{2} (\mathbf{G}_i) \right] = q \mathbf{F} \quad (12.193)$$

$$\mathbf{F}^T \boldsymbol{\delta} = 1 \quad (12.194)$$

By solving the above system of linear equations, we can obtain the initial nodal velocity vector  $\boldsymbol{\delta}_0$ , from which the initial load multiplier can be derived by using the following equation

$$m_0 = \sum_{i=1}^{NG \times e} \varrho_i |J|_i \left[ \frac{1}{2} (\boldsymbol{\delta}_0^T \mathbf{K}_i \boldsymbol{\delta}_0) \cdot (4 + \mathbf{Q}^T \mathbf{P}^{-1} \mathbf{Q}) - \frac{1}{2} (\boldsymbol{\delta}_0^T \mathbf{G}_i) \right] \quad (12.195)$$

*Step k+1 (k=0,1,2..): identifying the rigid regions to modify objective function*

At step  $k$ , the value of  $\omega^{ICP}$  needs to be calculated at every integration point in order to check if it is in a nondifferentiable area. Then the integration point set I will be subdivided into two subsets: (a) the subset  $(I_R)_{k+1}$  where the objective function is not differentiable and, (b) the subset  $(I_P)_{k+1}$  where the objective function is differentiable. Therefore

$$I = (I_R)_{k+1} \cup (I_P)_{k+1} \quad (12.196)$$

$$(I_R)_{k+1} = \{i \in I, \omega^{ICP} = 0\} \quad (12.197)$$

$$(I_P)_{k+1} = \{i \in I, \omega^{ICP} > 0\} \quad (12.198)$$

It should be noted that in actual calculations, the integration point is regarded as in the rigid region as long as  $\omega^{ICP}$  is smaller than a certain small value say  $\xi$  (which may range from  $10^{-8}$  to  $10^{-12}$ ).

The value of nodal velocity vector at step  $k$ ,  $\boldsymbol{\delta}_k$ , can then be determined by solving the following revised mathematical programming problem:

$$m_k = \min_{\boldsymbol{\delta}} \sum_{i \in (I_P)_{k+1}} \varrho_i |J|_i \left[ \frac{1}{2} \times \frac{(\boldsymbol{\delta}^T \mathbf{K}_i \boldsymbol{\delta}) \cdot (4 + \mathbf{Q}^T \mathbf{P}^{-1} \mathbf{Q})}{\omega^{ICP}} - \frac{1}{2} (\boldsymbol{\delta}^T \mathbf{G}_i) \right] \quad (12.199)$$

Subject to  $\mathbf{F}^T \boldsymbol{\delta} = 1$

$$\omega^{ICP} = \sqrt{(\boldsymbol{\delta}^T \mathbf{K}_i \boldsymbol{\delta}) \cdot (4 + \mathbf{Q}^T \mathbf{P}^{-1} \mathbf{Q})} = 0 \quad \text{if } i \in (I_R)_{k+1} \quad (12.200)$$

which is equivalent to the following minimum optimization problem

$$L(\boldsymbol{\delta}, q) = \sum_{i \in (I_P)_{k+1}} \varrho_i |J|_i \left[ \frac{1}{2} \frac{(\boldsymbol{\delta}^T \mathbf{K}_i \boldsymbol{\delta}) \cdot (4 + \mathbf{Q}^T \mathbf{P}^{-1} \mathbf{Q})}{(\omega^{ICP})_k} - \frac{1}{2} (\boldsymbol{\delta}^T \mathbf{G}_i) \right]$$

$$+ \eta \sum_{i \in (I_R)_{k+1}} \varrho_i |J|_i [(\delta^T \mathbf{K}_i \delta) \cdot (4 + \mathbf{Q}^T \mathbf{P}^{-1} \mathbf{Q})] + q(1 - \mathbf{F}^T \delta) \quad (12.201)$$

where  $\eta$  is a penalty factor and its value may vary from  $10^6$  to  $10^{12}$ .

Finally, the above minimum optimization problem can be transformed into the following system of linear equations by applying (12.192):

$$\begin{aligned} \sum_{i \in (I_P)_{k+1}} \varrho_i |J|_i \left[ \frac{1}{2} \frac{(\mathbf{K}_i \delta) \cdot (4 + \mathbf{Q}^T \mathbf{P}^{-1} \mathbf{Q})}{(\omega^{ICP})_k} - \frac{1}{2} (\mathbf{G}_i) \right] \\ + \eta \sum_{i \in (I_R)_{k+1}} \varrho_i |J|_i [(\mathbf{K}_i \delta) \cdot (4 + \mathbf{Q}^T \mathbf{P}^{-1} \mathbf{Q})] = q\mathbf{F} \end{aligned} \quad (12.202)$$

$$\mathbf{F}^T \delta = 1 \quad (12.203)$$

By solving the linear system of equations defined by (12.202) and (12.203), we can obtain the nodal velocity vector  $\delta_{k+1}$  at step  $k$ . The limit load multiplier at this step can then be determined by

$$m_{k+1} = \sum_{i \in I} \varrho_i |J|_i \left[ \frac{1}{2} (\delta_{k+1}^T \mathbf{K}_i \delta_{k+1}) \cdot (4 + \mathbf{Q}^T \mathbf{P}^{-1} \mathbf{Q}) - \frac{1}{2} (\delta_{k+1}^T \mathbf{G}_i) \right] \quad (12.204)$$

It is noted that the above iteration is repeated until the solution satisfies the following convergence criteria

$$\frac{|m_{k+1} - m_k|}{m_{k+1}} \leq ERR1 \quad (12.205)$$

$$\frac{\|\delta_{k+1} - \delta_k\|}{\|\delta_{k+1}\|} \leq ERR2 \quad (12.206)$$

where  $ERR1$  and  $ERR2$  are error tolerances given by the user.

Li and Yu (2005) present a number of numerical examples indicating that the procedure outlined here is very robust and can be used confidently to give accurate stability solutions for geotechnical problems involving complex loading conditions. The formulation has also been extended by Li and Yu (2006a) to composite materials. A major advantage of this nonlinear programming method is that it can be readily applied to three-dimensional problems because standard displacement finite elements are used in the formulation. This has been demonstrated by Liu *et al.* (1995) and Li and Yu (2006b) using three-dimensional numerical examples.

## REFERENCES

Alehossein H., Carter J.P. and Booker J.R. (1992). Finite element analysis of rigid footings on jointed rock. *Proc. 3rd Int. Conf. Computational Plasticity*, Vol. 2, 935-945.

Anderheggen, E. and Knopfel, H. (1972). Finite element limit analysis using linear programming. *Int. J. Solids and Structures.*, Vol. 8, 1413-1431.

Bishop, A.W. (1955). The use of the slip circle in the stability of slopes. *Geotechnique.*, Vol 5, 7-17.

Bottero, A., Negre, R., Pastor, J. and Turgeman, S. (1980). Finite element method and limit analysis theory for soil mechanics problems. *Comput. Meth. Appl. Mech. Eng.*, Vol. 22, 131-149.

Chen, W.F. (1975). *Limit Analysis and Soil Plasticity*, Elsevier, Amsterdam.

Chen W.F. and Drucker D.C. (1969). Bearing capacity of concrete blocks or rock. *J. Eng. Mech. Div., ASCE*, Vol 95, 955-979.

Chen, W.F. and Liu, X.L. (1990). *Limit Analysis in Soil Mechanics*, Elsevier, Amsterdam.

Collins, I.F. (1974). A note on the interpretation of Coulomb's analysis of the thrust on a rough retaining wall in terms of the limit theorems of plasticity theory. *Geotechnique.*, Vol. 24, 106-108.

Cousins, B.F. (1978). Stability charts for simple earth slopes. *J. Geotech. Eng. Div., ASCE*, Vol. 104, GT2, 267-279.

Davis, E.H. (1968). Theories of plasticity and the failure of soil masses, In: *Soil Mechanics: Selected Topics*, (Editor: I. K. Lee), Butterworths, London, 341-380.

Davis E.H. (1980). A note on some plasticity solutions relevant to the bearing capacity of brittle and fissured materials. *Proc. Int. Conf. Struct. Foundations on Rock*, Vol. 3, 83-90.

Davis, R.O. and Selvadurai, A.P.S. (2002). *Plasticity and Geomechanics*, Cambridge University Press.

Drescher, A. and Detournay, E. (1993). Limit load in translational failure mechanisms for associative and non-associative materials. *Geotechnique.*, Vol. 43, 443-456.

Drucker, D.C., Greenberg, H.J. and Prager, W. (1952). Extended limit design theorems for continuous media. *Quart. J. Appl. Maths.*, Vol. 9, 381-389.

Duncan, J.M. and Wright, S.G. (1980). The accuracy of equilibrium methods of slope stability analysis, *Eng. Geology*, Vol. 16, 5-17.

Duncan, J.M., Buchignani, A.L. and de Wet, M. (1987). An engineering manual for slope stability studies, *Internal Research Report, Department of Civil Engineering, Virginia Tech, USA*.

Fellenius, W.O. (1926). *Mechanics of Soils*, Statika Gruntov, Gosstrollzdat.

Fredlund, D.G. and Krahn, J. (1977). Comparison of slope stability methods of analysis, *Can. Geotech. J.*, Vol. 14, 429-439.

Gao, Y. (1988). Panpenalty finite element programming for plastic limit analysis, *Comput. Struct.*, Vol. 28, 749-755.

Gibson, R.E. and Morgenstern, N. (1962). A note on the stability of cuttings in normally consolidated clays. *Geotechnique*, Vol. 12, 212-216.

Graham, J. (1984). Methods of stability analysis. Chapter 6 In: *Slope Instability*, (Editors: D. Brunsden and D.B. Prior), Wiley.

Himmelblau, D.M. (1972). *Applied Nonlinear Programming*, McGraw-Hill Book Company, New York.

Huh, H. and Yang, W.H. (1991). A general algorithm for limit solutions of plane stress problems. *Int. J. Solids and Structures*, Vol. 28, 727-738.

Hunter, J.H. and Schuster, R.L. (1968). 'Stability of simple cuttings in normally consolidated clays'. *Geotechnique*, Vol. 18, 372-378.

Janbu, N. (1954). Stability analysis of slopes with dimensionless parameters, *Harvard Soil Mechanics Series*, No. 46.

Kim, J.K., Salgado, R. and Lovell, C.W. (1997). *STABL – Instructions for Use*. School of Civil Engineering, Purdue University.

Kim, J.M., Salgado, R. and Yu, H.S. (1999). Limit analysis of soil slopes subjected to pore pressures. *J. Geotech. Geoenviron. Eng.*, ASCE, Vol 125, 49-58.

Li, H.X. and Yu, H.S. (2005). Kinematic limit analysis of frictional materials using nonlinear programming. *Int. J. Solids and Structures*, Vol 42, 4058-4076.

Li, H.X. and Yu, H.S. (2006a). Limit analysis of composite materials based on an ellipsoid yield criterion. *Int. J. Plasticity* (in press).

Li, H.X. and Yu, H.S. (2006b). Limit analysis of 2D and 3D structures based on an ellipsoid yield criterion. *Int. J. Mech. Sci.* (in press).

Liu, Y.H., Cen, Z.Z. and Xu, B.Y. (1995). A numerical method for plastic limit analysis of 3D structures. *Int. J. Solids and Structures*, Vol 32, 1645-1658.

Lyamin, A. and Sloan S.W. (2002a). Upper bound limit analysis using linear finite elements and nonlinear programming. *Int. J. Num. Analy. Meth. Geomech*, Vol 26, 181-216.

Lyamin, A. and Sloan S.W. (2002b). Lower bound limit analysis using nonlinear programming. *Int. J. Num. Meth. Eng.*, Vol 55, 573-616.

Lyamin, A., Yu, H.S., Sloan, S.W and Hossain, M.Z. (1998). Lower bound limit analysis of jointed rocks using the Hoek-Brown criterion. *Australian Geomech. J.*, Vol 33, 46-62.

Lysmer, J. (1970). Limit analysis of plane problems in soil mechanics. *J. Soil Mech. and Found. Div.*, ASCE, Vol. 96, SM4, 1131-1334.

Maier, G., Carvelli, G. and Cocchetti, G. (2000). On direct methods of shakedown and limit analysis. *Plenary Lecture, 4th Euromech Solid Mechanics Conference*, Metz, June.

Merifield, R.S., Sloan, S.W. and Yu, H.S. (1999). Rigorous plasticity solutions for the bearing capacity of two layered clays. *Geotechnique*, Vol. 49, 471-490.

Merifield, R.S., Sloan, S.W. and Yu, H.S. (2001). Stability of plate anchors in undrained clay. *Geotechnique*, Vol. 51, 141-153.

Michalowski, R.L. (1989). Three-dimensional analysis of locally loaded slopes. *Geotechnique*, Vol. 39, 27-38.

Michalowski, R.L. (1994). Limit analysis of slopes subjected to pore pressure. *Computer Methods and Advances in Geomechanics*, (Editors: Siriwardane and Zaman), 2477-2482.

Miller, T.W. and Hamilton, J.H. (1989). A new analysis procedure to explain a slope failure at the Martin Lake mine. *Geotechnique*, Vol. 39, also see Discussion, Vol. 40, 145-147.

Morgenstern, N.R. and Price, V.E. (1965). The analysis of the stability of generalized slip surfaces. *Geotechnique*, Vol. 15, 79-93.

Nagtegaal, J., Parks, D.M. and Rice, J.R. (1974). On numerically accurate finite element solutions in the fully plastic range. *Comput. Meth. Appl. Mech. Eng.*, Vol. 4, 153-177.

Nash, D. (1987). A comparative review of limit equilibrium methods of stability analysis. Chapter 2 In: *Slope Stability*, (Editors: M.G. Anderson and K.S. Richards), John Wiley.

Ponter, A.R.S. and Boulbibane, M. (2006). The linear matching method for limit load and shakedown analysis, In: *Modern Trends in Geomechanics*, (Editors: W. Wu and H.S. Yu), Springer.

Potts, D. M. and Zdravkovic, L. (1999). *Finite Element Analysis in Geotechnical Engineering: Theory*, Thomas Telford, London.

Prager, W. and Hodge, P.G. (1951). *The Theory of Perfectly Plastic Solids*, John Wiley and Sons, New York.

Shield, R.T. (1954). Stress and velocity fields in soil mechanics, *Quart. Appl. Math.*, Vol 12, 144-156.

Sloan, S.W. (1988a). A steepest edge active set algorithm for solving sparse linear programming problems. *Int. J. Num. Meth. Eng.*, Vol. 26, 2671-2685.

Sloan, S.W. (1988b). Lower bound limit analysis using finite elements and linear programming. *Int. J. Num. Analy. Meth. Geomech.*, Vol. 12, 61-77.

Sloan, S.W. (1989). Upper bound limit analysis using finite elements and linear programming. *Int. J. Num. Analy. Meth. Geomech.*, Vol. 13, 263-282.

Sloan, S.W. (1995). 'Limit analysis in geotechnical engineering'. in: *Modern Developments in Geomechanics* (Editor: C.M. Haberfield), Proc. of Ian Donald Symposium, Monash University, Australia, 167-199.

Sloan, S.W. and Kleeman, P.W. (1995). Upper bound limit analysis using discontinuous velocity fields. *Computer Meth. Appl. Mech. Eng.*, Vol. 127, 293-314.

Sloan S.W. and Randolph M.F. (1982). Numerical prediction of collapse load using finite elements and linear programming. *Int. J. Num. Analy. Meth. Geomech.*, Vol 6, 47-76.

Spencer, E. (1967). A method of analysis of the stability of embankments assuming parallel inter-slice forces. *Geotechnique.*, Vol. 17, 11-26.

Sutcliffe, D.J., Yu, H.S. and Page, A.W. (2001). Lower bound limit analysis of unreinforced masonry shear walls, *Comput. Struct.*, Vol. 79, 1295-1312.

Sutcliffe, D.J., Yu, H.S. and Sloan, S.W. (2004). Lower bound solutions for bearing capacity of jointed rock. *Comput. Geotech.*, Vol. 31, 23-36.

Taylor, D.W. (1948). *Fundamentals of Soil Mechanics*, Wiley, New York.

Terzaghi, K. (1943). *Theoretical Soil Mechanics*, Wiley, New York.

Whitman, R.W. and Bailey, W.A. (1967). Use of computers for slope stability analysis. *J. Soil Mech. and Found. Div.*, ASCE, Vol. 93, SM4, 475-498.

Yu, H.S. and Netherton, M. (2000). Performance of displacement finite elements for modelling incompressible materials. *Int. J. Num. Analy. Meth. Geomech.*, Vol. 24, 627-653.

Yu, H.S. and Sloan, S.W. (1991a). Lower bound limit analysis of axisymmetric problems using finite elements and linear programming, *Proc. 6th Int. Conf. in Australia on Finite Elements*, Sydney, Vol. 1, 48-52.

Yu, H.S. and Sloan, S.W. (1991b). Lower bound limit analysis of plane problems in soil mechanics, *Proc. Int. Conf. of Nonlinear Engineering Computations*, Swansea, 329-338.

Yu, H.S. and Sloan, S.W. (1994a). A note on bearing capacity of soft clays under embankments, *J. Geotech. Eng.*, ASCE, Vol. 120 (1), 246-255.

Yu, H.S. and Sloan, S.W. (1994b). Upper bound limit analysis of a rigid-plastic body with frictional interfaces. *Int. J. Mech. Sci.*, Vol. 36, 219-229.

Yu, H.S. and Sloan, S.W. (1994c). Bearing capacity of jointed rock. In: *Compter methods and Advances in Geomechanics*, (Editors: Siriwardane and Zaman), 2403-2408.

Yu, H.S. and Sloan, S.W. (1995). Limit analysis of anisotropic soils using finite elements and linear programming. *Mech. Res. Commu.*, Vol. 21 545-554.

Yu, H.S. and Sloan, S.W. (1997). Finite element limit analysis of reinforced soils. *Comput. Struct.*, Vol 63, 567-577.

Yu H.S., Houlsby, G.T. and Burd, H.J. (1993). A novel isoparametric finite element displacement formulation for axisymmetric analysis of nearly incompressible materials. *Int. J. Num. Meth. Eng.*, Vol 36, 2453-2472.

Yu, H.S., Salgado, R., Sloan, S.W. and Kim, J.M. (1998). Limit analysis versus limit equilibrium for slope stability. *J. Geotech. Geoenviro. Eng.*, ASCE, Vol 124, 1-11.

Yu, H.S., Sloan, S.W. and Kleeman, P.W. (1994). A quadratic element for upper bound limit analysis. *Engineering Computations*, Vol. 11, 195-212.

Zhang, P.X., Lu, M.W. and Hwang, K. (1991). A mathematical programming algorithm for limit analysis. *Acta Mechanica Sinica*, Vol. 7, 267-274.

Zouain, N., Herskovits, J. and Borges, L.A. (1993). An iterative algorithm for limit analysis with nonlinear yield functions. *Int. J. Solids and Structures*, Vol. 32, 1645-1658.

## CHAPTER 13

### SHAKEDOWN ANALYSIS

#### 13.1 INTRODUCTION

In the previous chapter, we were concerned with direct methods of determining plastic collapse loads of geotechnical structures under static loading conditions. In particular, two fundamental theorems have been found extremely useful. These are the lower and upper bound theorems of plastic collapse for perfectly plastic materials (Gvozdev, 1936; Hill, 1951; Drucker *et al.*, 1952). These theorems allow the collapse load to be determined directly without using an incremental analysis.

This chapter is concerned with a more general case involving structures that are subjected to variable loads. In particular we are interested in the direct methods that can be used to assess the stability of structures under variable loads. When an elastic-plastic structure is subjected to a cyclic load, three distinctive situations may occur (Yu, 2005). First, if the load magnitude applied is so low (i.e. lower than the elastic limit of the structure) that nowhere in the structure is deforming plastically, then the behaviour will be entirely elastic. Second, if the load is larger than the elastic limit (or the first yield limit) so that some part of the structure is deforming plastically but is less than a critical limit, then the plastic deformation will cease to occur after a number of load cycles. In other words, after a number of cycles with plastic deformation, the whole structure will respond purely elastically to the remaining load cycles. If this happens, then we consider the structure to have ‘shaken down’, and the critical limit (below which shakedown can occur) is termed a ‘shakedown (or elastic shakedown) limit’. Third, if the applied load is greater than the shakedown limit, then the structure will continue to exhibit plastic strains for however long the load cycles are applied. If this occurs, then the structure would eventually fail owing to fatigue or excessive plastic deformation. Therefore for structures under variable loads, the shakedown limit provides a rational criterion for design (Kachanov, 1974; Konig, 1987; Johnson, 1985, 1992; Maier *et al.*, 2000).

Over the last two decades, there has been growing interest in the application of the fundamental shakedown theorems of Bleich (1932), Melan (1938), Symonds and Neal (1951) and Koiter (1960) to study the behaviour of elastic-plastic structures subjected to repeated or cyclic loading conditions (e.g. Johnson, 1985; Konig, 1987). In the field of geotechnical engineering, the theory of shakedown is particularly useful for solving problems in the design of foundations under cyclic loads

(Aboustit and Reddy, 1980; Pande, 1982) and pavements under moving traffic loads (Sharp, 1983; Sharp and Booker, 1984; Collins and Cliffe, 1987; Collins *et al.*, 1993; Raad *et al.*, 1988; Yu and Hossain, 1998; Shiau and Yu, 2000a,b; Yu, 2005; Boulbibile and Ponter, 2006; Li and Yu, 2006a, b, c).

## 13.2 THE CONCEPT AND THEOREMS OF SHAKEDOWN

### 13.2.1 Simple illustration of the concept of shakedown

To provide a simple illustration of the basic concept of shakedown, we follow Hill (1950) and Calladine (1985) in considering the behaviour of loading-unloading-reloading in a simple one-dimensional cavity expansion problem in a Tresca material.

For simplicity let us consider a spherical shell with internal and external radii of  $a$  and  $b$ . The shell is subjected to an internal pressure  $p$  and the external boundary is stress-free. This is a special case of the problem considered in section 10.3 of Chapter 10. The solutions for this problem using the Tresca yield criterion can also be found in Hill (1950).

#### *The loading stage - elastic limit and plastic limit*

When the internal pressure  $p$  is increased from zero, the shell is initially elastic until the pressure reaches the following elastic limit

$$p_e = \frac{2Y}{3} \left(1 - \left(\frac{a_0}{b_0}\right)^3\right) \quad (13.1)$$

where  $Y = 2S_u$  and  $S_u$  is known as the undrained shear strength.

The elastic stress field is obtained as follows

$$\sigma_r = -p \frac{\left(\frac{b_0}{r}\right)^3 - 1}{\left(\frac{b_0}{a_0}\right)^3 - 1} \quad (13.2)$$

$$\sigma_\theta = \sigma_\phi = p \frac{\frac{1}{2} \left(\frac{b_0}{r}\right)^3 + 1}{\left(\frac{b_0}{a_0}\right)^3 - 1} \quad (13.3)$$

Once the internal pressure exceeds  $p_e$ , a plastic region will be formed starting from the internal boundary. As detailed in Chapter 10, the following solution for stresses in the plastic region ( $a \leq r \leq c$ ) can be obtained:

$$\sigma_r = -2Y \ln\left(\frac{c}{r}\right) - \frac{2Y}{3} \left[1 - \left(\frac{c}{b_0}\right)^3\right] \quad (13.4)$$

$$\sigma_\theta = \sigma_\phi = Y - 2Y \ln\left(\frac{c}{r}\right) - \frac{2Y}{3} \left[1 - \left(\frac{c}{b_0}\right)^3\right] \quad (13.5)$$

where  $c$  is the radius of the plastic zone. The stresses in the outer elastic region ( $c \leq r \leq b$ ) are

$$\sigma_r = -\frac{2Yc^3}{3b_0^3} \left[\left(\frac{b_0}{r}\right)^3 - 1\right] \quad (13.6)$$

$$\sigma_\theta = \sigma_\phi = \frac{2Yc^3}{3b_0^3} \left[\frac{1}{2} \left(\frac{b_0}{r}\right)^3 + 1\right] \quad (13.7)$$

By substituting  $r = a$  in equation (13.4), the internal pressure needed to produce plastic flow to a radius  $c$  is found to be

$$p = 2Y \ln\left(\frac{c}{a}\right) + \frac{2Y}{3} \left[1 - \left(\frac{c}{b_0}\right)^3\right] \quad (13.8)$$

As a special case, when the whole shell becomes plastic (i.e.  $c=b$ ), then the internal pressure reaches a true maximum (i.e. plastic limit), which can be obtained simply from equation (13.8):

$$p_p = 2Y \ln\left(\frac{b}{a}\right) \quad (13.9)$$

which would decrease during the subsequent expansion due to the geometry change.

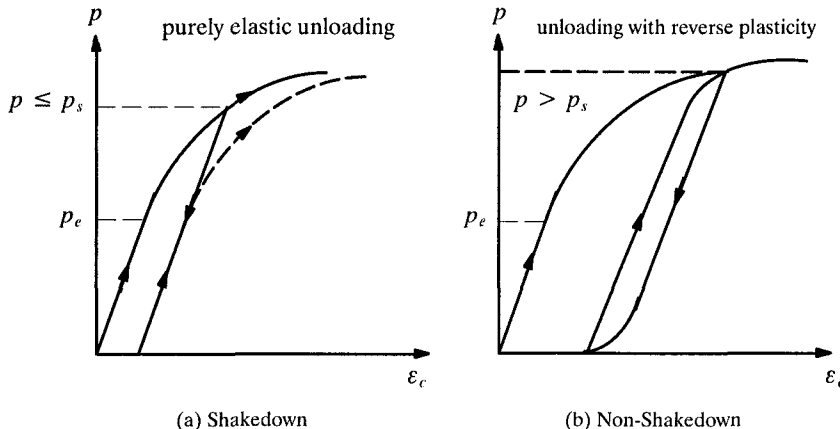


Figure 13.1: The behaviour of shakedown for cavity loading-unloading-reloading

*The unloading stage - residual stresses and shakedown limit*

If a pressure  $p > p_e$  is applied to the internal boundary of the shell and then reduced to zero, the unloading process is purely elastic if  $p$  is not too great (see Figure 13.1a). The resulting field of residual stresses is obtained by subtracting from (13.4)-(13.7) the elastic stresses (13.2)-(13.3) due to the removal of the internal pressure. The residual stress field in the outer elastic region ( $c \leq r \leq b$ ) is

$$\sigma_r = -\frac{2Y}{3} \left[ \frac{c^3}{a_0^3} - \frac{p}{p_e} \right] \left[ \frac{a_0^3}{r^3} - \frac{a_0^3}{b_0^3} \right] \quad (13.10)$$

$$\sigma_\theta = \frac{2Y}{3} \left[ \frac{c^3}{a_0^3} - \frac{p}{p_e} \right] \left[ \frac{a_0^3}{2r^3} + \frac{a_0^3}{b_0^3} \right] \quad (13.11)$$

and the residual stress field in the inner plastic region ( $a \leq r \leq c$ ) is

$$\sigma_r = -\frac{2Y}{3} \left[ \frac{p}{p_e} \left( 1 - \frac{a_0^3}{r^3} \right) - 3 \ln \left( \frac{r}{a_0} \right) \right] \quad (13.12)$$

$$\sigma_\theta = \frac{2Y}{3} \left[ \frac{3}{2} + 3 \ln \left( \frac{r}{a_0} \right) - \frac{p}{p_e} \left( 1 + \frac{a_0^3}{2r^3} \right) \right] \quad (13.13)$$

where

$$p = 2Y \ln \left( \frac{c}{a} \right) + \frac{2Y}{3} \left[ 1 - \left( \frac{c}{b_0} \right)^3 \right]$$

$$p_e = \frac{2Y}{3} \left( 1 - \left( \frac{a_0}{b_0} \right)^3 \right)$$

As stated in Hill (1950), the contraction of the outer layers of the shell compresses the inner layers, and leaves the internal surface in a state of tangential compression of magnitude  $Y(p/p_0 - 1)$ . A subsequent application of pressure (i.e. reloading to a pressure less than the original maximum) only strains the shell elastically, as shown in Figure 13.1a. In this way, the shell is strengthened by pre-stressing (as reloading from a stress-free state will follow the stress path marked by the dashed line). This simple example illustrates that certain residual stresses (in this case caused by prior pressurisation of the shell) raises the load to cause first yield.

It is noted that the behaviour shown in Figure 13.1a is only possible if the unloading process is purely elastic. In other words, no elements of the shell are unloaded and stressed to yield in the reverse direction during the removal of the applied load. For the Tresca yield condition, it is the quantity  $\sigma_\theta - \sigma_r$  that governs yielding. The largest difference occurs on the internal boundary, where it equals

$$\sigma_\theta - \sigma_r = Y(1 - \frac{p}{p_e}) \quad (13.14)$$

For reverse yielding to occur we have

$$\sigma_\theta - \sigma_r = -Y \quad (13.15)$$

and by combining equations (13.14) and (13.15) we know that the condition for reverse yielding to occur during unloading is evidently

$$p = p_s \leq 2p_e = \frac{4Y}{3}(1 - \frac{a_0^3}{b_0^3}) \quad (13.16)$$

The unloading is accordingly purely elastic if the pressure is less than two times the elastic limit, and this occurs for all pressures  $p$  up to the plastic limit

$$p = p_s \leq p_p = 2Y \ln(\frac{b_0}{a_0}) \quad (13.17)$$

We may define the shakedown limit as  $p_s = \min(p_p, 2p_e)$ , and for  $p \leq p_s$  both the initial unloading and any subsequent reloading will be purely elastic, which is shown in Figure 13.1a. It is easy to work out that the shakedown condition (13.16) controls as long as  $b_0/a_0 > 4.92$ . The analysis we have done shows that a single application of pressure  $p$  (that is less than  $p_s$ ) induces residual stresses which enable the shell to respond to repeated pressure application up to this level by purely elastic action. We say the structure will shake down to elastic behaviour for repeated pressurisation between  $0 < p \leq p_s$ .

Finally we note that for pressure  $p > p_s$ , yielding and therefore plastic deformation will occur during both unloading and reloading processes as shown in Figure 13.1b. If this occurs, the structure will not shake down to elastic behaviour. As stressed by Calladine (1985), these conclusions depend critically on our assumption that there is no hysteresis and there is no Bauschinger effect.

### 13.2.2 The lower and upper bound theorems of shakedown

It should be acknowledged that the preceding example of shakedown has been extremely simple: a simple structure subject to only one kind of loading whose sign never changed. In reality, however, shakedown problems of practical interest would be much more complicated, particularly involving two- or three- dimensional formulations. In these cases, it is hardly possible to derive the exact shakedown limits.

To overcome the potential difficulties of applying the shakedown concept to engineering design, we can make use of two fundamental shakedown theorems (similar to the lower and upper bound theorems of plastic collapse) developed by Melan

(1938) and Koiter (1960). These theorems, presented and proved in Section 4.6 of Chapter 4, enable the shakedown limit of a general elastic-plastic structure to be estimated in a direct manner.

*The lower bound shakedown theorem (Melan, 1938)*

Melan's static or lower bound shakedown theorem states that if any self-equilibrated residual stress field  $\varrho_{ij}$  can be found, which, when combined with the elastic stress field produced by the applied loads, does not violate the yield condition anywhere, then shakedown will occur. If the applied load is denoted by  $\lambda p_0$  (where  $p_0$  may be conveniently set as the unit pressure in the actual calculation), and  $\lambda$  is a dimensionless scale parameter, then all the induced elastic stress components are also proportional to  $\lambda$ . Melan's shakedown theorem hence demands

$$f(\lambda \sigma_{ij}^e + \varrho_{ij}) \leq 0 \quad (13.18)$$

where  $\sigma_{ij}^e$  is the elastic stress field due to the applied pressure  $p_0$ , and  $f(\sigma_{ij}) = 0$  is the yield condition for the material. The largest value of  $\lambda$  obtained by searching all possible self-equilibrated residual stress fields,  $\varrho_{ij}$ , will give the actual shakedown limit  $p_s = \lambda_s p_0$ .

*The upper bound shakedown theorem (Koiter, 1960)*

Koiter's kinematic or upper bound theorem can be stated as follows: an elastic-perfectly plastic structure will not shakedown for given extreme load values (i.e. it will fail ultimately due to progressive plastic flow) if any kinematically admissible plastic strain rate cycle  $\dot{\varepsilon}_{ij}^k$  and any external loads  $T_{0i}$  within the prescribed limits can be found so that

$$\int_0^t dt \iint_{S_T} T_{0i} \dot{u}_i^k dS > \int_0^t dt \iiint_V \sigma_{ij}^k \dot{\varepsilon}_{ij}^k dV \quad (13.19)$$

which provides an upper bound for the shakedown limit.

Alternatively, Koiter (1960) pointed out that the upper bound theorem can be stated as follows: the structure will shakedown if the inequality sign in (13.19) is reversed for all kinematically admissible strain rate cycles

$$\lambda_s \int_0^t dt \iint_{S_T} p_{0i} \dot{u}_i^k dS \leq \int_0^t dt \iiint_V \sigma_{ij}^k \dot{\varepsilon}_{ij}^k dV \quad (13.20)$$

which provides an upper bound to the shakedown load multiplier  $\lambda_s$ .

$$\lambda_s \leq \frac{\int_0^t dt \iint_V \sigma_{ij}^k \dot{\varepsilon}_{ij}^k dV}{\int_0^t dt \iint_{S_T} p_{0i} \dot{u}_i^k dS} \quad (13.21)$$

### 13.3 SHAKEDOWN OF ROLLING AND SLIDING LINE CONTACTS

Shakedown involving a repeated rolling and sliding contact proves to be fundamental to the analysis and design of several engineering problems. In particular, it has applications to the simulation of railway foundations, roads and pavements under moving traffic loads (e.g. Johnson, 1962, 1985; Sharp and Booker, 1984; Collins and Cliffe, 1987; Radovsky and Murashina, 1996; Yu and Hossain, 1998; Yu, 2005).

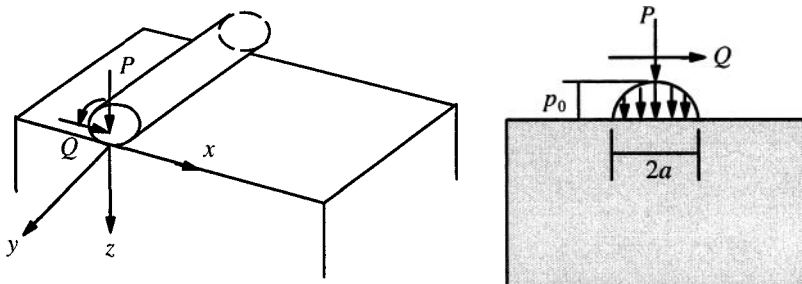


Figure 13.2: Rolling/sliding contact of a cylinder with an elastic-plastic half space

#### 13.3.1 Elastic stress fields

##### *The contact tractions due to a rolling and sliding cylinder*

In order to use the lower bound shakedown theorem, we need to evaluate the elastic stress distribution due to the surface tractions. Therefore we have to assume a form of surface pressure distribution. According to Johnson (1985), the contact stresses due to a moving cylinder may be assumed to consist of a normal and a tangential traction for rolling and sliding contact. If the normal load per unit length in the y-direction is denoted as  $P$  and its tangential counterpart as  $Q$ , we may define a surface friction coefficient

$$\mu = \frac{Q}{P} \quad (13.22)$$

If we assume that the contact pressure is limited to a width of  $2a$  in the x-direction, the Hertz theory leads to the following normal and tangential contact tractions

$$\sigma_{zz} = -\frac{2P}{\pi a^2} \sqrt{(a^2 - x^2)} \quad (13.23)$$

$$\sigma_{xz} = -\frac{2\mu P}{\pi a^2} \sqrt{(a^2 - x^2)} \quad (13.24)$$

As shown in Figure 13.2, the maximum vertical stress occurs at  $x=z=0$ , which is obtained from equation (13.23) as follows

$$p_0 = \frac{2P}{\pi a} \quad (13.25)$$

On the other hand, the mean or average vertical stress is

$$\bar{p} = \frac{P}{2a} \quad (13.26)$$

The width of loading is also linked to the normal load  $P$  as follows (Johnson, 1985):

$$a = \sqrt{\frac{4PR}{\pi E^*}} \quad (13.27)$$

in which  $1/R = 1/R_1 + 1/R_2$  and  $E^*$  depends on material properties.

By combining equations (13.25)-(13.27), we may obtain the direct expression for the maximum pressure from the normal load  $P$ :

$$p_0 = \frac{2P}{\pi a} = \frac{4}{\pi} \bar{p} = \sqrt{\frac{PE^*}{\pi R}} \quad (13.28)$$

which indicates that the normal load  $P$  is proportional to  $(p_0)^2$ .

#### *The elastic stress fields due to contact pressures*

The elastic stresses in the half-space due to the normal load  $P$  can be expressed in closed form as follows (Johnson, 1985):

$$(\sigma_{xx})_p = -\frac{p_0}{a} \left\{ m \left( 1 + \frac{z^2 + n^2}{m^2 + n^2} \right) - 2z \right\} \quad (13.29)$$

$$(\sigma_{zz})_p = -\frac{p_0}{a} m \left( 1 - \frac{z^2 + n^2}{m^2 + n^2} \right) \quad (13.30)$$

$$(\sigma_{xz})_p = -\frac{p_0}{a} n \left( \frac{m^2 - z^2}{m^2 + n^2} \right) \quad (13.31)$$

where  $m$  and  $n$  are defined by

$$m^2 = \frac{1}{2} \left\{ \sqrt{(a^2 - x^2 + z^2)^2 + 4x^2z^2} + (a^2 - x^2 + z^2) \right\} \quad (13.32)$$

$$n^2 = \frac{1}{2} \left\{ \sqrt{(a^2 - x^2 + z^2)^2 + 4x^2z^2} - (a^2 - x^2 + z^2) \right\} \quad (13.33)$$

in which the signs of  $m$  and  $n$  are the same as the signs of  $z$  and  $x$  respectively.

Now we present the elastic stresses due to the tangential traction

$$(\sigma_{xx})_q = \frac{q_0}{a} \left\{ n \left( 2 - \frac{z^2 - m^2}{m^2 + n^2} \right) - 2x \right\} \quad (13.34)$$

$$\frac{(\sigma_{zz})_q}{q_0} = \frac{(\sigma_{xz})_p}{p_0} \quad (13.35)$$

$$\frac{(\sigma_{xz})_q}{q_0} = \frac{(\sigma_{xx})_p}{p_0} \quad (13.36)$$

where  $q_0 = \mu p_0$  is the maximum shear stress at  $x=z=0$ .

The total elastic stresses due to both the normal and tangential loads are the sum of those given in equations (13.29)-(13.31) and those given in equations (13.34)-(13.36).

### 13.3.2 Shakedown solutions in Tresca materials

Johnson (1962) took the first step in deriving the shakedown limit for a half space with an infinitely long cylinder rolling and/or sliding on the surface as shown in Figure 13.2. The material is assumed to be cohesive in nature and the Tresca yield criterion was used.

#### (a) The lower bound approach

##### *The residual stress field and shakedown condition*

To use Melan's lower bound theorem, we need to search for possible residual stress fields. For the case of an elastic cylinder rolling or sliding on an elastic-perfectly plastic half-space, Johnson (1962) was the first to study its residual stress fields.

A possible residual stress field is such that can remain in the half-space after the load has passed. It must also satisfy the equations of stress equilibrium. The assumption of plane deformation in the  $y$ -direction eliminates  $\sigma_{xy}$  and  $\sigma_{yz}$ , and makes the remaining components independent of  $y$ . As noted by Johnson (1985), if the plastic deformation is assumed to be steady and continuous, the surface of the half-space must remain flat and the residual stresses must be independent of  $x$ . Finally for the residual stresses to be in equilibrium with a traction free surface,  $\sigma_{zz}$  and  $\sigma_{xz}$

must be zero. After these considerations, the only possible system of residual stresses is defined by

$$\varrho_{xx} = f(z); \quad \varrho_{yy} = g(z); \quad \varrho_{zz} = \varrho_{xy} = \varrho_{yz} = \varrho_{zx} = 0 \quad (13.37)$$

According to Melan's lower bound shakedown theorem, we can choose the residual stresses to have any value at any depth to avoid violating the yield condition. We can then choose  $\varrho_{yy}$  to ensure that the total stress in the  $y$ -direction is the intermediate principal stress. If the yield condition of the material is assumed to obey the Tresca criterion, which is expressed in terms of the total stresses (including both the elastic stresses and residual stresses) as follows:

$$\frac{1}{4}(\lambda\sigma_{xx}^e + \varrho_{xx} - \lambda\sigma_{zz}^e)^2 + (\lambda\sigma_{xz}^e)^2 \leq (S_u)^2 \quad (13.38)$$

from which, we can conclude that the yield condition cannot be satisfied if  $\lambda\sigma_{xz}^e$  exceeds the undrained shear strength. Therefore the best lower bound would be to determine the following load multiplier

$$\lambda_s = \min_{(x,z)} \frac{S_u}{\sigma_{xz}^e(x,z)} = \frac{S_u}{\max_{(x,z)} \sigma_{xz}^e(x,z)} \quad (13.39)$$

In other words, the shakedown limit is controlled by the maximum elastic shear stress  $\sigma_{xz}^e$ . For example for the case of normal loads only (i.e. pure rolling), equation (13.31) can be used to give the maximum shear stress as  $\max \sigma_{xz}^e(x,z) = 0.25p_0$  at points  $(0.87a, 0.5a)$  and  $(-0.87a, 0.5a)$ . Hence the shakedown limit can be represented by the following normalised form

$$\frac{\lambda_s p_0}{S_u} = \frac{1}{0.25} = 4.0 \quad (13.40)$$

### *Influence of tangential traction*

The same analysis can be performed for cases with both normal and tangential tractions (i.e.  $\mu > 0$ ). This type of analysis was first considered by Johnson and Jeffries (1963). It is important to note that in this case the residual stress field defined by equation (13.37) is still valid, and therefore the shakedown limit is also determined by the maximum elastic shear stress  $\sigma_{xz}^e$ , as defined in equation (13.39). The only difference is that in calculating the elastic stress, the contribution due to the tangential traction must be added. It is found that the point of maximum  $\sigma_{xz}^e$  lies below the surface as long as  $\mu = Q/P \leq 0.367$ . At larger values of tangential traction, the point of maximum shear stress lies in the surface layer. Figure 13.3 shows the shakedown limits obtained by Yu (2005) for a range of  $\mu$  values. It is evident that the shakedown limit tends to reduce with increasing value of tangential traction.

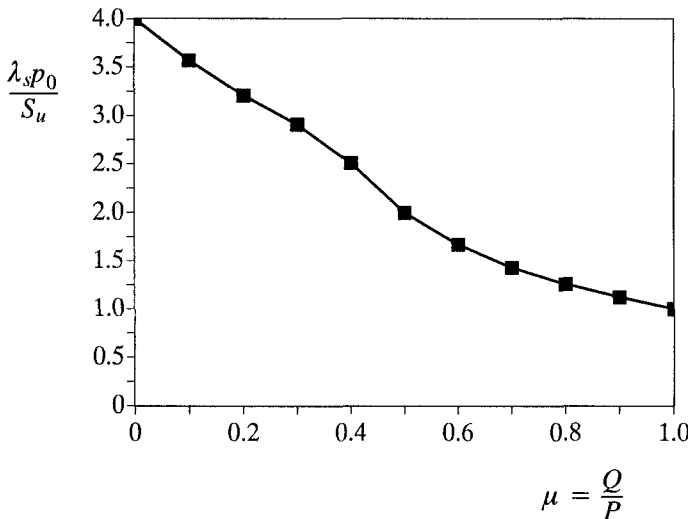


Figure 13.3: Shakedown solutions for line contact in Tresca materials (Yu, 2005)

### (b) The upper bound approach

As stated by Johnson (1992), the first attempt appears to be made by Belyakov (see Gokhfeld and Cherniavski, 1980) for the preceding shakedown problem. To apply Koiter's upper bound shakedown theorem, we may assume a mechanism of incremental collapse comprising simple plastic shear along a plane  $z = z_0 = \text{constant}$ . If the increment of plastic tangential displacement is  $\Delta u_{xx}^p$ , the work done by the elastic stresses is  $\sigma_{xz}^e \times \Delta u_{xx}^p$  and the internal dissipation is given by  $S_u \times \Delta u_{xx}^p$ . From Koiter's upper bound theorem we have

$$\lambda_s \leq \frac{\int_0^t dt \iint_V \int_V \sigma_{ij}^k \varepsilon_{ij}^k dV}{\int_0^t dt \iint_{S_T} p_{0i} \dot{u}_i^k dS} = \frac{S_u \times \Delta u_{xx}^p}{\sigma_{xz}^e \times \Delta u_{xx}^p} = \frac{S_u}{\sigma_{xz}^e} \quad (13.41)$$

The optimum upper bound may be obtained by searching  $z_0$  a depth where the elastic shear stress  $\sigma_{xz}^e$  becomes maximum. This is clearly the same as the lower bound solution defined by (13.39). Therefore the shakedown solutions presented in Figure 13.3 may be regarded as the true shakedown solutions for the problem considered (Johnson, 1992).

### 13.3.3 Shakedown solutions in Mohr-Coulomb materials

In this subsection, we will derive the shakedown limits for a half-space that is made of cohesive-frictional materials obeying the Mohr-Coulomb yield condition. As for cohesive materials we will make use of both the lower bound and upper bound approaches.

#### (a) The lower bound approach

##### *The residual stress field and shakedown condition*

A possible residual stress field is such that can remain in the half-space after the load has passed. It must also satisfy the equations of stress equilibrium. The assumption of plane deformation in the  $y$ -direction eliminates  $\varrho_{xy}$  and  $\varrho_{yz}$ , and makes the remaining components independent of  $y$ . As noted by Johnson (1985), if the plastic deformation is assumed to be steady and continuous, the surface of the half-space must remain flat and the residual stresses must be independent of  $x$ . Finally for the residual stresses to be in equilibrium with a traction free surface,  $\varrho_{zz}$  and  $\varrho_{xz}$  must be zero. After these considerations, the only possible system of residual stresses is defined by

$$\varrho_{xx} = f(z); \quad \varrho_{yy} = g(z); \quad \varrho_{zz} = \varrho_{xy} = \varrho_{yz} = \varrho_{zx} = 0 \quad (13.42)$$

According to Melan's lower bound shakedown theorem, we can choose the residual stresses to have any value at any depth to avoid violating the yield condition. We can then choose  $\varrho_{yy}$  to ensure that the total stress in the  $y$ -direction is the intermediate principal stress. If the yield condition of the material is assumed to obey the Mohr-Coulomb criterion, which is expressed in terms of the total stresses (including both the elastic stresses and residual stresses) as follows:

$$\sqrt{(\lambda\sigma_{xx}^e + \varrho_{xx} - \lambda\sigma_{zz}^e)^2 + 4(\lambda\sigma_{xz}^e)^2} + (\lambda\sigma_{xx}^e + \varrho_{xx} + \lambda\sigma_{zz}^e) \sin \phi \leq 2c \cos \phi \quad (13.43)$$

which can be satisfied only if the following condition is met (Yu, 2005; Radovsky and Murashina, 1996):

$$\lambda \leq \frac{c}{|\sigma_{xz}^e| + \sigma_{zz}^e \tan \phi} \quad (13.44)$$

Therefore the best lower bound would be to determine a load multiplier so that

$$\lambda_s = \min_{(x,z)} \frac{c}{|\sigma_{xz}^e| + \sigma_{zz}^e \tan \phi} = \frac{c}{\max_{(x,z)} [|\sigma_{xz}^e| + \sigma_{zz}^e \tan \phi]} \quad (13.45)$$

In other words, the shakedown limit is controlled by the maximum elastic stress function  $|\sigma_{xz}^e| + \sigma_{zz}^e \tan \phi$ .

Whilst some results are given by Radovsky and Murashina (1996) for the case of pure rolling, a complete set of results has been obtained by Yu (2005) for cases with both normal and tangential tractions. Figure 13.4 shows the shakedown limits for the cases of  $\phi = 0^0, 15^0, 30^0, 45^0$ . It is found that the shakedown limit increases with internal friction angle but decreases with the surface friction coefficient  $\mu$ .

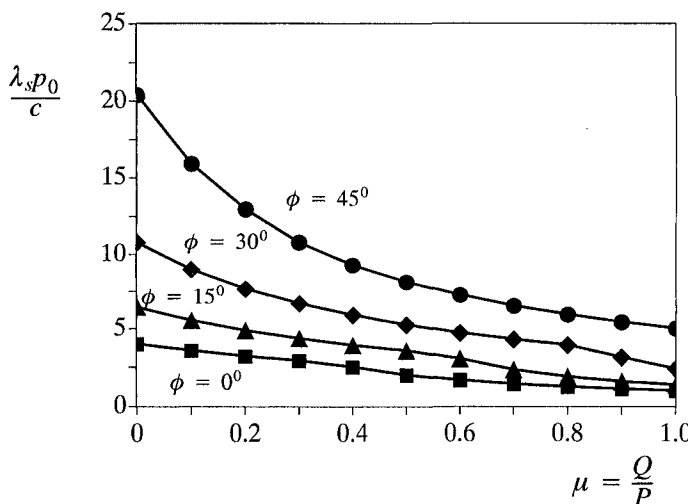


Figure 13.4: Shakedown solutions for line contact in Mohr-Coulomb materials for friction angle ranges from zero to 45 degrees (Yu, 2005)

### (b) The upper bound approach

To apply Koiter's upper bound shakedown theorem, we may assume a mechanism of incremental collapse comprising simple plastic shear along a plane  $z = z_0 = \text{constant}$ . As pointed out by Collins and Cliffe (1987), due to the dilatant nature of the associated flow rule of a Mohr-Coulomb material, a shear velocity must be accompanied by a normal component, such that the resultant velocity vector is inclined at an angle  $\phi$  to the slip line. The rate of plastic work per unit length on such a slip line is the product of the cohesion  $c$  with the tangential velocity jump  $V \cos \phi$ . The work done by the elastic stresses is  $|\sigma_{xz}^e| \times V \cos \phi + \sigma_{zz}^e \times V \sin \phi$ . From Koiter's upper bound theorem we have

$$\begin{aligned}
 \lambda_s \leq & \frac{\int_0^t dt \iint_V \sigma_{ij}^k \dot{\varepsilon}_{ij}^k dV}{\int_0^t dt \iint_{S_T} p_{0i} \dot{u}_i^k dS} = \frac{c \times V \cos \phi}{|\sigma_{xz}^e| \times V \cos \phi + \sigma_{zz}^e \times V \sin \phi} \\
 & = \frac{c}{|\sigma_{xz}^e| + \sigma_{zz}^e \tan \phi} \quad (13.46)
 \end{aligned}$$

The optimum upper bound may be obtained by searching  $z_0$  at a depth where the elastic shear stress function  $|\sigma_{xz}^e| + \sigma_{zz}^e \tan \phi$  becomes maximum. This is clearly the same as the lower bound solution defined by (13.44). As a result, the shakedown solutions presented in Figure 13.4 for Mohr-Coulomb materials can be regarded as the true shakedown solutions.

### 13.4 SHAKEDOWN OF ROLLING AND SLIDING POINT CONTACTS

In the previous section, we considered the shakedown of a half-space under a rolling and sliding line load, as shown in Figure 13.2. Because of its two-dimensional nature (i.e. plane strain), it can only be considered as an approximate solution to pavement or railway foundations under moving traffic loads. A better approximation of the traffic loading would be to use a surface contact loading limited to a circle (Yu, 2005; Collins and Cliffe, 1987). With this assumption, however, the problem becomes three-dimensional and as a consequence it is much more difficult to derive relevant shakedown solutions.

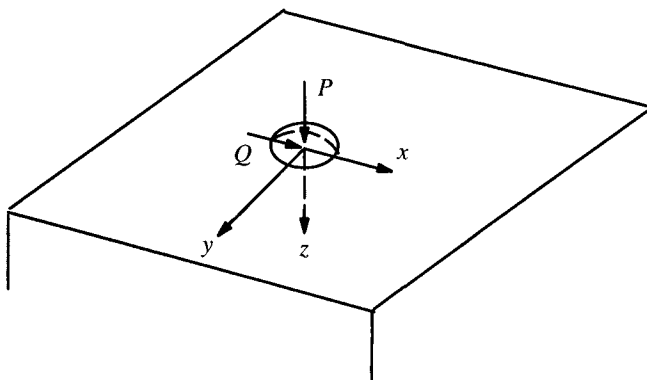


Figure 13.5: Rolling/sliding point contact with an elastic-plastic half space

### 13.4.1 Problem definition of a point contact

We now follow Yu (2005) to consider a cohesive-frictional half-space that is subjected to a surface contact loading limited to a circle of radius,  $a$ , (i.e.  $x^2 + y^2 \leq a^2$ ), as shown in Figure 13.5. If the tensile stresses are treated as positive, then the boundary stresses on the surface are given as follows:

$$\sigma_{zz} = -\frac{3P}{2\pi a^3} \sqrt{(a^2 - x^2 - y^2)} \quad (13.47)$$

$$\sigma_{xz} = -\frac{3Q}{2\pi a^3} \sqrt{(a^2 - x^2 - y^2)} \quad (13.48)$$

$$\sigma_{yz} = 0 \quad (13.49)$$

where  $P$  is the total normal load applied in the  $z$ -direction (i.e. the vertical direction), and  $Q$  is the total shear force applied in the  $x$ -direction (i.e. the moving load direction). All the boundary stresses outside the circle of contact are assumed to be zero. It is also common to link the normal and shear loads by a friction coefficient  $\mu = Q/P$ .

The stress distribution defined by equations (13.47)-(13.49), often referred to as the three-dimensional Hertz load distribution (Johnson, 1985; Collins and Cliffe, 1987), is found to model the loaded region between a tyre and a pavement reasonably well (Sharp and Booker, 1984). If the circular load moves along the  $x$ -direction, then we wish to determine the load condition (i.e. the value of  $P$  for a given  $\mu$ ) at which shakedown of cohesive-frictional materials can occur.

### 13.4.2 The elastic stress field caused by a Hertz stress distribution

The analytical solutions for elastic stress fields at any point  $(x,y,z)$  in the half-space, due to the three-dimensional Hertz stress distribution, defined in equations (13.47)-(13.49), were given by Hamilton (1983). The stress expressions that are relevant to this study are given below.

#### *The stresses due to the normal load*

The elastic stresses due to the normal load  $P$  are given as follows:

$$\sigma_{zz} = \frac{3P}{2\pi a^3} \left[ -N + \frac{azM}{S} \right] \quad (13.50)$$

$$\sigma_{xz} = \frac{3P}{2\pi a^3} \left[ -z \left\{ \frac{xN}{S} - \frac{xzH}{G^2 + H^2} \right\} \right] \quad (13.51)$$

#### *The stresses due to the shear load*

The elastic stresses due to the shear load  $Q$  are given as follows:

$$\sigma_{zz} = \frac{3Q}{2\pi a^3} \left[ \frac{xzN}{2r^2} \left\{ 1 - \frac{r^2 + z^2 + a^2}{S} \right\} \right] \quad (13.52)$$

$$\begin{aligned} \sigma_{xz} = & \frac{3Q}{2\pi a^3} \left[ \frac{3z\Phi}{2} + \frac{azM}{r^2} \left\{ 1 + \frac{x^2}{r^2} - \frac{x^2}{S} \right\} \right] \\ & + \frac{3Q}{2\pi a^3 r^2} \left[ -\frac{3}{4}(S + 2A) + z^2 - \frac{3}{4}a^2 - \frac{1}{4}r^2 + \frac{z^2}{2} \left( \frac{1}{2} - \frac{2x^2}{r^2} \right) \right] \end{aligned} \quad (13.53)$$

where the quantities  $A$ ,  $S$ ,  $M$ ,  $N$ ,  $G$ ,  $H$ ,  $r$  and  $\Phi$  in equations (13.50)-(13.53) are defined below:

$$A = r^2 + z^2 - a^2, \quad S = (A^2 + 4a^2z^2)^{1/2}, \quad r^2 = x^2 + y^2 \quad (13.54)$$

$$M = \left( \frac{S + A}{2} \right)^{1/2}, \quad N = \left( \frac{S - A}{2} \right)^{1/2}, \quad \Phi = \tan^{-1} \left( \frac{a}{M} \right) \quad (13.55)$$

$$G = M^2 - N^2 + zM - aN \quad (13.56)$$

$$H = 2MN + aM + zM \quad (13.57)$$

### 13.4.3 The residual stress field and static shakedown condition

To determine a lower bound shakedown limit, we need to consider a residual stress field. Any residual stress fields must satisfy the equations of equilibrium and stress boundary conditions upon removal of applied surface loads. A general material point may have all the six components of residual stresses, but symmetry and other considerations impose some constraints. This has been discussed in detail by Sharp (1983), Hills and Sackfield (1984), Johnson (1985) and Kapoor and Johnson (1992). As noted by Hills and Sackfield (1984), it is also useful to remember that, in some cases, one can conceive of alternative sets of residual stresses that result in the same shakedown limit, although some will be more physically reasonable than others. The closeness of a lower bound solution to the true shakedown limit depends on our ability to propose a residual stress field as close as possible to the true one.

For the problem considered here, in which the material is assumed to be isotropic and homogenous, the resulting permanent deformation and therefore the residual stress field will be independent of the travel ( $x$ ) direction. It is reasonable to assume that under a moving three-dimensional Hertz pressure distribution, the most critical plane is one of the  $xz$  planes defined by  $y=\text{constant}$ . On these planes, the only non-zero residual stress that may increase the shakedown limit would be  $\sigma_{xz}$ . This is

because for the case of normal loading, the shear stress  $\sigma_{xz}^e$  is antisymmetric in  $x$ , as it has peaks that are equal in magnitude but opposite in sign on either side of  $x=0$ . It is therefore not possible to increase the shakedown limit by introducing a residual shear stress distribution  $\varrho_{xz}$ , which must be independent of  $x$  (Johnson, 1985; Kapoor and Johnson, 1992). Of course, in the  $y$ -direction, a non-zero normal residual stress  $\varrho_{yy}$  may well exist. Given that the residual stress field must be independent of the travel ( $x$ ) direction, the equations of equilibrium would require that

$$\varrho_{xx} = f(y, z); \quad \varrho_{yy} = g(z); \quad \varrho_{zz} = \varrho_{xy} = \varrho_{yz} = \varrho_{zx} = 0 \quad (13.58)$$

This assumed residual stress field has been proved valid by a numerical study of Shiau (2001) supervised by the author.

Therefore the total stress field due to a moving Hertz load distribution for an element on any  $xz$  plane (i.e.  $y=\text{constant}$  plane) at any given moment can be defined as the sum of elastic stresses and residual stresses

$$\sigma_{zz} = \lambda\sigma_{zz}^e \quad (13.59)$$

$$\sigma_{xx} = \lambda\sigma_{xx}^e + \varrho_{xx} \quad (13.60)$$

$$\sigma_{xz} = \lambda\sigma_{xz}^e \quad (13.61)$$

According to Melan's lower bound shakedown theorem, the material shak-  
down if the total stress field does not violate the yield condition anywhere. If we  
assume that the yield condition for the half-space can be described by the Mohr-  
Coulomb criterion, and the normal stress in the  $y$ -direction, then  $\sigma_{yy} = \lambda\sigma_{yy}^e + \varrho_{yy}$ ,  
is the intermediate stress (which is possible as the residual stress  $\varrho_{yy}$  is an arbitrary  
function of  $z$ ), then the necessary condition for shakedown to occur is that the stress  
field defined by equations (13.59)-(13.61) satisfies the following inequality

$$\sqrt{(\lambda\sigma_{xx}^e + \varrho_{xx} - \lambda\sigma_{zz}^e)^2 + 4(\lambda\sigma_{xz}^e)^2} + (\lambda\sigma_{xx}^e + \varrho_{xx} + \lambda\sigma_{zz}^e) \sin \phi \leq 2c \cos \phi \quad (13.62)$$

which may be rewritten as follows:

$$(X + Y)^2 + Z \leq 0 \quad (13.63)$$

with

$$X = \frac{1}{2}(\lambda\sigma_{xx}^e + \varrho_{xx} - \lambda\sigma_{zz}^e) \quad (13.64)$$

$$Y = (c - \lambda\sigma_{zz}^e \tan \phi) \tan \phi \quad (13.65)$$

$$Z = (1 + \tan^2 \phi)[(\lambda\sigma_{xz}^e)^2 - (c - \lambda\sigma_{zz}^e \tan \phi)^2] \quad (13.66)$$

It then follows that in order to satisfy the shakedown condition (13.63), the following must be met

$$Z \leq 0 \Rightarrow \lambda \leq \frac{c}{|\sigma_{xz}^e| + \sigma_{zz}^e \tan \phi} \quad (13.67)$$

The best possible lower bound would be to determine a load multiplier so that

$$\lambda_s = \min_{(x,y,z)} \frac{c}{|\sigma_{xz}^e| + \sigma_{zz}^e \tan \phi} = \frac{c}{\max_{(x,y,z)} [|\sigma_{xz}^e| + \sigma_{zz}^e \tan \phi]} \quad (13.68)$$

The shakedown condition (13.63) cannot be satisfied if the condition (13.67) is violated, but can simply be satisfied with  $Z=0$  if the residual stress  $\sigma_{xx}$  were chosen to make the first term of (13.63) vanish (i.e.  $X+Y=0$ ; which should be possible as the residual stress  $\sigma_{xx}$  is an arbitrary function of  $y$  and  $z$ ). The limiting condition for shakedown occurs at the point in the half-space where  $|\sigma_{xz}^e| + \sigma_{zz}^e \tan \phi$  is a maximum. By using the elastic stress solutions (13.50)-(13.53), it is a simple matter to search for the most critical plane (defined by the  $y$  coordinate) on which  $|\sigma_{xz}^e| + \sigma_{zz}^e \tan \phi$  is a maximum at a critical point (defined by the  $x$  and  $z$  coordinates). Because the elastic stresses are symmetric along the central plane ( $y=0$ ), it is sufficient only to search for either  $y \leq 0$  or  $y \geq 0$  for the most critical plane (i.e. the critical  $y$  value).

The procedure outlined above satisfies all the requirements of Melan's shakedown theorem and therefore is a rigorous lower bound analysis for cohesive-frictional materials. By making an a priori assumption that shakedown is controlled by the stress condition on the central plane ( $y=0$ ), some shakedown solutions were obtained previously by Johnson and Jefferies (1963) and Johnson (1985) for three-dimensional rolling/sliding contact problems in a purely cohesive material. It is stressed that no such assumption is needed in the analysis developed by Yu (2005), which is valid for a more general cohesive-frictional material.

#### 13.4.4 Numerical results and discussion

For a Hertz stress distribution, the maximum compressive pressure occurs at the centre of the loading area ( $x=y=z=0$ ), and is obtained from equation (13.47) as  $p_0 = 3P/2\pi a^2$ . The shakedown limit determined by the condition (13.68) may be represented by a dimensionless shakedown limit parameter  $k_{\max} = \lambda_s p_0/c$ . Alternatively, the shakedown limits may also be defined in terms of the mean or average pressure acting on the circular area,  $\bar{p} = P/\pi a^2$ . In the latter case, the dimensionless shakedown limit parameter is  $k_{\text{mean}} = \lambda_s \bar{p}/c = (2/3)k_{\max}$ . These dimensionless shakedown limit parameters are dependent on material properties including the angle of internal soil friction  $\phi$  and the surface shear coefficient  $\mu$ .

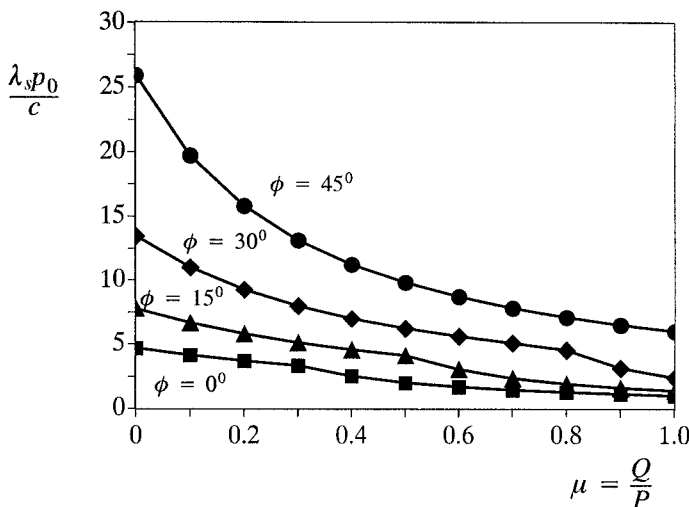


Figure 13.6: Shakedown solutions for point contact in Mohr-Coulomb materials for friction angle ranges from zero to 45 degrees (Yu, 2005)

Figure 13.6 presents the numerical results demonstrating the dependence of the shakedown limit on both the angle of internal friction and tangential frictional coefficient. It is evident that the shakedown limit of a cohesive-frictional half-space increases with increasing friction angle. In addition, the presence of surface shear stress tends to reduce the vertical shakedown load significantly. This effect is important as a real traffic load generally has a non-zero tangential (shear) component. It is noted that for the special case of zero friction angle (i.e. purely cohesive materials with the Tresca yield criterion), the solutions presented here are identical to the well-known solutions presented by Johnson and Jefferies (1963) and Johnson (1985). In particular, the shakedown limit parameter for the case of normal loading only is found to be  $k_{\max} = \lambda_s p_0 / c = 4.68$ . This analytical shakedown limit is almost identical to an upper bound solution of  $k_{\max} = 4.7$  derived by Ponter *et al.* (1985). This closeness would suggest that the lower bound solutions obtained by Yu (2005) for frictional materials may be very close to the true shakedown limits.

A most interesting and useful conclusion obtained by Yu (2005) is that the numerical search for the most critical point throughout the half-space that controls the yield condition suggests that it always lies on the central plane  $y=0$ . In fact, this condition was assumed previously by Johnson and Jefferies (1963) and Johnson (1985), without rigorous proof, in deriving lower bound solutions for rolling/sliding contact problems in purely cohesive materials.

To illustrate the need to ensure that the yield condition is not violated anywhere in the half-space in shakedown analysis, Figure 13.7 presents shakedown limit results for two different cases:

- (1) The yield condition is satisfied everywhere in the half-space  $-\infty \leq y/a \leq \infty$ ;
- (2) The yield condition is satisfied in a large part of the half-space defined by  $-\infty \leq y/a \leq -0.1$  and  $+0.1 \leq y/a \leq \infty$ .

where  $a$  is the radius of the surface contact loading area. As expected, Figure 13.7 shows that the shakedown limits for case 1 are generally smaller than the results for case 2 in which the yield criterion is violated in the region  $-0.1 \leq y/a \leq +0.1$ . Obviously the difference will increase if the region where the yield condition is violated becomes larger. For situations where the critical stress location lies on the loading surface  $z=0$  (i.e. for a case when  $\mu$  is close to 1.0), the difference becomes very small.

$\mu = Q/P$	$\phi = 20^\circ$ Case 1	$\phi = 20^\circ$ Case 2	$\phi = 45^\circ$ Case 1	$\phi = 45^\circ$ Case 2
0	9.25	9.32	25.89	26.12
0.2	6.72	6.77	15.79	15.96
0.4	5.23	5.26	11.23	11.35
0.6	4.26	4.29	8.69	8.77
0.8	2.31	2.33	7.07	7.14
1.0	1.58	1.59	5.97	6.02

Figure 13.7: Effect of partial violation of the yield condition on shakedown limit  $\lambda_s p_0/c$  for two values of friction angle

It is noted that the analytical shakedown solution of Yu (2005) for a single layer material has been extended by Li and Yu (2006c) to obtain solutions for a layered material with the aid of numerical solutions for elastic stress fields.

### 13.5 SHAKEDOWN ANALYSIS USING LINEAR PROGRAMMING

As in limit analysis, numerical procedures have been developed for many years for performing shakedown analysis involving complex geometry and loading conditions. These numerical methods are based on mathematical programming and finite elements (e.g. Maier, 1969; Belytschko, 1972; Raad *et al.*, 1988; Yu and Hossain, 1998). In this section we present the linear programming formulation developed by

Yu and Hossain (1998) for lower bound shakedown analysis using finite elements and discontinuous stress fields.

### 13.5.1 Finite element formulation

Melan's lower bound shakedown theorem states that 'if the combination of a time independent, self-equilibrated residual stress field,  $\varrho_{ij}$ , and the elastic stresses  $\sigma_{ij}$  can be found which does not violate the yield condition anywhere in the region, the material will shakedown'. Hence the main task of a lower bound shakedown analysis is to search for a residual stress field that would lead to a maximum possible applied load.

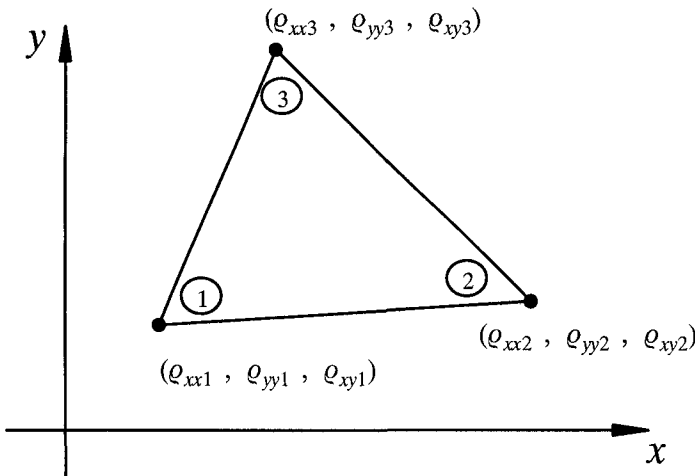


Figure 13.8: Three-noded linear stress triangle with 3 unknown residual stresses at each node.

The finite element formulation of the lower bound theorem of Yu and Hossain (1998) makes use of three-noded triangular elements to model the variation of residual stress fields, Figure 13.8. Each node is associated with three residual stresses,  $\varrho_{xx}$ ,  $\varrho_{yy}$ ,  $\varrho_{xy}$  and with the variation of stresses throughout each element assumed to be linear, namely:

$$\varrho_{xx} = \sum_{i=1}^3 N_i \varrho_{xxi} \quad (13.69)$$

$$\varrho_{yy} = \sum_{i=1}^3 N_i \varrho_{yyi} \quad (13.70)$$

$$\varrho_{xy} = \sum_{i=1}^3 N_i \varrho_{xyi} \quad (13.71)$$

where  $\varrho_{xxi}$ ,  $\varrho_{yyi}$ ,  $\varrho_{xyi}$  are the nodal residual stresses and  $N_i$  are linear shape functions. These shape functions are

$$N_1 = (\xi_1 + \eta_1 + \varsigma_1)/(2A) \quad (13.72)$$

$$N_2 = (\xi_2 + \eta_2 + \varsigma_2)/(2A) \quad (13.73)$$

$$N_3 = (\xi_3 + \eta_3 + \varsigma_3)/(2A) \quad (13.74)$$

in which

$$\xi_1 = x_2y_3 - x_3y_2; \quad \eta_1 = y_2 - y_3; \quad \varsigma_1 = x_3 - x_2 \quad (13.75)$$

$$\xi_2 = x_3y_1 - x_1y_3; \quad \eta_2 = y_3 - y_1; \quad \varsigma_2 = x_1 - x_3 \quad (13.76)$$

$$\xi_3 = x_1y_2 - x_2y_1; \quad \eta_3 = y_1 - y_2; \quad \varsigma_3 = x_2 - x_1 \quad (13.77)$$

and  $2A = |\eta_1\varsigma_2 - \eta_2\varsigma_1|$  is twice the area of the element. Unlike the elements used in displacement finite element analysis, several nodes may share the same coordinate and each node is associated with only one element. In this way statically admissible stress discontinuities can occur at all edges between adjoining triangles. If  $E$  is the number of triangular elements in a mesh, then there are  $3E$  nodes and  $9E$  unknown residual stresses. By ensuring the equations of equilibrium and the stress boundary conditions are satisfied by the residual stresses and the yield condition is not violated by the total stresses, a rigorous lower bound on the shakedown load may be obtained.

#### *Element equilibrium by the residual stresses*

To ensure that the residual stresses satisfy equilibrium, the residual stresses throughout each triangle must obey the following equations:

$$\frac{\partial \varrho_{xx}}{\partial x} + \frac{\partial \varrho_{xy}}{\partial y} = 0 \quad (13.78)$$

$$\frac{\partial \varrho_{yy}}{\partial y} + \frac{\partial \varrho_{xy}}{\partial x} = \gamma \quad (13.79)$$

where tensile stresses are taken positive, a right handed Cartesian coordinate system is adopted and  $\gamma$  is the unit weight of the material. This results in two equality constraints on nodal residual stresses for each element.

#### *Discontinuity equilibrium*

It is necessary to impose additional constraints on the nodal residual stresses at the edges of adjacent triangles in order to permit admissible discontinuities. For a discontinuity to be statically admissible only the normal stress parallel to the discontinuity may be discontinuous, with continuity of the corresponding shear stresses and normal stresses perpendicular to the discontinuity maintained.

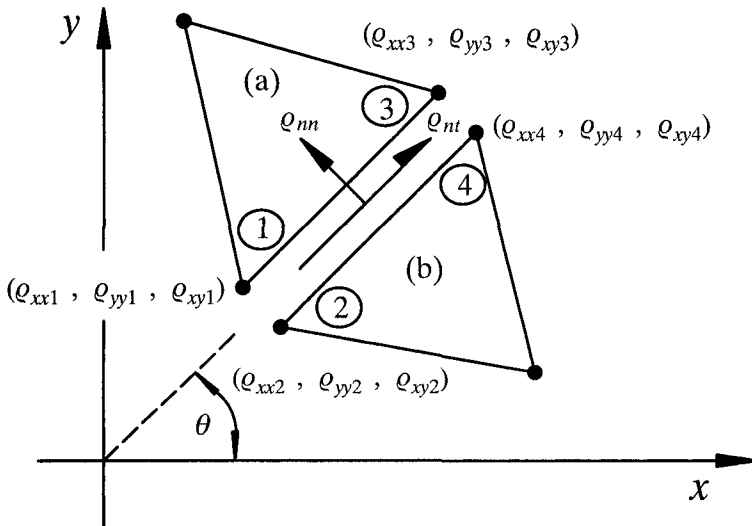


Figure 13.9: Statically admissible residual stress discontinuity between adjacent triangles

Looking at Figure 13.9, for triangles *a* and *b*, equilibrium along the discontinuity (or common side) requires that at every point along this side:

$$\rho_{nn}^a = \rho_{nn}^b ; \quad \rho_{nt}^a = \rho_{nt}^b \quad (13.80)$$

Since stresses are confined to varying linearly along any element edge, an equivalent condition is achieved by enforcing the constraints:

$$\rho_{nn1}^a = \rho_{nn2}^b ; \quad \rho_{nn3}^a = \rho_{nn4}^b \quad (13.81)$$

$$\rho_{nt1}^a = \rho_{nt2}^b ; \quad \rho_{nt3}^a = \rho_{nt4}^b \quad (13.82)$$

As such, each statically admissible discontinuity along an element edge results in four equality constraints on the nodal stresses (Yu and Hossain, 1998).

#### *Boundary conditions by residual stresses*

Residual stresses also need to satisfy certain boundary conditions, which typically take the following form:

$$\varrho_{nn} = q = \text{constant} ; \quad \varrho_{nt} = t = \text{constant} \quad (13.83)$$

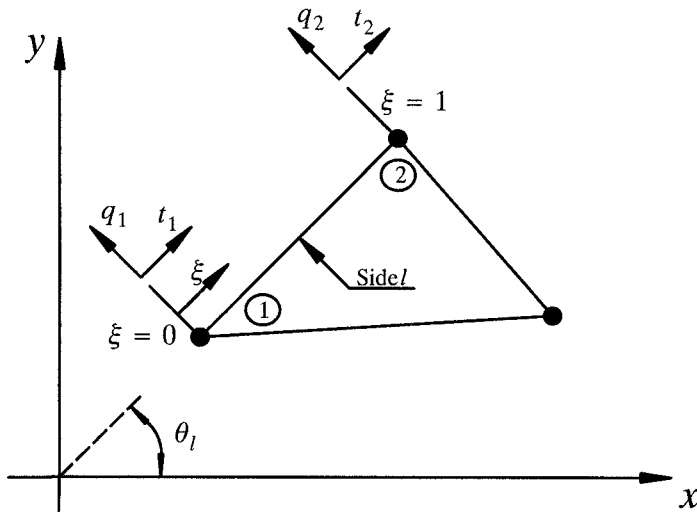


Figure 13.10: Residual stress boundary conditions

Given a linear variation of the residual stress components along the edge of each triangle, a more general boundary condition may be imposed, in the form of (see Figure 13.10):

$$\varrho_{nn}^l = q_1 + (q_2 - q_1)\xi ; \quad \varrho_{nt}^l = t_1 + (t_2 - t_1)\xi \quad (13.84)$$

where

$l$  = edge of triangle  $e$  where boundary tractions are specified

$\xi$  = local coordinate along  $l$

$q_1, q_2$  = normal stresses specified at nodes 1 and 2 (tension positive)

$t_1, t_2$  = shear stresses specified at nodes 1 and 2 (clockwise shears positive)

The boundary conditions of equation (13.84) are satisfied then by requiring

$$\varrho_{nn1}^e = q_1 ; \quad \varrho_{nn2}^e = q_2 ; \quad \varrho_{nt1}^e = t_1 , \quad \varrho_{nt2}^e = t_2 \quad (13.85)$$

So for each edge where a boundary traction is specified, a maximum of four equality constraints on the nodal stresses are generated.

#### *Yield condition*

Under conditions of plane strain, the Mohr-Coulomb yield criterion may be written as

$$F = (\sigma_{xx} - \sigma_{yy})^2 + 4\sigma_{xy}^2 - (2c \cos \phi - (\sigma_{xx} + \sigma_{yy}) \sin \phi)^2 = 0 \quad (13.86)$$

where  $c$  is the cohesion and  $\phi$  is the friction angle. In terms of the quantities  $(\sigma_{xx} - \sigma_{yy})$  and  $2\sigma_{xy}$ , this yield function plots as a circle, as shown in Figure 13.11.

A key feature of formulating limit analysis as a linear programming problem is the use of a linearized yield surface. With reference to Figure 13.11, if  $p$  is the number of sides used to approximate the yield function (13.86), then the linearized yield function can be shown to be:

$$A_k \sigma_{xx} + B_k \sigma_{yy} + C_k \sigma_{xy} \leq E, \quad k = 1, 2, \dots, p \quad (13.87)$$

where

$$A_k = \cos\left(\frac{2\pi k}{p}\right) + \sin \phi \cos\left(\frac{\pi}{p}\right)$$

$$B_k = -\cos\left(\frac{2\pi k}{p}\right) + \sin \phi \cos\left(\frac{\pi}{p}\right)$$

$$C_k = 2 \sin\left(\frac{2\pi k}{p}\right)$$

$$E = 2c \cos \phi \cos\left(\frac{\pi}{p}\right)$$

The yield condition (13.87) must be satisfied by the total stresses which may be written as follows

$$\sigma_{ij} = \lambda \sigma_{ij}^e + \varrho_{ij} \quad (13.88)$$

where  $\lambda$  is the shakedown factor and  $\sigma_{ij}^e$  is the elastic stress field resulting from the application of a unit load distribution, which can be determined either analytically or numerically.

By using equation (13.88), the yield condition (13.87) can be rewritten as follows:

$$A_k \varrho_{xx} + B_k \varrho_{yy} + C_k \varrho_{xy} + \lambda(A_k \sigma_{xx}^e + B_k \sigma_{yy}^e + C_k \sigma_{xy}^e) \leq E \quad (13.89)$$

It is noted that although the residual stress field varies linearly across the element, the elastic stresses may not. As a result, it may not be sufficient to enforce the yield condition (13.89) at three corner nodes. To ensure that the yield condition is satisfied across the element, the yield condition may need to be enforced at many sampling points within the element. Numerical studies by Yu and Hossain (1998) indicate, however, that the use of three corner nodes plus three middle points of the triangle arms is satisfactory, as a further increase in number of points used for enforcing the yield criterion does not have a significant effect on the derived shakedown results.

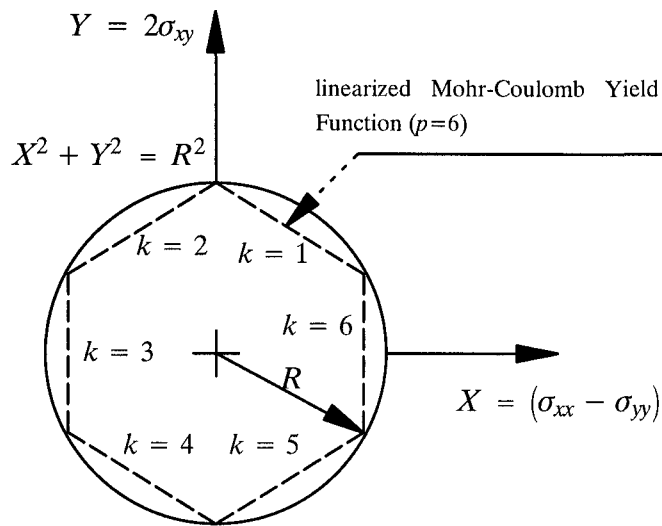


Figure 13.11: Linearized Mohr-Coulomb yield function ( $p=6$ )

Apart from ensuring the total stresses are within the yield surface, it is also necessary to ensure that the residual stresses alone do not violate the yield criterion (Yu and Hossain, 1998). This condition is given below:

$$A_k \varrho_{xx} + B_k \varrho_{yy} + C_k \varrho_{xy} \leq E \quad (13.90)$$

Because the residual stress field varies linearly across the element, the yield condition (13.90) is exactly satisfied across the whole element provided it is enforced at three corner nodes.

#### *Objective function and linear programming problem*

We aim to find a residual stress distribution with a maximum possible load factor,  $\lambda$ , which with the elastic stresses will satisfy yield criterion all over the mesh. The problem can then be stated as:

$$\text{Minimize} \quad -\lambda \quad (13.91)$$

$$\text{Subject to} \quad A_1 X = B_1$$

$$A_2 X \leq B_2$$

where  $A_1, B_1$  represent the coefficients due to equilibrium and stress boundary conditions;  $A_2, B_2$  represent the coefficients for the yield conditions;  $X$  is the global vector of unknown stresses and the shakedown factor. An active set algorithm is

used to solve the above linear programming problem, the details of which can be found in Sloan (1988). The solution for the unknown stresses  $X$  from (13.91) defines a statically admissible residual stress field that gives the best lower bound shakedown load.

### 13.5.2 Numerical application to shakedown analysis of pavements

The purpose of pavement shakedown analysis is to derive the shakedown limit for layered pavements under traffic loading. Pavements operating at loads below this shakedown limit would behave elastically after some initial permanent deformation. To provide an example, we present some of the numerical work carried out by Yu and Hossain (1998) and Shiau and Yu (1999, 2000a,b) on a parametric study of shakedown of pavements under moving surface loads.

#### *Plane strain pavement model*

Following Sharp and Booker (1984), a trapezoidal traffic load distribution is assumed in a vertical plane along the travel direction. It is further assumed that the resulting deformation is plane strain by replacing the wheel load as an infinite wide roller (Figure 13.12(a)). The normal stress ( $P_V$ ) and longitudinal shear stress ( $P_H$ ) are related by a surface friction parameter  $\mu = P_H/P_V$ . For simplicity, this coefficient is assumed to be constant so that the longitudinal shear stresses are also trapezoidal (Figure 13.12(b)).

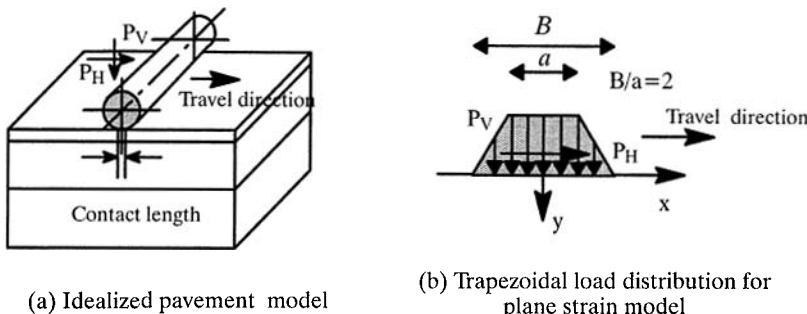
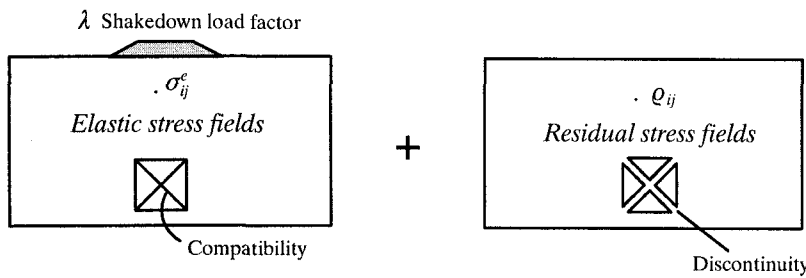


Figure 13.12: Pavements under traffic loads

#### *Melan's static shakedown theorem*

Melan's static (i.e. lower bound) shakedown theorem states that “If the combination of a time independent, self-equilibrated residual stress field  $\sigma_{ij}$  and the elastic

stresses  $\lambda\sigma_{ij}^e$  can be found which doesn't violate the yield condition anywhere in the region, then the material will shakedown".



$\lambda\sigma_{ij}^e + \varrho_{ij}$  are to satisfy the Mohr-Coulomb yield criterion

Figure 13.13: Shakedown condition in terms of stresses

Referring to Figure 13.13 and supposing that the elastic stresses are proportional to a load factor  $\lambda$ , the total stresses are therefore  $\sigma_{ij}^t = \lambda\sigma_{ij}^e + \varrho_{ij}$ , where  $\lambda$  is the shakedown load factor,  $\sigma_{ij}^e$  are the elastic stresses and  $\varrho_{ij}$  are the residual stresses. By insisting that both the total stresses and the residual stresses do not violate a linearized Mohr-Coulomb yield condition in the mesh, Melan's static shakedown theorem can be implemented using finite elements and linear programming techniques.

#### *Finite elements for elastic stresses and residual stress fields*

The displacement finite element method is used to determine the elastic stress field. In this section, the 6-noded triangular displacement elements are utilised so that the elastic stress field is assumed to be linear across each element as shown in Figure 13.14(a). On the other hand, the residual stress field is modelled by the 3-noded triangular stress finite elements described earlier. Statically admissible stress discontinuities are permitted at shared edges between adjacent stress triangles. Unlike the usual form of the displacement finite element, each node is unique to a particular element and more than one node share the same coordinates as shown in Figure 13.14. If  $E$  denotes the number of triangles in the mesh, then there are  $3E$  nodes and  $9E$  unknown residual stresses.

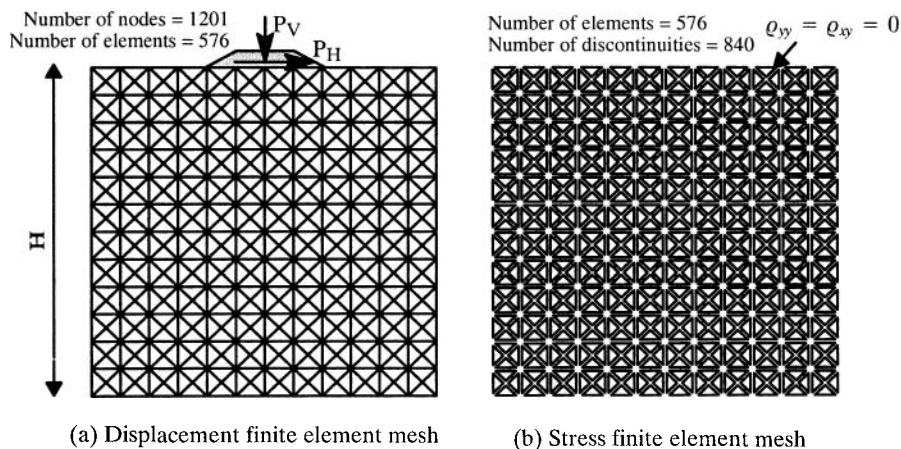


Figure 13.14: Finite element meshes for elastic stress and residual stress fields

#### *The Mohr-Coulomb yield criterion*

The Mohr-Coulomb yield criterion for plane strain condition can be approximated as a linear function of the unknown stresses and details of this linearization can be found in Yu and Hossain (1998). The linearized yield surface must be internal to the original Mohr-Coulomb yield circle to ensure that the solutions obtained are rigorous lower bounds. In each element, both the elastic and residual stress variations are linearly distributed across the mesh. The yield conditions in terms of both residual and total stresses will be satisfied everywhere within an element as long as the yield criterion is enforced at corner nodes. As a result, the condition of not violating the yield criterion in the mesh can be replaced by enforcing the following inequality constraints: (a) yield criterion at corner nodes by the residual stresses, (b) yield criterion at corner nodes by the total stresses. This differs slightly from the formulation by Yu and Hossain (1998) where the total stresses are enforced at several sampling points within each element.

#### *Verification of the numerical formulation for a single-layered pavement*

For the purpose of verification, only the vertical load is considered. The results of dimensionless shakedown limits with the variation of soil internal friction angle from  $0^\circ$  to  $30^\circ$  are presented in Figure 13.15. It is shown that the values of  $\lambda P_V/c$  derived here are very close to those obtained by Sharp and Booker (1984) and this is particularly true for the case of a purely cohesive clay which gives a value of 3.696.

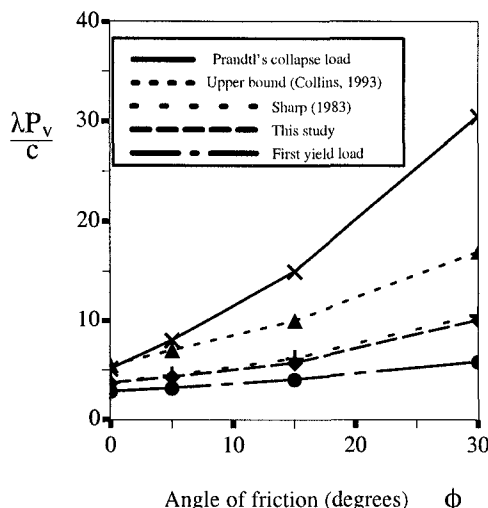


Figure 13.15: Effects of friction angle on dimensionless shakedown limit

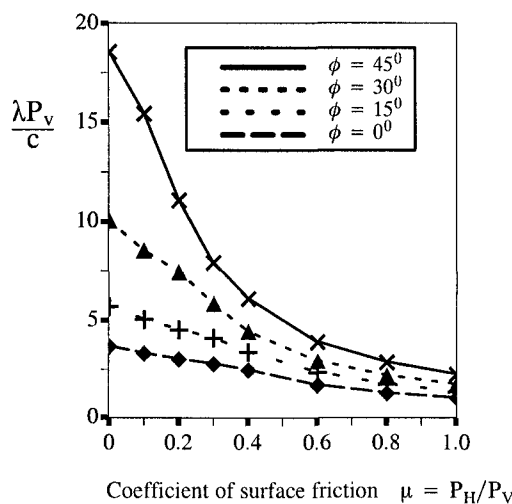


Figure 13.16: Effects of surface friction on dimensionless shakedown limit

As shown in Figure 13.16, the dimensionless shakedown limit decreases dramatically with the coefficient of surface friction  $\mu$ . This is due to the existence of high elastic shear stresses in the top layer which will result in a type of shear failure of that layer when the value of  $\mu$  is high. In this figure, it is also found that the results

from this formulation yield smaller values than that in Sharp and Booker (1984) at higher frictional angle of soil. The present formulation uses many more elements to model both the elastic and residual stress fields and therefore should give more accurate shakedown loads.

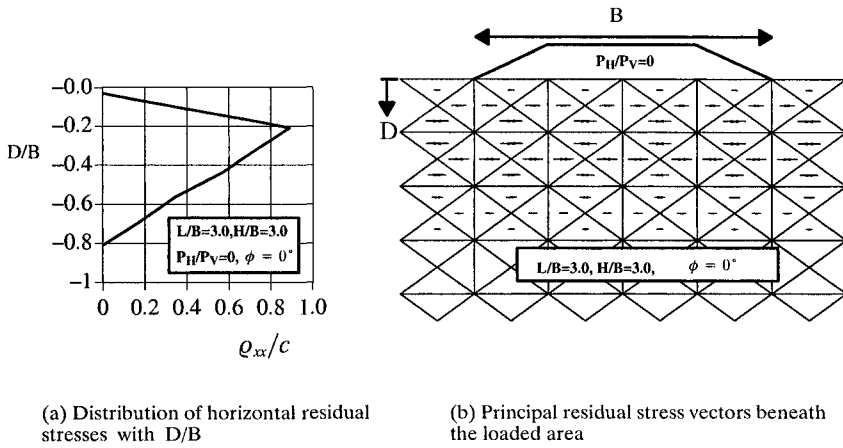


Figure 13.17: Numerical residual stress fields

Figure 13.17(a) shows the distribution of horizontal residual stresses with depth for the case of  $\phi = 0$ ,  $\mu = 0$ . The value of  $\sigma_{xx}/c$  reaches a maximum at  $D/B=0.21$  with  $\sigma_{xx} = 0.9c$ . This value converges to zero at a depth of  $D/B=0.8$ . This result is in good agreement with the experimental data presented in Radovský and Murashina (1996) on the residual stress field. Figure 13.17(b) presents the principal residual stress vectors beneath the loaded area and shows that only  $\sigma_{xx}$  exists in the medium under the traffic load. As expected, for the plane strain assumption used here residual stresses vary only with the depth and are uniform over any horizontal plane (i.e. travel direction).

#### *Parametric study on shakedown of three-layered pavements*

Figure 13.18 shows the problem notation of a three layered pavement. A purely cohesive subgrade ( $\phi_3 = 0$ ) is considered in this section and the internal friction angles for the first and second layers are assumed to be 50 and 20 degrees respectively. The influence of relative stiffness ratio ( $E_1/E_2$ ) on the dimensionless shakedown limit for different values of relative cohesive strength ratio ( $C_1/C_2$ ) for both soft and stiff subgrades is presented in Figure 13.19. It is clear from the figure that,

at a given value of relative strength ratio, there exists an optimum relative stiffness ratio at which the resistance to incremental collapse is maximised. Further increase in relative stiffness ratio does not contribute to an increase in the shakedown limit. Results for the case of a stiff subgrade are higher than those from a soft subgrade.

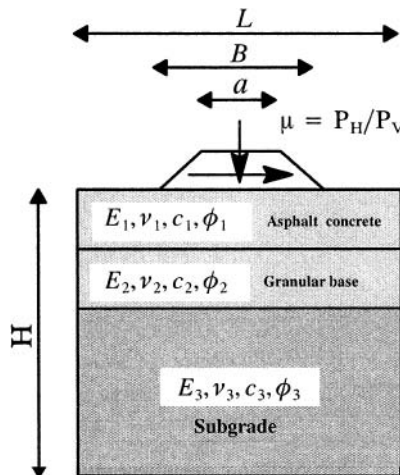


Figure 13.18: Problem definition of three-layered pavements

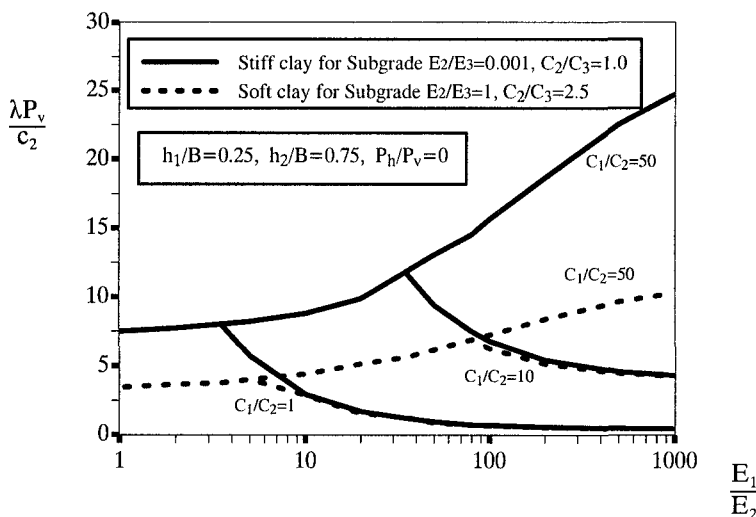


Figure 13.19: Effects of relative stiffness and cohesion on dimensionless shakedown limit

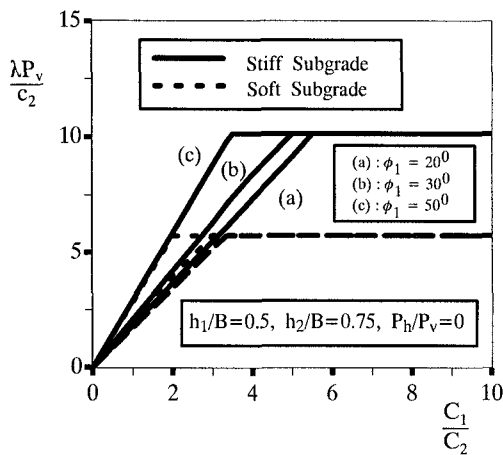


Figure 13.20: Effects of relative cohesion on dimensionless shakedown limit for a given stiffness ratio ( $E_1/E_2 = 10$ )

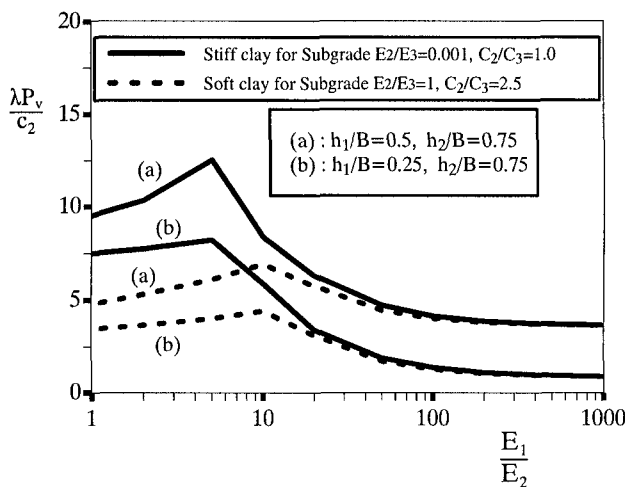


Figure 13.21: Effects of relative stiffness on dimensionless shakedown limit for a given cohesion ratio ( $C_1/C_2 = 2$ )

As shown in Figure 13.20, it is important to note that for a lower value of  $E_1/E_2$  the dimensionless shakedown limit ceases to increase at a particular value of  $C_1/C_2$  for both soft and stiff subgrades. This may indicate a transfer of failure mode from the top layer to the bottom layer when the value of  $E_1/E_2$  is low. Thus further in-

crease in basecourse strength will not improve the shakedown capacity. In Figure 13.21, the dimensionless shakedown limit increases with the increase in surface layer thickness ( $h_1/B$ ) for both soft and stiff subgrades.

### *Shakedown charts for pavement thickness design*

For a given layered pavement with known material parameters, the shakedown limit can be determined from shakedown analysis and compared against the design traffic load. The design traffic load has to be less than the shakedown load to ensure that accumulation of permanent strains will not occur. In the case that the design traffic load is much smaller than the shakedown load, the design of the pavement is conservative and the adjustment of basecourse thickness should be made.

For a given design traffic load and various material properties for the surface course, base course and subgrade, shakedown-based design charts (either for two or three-layered pavements) can be developed (e.g. Shiau and Yu, 1999, 2000a, b; Li and Yu, 2006c) for use to determine the minimum thickness for basecourse so that the pavement designed would 'shake down' under the given design traffic load.

## 13.6 SHAKEDOWN ANALYSIS USING NONLINEAR PROGRAMMING

In this section, we present a nonlinear programming approach developed most recently by Li and Yu (2006a) for performing shakedown analysis based on Koiter's upper bound theorem. This is an extension of the limit analysis procedure developed by Li and Yu (2005). The main advantage of this approach over other nonlinear programming procedures is that it makes use of the standard displacement finite elements and is therefore easier to apply in practice.

### **13.6.1 Shakedown analysis for a general yield criterion**

#### *A general yield criterion*

Many widely used yield criteria for cohesive-frictional materials can be expressed in a general form as follows

$$F(\sigma) = \sigma^T P \sigma + \sigma^T Q - 1 = 0 \quad (13.92)$$

where  $\sigma$  is the stress vector,  $P$  and  $Q$  are coefficient matrix and vector that are related to strength properties of the material (i.e. cohesion and frictional angle).

As shown in the previous chapter (Section 12.5.1), the Mohr-Coulomb criterion in plane strain can be expressed in the form of (13.92) with the following coefficient matrix and vector:

$$\mathbf{P} = \begin{bmatrix} \frac{1}{4c^2} & \frac{-1 - \sin^2\phi}{4c^2 \cos^2\phi} & 0 \\ \frac{-1 - \sin^2\phi}{4c^2 \cos^2\phi} & \frac{1}{4c^2} & 0 \\ 0 & 0 & \frac{1}{c^2 \cos^2\phi} \end{bmatrix} \quad (13.93)$$

$$\mathbf{Q} = \begin{bmatrix} \frac{\sin\phi}{c \cos\phi} \\ \frac{\sin\phi}{c \cos\phi} \\ 0 \end{bmatrix} \quad (13.94)$$

where  $c$  and  $\phi$  are cohesion and frictional angle respectively. Taking tensile stresses as positive, the Drucker-Prager criterion is written as follows:

$$F(\sigma_{ij}) = \alpha I_1 + \sqrt{J_2} - k = 0 \quad (13.95)$$

where  $I_1$  is the first invariant of stress tensor,  $J_2$  is the second invariant of the deviatoric stress tensor,  $\alpha$  and  $k$  are material strength parameters.

It can be shown that for a three-dimensional stress state, the Drucker-Prager yield function (13.95) can also be expressed in the form of (13.92) provided we set

$$\mathbf{P} = \begin{bmatrix} p_1 & p_2 & p_2 & 0 & 0 & 0 \\ p_2 & p_1 & p_2 & 0 & 0 & 0 \\ p_2 & p_2 & p_1 & 0 & 0 & 0 \\ 0 & 0 & 0 & p_3 & 0 & 0 \\ 0 & 0 & 0 & 0 & p_3 & 0 \\ 0 & 0 & 0 & 0 & 0 & p_3 \end{bmatrix} \quad (13.96)$$

$$\mathbf{Q} = [q_0, q_0, q_0, 0, 0, 0]^T \quad (13.97)$$

where

$$p_1 = \frac{1 - 3\alpha^2}{3k^2}, \quad p_2 = -\frac{1 + 6\alpha^2}{6k^2}, \quad p_3 = \frac{1}{k^2}, \quad q_0 = \frac{2\alpha}{k} \quad (13.98)$$

### The kinematic theorem of shakedown analysis

An upper bound to the shakedown limit of a structure can be obtained using Koiter's kinematic shakedown theorem. The kinematic shakedown theorem states that shakedown will occur only if

$$m_{sd} \int_0^T \int_{S_T} \int T_i \dot{u}_i \, dS \, dt \leq \int_0^T \int \int_V \sigma_{ij} \dot{\epsilon}_{ij} \, dV \, dt - \int_0^T \int \int_V f_i \dot{u}_i \, dV \, dt \quad (13.99)$$

where  $m_{sd}$  is the shakedown load multiplier,  $T_i$  is the basic load of surface tractions (may be set as a unit value),  $f_i$  is the body force,  $\dot{u}_i$  and  $\dot{\epsilon}_{ij}$  are kinematically admissible

sible displacement increment and strain rate fields,  $S_T$  denotes the traction boundary and  $V$  denotes the space domain of the structure. The basic load of surface tractions  $T_i$  is cycled over a time interval  $t=[0,T]$ , amplified by the load multiplier  $m_{sd}$  to form a load domain  $\Omega$ .

As shown by Li and Yu (2006a), the integral on the left hand side of (13.99) can be re-expressed using the virtual work equation as follows

$$\int_0^T \int \int_{S_T} T_i \dot{u}_i \, dS_T dt = \int_0^T \int \int \int_V \sigma_{ij}^e \dot{\epsilon}_{ij} \, dV dt \quad (13.100)$$

where  $\sigma_{ij}^e$  is the linear elastic stress field in the structure caused by the external surface traction  $T_i$ .

With equation (13.100), the shakedown expression (13.99) can be reduced to

$$m_{sd} \int_0^T \int \int_V \sigma_{ij}^e \dot{\epsilon}_{ij} \, dV dt \leq \int_0^T \int \int \int_V \sigma_{ij} \dot{\epsilon}_{ij} \, dV dt - \int_0^T \int \int \int_V f_i \dot{u}_i \, dV dt \quad (13.101)$$

According to the mathematical programming theory, the kinematic theorem (13.101) can be formulated as follows in the absence of body force  $f_i$ :

$$m_{sd} = \min \int_0^T \int \int \int_V \sigma_{ij} \dot{\epsilon}_{ij} \, dV dt = \int \int \int_V D(\dot{\epsilon}_{ij}) \, dV \quad (13.102)$$

$$\text{Subject to } \int_0^T \int \int \int_V \sigma_{ij}^e \dot{\epsilon}_{ij} \, dV = 1 \quad (13.103)$$

$$\Delta \epsilon_{ij} = \int_0^T \dot{\epsilon}_{ij} dt = \frac{1}{2} (\Delta u_{ij} + \Delta u_{ji}) \quad \text{in } V \quad (13.104)$$

$$\Delta u_i = \int_0^T \dot{u}_i dt \quad \text{in } V \quad (13.105)$$

$$\Delta u_i = 0 \quad \text{on } S_U \quad (13.106)$$

where

$$D(\dot{\epsilon}_{ij}) = \sigma_{ij} \dot{\epsilon}_{ij} \quad (13.107)$$

is the rate of plastic dissipation power in terms of the admissible strain rate  $\dot{\epsilon}_{ij}$  and  $\Delta \epsilon_{ij}$  and  $\Delta u_i$  denote the cumulative plastic strain and displacement fields at the end of one loading cycle over the time cycle  $[0,T]$  respectively.  $S_U$  denotes the displacement boundary.

Hence the kinematic shakedown analysis of a structure has been reduced to the calculation of the smallest shakedown load multiplier  $m_{sd}$  as the shakedown load is equal to  $m_{sd}T_i$ .

*Dissipation power for a general yield criterion*

From equation (13.107), it is clear that the plastic dissipation power depends on both stress and strain rate fields. It should be noted that the stress field is linked to the plastic strain rate field through the associated flow rule, namely

$$\dot{\epsilon}_{ij} = \lambda \frac{\partial F(\sigma_{ij})}{\partial \sigma_{ij}} \quad (13.108)$$

which is reduced to the following by using the general yield equation (12.147)

$$\dot{\epsilon} = 2\lambda \mathbf{P}\sigma + \lambda \mathbf{Q} \quad (13.109)$$

from which we can express the stress field in terms of the strain field

$$\sigma = \frac{1}{2\lambda} \mathbf{P}^{-1} \dot{\epsilon} - \frac{1}{2} \mathbf{P}^{-1} \mathbf{Q} \quad (13.110)$$

If the matrix  $\mathbf{P}$  is non-singular,  $\mathbf{P}^{-1}$  can be determined uniquely. However for the case of a singular  $\mathbf{P}$  matrix, we can use  $\mathbf{P} + \gamma$  to replace  $\mathbf{P}$ , where  $\gamma$  is a very small real value.

Given that the stress field is on the yield surface, equations (13.110) and (13.92) can be combined to determine the plastic multiplier rate  $\dot{\lambda}$ :

$$\dot{\lambda} = \sqrt{\frac{\dot{\epsilon}^T \mathbf{P}^{-1} \dot{\epsilon}}{4 + \mathbf{Q}^T \mathbf{P}^{-1} \mathbf{Q}}} \quad (13.111)$$

Now we can express the rate of plastic dissipation power purely in terms of the plastic strain rate field:

$$\begin{aligned} D(\dot{\epsilon}_{ij}) &= \sigma_{ij} \dot{\epsilon}_{ij} = \sigma^T \dot{\epsilon} \\ &= \frac{1}{2} \sqrt{(\dot{\epsilon}^T \mathbf{P}^{-1} \dot{\epsilon}) \cdot (4 + \mathbf{Q}^T \mathbf{P}^{-1} \mathbf{Q})} - \frac{1}{2} \dot{\epsilon}^T \mathbf{P}^{-1} \mathbf{Q} \end{aligned} \quad (13.112)$$

Therefore once the kinematically admissible velocity field is obtained, the plastic dissipation power can also be calculated. The key result is that there is no need to evaluate plastic stress fields in kinematic shakedown analysis which simplifies the numerical procedure considerably.

*The nonlinear programming problem*

Based on the above expression for the rate of plastic dissipation power, the kinematic shakedown analysis of frictional materials can be formulated as the following mathematical programming problem:

$$m_{sd} = \min \int \int \int_V \left[ \frac{1}{2} \sqrt{(\dot{\epsilon}^T \mathbf{P}^{-1} \dot{\epsilon}) \cdot (4 + \mathbf{Q}^T \mathbf{P}^{-1} \mathbf{Q})} - \frac{1}{2} \dot{\epsilon}^T \mathbf{P}^{-1} \mathbf{Q} \right] dV \quad (13.113)$$

$$\text{Subject to} \quad \int \int \int_V (\sigma^e)^T \epsilon \, dV = 1 \quad (13.114)$$

$$\Delta \epsilon_{ij} = \int_0^T \dot{\epsilon}_{ij} dt = \frac{1}{2} (\Delta u_{i,j} + \Delta u_{j,i}) \quad \text{in } V \quad (13.115)$$

$$\Delta u_i = \int_0^T \dot{u}_i dt \quad \text{in } V \quad (13.116)$$

$$\Delta u_i = 0 \quad \text{on } S_U \quad (13.117)$$

*The removal of the time integration*

To apply the mathematical programming formulations (13.113)-(13.117) to a real structure, the time integration must be removed as it will be difficult to calculate the integration along a deformation path. To overcome this potential difficulty, we may follow the technique proposed by Konig (1987).

Due to cyclic loading, a load domain  $\mathcal{Q}$  can be regarded as a load space and the shape of which is a hyper polyhedron defined by a convex linear combination of load vertices  $P_k (k = 1, 2, 3, \dots, l)$ . It is assumed that if a structure reaches a state of shakedown under any load vertices, then it will shakedown under the whole load domain  $\mathcal{Q}$ . The cyclic loading remains constant over a time interval  $t_k$  ( $\sum_{k=1}^l t_k = T$ ) on each vertex, and the admissible plastic strain cycles on these vertices can generate a plastic strain increment:

$$\epsilon_k = \int_{t_k} \dot{\epsilon} \, dt \quad (k = 1, 2, 3, \dots, l) \quad (13.118)$$

Then the cumulative plastic strain at the end of one load cycle over the time interval  $[0, T]$  can be derived as follows:

$$\Delta \boldsymbol{\varepsilon} = \sum_{k=1}^l \boldsymbol{\varepsilon}_k \quad (13.119)$$

Finally the kinematic shakedown analysis of a structure subject to repeated loads can be expressed as the following nonlinear mathematical programming problem:

$$m_{sd} = \min \sum_{k=1}^l \int \int_V \left[ \frac{1}{2} \sqrt{(\boldsymbol{\varepsilon}_k^T \mathbf{P}^{-1} \boldsymbol{\varepsilon}_k) \cdot (4 + \mathbf{Q}^T \mathbf{P}^{-1} \mathbf{Q})} - \frac{1}{2} \boldsymbol{\varepsilon}_k^T \mathbf{P}^{-1} \mathbf{Q} \right] dV \quad (13.120)$$

$$\text{Subject to } \sum_{k=1}^l \int \int_V (\boldsymbol{\sigma}^e)^T \boldsymbol{\varepsilon}_k dV = 1 \quad (13.121)$$

$$\Delta \boldsymbol{\varepsilon} = \sum_{k=1}^l \boldsymbol{\varepsilon}_k dt = \frac{1}{2} (\Delta u_{i,j} + \Delta u_{j,i}) \quad \text{in } V \quad (13.122)$$

$$\Delta u_i = 0 \quad \text{on } S_U \quad (13.123)$$

### 13.6.2 Finite element approximation of velocity fields

To describe the variation of kinematically admissible velocity (or displacement increment) fields, the standard displacement-based finite elements are used. In the finite element method, the structure is divided into a large number of small elements, in which the velocity (or displacement increments) is assumed to vary in a certain manner (e.g. linear or quadratic variations).

The velocity field  $\Delta \mathbf{u}$  within an element,  $e$ , is linked to its nodal velocity vector  $\Delta \boldsymbol{\delta}$  through shape functions  $\mathbf{N}$ , namely

$$\Delta \mathbf{u}_e = \mathbf{N}_e \Delta \boldsymbol{\delta}_e \quad (13.124)$$

from which we can determine the strain field from the velocity field as follows

$$\Delta \boldsymbol{\varepsilon}_e = \mathbf{L} \Delta \mathbf{u} = \mathbf{L} \mathbf{N}_e \Delta \boldsymbol{\delta}_e = \mathbf{B}_e \Delta \boldsymbol{\delta}_e \quad (13.125)$$

in which

$$\mathbf{B}_e = [\mathbf{B}_1, \mathbf{B}_2, \dots, \mathbf{B}_m] \quad (13.126)$$

and

$$\mathbf{B}_i = \begin{bmatrix} \frac{\partial N_i}{\partial x} & 0 & 0 \\ 0 & \frac{\partial N_i}{\partial y} & 0 \\ 0 & 0 & \frac{\partial N_i}{\partial z} \\ \frac{\partial N_i}{\partial y} & \frac{\partial N_i}{\partial x} & 0 \\ 0 & \frac{\partial N_i}{\partial z} & \frac{\partial N_i}{\partial y} \\ \frac{\partial N_i}{\partial z} & 0 & \frac{\partial N_i}{\partial x} \end{bmatrix} \quad (i = 1, 2, \dots, m) \quad (13.127)$$

where  $m$  is the number of nodes in each element.

By using the Gaussian integration technique, the objective function in equation (13.113) can be further reduced to

$$\begin{aligned} & \sum_{k=1}^l \int \int \int_V \left[ \frac{1}{2} \sqrt{(\boldsymbol{\varepsilon}_k^T \mathbf{P}^{-1} \boldsymbol{\varepsilon}_k) \cdot (4 + \mathbf{Q}^T \mathbf{P}^{-1} \mathbf{Q})} - \frac{1}{2} \boldsymbol{\varepsilon}_k^T \mathbf{P}^{-1} \mathbf{Q} \right] dV \\ &= \sum_{k=1}^l \sum_{e=1}^N \sum_{i=1}^{NG} (\varrho_e)_i |J|_i \left[ \frac{1}{2} \sqrt{(\boldsymbol{\varepsilon}_{ek}^T \mathbf{P}^{-1} \boldsymbol{\varepsilon}_{ek}) \cdot (4 + \mathbf{Q}^T \mathbf{P}^{-1} \mathbf{Q})} - \frac{1}{2} (\boldsymbol{\varepsilon}_{ek})^T \mathbf{P}^{-1} \mathbf{Q} \right] \\ &= \sum_{k=1}^l \sum_{r=1}^n \varrho_r |J|_r \left[ \frac{1}{2} \sqrt{(\boldsymbol{\varepsilon}_{kr}^T \mathbf{P}^{-1} \boldsymbol{\varepsilon}_{kr}) \cdot (4 + \mathbf{Q}^T \mathbf{P}^{-1} \mathbf{Q})} - \frac{1}{2} (\boldsymbol{\varepsilon}_{kr})^T \mathbf{P}^{-1} \mathbf{Q} \right] \end{aligned} \quad (13.128)$$

where, with reference to the  $r$ -th Gaussian integral point,  $\varrho_r$  is the Gaussian integral weight,  $|J|_r$  is the determinant of the Jacobian matrix,  $NG$  is the number of integration points within each element and  $n$  is the total number of Gaussian integral points of the whole finite element mesh. We also have

After the discretization, the normalization condition in (13.121) can be rewritten as follows:

$$\sum_{k=1}^l \int \int \int_V (\boldsymbol{\sigma}^e)^T \boldsymbol{\varepsilon}_k dV = \sum_{k=1}^l \sum_{e=1}^N \int \int \int_{V_e} (\boldsymbol{\sigma}_{ek}^e)^T \boldsymbol{\varepsilon}_{ek} dV \quad (13.129)$$

$$= \sum_{k=1}^l \sum_{e=1}^N \sum_{i=1}^{NG} (\varrho_e)_i |J|_i (\boldsymbol{\sigma}_{ek}^e)^T \boldsymbol{\varepsilon}_{ek} \quad (13.130)$$

$$= \sum_{k=1}^l \sum_{r=1}^n \varrho_r |J|_r (\boldsymbol{\sigma}_{kr}^e)^T \boldsymbol{\varepsilon}_{kr} = 1 \quad (13.131)$$

In addition, the geometric compatibility condition of the cumulative plastic strains in equation (13.122) can be written as

$$\Delta \boldsymbol{\epsilon}_r = \sum_{k=1}^l \boldsymbol{\epsilon}_{kr} = \mathbf{B}_r \Delta \boldsymbol{\delta} \quad (r = 1, 2, \dots, n) \quad (13.132)$$

where  $\Delta \boldsymbol{\delta}$  is a global nodal cumulative velocity vector over a loading cycle and  $\mathbf{B}_r$  is the strain-velocity matrix at the  $r$ -th Gaussian integral point and

$$\mathbf{B}_r = \mathbf{B}_e \times \mathbf{C}_e \quad (13.133)$$

in which  $\mathbf{C}_e$  is a transformation matrix.

With the above finite element formulations, the kinematic shakedown analysis may be expressed as the following nonlinear programming problem:

$$m_{sd} = \min \sum_{k=1}^l \sum_{r=1}^n \varrho_r |J_r| \left[ \frac{1}{2} \sqrt{(\boldsymbol{\epsilon}_{kr}^T \mathbf{P}^{-1} \boldsymbol{\epsilon}_{kr}) \cdot (4 + \mathbf{Q}^T \mathbf{P}^{-1} \mathbf{Q})} - \frac{1}{2} (\boldsymbol{\epsilon}_{kr}^T \mathbf{P}^{-1} \mathbf{Q}) \right] \quad (13.134)$$

$$\text{Subject to } \sum_{k=1}^l \sum_{r=1}^n \varrho_r |J_r| r (\boldsymbol{\sigma}_{kr}^e)^T \boldsymbol{\epsilon}_{kr} = 1 \quad (13.135)$$

$$\Delta \boldsymbol{\epsilon}_r = \sum_{k=1}^l \boldsymbol{\epsilon}_{kr} = \mathbf{B}_r \Delta \boldsymbol{\delta} \quad (r = 1, 2, \dots, n) \quad (13.136)$$

where  $\boldsymbol{\sigma}_{kr}^e$  is the elastic stress field due to the specific surface traction  $T_i$  which may take a unit value. After the displacement boundary condition is imposed by means of the standard finite element method, the above nonlinear programming problem can be solved to obtain the lowest load multiplier  $m_{sd}$ . The shakedown limit of the structure is then given by  $m_{sd} T_i$ .

### 13.6.3 The iterative solution algorithm

The kinematic shakedown analysis defined by equations (13.134)-(13.136) is a minimum optimisation problem with a single equality constraint. The objective function is nonlinear, continuous but may be nondifferentiable. For a continuous and differentiable quadratic mathematical programming problem, several effective methods can be used to solve it (Himmelblau, 1972).

For the mathematical programming problem (13.134), there is a calculation of square root which could make the objective function unsMOOTH and nondifferentiable. This would cause difficulties in solving the programming problem. The nonlinear objective function becomes nondifferentiable in rigid areas (where the strain fields are zero) for shakedown analysis. This difficulty can be overcome by using

an iterative algorithm that has been developed by Li and Yu (2005) for limit analysis of cohesive-frictional materials. This technique is concerned with how to distinguish rigid and deforming plastic areas.

### *Minimum optimization strategy*

By using the Lagrangian method (Himmelblau, 1972), the equality constraint can be removed so that the equations (13.135) and (13.136) can be combined to give an unconstrained minimum optimization problem with the following new objective function:

$$\begin{aligned}
 L(\boldsymbol{\varepsilon}_{kr}, \Delta\boldsymbol{\delta}, q, \mathbf{L}_r) &= \sum_{k=1}^l \sum_{r=1}^n \varrho_r |J|_r \left[ \frac{1}{2} \sqrt{(\boldsymbol{\varepsilon}_{kr}^T \mathbf{P}^{-1} \boldsymbol{\varepsilon}_{kr}) \cdot (4 + \mathbf{Q}^T \mathbf{P}^{-1} \mathbf{Q})} - \frac{1}{2} (\boldsymbol{\varepsilon}_{kr})^T \mathbf{P}^{-1} \mathbf{Q} \right] \\
 &\quad + q \left( 1 - \sum_{k=1}^l \sum_{r=1}^n \varrho_r |J|_r (\boldsymbol{\sigma}_{kr}^e)^T \boldsymbol{\varepsilon}_{kr} \right) \\
 &\quad + \sum_{r=1}^n \mathbf{L}_r^T \left( \sum_{k=1}^l \boldsymbol{\varepsilon}_{kr} - \mathbf{B}_r \Delta\boldsymbol{\delta} \right) \tag{13.137}
 \end{aligned}$$

where  $q$  and  $\mathbf{L}_r$  are the Lagrangian multipliers.

According to the Kuhn-Tucker conditions, the shakedown analysis problem (13.134) can be solved by applying the following conditions to equation (13.137):

$$\frac{\partial L}{\partial \boldsymbol{\varepsilon}_{kr}} = 0 \tag{13.138}$$

$$\frac{\partial L}{\partial \Delta\boldsymbol{\delta}} = 0 \tag{13.139}$$

$$\frac{\partial L}{\partial q} = 0 \tag{13.140}$$

$$\frac{\partial L}{\partial \mathbf{L}_r} = 0 \tag{13.141}$$

which can be shown to be as follows:

$$\frac{\mathbf{P}^{-1}(4 + \mathbf{Q}^T \mathbf{P}^{-1} \mathbf{Q})}{2 \sqrt{\boldsymbol{\varepsilon}_{kr}^T \mathbf{P}^T \boldsymbol{\varepsilon}_{kr} \cdot (4 + \mathbf{Q}^T \mathbf{P}^{-1} \mathbf{Q})}} \boldsymbol{\varepsilon}_{kr} - q \boldsymbol{\sigma}_{kr}^e + (\varrho_r |J|_r)^{-1} \mathbf{L}_r - \frac{1}{2} \mathbf{P}^{-1} \mathbf{Q} = 0$$

$$(k=1, 2, \dots, l; r=1, 2, \dots, n) \tag{13.142}$$

$$\sum_{r=1}^n (\mathbf{B}_r^T \mathbf{L}_r) = 0 \tag{13.143}$$

$$\sum_{k=1}^l \sum_{r=1}^n |J|_r (\sigma_{kr}^e)^T \varepsilon_{kr} = 1 \quad (13.144)$$

$$\sum_{k=1}^l \varepsilon_{kr} - B_r \Delta \delta = 0 \quad (r = 1, 2, \dots, n) \quad (13.145)$$

The above set of equations are difficult to solve as it is nonlinear and also nondifferentiable. However, an iterative technique can be used to find solutions for the above equations. In order to perform this iterative technique, we will re-express the above equations in the following form:

$$H_{kr}^{ICP} \varepsilon_{kr} - q \sigma_{kr}^e + (Q_r |J|_r)^{-1} L_r - \frac{1}{2} P^{-1} Q = 0 \quad (k=1, 2, \dots, l; r=1, 2, \dots, n) \quad (13.146)$$

$$\sum_{r=1}^n (B_r^T L_r) = 0 \quad (13.147)$$

$$\sum_{k=1}^l \sum_{r=1}^n |J|_r (\sigma_{kr}^e)^T \varepsilon_{kr} = 1 \quad (13.148)$$

$$\sum_{k=1}^l \varepsilon_{kr} - B_r \Delta \delta = 0 \quad (r = 1, 2, \dots, n) \quad (13.149)$$

in which we have

$$H_{kr}^{ICP} = \frac{1}{2} P^{-1} (4 + Q^T P^{-1} Q) (z_{kr})^{-1} \quad (13.150)$$

$$z_{kr} = \sqrt{(\varepsilon_{kr}^T P^{-1} \varepsilon_{kr}) \cdot (4 + Q^T P^{-1} Q)} \quad (13.151)$$

and the superscript 'ICP' indicates that the variable is an iterative control parameter.

Once the equations (13.146)-(13.149) are solved for the variables  $\varepsilon_{kr}$ , the shake-down load multiplier can be determined by

$$m_{sd} = \sum_{k=1}^l \sum_{r=1}^n Q_r |J|_r \left[ \frac{1}{2} \sqrt{(\varepsilon_{kr}^T P^{-1} \varepsilon_{kr}) \cdot (4 + Q^T P^{-1} Q)} - \frac{1}{2} (\varepsilon_{kr})^T P^{-1} Q \right] \quad (13.152)$$

### Iterative strategy

To overcome the difficulties which may arise from an unsMOOTH objective function, all the nondifferentiable areas need to be identified where the first part of the objective function becomes zero (i.e.  $z_{kr} = 0$ ). In order to find all nondifferentiable

regions, an iterative technique is needed. The iteration begins with the assumption that the plastic strain field is non-zero everywhere and therefore the nondifferentiable region does not exist at the first iteration step. However from the second step, the plastic strain field will be updated and the nondifferentiable areas can be identified by checking if  $z_{kr} = 0$ .

Once a nondifferentiable area is identified at an iteration step, the condition  $z_{kr} = 0$  will be introduced as a constraint into the nonlinear programming problem using the penalty method. Hence the objective function will be modified at each iteration step until the limit load multiplier is determined.

As discussed in Li and Yu (2006a), an iterative solution algorithm for calculating the shakedown multiplier is proposed as follows:

*Step 0: initializing the nonlinear objective function*

It may be proved that from any initial trial solution, the subsequent iterations are locked in a certain convex hull that contains the exact solution of the problem (Huh and Yang, 1991). For simplicity, we can begin the iteration by setting  $(Z_{kr})_0 = 1$ . Then we can obtain

$$(H_{kr})_0 = \frac{1}{2} P^{-1} (4 + Q^T P^{-1} Q) \quad (13.153)$$

By solving the system of linear equations (13.146)-(13.149), we can obtain the initial plastic strain vector  $(\epsilon_{kr})_0$ , at this step, from which the initial shakedown load multiplier can be derived by using the following equation

$$m_{sd}^0 = \sum_{k=1}^l \sum_{r=1}^n \varrho_r |J|_r \left[ \frac{1}{2} \sqrt{((\epsilon_{kr})_0^T P^{-1} (\epsilon_{kr})_0) \cdot (4 + Q^T P^{-1} Q)} - \frac{1}{2} (\epsilon_{kr})_0^T P^{-1} Q \right] \quad (13.154)$$

*Step  $h+1$  ( $h=0,1,2,\dots$ ): identifying the rigid regions to modify objective function*

At step  $h$ , the value of  $z_{kr}$  needs to be calculated at every integration point in order to check if it is in a nondifferentiable area. Then the integration point set I will be subdivided into two subsets: (a) the subset  $(I_R)_{h+1}$  where the objective function is not differentiable and, (b) the subset  $(I_P)_{h+1}$  where the objective function is differentiable. Therefore

$$I = (I_R)_{h+1} \cup (I_P)_{h+1} \quad (13.155)$$

$$(I_R)_{h+1} = \{r \in I, z_{kr} = 0\} \quad (13.156)$$

$$(I_P)_{h+1} = \{r \in I, z_{kr} > 0\} \quad (13.157)$$

It should be noted that in actual calculations, the integration point is regarded as in the rigid region as long as  $z_{kr}$  is smaller than a certain small value say  $\xi$  (which may range from  $10^{-8}$  to  $10^{-12}$ ).

Once a nondifferentiable region is found, the objective function (13.134) will be modified by removing it from the calculation. The constraint that  $z_{kr} = 0$  can be introduced into the programming problem by a penalization function. Hence the coefficient matrix  $\mathbf{H}_{kr}$  at this iteration step will be updated as follows:

$$(\mathbf{H}_{kr})_{h+1} = \frac{1}{2} \mathbf{P}^{-1} (4 + \mathbf{Q}^T \mathbf{P}^{-1} \mathbf{Q}) (z_{kr})^{-1} \quad r \in (I_P)_{h+1} \quad (13.158)$$

$$(\mathbf{H}_{kr})_{h+1} = \beta \mathbf{P}^{-1} \quad r \in (I_R)_{h+1} \quad (13.159)$$

where  $\beta$  is a penalization factor which is used to introduce the nondifferentiable area (i.e. rigid region) as a constraint into the programming problem. In practice it is satisfactory to choose a value for  $\beta$  between  $10^6$  and  $10^{12}$ .

By solving the linear system of equations defined by (13.146)-(13.149) using the procedure outlined in Li and Yu (2006a), we can obtain the plastic strain vector  $(\varepsilon_{kr})_{h+1}$  at step  $h+1$ . The shakedown load multiplier at this step can then be determined by

$$m_{sd}^{h+1} = \frac{1}{2} \sum_{k=1}^l \sum_{r=1}^n \varrho_r |J|_r \sqrt{((\varepsilon_{kr})_{h+1}^T \mathbf{P}^{-1} (\varepsilon_{kr})_{h+1}) \cdot (4 + \mathbf{Q}^T \mathbf{P}^{-1} \mathbf{Q})} \\ - \frac{1}{2} \sum_{k=1}^l \sum_{r=1}^n \varrho_r |J|_r (\varepsilon_{kr})_{h+1}^T \mathbf{P}^{-1} \mathbf{Q} \quad (13.160)$$

It is noted that the above iteration is repeated until the solution satisfies the following convergence criteria

$$\frac{|m_{sd}^{h+1} - m_{sd}^h|}{m_{sd}^{h+1}} \leq ERR1 \quad (13.161)$$

$$\frac{\|\Delta \delta_{h+1} - \Delta \delta_h\|}{\|\Delta \delta_{h+1}\|} \leq ERR2 \quad (13.162)$$

where  $ERR1$  and  $ERR2$  are error tolerances given by the user.

The numerical procedure outlined above has been shown by Li and Yu (2006a) to give accurate shakedown load multipliers through a monotonically decreasing convergence sequence. This numerical procedure has been further extended by Li and Yu (2006b) to carry out shakedown analysis of composite materials.

## REFERENCES

Aboustit, B.L. and Reddy, D.V. (1980). Finite element linear programming approach to foundation shakedown, *Soils Under Cyclic and Transient Loading*, (Editors: G.N. Pande and O.C. Zienkiewicz).

Belytschko, T. (1972). Plane stress shakedown analysis by finite elements. *Int. J. Mech. Sci.*, Vol 14, 619-625.

Bleich, H. (1932). Über die Bemessung statisch unbestimmter Stahltragwerke unter Berücksichtigung des elastisch-plastischen Verhaltens des Baustoffes, *Bauingenieur*, Vol 19/20, 261.

Boulbibane, M. and Ponter, A.R.S. (2006). The linear matching method for the shakedown analysis of geotechnical problems. *Int. J. Num. Analy. Meth. Geomech.*, Vol 30, 157-179.

Calladine, C.R. (1985). *Plasticity for Engineers*, Ellis Horwood.

Capurso, M. (1974). A displacement bounding principle in shakedown of structures subjected to cyclic loads. *Int. J. Solids Structures*, Vol 10, 77-92.

Collins, I.F. and Cliffe, P.F. (1987). Shakedown in frictional materials under moving surface loads. *Int. J. Num. Analy. Meth. Geomech.*, Vol 11, 409-420.

Collins, I.F., Wang, A.P. and Saunders, L.R. (1993). Shakedown in layered pavements under moving surface loads. *Int. J. Num. Analy. Meth. Geomech.*, Vol 17, 165-174.

Drucker, D.C., Prager, W. and Greenberg, H.J. (1952). Extended limit design theorems for continuous media, *Quart. Appl. Math.*, Vol 9, 381-389.

Gokhfeld, D.A. and Cherniavski, O.F. (1980). *Limit Analysis at Thermal Cycling*, Shjhoff and Noordhoff.

Gvozdev, A.A. (1936). La determination de la charge de ruine pour les systemes hyperstatiques subissant des deformations plastiques, *Proc. Conf. Plastic Deformation, Ac Sc. USSR*, 19.

Hamilton, G.M. (1983). Explicit equations for the stresses beneath a sliding spherical contact, *Proc. Inst. Mech. Eng.*, Vol 197c, 53-59.

Hill, R. (1950). *The Mathematical Theory of Plasticity*, Clarendon Press, Oxford.

Hill, R. (1951). On the state of stress in a plastic-rigid body at the yield point, *Phil. Mag.*, Vol 42, 868-875.

Hills, D.A. and Sackfield, A. (1984). Yield and shakedown states in the contact of generally curved bodies, *J. Strain Analy.*, Vol 19, 9-14.

Himmelblau, D.M. (1972). *Applied Nonlinear Programming*, McGraw-Hill Book Company, New York.

Huh, H. and Yang, W.H. (1991). A general algorithm for limit solutions of plane stress problems. *Int. J. Solids and Structures.*, Vol. 28, 727-738.

Johnson, K.L. (1962). A shakedown limit in rolling contact, *Proc. 4th US Nat. Congress Appl. Mech.*, ASME, Berkeley, 28.

Johnson, K.L. (1985). *Contact Mechanics*, Cambridge University Press.

Johnson, K.L. (1992). The application of shakedown principles in rolling and sliding contact, *Eur. J. Mech. A/Solids*, Vol 11, 155-172.

Johnson, K.L. and Jefferis, J.A. (1963). Plastic flow and residual stresses in rolling and sliding contact, *Proc. Inst. Mech. Eng: Symp. Fatigue in Rolling Contact*, Vol 177, 54-65.

Kachanov, L.M. (1974). *Fundamentals of the Theory of Plasticity*. Mir Publishers, Moscow.

Kapoor, A. and Johnson, K.L. (1992). Effect of changes in contact geometry on shakedown of surfaces in rolling/sliding/ contact. *Int. J. Mech. Sci.*, Vol 34, 223-239.

Koiter, W.T. (1960). General theorems for elastic-plastic solids, In: *Progress in Solid Mechanics*, (Editors: I.N. Sneddon and R. Hill), Vol 1, 167-221.

Konig, J.A. (1987). *Shakedown of Elastic-Plastic Structures*. Elsevier.

Li, H.X. and Yu, H.S. (2005). Kinematic limit analysis of frictional materials using nonlinear programming. *Int. J. Solids Structures*, Vol 42, 4058-4076.

Li, H.X. and Yu, H.S. (2006a). A nonlinear programming approach to kinematic shakedown analysis of frictional materials. *Int. J. Solids Structures* (in press).

Li, H.X. and Yu, H.S. (2006b). A nonlinear programming approach to kinematic shakedown analysis of composite materials. *Int. J. Num. Meth. Eng.*, Vol 66, 117-146.

Li, H.X. and Yu, H.S. (2006c). Three-dimensional solutions for shakedown of layered pavements under moving surface loads. *Int. J. Num. Analy. Meth. Geomech.* (under review).

Liu, Y.H., Cen, Z.Z. and Xu, B.Y. (1995). A numerical method for plastic limit analysis of 3D structures. *Int. J. Solids and Structures*, Vol. 32, 1645-1658.

Maier, G. (1969). Shakedown theory in perfect elastoplasticity with associated and non-associated flow laws: a finite element linear programming approach. *Meccanica*, Vol 4, 250-260.

Maier, G, Carvelli, G. and Cocchetti, G. (2000). On direct methods of shakedown and limit analysis. *Plenary Lecture, 4th Euromech Solid Mechanics Conference*, Metz, June.

Melan, E (1938). Zur plastizitat des raumlichen Kontinuums, *Ing. Arch.*, Vol 9, 116-125.

Pande, G.N. (1982). Shakedown of foundations subjected to cyclic loads, *Soil Mechanics – Transient and Cyclic Loads*, (Editors: G.N. Pande and O.C. Zienkiewicz), 469-489.

Ponter, A.R.S. (1972). An upper bound on the small displacement of elastic perfectly plastic structures. *J. Appl. Mech.*, Vol 39, 959-963.

Ponter, A.R.S. (1976). A general shakedown theorem for inelastic materials. *Proc. 3rd Int. Conf. Struct. Mech. Reactor Technology*, Section L, Imperial College, London.

Ponter, A.R.S., Hearle, A.D. and Johnson, K.L. (1985). Application of the kinematical shakedown theorem to rolling and sliding point contacts. *J. Mech. Phys. Solids*, Vol 33, 339-362.

Prager, W. and Hodge, P.G. (1951). *The Theory of Perfectly Plastic Solids*, John Wiley and Sons, New York.

Radd, L., Weichert, D. and Najm, W. (1988). Stability of multilayer system under repeated loads. *Transport. Res. Rec.*, Vol 1207, 181-186.

Radovsky, B.S. and Murashina, N.V. (1996). Shakedown of subgrade soil under repeated loading. *Transport. Res. Rec.*, Vol 1547, 82-88.

Sharp, R.W. (1983). *Shakedown Analysis and Design of Pavements*, PhD Thesis, Sydney University, Australia.

Sharp, R.W. and Booker, J.R. (1984). Shakedown of pavements under moving surface loads. *J. Transp. Eng.*, ASCE, Vol 110, 1-14.

Shiau, S.H. (2001). *Numerical Methods for Shakedown Analysis of Pavements*, PhD Thesis, University of Newcastle, Australia.

Shiau, S.H. and Yu, H.S. (1999). Shakedown of three-layered pavements. *Proc. 7th Int. Conf. on Structural Failure and Plasticity*, Melbourne, Australia.

Shiau, S.H. and Yu, H.S. (2000a). Load and displacement predictions for shakedown analysis of layered pavements. *Transport. Res. Rec.*, Vol 1730, 117-124.

Shiau, S.H. and Yu, H.S. (2000b). Shakedown analysis of flexible pavements. *Proc. John Booker Memorial Symp.*, 643-653.

Sloan, S.W. (1988). A steepest edge active set algorithm for solving sparse linear programming problems. *Int. J. Num. Meth. Eng.*, Vol. 26, 2671-2685.

Symonds, P.S. and Neal, B.G. (1951). Recent progress in the plastic methods of structural analysis. *J. Franklin. Inst.*, Vol 252, 383-407.

Yu, H.S. (2005). Three-dimensional analytical solutions for shakedown of cohesive frictional materials under moving surface loads. *Proc. R. Soc. A.*, Vol 461, 1951-1964.

Yu, H.S. and Hossain, M.Z. (1998). Lower bound shakedown analysis of layered pavements using discontinuous stress fields. *Comput. Meth. Appl. Mech. Eng.*, Vol 167, 209-222.

## CHAPTER 14

### FINITE ELEMENT ANALYSIS

#### 14.1 INTRODUCTION

Over the last forty years, the finite element method has been developed as the most powerful and general numerical method for the analysis of nonlinear engineering problems. Its use and application to geotechnical engineering is now very widespread. Whilst the use of finite elements for linear, elastic analysis of geotechnical problems is relatively trouble-free, its application to nonlinear, plastic geotechnical analysis is not very straightforward as several difficult issues still cause potential numerical problems that may lead to significant errors in solutions (e.g. Sloan and Randolph, 1982; Naylor *et al.*, 1981; Crisfield, 1991, 1997; Yu *et al.*, 1993; Zienkiewicz *et al.*, 1998; Potts and Zdravkovic, 1999; Carter *et al.*, 2000).

In the present chapter, we will first present the basic procedures of nonlinear finite element analysis involving elastic-plastic stress-strain relations. Then we will focus on addressing the following issues that are essential for accurate finite element analysis of geotechnical applications but have not yet been fully covered in the geotechnical literature:

- (1) Accurate finite elements for modelling incompressible and dilatant plastic material behaviour (e.g. Nagtegaal *et al.*, 1974; Naylor, 1974; Sloan, 1981; Yu, 1990, 1991; Yu *et al.*, 1993; Yu and Netherton, 2000);
- (2) Solutions schemes for nonlinear load-displacement and stress-strain relations (e.g. Crisfield, 1991; Sloan, 1987; Abbo, 1997; Simo and Hughes, 1998);
- (3) Finite element formulations for problems involving large deformation (e.g. Hibbit *et al.*, 1970; McMeeking and Rice, 1975; Carter *et al.*, 1977; Burd, 1986; Teh, 1987; Yu, 1990; Chen and Mizuno, 1990).

Finally we will present some numerical examples where finite elements and plasticity models (as described in this book) are applied in geotechnical analysis (e.g. Yu, 1990; Khong, 2004; Yuan, 2005; Tan, 2006; Xu, 2006; Walker and Yu, 2006; Yang and Yu, 2006a,b).

#### 14.2 PROCEDURES OF NONLINEAR FINITE ELEMENT ANALYSIS

In this section, we give a brief introduction on the basic elements of nonlinear finite element analysis particularly involving plasticity. Nonlinear finite elements deal

with either nonlinear material behaviour (i.e. stress-strain relations) or geometric (e.g. large deformation formulations) behaviour or their combined effects.

When plasticity is used to describe material behaviour, non-linearity occurs at two different levels. First of all, it occurs at the element level when stresses at the integration points need to be updated after the strain rates are calculated from the nodal displacement increments. The stress update is obtained by solving a nonlinear incremental stress-strain equation. Secondly it occurs at the structural level when the nonlinear incremental nodal load-displacement equation needs to be solved subject to given boundary conditions. These two sets of nonlinear relations are shown in Figure 14.1.

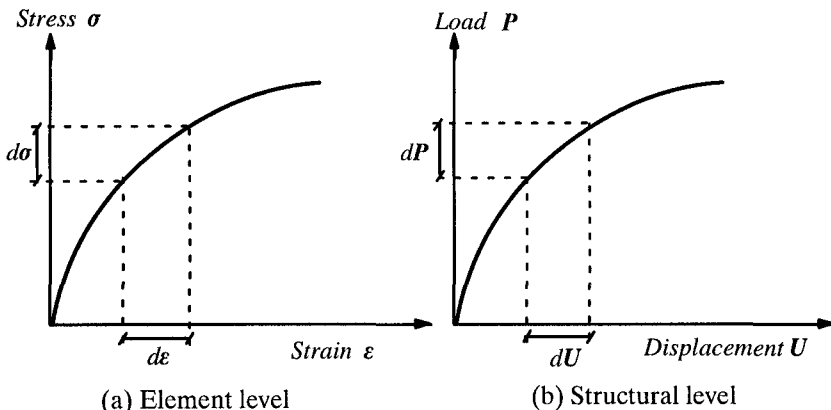


Figure 14.1: Nonlinear relations in finite element analysis

In a nonlinear finite element analysis, we may follow the essential steps given below:

- (1) To select a finite element type and discretize the domain of interest into a large number of elements;
- (2) To use the virtual work equation to formulate incremental nodal load-displacement equations at the element level. The elemental stiffness matrix can then be obtained;
- (3) To assemble the global stiffness matrix so that the incremental load-displacement equations are obtained;
- (4) To use an incremental or iterative strategy to solve the resulting nonlinear incremental load-displacement equations subject to given boundary conditions;

- (5) With the solutions of displacement increments at all nodes obtained from the last step, the stresses at integration points are updated using given stress-strain relations of the material.
- (6) For the next load or displacement increment, repeat steps (1)-(5) with new initial values of all relevant quantities (e.g. nodal forces, nodal displacements, stresses and strains at integration points).

### 14.3 ACCURATE FINITE ELEMENTS FOR SOIL PLASTICITY

It is well known that severe numerical difficulties may arise when displacement finite elements are used to model the behaviour of incompressible or nearly incompressible materials (e.g. undrained or critical state soil behaviour) and this is particularly true for axisymmetric problems. These numerical difficulties are caused by excessive kinematic constraints (due to incompressible plastic flow rules) and are reflected by strong oscillations in the calculated stress distribution and overestimations of plastic collapse loads. As noted by Sloan (1981) and Yu (1990), the same numerical difficulties exist when finite elements are used to analyse frictional materials with constant dilation. The purpose of this section is to present a new displacement finite element formulation which is particularly suitable for axisymmetric analysis of incompressible or nearly incompressible behaviour.

#### 14.3.1 Introduction

Finite element analysis of undrained geotechnical problems has encountered severe numerical difficulties over the years. One notable example is that the conventional displacement finite element method suffers from the disadvantages that the accuracy of the calculated stresses reduces dramatically as the compressibility approaches zero. This phenomenon, which is widely known as 'locking', has been reported in the literature by many researchers (see, for example, Herrmann, 1965; Christian, 1968; Naylor, 1974; Nagtegaal *et al.*, 1974; Zienkiewicz *et al.*, 1971; Burd and Housby, 1990).

In 1974, Nagtegaal *et al.* published a landmark paper on the theoretical analysis of the difficulties associated with finite element calculations in the fully plastic range involving incompressible behaviour. By considering the limiting case of a very fine mesh, they proved that most displacement finite elements which employ low order polynomials to model the displacement field are not suitable for incompressibility computations, and this is particularly true for axisymmetric problems. This is because the incremental incompressibility condition typically imposes a large number of constraints on the nodal velocities which, effectively, reduces the available number of degrees of freedom. Since these constraints may multiply at

a faster rate than the new degrees of freedom as the mesh is refined, it may not be possible to ensure that there are sufficient degrees of freedom available to accommodate the constant volume condition, regardless of how many elements are used in the grid.

One of the earlier approaches used to overcome this problem is the reduced integration rule suggested by Zienkiewicz *et al.* (1971). The typical element used in this type of approach is the 8-noded rectangle with 4-point integration. As discussed by Naylor (1974) and Sloan and Randolph (1982), reduced integration has the beneficial effect of decreasing the total number of incompressibility constraints on the nodal degrees of freedom. This is clearly seen by noting that the maximum number of constraints per element must be less than, or equal to, the total number of integration points used in the calculation of the element stiffness matrices. A theoretical justification of using reduced integration in analysing incompressible materials has been given by Malkus and Hughes (1978). They proved that displacement formulations with reduced integration are, in certain cases, equivalent to mixed formulations where both stresses and displacements are treated as variables. This equivalence typically holds in plane strain and three-dimensional analysis. However, the equivalence breaks down for the case of axisymmetric loading.

Although it was once widely used in the finite element community, the reduced integration method can produce spurious stress and displacement oscillations and this is caused by the formation of zero-energy modes. To illustrate the limitations of the reduced integration method, Sloan and Randolph (1983) presented a number of numerical examples on footings and vertical cuts in which the reduced integration approach leads to incorrect or unacceptable deformation predictions. In particular, the initial and deformed meshes shown in Sloan and Randolph (1983) for a rigid circular footing that were obtained using the reduced integration method indicate that the finite elements in the vicinity of the footing deform in a bulging mode and numerical problems are clearly evident. Recently, Naylor (1994) also demonstrated that even a high order element (cubic triangles), when used with 6 integration points (reduced integration), produces a zero-energy mechanism. These shortcomings are relatively well known in the area of computational geomechanics and a number of other important cases have also been discussed by Sloan (1981) and de Borst & Vermmer (1984) among others. At a more fundamental level, the major limitation of using the reduced integration technique is that the incompressibility condition is satisfied only at a limited number of integration points, rather than everywhere within the element. In other words, even though the reduced integration may give reasonably accurate stress prediction at a limited number of integration

points within an element, the numerical stress field in the remaining part of the element would be highly incorrect.

Another method for the analysis of incompressible materials, which does not have the drawbacks associated with reduced integration, is to use a high order element as suggested by Sloan and Randolph (1982). Using the analysis of Nagtegaal *et al.* (1974), they proved that high order elements can provide a sufficient number of degrees of freedom to satisfy the constant volume condition. This is so because the number of degrees of freedom per element increases faster than the number of incompressibility constraints when the order of an element increases. According to Sloan (1981), the lowest order of triangular element for axisymmetric problems suitable for this approach is a 15-noded cubic strain element. Although this approach works well, it suffers from the drawback that the high order elements cause a large bandwidth in the stiffness matrix, which may require some sophisticated equation solvers.

Yu (1990, 1991) later proved that the number of incompressibility constraints may also be reduced by choosing appropriate displacement interpolation functions. In particular, Yu (1990, 1991) proposed a modified displacement interpolation function which can be used to develop suitable displacement finite elements for axisymmetric analysis of incompressible materials. The application of this new displacement interpolation function to a 6-noded triangular element presented by Yu *et al.* (1993) suggests that this novel approach permits low order elements to be successfully used for axisymmetric analysis of incompressible materials. Yu's new formulation is also simple to implement in a standard finite element program. Since Yu's approach employs full integration to evaluate the element stiffness matrices, the numerical examples (including footing problems) presented in Yu (1990, 1991) and Yu *et al.* (1993) show that no problems are experienced with barrelling or zero-energy mechanisms. It is noted that Yu's displacement interpolation function has also been used successfully by Jinka and Lewis (1994) to develop a modified mixed and penalty formulation for axisymmetric analysis of incompressible materials.

A major objective of this section is to present a general finite element formulation which can be used to implement Yu's displacement interpolation function in any type of displacement finite elements. The presentation is based on the work of Yu and Netherton (2000). Further, in this study, we have also detailed the way by which the new formulations of 3, 6, 10, 15-noded triangular elements and 4, 8-noded quadrilateral elements can be implemented in a standard displacement finite element program. The performance of these new elements will be investigated by comparing the numerical results with exact solutions.

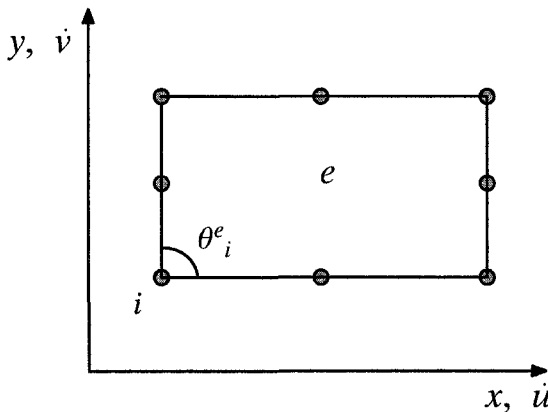


Figure 14.2: An eight-noded rectangle in plane strain

### 14.3.2 Theory

#### *Plane strain loading conditions*

To illustrate the difficulties associated with the analysis of incompressible materials, consider the 8-noded rectangle shown in Figure 14.2. The conventional displacement interpolation function for this element is given by:

$$\dot{u} = c_1 + c_2x + c_3y + c_4x^2 + c_5xy + c_6y^2 + c_7x^2y + c_8xy^2 \quad (14.1)$$

$$\dot{v} = c_9 + c_{10}x + c_{11}y + c_{12}x^2 + c_{13}xy + c_{14}y^2 + c_{15}x^2y + c_{16}xy^2 \quad (14.2)$$

where  $\dot{u}$  and  $\dot{v}$  are the velocities in the x- and y-directions, and  $c_1, c_2, \dots, c_{16}$  are unknown coefficients which are functions of the nodal velocities and the nodal coordinates.

Under the conditions of plane strain, the incremental constant volume condition may be written as:

$$\frac{\partial \dot{u}}{\partial x} + \frac{\partial \dot{v}}{\partial y} = 0 \quad (14.3)$$

Substituting (14.1) and (14.2) into (14.3) gives another form of the incompressibility condition:

$$(c_2 + c_{11}) + (2c_4 + c_{13})x + (c_5 + 2c_{14})y + (2c_7 + 2c_{16})xy + c_{15}x^2 + c_8y^2 = 0 \quad (14.4)$$

In the displacement finite element method, the element stiffness matrices and stresses are normally evaluated at a discrete number of integration points. The

number of integration points used in each element is denoted by  $N_g$ . For the 8-noded rectangle a 9-point integration rule (i.e.  $N_g = 9$ ), which is generally regarded as 'full integration', should be employed. This means that equation (14.4) must be satisfied at 9 independent locations within the element. Using the method suggested by Sloan (1981), it may easily be shown that satisfaction of (14.4) at 9 independent locations imposes 6 incompressibility constraints on the nodal degrees of freedom. These constraints are:

$$\begin{aligned} (c_2 + c_{11}) &= (2c_4 + c_{13}) = (c_5 + 2c_{14}) = (2c_7 + 2c_{16}) \\ &= c_{15} = c_8 = 0 \end{aligned} \quad (14.5)$$

	Lagrangian Rectangles	Lagrangian Triangles
Plane strain	$N(N + 2)$	$0.5N(N + 1)$
Axisymmetry	$N(N + 3) + 1$	$0.5(N + 1)(N + 2)$

Figure 14.3: Formulae for the number of incompressibility constraints per element  $C_e$

The above analysis, which is valid for the 8-noded rectangle under conditions of plane strain, may be extended to axisymmetric loading and other types of elements. For the Lagrange family of elements, Sloan (1981) has derived formulae which give the maximum number of constraints per element,  $C_e$ , arising from the incompressibility condition. These are shown in Figure 14.3 and are expressed in terms of  $N$ , the order of the highest complete polynomial in the velocity expansion. Unfortunately, similar formulae for the serendipity family of elements are not readily apparent due to the *ad hoc* nature in which the high order terms are accumulated as the element order is increased.

For an element to be suitable for modelling incompressible behaviour, it must have a sufficient number of degrees of freedom to satisfy the incompressibility constraints. Following Nagtegaal *et al.* (1974), the suitability of a particular type of element may be determined by considering the limiting case of a very fine mesh to find the number of degrees of freedom per constraint. This ratio, which must be greater than or equal to 1 for good performance, is given as  $f_e/C_e$ , where  $f_e$  is the limiting

value of degrees of freedom per element. The quantity  $f_e$  is defined uniquely for each type of element, regardless of the mesh arrangement, according to:

$$f_e = \frac{1}{\pi} \sum_{i=1}^{i=n} \theta_i^e \quad (14.6)$$

where  $\theta_i^e$  represents the internal angle for node  $i$  of element  $e$  and  $n$  is the number of nodes per element.

For the 8-noded rectangle, from (14.5) and (14.6) we can see that  $c_e = 6$  and  $f_e = 6$ . Hence the number of degrees of freedom per constraint in the limiting case of a very fine mesh is equal to  $f_e/c_e = 6/6 = 1$ . Since this value is not less than 1, the 8-noded rectangle is deemed to be suitable for analysis of incompressible behaviour under plane strain conditions.

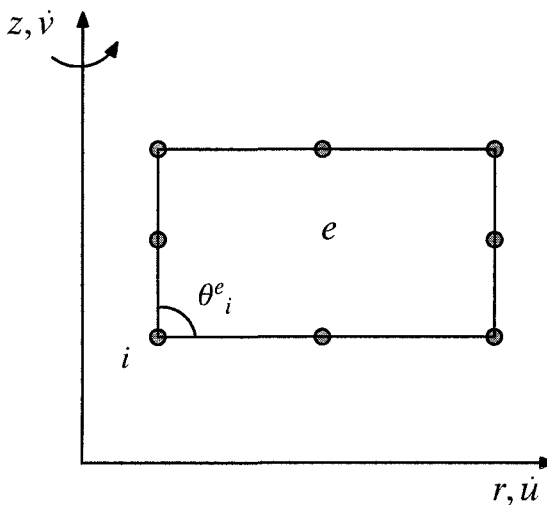


Figure 14.4: An eight-noded rectangle in axisymmetry

#### Axisymmetric loading conditions

For axisymmetric loading, let us consider the 8-noded rectangle shown in Figure 14.4. Following the usual convention of using  $(r, z)$  to denote the coordinates of axisymmetric problems, the conventional displacement interpolation function for the axisymmetric version of this element is as follows:

$$u = c_1 + c_2r + c_3z + c_4r^2 + c_5rz + c_6z^2 + c_7r^2z + c_8rz^2 \quad (14.7)$$

$$v = c_9 + c_{10}r + c_{11}z + c_{12}r^2 + c_{13}rz + c_{14}z^2 + c_{15}r^2z + c_{16}rz^2 \quad (14.8)$$

where  $\dot{u}$  and  $\dot{v}$  are the velocities in the  $r$ - and  $z$ -directions, and  $c_1, c_2, \dots, c_{16}$  are unknown coefficients which are functions of the nodal velocities and the nodal coordinates.

Under the conditions of axisymmetry, the incremental constant volume condition may be written as follows:

$$\frac{\partial \dot{u}}{\partial r} + \frac{\partial \dot{v}}{\partial z} + \frac{\dot{u}}{r} = 0 \quad (14.9)$$

By substituting (14.7) and (14.8) into (14.9), we obtain the following incompressibility condition:

$$(2c_2 + c_{11}) + (3c_4 + c_{13})r + (2c_5 + 2c_{14})z + (3c_7 + 2c_{16})rz + c_{15}r^2 + 2c_8z^2 + c_1 \frac{1}{r} + c_3 \frac{z}{r} + c_6 \frac{z^2}{r} = 0 \quad (14.10)$$

If 9-point integration is used to evaluate the element stiffness, then equation (14.10) imposes the following constraints on the nodal velocities:

$$(2c_2 + c_{11}) = (3c_4 + c_{13}) = (2c_5 + 2c_{14}) = (3c_7 + 2c_{16}) = c_{15} = 2c_8 = c_1 = c_3 = c_6 = 0 \quad (14.11)$$

This gives 9 constraints for each element, i.e.  $c_e = 9$ . On the other hand, the number of degrees of freedom per element is  $f_e = 6$ . Hence the limiting number of degrees of freedom per constraint, with a 9-point integration (i.e. full integration), is equal to the unacceptable low value of  $f_e/c_e = 6/9 = 0.67$ . According to the criterion of Nagtegaal *et al.* (1974), the 8-noded rectangle with a full integration is not suitable for analysis of incompressible materials under axisymmetric loading conditions.

The above analysis can be applied to all types of displacement elements to assess their suitability for modelling incompressible materials. Figure 14.5 presents the results derived by Sloan (1981) on the suitability of some triangular and rectangular elements under both plane strain and axisymmetric conditions.

As the number of incompressibility constants per element must be less than or equal to the number of integration points used to evaluate the element stiffness matrices, the integration rule has a direct effect on the limiting ratio of degrees of freedom to constraints. In Figure 14.5, the integration rules have been selected so that the stiffness for an elastic element with straight sides is evaluated exactly under conditions of plane strain. This is generally referred to as 'full integration' rather than 'exact integration', since it is generally not possible to compute the stiffness exactly for an element with curved sides. Due to the presence of hoop strain terms,

none of the schemes can evaluate the element stiffness exactly for axisymmetric problems. To ensure that the element stiffness can be calculated accurately, most finite element codes use the same order or a slightly higher order of integration rule than that for plane strain (e.g. Larsen and Gellert, 1978).

Elements	$f_e$	Plane Strain				Axisymmetry			
		$N_g$	$c_e$	$f_e/c_e$	Suitable	$N_g$	$c_e$	$f_e/c_e$	Suitable
3-noded triangle	1	1	1	1	Yes	3	3	1/3	No
6-noded triangle	4	3	3	4/3	Yes	6	6	2/3	No
10-noded triangle	9	6	6	3/2	Yes	12	10	9/10	No
15-noded triangle	16	12	10	8/5	Yes	16	15	16/15	Yes
4-noded rectangle	2	4	3	2/3	No	9	5	2/5	No
8-noded rectangle	6	9	6	1	Yes	9	9	2/3	No

Figure 14.5: Suitability of plane strain and axisymmetric elements for incompressible analysis with full-integration (after Sloan, 1981)

### 14.3.3 The use of new displacement interpolation functions

The results presented in Figure 14.5 indicate that although all the displacement elements (with exception of the 4-noded rectangle) are suitable for plane strain problems, they are generally not suited for analysis of axisymmetric problems. There is only one element that is found to be suitable for axisymmetric incompressible analysis and that is the 15-noded cubic triangular element. This has led Sloan and Randolph (1982) to propose the use of high order elements for analysis of incompressible materials under both plane strain and axisymmetric loading conditions.

As an alternative to using high order elements, Yu (1990, 1991) has proposed the use of a new interpolation function. This reduces the number of incompressibility constraints on the nodal degrees of freedom and permits low order elements to be

used successfully. To illustrate this approach, once again we will consider the axisymmetric 8-noded rectangle shown in Figure 14.4.

Comparing the incompressibility condition (14.3) for plane strain conditions, and (14.9) for axisymmetric conditions, it may be seen that the three additional constraints imposed in the axisymmetric formulation are caused by the additional hoop strain term. As shown in Yu (1990, 1991), these additional constraints may be removed if the formulation is based on the generalized radial coordinate  $R$  and its velocities  $\dot{R}$ , which satisfy the following condition:

$$\frac{\partial \dot{R}}{\partial R} = \frac{\partial \dot{u}}{\partial r} + \frac{\dot{u}}{r} = \frac{\partial \dot{r}}{\partial r} + \frac{\dot{r}}{r} = 0 \quad (14.12)$$

The incompressibility condition for axisymmetric cases, equation (14.12), may now be cast in the same form as the incompressibility condition for plane strain:

$$\frac{\partial \dot{R}}{\partial R} + \frac{\partial \dot{z}}{\partial z} = 0 \quad (14.13)$$

If the formulation is based on the use of a 8-noded rectangular element, then the expansion for the velocities should be:

$$\dot{U} = \dot{R} = c_1 + c_2R + c_3z + c_4R^2 + c_5Rz + c_6z^2 + c_7R^2z + c_8Rz^2 \quad (14.14)$$

$$\dot{v} = \dot{z} = c_9 + c_{10}R + c_{11}z + c_{12}R^2 + c_{13}Rz + c_{14}z^2 + c_{15}R^2z + c_{16}Rz^2 \quad (14.15)$$

By substituting (14.14)-(14.15) into the incompressibility condition (14.13), it may easily be shown that the number of incompressibility constraints is  $c_e = 6$ , rather than 9 that is obtained if the conventional displacement interpolation function is used. Equation (14.12) can be solved to give solutions for the generalized radial coordinate  $R$  and its velocity  $\dot{R}$  as follows:

$$R = r^2 \quad ; \quad \dot{R} = \dot{U} = 2\dot{r}r = 2\dot{u}r \quad (14.16)$$

Following the above analysis for other displacement finite elements, we can derive a new set of values of the limiting ratio of degrees of freedom per constraint when the new displacement interpolation functions are used. The results of such an analysis are summarized in Figure 14.6. It is found that all the elements (with exception of the 4-noded rectangle) are suitable for axisymmetric analysis of incompressible materials provided the new displacement interpolation functions are used.

In summary, it has been found that if the 'full integration' is used most displacement finite elements (with the exception of the 15-noded triangular element) fail to satisfy the suitability criterion of Nagtegaal *et al.* (1974) for axisymmetric loading conditions, and therefore are not suitable for axisymmetric analysis of incompressible materials. Using the 8-noded rectangle as an example, it has been demon-

strated that the problem can be removed by using the generalized radial coordinate and its velocities in the finite element formulation.

Elements	$f_e$	Axisymmetry (new formulations)				Axisymmetry (conventional formulations)			
		$N_g$	$c_e$	$f_e/c_e$	Suitable	$N_g$	$c_e$	$f_e/c_e$	Suitable
3-noded triangle	1	3	1	1	Yes	3	3	1/3	No
6-noded triangle	4	6	3	4/3	Yes	6	6	2/3	No
10-noded triangle	9	12	6	3/2	Yes	12	10	9/10	No
15-noded triangle	16	16	10	8/5	Yes	16	15	16/15	Yes
4-noded rectangle	2	9	3	2/3	No	9	5	2/5	No
8-noded rectangle	6	9	6	1	Yes	9	9	2/3	No

Figure 14.6: Suitability of modified and conventional axisymmetric elements for incompressible analysis with full-integration

#### 14.3.4 Finite element formulations

Yu (1990) and Yu *et al.* (1993) have proposed two alternative formulations of 6-noded triangular elements that can be used to implement the new displacement interpolation function into a standard finite element code. To minimise the modifications to the standard finite element code, we will focus on the procedure in which the conventional displacement variables are retained but modifications are made to the shape functions. Figure 14.7 shows an example element (e.g. 3-noded triangular element) plotted in the original coordinates ( $r, z$ ), the generalised coordinates ( $R, z$ ) and the area coordinates ( $\alpha, \beta$ ).

##### *The strain rate - velocity relationship*

The velocity field vector,  $\mathbf{u}$ , is defined in the conventional way:

$$\mathbf{u} = [\dot{r}, \dot{z}]^T = [\dot{u}, \dot{v}]^T \quad (14.17)$$

The strain rate vector,  $\boldsymbol{\varepsilon}$ , is written in terms of the velocity vector:

$$\boldsymbol{\varepsilon} = [\dot{\varepsilon}_r, \dot{\varepsilon}_z, \dot{\varepsilon}_{rz}, \dot{\varepsilon}_\theta]^T = \mathbf{L}_n \mathbf{u} \quad (14.18)$$

where the linear operator matrix  $\mathbf{L}_n$  is

$$\mathbf{L}_n = \begin{bmatrix} \frac{\partial}{\partial r} & 0 \\ 0 & \frac{\partial}{\partial z} \\ \frac{\partial}{\partial z} & \frac{\partial}{\partial r} \\ \frac{1}{r} & 0 \end{bmatrix} \quad (14.19)$$

### The strain rate - nodal velocity relationship

The conventional nodal velocity vector,  $\mathbf{a}^e$ , is retained:

$$\mathbf{a}^e = [\dot{u}_1, \dot{v}_1, \dots, \dot{u}_{nd}, \dot{v}_{nd}]^T \quad (14.20)$$

where  $nd$  = the number of nodes per element.

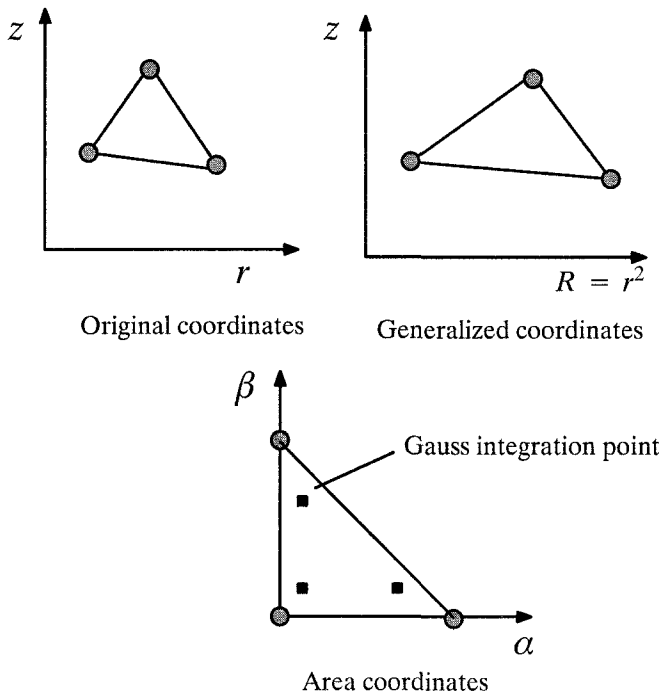


Figure 14.7: Mapping of a 3-noded triangular element

The proposed new displacement interpolation function can be used to relate the velocity field vector  $\mathbf{u}$  to the nodal velocity vector  $\mathbf{a}^e$  as follows:

$$\mathbf{u} = N_n \mathbf{a}^e \quad (14.21)$$

where the general new shape function matrix  $N_n$ , which is valid for all element types, can be derived as:

$$N_n = \begin{bmatrix} \bar{N}_1 & 0 & \dots & \bar{N}_{nd} & 0 \\ 0 & N_1 & \dots & 0 & N_{nd} \end{bmatrix} \quad (14.22)$$

and

$$\bar{N}_i = \frac{N_i r_i}{r} \quad (14.23)$$

where

$N_i$  = conventional shape function at node i;

$\bar{N}_i$  = modified shape function at node i;

$r_i$  = radius of node i;

$r$  = radius of integration points.

Substituting equations (14.21) in (14.18) results in:

$$\boldsymbol{\varepsilon} = \mathbf{L}_n \mathbf{u} = \mathbf{L}_n N_n \mathbf{a}^e = \mathbf{B}_n \mathbf{a}^e \quad (14.24)$$

where the general new strain rate-nodal velocity matrix  $\mathbf{B}_n$  which is valid for all element types is as follows:

$$\mathbf{B}_n = \begin{bmatrix} \frac{\partial \bar{N}_1}{\partial r} & 0 & \dots & \frac{\partial \bar{N}_{nd}}{\partial r} & 0 \\ 0 & \frac{\partial N_1}{\partial z} & \dots & 0 & \frac{\partial N_{nd}}{\partial z} \\ \frac{\partial \bar{N}_1}{\partial z} & \frac{\partial N_1}{\partial r} & \dots & \frac{\partial \bar{N}_{nd}}{\partial z} & \frac{\partial N_{nd}}{\partial r} \\ \frac{\bar{N}_1}{r} & 0 & \dots & \frac{\bar{N}_{nd}}{r} & 0 \end{bmatrix} \quad (14.25)$$

and

$$\frac{\bar{N}_i}{r} = r_i \frac{N_i}{R} \quad (14.26)$$

$$\frac{\partial \bar{N}_i}{\partial z} = \frac{r_i}{R} \frac{\partial N_i}{\partial z} \quad (14.27)$$

$$\frac{\partial \bar{N}_i}{\partial r} = -r_i \frac{N_i}{R} + 2r_i \frac{\partial N_i}{\partial R} \quad (14.28)$$

### *The nodal force - nodal velocity relationship*

The application of the principle of virtual displacement to an element in the original coordinates (r,z) can be used to give the following nodal force-nodal velocity relationship, which may be expressed in terms of the variables in the generalised coordinates (R,z) as follows:

$$\dot{\mathbf{P}}^e = \pi \int \int_{V^e} \mathbf{B}_n^T \dot{\mathbf{a}} \, dR dz = \mathbf{K}_n \mathbf{a}^e \quad (14.29)$$

where the nodal force vector is defined by

$$\dot{\mathbf{P}}^e = [(2\pi r p_h)_1, (2\pi r p_v)_1, \dots, (2\pi r p_h)_{nd}, (2\pi r p_v)_{nd}]^T \quad (14.30)$$

in which  $p_h$  and  $p_v$  represent nodal force increments per unit length in radial and axial directions respectively. The element stiffness matrix  $\mathbf{K}_n$  is given by

$$\mathbf{K}_n = \pi \int \int_{(\alpha, \beta)} \mathbf{B}_n^T \mathbf{D}^{ep} \mathbf{B}_n \det J \, d\alpha d\beta \quad (14.31)$$

where  $\mathbf{D}^{ep}$  is the elastic-plastic stress strain matrix and  $J$  is the Jacobian of the transformation from (R, z) to ( $\alpha, \beta$ ) coordinates.

### *The nodal force vectors*

Following the procedure of Yu (1990) and Yu *et al.* (1993) for the 6-noded triangle, we can derive the general expressions for the following three types of nodal force vectors that are valid for all axisymmetric displacement elements.

#### (a) Residual Stresses

By using equation (14.29), the element nodal force vector due to a residual stress vector  $\sigma_0$  is:

$$\mathbf{P}^e_{\sigma_0} = \pi \int \int_{(\alpha, \beta)} \mathbf{B}_n^T \sigma_0 \det J \, d\alpha d\beta \quad (14.32)$$

#### (b) Body Forces

The body forces per unit volume in the radial and axial directions are defined by  $b_r$  and  $b_z$  respectively. The corresponding nodal force vector is obtained by applying the virtual work principle to an element:

$$\mathbf{P}^e_b = \pi \int \int_{(\alpha, \beta)} \mathbf{N}_n^T \mathbf{b} \det J \, d\alpha d\beta \quad (14.33)$$

where the body force vector  $\mathbf{b} = [b_r, b_z]^T$ .

(c) Surface Tractions

Applying the virtual displacement principle to an element such as the one shown in Figure 14.8, the equivalent nodal force vector may be shown to be:

$$\mathbf{P}_s^e = 2\pi \int_{\xi} N_n^T r \begin{bmatrix} \frac{q}{2r} \frac{\partial R}{\partial \xi} - p \frac{\partial z}{\partial \xi} \\ q \frac{\partial z}{\partial \xi} + p \frac{\partial R}{2r \partial \xi} \end{bmatrix} d\xi \quad (14.34)$$

where the shape function matrix  $N_n$  depends on element types and the number of nodes per side for the element upon which the surface traction is applied.  $\xi$  is the one-dimensional coordinate along the loaded element side whose values are zero at the middle point of the element side, and  $-1$  and  $+1$  at two end points.

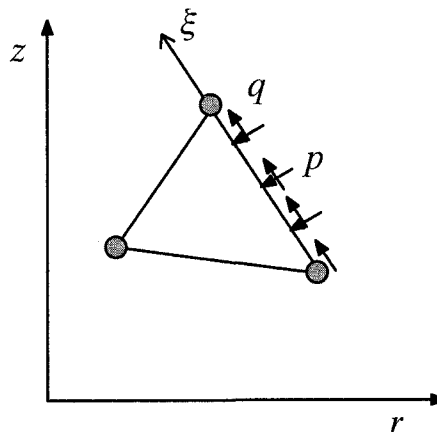


Figure 14.8: Calculation of nodal force vectors due to distributed surface tractions

#### 14.3.5 Implementation in a standard finite element code

This section details the way by which the new finite element formulations described in the previous section can be implemented in a standard finite element program. Specific examples of where the modification is needed to the conventional finite element code are given below.

##### *Discretization of region and transformation of coordinates*

The new finite element formulations presented here are based on the use of the generalized coordinates  $(R, z)$ , where  $R = r^2$ . Thus, any mesh to be analysed with the

new displacement interpolation functions must first be transformed into the generalised coordinates. Although two alternatives exist (e.g. Yu *et al.*, 1993), the following method, that has been found to be entirely satisfactory and also very easy to implement, will be presented here:

- (1) For each element, the corner nodes are directly transformed into  $(r,z)$  space to  $(R,z)$  space;
- (2) The remaining boundaries are then positioned in  $(R,z)$  coordinates so that they are linearly equidistant between corner nodes;
- (3) Any remaining internal nodes are positioned so that they are linearly equidistant between relevant boundary nodes.

The effect of this transformation is to generate straight sided triangular or rectangular elements, rather than curved sided elements in the generalised  $(R,z)$  space. This is desirable as the element stiffness matrix, as defined by equation (14.31), should be calculated using an element geometry defined in the generalised coordinates  $(R,z)$ .

#### *Modifications to element stiffness matrix calculation*

##### (a) Conventional Element Stiffness Matrix

For axisymmetric loading, the element stiffness is calculated by the following equation:

$$\mathbf{K} = 2\pi \iint_{(\alpha, \beta)} r \mathbf{B}^T \mathbf{D}^{ep} \mathbf{B} \det J \, da \, d\beta \quad (14.35)$$

where the conventional strain-displacement matrix  $\mathbf{B}$  is of the form:

$$\mathbf{B} = \begin{bmatrix} \frac{\partial N_1}{\partial r} & 0 & \dots & \frac{\partial N_{nd}}{\partial r} & 0 \\ 0 & \frac{\partial N_1}{\partial z} & \dots & 0 & \frac{\partial N_{nd}}{\partial z} \\ \frac{\partial N_1}{\partial z} & \frac{\partial N_1}{\partial r} & \dots & \frac{\partial N_{nd}}{\partial z} & \frac{\partial N_{nd}}{\partial r} \\ \frac{N_1}{r} & 0 & \dots & \frac{N_{nd}}{r} & 0 \end{bmatrix} \quad (14.36)$$

The calculations are performed based on the element geometries in the original coordinates  $(r,z)$ .

##### (b) New Element Stiffness Matrix

The new element stiffness is calculated by equation (14.31):

$$\mathbf{K}_n = \pi \int \int_{(\alpha, \beta)} \mathbf{B}_n^T \mathbf{D}^{ep} \mathbf{B}_n \det J \, d\alpha d\beta$$

where the new strain-displacement matrix  $\mathbf{B}_n$  is given by equation (14.25):

$$\mathbf{B}_n = \begin{bmatrix} \frac{\partial \bar{N}_1}{\partial r} & 0 & \dots & \frac{\partial \bar{N}_{nd}}{\partial r} & 0 \\ 0 & \frac{\partial \bar{N}_1}{\partial z} & \dots & 0 & \frac{\partial \bar{N}_{nd}}{\partial z} \\ \frac{\partial \bar{N}_1}{\partial z} & \frac{\partial \bar{N}_1}{\partial r} & \dots & \frac{\partial \bar{N}_{nd}}{\partial z} & \frac{\partial \bar{N}_{nd}}{\partial r} \\ \bar{N}_1 & 0 & \dots & \bar{N}_{nd} & 0 \end{bmatrix}$$

It should be stressed that the calculations for the element stiffness in the new formulations are performed based on the element geometries in the generalised coordinates (R, z).

#### *Modifications to nodal force vector calculation*

The expressions for calculating nodal forces due to residual stresses, body forces and surface tractions are given by equations (14.32)-(14.34) respectively. Since the surface tractions will often be used, the modifications required to calculate the nodal forces due to the surface tractions are given here.

For an application of distributed loads on an element edge, it is necessary to determine the components of the applied forces at each of the nodes along that edge and then assemble each load into the global nodal force vector.

#### (a) Conventional Formulation of Nodal Force Vector Due to Surface Traction

In the conventional formulation of the nodal force vector due to distributed loads, the nodal force vector due to the surface shear and normal tractions of  $q$  and  $p$  is given by:

$$\mathbf{P}_s^e = 2\pi \int_{\xi} N^T r \begin{bmatrix} q \frac{\partial r}{\partial \xi} - p \frac{\partial z}{\partial \xi} \\ q \frac{\partial z}{\partial \xi} + p \frac{\partial r}{\partial \xi} \end{bmatrix} d\xi \quad (14.37)$$

Note that the nodal force vector in the left hand side of the above equation is defined by equation (14.30), and the shape function matrix  $\mathbf{N}$  contains the conventional shape functions.

#### (b) New Formulation of Nodal Force Vector Due to Surface Traction

In the new formulation of the nodal force vector due to distributed loads, the nodal force vector due to the surface tractions (q,p) is given by equation (14.34):

$$\mathbf{P}_s^e = 2\pi \int_{\xi} N_n^T r \begin{bmatrix} \frac{q}{2r} \frac{\partial R}{\partial \xi} - p \frac{\partial z}{\partial \xi} \\ q \frac{\partial z}{\partial \xi} + \frac{p}{2r} \frac{\partial R}{\partial \xi} \end{bmatrix} d\xi$$

where the shape function matrix  $N_n$  contains the modified shape functions. For simplicity, the above equation may also be expressed in terms of the conventional shape functions and in a similar form as (14.37):

$$\mathbf{P}_s^e = 2\pi \int_{\xi} N^T r \begin{bmatrix} \frac{r_i}{r} \left( \frac{q}{2r} \frac{\partial R}{\partial \xi} - p \frac{\partial z}{\partial \xi} \right) \\ q \frac{\partial z}{\partial \xi} + \frac{p}{2r} \frac{\partial R}{\partial \xi} \end{bmatrix} d\xi \quad (14.38)$$

where  $i$  denotes the node number along the element side with applied surface shear and normal tractions of  $q$  and  $p$ .

#### *Summary of the necessary modifications*

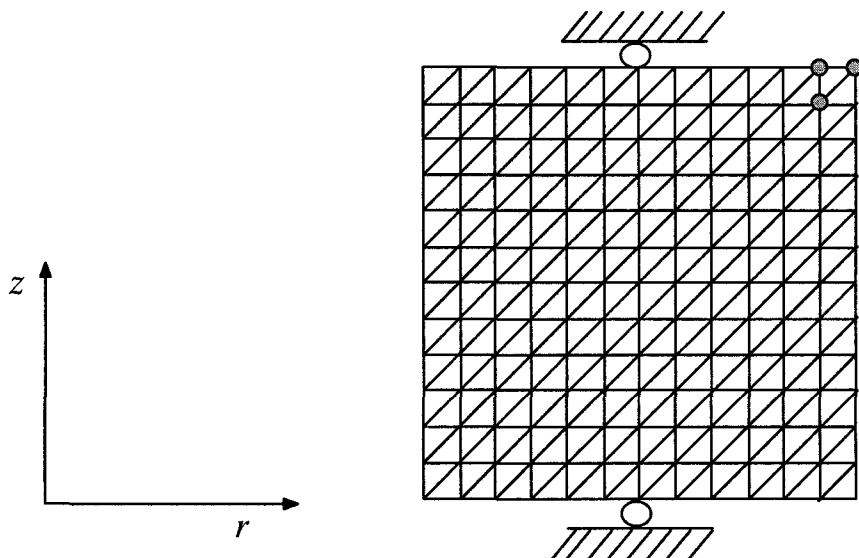
To implement the new finite element formulations into a standard displacement finite element program, the following changes are required:

- (1) Discretization of meshes into the generalized coordinates (R,z);
- (2) Modification to the expression for calculating element stiffness matrix;
- (3) Modification to the expression for calculating nodal force vectors.

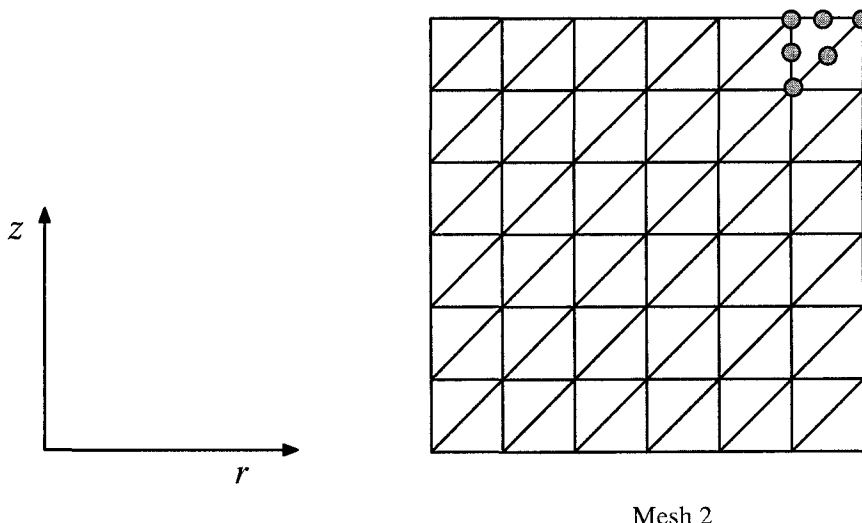
As can be seen in this section, the overall changes to a standard finite element program are not extensive and numerical implementation of the new formulations is therefore relatively straight forward.

#### **14.3.6 Numerical examples**

In this section, some numerical results are presented to illustrate the performance of the conventional and Yu's modified displacement finite elements for axisymmetric stress analysis of incompressible elastic-plastic materials. A thick-walled cylinder subject to a uniform internal pressure has been used as the test problem because exact solutions are available for stress distributions which can be used to compare with the finite element results. The solutions for both purely elastic and elastic-plastic materials are given by Yu and Netherton (2000). Here only elastic-plastic solutions are presented.



Mesh 1



Mesh 2

Figure 14.9: Finite element meshes 1 and 2 (with 3-noded and 6-noded triangles)

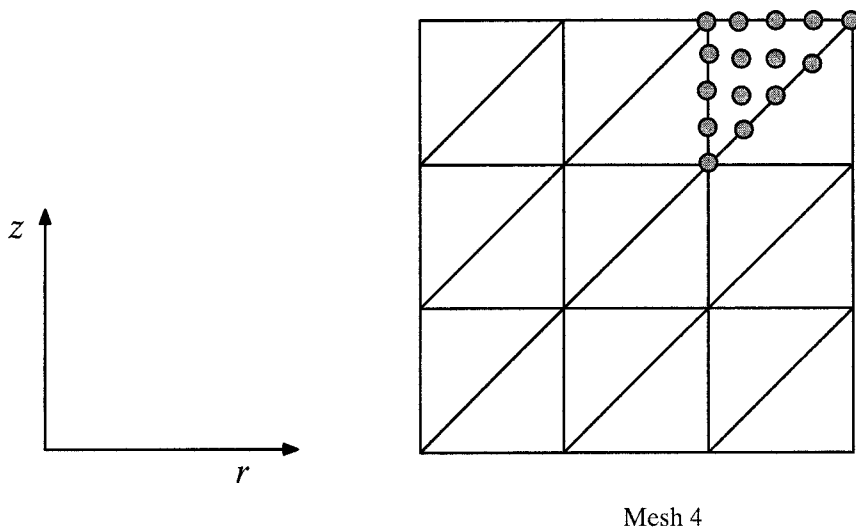
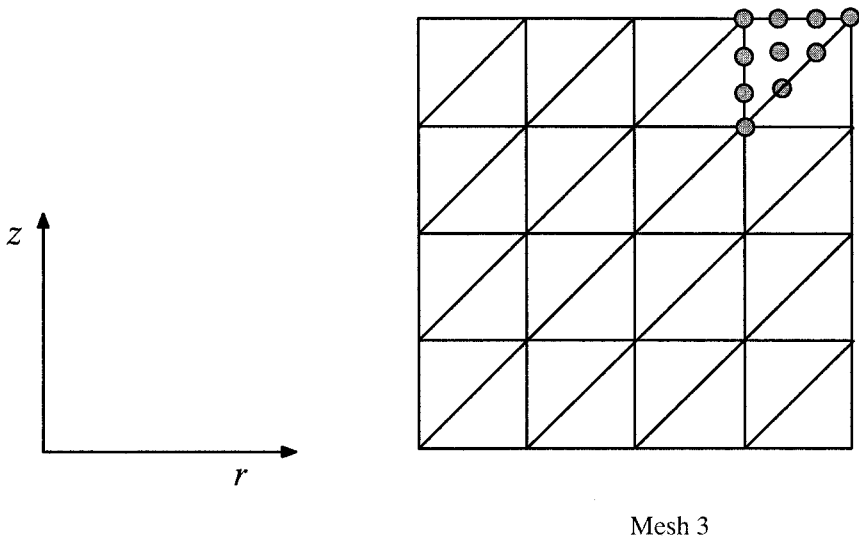
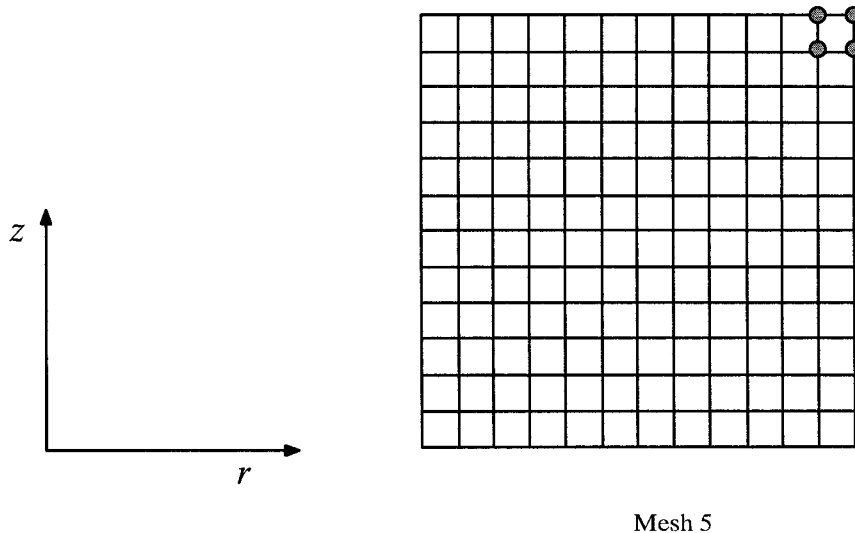
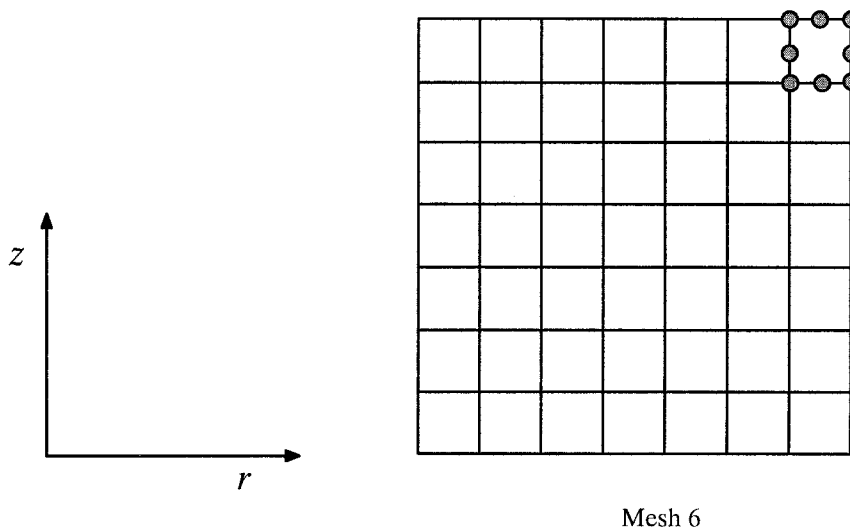


Figure 14.10: Finite element meshes 3 and 4 (with 11-noded and 15-noded triangles)



Mesh 5



Mesh 6

Figure 14.11: Finite element meshes 5 and 6 (with 4-noded and 8-noded rectangles)

### *Elastic-plastic expansion of a thick cylinder*

This example is concerned with the detailed analysis of the stresses within an elastic-plastic thick-walled cylinder subject to internal pressure. The numerical stresses from both conventional and modified formulations will be compared with the closed form solutions given by Hill (1950). The Tresca yield criterion is used to define the onset of plastic yielding. For a cylinder with the ratio of external to internal radii of 2, the value of internal pressure at initial yielding is  $0.75c$ , where  $c$  is the cohesion of the material. The entire cylinder becomes plastic when the internal pressure is equal to  $1.38c$ . In this study, the stresses at each Gauss point when the internal pressure is equal to  $0.95c$  are used to compare with the exact solutions.

Six meshes of different element types with the same or similar number of degrees of freedom as shown in Figure 14.9, Figure 14.10 and Figure 14.11 are used in the analysis so that the performance of different elements can be compared. The geometry of the cylinder is defined by a value of the ratio of external to internal radii of 2. Specifically, Meshes 1-4 consist of 3, 6, 10 and 15-noded triangular elements respectively and have the same number of degrees of freedom of 169. Meshes 5 and 6 are arranged with the 4 and 8-noded rectangular elements and the number of degrees of freedom for Meshes 5 and 6 is equal to 176. Analyses have been carried out for Meshes 1-6 with both the conventional and Yu's modified displacement interpolation functions. In the elastic-plastic analyses, three different values of Poisson's ratio  $\mu$  are used to illustrate the behaviour of the different elements as material incompressibility is approached. For each of the element types, different integration rules are again used to observe the effect of reduced integration.

In order to assess the quality of the calculated stresses, an error is calculated for each analysis. The percentage errors, for both radial and hoop stresses, are defined as:

$$e_r = 100 \times \left[ \frac{1}{n} \sum_{i=1}^{i=n} \left( \frac{\sigma_{ri}^* - \sigma_{ri}}{p_{in}} \right)^2 \right]^{1/2} \quad (14.39)$$

$$e_\theta = 100 \times \left[ \frac{1}{n} \sum_{i=1}^{i=n} \left( \frac{\sigma_{\theta i}^* - \sigma_{\theta i}}{p_{in}} \right)^2 \right]^{1/2} \quad (14.40)$$

where  $p_{in}$  is the applied internal pressure;  $\sigma_{ri}^*$  and  $\sigma_{\theta i}^*$  are the radial and hoop stresses obtained from the finite element solution at Gauss point  $i$ ;  $\sigma_{ri}$  and  $\sigma_{\theta i}$  are the exact values of the radial and hoop stresses at Gauss point  $i$  and  $n$  is the total number of Gauss points in the mesh.

Elastic-plastic results in terms of the percentage errors for Meshes 1-6 with both conventional and modified displacement interpolation functions are presented in

Figure 14.12, Figure 14.13 and Figure 14.14. Generally speaking, the following conclusions can be made:

(a) Effect of Incompressibility and Element Types

For the elements based on the conventional displacement interpolation functions, the errors increase rapidly as the value of Poisson's ratio approaches 0.5. When Poisson's ratio is equal to 0.499995, the errors from the 3, 6 and 10-noded triangular elements and the 4 and 8-noded rectangular elements are in the order of 1000%-10000%. In contrast, the 15-noded triangular element performs significantly better with typical errors of 300% when the 'full integration' is used.

On the other hand, when Yu's modified displacement interpolation functions are used, the errors are largely independent of the value of Poisson's ratio (i.e. incompressibility). The values of the error obtained from all the analyses are less than a few percent when the 'full integration' is used with the 4-noded triangle giving the highest error (around 10%).

(b) Effect of Integration Schemes

For the meshes using the conventional displacement interpolation functions, the errors increase when the number of Gauss integration points increases. For example, when Poisson's ratio is equal to 0.499995, the errors from the 8-noded rectangular elements, when a 4-point integration (i.e. reduced integration) is used, are less than 7%. In contrast, when a 9-point integration (i.e. full integration) is used, the errors are over 6000%. The errors increase with the number of Gauss points used in the calculation of the element stiffness matrix. This suggests that although the reduced integration may be used to improve the stresses at a fewer number of points within the element, it fails to satisfy the incompressibility condition everywhere in the element.

Although the errors for all the elements based on the modified displacement interpolation functions are very small, it is interesting to note that they tend to decrease slightly when the number of Gauss points increases. This is because as the order of integration is increased, the element stiffness matrix is calculated increasingly more accurately without introducing additional incompressibility constraints. This indicates that the incompressibility condition is satisfied everywhere in the element when the new displacement interpolation functions are used.

### 14.3.7 Conclusions

The theoretical criterion originally developed by Nagtegaal *et al.* (1974) has been used to assess the suitability of displacement finite elements when used to analyse incompressible materials. It was found that the 3, 6, 10, 15-noded triangular ele-

ments and the 8-noded rectangle are able to satisfy the Nagtegaal criterion under axisymmetric loading conditions provided that the new displacement interpolation functions proposed by Yu (1990, 1991) are used. Yu's new displacement interpolation functions can be used in conjunction with various triangular and rectangular displacement elements. It has been shown that the new formulations can be readily implemented in an existing displacement-based finite element code, with only few changes to expressions for the shape function matrix and nodal force vectors. The results of the numerical analyses of elastic-plastic incompressible behaviour confirm the theoretical predictions. A detailed comparison between the numerical and analytical stresses indicates that when the incompressibility condition is approached, most conventional displacement finite elements failed completely in predicting the stresses, while the new finite element formulations give a very high accuracy in the calculated stresses.

mesh	nd	Ng	$\mu = 0.125$	$\mu = 0.495$		$\mu = 0.499995$		
			error		error		error	
			$e_r$ (%)	$e_\theta$ (%)	$e_r$ (%)	$e_\theta$ (%)	$e_r$ (%)	$e_\theta$ (%)
1	3	1	2.4	2.4	53.3	52.6	188.5	188.0
1	3	3	4.2	3.5	128	127	5050	5046
1(m)	3	1	1.1	1.1	0.6	0.6	0.9	0.9
1(m)	3	3	1.8	1.8	1.6	1.7	1.5	1.5
2	6	3	0.2	0.2	2.8	2.7	5.1	5.0
2	6	6	0.4	0.3	13.2	13.1	7951	7948
2(m)	6	3	0.1	0.1	0.2	0.2	0.2	0.3
2(m)	6	6	0.1	0.2	0.3	0.4	0.4	0.4

*Note: nd = number of nodes per element*

*Ng = number of integration points used per element*

Figure 14.12: Errors of finite element analysis of elastic-plastic cylinder expansion for Meshes 1 and 2

mesh	nd	Ng	$\mu = 0.125$		$\mu = 0.495$		$\mu = 0.499995$	
			error		error		error	
			$e_r$ (%)	$e_\theta$ (%)	$e_r$ (%)	$e_\theta$ (%)	$e_r$ (%)	$e_\theta$ (%)
3	10	6	0.2	0.2	0.4	0.4	0.6	0.5
3	10	12	0.6	0.5	1.6	1.6	1306	1306
3	10	16	0.6	0.4	2.0	2.0	1526	1526
3	10	25	0.5	0.4	2.4	2.3	1697	1697
3(m)	10	6	0.2	0.2	0.2	0.2	0.3	0.3
3(m)	10	12	0.6	0.5	0.5	0.5	0.5	0.5
3(m)	10	16	0.6	0.4	0.5	0.5	0.5	0.5
3(m)	10	25	0.5	0.5	0.5	0.5	0.6	0.6
4	15	6	1.2	3.8	1.2	3.8	1.2	3.8
4	15	12	0.4	0.5	0.3	0.3	57.2	57.3
4	15	16	0.8	0.5	0.5	0.5	294.1	294.2
4	15	25	0.7	0.4	0.4	0.5	311.8	311.9
4(m)	15	6	4.2	7.4	4.4	7.6	4.4	7.6
4(m)	15	12	0.6	0.5	0.5	0.5	0.5	0.6
4(m)	15	16	0.7	0.5	0.6	0.6	0.6	0.6
4(m)	15	25	0.6	0.4	0.5	0.5	0.5	0.5

*Note: nd = number of nodes per element*

*Ng = number of integration points used per element*

Figure 14.13: Errors of finite element analysis of elastic-plastic cylinder expansion for Meshes 3 and 4

mesh	nd	Ng	$\mu = 0.125$		$\mu = 0.495$		$\mu = 0.499995$	
			error		error		error	
			$e_r$ (%)	$e_\theta$ (%)	$e_r$ (%)	$e_\theta$ (%)	$e_r$ (%)	$e_\theta$ (%)
5	4	4	6	8	142.4	141.5	3825	3819
5	4	9	6.4	8.2	156	155	4190	4184
5	4	16	6.5	8.3	161	160	4338	4331
5	4	25	6.6	8.3	164	163	4417	4411
5(m)	4	4	4.5	7.3	6.7	9.3	9	11.2
5(m)	4	9	4.6	7.4	7.1	9.6	9.7	11.7
5(m)	4	16	4.7	7.5	7.3	9.7	9.9	11.9
5(m)	4	25	4.8	7.5	7.4	8.3	10.1	12
6	8	4	3.2	6.9	3.2	7	3.3	7.1
6	8	9	3.2	7.1	11	12	6008	6004
6	8	16	3.2	7.1	12.4	13.1	6794	6789
6	8	25	3.3	7.1	13	13.5	7360	7354
6(m)	8	4	3.2	6.9	3.2	7.0	3.4	7.1
6(m)	8	9	3.1	7.1	3.1	7.1	3.1	7.1
6(m)	8	16	3.1	7.1	3.1	7.2	3.2	7.2
6(m)	8	25	3.2	7.2	3.2	7.1	3.2	7.2

Note:  $nd$  = number of nodes per element

$Ng$  = number of integration points used per element

Figure 14.14: Errors of finite element analysis of elastic-plastic cylinder expansion for Meshes 5 and 6

## 14.4 SOLUTION SCHEMES FOR LOAD-DISPLACEMENT EQUATIONS

As discussed in an earlier section, there are two systems of nonlinear equations that need to be solved in a nonlinear finite element analysis. They include the load-displacement equation at the structural level and stress-strain relations at the element level (i.e. at the integration points). The methods that have been used to solve the nonlinear governing load-displacement equation may be broadly classified as either iterative or incremental (e.g. Crisfield, 1991; Abbo and Sloan, 1996). Iterative schemes solve the governing equation by applying unbalanced forces, computing the corresponding displacement increments and iterating until the drift from equilibrium is tolerable. Examples of iterative schemes are Newton-Raphson, modified Newton-Raphson, and initial stress methods. Incremental schemes treat the governing equations as a system of ordinary differential equations and involve no iteration as the solution is generated using a series of piece-wise linear steps which approximate the nonlinear load-displacement curve of the structure.

### 14.4.1 Incremental solution strategy

Assume that the governing load-displacement equation is written as follows

$$\mathbf{P} = \mathbf{K}(\mathbf{U}) \mathbf{U} = \left(\frac{d\mathbf{P}}{d\mathbf{U}}\right) \mathbf{U} \quad (14.41)$$

where  $\mathbf{K}$  is the global stiffness matrix that depends on the level of displacement for a nonlinear problem. As shown in Figure 14.15, an incremental solution to the governing equation involves applying a large number of small load increments and repeated application of the following equation

$$\Delta \mathbf{U}_i = \left(\frac{d\mathbf{P}}{d\mathbf{U}}\right)^{-1} \Delta \mathbf{P}_i \quad (14.42)$$

As can be clearly seen from Figure 14.15, the incremental solution strategy is accurate only if the number of load increments is sufficiently large. In other words, the load increments used must be small enough for the piece-wise approximation to be sufficiently close to the real load-displacement curve.

### 14.4.2 Iterative solution strategy

To use an iterative solution strategy, the governing load-displacement equation is rewritten as follows

$$g(\mathbf{U}) = \mathbf{K}(\mathbf{U}) \mathbf{U} - \mathbf{P} = 0 \quad (14.43)$$

where  $\mathbf{K}$  is the global stiffness matrix that depends on the level of displacement for a nonlinear program. As shown in Figure 14.16, an iterative solution to the govern-

ing equation involves finding a displacement solution that would satisfy equation (14.43) using the well-known Newton-Raphson iterative technique. For a given load level, the procedure is used to determine a better solution  $\mathbf{U}_{i+1}$  from an earlier estimate  $\mathbf{U}_i$  for displacements

$$\mathbf{U}_{i+1} = \mathbf{U}_i - \left( \frac{dg_i}{d\mathbf{U}} \right)^{-1} g_i(\mathbf{U}_i) \quad (14.44)$$

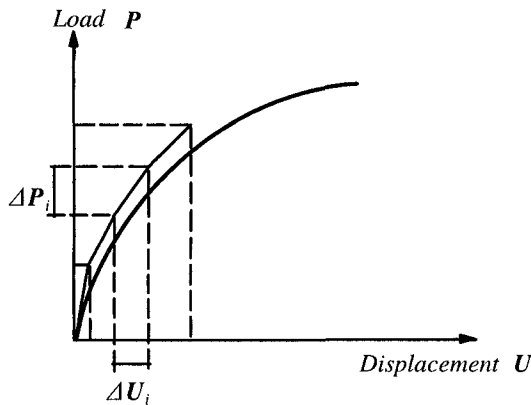


Figure 14.15: An incremental solution to nonlinear load-displacement equations

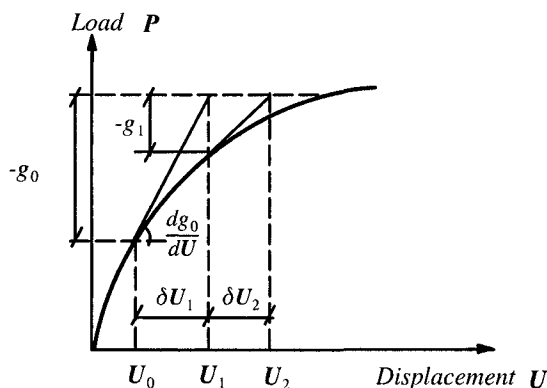


Figure 14.16: An iterative solution to nonlinear load-displacement equations (Newton-Raphson scheme)

The Newton-Raphson procedure is generally robust but is relatively expensive as at each estimate for the displacement field, the stiffness matrix  $dg_i/dU$  needs to be calculated. To reduce the computational cost, a modified Newton-Raphson procedure, shown in Figure 14.17, may be used.

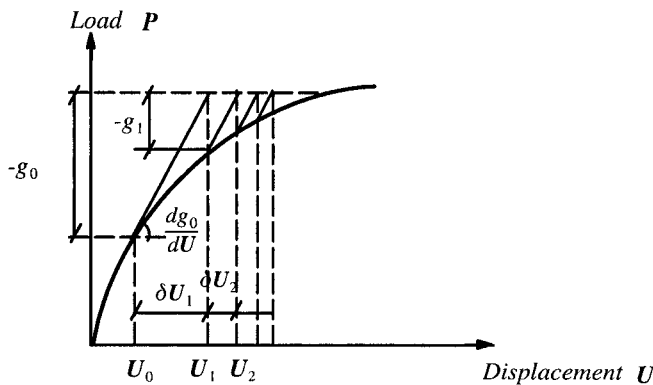


Figure 14.17: An iterative solution to nonlinear load-displacement equations (modified Newton-Raphson scheme)

It is noted that it is possible that the Newton-Raphson type of solution procedures may also not converge, particularly when the behaviour is strongly nonlinear. If this happens, some stabilising measures, such as line searches or arc length control, will have to be used (e.g. Crisfield, 1991, 1997).

#### 14.4.3 Incremental solution strategy with automatic step size control

##### *Explicit Incremental Methods*

As discussed earlier, the load step size must be very small for the incremental solution procedure to be accurate. However selecting a suitable step size does provide a challenge particularly to those who are not very experienced in nonlinear analysis. To help overcome this potential problem, Abbo and Sloan (1996) proposed an incremental solution procedure with automatic step size control. The integration process selects each step so that the local truncation error in the computed displacements is below a prescribed value. The attractive feature of this revised strategy is that by automatically controlling the load path, the load path error in the resulting final displacements can be constrained to be close to a user-specified tolerance.

For each load increment the system of differential equations to be solved may be expressed in rate form as follows

$$\dot{\mathbf{U}} = [\mathbf{K}(\mathbf{U})]^{-1} \dot{\mathbf{P}} = [\mathbf{K}(\mathbf{U})]^{-1} \frac{\Delta \mathbf{P}}{\Delta t} \quad (14.45)$$

where  $\mathbf{K}$  is the global tangential stiffness matrix that depends on the level of displacement for a nonlinear problem. If we introduce a dimensionless time  $T$ , such that

$$T = \frac{t - t_0}{\Delta t} \quad (14.46)$$

where  $t_0$  and  $t_0 + \Delta t$  are the time at the start and end of the current load increment and it is clear  $0 \leq T \leq 1$ . Using (14.46), equation (14.45) can be re-written as follows:

$$\frac{d\mathbf{U}}{dT} = [\mathbf{K}(\mathbf{U})]^{-1} \Delta \mathbf{P} \quad (14.47)$$

which is of the form of a classical initial value problem since  $\Delta \mathbf{P}$  is known. The simplest method for solving such a system of equations is the first-order forward Euler scheme. For a given displacement vector  $\mathbf{U}_0$  at the start of the increment, the forward Euler scheme gives the displacement at the end of an increment as follows

$$\mathbf{U} = \mathbf{U}_0 + [\mathbf{K}(\mathbf{U}_0)]^{-1} \Delta \mathbf{P} \quad (14.48)$$

This simple approach is however only accurate when the load step is very small. As noted by Sloan (1981), the accuracy of this simple approach can be improved greatly by computing the unbalanced forces at the end of each load increment and adding to the applied load for the next load increment according to

$$\mathbf{U} = \mathbf{U}_0 + [\mathbf{K}(\mathbf{U}_0)]^{-1} [\Delta \mathbf{P} + \mathbf{P}^{unb}(\mathbf{U}_0)] \quad (14.49)$$

Of course, the accuracy of the above procedure can be further improved by dividing the applied load increment into  $N$  subincrements of equal size. In this case, Equation (14.49) is replaced by the recurrence relationship with  $i = 1, 2, \dots, N$ :

$$\mathbf{U}_i = \mathbf{U}_{i-1} + [\mathbf{K}(\mathbf{U}_{i-1})]^{-1} [\Delta \mathbf{P}_i + \mathbf{P}^{unb}(\mathbf{U}_{i-1})] \quad (14.50)$$

in which  $\Delta \mathbf{P}_i = \Delta \mathbf{P} \Delta T_i$  and  $\Delta T_i = 1/N$ .

#### *Modified Euler scheme with adaptive load substepping*

As discussed by Abbo (1997) and Abbo and Sloan (1996), an even better procedure than what is described by (14.50) is to use an adaptive integration scheme, where the load subincrement size is automatically chosen to ensure that the local truncation error is near a specified tolerance. The key idea behind this type of scheme is to use two integration schemes, whose order of accuracy differs by one, to predict the solution at the end of each step. The difference between these two solutions provides an estimate of the local truncation error for the current load step size.

Abbo (1997) and Abbo and Sloan (1996) described a modified Euler scheme with adaptive load substepping. The essence of this scheme is given here as an example of substepping methods. For clarity, the presentation ignores the effect of unbalanced loads in this example although it can also be included.

For a load increment  $\Delta \mathbf{P}$ , we will divide it into  $N$  substeps (not equal size) for integration so that

$$\Delta \mathbf{P}_i = \Delta \mathbf{P} \Delta T_i \quad (14.51)$$

$$\sum_{i=1}^N \Delta T_i = 1 \quad (14.52)$$

We now use the Euler and modified Euler formulae to estimate the displacements as follows

$$\Delta \mathbf{U}_1 = [\mathbf{K}(\mathbf{U}_{i-1})]^{-1} \Delta \mathbf{P}_i \quad (14.53)$$

$$\Delta \mathbf{U}_2 = [\mathbf{K}(\mathbf{U}_{i-1} + \Delta \mathbf{U}_1)]^{-1} \Delta \mathbf{P}_i \quad (14.54)$$

and therefore

$$\mathbf{U}_i = \mathbf{U}_{i-1} + \Delta \mathbf{U}_1 \quad (14.55)$$

$$\bar{\mathbf{U}}_i = \mathbf{U}_{i-1} + \frac{1}{2}(\Delta \mathbf{U}_1 + \Delta \mathbf{U}_2) \quad (14.56)$$

If we define the following difference between the two displacement solutions

$$\| \mathbf{E}_i \| = \frac{1}{2} \| (\Delta \mathbf{U}_2 - \Delta \mathbf{U}_1) \| \quad (14.57)$$

where any convenient norm may be used, this difference represents the absolute truncation error, that can be normalised by dividing  $\| \bar{\mathbf{U}}_i \|$ , so that we have a dimensionless relative error measure

$$R_r = \frac{\| \mathbf{E}_i \|}{\| \bar{\mathbf{U}}_i \|} \quad (14.58)$$

The current load substep  $\Delta T_i$  will be accepted if the relative error measure is less than a user-specified tolerance,  $TOL$ , and rejected otherwise. In both cases, the size of the next time step is given by

$$\Delta T_{i+1} = m \Delta T_i \quad (14.59)$$

and the factor  $m$  is estimated using the following equation (Abbo and Sloan, 1996):

$$m = 0.7 \sqrt{\frac{TOL}{R_r}} \quad \text{and} \quad 0.1 \leq m \leq 1.1 \quad (14.60)$$

## 14.5 INTEGRATION OF STRESS-STRAIN EQUATIONS

## 14.5.1 Elastic-plastic stress-strain relationship

In finite element analysis of plastic materials, a key step is to update the stress state at each Gauss point. At the end of each load increment, the corresponding strain increments at each Gauss point can be determined. If such strain increments cause no plastic yielding, the stress increments can be determined by the following simple (often linear) elastic stress-strain relationship:

$$\dot{\sigma} = D_e \dot{\epsilon} \quad (14.61)$$

On the other hand, if such strain increments cause plastic yielding, the stress increments can be expressed by the following elastic-plastic stress-strain relationship:

$$\dot{\sigma} = D_{ep} \dot{\epsilon} \quad (14.62)$$

If we introduce a pseudo time,  $T$ , as defined by (14.46), the following initial value problem will be obtained

$$\frac{d\sigma}{dT} = D_{ep} \Delta\epsilon \quad (14.63)$$

which is in the same form as the load-displacement relation (14.47). In the above equation, the strain increments  $\Delta\epsilon$  are known and the elastic-plastic stiffness matrix  $D_{ep}$  is a function of stresses and also the hardening parameter for a hardening plasticity. The above equation can be further written as follows

$$\frac{d\sigma}{dT} = D_{ep} \Delta\epsilon = [D_e - \frac{D_e b a^T D_e}{h + a^T D_e b}] \Delta\epsilon = \Delta\sigma_e - \Delta\lambda D_e b \quad (14.64)$$

in which  $D_e$  is the elastic stress-strain stiffness matrix, and  $a = \partial f / \partial \sigma$ ,  $b = \partial g / \partial \sigma$  where  $f$  and  $g$  represent the yield function and plastic potential respectively. The plastic multiplier  $\Delta\lambda$  is given by

$$\Delta\lambda = \frac{a^T D_e \Delta\epsilon}{h + a^T D_e b} = \frac{a^T \Delta\sigma_e}{h + a^T D_e b} \quad (14.65)$$

If the hardening parameter is denoted by  $\alpha$ , the hardening modulus  $h$  in (14.64) and (14.65) can be obtained as shown in Chapter 3:

$$h = - \frac{\partial f}{\partial \alpha} \frac{\partial \alpha}{\partial \epsilon^p} \frac{\partial g}{\partial \sigma} \quad (14.66)$$

Two classes of methods have been used to integrate the nonlinear elastic-plastic stress-strain relationship (14.63). They are explicit methods (e.g. Sloan, 1987; Abbo, 1997) and implicit methods (e.g. Crisfield, 1991; Simo and Hughes, 1998).

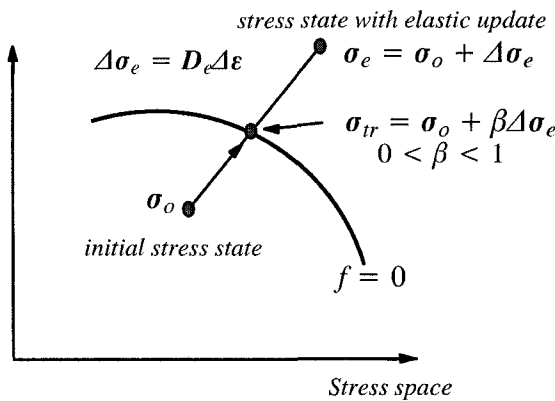


Figure 14.18: Yield surface intersection when material makes an elastic to plastic transition

#### 14.5.2 Explicit integration method

##### *Determination of initial yielding - yield surface intersection*

In using the explicit integration methods, it is necessary to locate the yield surface intersection when materials make a transition from a purely elastic behaviour to an elastic-plastic behaviour during the current load increment. In other words, the material is elastic at the start of the increment and the stress update based on the elastic stiffness matrix will give a stress state that lies outside of the yield surface. Therefore we need to find the portion of the strain increments that only causes elastic behaviour and the remaining portion of the strain increments will cause elastic-plastic deformation, see Figure 14.18. It is noted that only for the portion of the strain increments that causes elastic-plastic behaviour we can use (14.63) to update stresses.

The transition from elastic loading to plastic loading occurs as long as

$$f(\sigma_0, \alpha_0) < 0 \quad (14.67)$$

$$f(\sigma_e, \alpha_0) > 0 \quad (14.68)$$

The problem of locating the stress state at the intersection point,  $\sigma_{tr}$ , is to find the scalar quantity  $\beta$  that satisfies the following nonlinear equation

$$f(\sigma_0 + \beta \Delta \sigma_e, \alpha_0) = 0 \quad (14.69)$$

which can be solved by using the Newton-Raphson method (Sloan, 1987). Once the scalar quantity  $\beta$  is determined, the portion of the strain increment that causes plastic deformation is  $\Delta \epsilon_p = (1 - \beta) \Delta \epsilon$ .

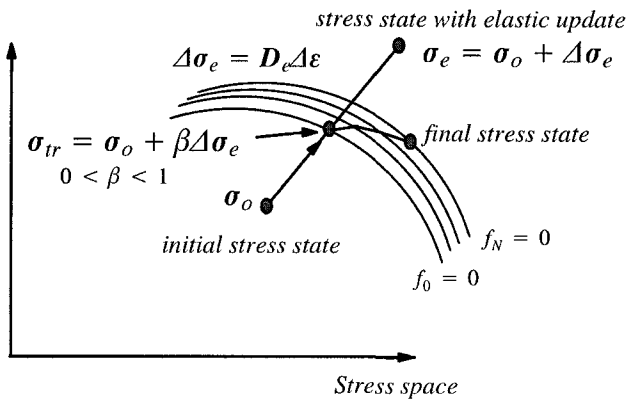


Figure 14.19: Explicit stress update with substepping

### Modified Euler method with substepping

The substepping method to be described here is based on the scheme of Sloan (1987) and Abbo (1997). This approach is attractive because it controls the errors in the stresses and hardening parameter in the numerical integration of stress-strain relations. For an isotropic work-hardening material, the elastic-plastic stress-strain relationship is defined by

$$\frac{d\sigma}{dT} = D_{ep}(\sigma, \alpha) \quad \Delta\epsilon_p = D_{ep}(\sigma, \alpha) (1 - \beta) \Delta\epsilon \quad (14.70)$$

where the hardening parameter  $\dot{\alpha} = \dot{W}_p$  and its evolution with time can be shown to be of the following form

$$\frac{d\alpha}{dT} = \Delta\lambda \quad a^T b \quad (14.71)$$

in which the plastic multiplier  $\Delta\lambda$  is given by (14.65). Therefore

$$\Delta\lambda = \frac{a^T D_e (1 - \beta) \Delta\epsilon}{h + a^T D_e b} = \frac{a^T (1 - \beta) \Delta\sigma_e}{h + a^T D_e b} \quad (14.72)$$

For a plastic strain increment  $\Delta\epsilon_p$ , we will divide it into  $N$  substeps (not equal size) for integration (Figure 14.19) so that

$$\Delta\epsilon_p^i = \Delta\epsilon_p \Delta T_i \quad (14.73)$$

$$\sum_{i=1}^N \Delta T_i = 1 \quad (14.74)$$

We now use the first order Euler method to estimate the stresses and hardening parameter

$$\sigma_i = \sigma_{i-1} + \Delta\sigma_1 \quad (14.75)$$

$$\alpha_i = \alpha_{i-1} + \Delta\alpha_1 \quad (14.76)$$

where

$$\Delta\sigma_1 = D_{ep}(\sigma_{i-1}, \alpha_{i-1}) \Delta\epsilon_p^i \quad (14.77)$$

$$\Delta\alpha_1 = \Delta\lambda(\sigma_{i-1}, \alpha_{i-1}, \Delta\epsilon_p^i) \sigma_{i-1}^T b(\sigma_{i-1}) \quad (14.78)$$

A more accurate estimate of the stresses and hardening parameter can be obtained using the modified Euler method that gives

$$\bar{\sigma}_i = \sigma_{i-1} + \frac{1}{2}(\Delta\sigma_1 + \Delta\sigma_2) \quad (14.79)$$

$$\bar{\alpha}_i = \alpha_{i-1} + \frac{1}{2}(\Delta\alpha_1 + \Delta\alpha_2) \quad (14.80)$$

in which

$$\Delta\sigma_2 = D_{ep}(\sigma_i, \alpha_i) \Delta\epsilon_p^i \quad (14.81)$$

$$\Delta\alpha_2 = \Delta\lambda(\sigma_i, \alpha_i, \Delta\epsilon_p^i) \sigma_i^T b(\sigma_i) \quad (14.82)$$

If we define the following difference between the two stress solutions

$$\| \epsilon_i \| = \frac{1}{2} \| (\Delta\sigma_2 - \Delta\sigma_1) \| \quad (14.83)$$

where any convenient norm may be used, this difference represents the absolute truncation error, that can be normalised by dividing  $\| \bar{\sigma}_i \|$ , so that we have a dimensionless relative error measure

$$R_r = \frac{\| \epsilon_i \|}{\| \bar{\sigma}_i \|} \quad (14.84)$$

The current load substep  $\Delta T_i$  will be accepted if the relative error measure is less than a user-specified tolerance,  $TOL$ , and rejected otherwise. In both cases, the size of the next time step is given by

$$\Delta T_{i+1} = m \Delta T_i \quad (14.85)$$

and the factor  $m$  is estimated using the following equation (Abbo, 1997):

$$m = 0.9 \sqrt{\frac{TOL}{R_r}} \quad \text{and} \quad 0.1 \leq m \leq 1.1 \quad (14.86)$$

### 14.5.3 Implicit integration method

Crisfield (1991) describes a number of implicit methods for integrating stress-strain relations. In this section, a very simple scheme of this kind is presented.

#### *Elastic stress predictor*

As discussed before, the transition from elastic loading to plastic loading occurs as long as

$$f(\sigma_0, \alpha_0) < 0 \quad (14.87)$$

$$f(\sigma_e, \alpha_0) > 0 \quad (14.88)$$

The stress state obtained using an elastic stress update will lie outside of the yield surface, as shown in Figure 14.20.

#### *Single step backward Euler method*

A single step backward Euler method may be used to return the stress state from the point reached by the elastic stress update. To derive the backward Euler return, the yield function  $f$  is expanded in a truncated Taylor series about  $\sigma_e$  to give

$$f = f_e + \mathbf{a}^T \Delta \sigma + \frac{\partial f}{\partial \alpha} \Delta \alpha \quad (14.89)$$

The stress increment can be determined from the usual equation

$$\Delta \sigma = D_e \Delta \varepsilon - \Delta \lambda D_e \mathbf{b} \quad (14.90)$$

Given the strain increment has all be applied to arrive at the elastic stress predictor, the backward Euler return will involve zero strain increment. Hence from (14.90), we obtain

$$\Delta \sigma = - \Delta \lambda D_e \mathbf{b} \quad (14.91)$$

and

$$\Delta \alpha = \Delta \lambda \sigma_e^T \mathbf{b} \quad (14.92)$$

If we insist that the yield function (14.89) is zero and by using equations (14.90)-(14.91) we have

$$\Delta \lambda = \frac{f_e}{h + \mathbf{a}^T D_e \mathbf{b}} \quad (14.93)$$

and the updated stresses and hardening parameter can then be calculated using the following equations

$$\sigma_1 = \sigma_e - \Delta \lambda D_e \mathbf{b} \quad (14.94)$$

$$\alpha_1 = \alpha_0 + \Delta \lambda \sigma_e^T \mathbf{b} \quad (14.95)$$

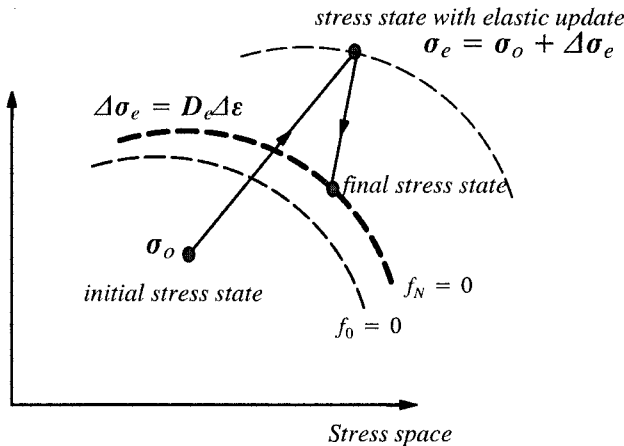


Figure 14.20: Implicit stress update with single step backward Euler method

## 14.6 LARGE DEFORMATION ANALYSIS

### 14.6.1 Introduction

In recent years, there has been growing interest in finite element analysis of large deformation involving soil plasticity. This is because many practical problems in geotechnical engineering are concerned with large deformations. Examples include embankments on soft ground and deep penetration problems (e.g. Burd, 1986; Teh, 1987; Yu, 1990; Walker and Yu, 2006). It is well known that the analysis of large strain soil plasticity problems is much more difficult than small strain analysis. The first difficulty lies in the choice of the appropriate definition for stresses and strains. In the infinitesimal theory of elastic-plastic deformations, it is possible to define strains in a unique and unambiguous way. This is not possible when the deformation becomes large since a variety of coordinate systems may be used which will inevitably lead to different strain definitions. In continuum mechanics, the deformation of a body subject to large displacements is usually described by either a Lagrangian (material) reference system or an Eulerian (spatial) reference system (Malvern, 1969). In some applications, the Lagrangian approach would be more advantageous than an Eulerian formulation since, in the former, the boundary conditions and configuration are well defined. In the latter, the geometric variables are not known *a priori*. In geotechnical engineering, however, the loading proced-

ure often takes the form of addition or removal of material, thus making the definition of the undeformed configuration in the Lagrangian approach less useful.

Indeed in many previous finite deformation studies of geomaterials, an Eulerian approach, based on a mesh representing the current state of deformation, has been preferred (e.g. Carter *et al.*, 1977; Burd, 1986; Teh, 1987; Yu, 1990). This is partly due to the fact that an Eulerian description is well suited to the analysis of material for which the constitutive laws are conveniently expressed in terms of stress and strain rates, as is often the case in geotechnical engineering. An Eulerian approach, however, poses considerable difficulties with moving boundaries and stress boundaries whilst it simplifies the equilibrium equations. It is therefore necessary for an Eulerian approach to make some assumptions regarding configuration changes during each increment.

The method which perhaps gives the most advantages is the updated Lagrangian method in which, after each increment of a calculation, new coordinates of the nodal points and the reference state are updated from the nodal displacements.

For a mathematical description of material behaviour to be consistent within the framework of continuum mechanics, it is necessary that the stress rate used in the constitutive equation is 'objective'. This condition requires that the stress rate must vanish under conditions of rigid body motion. It was shown by Prager (1961) that the definition of 'objectivity' is not sufficiently restrictive to give a unique definition of stress rate. As a result, several different objective stress rates have been proposed (Jaumann, 1911; Truesdell, 1953; Oldroyd, 1950). Amongst these, the Jaumann definition has been more widely used in large deformation computations. This popularity stems from the desirable feature of the Jaumann definition that vanishing of the stress rate implies stationary behaviour of the stress invariants. It should also be noted that some drawbacks for the use of the Jaumann stress rate have been reported. In particular, it is found that the Jaumann stress rate may give rise to physically unrealistic solutions to problems where shear strains are very large (e.g. Dienes, 1979).

#### 14.6.2 Finite element formulations for large deformation

Two key papers on finite element analysis of large deformation are those by Hibbit *et al.* (1971) and McMeeking and Rice (1975). The first paper is concerned with the Lagrangian formulation and the latter is concerned with either a Lagrangian or an Eulerian formulation. In this section we closely follow McMeeking and Rice (1975) and present a general procedure for deriving finite element equations from the virtual work equation using either Lagrangian or Eulerian formulation. A more

detailed treatment of large deformation finite elements can be found in Bathe (1982), Chen and Mizuno (1990) and Crisfield (1991, 1997) among others.

If we denote a material strain tensor by  $\mathbf{e}$  (or  $e_{ij}$ ) that is defined on a coordinate system  $\mathbf{X}$  in the adopted reference state such that the principal directions of  $\mathbf{e}$  coincide with fibres of principal stretch from that state (Malvern, 1969). Any strain measure so defined accords with the small strain  $\boldsymbol{\varepsilon}$  at small displacement gradients and  $\dot{\mathbf{e}}$  is equal to the rate of deformation tensor.

The most widely used material strain tensor is Green strain defined as follows

$$e_{ij}^G = \frac{1}{2}(u_{ij} + u_{ji} + u_{kk}) \quad (14.96)$$

where  $\mathbf{u} = \mathbf{x} - \mathbf{X}$  is the displacement from the reference state and  $u_{ij} = \partial u_i / \partial X_j$ .

Following Hill (1968), we may define a corresponding family of symmetric conjugate stress measures  $\mathbf{s}$  (or  $s_{ij}$ ) so that  $s_{ij}\delta e_{ij}$  is the stress working per unit volume of reference state for arbitrary virtual deformations  $\delta \mathbf{e}$  (or  $\delta e_{ij}$ ). It is well known that the second Piola-Kirchhoff stress  $s_{ij}^{PK}$  is the conjugate to Green strain  $e_{ij}^G$ , where

$$s_{ij}^{PK} = J \frac{\partial X_i}{\partial x_k} \sigma_{kl} \frac{\partial X_j}{\partial x_l} \quad \text{and} \quad J = \det(\frac{\partial \mathbf{x}}{\partial \mathbf{X}}) \quad (14.97)$$

To derive incremental finite element formulations, either Lagrangian or Eulerian, we can start from a virtual work equation in conjugate deformation variables:

$$\int \int \int_{V^0} \delta \mathbf{e}^T \mathbf{s} \, dV^0 = \int \int \int_{V^0} \delta \mathbf{u}^T \mathbf{b} \, dV^0 + \int \int \int_{S^0} \delta \mathbf{u}^T \mathbf{f} \, dS^0 \quad (14.98)$$

where  $\delta \mathbf{u}$  and  $\delta \mathbf{e}$  are associated virtual displacements and strains, the forces are nominal and  $\mathbf{s}$  and  $\mathbf{e}$  are any conjugate measures. Assuming that the vector of nodal displacements is denoted by  $\delta \mathbf{u}_n$ , we have

$$\delta \mathbf{u} = \mathbf{N} \delta \mathbf{u}_n \quad (14.99)$$

in which  $\mathbf{N}$  is known as the shape function matrix. Hence the virtual strain vector can be expressed in terms of the nodal displacement vector

$$\delta \mathbf{e} = \mathbf{L} \delta \mathbf{u} = \mathbf{L} \mathbf{N} \delta \mathbf{u}_n = \mathbf{B} \delta \mathbf{u}_n \quad (14.100)$$

in which  $\mathbf{B}$  is a matrix linking the nodal displacements to the strains within elements. It is noted that this matrix is now a function of  $\delta \mathbf{u} / \partial \mathbf{X}$  that varies with the strain measure adopted. However it becomes identical when the current and reference states coincide. Therefore, in the usual manner, the virtual work equation (14.98) becomes

$$\mathbf{P} = \int \int \int_{V^0} \mathbf{B}^T \mathbf{s} \, dV^0 \quad (14.101)$$

where

$$\mathbf{P} = \int \int \int_{V^0} \mathbf{N}^T \mathbf{b} \, dV^0 + \int \int_{S^0} \mathbf{N}^T \mathbf{f} \, dS^0 \quad (14.102)$$

The incremental form of the virtual work equation (14.101) can be shown to be as follows:

$$\dot{\mathbf{P}} = \int \int \int_{V^0} [\mathbf{B}^T \dot{\mathbf{s}} + \dot{\mathbf{B}}^T \mathbf{s}] \, dV^0 \quad (14.103)$$

in which

$$\dot{\mathbf{P}} = \int \int \int_{V^0} \mathbf{N}^T \dot{\mathbf{b}} \, dV^0 + \int \int_{S^0} \mathbf{N}^T \dot{\mathbf{f}} \, dS^0 \quad (14.104)$$

It is then easy to show that the incremental finite element equilibrium equations are given below

$$\dot{\mathbf{P}} = [\mathbf{K}_c + \mathbf{K}_s] \dot{\mathbf{u}}_n \quad (14.105)$$

where the usual incremental stiffness  $\mathbf{K}_c$  is defined by

$$\mathbf{K}_c = \int \int \int_{V^0} \mathbf{B}^T \mathbf{D} \mathbf{B} \, dV^0 \quad (14.106)$$

and  $\mathbf{D}$  defines the incremental relationship between conjugate stress and strain measures, namely

$$\dot{\mathbf{s}} = \mathbf{D} \dot{\mathbf{e}} \quad (14.107)$$

The second stiffness matrix  $\mathbf{K}_s$  in equation (14.105) depends on initial stress states. If we choose Green strain and second Piola-Kirchhoff stress as measures, then the initial stress stiffness takes a simple form

$$\mathbf{K}_s = \int \int \int_{V^0} [N_k^T]_i s_{ij}^{PK} [N_k]_j \, dV^0 \quad (14.108)$$

which would be the most suitable basis for a Lagrangian method.

#### *Eulerian finite element formulations*

As shown in McMeeking and Rice (1975), an Eulerian finite element formulation can be obtained for any choice of measure by taking the reference state to coincide

instantaneously with the current state. In this case,  $s = \sigma$  and  $\dot{e} = \dot{\epsilon}$  and  $\dot{\epsilon}$  is the rate of deformation tensor (i.e. strain rate). The matrix  $\mathbf{B}$  is therefore the same as for the case of small deformation

$$[B_{ij}] = \frac{1}{2} [N_i]_j + \frac{1}{2} [N_j]_i \quad (14.109)$$

and the finite element equilibrium equation (14.101) becomes

$$\mathbf{P} = \int \int \int_V \mathbf{B}^T \sigma \, dV \quad (14.110)$$

The incremental form of the virtual work equation (14.110) can be obtained as follows:

$$\dot{\mathbf{P}} = \int \int \int_V [\mathbf{B}^T \dot{\sigma} + \dot{\mathbf{B}}^T \sigma] \, dV \quad (14.111)$$

As an example, let us adopt the objective Jaumann stress rate given below

$$\dot{\sigma}_{ij}^J = \dot{\sigma}_{ij} - \sigma_{ik} \dot{\omega}_{jk} - \sigma_{jk} \dot{\omega}_{ik} \quad (14.112)$$

where  $\dot{\omega}_{ij}$  is the skew-symmetric spin tensor. The constitutive equation is then used to link the Jaumann stress rate and the rate of deformation tensor, namely

$$\dot{\sigma}^J = \mathbf{D}^{ep} \dot{\epsilon} \quad (14.113)$$

The objective Jaumann stress rate defined by (14.112) can also be expressed as follows

$$\dot{\sigma}^J = \dot{\sigma} - \mathbf{R} \dot{\epsilon} \quad (14.114)$$

where  $\mathbf{R}$  is a simple matrix. By comparing equations (14.113) and (14.114) we obtain

$$\dot{\sigma} = (\mathbf{D}^{ep} + \mathbf{R}) \dot{\epsilon} \quad (14.115)$$

By using the above equation and the usual procedure, the rate form of the virtual work equation (14.111) can be written in the following form

$$\dot{\mathbf{P}} = [\mathbf{K}_c + \mathbf{K}_s] \dot{\mathbf{u}}_n \quad (14.116)$$

where the usual incremental stiffness  $\mathbf{K}_c$  and the initial stress stiffness are defined by

$$\mathbf{K}_c = \int \int \int_V \mathbf{B}^T (\mathbf{D}^{ep} + \mathbf{R}) \mathbf{B} \, dV \quad (14.117)$$

$$\mathbf{K}_s = \int \int \int_V \mathbf{C} \, dV \quad (14.118)$$

and the matrix  $\mathbf{C}$  can be determined from the following equation

$$\mathbf{C}\dot{\mathbf{u}}_n = \mathbf{B}^T \boldsymbol{\sigma} \quad (14.119)$$

The Eulerian finite element formulation presented here has been applied successfully by Burd (1986) to analyse plane strain unpaved road problems and by Teh (1987) and Yu (1990, 1991) to analyse axisymmetric cone penetration and pressurometer problems. The reader is referred to these references for further details.

## 14.7 NUMERICAL EXAMPLES

In this section, some examples are given on the application of finite elements and advanced plasticity models to the solution of some of the common geotechnical boundary value problems.

### 14.7.1 Finite element analysis of critical state geomaterials

In Chapter 6, we described the critical state concept and a unified model CASM for clay and sand (Yu, 1995, 1998) and its variants. Yu and Khong (2002), Khong and Yu (2002), Khong (2004) and Tan (2006) present a detailed treatment of finite element implementation of CASM into the finite element code CRISP (Britto and Gunn, 1987) together with its application to the analysis of footings, pressurometers, anchors and pavements (Khong, 2004; Yu, 2004) and bonded geomaterials (Tan, 2006). The model CASM has also been implemented into the commercial finite element code ABAQUS using its material subroutine UMAT with application to the analysis of wellbore stability (Xu, 2006) and non-coaxial materials (Yang and Yu, 2006b). Here we only present a few results to illustrate the capability of the CASM models when used in finite element analysis.

#### (a) Analysis of horizontal strip anchors in clay and sand

In this sub-section, a finite element study of horizontal anchors subject to uplift forces is presented. The soil is modelled by CASM. The effects of the depth to width ratio of the anchor and the stress history of the soil are examined. The analyses are displacement-controlled and the applied vertical load is calculated from the nodal reaction forces.

A general layout of the anchor problem is shown Figure 14.21. The ultimate pullout capacity of an anchor depends on factors such as initial stresses, soil stress

history (i.e. OCR for clay and state parameter for sand), soil strength and the depth to width ratio (H/B).

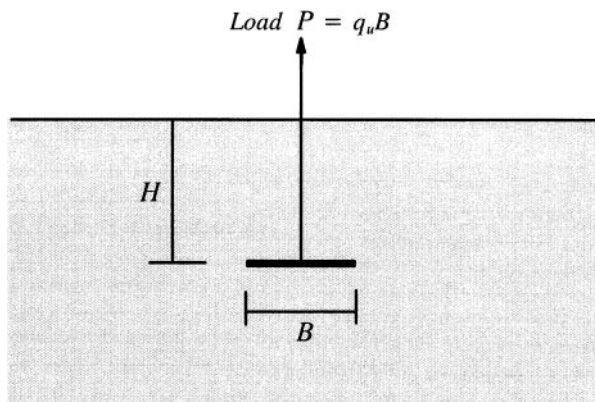


Figure 14.21: A strip plate anchor subject to an uplift force

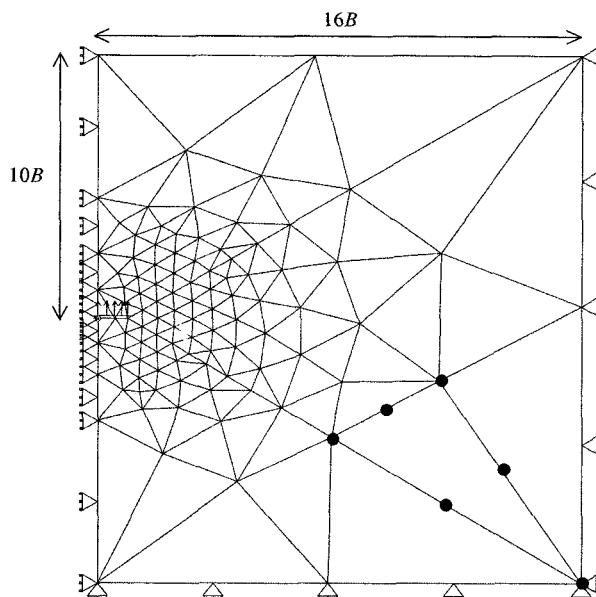


Figure 14.22: A finite element mesh for anchor analysis

For simplicity, the anchor is assumed to be very thin and rigid. The initial stress state is assumed to be isotropic with a value of  $\sigma_0$ . The finite element mesh used in the calculation for the case of  $H/B=10$  is shown in Figure 14.22.

*Solutions for plate anchors in London clay under undrained conditions*

For London clay, the model constants for CASM are given below

$$M = 0.89; \lambda = 0.161; \kappa = 0.062; \mu = 0.3; \Gamma = 2.759; n = 2; r = 2.718$$

The finite element analyses have been performed using various embedment ratios ( $H/B=1$  to 12) and soil stress histories ( $OCR=1$  to 20). The uplift load-displacement curves for various cases are shown in Figure 14.23. It is evident that the anchor behaviour (both deformation and stability aspects) depends on both anchor embedment ratio  $H/B$  and soil stress history  $OCR$ .

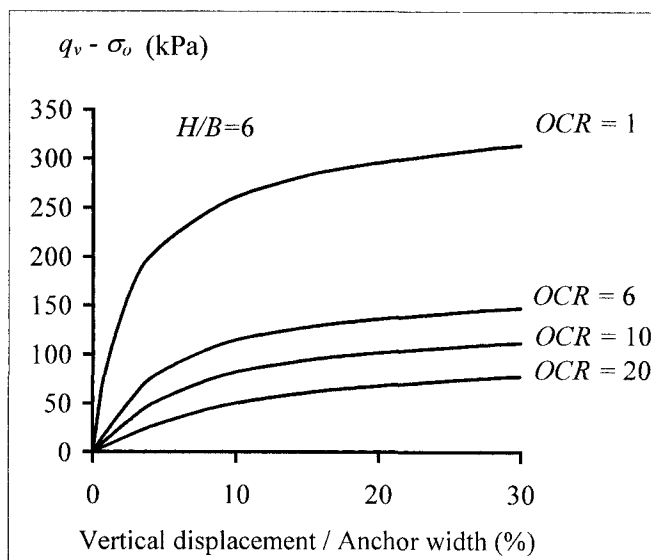
*Solutions for plate anchors in Ticino sand under drained conditions*

For Ticino sand, the model constants for CASM are given below

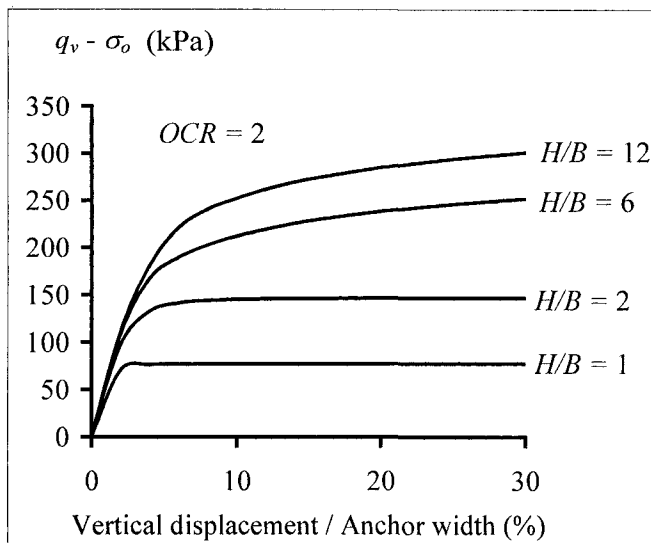
$$M = 1.3; \lambda = 0.04; \kappa = 0.01; \mu = 0.3; \Gamma = 1.986; n = 2; r = 4$$

The finite element analyses for anchors embedded in Ticino sand have been performed using various embedment ratios ( $H/B=1$  to 12) and initial state parameters ( $\xi_0 = 0.02, 0, -0.02, -0.04, -0.06, -0.08$ ). The uplift load-displacement curves for various cases are shown in Figure 14.24. It is evident that the anchor behaviour (both deformation and stability aspects) depends on both anchor embedment ratio  $H/B$  and soil initial state parameter  $\xi_0$ .

A summary of the anchor pull-out capacity in sand is shown in Figure 14.25. The normalised pull-out limit load has been plotted as a function of the embedment ratio and initial state parameter. It is clear that for a given initial state parameter, the pull-out capacity increases approximately linearly with the embedment ratio. On the other hand, for a given embedment ratio, the pull-out capacity decreases with the initial state parameter.

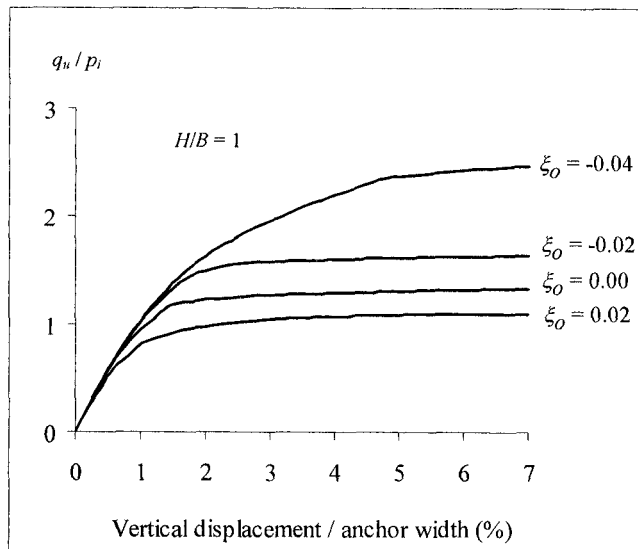


(a)

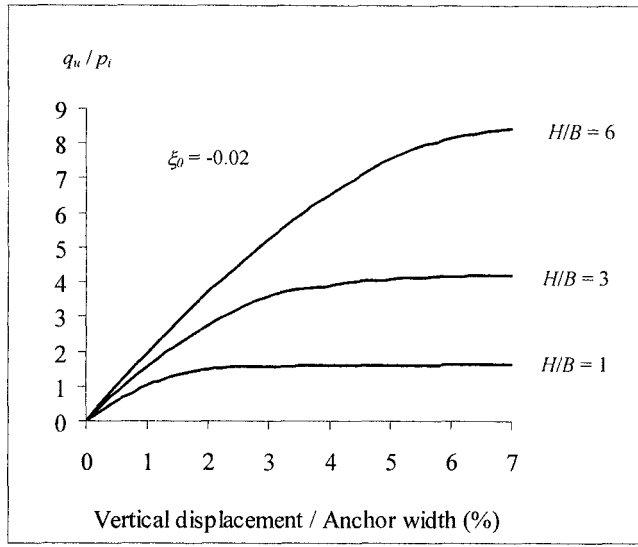


(b)

Figure 14.23: Uplift load-displacement curves for strip anchors in London clay

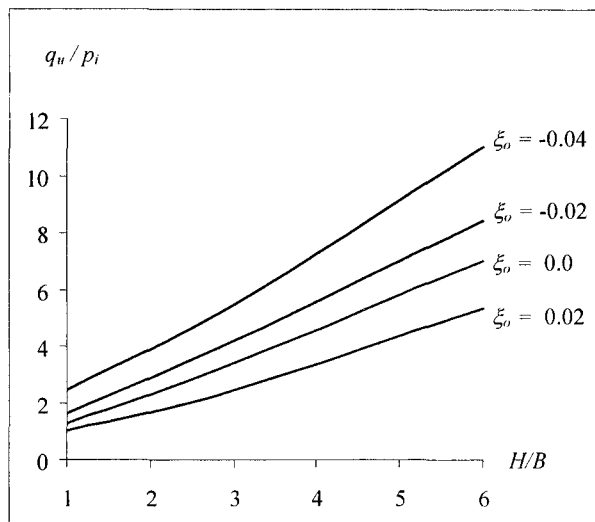


(a)

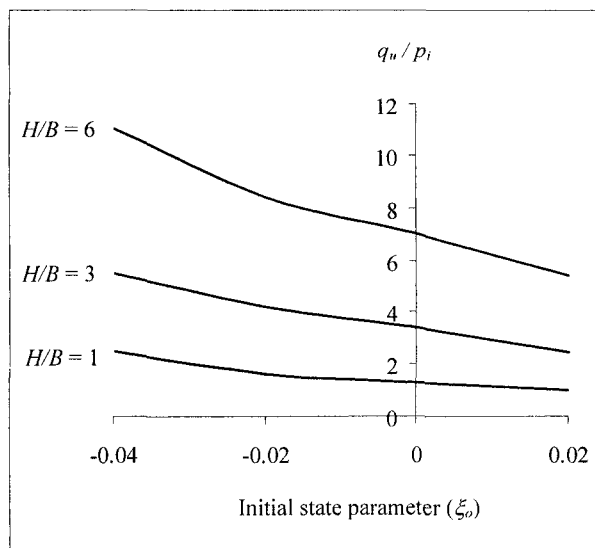


(b)

Figure 14.24: Uplift load-displacement curves for strip anchors in Ticino sand



(a)



(b)

Figure 14.25: Pull-out capacity factor versus embedment ratio and initial state parameter for anchors in Ticino sand

### (b) Analysis of pressuremeter tests in clay and sand

In this sub-section, a finite element study of pressuremeter tests in soils is presented. The soil is modelled by CASM. The effects of the pressuremeter geometry and the stress history of the soil are examined.

The finite element mesh used was made up of 15-noded triangular elements as this element was shown earlier in this chapter to be able to give accurate results for axisymmetric problems. Due to symmetry, only half of the soil mass needs to be modelled. A schematic diagram of a typical mesh is plotted in Figure 14.26. The radius of the pressuremeter was set to one unit, with the length of the mesh in both the radial and axial directions being 200 units.

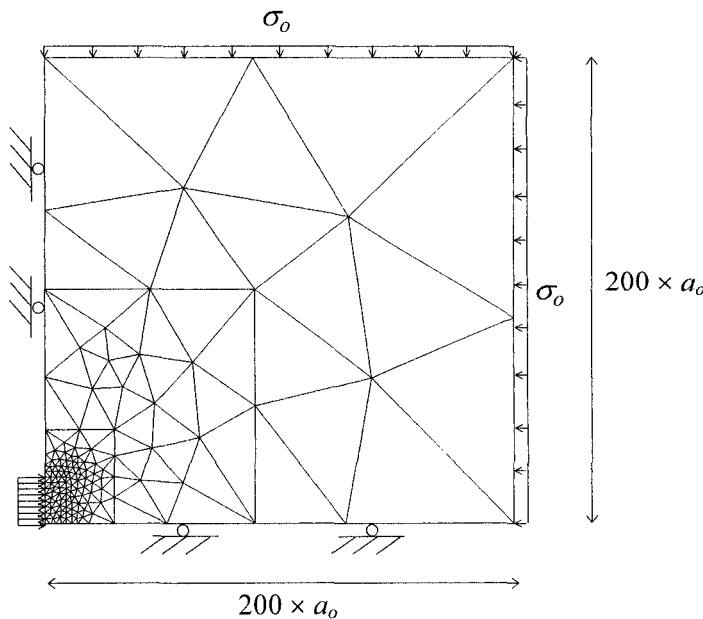


Figure 14.26: Finite element mesh for pressuremeter analysis

#### *Pressuremeter tests in undrained London clay*

To study the effect of two-dimensional geometry of the pressuremeter, four pressuremeter length to diameter ratios of 20, 15, 10 and 5 were used. One-dimensional cylindrical cavity expansions were used to model pressuremeter tests with an infinitely large length to diameter ratio.

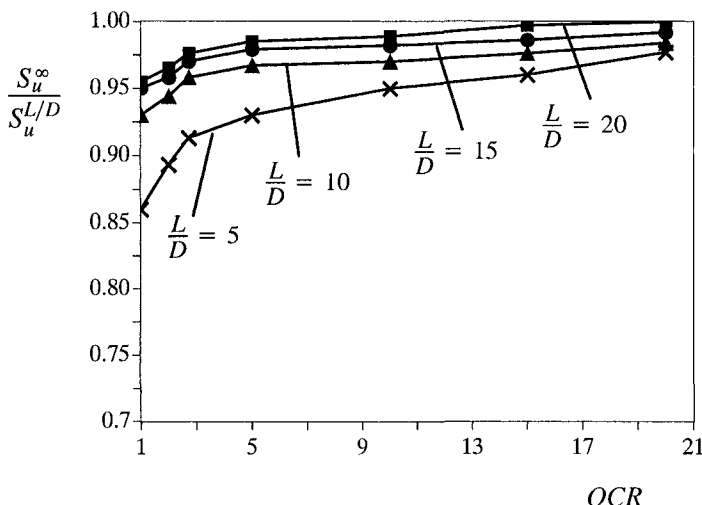


Figure 14.27: Pressuremeter geometry effects on derived undrained strength from tests in London clay (after Yu *et al.*, 2005)

Figure 14.27 shows the effect of pressuremeter length to diameter ratio ( $L/D$ ) on derived undrained shear strength ( $S_u$ ) as a function of stress history OCR value. It is expected that the geometry effect is larger for a smaller pressuremeter length to diameter ratio. The results also suggest that for heavily overconsolidated clays with a large OCR value the pressuremeter geometry effect becomes much smaller.

#### *Drained pressuremeter tests in Ticino sand*

For sand, the effect of spacing ratio  $r$  was also investigated in detail for purposes of comparison. This is because the yield surface of CASM would be similar to the Mohr-Coulomb or Matsuoka-Nakai type when the spacing ratio takes a very large value, see Figure 14.28.

To illustrate the effect of the yield surface, we present the numerical correlations between the initial state parameter and pressuremeter loading slope for the case when the pressuremeter is infinitely long. For this case, Yu (1994) presented a numerical correlation using a Matsuoka-Nakai type of yield surface, indicating that there is a linear relationship between the initial soil state parameter ( $\xi_0$ ) and pressuremeter loading slope ( $S_d$ ).

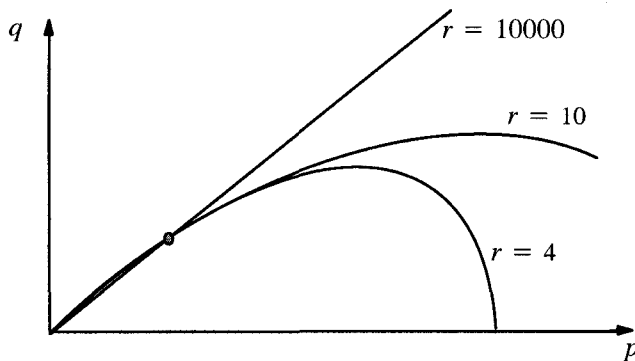


Figure 14.28: CASM yield surfaces with three different spacing ratios

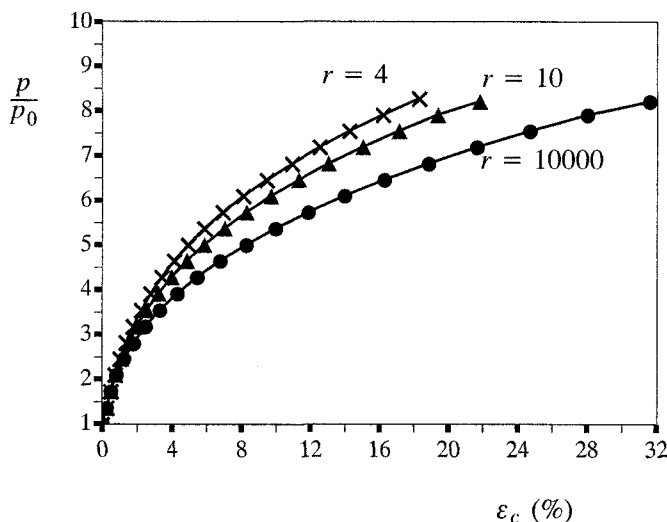


Figure 14.29: Effect of spacing ratios on pressuremeter curves in soils with the initial state parameter of  $\xi_0 = - 0.06$

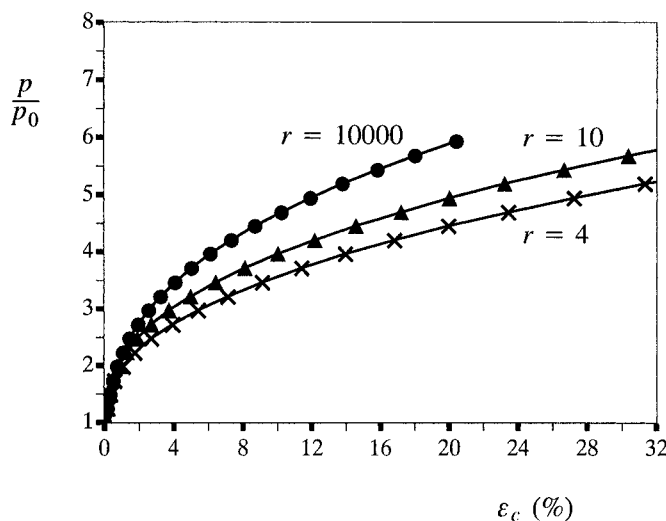


Figure 14.30: Effect of spacing ratios on pressuremeter curves in soils with the initial state parameter of  $\xi_0 = 0.02$

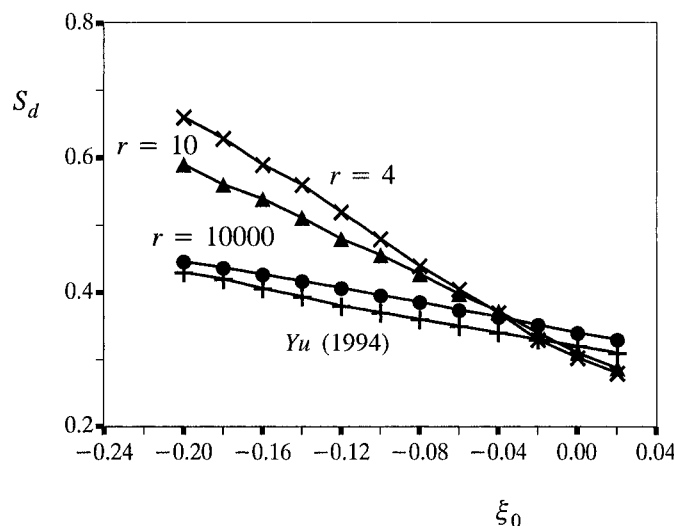


Figure 14.31: Effect of spacing ratios on pressuremeter slope correlations

Figure 14.29 and Figure 14.30 show the effect of the spacing ratio on pressuremeter curves for dense and loose sand respectively (where  $p$  is cavity pressure,  $p_0$  is the initial soil stress and  $\varepsilon_c$  is cavity strain). Figure 14.31 shows the numerical correlations for three different spacing ratios ( $r=4, 10, 10000$ ). For comparison, the numerical correlation derived by Yu (1994) for a hardening plasticity model based on the Matsuoka-Nakai yield surface (where the consolidation hardening is not taken into account) is also plotted in the figure. There are two points that should be noted. First, it is evident from these figures that the inclusion of consolidation hardening (i.e. with a smaller value of the spacing ratio  $r$ ) has a considerable effect on the derived numerical results. It is also shown that the solutions from CASM with a very large spacing ratio (i.e.  $r=10000$ ) is similar to that obtained by Yu (1994) using the Matsuoka-Nakai yield surface. In particular, Figure 14.31 shows that the slope for the numerical correlation between the pressuremeter slope  $S_d$  and initial soil state parameter  $\xi_0$  is almost the same for the two models used.

#### 14.7.2 Finite element analysis of non-coaxial geomaterials

Most recently Yu and Yuan (2005, 2006), Yu *et al.* (2005), Yuan (2005) and Yang and Yu (2006a,b) have applied the non-coaxial plasticity models described in Chapter 8 to analyse a number of soil-structure interaction problems. The explicit substepping scheme with error control, as described in Section 14.5.2, has been used to update stresses. Here one of these examples is given.

##### *Surface strip footings under a vertical load*

The load-deformation response of a surface footing under a vertical load is one of the most important boundary value problems in geotechnical engineering. It is directly related to the design of shallow foundations on soils. The solution to the problem with the coaxial Mohr-Coulomb model is well known. However, geotechnical solutions that account for non-coaxial soil behaviour are very rare.

Yu and Yuan (2005) have analysed the rigid footing problem using the non-coaxial plasticity theory developed by Yu and Yuan (2006) (also presented in Chapter 8). The footing loading is simulated by prescribing the vertical displacement at nodes beneath the footing to ensure that all the nodes move vertically by the same amount. Soil is idealised in the analysis as an elastic perfectly plastic material obeying the Mohr-Coulomb criterion. Typical elastic constants are assumed: Young's modulus  $E = 8 \times 10^4 \text{ kN/m}^2$ , Poisson's ratio  $\mu = 0.3$ , and soil cohesion  $c = 10 \text{ kN/m}^2$  is considered.

Figure 14.32 shows numerical load-displacement curves for both coaxial and non-coaxial models for weightless cohesive-frictional soils with no surcharge. For

the results shown in this figure, an associated flow rule is used with the angles of internal friction and dilation as 30 degrees. It is evident from the figure that the ultimate loads may become very close at very large deformation. For a given working load, however, the deformation induced for a non-coaxial soil is much larger than that for a coaxial soil. For example, when the vertical footing at  $q/c = 25$ , the vertical footing displacement for a non-coaxial soil with  $\Lambda = 0.1$  is about twice as large as that for a coaxial soil ( $\Lambda = 0.0$ ). In other words, the soil becomes much softer when its non-coaxial behaviour is accounted for. Figure 14.33 shows a comparison of the enlarged velocity fields for both cases.

The studies carried out by Yu and Yuan (2005), Yu *et al.* (2005), Yuan (2005) and Yang and Yu (2006a,b) for footings under combined loads and other boundary problems lead to similar conclusions about the importance of including non-coaxial behaviour in soil-structure interaction analysis. This is particularly true for problems involving strong stress rotations.

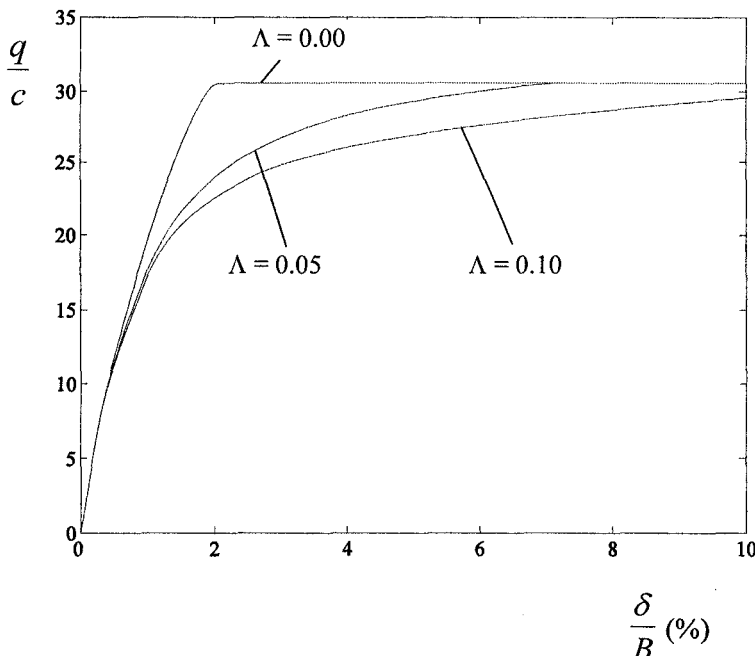
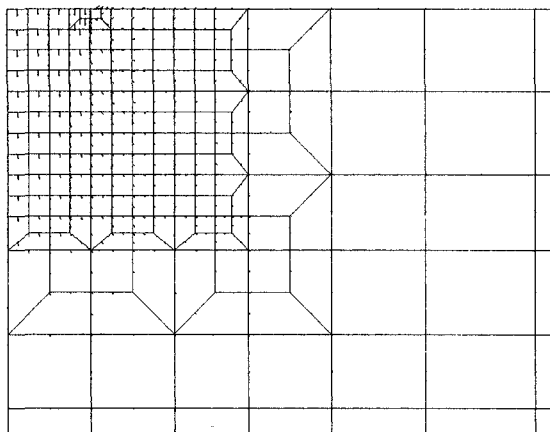
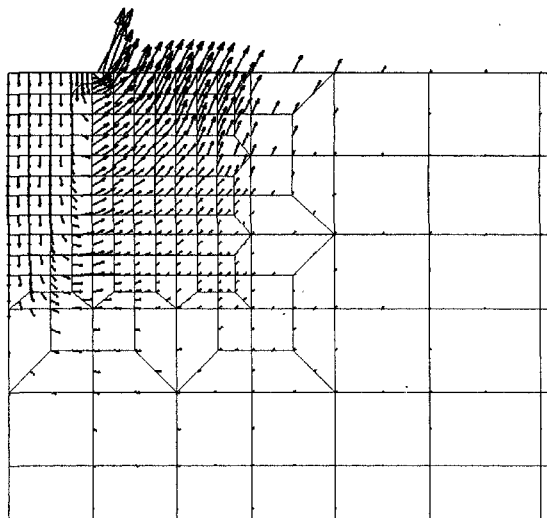


Figure 14.32: Footing load-displacement curves with different non-coaxiality coefficients (after Yu and Yuan, 2005)



(a) Coaxial model



(b) Non-coaxial model

Figure 14.33: Comparison of velocity fields around the footing for both coaxial and non-coaxial models (after Yu and Yuan, 2005)

#### 14.7.3 Finite element analysis of bonded geomaterials

In Section 6.9, the unified critical state model CASM has been extended to model the behaviour of bonded geomaterials. In particular, two important effects are con-

sidered. First of all, the presence of bonding tends to increase the size of elastic domains and therefore affects the size of the yield surface. Secondly bonding is also shown to delay or prevent the tendency for the soil to dilate. This latter effect can be accounted for, for example, by adopting Rowe's stress-dilatancy relation that includes the effect of cohesion.

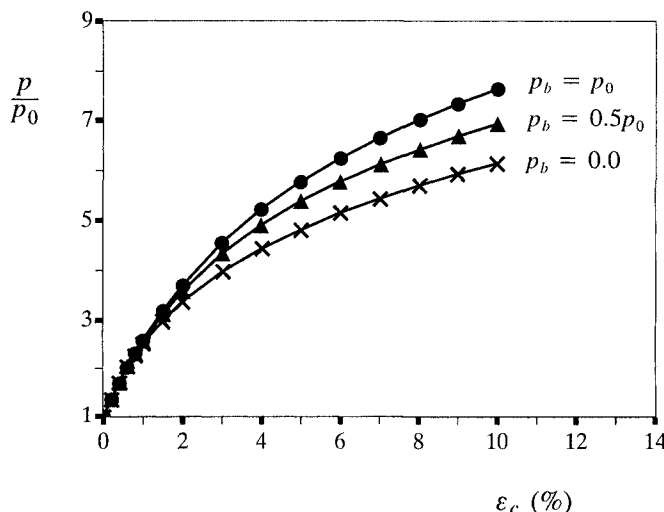


Figure 14.34: Effect of bonding on pressuremeter curves due to enlargement of the elastic domain ( $r=4$ )

In this section, for illustration purpose we present a few results of finite element analysis of a simple boundary value problem of infinitely long pressuremeter tests in bonded geomaterials. More examples of numerical modelling of bonded geomaterials can be found in Tan (2006). For simplicity, the model constants relevant to Ticino sand are used in the finite element calculations. The initial state of the soil is on the dense side of the critical state line with the initial state parameter being equal to  $\xi_0 = -0.04$ . Figure 14.34 shows the effect of bonding on the pressuremeter loading curve and it is expected that the enlargement of the elastic domain makes the material stronger.

Pressuremeter analyses have also been carried out to assess the effect of bonding due to its tendency to delay or prevent dilatancy. The results are plotted in Figure 14.35, which shows that the presence of bonding tends to make the material response slightly softer. As defined in Chapter 6,  $D_c$  is the model parameter used to control the degradation of cohesion with plastic straining.

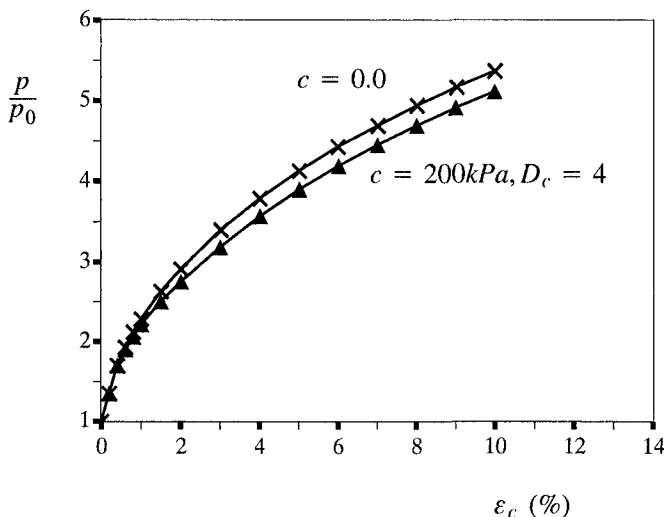


Figure 14.35: Effect of bonding on pressuremeter curves due to its influence on dilatancy ( $r=10000$ )

## REFERENCES

Abbo, A.J. (1997). *Finite Element Algorithms for Elastoplasticity and Consolidation*, PhD Thesis, University of Newcastle, NSW.

Abbo, A.J. and Sloan, S.W. (1996). An automatic load stepping algorithm with error control. *Int. J. Num. Meth. Eng.*, Vol. 39, 1737-1759.

Bathe, K.J. (1982). *Finite Element Procedures in Engineering Analysis*, Prentice Hall.

Britto, A.M. and Gunn, M.J. (1987). *Critical State Soil Mechanics via Finite Elements*, Ellis Horwood, Chichester.

Burd, H.J. (1986). *A Large Displacement Finite Element Analysis of a Reinforced Unpaved Road*, DPhil Thesis, University of Oxford, UK.

Burd, H.J. and Housby, G.T. (1990). Finite element analysis of two cylindrical expansion problems involving near incompressible material behaviour. *Int. J. Num. Anal. Meth. Geomech.*, Vol. 14, 351-366.

Carter, J.P., Booker, J.R. and Davis, E.H. (1977). Finite deformation of an elasto-plastic soil. *Int. J. Num. Anal. Meth. Geomech.*, Vol. 1, 25-43.

Carter, J.P., Desai, C.S., Potts, D.M., Schweiger, H.F. and Sloan, S.W. (2000). Computing and computer modelling in geotechnical engineering, *Proc. of GeoEng2000*, Vol I, 1157-1252.

Chen, W.F. and Mizuno, E. (1990). *Nonlinear Analysis in Soil Mechanics*. Elsevier, Amsterdam.

Christian, J.T. (1968). Undrained stress distribution by numerical methods. *J. Soil Mech. Found. Div., ASCE*, Vol. 96, 1289-1310.

Crisfield, M.A. (1991). *Non-linear Finite Element Analysis of solids and Structures*, Vol I, John Wiley and Sons, Chichester.

Crisfield, M.A. (1997). *Non-linear Finite Element Analysis of solids and Structures*, Vol II, John Wiley and Sons, Chichester.

de Borst, R. and Vermeer, P.A. (1984). Possibilities and limitations of finite elements for limit analysis, *Geotechnique*, Vol. 34, 199-210.

Dienes, J.K. (1979). On the analysis of rotation and stress rate in deforming bodies, *Acta Mechanica*, Vol. 32, 217-232.

Herrmann, L.R. (1965). Elasticity equations for incompressible and nearly incompressible materials by a variational theorem. *J. Am. Inst. Aeronautics and Astronautics*, Vol. 3, 1896-1900.

Hibbitt, H.D., Marcal, P.V. and Rice, J.R. (1970). A finite element formulation for problems of large strain and large displacement. *Int. J. Solids and Structures*, Vol. 6, 1069-1086.

Hill, R. (1950). *The Mathematical Theory of Plasticity*, Clarendon Press, Oxford.

Hill, R. (1968). On constitutive inequalities for simple materials. *J. Mech. Phys. Solids*, Vol 16, 229-242.

Jaumann, G. (1911). Sitzungsberichte akad. Wiss. Wien., Vol 120, 385.

Jinka, A.G.K. and Lewis, R.W. (1994). Incompressibility and axisymmetry: a modified mixed and penalty formulation. *Int. J. Num. Meth. Eng.*, Vol. 37, 1623-1649.

Khong, C.D. (2004). *Development and Numerical Evaluation of Unified Critical State Models*, PhD Thesis, University of Nottingham, UK.

Khong, C.D. and Yu, H.S. (2002). Computational aspects of a unified critical state model for clay and sand, *Proc. of 8th NUMOG*, Rome, 271-277.

Laursen, M.E. and Gellert, M. (1978). Some criteria for numerically integrated matrices and quadrature formulas for triangles. *Int. J. Num. Meth. Eng.*, Vol. 12, 167-176.

Malkus, D.S. and Hughes, T.J.R. (1978). Mixed finite element methods - reduced and selective integration techniques: a unification of concepts. *Comp. Methods Appl. Mech. Eng.*, Vol. 15, 63-81.

Malvern, L.E. (1969). *Introduction to the Mechanics of a Continuous Medium*. Prentice Hall, New Jersey.

McMeeking, R.M. and Rice, J.R. (1975). Finite element formulations for problems of large elastic-plastic deformation. *Int. J. Solids and Structures*, Vol. 11, 601-616.

Naylor, D.J. (1974). Stresses in nearly incompressible materials by finite elements with application to the calculation of excess pore pressures. *Int. J. Num. Meth. Eng.*, Vol 8, 443-460.

Naylor, D.J. (1994). On integrating rules for triangles, *Numerical Methods in Geotechnical Engineering*, Smith (ed.), Balkema, 111-114.

Naylor, D.J., Pande, G.N., Simpson, B. and Tabb, R. (1981). *Finite Elements in Geotechnical Engineering*, Pineridge Press, Swansea.

Nagtegaal, J.C., Parks, D.M. and Rice, J.R. (1974). On numerically accurate finite element solutions in the fully plastic range. *Comp. Methods Appl. Mech. Eng.*, Vol. 4, 153-177.

Oldroyd, J.G. (1950). On the formulation of rheological equations of state. *Proc. R. Soc. A*, Vol 200, 523-541.

Potts, D. M. and Zdravkovic, L. (1999). *Finite Element Analysis in Geotechnical Engineering: Theory*, Thomas Telford, London.

Prager, W. (1961). An elementary discussion of definitions of stress rate. *Quart. Appl. Math.*, Vol. 18, 403-407.

Simo, J.C. and Hughes, T.J.R. (1998). *Computational Inelasticity*, Springer.

Sloan, S.W. (1981). *Numerical Analysis of Incompressible and Plastic Solids Using Finite Elements*. PhD Thesis, University of Cambridge.

Sloan, S.W. (1987). Substepping schemes for the numerical integration of elastoplastic stress-strain relations. *Int. J. Num. Meth. Eng.*, Vol 24, 893-912.

Sloan, S.W. and Randolph, M.F. (1982). Numerical prediction of collapse loads using finite element methods. *Int. J. Num. Anal. Meth. Geomech.*, Vol. 6, 47-76.

Sloan, S.W. and Randolph, M.F. (1983). Discussion on 'Elasto-plastic analysis of deep foundations in cohesive soils' by D.V. Griffiths. *Int. J. Num. Anal. Meth. Geomech.*, Vol. 7, 385-393.

Tan, S.M. (2006). *Constitutive and Numerical Modelling of Bonded Geomaterials*, Forthcoming PhD Thesis, University of Nottingham, UK.

Teh, C.I. (1987). *An Analytical Study of the Cone Penetration*, DPhil Thesis, University of Oxford, UK.

Truesdell, C. (1953). The mechanical foundations of elasticity and fluid dynamics. *J. Rat. Mech. Analys.*, Vol. 2, 593-616.

Walker, J. and Yu, H.S. (2006). Adaptive finite element analysis of cone penetration in clay. *Acta Geotechnica*, Vol. 1 (in press).

Xu, G.Q. (2006). *Wellbore Stability in Geomechanics*, Forthcoming PhD Thesis, University of Nottingham, UK.

Yang, Y. and Yu, H.S. (2006a). Numerical simulations of simple shear with non-coaxial soil models, *Int. J. Num. Analy. Meth. Geomech.*, Vol 30, 1-19.

Yang, Y. and Yu, H.S. (2006b). A non-coaxial critical state soil model and its application to simple shear simulations, *Int. J. Num. Analy. Meth. Geomech.* (in press).

Yu, H.S. (1990). *Cavity Expansion Theory and its Application to the Analysis of Pressuremeters*. DPhil. Thesis, University of Oxford.

Yu, H.S. (1991). A rational displacement interpolation function for axisymmetric finite element analysis of incompressible materials. *Finite Elements in Analysis and Design*, Vol. 10, 205-219.

Yu, H.S. (1994). State parameter from self-boring pressuremeter tests in sand. *J. Geotech. Eng.*, ASCE, Vol. 120, 2118-2135.

Yu, H.S. (1995). A unified critical state model for clay and sand. *Civil Engineering Research Report No 112.08.1995*, University of Newcastle, NSW.

Yu, H.S. (1998). CASM: A unified state parameter model for clay and sand. *Int. J. Num. Analy. Meth. Geomech.*, Vol 22, 621-653.

Yu, H.S. (2004). In situ soil testing: from mechanics to interpretation - First J.K. Mitchell Lecture, *Proc. 2nd International Conference on Site Characterisation (ISC2)*, Porto, Vol. 1, 3-38.

Yu, H.S. and Khong, C.D. (2002). Application of a unified critical state model in finite element analysis, *Proc. 3rd Conf. on 3D Finite Elements for Pavement Analysis Design and Research*, Amsterdam, 253-267.

Yu, H.S. and Netherton, M.D. (2000). Performance of displacement finite elements for modelling incompressible materials. *Int. J. Num. Analy. Meth. Geomech.*, Vol. 24, 627-653.

Yu, H.S. and Yuan, X. (2005). The importance of accounting for non-coaxial behaviour in modelling soil-structure interaction, *Proc. 11th Int Conf. of IACMAG*, (Editors: G Barla and M. Barla), Patron Editore, Invited Issue Paper, Vol 4, 709-718.

Yu, H.S. and Yuan, X. (2006). On a class of non-coaxial plasticity models for granular soils, *Proc. R. Soc. A.*, Vol 462, 725-748.

Yu, H.S., Charles, M.T. and Khong, C.D. (2005). Analysis of pressuremeter geometry effects in clay using critical state models. *Int. J. Num. Analy. Meth. Geomech.*, Vol. 29, 845-859.

Yu, H.S., Houlsby, G.T. and Burd, H.J. (1993). A novel isoparametric finite element displacement formulation for axisymmetric analysis of nearly incompressible materials. *Int. J. Num. Meth. Eng.*, Vol. 36, 2453-2472.

Yu, H.S., Yang, Y. and Yuan, X. (2005). Application of non-coaxial plasticity models in geotechnical analysis. *Proc. of 16th Int. Conf. of ISSMGE*, Osaka, Vol. 2, 993-996.

Yuan, X. (2005). *Non-Coaxial Plasticity for Granular Soils*, PhD Thesis, University of Nottingham, UK.

Zienkiewicz, O.C., Taylor, R.L. and Too, T.M. (1971). Reduced integration technique in general analysis of plates and shells. *Int. J. Num. Meth. Eng.*, Vol. 3, 275-290.

Zienkiewicz, O.C., Chan, A.H.C., Pastor, M., Schrefler, B.A. and Shiomi, T. (1998). *Computational Geomechanics*, Wiley.

## INDEX

Accurate finite elements, 458  
Active set algorithm, 345, 391  
Admissible stress fields, 51, 333  
 $\alpha$ -lines, 296  
 $\alpha'$ -lines, 307  
Anchors, 498  
Angle of friction, 76  
Angle of dilation, 77  
Anisotropic cohesive-frictional material, 323  
Anisotropic Mohr-Coulomb criterion, 323  
Anisotropic strength theory, 359  
Anisotropic soils, 359  
Anisotropy, 322  
Associated flow rule, 91, 303  
Axisymmetric problems, 209, 326, 463

Bauschinger effect, 30, 412  
Bearing capacity, 310, 355  
 $\beta$ -lines, 296  
 $\beta'$ -lines, 307  
Body forces, 13  
Bonded geomaterials, 139  
Bonding, 140  
Bonding degradation, 141  
Boundary value problems, 251, 301  
Bounding surface plasticity, 153  
Bubble model, 175

Bulk modulus, 91  
Cam clay, 88  
Cap-model, 86  
CASM, 105, 498  
CASM-b, 183  
CASM-c, 186  
Cavity expansion, 251,  
Characteristic directions, 296  
Clay, 111, 192  
Coaxiality, 2, 197  
Cohesive-frictional soil, 315  
Cohesive soils, 72  
Cohesionless soils, 241  
Collapse, 54, 56, 58  
Collapse load theorems, 54  
Collins' generalised upper bound theorem, 60  
Complementary energy function, 71  
Complete solution, 316  
Compatibility condition, 18  
Consistency conditions, 32, 34  
Constant volume condition, 461, 464  
Convected part of stress rate, 270  
Continuum mechanics, 10  
Convex yield surface, 24  
Creep strains, 133  
Critical state, 87, 223, 498  
Cyclic loading, 153, 186  
Cyclic triaxial tests, 188

Deformation analysis, 3

Design charts, 441  
Deviatoric plane, 16, 73, 76, 79, 81, 144  
Deviatoric stresses, 15, 233  
Discontinuities in velocity, 307  
Discrete approach, 4  
Discrete element methods, 3, 201  
Disturbed states, 88  
Displacements, 18  
Displacement bounding theorems, 66  
Displacement interpolation function, 465  
Dissipation function, 234, 245  
Dilation, 77  
Double hardening, 95  
Double shearing theory, 205, 285  
Drucker's stability postulate, 27  
Drucker-Prager model, 78

Elasticity, 19, 70  
Elastic material, 47  
Elastic models, 70  
Elastic stress fields, 414  
Elastic stress-strain relations, 19  
Elastic-plastic material, 51  
Elastic-plastic problems, 251  
Elastic-viscoplastic model, 132  
Embankments, 310  
Endochronic theory, 237  
Energy balance, 234  
Engineering shear strain, 18  
Equilibrium, 17, 337, 346  
Eulerian formulations, 496  
Explicit integration methods, 489  
Factor of safety, 373, 378, 380  
Failure, 310, 361  
Failure surface, 353  
Finite element analysis, 456  
Finite element formulations, 467  
Finite medium, 259  
Flow rules, 23, 91, 235, 246  
Footings, 355, 508  
Friction angles, 76  
Frictional material, 75  
Frictional soil, 164  
Full integration, 464

General elastic-plastic theorems, 40  
General stress states, 142  
General stress-state relation, 100  
Geomaterial, 1  
Geotechnical analysis, 1  
Geotechnical stability, 310  
Green strain tensor, 495  
Granular assembly, 201

Hardening, 25  
Hertz load distribution, 422  
Hill's mechanism, 313  
Hoek-Brown model, 82  
Hollow cylinder apparatus, 199  
Hooke's law, 19  
Hyperelasticity, 71  
Hyperplasticity, 245  
Hypoelasticity, 72  
Hypoplasticity, 242  
Hysteresis, 412

Implicit integration methods, 492

Incomplete stress solution, 317  
Incompressible behaviour, 458  
Incompressible materials, 458  
Incompressible plastic flow rule, 458  
Incompressibility constraints, 460  
Incremental solution strategy, 483  
Infinite media, 251  
Infinitesimal theory, 493  
Intermediate principal stress, 290  
Internal state variables, 238  
Intrinsic time measure, 239  
Invariants, 15  
Isotropic hardening, 29, 86  
Iterative solution strategy, 483  
Iwan's translation rule, 159

Jaumann stress rate, 494, 497  
Jointed media, 351  
Joints, 351, 355

Kinematic constraints, 458  
Kinematic hardening, 30, 153  
Kinematic theorem of limit analysis, 395  
Kinematic theorem of shakedown analysis, 443  
Kinematically admissible strain rate fields, 51  
Kinematically admissible velocity fields, 58  
Koiter's upper bound shakedown theorem, 64  
Kronecker delta, 15, 82, 161, 233

Lagrangian formulation, 494  
Lade-Duncan model, 80  
Large deformation analysis, 493  
Large strain, 255  
Linear elasticity, 70  
Linear programming, 339, 364  
Linearized Mohr-Coulomb yield function, 344, 365  
Limit cavity pressure, 257  
Limit analysis, 54, 331  
Limit equilibrium analysis, 337  
Load-path analysis, 331  
Loading surface, 25, 156, 161  
Locked-in energy, 107  
Locking, 458  
Lode angle, 17, 143  
Logarithmic strains, 255  
London clay, 504  
Lower bound analysis, 339  
Lower bound theorem of plastic collapse, 56  
Lower bound shakedown theorem, 63

Major principal stress, 11, 327  
Matsuoka-Nakai model, 80  
Maximum plastic work, 24  
Mean pressure, 15  
Melan's lower bound shakedown theorem, 63  
Method of characteristics, 296, 328  
Micromechanics, 3  
Minimum principles, 47  
Minor principal stress, 11, 327  
Mixed finite element formulation, 459  
Mixed hardening, 31

Modified Cam clay, 88  
 Modified Euler scheme, 486  
 Modified Newton-Raphson scheme, 485  
 Mohr circle, 12  
 Mohr-Coulomb model, 76  
 Mohr-Coulomb yield condition, 252  
 Monotonic loading, 183  
 Mroz's translation rule, 156  
 Multi-surface plasticity, 153

Newton-Raphson scheme, 484  
 Neutral loading, 26, 28  
 Non-associated flow rule, 23, 320  
 Non-coaxial CASM model, 223  
 Non-coaxial plasticity, 197  
 Non-coaxial soil behaviour, 197  
 Nonlinear finite element analysis, 456  
 Nonlinear programming, 393, 442  
 Normality, 23  
 Numerical examples, 498  
 Numerical methods, 3

Objective stress rates, 494  
 Objectivity, 494  
 Onsager's principle, 38  
 Overconsolidation ratio (OCR), 96

Partially saturated soils, 133  
 Particle distortion, 235  
 Particle fracture, 107  
 Particle rearrangement, 234

Passive loading of a retaining wall, 317  
 Pavements, 434  
 Pavement model, 434  
 Perfect plasticity, 25, 69  
 Plane strain, 20  
 Plane strain wedge, 276  
 Plane stress, 19  
 Plastic anisotropy, 322  
 Plastic collapse, 54  
 Plastic deformation, 22  
 Plastic potential, 23  
 Plastic work, 24  
 Plasticity, 1, 22, 69, 153, 197, 232  
 Poisson's ratio, 20  
 Power dissipation, 369  
 Prager's kinematic hardening, 30  
 Prandtl's solution, 316  
 Pressuremeter analysis, 504  
 Principal stresses, 11, 15  
 Pure shear, 73, 277

Radenkovic's upper bound theorem, 59  
 Radial mapping, 177  
 Reduced integration, 459  
 Reference state, 494  
 Reference time line, 133  
 Reinforced soils, 361  
 Residual stresses, 63, 416, 423  
 Retaining walls, 317, 332  
 Reverse plasticity, 410  
 Rock joints, 355  
 Rock mass, 355

Rolling and sliding line contact, 414  
Rolling and sliding point contact, 421  
Rigid infinite cone, 281  
Rigorous analysis, 251

Sand, 1, 123, 500  
Second Piola-Kirchoff stress, 495  
Shakedown theorems, 62  
Shakedown theorems, 62  
Shakedown analysis, 408  
Shallow foundations, 315  
Shear hardening, 129  
Shear modulus, 21  
Shear strains, 18  
Shear stresses, 10  
Similarity solutions, 263  
Simple shear, 198  
Simple slope, 371  
Slip line analysis, 293  
Slip line fields, 300, 301  
Slope stability, 370  
Solution schemes, 483  
Spacing ratio, 96, 504  
Specific dissipation function, 245  
Specific free energy, 245  
Specific volume, 87  
Spherical polar coordinates, 285  
Spherical cavity, 251  
Stable, 27  
Stable plastic material, 28  
Stability analysis, 3  
Stability postulate, 27  
State parameter, 95

Static shakedown theorem, 434  
Statically admissible stress rate fields, 51  
Statically admissible stress fields, 57, 333  
Steady state, 88  
Strain energy function, 71  
Strain space plasticity, 2, 153  
Streamlines for plastic flow, 282  
Stress conditions on velocity characteristics, 309  
Stress-dilatancy relation, 107, 141  
Stress discontinuity, 333  
Stress extension, 317  
Stress fields in plastic regions, 294  
Stress space plasticity, 2  
Stress-state coefficient, 111  
Stress-strain relations, 2, 32  
Stress invariants, 16  
Strip footings, 508  
Structured material, 139  
Substepping, 486, 490

Tangential traction, 414  
Tresca model, 72  
Theorems of plastic collapse, 54  
Theory of envelopes, 232  
Thermodynamics, 238  
Thermomechanical approach, 232  
Three-surface plasticity, 180  
Time-dependent stress-strain behaviour, 132  
Torsional shear, 199  
Traction, 41  
Triaxial tests, 88

Two-surface plasticity, 170

Ultimate states, 87

Undrained shear strength, 73

Uniqueness theorems, 43, 317

Unloading, 186, 409

Unsaturated soils, 133

Unstable, 27

Upper bound analysis, 335, 364

Upper bound theorem of plastic collapse, 58

Upper bound shakedown theorem, 64, 443

Variational principles, 47

Velocity discontinuities, 335, 337

Velocity fields in plastic regions, 303

Vertical cut, 351

Virtual work, 40

Viscoplasticity, 132

Void ratio, 87

Volumetric hardening, 91

Volumetric strains, 91

von Mises model, 74, 246

Wedge penetration, 318

Wellbore stability, 498

Work equation, 89

Work hardening, 30, 86

Yield criterion, 22, 232

Yield surfaces, 22, 25

Yield surface intersection, 489

Yield vertex theory, 202

Young's modulus, 20

Yu's unified critical state model, 99

Zero energy mode, 459

Ziegler's kinematic hardening, 31

Ziegler's orthogonality principle, 246